



**UNIVERSIDADE FEDERAL DO PARÁ  
CENTRO DE GEOCIÊNCIAS  
PROGRAMA DE PÓS-GRADUAÇÃO EM GEOLOGIA E GEOQUÍMICA**

---

**TESE DE DOUTORADO**

**GEOCRONOLOGIA  $^{207}\text{Pb}/^{206}\text{Pb}$ , Sm-Nd, U-Th-Pb E  $^{40}\text{Ar}-^{39}\text{Ar}$  DO  
SEGMENTO SUDESTE DO ESCUDO DAS GUIANAS: EVOLUÇÃO  
CRUSTAL E TERMOCRONOLOGIA DO EVENTO TRANSAMAZÔNICO**

**Tese apresentada por:**

**LÚCIA TRAVASSOS DA ROSA-COSTA**

---

**BELÉM  
2006**

Dados Internacionais de Catalogação-na-Publicação(CIP)  
Biblioteca Geól. Rdº Montenegro G. de Montalvão

---

Rosa-Costa, Lúcia Travassos da

**Geocronologia  $^{207}\text{Pb}/^{206}\text{Pb}$ , Sm-Nd, U-Th-Pb e  $^{40}\text{Ar}$ - $^{39}\text{Ar}$  do Segmento Sudeste do Escudo das Guianas:** Evolução Crustal e Termocronologia do Evento Transamazônico. / Lúcia Travassos da Rosa-Costa; Orientador, Jean-Michel Lafon – 2006

226 f. : il

Tese (Doutorado em Geoquímica e Petrologia) – Universidade Federal do Pará, CG, Curso de Pós-Graduação em Geologia e Geoquímica, Belém, 2006.

1. Geocronologia. 2. Evolução Crustal. 3. Termocronologia. 4. Arqueano. 5. Evento Transamazônico. 6. Escudo das Guianas. 7. Cráton Amazônico. I. Universidade Federal do Pará. II. Lafon, Jean-Michel, Orient. II. Título.

**CDD 20. ed.: 551.7**

---



**Universidade Federal do Pará**

**Centro de Geociências**

**Programa de Pós-Graduação em Geologia e Geoquímica**

**GEOCRONOLOGIA  $^{207}\text{Pb}/^{206}\text{Pb}$ , Sm-Nd, U-Th-Pb E  $^{40}\text{Ar}-^{39}\text{Ar}$  DO  
SEGMENTO SUDESTE DO ESCUDO DAS GUIANAS: EVOLUÇÃO  
CRUSTAL E TERMOCRONOLOGIA DO EVENTO TRANSAMAZÔNICO**

TESE APRESENTADA POR

**LÚCIA TRAVASSOS DA ROSA-COSTA**

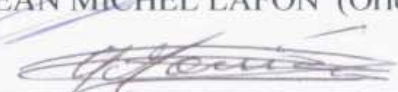
Como requisito parcial à obtenção do Grau de Doutor em Ciências  
na Área de GEOQUÍMICA E PETROLOGIA.

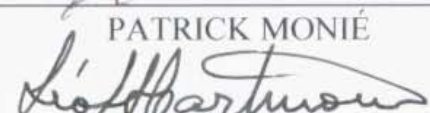
Data de Aprovação: **06 / 07 / 2006**

**Comitê de Tese**

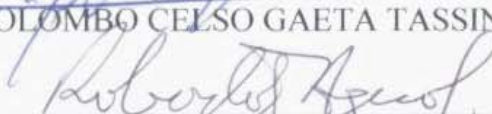


  
JEAN-MICHEL LAFON (Orientador)

  
PATRICK MONIÉ

  
LÉO AFRANEO HARTMANN

  
COLOMBO CELSO GAETA TASSINARI

  
ROBERTO DALL'AGNOL

Belém

*“....amor sem fim, amor  
incondicional, amor maior....  
À Luna e Gabriel, por tantas  
possibilidades no amor”*

## AGRADECIMENTOS

Várias pessoas e instituições contribuíram para o desenvolvimento deste trabalho em suas diversas etapas, às quais desejo expressar meu “muito obrigada”.

Agradeço inicialmente à CPRM, na pessoa do seu presidente, Agamenon Dantas, por ter permitido e, algumas vezes, viabilizado meu desenvolvimento profissional.

À Universidade Federal do Pará, através do Centro de Geociências, pela infra-estrutura.

À CAPES (processo BEX2639/03-3) pelo suporte financeiro para o desenvolvimento do estágio sanduíche no exterior.

Ao Projeto PRONEX (FADESP/CNPq, proj. n°103/98), através de seu coordenador Roberto Dall’Agnol, grande incentivador, por ter possibilitado em diversas ocasiões a divulgação deste trabalho.

A Jean-Michel Lafon eu agradeço pela orientação, pela agradável convivência, por ter confiado em mim, respeitado meu trabalho e meus limites.

Je remercie Patrick Monié pour avoir conduit mon stage à l’Université Montpellier II, et les autres personnes qui ont rendu, pour diverses raisons, mon séjour plus agréable et productif: Rémi Enjolvy, Nicolas Arnaud, Laurent Dezileau, Françoise Roger, André Leyreloup, José Ramos et Jacques Freulon.

Mes remerciements à Claude Delor, pour sa collaboration et pour les discussions géologiques très stimulantes, dès le début de cette thèse.

À Alain Cocherie, pour les discussions productives sur les mystères cachés des monazites.

Aos colegas do Laboratório Pará-Iso (CG-UFPa), Marco Antônio Galarza, Thomas Scheller, Rosemary Monteiro, Elma Oliveira, Roberta Florêncio e Keila Teixeira, pela grande ajuda dispensada durante as análises laboratoriais.

Agradeço Cláudio Lamarão (CG-UFPa), Hilton Costi (Museu Emílio Goeldi), Jean Breton e Claire Bény (BRGM), pelas análises em MEV e “revelação” das adoráveis monazitas.

A vários colegas da CPRM que prestaram imprescindível auxílio em diversas fases deste trabalho: Tomaz e Denise Lobato, Edilberto Leão, Alexandre Carvalho, Raimundo Lourenço, João Inácio, Manoel Soares, Avelino Moraes, Sebastião Benjamin, Reginaldo Cavalcante e Luiz Alberto Costa e Silva.

Aos colegas José Maria Carvalho, Marcelo Vasquez, Evandro Klein e Jaime Passos, pelo incentivo, provocações, o que não deixa de ser um grande incentivo, e por se mostrarem sempre dispostos a ouvir meus devaneios geológicos.

Aos amigos que a França me deu: Beatrix Reynaud, Maria « Guta » Nunes, Sérgio e Olga Neves, pelo apoio constante e por tantos momentos felizes.

À Cíntia Gaia e Alayde Barbosa, pela amizade, sempre (agora me incluam no grupo!). À Cíntia também pela grande e precisa ajuda no final desta jornada.

Aos meus pais José e Terezinha, e irmãos Daniel, Leina, Zilda e Rosa, meu porto seguro, por estarem sempre comigo.

Finalmente, agradeço especialmente ao Paulo Gorayeb, pelo carinho, compreensão e dedicação, que fazem dele um grande companheiro e me permitem seguir em frente.

## SUMÁRIO

	<b>Pág.</b>
<b>DEDICATÓRIA</b> .....	i
<b>AGRADECIMENTOS</b> .....	ii
<b>RESUMO</b> .....	1
<b>ABSTRACT</b> .....	3
<b>1 – APRESENTAÇÃO</b> .....	5
<b>2 – SITUAÇÃO GEOLÓGICA REGIONAL E CONTEXTUALIZAÇÃO TECTÔNICA DA ÁREA DE TRABALHO</b> .....	8
2.1 – MODELOS DE EVOLUÇÃO TECTÔNICA DO CRÁTON AMAZÔNICO.....	8
2.2 – A FAIXA OROGÊNICA PALEOPROTEROZÓICA DO NORTE DO CRÁTON AMAZÔNICO (PROVÍNCIA MARONI-ITACAIÚNAS vs. PROVÍNCIA TRANSAMAZÔNICA) .....	13
<b>3 – CONTEXTO GEOLÓGICO LOCAL</b> .....	21
3.1 – COMPARTIMENTAÇÃO TECTÔNICA .....	21
3.2 – UNIDADES LITOESTRATIGRÁFICAS .....	25
<b>3.2.1 – Assembléia de Embasamento</b> .....	26
3.2.1.1 – Domínio Cupixi .....	26
3.2.1.1.1 – Complexo Tumucumaque .....	26
3.2.1.2 – Domínio Jari .....	27
3.2.1.2.1 – Complexo Jari-Guaribas .....	27
3.2.1.2.2 – Complexo Baixo-Mapari .....	29
3.2.1.2.3 – Suíte Intrusiva Noucouru .....	30
3.2.1.2.4 – Complexo Guianense .....	30
3.2.1.2.5 – Complexo Iratapuru .....	33
3.2.1.2.6 – Complexo Indiferenciado .....	35
3.2.1.3 – Domínio Carecuru.....	36

3.2.1.3.1 – Complexo Paru-Maratiá.....	36
3.2.1.4 – Domínio Paru .....	37
3.2.1.4.1 –Complexo Ananái.....	37
<b>3.2.2 – Seqüências Metavulcano-sedimentares.....</b>	<b>39</b>
<b>3.2.3 – Magmatismo Plutônico Orogênico .....</b>	<b>42</b>
3.2.3.1 – Complexo Máfico-Ultramáfico Bacuri .....	42
3.2.3.2 – Suíte Intrusiva Carecuru.....	43
3.2.3.1.1 – Suíte Intrusiva Igarapé Urucu.....	44
3.2.3.3 – Suíte Intrusiva Parintins.....	46
3.2.3.4 – Granitóides Indiferenciados.....	46
3.2.3.5 – Corpos Máficos-Ultramáficos Indiferenciados.....	48
<b>3.2.4 - Magmatismo Anorogênico.....</b>	<b>48</b>
3.2.4.1 – Granito Waiãpi.....	48
3.3 – PADRÕES ESTRUTURAIS E ASSINATURAS AEROGEOFÍSICAS DOS DOMÍNIOS TECTÔNICOS.....	49
<b>4 – MOTIVAÇÃO DO TRABALHO E OBJETIVOS .....</b>	<b>54</b>
<b>5 – ATIVIDADES E PROCEDIMENTOS ANALÍTICOS .....</b>	<b>57</b>
5.1 – TRABALHOS DE CAMPO E AMOSTRAGEM .....	57
5.2 – ESTUDO PETROGRÁFICO.....	59
5.3 – PREPARAÇÃO DE AMOSTRAS .....	59
5.4 – MICROSCOPIA ELETRÔNICA.....	60
5.5 – GEOCRONOLOGIA E GEOLOGIA ISOTÓPICA.....	61
5.5.1 – Evaporação de Pb em Monocristais de Zircão.....	62
5.5.2 – Sm-Nd em Rocha Total.....	63
5.5.3 – U-Th-Pb em Monazitas.....	64
5.5.4 – $^{40}\text{Ar}$ - $^{39}\text{Ar}$ em Anfibólios e Biotitas.....	65
<b>6 – GEOCRONOLOGIA Pb-Pb POR EVAPORAÇÃO EM ZIRCÃO E GEOLOGIA ISOTÓPICA Sm-Nd EM ROCHA TOTAL.....</b>	<b>67</b>

6.1 – ZIRCON GEOCHRONOLOGY AND Sm-Nd ISOTOPIC STUDY: FURTHER CONSTRAINTS FOR THE ARCHEAN AND PALEOPROTEROZOIC GEODYNAMICAL EVOLUTION OF THE SOUTHEASTERN GUIANA SHIELD, NORTH OF AMAZONIAN CRATON, BRAZIL .....	67
<b>7 – GEOCRONOLOGIA U-Th-Pb EM MONAZITAS.....</b>	<b>114</b>
7.1 – ELECTRON MICROPROBE U-Th-Pb MONAZITE DATING OF THE TRANSAMAZONIAN HIGH-GRADE METAMORPHIC OVERPRINT ON ARCHEAN ROCKS FROM AMAPÁ BLOCK, SOUTHEASTERN GUIANA SHIELD, NORTHERN BRAZIL.....	114
<b>8 – GEOCRONOLOGIA <sup>40</sup>Ar-<sup>39</sup>Ar EM ANFIBÓLIO E BIOTITA.....</b>	<b>158</b>
8.1- <sup>40</sup> Ar- <sup>39</sup> Ar GEOCHRONOLOGY ACROSS ARCHEAN AND PALEOPROTEROZOIC TERRANES FROM SOUTHEASTERN GUIANA SHIELD (NORTH OF AMAZONIAN CRATON, BRAZIL): EVIDENCE FOR CONTRASTING COOLING AND EXHUMATION HISTORIES .....	158
<b>9 – CONSIDERAÇÕES FINAIS .....</b>	<b>198</b>
<b>REFERÊNCIAS BIBLIOGRÁFICAS .....</b>	<b>205</b>

## ANEXOS

ANEXO I – MAPA GEOLÓGICO

ANEXO II –TABELAS ANALÍTICAS

## RESUMO

A região sudeste do Escudo das Guianas é parte de uma das mais expressivas faixas orogênicas paleoproterozóicas do mundo, cuja evolução está relacionada ao Ciclo Orogênico Transamazônico (2,26 – 1,95 Ga). Neste segmento foram estudados distintos terrenos tectônicos, denominados Jari, Carecuru e Paru, reconhecidos em estudos anteriores em função de seus notáveis contrastes em termos de idade, conteúdo litológico e assinatura geofísico-estrutural. O Domínio Jari é constituído por uma assembléia de embasamento do tipo granulito-gnaiss-migmatito com protólitos arqueanos, enquanto o Domínio Carecuru é composto basicamente por rochas cálcio-alcálicas e seqüências metavulcano-sedimentares, com evolução relacionada ao Evento Transamazônico. O Domínio Paru foi delimitado no interior do Domínio Carecuru, e é formado por gnaisses granulíticos com protólitos arqueanos, que hospedam plútons charnoquíticos paleoproterozóicos.

Neste estudo, quatro métodos geocronológicos foram empregados em rochas provenientes dos distintos domínios tectônicos, com o objetivo de entender significado tectônico de cada um deles, definir os processos de evolução crustal que atuaram no Arqueano e no Paleoproterozóico e avaliar a extensão de crosta arqueana neste setor da faixa orogênica em questão.

Os métodos de evaporação de Pb em zircão e Sm-Nd em rocha total demonstram que a evolução do Domínio Jari envolve vários estágios de acreção e retrabalhamento crustal, do Arqueano ao Paleoproterozóico. Atividade magmática ocorreu principalmente na transição Meso-Neoarqueano (2,80-2,79 Ga) e durante o Neoarqueano (2,66-2,60 Ga). O principal período de formação de crosta continental ocorreu a partir do final do Paleoarqueano e ao longo do Mesoarqueano (3,26-2,83 Ga), enquanto retrabalhamento crustal prevaleceu no Neoarqueano. Durante o Evento Transamazônico, dominaram processos de retrabalhamento de crosta arqueana, com vários pulsos de magmatismo granítico, datados entre 2,22 Ga e 2,03 Ga, que marcam distintos estágios da evolução orogenética.

Os dados geocronológicos obtidos neste estudo, conjugados aos disponíveis na literatura, indicam que o Domínio Jari é parte do mais expressivo segmento de crosta arqueana conhecido no Escudo das Guianas, aqui definido e denominado de Bloco Amapá.

No Domínio Carecuru foram definidos dois pulsos de magmatismo cálcio-alcálico, entre 2,19 e 2,18 Ga e entre 2,15 e 2,14 Ga, enquanto magmatismo granítico foi datado em 2,10 Ga. Acreção crustal juvenil cálcio-alcálica foi reconhecida em torno de 2,28 Ga. No entanto, idades

$T_{DM}$  (2,50-2,38 Ga), preferencialmente interpretadas como idades mistas, e  $\epsilon_{Nd} < 0$ , indicam a participação de componentes arqueanos na fonte das rochas paleoproterozóicas. Os dados isotópicos, somados à associação litológica deste domínio, sugerem uma evolução relacionada a sistema de arco magmático em margem continental ativa, que foi acrescido ao Bloco Amapá durante o Evento Transamazônico.

No Domínio Paru, magmatismo neoarqueano datado em torno de 2,60 Ga, foi produzido por retrabalhamento de crosta mesoarqueana, assim como no Bloco Amapá. Adicionalmente, acreção crustal juvenil e magmatismo cálcio-alcálico foram reconhecidos, em torno de 2,32 Ga e 2,15 Ga, respectivamente, além de magmatismo charnoquítico em 2,07 Ga.

Idades U-Th-Pb obtidas em monazitas provenientes da assembléia de alto grau do sudoeste do Bloco Amapá, revelaram dois estágios distintos da evolução orogênica transamazônica. O primeiro ocorreu em torno de 2,09 Ga, que marca a idade do metamorfismo de fácies granulito, contemporâneo ao desenvolvimento de um sistema de cavalgamento oblíquo, relacionado ao estágio colisional da orogênese. O outro ocorreu em torno de 2,06 Ga e 2,04 Ga, e é consistente com o estágio tardi-colisional, marcado por migmatização do embasamento e colocação de granitos ao longo de zonas de cisalhamento transcorrentes.

Finalmente, análises  $^{40}\text{Ar}/^{39}\text{Ar}$  em anfibólios e biotitas de unidades estratigráficas representativas, principalmente do Bloco Amapá e do Domínio Carecuru, revelam distintos padrões de resfriamento e exumação para estes dois segmentos crustais. No Bloco Amapá, as idades de anfibólios variam entre 2,13 e 2,09 Ga, enquanto as biotitas forneceram idades principalmente entre 2,10 e 2,05 Ga. No Domínio Carecuru, anfibólios e biotitas apresentaram idades entre 2,16 e 2,06 Ga e entre 1,97 e 1,85 Ga, respectivamente. Taxas de resfriamento da ordem 67 °C/Ma e 40 °C/Ma foram calculadas para o Bloco Amapá, indicando resfriamento rápido e exumação controlada por tectonismo, possivelmente relacionada ao estágio colisional do Evento Transamazônico. Em contrapartida, no Domínio Carecuru, as taxas de resfriamento regional variam em torno de 3-2,3 °C/Ma, sugerindo resfriamento lento e exumação gradual, o que é consistente com o modelo de arco magmático, no qual, crescimento de crosta continental resulta principalmente de acreção magmática lateral, sem espessamento crustal significativo.

## ABSTRACT

The southeastern portion of the Guiana Shield is part of a large Paleoproterozoic orogenic belt, with evolution related to the Transamazonian Orogenic Cycle (2.26 – 1.95 Ga). In this area, previous works defined distinct tectonic domains, named Jari, Carecuru and Paru, which present outstanding differences in terms of age, lithological content, structural pattern and geophysical signature. The Jari Domain is constituted of a granulite-gneiss-migmatite basement assemblage derived from Archean protoliths, and the Carecuru Domain is composed mainly of calc-alkaline rocks and metavolcano-sedimentary sequences, developed during the Transamazonian Event. The Paru Domain is an oval-shaped granulitic nucleus, located within the Carecuru Domain, formed by granulitic gneisses with Archean precursors and Paleoproterozoic charnockitic plutons.

In this study, distinct geochronological methods were employed in rocks from the distinct domains, in order to define their tectonic meaning and crustal evolution processes during Archean and Paleoproterozoic times.

Pb-evaporation on zircon and Sm-Nd on whole rock dating were provided on magmatic and metamorphic units from the Jari Domain, defining its long-lived evolution, marked by several stages of crustal accretion and crustal reworking. Magmatic activity occurred mainly at the Meso-Neoproterozoic transition (2.80-2.79 Ga) and during the Neoproterozoic (2.66-2.60 Ga). The main period of crust formation occurred during a protracted episode at the end of Paleoproterozoic and along the whole Mesooproterozoic (3.26-2.83 Ga). Conversely, crustal reworking processes have dominated in Neoproterozoic times. During the Transamazonian Event, the main geodynamic processes were related to reworking of older Archean crust, with minor juvenile accretion at about 2.3 Ga, during an early orogenic phase. Transamazonian magmatism consisted of syn- to late-orogenic granitic pulses, which were dated between 2.22 and 2.03 Ga. Most of the  $\epsilon_{\text{Nd}}$  values and  $T_{\text{DM}}$  model ages (2.52-2.45 Ga) indicate an origin of the Paleoproterozoic granites by mixing of juvenile Paleoproterozoic magmas with Archean components.

The new geochronological results, added to data from previous studies, revealed that the Jari Domain represents the southwestern part of the most expressive Archean continental landmass of the Guiana Shield, here defined and named Amapá Block. The recognition of an extended Archean block precludes previous statements that the Archean in the southeast of the Guiana Shield, was restricted to isolated remnants or inliers within Paleoproterozoic terrains.

In the Carecuru Domain the widespread calc-alkaline magmatism occurred at 2.19-2.18 Ga and at 2.15-2.14 Ga, and granitic magmatism was dated at 2.10 Ga. Crustal accretion was recognized at about 2.28 Ga, in agreement with the predominantly Rhyacian crust-forming pattern of the Guiana Shield. Nevertheless,  $T_{DM}$  model ages (2.50-2.38 Ga), preferentially interpreted as mixed ages, and  $\epsilon_{Nd} < 0$ , point to some participation of Archean components in the source of the Paleoproterozoic rocks. The lithological association and the available isotopic data registered in the Carecuru Domain, suggests a geodynamic evolution model based on the development of a magmatic arc system during the Transamazonian Orogenic Cycle, which was accreted to the southwest border of the Archean Amapá Block.

In the Paru Domain, Neoproterozoic magmatism at about 2.60 Ga was produced by reworking of Mesoproterozoic crust, as registered in the Amapá Block. Crustal accretion events and calc-alkaline magmatism were recognized at 2.32 Ga and at 2.15 Ga, respectively, as well as charnockitic magmatism at 2.07 Ga.

U-Th-Pb chemical ages in monazites from high-grade rocks of the southwestern part of Amapá Block, dated two main tectono-thermal events. The first one was revealed by the monazite ages of about 2.09 Ga and marks the age of the granulite-facies metamorphism. These data, added to petro-structural information, indicate that the granulite-facies metamorphism was contemporaneous to the development of a thrusting system associated to the collisional stage of the Transamazonian Orogeny. The later event was testified by monazite ages at about 2.06 Ga and 2.04 Ga, and is consistent with a late-orogenic stage marked by granitic emplacement and coeval migmatization of the Archean basement along strike-slip zones.

Finally,  $^{40}\text{Ar}/^{39}\text{Ar}$  geochronological study on amphibole and biotite from representative units of the Amapá Block and of the Carecuru Domain delineated contrasting cooling and exhumation stories. In the former amphibole vary from 2.13 to 2.09 Ga, and biotite ages range mainly between 2.10 and 2.05 Ga. In the later, amphibole and biotite ages are between 2.16 and 2.06 Ga, and 1.97 and 1.85 Ga, respectively. In the Amapá Block, fast cooling rates around 67 °C/m.y. and 40 °C/m.y indicate a tectonically controlled exhumation, related to collisional stages of the Transamazonian Event. Conversely, in the Carecuru Domain, regional cooling rates in the order of 3-2.3 °C/m.y. suggest slow cooling and gradual uplift, which is consistent with the magmatic arc model, where continental growth results mainly from lateral magmatic accretion, precluding significant tectonic crustal thickening.

## 1 - APRESENTAÇÃO

Na região sudeste do Escudo das Guianas, norte do Cráton Amazônico, a CPRM-Serviço Geológico do Brasil realizou, através do Projeto Promin-RENCA, mapeamento geológico de semi-detalhe (escala 1:250.000) em uma área de aproximadamente 33.000 km<sup>2</sup>, posicionada na fronteira entre os estados do Pará e Amapá, norte do Brasil (Figura 1.1).

A área mapeada inclui grande parte da Reserva Nacional do Cobre e Associados (RENCA), área restritiva para pesquisa geológica pelo setor privado, e é recoberta por uma densa floresta equatorial e por um espesso perfil de solos lateríticos, desenvolvidos sobre substrato rochoso pré-cambriano, apresentando grande dificuldade de acesso. Estas características fisiográficas, somadas ao fato de que os últimos levantamentos geológicos sistemáticos realizados na área datam do início dos anos 80, mantiveram esta região resguardada do avanço do entendimento geológico, a despeito de ser reconhecida como uma área com grande potencial metalogenético, tornando-se um dos setores mais desconhecidos, ou de conhecimento mais defasado do território brasileiro.

O novo levantamento geológico, iniciado no ano 2000, foi subsidiado por aerogeofísica de alta resolução (magnetometria e gamaespectrometria), trabalhos de campo, investigações petrográficas e algumas determinações geocronológicas. Os resultados alcançados pelo referido projeto propiciaram avanços significativos no conhecimento geológico daquela região, no entanto, dentro dos limites impostos por trabalhos de cunho regional.

Uma das mais significativas contribuições foi o reconhecimento de terrenos tectônicos, que se caracterizam individualmente por apresentarem conteúdo litológico, estilo estrutural e padrões geocronológicos particulares (arqueanos ou paleoproterozóicos) e distintos em relação aos terrenos adjacentes. Esta compartimentação tectônica orientou a sistematização das unidades litoestratigráficas regionais, através da redefinição de unidades amplamente comentadas na literatura e da proposição de novas unidades. Entretanto, a descoberta de novos registros de rochas arqueanas e, conseqüentemente, a possibilidade de existência de grandes segmentos crustais arqueanos, fomentaram discussões sobre a natureza e extensão de crosta arqueana no sudeste do Escudo das Guianas, região reconhecida como integrante de um dos mais expressivos orógenos paleoproterozóicos do mundo, que engloba toda a porção nordeste do referido escudo.

---

Objetivando contribuir para o avanço do conhecimento deste segmento do Cráton Amazônico, foi realizada esta pesquisa no nível de tese de doutorado, iniciada em 2002 e vinculada ao Programa de Pós-Graduação em Geologia e Geoquímica da Universidade Federal do Pará. A área selecionada para estudo é parte da área do Projeto Promin-RENCA, recobrando cerca de 2/3 da mesma, e tem como principais cursos d'água os rios Jari, Mapari, Iratapuru, Ipitinga, Carecuru e Paru, que foram utilizados como as principais vias de acesso durante o mapeamento (Figura 1.1).

A estrutura organizacional deste documento inclui preliminarmente a contextualização geológica regional (Capítulo 2), destacando-se os principais modelos de evolução propostos para o Cráton Amazônico, com ênfase nos mais relevantes aspectos geológicos e geocronológicos da porção oriental do referido cráton, onde está inserida a área deste estudo. Em seguida, será descrita, mais detalhadamente, a geologia da área em questão (Capítulo 3), e com a caracterização do estado da arte do conhecimento geológico da região de interesse, serão definidos os principais problemas geológicos que motivaram a proposição deste trabalho, a partir dos quais foram definidos os objetivos da pesquisa (Capítulo 4). As atividades e procedimentos metodológicos que viabilizaram o cumprimento dos objetivos propostos serão sinteticamente descritos (Capítulo 5). Os resultados alcançados neste trabalho serão apresentados e discutidos na forma de três artigos científicos (Capítulos 6, 7 e 8), e abordados de forma integrada no capítulo final (Capítulo 9).

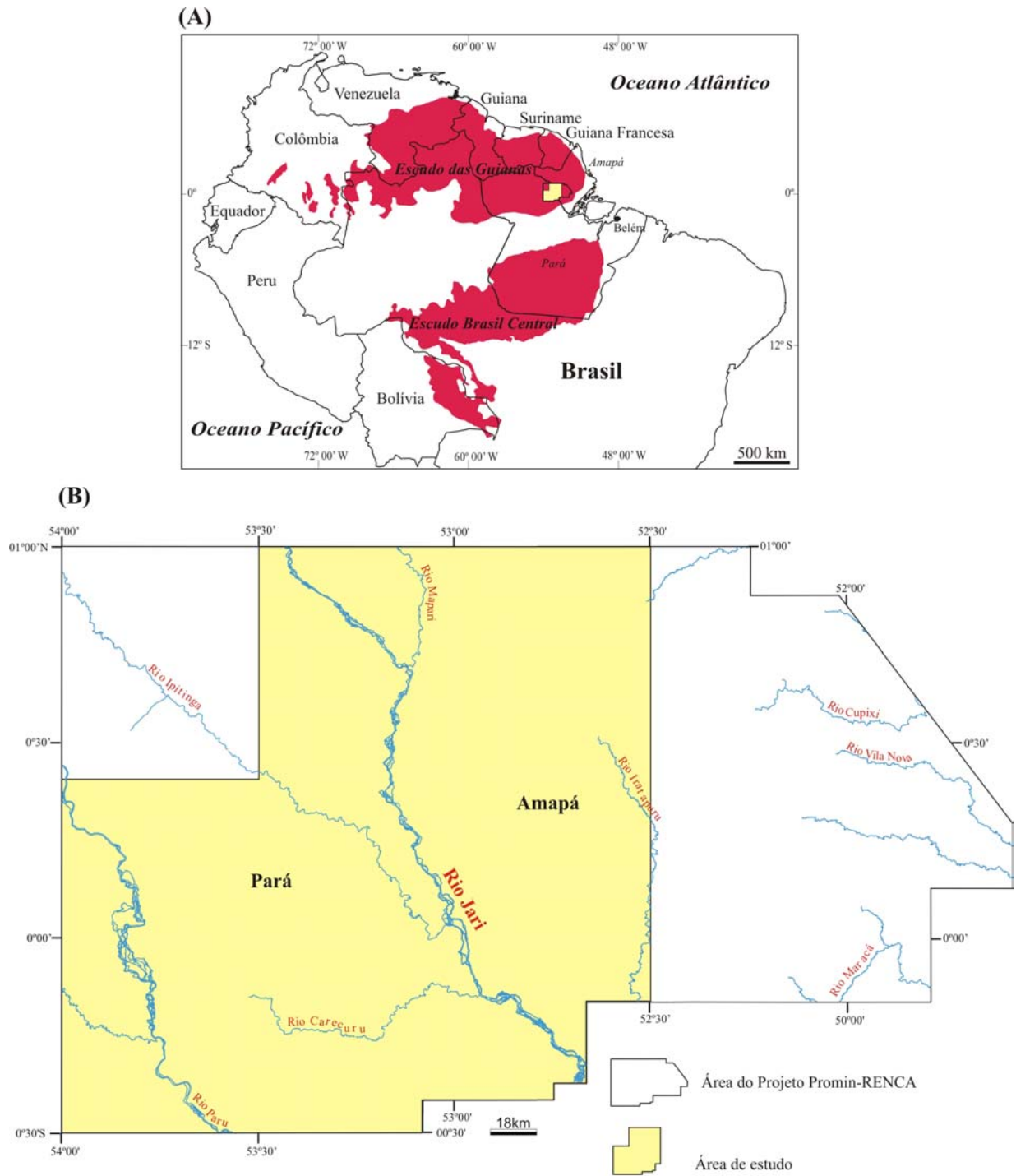


**Figura 1 - (A)** Localização do área de estudo no Escudo das Guianas, porção setentrional do Cráton Amazônico. **(B)** Situação da área no polígono mapeado pelo Projeto Promin-RENCA, com destaque aos principais cursos d'água da região.

## 2 – SITUAÇÃO GEOLÓGICA REGIONAL E CONTEXTUALIZAÇÃO TECTÔNICA DA ÁREA DE TRABALHO

### 2.1 – MODELOS DE EVOLUÇÃO TECTÔNICA DO CRÁTON AMAZÔNICO

Três grandes unidades geotectônicas constituem o continente sul-americano, ou porção continental (emersa) da Placa Sul-Americana: a Plataforma Sul-Americana, a Faixa Orogênica Andina e a Plataforma Patagônica (Almeida et al. 1981). O território brasileiro ocupa grande parte da Plataforma Sul-Americana, definida por três escudos pré-cambrianos, o Escudo das Guianas, o Escudo Brasil Central ou Guaporé, e o Escudo Atlântico, além de extensas áreas de coberturas plataformais fanerozóicas, acumuladas principalmente nas bacias sedimentares paleozóicas do Amazonas-Solimões, do Paraná e do Parnaíba (Figura 2.1).

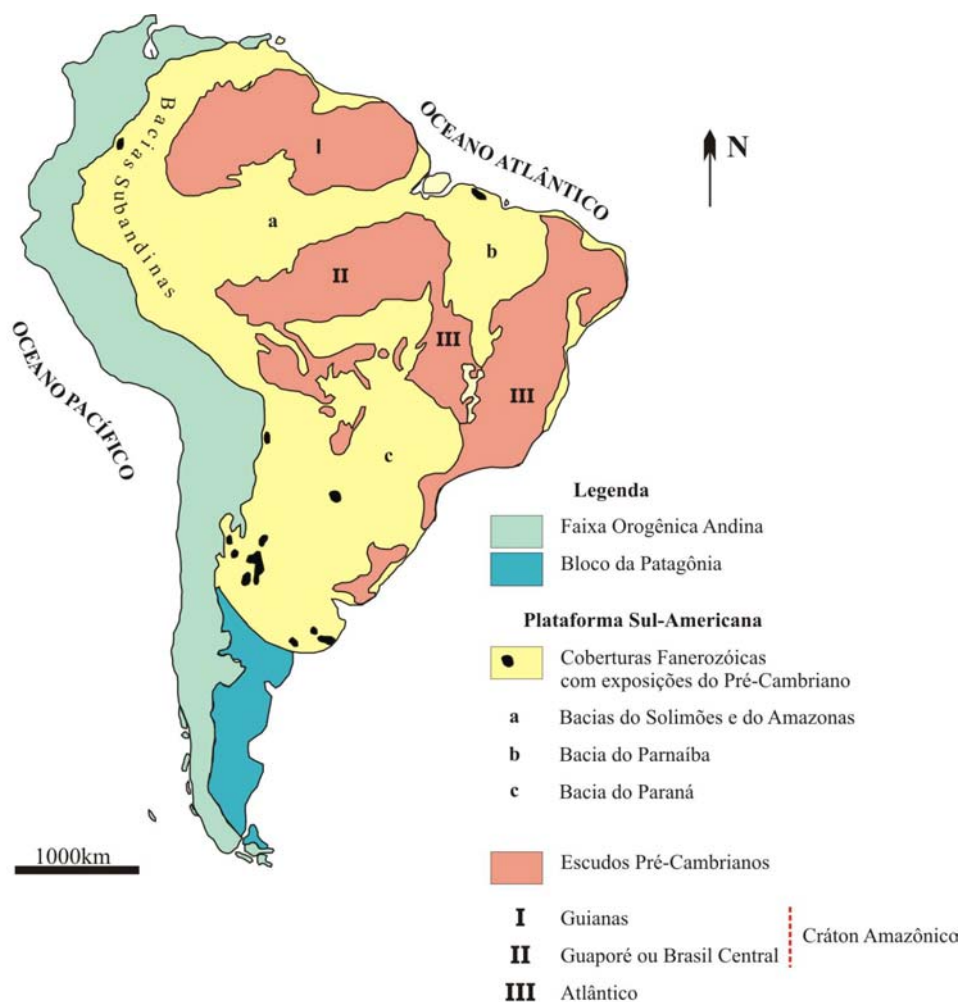


**Figura 2.1** - Províncias geotectônicas da América do Sul, segundo Cordani et al. (2000).

O Cráton Amazônico, representando uma das principais unidades tectônicas da Plataforma Sul-Americana, encerra dois escudos pré-cambrianos, o Escudo das Guianas, a norte, e o Escudo Brasil Central, a sul da bacia do Amazonas-Solimões (Figura 2.1). Localizado na porção norte da América do Sul, cobre uma área de aproximadamente 4.500.000 km<sup>2</sup>, que inclui parte do Brasil, Guiana Francesa, Guiana, Suriname, Venezuela, Colômbia e Bolívia. É limitado a norte pela margem atlântica, e em suas bordas oriental e meridional por faixas orogênicas neoproterozóicas marginais do Escudo Atlântico (Paraguai- Araguaia-Tocantins), geradas durante o Ciclo Orogrênico Brasileiro (Tassinari et al. 2000). O limite ocidental com a Faixa Orogrênica Andina é em grande parte convencional, visto que geralmente está encoberto por depósitos cenozóicos das bacias de antepaís subandinas, que se estendem desde a Venezuela até o sul da Argentina (Schobbenhaus & Brito Neves 2003).

O Cráton Amazônico representa uma grande placa litosférica continental, composta por várias províncias crustais de idades arqueana a mesoproterozóica, que foi estabilizada tectonicamente em torno de 1,0 Ga, tendo se comportado como uma placa estável no Neoproterozóico, durante o desenvolvimento das faixas orogênicas marginais brasileiras (Brito Neves & Cordani 1991).

Vários modelos de evolução tectônica têm sido propostos para o Cráton Amazônico, os quais contrapõem basicamente duas escolas teóricas principais, a fixista e a mobilista. Em linhas gerais, a escola fixista considera o referido cráton como uma grande plataforma continental arqueana, afetada por diversos episódios de retrabalhamento crustal e rejuvenescimento termal paleo e mesoproterozóicos. Seguindo os preceitos da tectônica fixista, destacam-se os trabalhos de Hasui et al. (1984), Hasui & Almeida (1985) e Costa & Hasui (1997). Estes autores definem o Cráton Amazônico como um mosaico de doze blocos tectônicos justapostos, ou paleoplacas, que se agregaram através de colisões diacrônicas no Arqueano e Paleoproterozóico, compondo parte de um megacontinente. Os blocos seriam constituídos, basicamente, por complexos gnáissicos de médio grau metamórfico e sequências meta-supracrustais, definindo terrenos do tipo *granito-greenstone*. Os limites dos blocos seriam marcados por suturas colisionais, delineadas pela gravimetria, às quais estariam associados cinturões granulíticos, ou por cinturões de cisalhamento, que envolveriam cavalgamentos, associados ou não a transcorrências tardias, igualmente condizentes com a tectônica colisional (Figura 2.2). Segundo este modelo, ao final do

Paleoproterozóico e início do Mesoproterozóico haveria uma grande massa continental consolidada, sobre a qual atuaram apenas eventos de tectônica intraplaca do tipo extensional.

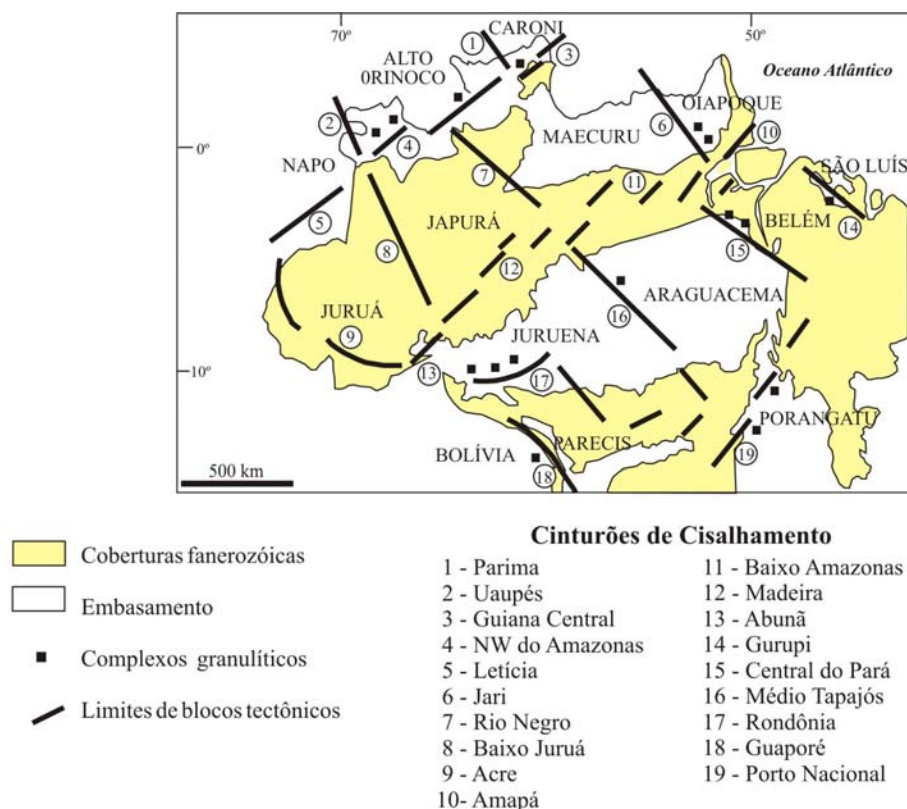


**Figura 2.2** - Modelo de compartimentação tectônica da região amazônica no Brasil, segundo a proposta de Hasui *et al.* (1984).

O modelo fixista baseou-se fundamentalmente em dados geofísicos (gravimetria e magnetometria), em interpretações de informações geológicas e estruturais disponíveis na época, e em dados radiométricos escassos e, sobretudo, obtidos pelos métodos geocronológicos K-Ar e Rb-Sr. Além disso, o modelo considerou apenas o processo colisional do tipo himalaiano (crosta continental vs. crosta continental) para explicar o crescimento da plataforma continental durante o Arqueano e Paleoproterozóico. Todavia, levantamentos geológicos realizados em diversos setores do Cráton Amazônico nas últimas décadas, os quais são geralmente acompanhados por determinações geocronológicas utilizando métodos mais adequados (U-Pb, Pb-Pb e Sm-Nd), não fornecem sustentação ao modelo fixista, pois demonstram que grande parte dos blocos crustais é mais jovem que Arqueano-Paleoproterozóico, e ainda que acreção crustal juvenil relacionada a

ambientes de subducção representou um mecanismo fundamental de crescimento continental deste cráton.

Alternativamente, a escola mobilista pontua que a evolução do Cráton Amazônico é resultante de sucessivos episódios de acreção crustal no Paleo- e Mesoproterozóico, em volta de um núcleo mais antigo, estabilizado no final do Arqueano. Como precursor dos modelos mobilistas, destaca-se o trabalho de Cordani et al. (1979), o qual vem sofrendo modificações à medida que novos dados geológicos e geocronológicos estão sendo produzidos em diversos segmentos do referido cráton (ex. Cordani & Brito Neves 1982, Teixeira et al. 1989, Tassinari 1996, Sato & Tassinari 1997, Cordani & Sato 1999, Tassinari & Macambira 1999, Tassinari et al. 2000), sendo a mais recente síntese apresentada por Tassinari & Macambira (2004).

Segundo esta proposta, o Cráton Amazônico pode ser dividido em grandes províncias geocronológicas, definidas a partir de padrões geocronológicos característicos, assembléias litológicas, *trends* estruturais e histórias geológicas particulares e distintas em relação às províncias adjacentes. Desta forma, foram individualizadas as províncias Amazônia Central (> 2,5 Ga), que compreende os núcleos arqueanos Carajás e Iricoumé, e as províncias paleo e mesoproterozóicas denominadas Maroni-Itacaiúnas (2,2 – 1,9 Ga), Ventuari-Tapajós (1,9 – 1,8 Ga), Rio Negro-Juruena (1,8 – 1,55 Ga), Rondoniana-San Ignácio (1,55 – 1,3 Ga) e Sunsás (1,25 – 1,0 Ga) (Figura 2.3).

O modelo evolutivo para o Cráton Amazônico consoante às propostas mobilistas admite que havia inicialmente um protocráton arqueano, composto por microcontinentes independentes, representados pelos blocos Carajás-Iricoumé e Imataca, que foram amalgamados entre 2,2 e 1,95 Ga através de faixas orogênicas paleoproterozóicas, que compõem a Província Maroni-Itacaiúnas. A aglutinação dos blocos arqueanos teria acontecido concomitantemente à acreção crustal juvenil iniciada na margem oeste do proto-cráton. Neste contexto, as províncias Ventuari-Tapajós, Rio Negro-Juruena e parte da Rondoniana-San Ignácio, representam um extenso domínio de crosta continental juvenil desenvolvida entre 1,9 e 1,55 Ga, através de sistemas de arcos magmáticos sucessivos, produzidos em função da subducção de litosfera oceânica para leste, resultante da convergência entre o proto-cráton Amazônico e outra massa continental a oeste. Finalmente, a evolução orogênica das províncias Rondoniana-San Ignácio e Sunsás, entre 1,4 e 1,0 Ga, se deu em ambiente ensiálico, devido à colisão continental entre o Cráton

Amazônico e a Laurentia (Provincia Greenville, América do Norte), em conformidade com proposições de Sadowski & Bettencourt (1996).

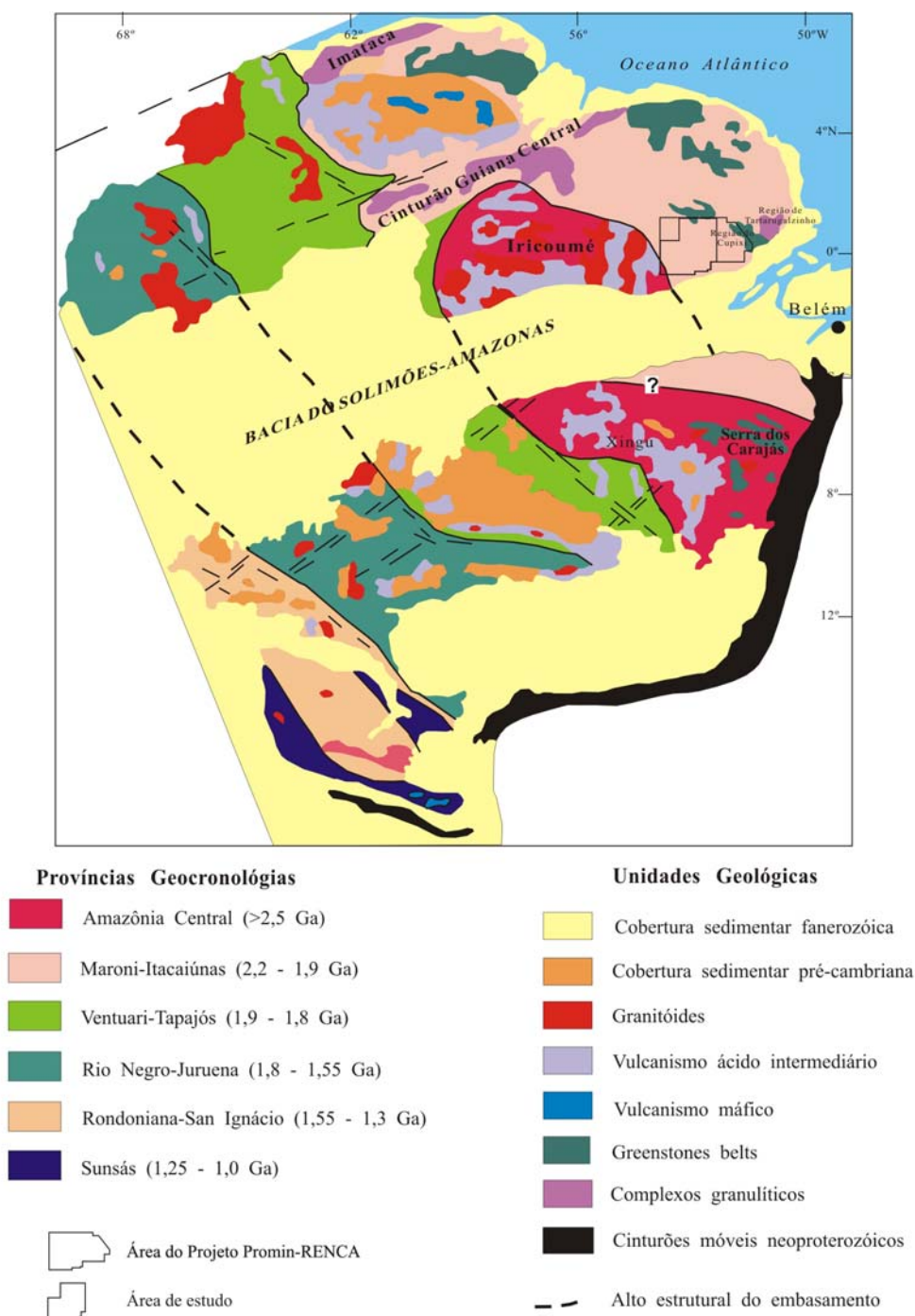


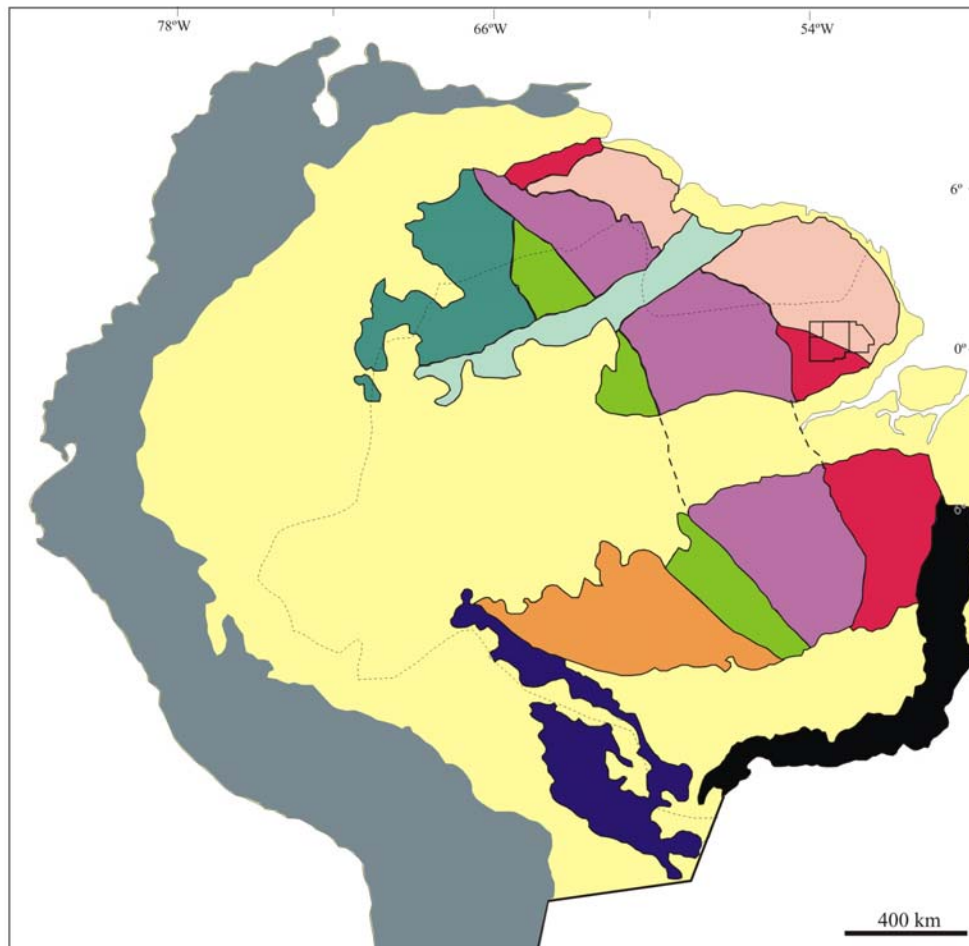
**Figura 2.3** - Províncias geocronológicas do Cráton Amazônico, de acordo com Tassinari & Macambira (2004).

Santos et al. (2000), baseando-se na interpretação de novos dados U-Pb e Sm-Nd obtidos na porção ocidental e central do cráton, e na reavaliação de dados geocronológicos disponíveis na literatura, propuseram algumas modificações ao modelo mobilista anterior, sobretudo no que diz respeito à denominação e posicionamento de limites entre províncias. Estes autores reconheceram a existência de sete províncias tectônicas, com idades entre 3,1 e 0,99 Ga, assim denominadas: Carajás-Imataca (3,10–2,53 Ga), Transamazônica (2,25 - 2,00 Ga), Tapajós–Parima (2,10 – 1,87 Ga), Amazônia Central (1,88 – 1,77 Ga), Rondônia–Juruena (1,75 – 1,47 Ga), Rio Negro (1,86 – 1,52 Ga) e Sunsás (1,33 – 0,99 Ga) (Figura 2.4). De acordo com esta proposta, os núcleos arqueanos estão representados pelos blocos Carajás, a sul, e Imataca, a norte; as províncias Transamazonas, Tapajós-Parima e Rondônia-Juruena representam províncias juvenis, geradas por sucessivos eventos de acreção crustal no Paleoproterozóico, relacionados a sistemas de arcos magmáticos; a Província Amazônia Central representa o prolongamento da crosta arqueana da Província Carajás para oeste, retrabalhada por *underplating* magmático; e as províncias Rio Negro e Sunsás seriam produzidas por reciclagem de crosta continental durante eventos colisionais. Adicionalmente, individualizaram a faixa K'Mudku (~ 1,2 Ga), que representa uma zona de cisalhamento de centenas de quilômetros de extensão, de direção NE-SW, que teria produzido deformação e fusões locais em pelo menos três províncias (Transamazônica, Tapajós-Parima e Rio Negro), afetando rochas de 2,0 a 1,52 Ga.

## 2.2 – A FAIXA OROGÊNICA PALEOPROTEROZÓICA DO NORTE DO CRÁTON AMAZÔNICO (PROVÍNCIA MARONI-ITACAIÚNAS vs. PROVÍNCIA TRANSAMAZÔNICA)

Ao longo da porção norte-nordeste do Cráton Amazônico ocorre uma expressiva faixa móvel paleoproterozóica, que se estende desde o segmento nordeste do Escudo Brasil Central, recobrando toda a porção setentrional do Escudo das Guianas, através do norte do Brasil, Guiana Francesa, Suriname, Guiana e leste da Venezuela. Em linhas gerais, esta faixa móvel tem evolução relacionada ao Ciclo Orogênico Transamazônico (2,26 – 1,95 Ga), e consiste em grandes extensões de crosta juvenil paleoproterozóica e alguns remanescentes arqueanos retrabalhados. É correlacionada aos terrenos Birimianos formados durante a orogênese

Eburneana do Cráton Oeste Africano (Onstott & Hargraves 1981, Onstott et al. 1984, Feybesse & Milesi 1994, Ledru et al. 1994, Zhao et al. 2002, Théveniaut et al. submetido).



**Províncias Geocronológicas**

- Carajás-Imataca (3,10 - 2,53 Ga)
- Amazônia Central (1,88 - 1,70 Ga)
- Transamazônica (2,25-2,00 Ga)
- Tapajós-Parima (2,10-1,87 Ga)
- Rio Negro (1,86 -1,52 Ga)
- Rondônia-Juruena (1,76 -1,47 Ga)
- Sunsás (1,33- 0,99 Ga)

- Faixa K'Mudku (1,33-1,10 Ga)

**Outras Unidades**

- Coberturas Fanerozoicas
- Faixas Orogênica Andina
- Cinturão Móvel Neoproterozoico
- Área do Projeto Promin-RENCA
- Área de estudo

**Figura 2.4** - Províncias geocronológicas do Cráton Amazônico, segundo a proposta de Santos et al. (2000).

As províncias Maroni-Itacaiúnas e Transamazônica, propostas por Tassinari & Macambira (2004) e Santos et al. (2000), respectivamente (Figuras 2.3 e 2.4), representam a referida faixa móvel paleoproterozóica nos modelos de compartimentação do Cráton Amazônico. No entanto, algumas diferenças na concepção das referidas províncias induziram à divergências em relação à extensão deste orógeno na porção oriental do cráton. Tais divergências são reflexos das premissas adotadas para definição das províncias. Enquanto a proposta de Tassinari & Macambira (2004) é baseada na idade da última orogênese que consolidou a Província Maroni-Itacaiúnas, no caso o Ciclo Orogênico Transamazônico, a de Santos et al. (2000) é fundamentada principalmente na idade das rochas, independente se as mesmas foram ou não afetadas pela referida orogênese. Desta forma, Tassinari & Macambira (2004) consideram o Bloco Arqueano Imataca (> 2,5 Ga) como parte da Província Maroni-Itacaiúnas, e posicionam o limite sul desta província com a Província Amazonia Central (> 2,5 Ga) logo a norte da região arqueana de Carajás, conforme indicado por Cordani et al. (1984). Adicionalmente, entendem que o Cinturão Guiana Central (estado da arte em Fraga 2002), uma faixa granulítica de direção NE-SW, que se estende desde o oeste do Suriname (Montanhas Bakhuis), através do sudeste da Guiana, até o estado de Roraima, também integra a Província Maroni-Itacaiúnas (Figura 2.3). Por sua vez, Santos et al. (2000) consideram o Bloco Imataca como um fragmento arqueano independente, a despeito do mesmo ter sido retrabalhado no Evento Transamazônico, e estendem a Província Arqueana de Carajás para norte, incorporando o então conhecido núcleo arqueano de Cupixi (Montalvão & Tassinari 1984, Sato & Tassinari 1997), na região central do Amapá, mas excluindo as rochas arqueanas de Tartarugalzinho (João & Marinho 1982, Lima et al. 1982, Lafon et al. 1998), na porção oriental desse estado, que continuam integrando a Província Transamazônica (Figura 2.4). Vale ressaltar que, nas duas propostas, as rochas arqueanas da região de Cupixi e Tartarugalzinho são freqüentemente consideradas como evidências da extensão da crosta arqueana de Carajás para norte.

Tassinari (1996), baseado em significativas variações do padrão geocronológico da Província Maroni-Itacaiúnas, definiu dois grandes domínios, denominando-os Simático e Ensiático, os quais estariam limitados pela Falha Oiapoque, de direção NE-SW, ao longo da qual foi estabelecido o rio homônimo, que delimita a fronteira entre o estado do Amapá e a Guiana Francesa. Segundo este autor, o domínio Simático representa a porção juvenil da referida

província, com evolução relacionada a eventos magmáticos e de acreção crustal paleoproterozóicos, ocorridos principalmente durante o Riaciano, como demonstravam os dados geocronológicos/isotópicos disponíveis naquela época (Priem et al. 1977 e 1980, Gibbs 1980, Gibbs & Olszewski 1982, Bosma et al. 1983, Ben Othman et al. 1984, Teixeira et al. 1984, Gruau et al. 1985, Vignol 1987, Olsewiski et al. 1989, Ledru et al. 1990, Egal et al. 1994, 1995, Milési et al. 1995).

O domínio ensialico por sua vez é constituído por protólitos arqueanos retrabalhados durante o Evento Transamazônico, e que são preservados como *inliers* em meio a rochas paleoproterozóicas. Para a concepção deste domínio, aquele autor fundamentou-se nos registros de rochas arqueanas obtidos nas regiões de Cupixi e Tartarugalzinho (João & Marinho 1982, Lima et al. 1982, Montalvão & Tassinari 1984, Sato & Tassinari 1997). O Complexo Imataca também foi considerado um domínio ensialico, uma vez que continha gnaisses de alto grau metamórfico com protólitos arqueanos, retrabalhados no Paleoproterozóico (Montgomery & Hurley 1978, Montgomery 1979, Onstott & York 1989, Swapp & Onstott 1989).

Diferentes setores da porção oriental da discutida província paleoproterozóica foram alvos de estudos na última década, os quais produziram grande aporte de novos dados geológicos e geocronológicos, que propiciaram significativo avanço no conhecimento da região, tanto no que diz respeito à descoberta de novos registros arqueanos nos domínios ensialicos (Sato & Tassinari 1997, Lafon et al. 1998, Ricci et al. 2001, 2002, Rosa-Costa et al. 2001, 2003, Tassinari et al. 2001, 2004, Pimentel et al. 2002, Avelar et al. 2003, Klein et al. 2003, Faraco et al. 2004a, Macambira et al. 2004), quanto à identificação de eventos magmáticos, de acreção e retrabalhamento crustal, que consolidaram esta província no Paleoproterozóico (Faraco 1997, McReath & Faraco 1997, Sato & Tassinari 1997, Vanderhaeghe et al. 1998, Lafrance et al. 1999, Nogueira et al. 2000, Norcross et al. 2000, Voicu et al. 2000, Delor et al. 2001, Macambira et al. 2001, 2003, Avelar 2002, Oliveira et al. 2002, Rosa-Costa et al. 2002a, Delor et al. 2003a,b, Roever et al. 2003, Santos 2003, Vasquez et al. 2005).

Na Guiana Francesa, durante a elaboração do mapa geológico na escala 1:500.000 pelo BRGM, foram realizados levantamentos geológicos em todo aquele território, e produzido um número expressivo de novos dados geocronológicos (Delor et al. 2001). Fundamentados pelo acervo das novas informações adquiridas e reavaliação de dados provenientes de estudos

anteriores, Delor et al. (2003a) propuseram um modelo de evolução geodinâmica para a Guiana Francesa, o qual foi refinado a partir do modelo de Vanderheaghe et al. (1998), que pode ser considerado como um domínio francamente juvenil do orógeno em questão.

Segundo o modelo proposto, a evolução geodinâmica dos terrenos paleoproterozóicos da Guiana Francesa é ordenada em quatro estágios principais, ilustrados na Figura 2.5:

1) Estágio Oceânico Eo-Riaciano (2,26 – 2,20 Ga) – corresponde à época de formação de crosta oceânica juvenil, decorrente da divergência de dois fragmentos continentais, inicialmente contíguos, representados por placas arqueanas do Cráton Oeste Africano e, supostamente, do norte do Cráton Amazônico. Evidências deste estágio na Guiana Francesa são as ocorrências de gabros e trondhjemitos com idades de cristalização em torno de 2,22-2,21 Ga, assumidos como derivados de magmas toleíticos meso-oceânicos. Este estágio foi estendido até 2,26 Ga, em função da ocorrência de uma idade isocrônica Sm-Nd obtida em rochas metamáficas de natureza basáltica toleítica pertencentes à seqüência supracrustal da Serra do Ipitinga (McReath & Faraco 1997), localizada em outro contexto tectônico, a ser posteriormente focado;

2) Estágio Meso-Riaciano D1 (2,18 – 2,13 Ga) – esta fase é caracterizada pela acreção de magmas cálcio-alcalinos e desenvolvimento de seqüências metavulcano-sedimentares em sistemas de arcos de ilhas, originados sobre uma zona de subdução entre placas litosféricas oceânicas, durante o início da convergência entre os blocos continentais arqueanos. Neste estágio ocorreram dois pulsos diacrônicos de magmatismo tipo TTG, entre 2,18-2,16 Ga e entre 2,15-2,13 Ga;

3) Estágio Neo-Riaciano D2a (2,11 – 2,08 Ga) – representa o final da fase convergente D1 e o início de um regime predominantemente transcorrente com cinemática sinistral, acompanhado de fusões locais (migmatização) dos granitóides tipo TTG, sob condições de baixa a moderada pressão. Simultaneamente, ocorreu a colocação de granitos com origem relacionada principalmente a retrabalhamento crustal, e o desenvolvimento de bacias do tipo *pull-apart*, conforme previamente sugerido por Vanderhaeghe et al. (1998). Adicionalmente, Mg-K magmatismo (granitos e granodioritos com anfibólio e/ou piroxênio) associado a este estágio é interpretado como reflexo de perturbações termais do manto, que favoreceriam a produção de magmas de alta temperatura;

4) Estágio Neo-Riaciano D2b (2,07 – 2,06 Ga) – representa a fase de colocação de granitos metaluminosos ao longo de zonas de cisalhamento transcorrentes dextrais. Neste estágio, os sedimentos depositados nas bacias *pull-apart* foram metamorfizados seguindo uma trajetória P-T anti-horária, similarmente àquela definida para os granulitos UHT (*Ultra High Temperature*) das Montanhas Bakhuis, no Suriname, cuja idade do metamorfismo granulítico foi definida em torno de 2,07-2,05 Ga (Roever et al. 2003). Segundo Delor et al. (2003b), a trajetória anti-horária do metamorfismo, que indica a ausência de significativo espessamento crustal, está relacionada a altos gradientes termais produzidos por *upwelling* mantélico, induzido por estiramento crustal em escala continental.

Avelar (2002), estudando a região centro-norte do estado do Amapá, definiu, a partir de datações Sm-Nd em rocha total e Pb-Pb em zircão, um domínio de transição entre a porção simática juvenil paleoproterozóica, que ocorre a partir da Guiana Francesa em direção oeste, e o domínio ensialico, cujo limite estaria posicionado logo a norte da área de ocorrência dos gnaisses com protólitos arqueanos da região de Tartarugalzinho. No domínio de transição, acreção crustal juvenil foi reconhecida apenas localizadamente por aquele autor, e ratificada por Nogueira et al. (2000), através da datação de granitóides cálcio-alcalinos em torno de 2,18 Ga e 2,16 Ga, os quais apresentam idades modelo  $T_{DM}$  entre 2,34 e 2,24 Ga, acompanhadas por valores positivos de  $\epsilon_{Nd}$ . No entanto, neste domínio prevalecem granitos com idades em torno de 2,10 Ga, que apresentam idades  $T_{DM}$  francamente arqueanas ou indicando mistura entre componentes arqueanos e paleoproterozóicos, atestando, em ambos os casos, origem envolvendo retrabalhamento de crosta arqueana durante o evento tectono-termal Transamazônico. Vale ressaltar que as idades do magmatismo cálcio-alcalino (2,18-2,16 Ga) e granítico (~ 2,10 Ga), são concordantes, respectivamente, aos estágios 2 e 3 de Delor et al. (2003a). Adicionalmente, na região de fronteira entre o norte do Amapá e a Guiana Francesa, porção norte do domínio de transição, magmatismo granítico e migmatização foram datados entre 2,11 e 2,08 Ga, e também associados ao estágio 2 daqueles mesmos autores (Lafon et al. 2003, Tavares et al. 2003)

A sul do domínio de transição, portanto em domínio ensialico, novos registros de rochas com protólitos arqueanos foram descobertos por Avelar et al. (2003) na região de Tartarugalzinho (gnaisse granulítico com 2,58 Ga) e nas cercanias da região do Cupixi (gnaisse tonalítico com 2,85 Ga), confirmando a presença de crosta arqueana naqueles setores, já indicada por estudos

---

anteriores (João & Marinho 1982, Lima et al. 1982, Montalvão & Tassinari 1984, Sato & Tassinari 1997). Processos de retrabalhamento das rochas arqueanas durante o Evento Transamazônico foram evidenciados tanto na região do Cupixi quanto em Tartarugalzinho, através da datação de leucossoma quartzo-feldspático, proveniente do gnaiss tonalítico de 2,85 Ga, e de pluton charnockítico intrusivo nos granulitos de 2,58 Ga, que forneceram, respectivamente, idades de 2,17 Ga e 2,06 Ga (Avelar et al. 2001 e 2003).

Situada na porção sudeste do Escudo das Guianas, a área enfocada nesta pesquisa localiza-se portanto no domínio ensialico da Província Maroni-Itacaiúnas, cujos aspectos geológicos mais relevantes serão discutidos no capítulo seguinte. Nesta região, determinações geocronológicas realizadas em ortognaisses de alto grau metamórfico indicaram que os mesmos apresentavam precursores magmáticos arqueanos (Rosa-Costa et al. 2003). Segundo Rosa-Costa et al. (2003), estes novos dados, conjugados com aqueles previamente obtidos nas regiões do Cupixi e Tartarugalzinho, sugerem que a crosta arqueana deste segmento do Cráton Amazônico está relacionada a extensos segmentos crustais, e não a *inliers* isolados em meio a rochas paleoproterozóicas. Desta forma, estes autores sugerem a existência de um segmento crustal arqueano, retrabalhado no Evento Transamazônico, que se estenderia desde a região NW do Pará/SW do Amapá até a região central do Amapá. Adicionalmente, sugerem que este segmento representaria um fragmento arqueano independente, portanto sem conexão com o segmento arqueano de Carajás. O registro sistemático de rochas paleoproterozóicas no segmento a norte de Carajás, inclusive com assinatura isotópica juvenil (Macambira et al. 2001, 2004, Santos 2003, Vasquez et al. 2005), é concordante com as suposições destes autores.

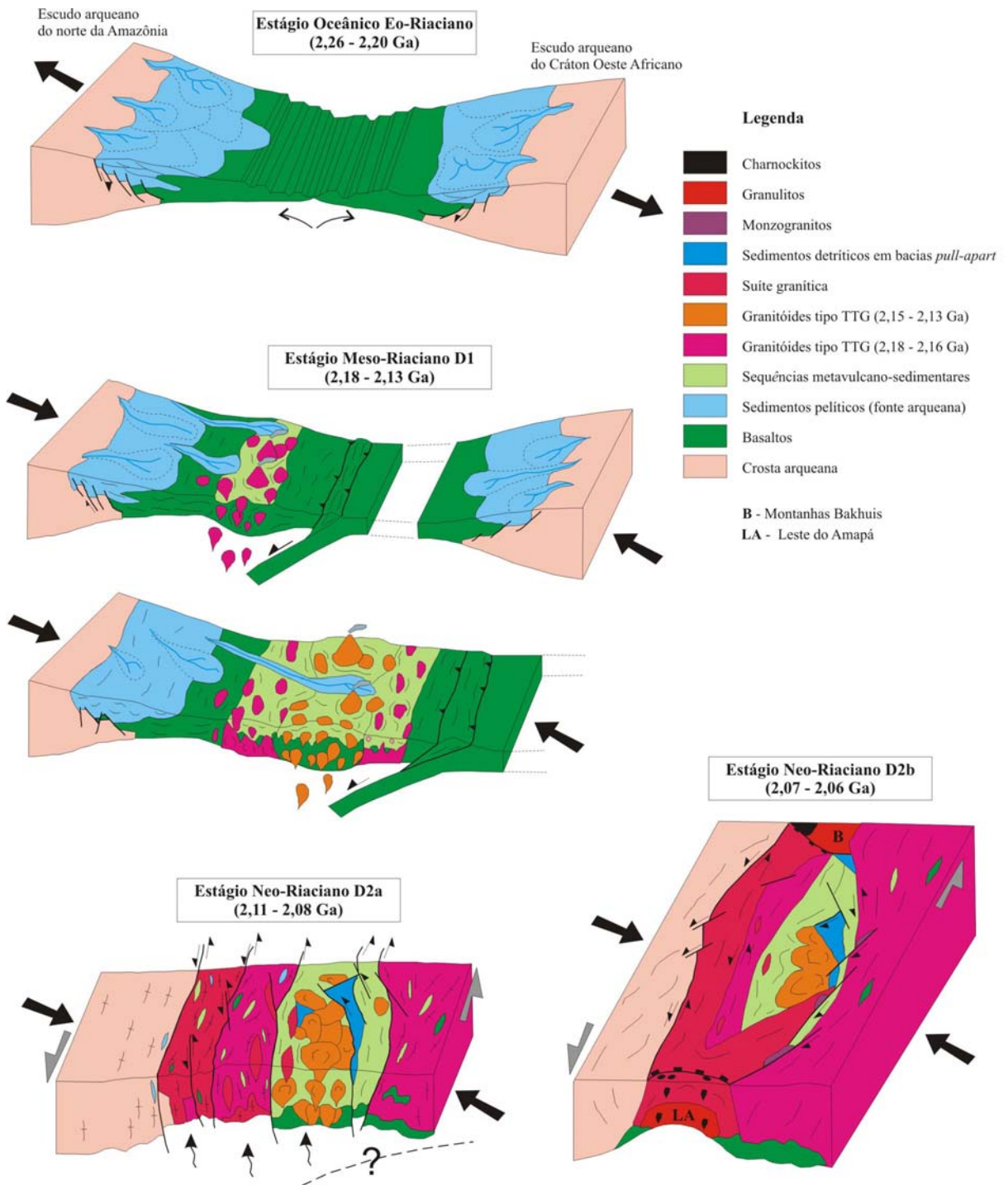


Figura 2.5 - Modelo de evolução geodinâmica, proposto por Delor et al. (2003a), para terrenos paleoproterozóicos da Guiana Francesa.

### 3 - CONTEXTO GEOLÓGICO LOCAL

#### 3.1 – COMPARTIMENTAÇÃO TECTÔNICA

A análise de informações de campo, interpretação de imagens aerogeofísicas e estudos petrográficos realizados no âmbito do Projeto Promim-RENCA, permitiram o reconhecimento de diferentes terrenos tectono-estratigráficos na região, justapostos e balizados por grandes lineamentos tectônicos (Ricci et al. 2001). Estes terrenos distribuem-se de nordeste para sudoeste conforme a denominação de Terreno Antigo Cupixi-Tartarugal Grande (TACTG), Cinturão Jari (CJ) e Orógeno Carecuru-Paru (OCP). Apresentam uma estruturação regional NW-SE e articulam-se através de zonas de cisalhamento transcorrentes, denominadas Lineamento Cupixi e Lineamento Ipitinga (Figuras 3.1 e 3.2). Segundo estes autores, contrastes significativos observados entre os terrenos, em termos de idade, conteúdo litológico e grau metamórfico dos complexos de embasamento, além de notáveis diferenças no padrão estrutural e, conseqüentemente, na assinatura geofísica, subsidiam esta proposta de compartimentação tectônica.

A compartimentação tectônica proposta por Ricci et al. (2001) foi inspirada na metodologia de análise de terrenos (*terrane analysis*), amplamente empregada em áreas tectonicamente complexas (Coney et al. 1980, Jones et al. 1986, Hamilton 1990, Wit et al. 1992, Howell 1995, Zhao et al. 2001, Friend & Nutman 2001, Kalsbeek 2001, St-Onge et al. 2001). Howell (1995) define um terreno tectono-estratigráfico como um compartimento tectônico limitado por grandes estruturas tectônicas, que apresenta estratigrafia e história evolutiva própria e distinta das unidades geológicas adjacentes ou terrenos contíguos.

Rosa-Costa et al. (2001) apresentaram dados geocronológicos obtidos pelo método Pb-Pb em zircão de rochas provenientes dos diferentes terrenos tectônicos, os quais, conjugados com dados da literatura (João & Marinho 1982, Lima et al. 1982, Montalvão & Tassinari 1984, Sato & Tassinari 1997, Lafon et al. 1998, Avelar et al. 2001), indicavam padrões de idades arqueanas para as rochas de embasamento do TACTG e CJ, e assinatura predominantemente paleoproterozóica para o DCR, o que foi considerado por Ricci et al. (2001) como um argumento fundamental para a individualização dos diferentes terrenos.

Segundo Ricci et al. (2001), o TACTG se estenderia a partir do Lineamento Cupixi para nordeste até a região central do Amapá. Entretanto, não inclui a propalada “região do Cupixi”, onde rochas arqueanas são reportadas desde o trabalho de Montalvão & Tassinari (1984), mas

engloba a região de Tartarugalzinho, também conhecida por conter granulitos com protólitos arqueanos (Lima et al. 1982, João & Marinho 1982, Lafon et al. 1998, Avelar et al. 2003). Foi interpretado como um “*ancient gneiss terrain*”, *sensu* Wit et al. (1992), uma vez que hospedava a rocha mais antiga do sudeste do Escudo das Guianas conhecida até aquele momento (gnaisse tonalítico com idade de zircão de 2,85 Ga – Avelar et al. 2001), coletada a nordeste do Lineamento Cupixi (Figura 3.2). No entanto, estudos posteriores revelaram a presença de rochas mais antigas que 2,85 Ga no CJ (gnaises tonalíticos com idade de zircão em 3,32 Ga - Klein et al. 2003).

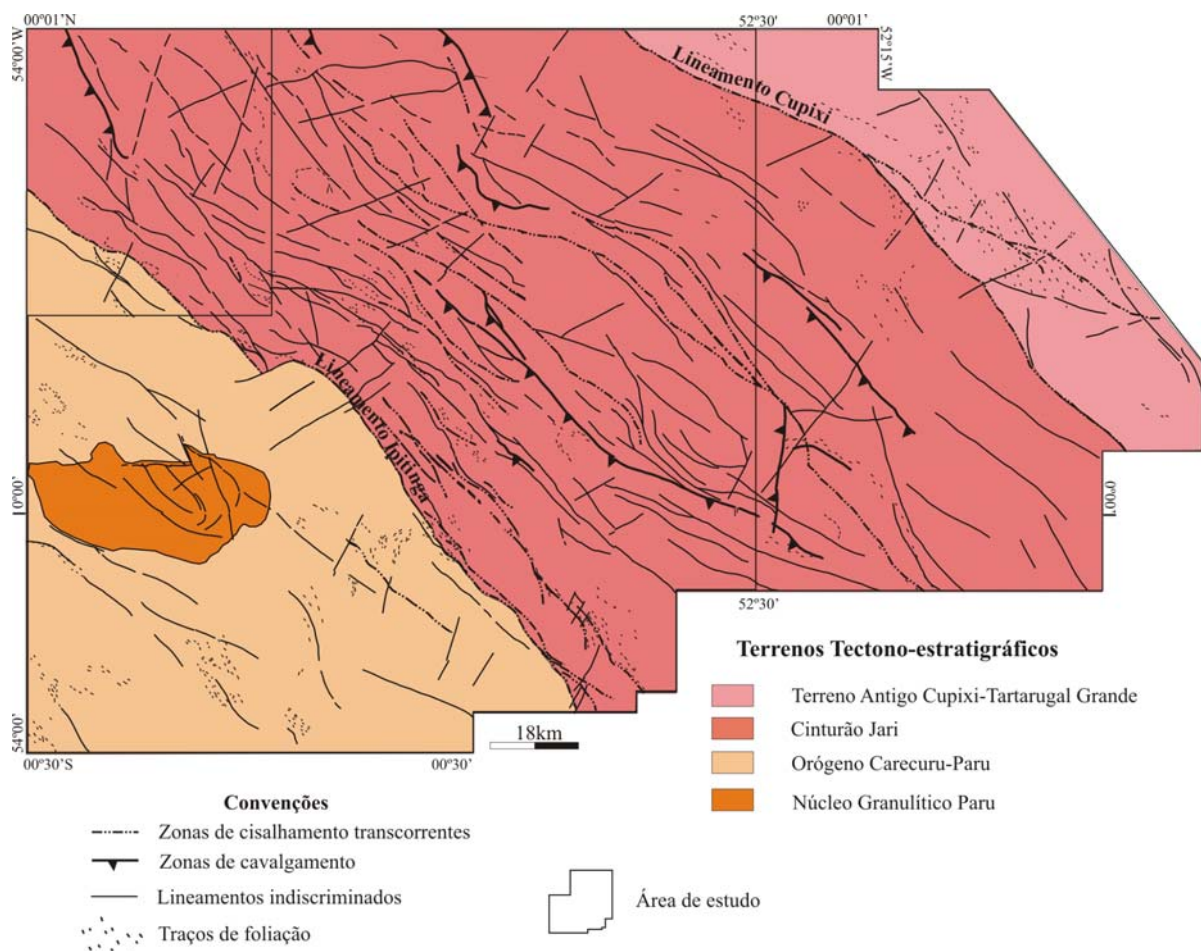


**Figura 3.1** - Compartimentação tectônica da área do Projeto Promin-RENCA, proposta por Ricci et al. (2001).

O terreno TACTG é dominado por ortognaisses cinza, metamorfizados sob condições de fácies anfíbolito (Complexo Tumucumaque), e derivados de protólitos ígneos mesoarqueanos, como indicado pela idade de 2,85 Ga obtida em gnaiss tonalítico (Avelar et al. 2001). Ricci et al. (2001) consideram ainda que, a ocorrência de granulitos, restrita a remanescentes isolados e não-lineares localizados na porção oriental deste terreno (nos rios Falsino e Tartarugal Grande, região de Tartarugalzinho), e a relativa escassez de maciços granitóides contrastam com a constituição litológica e o padrão metamórfico do CJ adjacente, dominado por rochas de alto grau, que ocorrem em faixas alongadas, e por um exuberante magmatismo orogênico evoluído. Aqueles autores destacam ainda que no TACTG a densidade de lineamentos estruturais, marcada em imagens de sensores remotos é consideravelmente menor que do CJ, e diminui em direção à sua porção central a nordeste, fora do polígono mapeado no Projeto RENCA.

O CJ apresenta-se como uma faixa linear NW-SE de aproximadamente 100 km de largura, onde dominam rochas de alto grau metamórfico na assembléia de embasamento, as quais ocorrem principalmente na porção sudoeste. São representadas por gnaisses granulíticos orto e paraderivados (complexos Jari-Guaribas e Iratapuru, respectivamente), ortognaisses graníticos da transição anfíbolito/granulito (Complexo Baixo Mapari), além de plútons charnoquíticos (Suíte Intrusiva Noucouru). Ortognaisses cinza de fácies anfíbolito também compõem a assembléia de embasamento (Complexo Guianense) do CJ. Determinações geocronológicas preliminares indicam que os gnaisses granulíticos derivam de precursores mesoarqueanos (~ 2,80 Ga), enquanto que idades neoarqueanas (2,65-2,60 Ga) foram obtidas para os protólitos ígneos dos ortognaisses cinza e para o magmatismo charnoquítico (Rosa-Costa et al. 2001, Ricci et al. 2002). Para Ricci et al. (2001), o CJ destaca-se como um grande corredor de deformação, onde é verificado, em imagens de sensores remotos, um número significativo de lineamentos sinuosos e contínuos, que ultrapassam por vezes 100 km de extensão longitudinal.

O DCR, posicionado a sudoeste da área, tem seu embasamento regional representado por gnaisses e granitóides cálcio-alcálicos (Complexo Paru-Maratiá e Suíte Intrusiva Carecuru) de idades paleoproterozóicas, situadas entre 2,15 e 2,14 Ga (Rosa-Costa et al. 2001). O *trend* NW-SE ainda é bem marcado no DCR, porém, os lineamentos radargamétricos não são tão abundantes quanto no CJ adjacente, ressaltando um dos seus contrastes comparativos (Ricci et al. 2001).

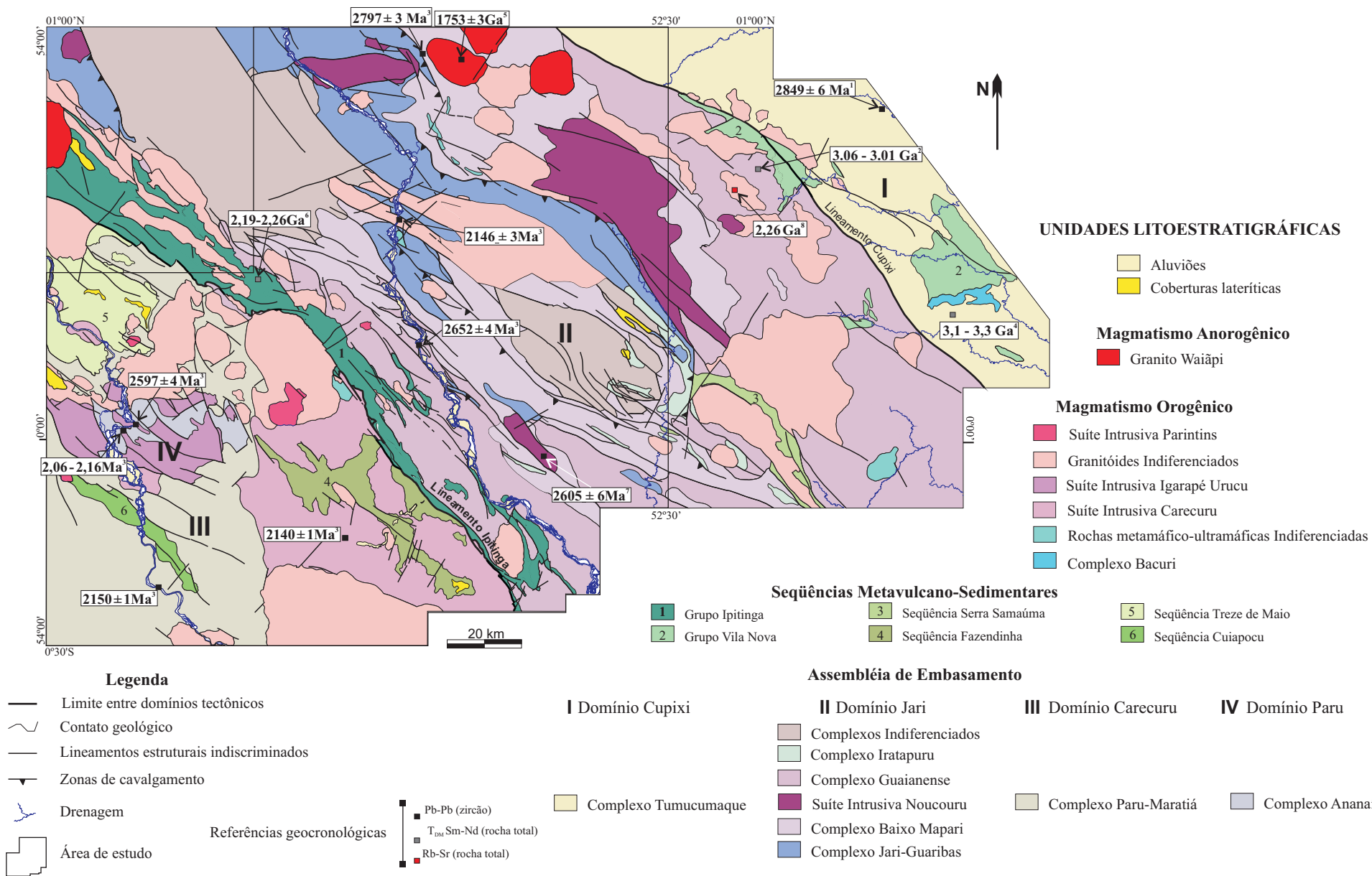


**Figura 3.2** - Mapa geológico simplificado da área do Projeto Promin-RENCA (modificado de Carvalho et al. 2001). Fonte dos dados geocronológicos: <sup>1</sup>Avelar et al. 2001, <sup>2</sup>Sato & Tassinari 1997, <sup>3</sup>Rosa-Costa et al. 2003, <sup>4</sup>Pimentel et al. 2002, <sup>5</sup>Vasquez & Lafon 2001, <sup>6</sup>Faraco 1997, <sup>7</sup>Ricci et al. 2002, <sup>8</sup>Montalvão & Tassinari 1984.

No interior do DCR, foi individualizado ainda o Núcleo Granulítico Paru (NGP), o qual é composto por ortognaisses granulíticos (Complexo Ananaí), que hospedam diversos plútons charnoquíticos (Suíte Intrusiva Igarapé Urucu). Dados geocronológicos disponíveis indicam idades neoarqueana (2,58 Ga) e paleoproterozóica (2,16-2,06 Ga) para os protólitos dos granulitos e para o magmatismo charnoquítico, respectivamente (Rosa-Costa et al. 2001).

Rosa-Costa et al. (2002b), a partir da análise de imagens aerogeofísicas magnetométricas e radiométricas, descrevem os padrões geofísicos característicos dos diferentes terrenos tectônicos, enfatizam as claras diferenças entre os padrões do CJ, OCR e NGP, e sugerem que, entre o CJ e o TACTG, tais diferenças não são evidentes. Isto corrobora com as observações de Rosa-Costa et al. (2003) que, discutindo mais detalhadamente os dados geocronológicos Pb-Pb em zircão obtidos em rochas provenientes do CJ, OCR e NGP, previamente divulgados em Rosa-Costa et al. (2001), sugerem a existência de um extenso e contínuo segmento crustal arqueano que se estenderia desde o Lineamento Ipitinga até a região central do Amapá, portanto englobando o TACTG e o CJ.

### 3.2 – UNIDADES LITOSTRATIGRÁFICAS

A partir do levantamento geológico realizado através do Projeto Promin RENCA, diversas unidades estratigráficas foram individualizadas, tendo sido propostas novas unidades ou redefinidas algumas já consagradas na literatura, as quais se encontram descritas em detalhe em Ricci et al. (2001). As unidades foram caracterizadas individualmente quanto a sua composição litológica, grau metamórfico, padrão estrutural e idade e, sobretudo aquelas que definem a assembléia de embasamento, foram consideradas como unidades tectono-estratigráficas, portanto com ocorrência restrita a um específico terreno tectônico. A utilização deste novo enfoque metodológico direcionou ao abandono de unidades litoestratigráficas macrorregionais, amplamente utilizadas em trabalhos anteriores de mapeamento realizados nas décadas de 70 e 80 (Lima et al. 1974, João et al. 1978, 1979, Barros et al. 1984, Machado Filho et al. 1986), as quais se estendiam por extensas regiões, embora estivessem em domínios tectônicos distintos.

Em virtude de se considerar que no estágio atual do conhecimento não existem dados suficientes para definição de terrenos tectono-estratigráficos, segundo os conceitos de Howell (1995), os terrenos tectono-estratigráficos definidos por Ricci et al. (2001) serão referidos simplesmente como “domínios”.

Adicionalmente, neste item as unidades estratigráficas serão agrupadas em grandes conjuntos litológicos, assim denominados: assembléia de embasamento, sendo específica para cada domínio tectônico; seqüências metavulcano-sedimentares, que recebem denominações distintas em cada domínio; e magmatismo plutônico orogênico e anorogênico, cujas unidades relacionadas podem ter ocorrência restrita a um determinado domínio tectônico ou ter ampla distribuição na área. O termo “orogênico” refere-se ao Ciclo Orogrênico Transamazônico.

A distribuição espacial das unidades estratigráficas enfocadas pode ser visualizada no mapa geológico simplificado da Figura 3.2, modificado a partir de Carvalho et al. (2001), onde também são apresentadas as referências geocronológicas disponíveis na literatura para algumas delas. No Anexo I, é apresentado o mapa geológico de detalhe da área de estudo na escala 1:250.000. Neste capítulo, as abreviações utilizadas para designar fases minerais estão em conformidade com Kretz (1983).

### **3.2.1 – Assembléia de Embasamento**

#### 3.2.1.1 – Domínio Cupixi

##### 3.2.1.1.1 - Complexo Tumucumaque

Scarpelli (1973 *apud* Barros et al. 1984) propôs a designação de Complexo Tumucumaque para reunir os gnaisses orto e paraderivados, estabilizados em fácies anfibolito a granulito, que afloram no sudeste do Escudo das Guianas, desde o rio Jari até a serra Lombarda, no centro-norte do Amapá. Essas rochas foram englobadas no Complexo Guianense, por Lima et al. (1974) e, posteriormente, Lima et al. (1982) redefiniram o Complexo Tumucumaque como um tectono-fácies do Complexo Guianense, que ocorreria ao longo do Cinturão Tumucumaque.

Segundo a concepção de Ricci et al. (2001), o Complexo Tumucumaque encerra um conjunto de ortognaisses cinza, metamorfizados em condições de fácies anfibolito, com ocorrência restrita ao Domínio Cupixi. Na área em questão, essa unidade é definida por gnaisses de composição diorítica a granítica, dominando os termos intermediários tonalíticos e granodioríticos, os quais exibem fraco a moderado grau de migmatização e contêm, freqüentemente, corpos anfibolíticos aleitados concordantemente ao bandamento gnáissico.

Uma datação Pb-Pb em zircão de um gnaisse tonalítico coletado a nordeste da área, forneceu a idade de  $2849 \pm 6$  Ma, interpretada como idade de cristalização do protólito ígneo (Avelar et al. 2001, 2003). Análises Sm-Nd em rocha total obtidas em gnaisses deste complexo

forneceram idades modelo  $T_{DM}$  entre 3,36 e 2,94 Ga (Avelar 2002, Pimentel et al. 2002, Avelar et al 2003), indicando que os mesmos derivam de fontes paleo a mesoarqueanas.

### 3.2.1.2 – Domínio Jari

#### 3.2.1.2.1 - Complexo Jari-Guaribas

Ricci et al. (2001) propõem a denominação de Complexo Jari-Guaribas para incorporar um conjunto expressivo de gnaisses metamorfizados na fácies granulito, cuja distribuição se restringe aos limites do Domínio Jari. Esta unidade distribui-se em corpos lentiformes e faixas alongadas segundo o *trend* estrutural regional NW-SE, que são balizados geralmente por grandes estruturas, que representam zonas transcorrentes ou de cavalgamento.

Neste complexo dominam amplamente ortogranulitos de composição enderbítica, charnoenderbítica e charnoquítica. São rochas de coloração rosada a acinzentada, de granulação média a grossa, com foliação bem definida através do bandamento gnáissico, evidenciado pela alternância regular de zonas quartzo-feldspáticas e outras mais ricas em minerais máficos (Figura 3.3 A e B).

Sob o microscópio, os gnaisses apresentam texturas granoblásticas e porfiroclásticas, podendo ocorrer até tipos miloníticos. A associação mineralógica principal é definida por plagioclásio, via de regra antipertítico, álcali-feldspato mesopertítico, quartzo e ortopiroxênio, podendo conter ainda clinopiroxênio, hornblenda e biotita. Como acessórios destacam-se os óxidos de Fe e Ti, zircão, apatita e mais raramente monazita.

Granulitos máficos ocorrem restritamente, na forma de leitos concordantes ao bandamento, contínuos ou rompidos, ou ainda como enclaves isolados nos gnaisses (Figura 3.3 C). São rochas de cor cinza escura, de granulação fina a média, geralmente maciças, ou localmente foliadas segundo a estruturação do gnaisse encaixante. São definidos mineralogicamente por ortopiroxênio, plagioclásio (raramente antipertítico), clinopiroxênio e quartzo, podendo conter ainda hornblenda e biotita. Os acessórios são óxidos, apatita e zircão. A microtextura é granoblástica, com contatos em ponto tríplice ou interlobados (Figura 3.3 D).

A associação mineral ortopiroxênio + clinopiroxênio + plagioclásio + hornblenda identificada nos gnaisses estudados permite a definição da fácies granulito. A presença de ortopiroxênio indica que temperaturas acima de 775°C foram atingidas durante o metamorfismo, enquanto a presença de hornblenda limita a 900°C o valor máximo de temperatura (Spear 1995).

Adicionalmente, a ausência de granada nos granulitos máficos aponta para condições de pressão médias a baixas (O'Brien & Rotzler 2003).

Evidências de transformações retrometamórficas para a fácies anfibolito, e até mesmo xisto-verde, são freqüentemente observadas, como por exemplo, a substituição parcial ou total dos piroxênios para anfibólio, biotita ou clorita.

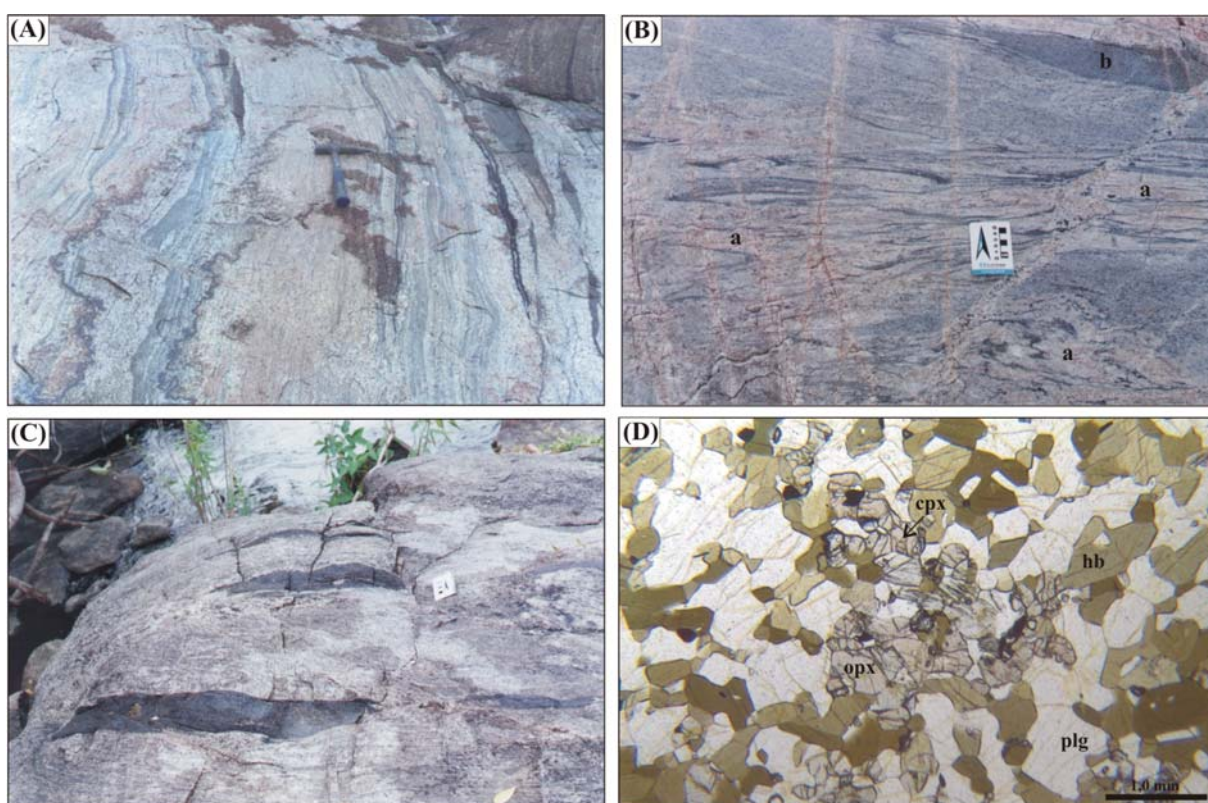


**Figura 3.3** - Complexo Jari-Guaribas. (A) Gnaiss charnoquítico com bandamento bem definido; (B) Gnaiss granulítico migmatizado, com leucossomas quartzo-feldspáticos (a) e leitossomas de granulito máfico (b) concordantes ao bandamento; (C) Enclaves de granulitos máficos alongados concordantemente à foliação; (D) Fotomicrografia de granulito máfico mostrando textura granoblástica com contatos em ponto tríplice, e associação mineral em equilíbrio representada por plagioclásio, hornblenda, ortopiroxênio e clinopiroxênio.

Condições de anatexia foram atingidas durante o metamorfismo granulítico, visto que é comum a presença de leucossomas, que ocorrem como bolsões ou lentes concordantes ao bandamento gnáissico, ou ainda como veios, concordantes ou não (Figura 3.3 B). Os leucossomas têm composição quartzo-feldspática, são ricos em plagioclásio antiperitítico, álcali-feldspato mesoperitítico e quartzo. Encontra-se por vezes o ortopiroxênio, o que caracteriza tipos charnoquíticos para os leucossomas e sugerem uma origem provavelmente associada a condições de pico metamórfico. Os leucossomas, quando ocorrem em corpos aleitados segundo a foliação

do gnaiss encaixante, apresentam-se geralmente deformados concordantemente àquela estruturação (Figura 3.3 B).

Um gnaiss enderbítico forneceu uma idade Pb-Pb em zircão de  $2797 \pm 3$  Ma, interpretada como a idade mínima de cristalização do protólito ígneo (Rosa-Costa et al. 2003), sugerindo que os granulitos deste complexo originaram-se a partir de precursores arqueanos.

#### 3.2.1.2.2 - Complexo Baixo-Mapari

Este complexo foi definido por Ricci et al. (2001) para englobar um conjunto de gnaisses de composição predominantemente granítica, estabilizados em condições da transição das fácies anfibolito – granulito, que ocorrem em extensas faixas alongadas na direção NW-SE, distribuídas principalmente na porção sudoeste do Domínio Jari. Dados geocronológicos inéditos produzidos no âmbito da CPRM-Belém indicam que os precursores magmáticos destes gnaisses têm idade neoarqueana.

São gnaisses leucocráticos, de coloração rosada, granulação média a grossa, conspicuamente bandados, de composição granítica (Figura 3.4A). A composição mineralógica principal é formada por feldspato mesopertítico, quartzo, plagioclásio antipertítico, sendo os minerais máficos a hornblenda e o clinopiroxênio. Os acessórios são óxidos, zircão, allanita e apatita. O ortopiroxênio ocorre esporadicamente, indicando que estas rochas atingiram excepcionalmente a fácies granulito. As rochas apresentam textura granoblástica, com contatos interlobados ou poligonais, ou porfiroclástica (Figura 3.4 B).

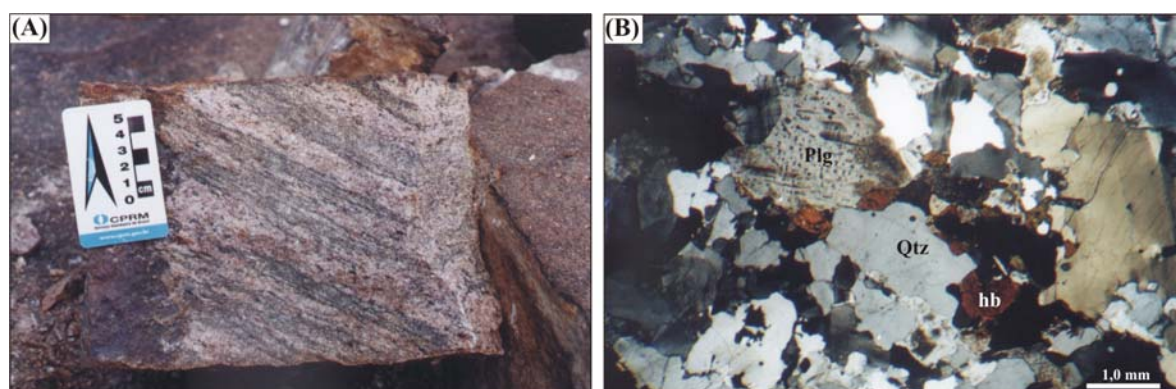


**Figura 3.4 - (A)** Aspecto textural típico dos gnaisses graníticos/charnoquíticos do Complexo Baixo Mapari; **(B)** Fotomicrografia de gnaiss com textura porfiroclástica, definida por porfiroclastos de quartzo e plagioclásio antipertítico em matriz quartzo-feldspática com hornblenda.

### 3.2.1.2.3 - Suíte Intrusiva Noucouru

Vários plutons charnoquíticos foram cartografados pelo Projeto Promin-RENCA, associados aos gnaisses granulíticos do Domínio Jari e do Núcleo Granulítico Paru, tendo sido agrupados indistintamente na Suíte Intrusiva Igarapé Urucu (Ricci et al. 2001). A datação de um desses plútons no Domínio Paru pelo método Pb-Pb em zircão sugere que, naquele domínio, estes corpos têm idade paleoproterozóica, uma vez que os zircões datados apresentaram idades principalmente entre 2,16 e 2,06 Ga (Rosa-Costa et al. 2001). Posteriormente, Ricci et al. (2002), utilizando o mesmo método de datação, obtiveram a idade de cristalização de  $2605 \pm 6$  Ma para um plúton charno-enderbítico do Domínio Jari. A partir desta idade, Ricci et al. (2003) definiram a Suíte Intrusiva Noucouru para englobar os diversos plútons charnoquíticos que ocorrem no Domínio Jari.

Esta suíte é definida por grandes batólitos, geralmente alongados segundo a estruturação regional, compostos por charnoquitos, enderbitos, charnoenderbitos e mesopertita-granitos (sem ortopiroxênio). São rochas de granulação média a grossa, coloração cinza esverdeada, amarronzada ou rosada, compostas por álcali-feldspato mesopertítico, quartzo, plagioclásio antipertítico, ortopiroxênio e biotita, além de óxidos, zircão, apatita e allanita. Os tipos enderbíticos apresentam ainda clinopiroxênio, hornblenda e, esporadicamente, granada. São rochas foliadas ou maciças, que apresentam ao microscópio textura porfiroclástica ou texturas ígneas preservadas do tipo porfirítica ou granular hipidiomórfica, com contatos retilíneos e interlobados (Figura 3.5).

### 3.2.1.2.4 - Complexo Guianense

O Complexo Guianense foi definido por Lima *et al.* (1974) para agrupar conjuntos de gnaisses, metagranitóides e inclusive granulitos, distribuídos por amplas regiões do Amapá e NW do Pará. João *et al.* (1978) propuseram a retirada dessa unidade das rochas granulíticas que ocorrem na região entre os rios Paru e Jari, inserindo-as no Complexo Ananaí. Ricci et al. (2001) redefinem o Complexo Guianense como um conjunto de ortognaisses cinza, metamorfizados sob condições de fácies anfíbolito, restringindo sua área de distribuição ao Domínio Jari.

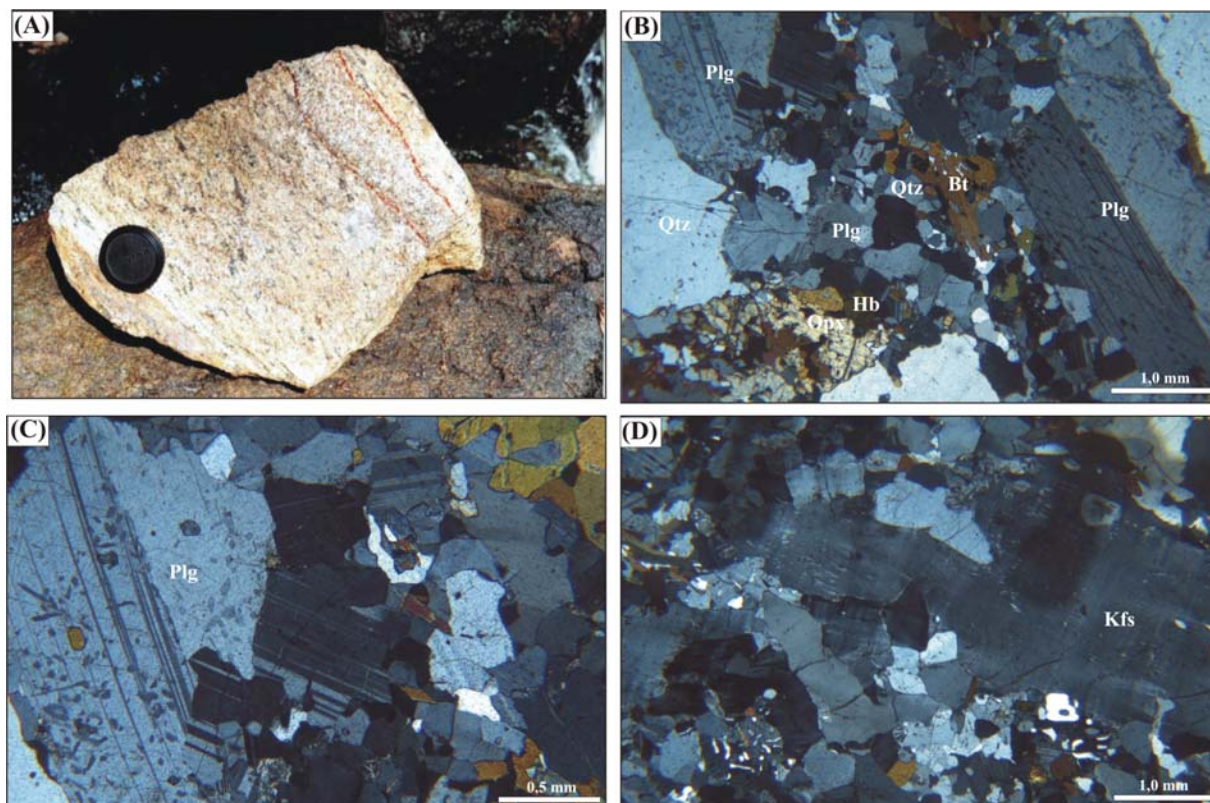


**Figura 3.5** - Aspectos texturais da Suite Intrusiva Noucouru. (A) Charnoquito foliado contendo veio granítico concordante à foliação; (B) Enderbito com textura porfírica preservada, definida por fenocristais de plagioclásio antiperfítico e quartzo em matriz granular, composta por plagioclásio, ortopiroxênio, hornblenda, quartzo e biotita; (C) Detalhe do plagioclásio antiperfítico; (D) Granito com porfirocristal de feldspato alcalino perfítico em matriz quartzo-feldspática granular, contendo núcleos quartzo-feldspáticos recristalizados.

Os gnaisses apresentam bandamento composicional bem definido, coloração diversificada, desde tipos cinza escuros a esbranquiçados, e apresentam geralmente granulação média (Figura 3.6 A). Augen gnaisses e gnaisses miloníticos de granulação grossa ocorrem localmente (Figura 3.6 B).

Predominam gnaisses com composição tonalítica a granodiorítica, com variações quartzodioríticos, trondhjemiticos e graníticos subordinados. Gnaisses graníticos peraluminosos são localmente registrados. Geralmente são rochas esbranquiçadas, com bandamento definido pela alternância regular de leitos quartzo-feldspáticos e bandas ricas em biotita e granada (Figura 3.6 C). Corpos anfibolíticos são freqüentemente encontrados nestes gnaisses, na forma de leitos contínuos ou enclaves, de dimensões decimétricas a métricas, aleitados concordantemente à foliação do gnaiss encaixante (Figura 3.6 A).

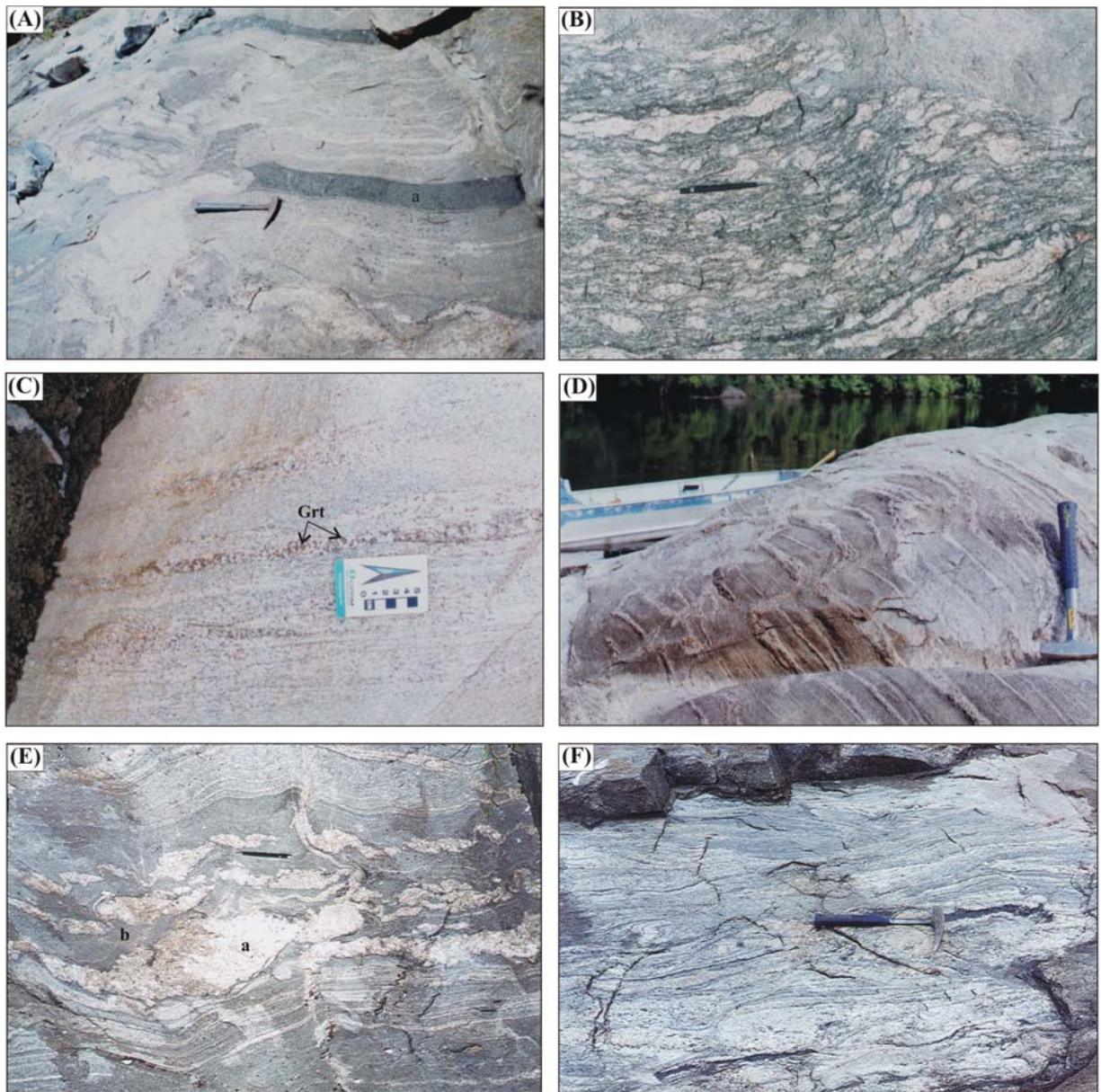


**Figura 3.6** - (A) Aspecto comumente observado nos gnaisses cinza do Complexo Guianense, apresentando bandamento composicional bem definido e leitossomas anfibolíticos (a) aleitados concordantemente; (B) Augen gneisse com ocelos de até 5 cm de feldspato alcalino ou definidos por agregados quartzo-feldspáticos; (C) Gneisse granítico com bandas ricas em granada, que ressaltam o bandamento; (D) Gneisse com leitossomas quartzo-feldspáticos concordantes ao bandamento; (E) Gneisse migmatizado, onde são individualizados leucossomas graníticos (a) e melanossomas dioríticos (b); (F) Gneisse migmatítico com estrutura estromatítica.

Ao microscópio, as texturas dominantes são as granolepidoblásticas, porfiroclásticas e localmente miloníticas. A mineralogia principal é definida por plagioclásio, quartzo, microclina, hornblenda, biotita, e a acessória por opacos, titanita, allanita, apatita e zircão. Nos litótipos

peraluminosos a hornblenda é ausente, mas ocorrem granada, biotita e muscovita. Nestas rochas também é comum a presença de monazita dentre os acessórios.

Os anfíbolitos têm textura nematoblástica, e são constituídos por plagioclásio, hornblenda e quartzo, além de titanita, apatita e opacos como fases acessórias.

Os gnaisses apresentam intensidades variáveis de migmatização, que é expressa pela presença de leucossomas quartzo-feldspáticos em leitos concordantes que ressaltam o bandamento (Figura 3.6 D), ou definem áreas extensivas, caracterizando verdadeiros migmatitos com estruturas complexas. Em domínios mais migmatizados individualizam-se claramente melanossomas dioríticos de leucossomas quartzo-feldspáticos (Figura 3.6 E), e são reconhecidas estruturas típicas de rochas migmatíticas, as quais, seguindo Mehnert (1968), poderiam ser classificadas como do tipo agmática, nebulítica, estromatítica e outras (Figura 3.6 F).

As rochas deste complexo são freqüentemente retrometamorfizadas a condições de fácies xisto-verde, sendo comum a ocorrência de epidoto, clorita, muscovita/sericita, carbonato, titanita secundária e minerais opacos associados à transformações, principalmente a partir da biotita, hornblenda e plagioclásio.

O posicionamento cronoestratigráfico no Neoarqueano do Complexo Guianense foi definido a partir da idade de  $2652 \pm 4$  Ma, obtida em gnaiss tonalítico, interpretada como idade de cristalização do protólito ígneo (Rosa-Costa et al. 2003).

#### 3.2.1.2.5 - Complexo Iratapuru

O Complexo Iratapuru foi definido por Ricci et al. (2001) para reunir conjuntos de rochas paraderivadas metamorfizadas em fácies granulito, que eram anteriormente considerados como integrantes do Grupo Vila Nova (Machado Filho *et al.* 1986). Este complexo ocorre como faixas estreitas e alongadas, segundo a estruturação regional, que apresentam contatos tectônicos com os complexos ortoderivados de alto grau adjacentes (complexos Jari-Guaribas e Baixo Mapari).

Os principais litocomponentes são paragnaisses aluminosos, cujos protólitos sedimentares correspondem provavelmente a composições pelíticas e semipelíticas. São rochas que freqüentemente apresentam pervasiva foliação dúctil, geralmente milonítica.

Os paragnaisses são rochas de granulação fina a média, coloração cinza a cinza escura, cuja associação mineral principal é quartzo, plagioclásio, álcali-feldspato, biotita titanífera,

granada, cordierita e silimanita, com ortopiroxênio ocorrendo ocasionalmente. Os acessórios reúnem óxidos, zircão, monazita, rutilo, e mais raramente grafita e espinélio.

Nas rochas menos deformadas a textura é porfiroblástica, definida por porfiroblastos de granada e ortopiroxênio com formas irregulares, com até 0,5 cm no comprimento maior, imersos em matriz granoblástica (Figura 3.7 A). Os tipos miloníticos são definidos por porfiroclastos amendoados de granada, com matriz contendo leitos poliminerálicos (microclina, plagioclásio, cordierita, quartzo e silimanita) alongados, cristais fitados de quartzo e trilhas anastomóticas ricas em biotita e silimanita. Nestas rochas, o isoalinhamento da silimanita prismática, acompanhada do quartzo fitado e dos porfiroblastos amendoados ou alongados de granada, definem uma clara lineação de estiramento mineral, provavelmente contemporânea ao metamorfismo granulítico (Figura 3.7 B).

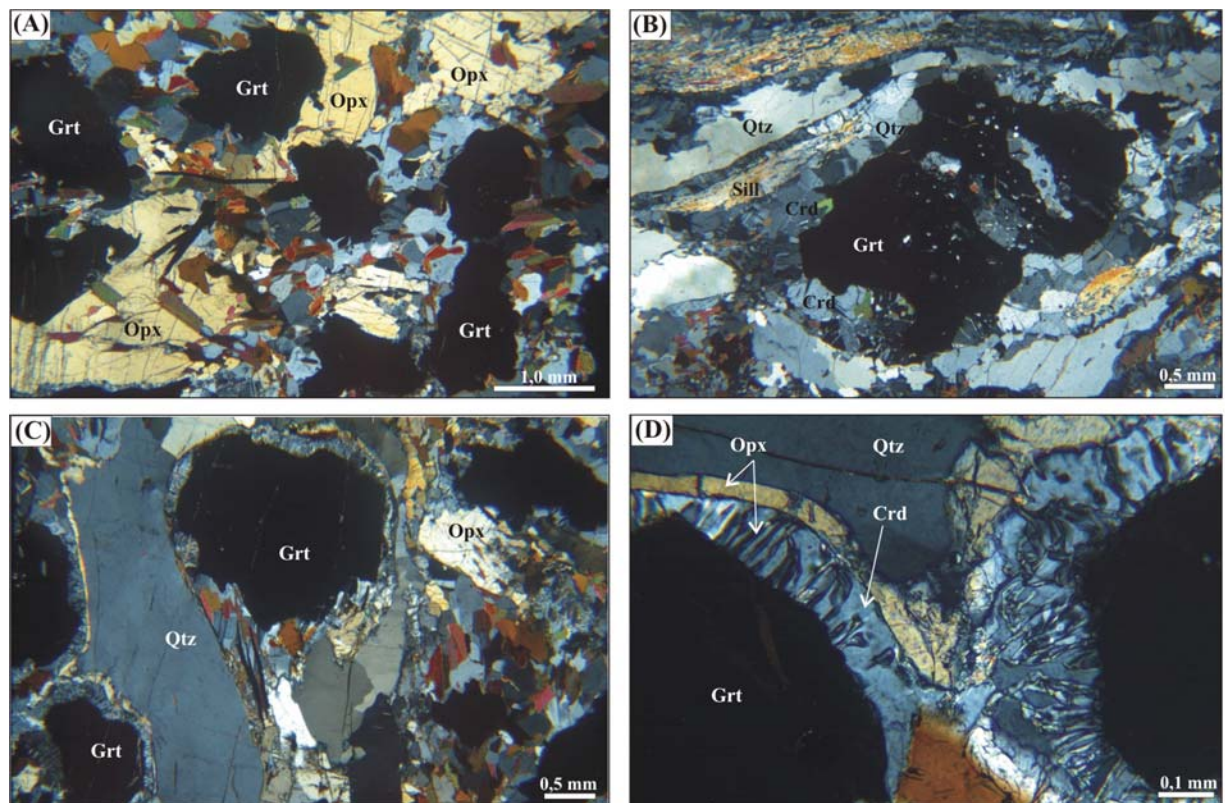


**Figura 3.7** - Fotomicrografias de gnaisses aluminosos do Complexo Iratapuru. (A) Porfiroblastos de granada e ortopiroxênio em matriz granoblástica; (B) Textura milonítica definida por porfiroclasto de granada amendoado, envolvido por manto recristalizado, composto principalmente por cordierita e quartzo. Notar a silimanita, o quartzo fitado e a granada + sombra de pressão marcando a lineação de estiramento; (C) Porfiroblastos circulares de granada em contato com quartzo, contornados por estruturas coroníticas; (D) Detalhe das coronas, constituídas por uma zona interna de simplectidos de ortopiroxênio e cordierita, envolvida por anéis de ortopiroxênio.

Estruturas coroníticas são frequentemente registradas em volta dos cristais de granada, preferencialmente quando este mineral está em contato com quartzo ou ortopiroxênio. As coronas são definidas por uma zona interna composta por simplectitos de ortopiroxênio e cordierita, e uma zona externa composta por anéis (*rims*) de ortopiroxênio (Figura 3.7 C e D).

A associação silimanita + álcali-feldspato e a presença de ortopiroxênio nos metapelitos são suficientes para indicar que o metamorfismo atingiu condições de fácies granulito. A ausência de cianita e a ampla ocorrência de cordierita sugerem que condições de pressão médias a baixas foram atingidas durante o metamorfismo granulítico (Spear 1995, O'Brien & Rotzler 2003). Adicionalmente, a associação granada + silimanita + quartzo sugere temperaturas de metamorfismo muito elevadas (Harley 1998).

Feições coroníticas similares às observadas nestas rochas são classicamente interpretadas como registros da história regressiva do metamorfismo e consideradas como indicativas de decompressão isotérmica pós-pico metamórfico (*near-isothermal decompression* – ITD, Harley 1989), associada à trajetórias horárias de pressão e temperatura (Ouzegane & Boumaza 1996, Raith et al. 1997, Harley 1998, Brandt et al. 2003). Segundo Harley (1989), os “ITD granulites” são formados em ambientes de crosta espessada por processos colisionais, com adições magmáticas funcionando como uma importante fonte de calor.

Nesta unidade também ocorrem quartzitos com silimanita e granada, e rochas ricas em quartzo, contendo clinopiroxênio, ou leitos contínuos de clinopiroxênio e porfiroblastos granada, as quais foram classificadas por Ricci et al. (2001) como formações ferríferas fácies silicato e aluminosa, respectivamente.

Transformações retrometamórficas mais comuns observadas em rochas deste complexo são a alteração de silimanita para muscovita, a pinitização parcial da cordierita e a sericitização do plagioclásio.

Embora ainda não datadas, uma idade arqueana é sugerida por Ricci et al. (2001) para as fontes sedimentares dos granulitos deste complexo.

#### 3.2.1.2.6 – Complexo Indiferenciado

Em alguns segmentos do Domínio Jari não foram realizados ainda levantamentos geológicos sistemáticos e, mesmo que já tenham sido registradas ocorrências de gnaisses de médio e alto grau metamórfico, não foi possível ainda vinculá-los a nenhuma unidade

estratigráfica formal. Estes segmentos apresentam padrão aerogeofísico e morfológico semelhante aos dos demais complexos metamórficos, e por isso também são supostamente considerados como integrantes da assembléia de embasamento.

### 3.2.1.3 – Domínio Carecuru

#### 3.2.1.3.1 - Complexo Paru-Maratiá

Esta unidade foi proposta por Ricci et al. (2001), para designar um conjunto de gnaisses com composições semelhantes à das séries cálcio-alcálicas, com ampla distribuição no Domínio Carecuru. São rochas de granulação média a grossa, coloração cinza a cinza-esbranquiçada, apresentando bandamento gnáissico (Figura 3.8 A) ou apenas uma foliação tectônica bem definida, dada pela iso-orientação dos minerais placóides. Prevaecem os gnaisses tonalíticos, dioríticos e granodioríticos, enquanto os trondhjemíticos e graníticos ocorrem bastante subordinadamente.

Neste complexo é muito comum a presença de enclaves anfíbolíticos, que ocorrem em corpos ou leitos tabulares alongados segundo a foliação, com dimensões por vezes ultrapassando 2 metros no comprimento maior (Figura 3.8 B). Estes corpos podem ser interpretados como diques, restos de rochas metavulcânicas máficas ou, alternativamente, como enclaves plutônicos representativos dos termos mais primitivos do magmatismo cálcio-alcálico.

Os gnaisses exibem textura sobretudo porfiroclástica. A mineralogia essencial é definida por plagioclásio, quartzo, biotita, hornblenda e microclina, e os minerais acessórios são os opacos, titanita, apatita, epidoto, allanita e zircão. A paragénese mineral indica metamorfismo compatível com a fácies anfíbolito, com transformações retrometamórficas observadas localmente, exemplificadas pela alteração da hornblenda para biotita e clorita e da biotita para clorita, com formação de titanita secundária e opacos associados. O plagioclásio também pode apresentar forte alteração para sericita e epidoto.

Feições de migmatização que indiquem que condições de anatexia foram atingidas durante o metamorfismo regional não são tão expressivas nas rochas deste complexo e, quando observadas, são representadas por discretos leitos de leucossomas concordantes à foliação. Injeções graníticas pegmatóides internamente foliadas e concordantes à foliação gnáissica são estruturas localmente observadas (Figura 3.8 C e D).

Um gnaiss tonalítico deste complexo datado forneceu uma idade de  $2150 \pm 1$  Ma (Rosa-Costa et al. 2003), indicando a evolução paleoproterozóica das rochas de embasamento do Domínio Carecuru.

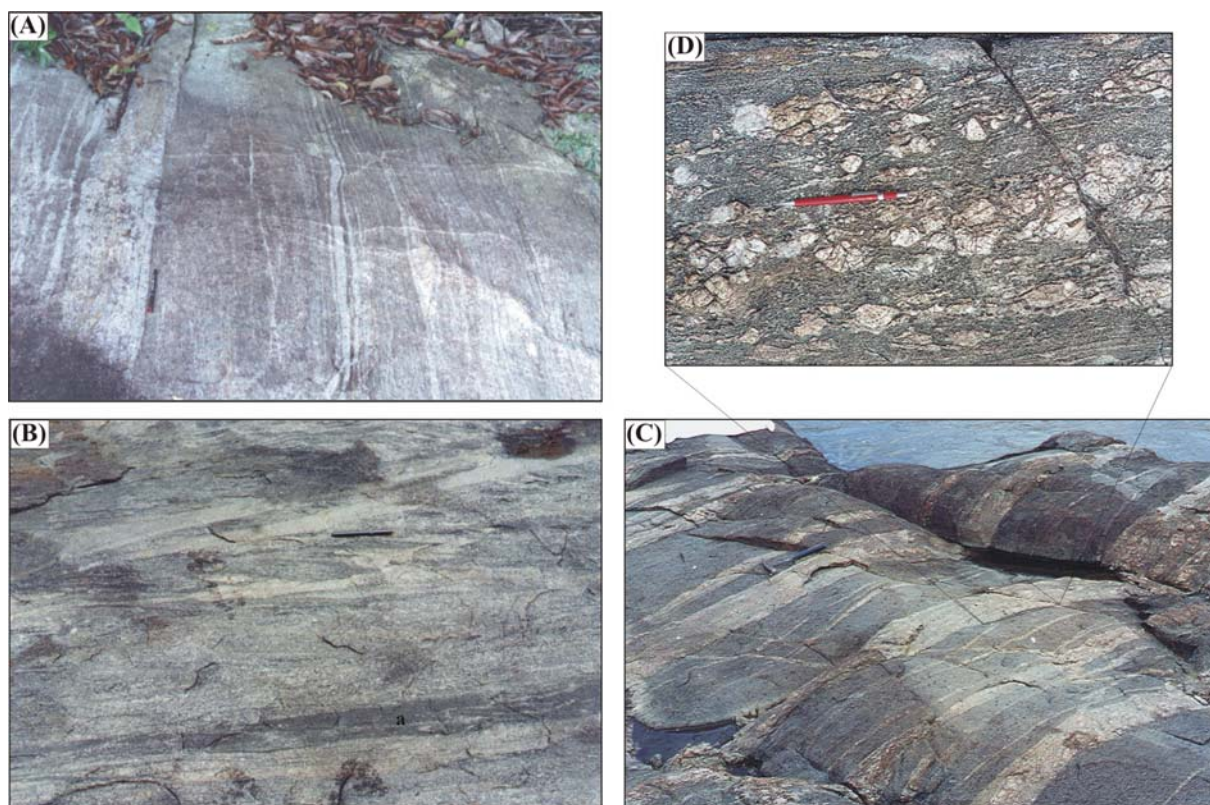


**Figura 3.8** - Complexo Paru-Maratiá. (A) Gnaiss trondhjemítico exibindo bandamento composicional bem definido, evidenciado pela presença de leitos de leucossoma concordantes; (B) Leito anfobolítico (a) concordante à foliação tecônica do gnaiss; (C) Gnaiss recortado por injeções/veios graníticos tabulares e concordantes à foliação; (D) Detalhe de um veio granítico onde se observa a foliação milonítica interna, dada por fenocristais amendoados de feldspato alcalino, contornados por matriz quartzo feldspática com padrão anastomótico.

#### 3.2.1.4 – Domínio Paru

##### 3.2.1.4.1 - Complexo Ananaí

João *et al.* (1978) denominaram de Suíte Metamórfica Ananaí as rochas granulíticas básicas (Piriclasito Mutum) e ácidas (Granoblastito Urucu) que ocorrem no médio curso do Rio Paru, na região Domínio Paru. Ricci et al. (2001) substituem o termo suíte metamórfica por complexo, considerando a ocorrência do Complexo Ananaí restrita apenas àquele núcleo granulítico.

Nesta unidade prevalecem gnaisses enderbíticos, charnoenderbíticos e granulitos máficos.

O bandamento é definido pela alternância regular de leitos de espessuras centimétricas, de composição enderbítica ou charnoenderbítica. Os granulitos máficos podem apresentar-se na forma de camadas regulares e contínuas que ressaltam o bandamento dos termos félsicos, e, neste caso, são internamente foliados (Figura 3.9 A e B). Ocorrem também como corpos isolados com dezenas de metros de extensão, geralmente isotrópicos, cujas relações de contato com os gnaisses são ainda desconhecidas.

As rochas gnáissicas apresentam granulação fina a média, coloração variando de cinza clara a cinza escura, com mobilizados restritos a esparsos leitos de aproximadamente 1cm de espessura, ou a leitos mais expressivos em quantidade e espessura, que lhes acentua o bandamento. Os gnaisses enderbíticos e charnoenderbíticos apresentam textura granoblástica poligonal ou porfiroclástica, e mineralogia definida por proporções variáveis de plagioclásio antipertítico, quartzo, ortopiroxênio, clinopiroxênio, feldspato mesopertítico, opacos apatita e zircão, podendo conter ainda hornblenda e/ou biotita (Figura 3.9 C). Os granulitos máficos têm textura granoblástica com contatos em ponto tríplice, e são constituídos por plagioclásio, clinopiroxênio, ortopiroxênio, hornblenda, quartzo, apatita e zircão (Figura 3.9 D). A biotita também pode ocorrer esporadicamente.

Os leucossomas são quartzo-feldspáticos, e ricos em plagioclásio antipertítico.

A associação mineral é semelhante à observada em granulitos do Complexo Jari-Guaribas, a qual é definida por ortopiroxênio + clinopiroxênio + plagioclásio + hornblenda, permitindo a caracterização de condições de fácies granulito, com estimativas de temperatura acima de 775°C e inferiores a 900°C, de acordo com Spear (1995). Da mesma forma, a ausência de granada nos granulitos máficos aponta para condições de pressão médias a baixas (O'Brien & Rotzler 2003).

Evidências de que, pelos menos localmente, estes granulitos foram retrometamorfizados até a fácies anfíbolito e/ou xisto verde, são cristais de piroxênio transformado para hornblenda ou biotita, além do plagioclásio alterado para sericita.

Uma análise geocronológica (Pb-Pb em zircão) realizada em um gnaisse enderbítico, forneceu uma idade média de  $2597 \pm 4$  Ga, que foi considerada como idade de cristalização do precursor ígneo, indicando que os granulitos deste complexo derivam de protólitos neoarqueanos (Rosa-Costa et al. 2003).

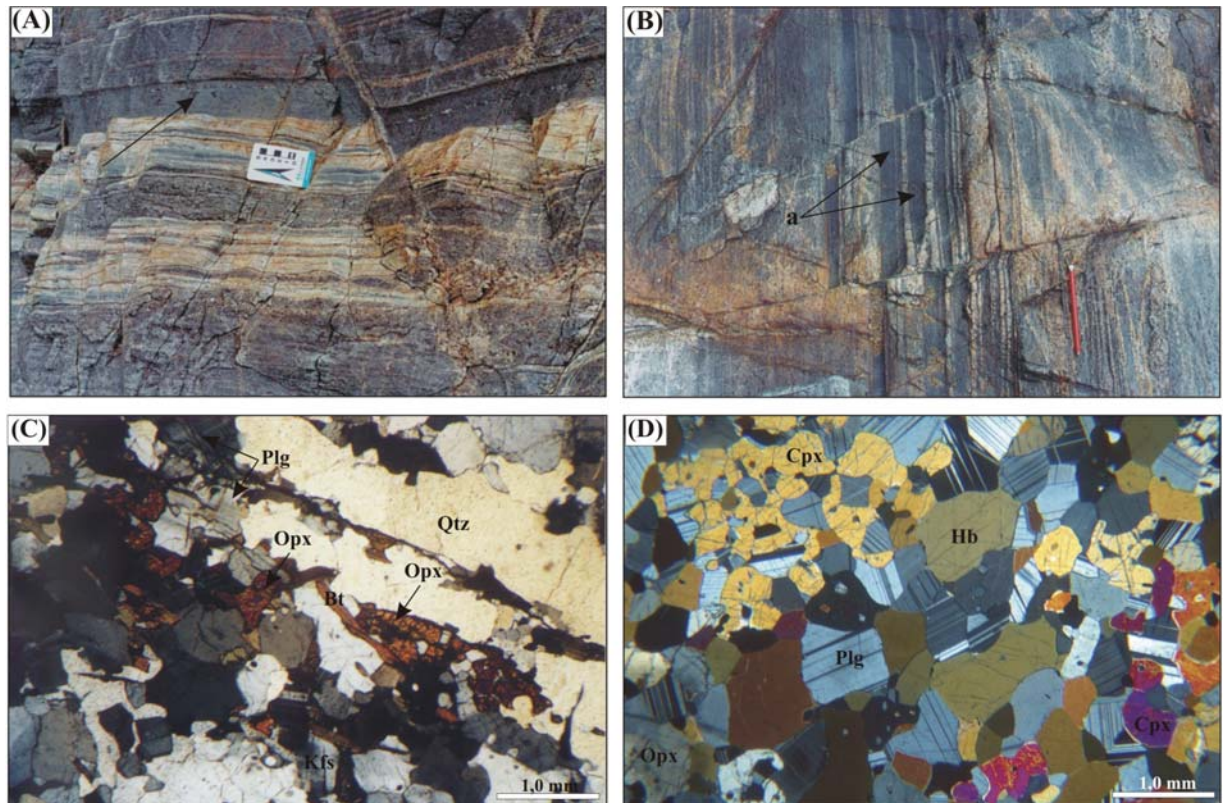


**Figura 3.9** - Complexo Ananai. (A) e (B) Aspecto estrutural dos gnaisses enderbíticos, contendo leitos tabulares concordantes e contínuos de granulitos máficos (a) que ressaltam o bandamento; (C) Aspecto textural de gnaiss charno-enderbítico, composto por quartzo, em fenocristais alongados, álcali-feldspato, plagioclásio, biotita e ortopiroxênio; (D) Textura granoblástica com contatos poligonais de granulito máfico, constituído essencialmente por plagioclásio, hornblenda, ortopiroxênio, clinopiroxênio e quartzo.

### 3.2.2 - Seqüências Metavulcano-Sedimentares

As diversas faixas de rochas metavulcano-sedimentares, metamorfizadas sob condições de fácies xisto verde a anfíbolito, e amplamente distribuídas ao longo do estado do Amapá e no noroeste do Pará, eram coletivamente agrupadas no Grupo Vila Nova (ex. Lima et al. 1974, João et al. 1978, Melo & Araújo 1982). Ricci et al. (2001) propuseram a restrição do uso do termo Grupo Vila Nova apenas para o conjunto supracrustal que ocorre ao longo da faixa NW-SE posicionada no limite entre os domínios Cupixi e Jari, na qual individualizaram dois grandes conjuntos rochosos, inserindo-os nas formações Igarapé Araújo (seqüência máfica-ultramáfica basal) e Serra das Coambas (seqüência sedimentar predominantemente clástica, com metavulcânicas félsicas e rochas químico exalativas subordinadas). Para englobar as rochas supracrustais que ocorrem ao longo de uma extensa e bem definida faixa NW-SE, que extrapola os limites da área mapeada e que marca o limite entre os domínios Jari e Carecuru, aqueles autores propuseram a

criação do Grupo Ipitinga, subdividindo-o nas formações Igarapé do Inferno (sequência máfica-ultramáfica basal), Igarapé dos Patos (sequência químico-exalativa intermediária) e Igarapé Fé em Deus (sequência sedimentar clástica superior). Adicionalmente, foram individualizados testemunhos supracrustais menores, que ocorrem como faixas desmembradas e com posição intra-domínio, as quais definem a Sequência Serra Samaúma, no Domínio Jari, e as sequências Cuiapocu, Fazendinha e Treze de Maio, no Domínio Carecuru.

As seqüências inter-domínio apresentam uma sucessão estratigráfica mais diversificada, com características semelhantes às das seqüências tipo *greenstone-belts*. Desenham grandes cinturões de rochas supracrustais, de centenas de quilômetros de extensão longitudinal, fortemente afetados pelas zonas transcorrentes Cupixi (Grupo Vila Nova) e Ipitinga (Grupo Ipitinga).

Segundo Ricci et al. (2001), a Formação Igarapé do Inferno do Grupo Ipitinga, predominam rochas metamáficas, além de metaultramáficas subordinadas. As metabásicas são, via de regra, foliadas, sendo representadas por plagioclásio-actinolita-tremolita xistos, plagioclásio-quartzo-actinolita xistos e plagioclásio-hornblenda xistos. Os principais representantes das metaultramáficas são rochas a piroxênio-anfibólio, tremolititos e anfibólio-xistos não-feldspáticos. Quando foliados, exibem textura nematoblástica e porfiroblástica.

A Formação Igarapé dos Patos é composta por formações ferríferas bandadas fácies óxido e, subordinadamente, fácies silicato.

Na Formação Igarapé Fé-em-Deus dominam muscovita-quartzitos e quartzitos puros, seguidos de muscovita-quartzo xistos, clorita-muscovita-quartzo xistos, clorita-biotita-muscovita-quartzo xistos e muscovita-quartzo-sericita xistos, com textura geralmente milonítica.

Devido ao forte controle estrutural imposto pelo Lineamento Ipitinga, estas rochas exibem comumente foliação com alto ângulo de mergulho, e no caso das formações ferríferas, apresentam um complexo padrão de dobramentos, atestando seu comportamento mais plástico à deformação (Figura 3.10).

Faraco (1997) admite que a deposição desta seqüência supracrustal está relacionada a ambiente de bacia retro-arco, formada no Paleoproterozóico. A evolução paleoproterozóica desta seqüência é indicada por idades modelo Sm-Nd de 2,26 Ga e 2,20 Ga obtidas em metamáficas, e pela idade de  $2264 \pm 34$  Ma (MSWD = 37,4) calculada a partir de uma errócrona Sm-Nd (McReath & Faraco 1997).

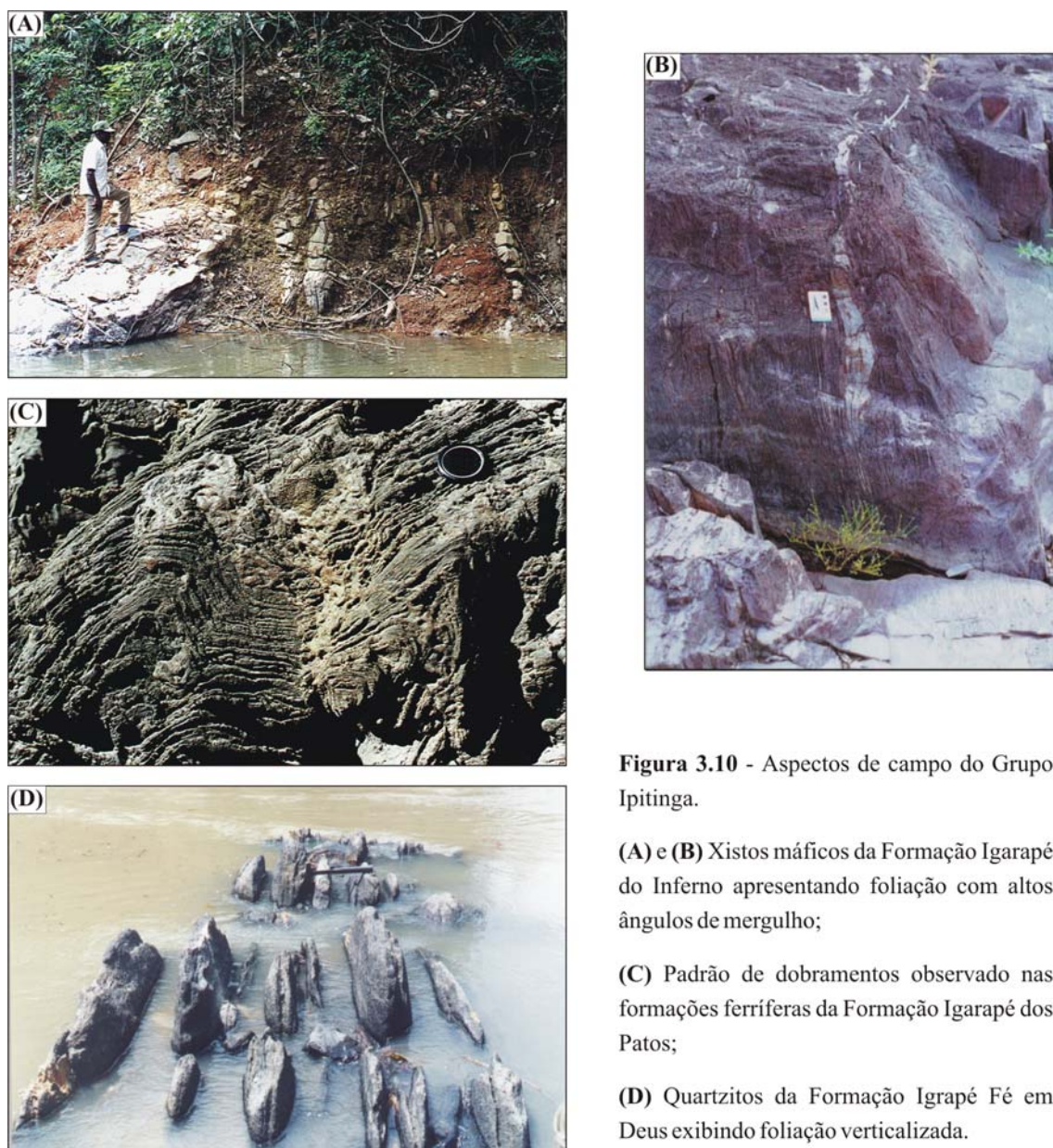


**Figura 3.10** - Aspectos de campo do Grupo Ipitanga.

(A) e (B) Xistos máficos da Formação Igarapé do Inferno apresentando foliação com altos ângulos de mergulho;

(C) Padrão de dobramentos observado nas formações ferríferas da Formação Igarapé dos Patos;

(D) Quartzitos da Formação Igarapé Fé em Deus exibindo foliação verticalizada.

Dentre as seqüências intra-domínio, a Sequência Serra Samaúma é a mais diversificada litologicamente, sendo constituída predominantemente por rochas metassedimentares clásticas (muscovita-quartzitos, quartzitos puros e ferruginosos) e químico-exalativas (formações ferríferas bandadas), seguidas de metaultramafitos (antofilita-serpentina, talco-hornblenda e tremolita-antofilita xistos) e metamafitos (clinopiroxênio-ortoanfibolitos bandados com piroxênio reliquiar e plagioclásio-antofilita-biotita xistos) subordinados (Ricci et al. 2001).

Por outro lado, as seqüências Fazendinha, Cuiapocu e Treze de Maio, no Domínio Carecuru, são constituídas essencialmente por rochas metavulcânicas máficas, xistosas ou isotrópicas. São rochas de granulação fina, cinza-esverdeadas a cinza-amarronzadas, podendo apresentar veios de quartzo de espessura até centimétrica, e vênulas preenchidas por pirita ou carbonato.

Rochas metavulcânicas intermediárias também ocorrem subordinadamente na Seqüência Fazendinha, com predominância de dacitos e andesitos, deformados ou não. Os tipos maciços preservam texturas ígneas porfíricas e glomeroporfíricas, e os anisotrópicos têm foliação desenhada por cordões de biotita iso-orientados ou apresentam foliação milonítica.

Os quartzitos são esporádicos nestas seqüências, e uma ocorrência de formação ferrífera foi registrada na Seqüência Treze de Maio.

Embora não haja dados geocronológicos em rochas destas unidades, lhes é inferida uma idade paleoproterozóica, uma vez que têm como embasamento o Complexo Paru-Maratiá, ou ainda apresentam relações estratigráficas que indicam que estas são intrudidas por granitóides da Suíte Intrusiva Carecuru, ambos comprovadamente paleoproterozóicos. A similaridade composicional entre os granitóide cálcio-alcálicos e as rochas vulcânicas destas seqüências, é indicativa que estes são correspondentes eruptivos daqueles.

### **3.2.3 – Magmatismo Plutônico Orogênico**

#### **3.2.3.1 - Complexo Máfico-Ultramáfico Bacuri**

O Complexo Máfico-Ultramáfico Bacuri está representado por um corpo alongado segundo E-W, localizado no Domínio Cupixi, intrusivo nos gnaisses do Complexo Tumucumaque e parcialmente recoberto por meta-supracrustais do Grupo Vila Nova (Spier & Ferreira Filho 1999).

Spier (1999) demonstrou que este complexo é resultante de um magmatismo primitivo originado de origem mantélica, com evolução balizada por processos de cristalização fracionada, associada a um mecanismo de intrusões múltiplas. É litologicamente definido, da base para o topo, por uma zona máfica inferior (leucoanfíbolitos), zona ultramáfica (serpentinóis, tremolitóis e cromitóis), sendo estes litotipos geralmente foliados segundo a estruturação regional e metamorfizados em condições da fácies anfíbolito.

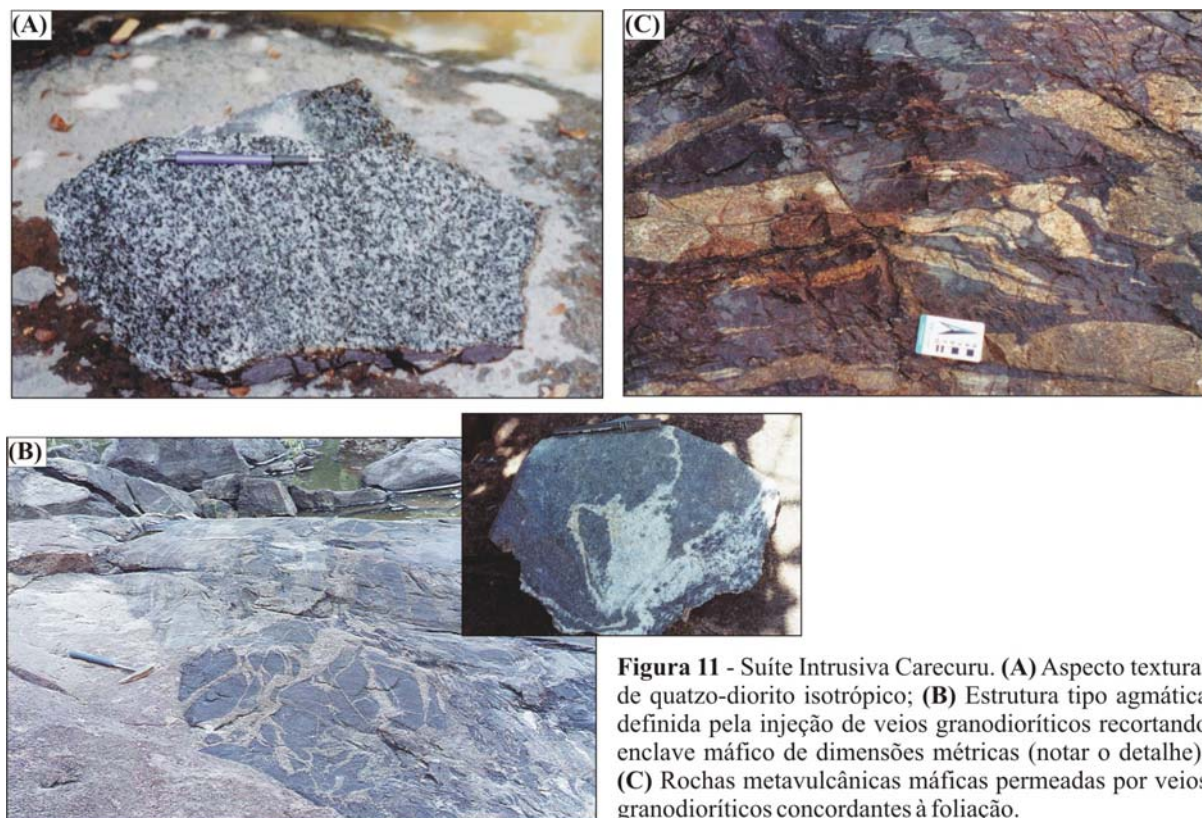
Pimentel et al. (2002), a partir de análises Sm-Nd em rocha total, apresentam uma errócrona onde foi calculada a idade de  $2220 \pm 12$  Ma (MSWD = 5.1), a qual é interpretada, devido à grande incerteza, apenas como idade aproximativa para cristalização deste complexo.

### 3.2.3.2 – Suíte Intrusiva Carecuru

Esta unidade, proposta por Ricci et al. (2001), engloba corpos plutônicos representados por dioritos e tonalitos, fundamentalmente, contendo ocasionais trondhjemitos e granitos, que são amplamente distribuídos no Domínio Carecuru, cujo conteúdo litológico é semelhante, em termos composicionais, ao do Complexo Paru-Maratiá. São rochas de coloração cinza escura a cinza esbranquiçada, de granulação média a grossa, geralmente isotrópicas, localmente milonitizadas (Figura 3.11 A). Os tipos isotrópicos exibem textura ígnea porfírica ou granular hipidiomórfica, enquanto os deformados desenham texturas porfiroclásticas e miloníticas. A associação mineralógica essencial é constituída por plagioclásio, quartzo, hornblenda, biotita e microclina, em proporções variáveis, e a acessória reúne minerais opacos, titanita, apatita e zircão. A hornblenda pode estar parcialmente transformada para biotita, clorita e epidoto, com formação secundária de opacos e titanita, assim como se observa localmente a biotita parcialmente substituída por clorita e o plagioclásio saussuritizado.

Enclaves máficos microgranulares de dimensões métricas são regularmente registrados, sendo recortados por veios e diques de composição tonalítica a granodiorítica, definindo uma estrutura tipo agmática (Figura 11 B). Adicionalmente, algumas estruturas observadas em afloramento apontam que estes granitóides são intrusivos nas rochas vulcânicas máficas das seqüências supracrustais, como por exemplo a presença de xenólitos de rochas vulcânicas, ou a ocorrência de veios destes granitóides permeando aquelas rochas (Figura 11 C).

Uma determinação geocronológica pelo método de evaporação de Pb em zircão proveniente de um diorito desta suíte forneceu idade de cristalização em  $2140 \pm 1$  Ma (Rosa-Costa et al. 2003), indicando que o magmatismo cálcio-alkalino que caracteriza esta unidade é pouco ( $\sim 10$  Ma) mais jovem que aquele do Complexo Paru-Maratiá. Entretanto, não foram observadas feições de campo que qualifiquem as relações de contato entre os plútons desta suíte e rochas daquele complexo. Considera-se que ambas as unidades representam pulsos temporalmente muito próximos do magmatismo cálcio-alkalino amplamente representado no Domínio Carecuru, sendo que as principais diferenças são de caráter estrutural.



### 3.2.3.3 - Suíte Intrusiva Igarapé Urucu

Esta unidade reúne vários plútons intrusivos nos granulitos do Complexo Ananaí, do Domínio Paru, os quais compreendem basicamente charnoquitos e granitos ricos em feldspato mesopertítico e plagioclásio antipertítico. São rochas de granulação grossa, leucocráticas, de coloração castanho-acinzentada, rosada ou esverdeada, freqüentemente isotrópicas, e localmente foliadas. Os tipos sem deformação predominam, apresentam textura ígnea granular hipidiomórfica ou porfírica, definida por fenocristais tabulares de mesopertita de até 3 cm isorientados, definindo uma estrutura de fluxo magmático (Figura 3.12 A). As rochas anisotrópicas caracterizam-se pelo desenvolvimento de uma foliação protomilonítica a milonítica, superimposta/concordante à foliação de fluxo magmático (Figura 3.12 B).

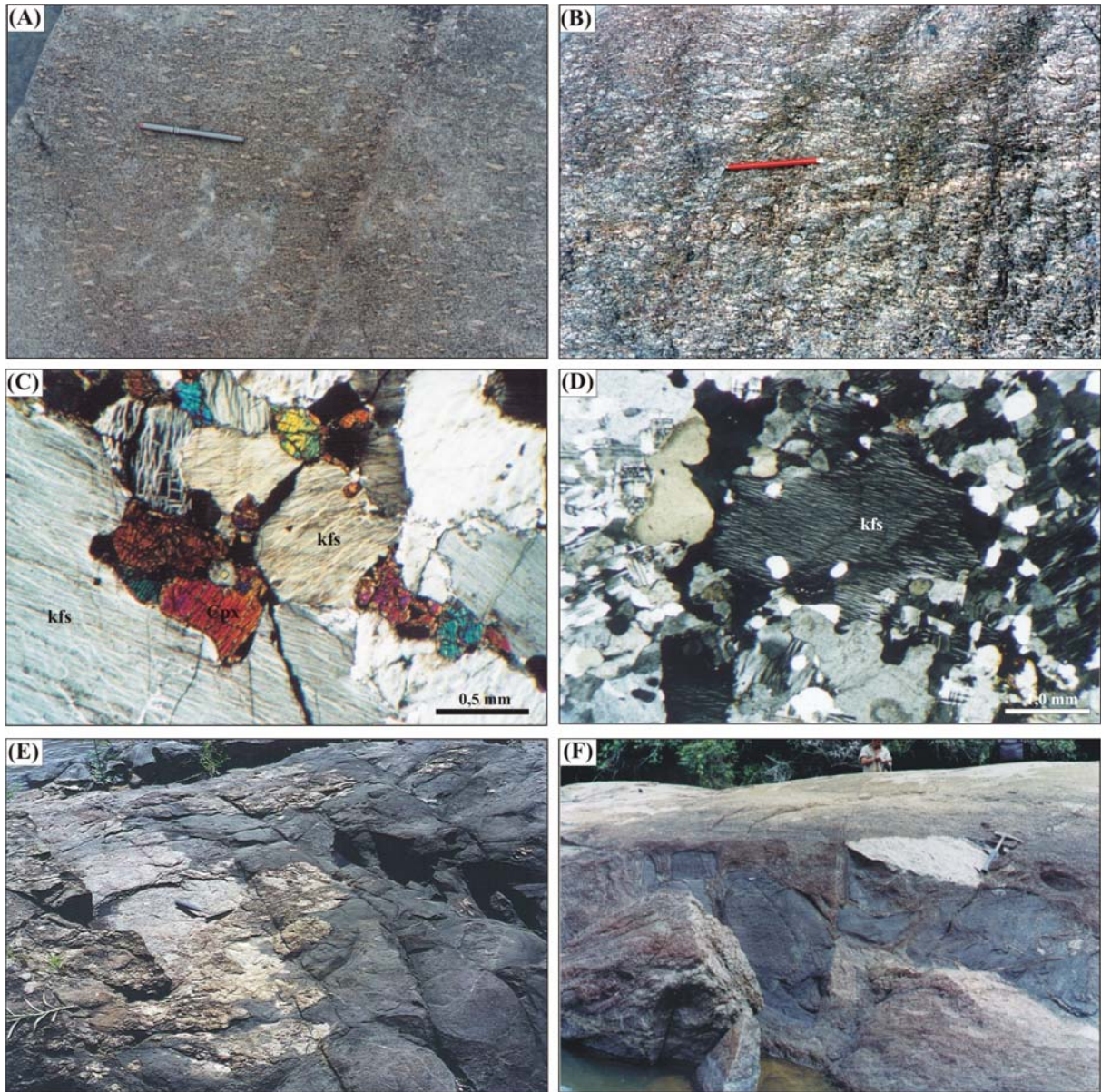


**Figura 3.12** - Suíte Intrusiva Igarapé Urucu. (A) Foliação de fluxo magmático definida pelo alinhamento de fenocristais tabulares de álcali-feldspato; (B) Charnquito protomilonítico, contendo fenocristais de álcali-feldspato amendoados, em matriz quartzo-feldspática; (C) Cristais de feldspato mesopertítico em contato com clinopiroxênio; (D) Microtextura porfirítica de mesopertita-granito, definida por fenocristal de feldspato mesopertítico em matriz quartzo-feldspática; (E) Contatos interlobados entre granitóides charnoquíticos e rocha máfica, indicando relação de mistura magmática; (F) Xenólito de gnaiss granulítico do Complexo Ananai em charnoquito.

Os constituintes mineralógicos essenciais são feldspato mesopertítico, quartzo, plagioclásio antipertítico, hornblenda, biotita, ortopiroxênio, clinopiroxênio, e os acessórios allanita, opacos, apatita e zircão (Figura 3.12 C). A granada ocorre esporadicamente e o ortopiroxênio é ausente nos mesopertita-granitos. A microtextura é geralmente porfirítica (Figura

3.12 D), e nas rochas deformadas torna-se porfiroclástica, com fenoclastos de mesopertita amendoados imersos em matriz inequigranular granoblástica.

Localmente, estas rochas encontram-se em relação de mistura magmática (*magma mingling*) com uma rocha máfica (Figura 3.12 E). Tais feições, somadas às texturas ígneas e à ocorrência de xenólitos de gnaisses granulíticos do Complexo Ananaí (Figura 3.12 F), atestam o caráter ígneo destes granitóides.

Datação em zircões obtidos de um charnoquito pelo método de evaporação de Pb, forneceu principalmente idades no intervalo de 2,16 a 2,06 Ga (Rosa-Costa et al. 2003). Estes resultados, embora imprecisos, indicam uma idade paleoproterozóica.

#### 3.2.3.4 - Suíte Intrusiva Parintins

João et al. (1978) definiram esta unidade para agrupar os granitóides tonalíticos a graníticos, isótipos ou com deformação incipiente, atribuindo-lhes um alojamento tardi-orogênico, conceito que foi incorporado por Ricci et al. (2001). Os plútons desta suíte têm distribuição indistinta entre os domínios tectônicos, formando corpos aproximadamente circulares, constituídos principalmente por monzogranitos e granodioritos, com tonalitos e sienogranitos subordinados, e com pegmatitos associados. As rochas são isotrópicas ou mostram uma discreta orientação dos minerais placóides. Têm coloração variando de cinza clara a rosada e granulação média, com texturas equigranular hipidiomórfica a porfírica.

#### 3.2.3.5 – Granitóides Indiferenciados

Esta denominação informal é empregada para agrupar várias suítes intrusivas (suítes Cupixi e Igarapé Careta) e corpos plutônicos (Granito Igarapé Castanhal e Alaskito Urucupatá), que foram propostas por Ricci et al. (2001) para caracterizar o magmatismo orogênico, predominantemente granítico, com idade paleoproterozóica inferida e localmente comprovada.

Em trabalhos anteriores, estes corpos plutônicos eram incorporados aos complexos metamórficos de embasamento por apresentarem, freqüentemente, tramas internas anisotrópicas. Ocorrem principalmente em maciços alongados segundo a estruturação regional, apresentando freqüentemente limites/contatos definidos por grandes lineamentos tectônicos. Corpos com formas elípticas e irregulares ocorrem em menor proporção.

Os tipos petrográficos dominantes são leucogranitos (monzogranitos, sienogranitos e álcali-feldspato granitos), com biotita-granitos, granodioritos e tonalitos subordinados. Alguns granitóides têm natureza peraluminosa, apresentando muscovita e biotita, granada e biotita ou granada e muscovita. Apresentam coloração variando entre avermelhada, acinzentada ou esbranquiçada, de acordo com sua composição mineralógica, granulação fina a média, sendo freqüentemente foliados e localmente isótropos. Os tipos deformados têm textura protomilonítica a milonítica, definidas por porfiroclastos de feldspato e quartzo, contornados por bandas/mosaicos alongados de composição quartzo-feldspática ou por trilhas anastomóticas de minerais máficos. Nas rochas miloníticas, fenocristais amendoados e bastonetes de quartzo definem a lineação de estiramento mineral. Os granitóides maciços exibem textura porfirítica ou granular hipidiomórfica.

Apresentam freqüentemente xenólitos dos gnaisses encaixantes, bem como ocorrem na forma de injeções ou diques naquelas rochas, concordantes ou não à sua estruturação (Figura 3.13 B e C e 3.8 C e D).

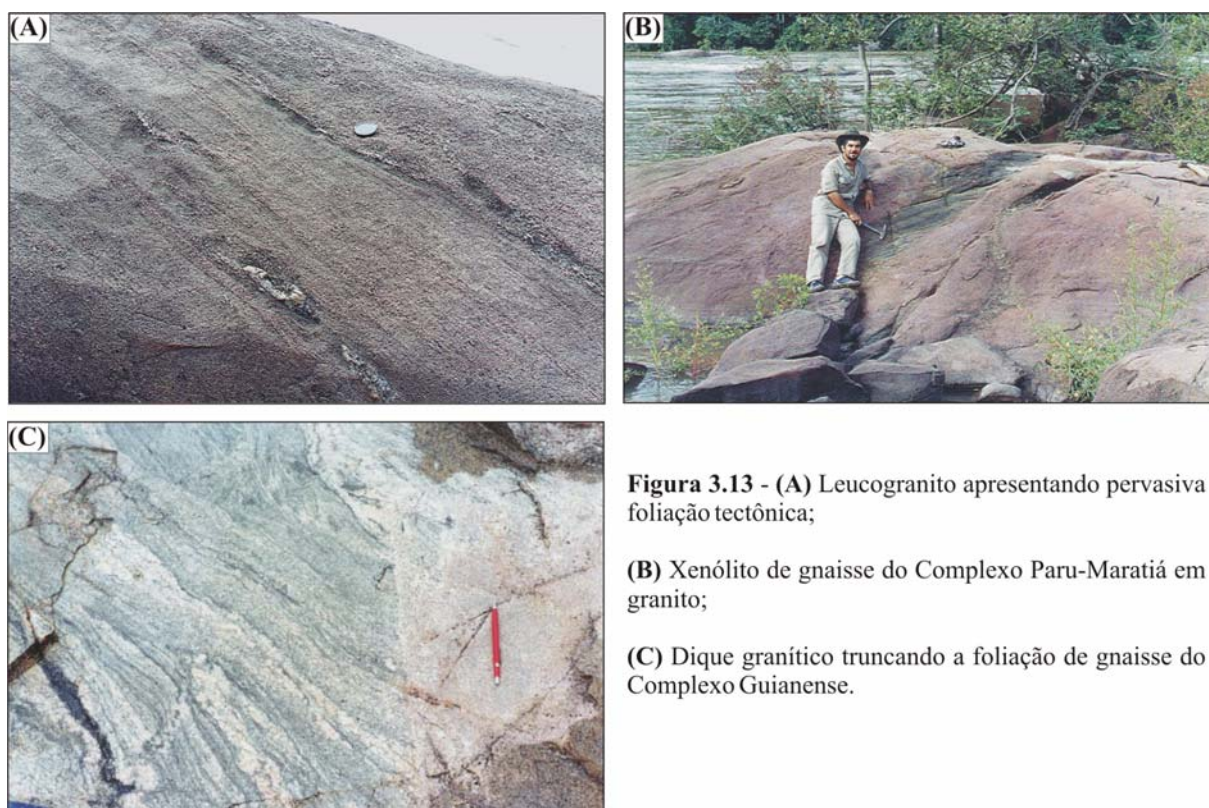


**Figura 3.13 - (A)** Leucogranito apresentando pervasiva foliação tectônica;

**(B)** Xenólito de gnaisse do Complexo Paru-Maratiá em granito;

**(C)** Dique granítico truncando a foliação de gnaisse do Complexo Guianense.

Dados geocronológicos que assegurem a evolução paleoproterozóica destes granitóides estão restritos a dois plútons datados, ambos localizados no âmbito do Domínio Jari (Figura 3.2). Montalvão & Tassinari (1984) obtiveram uma idade isocrônica Rb-Sr de 2,26 Ga em um plúton granítico intrusivo em gnaisses do Complexo Guianense, localizado na porção nordeste da área, enquanto um álcali feldspato-granito de um corpo intrusivo nos complexos Jari-Guaribas e Baixo-Mapari forneceu uma idade Pb-Pb em zircão de  $2146 \pm 3$  Ma (Rosa-Costa et al. 2003).

#### 3.2.3.6 – Corpos Máficos-Ultramáficos Indiferenciados

A esta unidade informal estão associados corpos plutônicos que ocorrem nos domínios Carecuru e Jari, compostos por metagabros, anfíbolitos e metaperidotitos, foliados ou maciços (Ricci et al. 2001). Faraco et al. (2004b) apresentam uma idade  $T_{DM}$  Sm-Nd de 2,46 Ga obtida no corpo que ocorre no Domínio Carecuru, vinculando sua evolução ao Paleoproterozóico.

### 3.2.4 - Magmatismo Anorogênico

#### 3.2.4.1 - Granito Waiãpi

Ricci et al. (2001) propuseram a designação de Granito Waiãpi, para englobar um conjunto de plútons graníticos, com características de granitos tipo A. São plútons com formas elípticas ou circulares, compostos por hastingsita-granitos, de granulação média a grossa, equigranulares, isótropos, e de coloração castanha a cinza-esbranquiçada. Localmente, ocorrem tipos porfíricos e/ou com textura rapakivi, além de microgranitos e aplitos. São compostos por plagioclásio, microclina, quartzo, hastingsita, biotita, opacos, apatita, zircão e fluorita, e exibem geralmente textura granular hipidiomórfica.

Em um plúton localizado no norte da área, no Domínio Jari, foi obtida a idade Pb-Pb em zircão de  $1753 \pm 3$  Ma, interpretada como idade do magmatismo granítico anorogênico (Vasquez & Lafon 2001).

### 3.3 – PADRÕES ESTRUTURAIS E ASSINATURAS AEROGEOFÍSICAS DOS DOMÍNIOS TECTÔNICOS

Rosa-Costa et al. (2002b), a partir da análise integrada de informações de campo, de imagens aerogeofísicas e de outros sensores remotos obtidos na área do Projeto Promin-RENCA, destacam a existência de diferentes domínios geofísicos, diretamente correlacionáveis aos domínios tectônicos individualizados naquela região. Segundo estes autores, as diferenças de assinaturas geofísicas são marcantes entre os domínios Jari, Carecuru e Paru, e pouco expressivas entre os domínios Jari e Cupixi, conforme pode ser visualizado nos mapas geofísicos da Figura 3.14. As assinaturas geofísicas características dos domínios tectônicos refletem não somente o conteúdo litológico distinto de cada um deles, o qual influenciaria diretamente os padrões radiométricos, mas também seus padrões estruturais diferenciados, bem marcados nos mapas radiométricos e magnetométricos.

O DJ destaca-se como um grande corredor de deformação, em que as rochas estão fortemente estruturadas, e nos quais as anomalias radiométricas e magnéticas apresentam-se como extensas faixas sigmoidais ou com formas lenticulares, alongadas segundo a direção NW-SE, que refletem a própria geometria dos grandes corpos rochosos, intensamente controlados por estruturas tectônicas. Nos mapas radiométricos caracteriza-se por apresentar um padrão de radiação heterogêneo, definido pela alternância de faixas com intensidades distintas de radiação (Figura 3.14 A e B), que reflete a diversidade litológica daquele domínio, com rochas de composição variando de diorítica à granítica. Nos mapas magnetométricos este domínio caracteriza-se pela grande incidência de anomalias magnéticas lineares de alta amplitude e alta frequência, que refletem a marcante presença de descontinuidades estruturais (Figura 3.14 C e D).

Este padrão geofísico-estrutural é característico sobretudo da porção sudoeste do Domínio Jari, onde ocorrem faixas de rochas granulíticas, intercaladas tectonicamente àquelas constituídas por gnaisses da fácies anfíbolito. Este segmento representa o Cinturão Jari, de Hasui et al. (1984), que, segundo estes autores, coincide com uma anomalia gravimétrica do tipo I, relacionada a um grande sistema de cavalgamento, que demarca o limite entre blocos crustais Oiapoque e Maecuru (Figura 2.2).

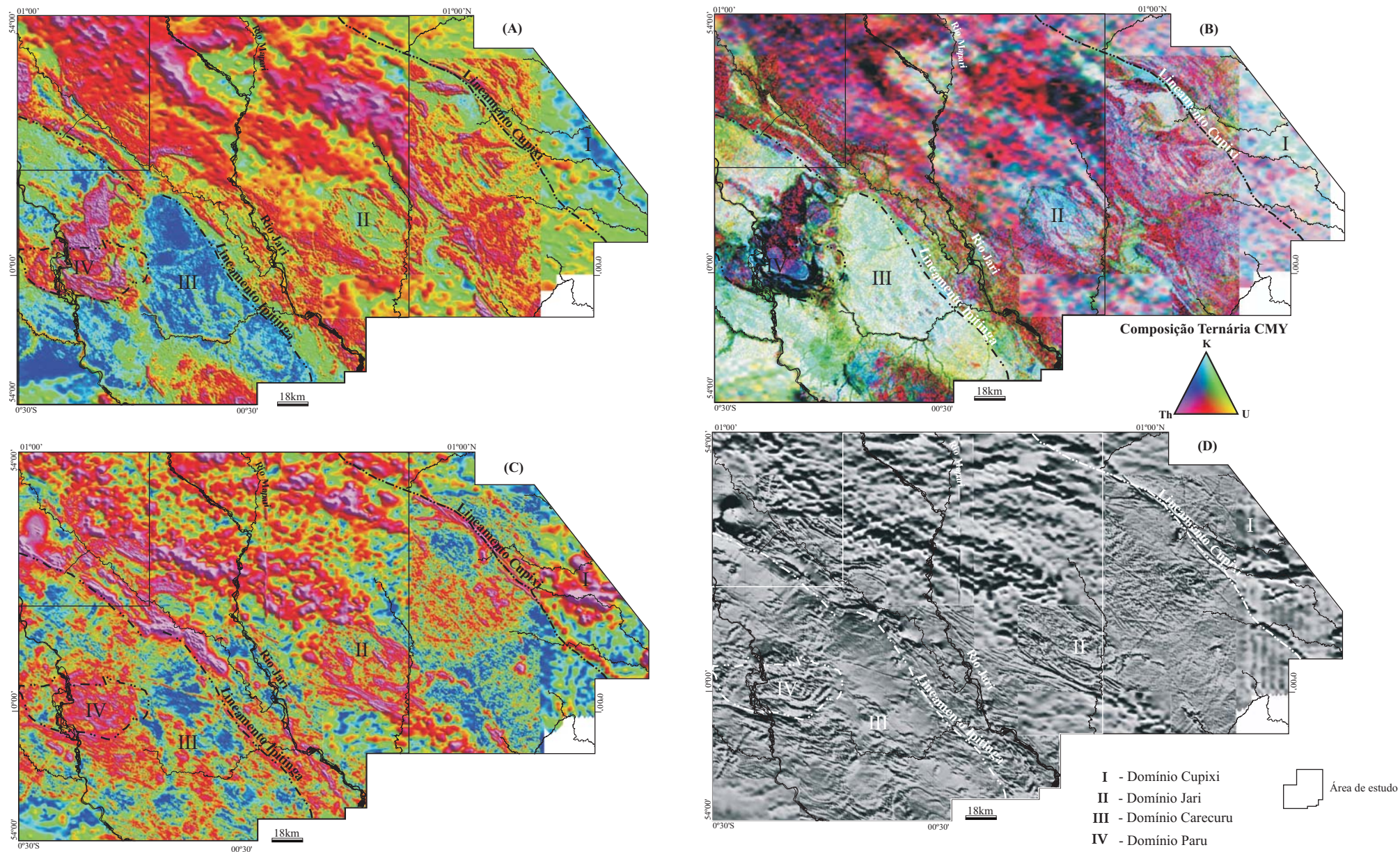


**Figura 3.14** - Imagens aerogeofísicas radiométricas e magnetométricas da área do Projeto Promin-RENCA, compiladas de Rosa-Costa et al. (2002b), com sobreposição dos limites entre os domínios tectônicos individualizados por Ricci et al. (2001): **(A)** Imagem radiométrica do canal do tório; **(B)** Imagem radiométrica de composição ternária Th-U-K em sistema de cores CMY; **(C)** Imagem magnética de amplitude do sinal analítico; **(D)** Imagem magnética da primeira derivada vertical do campo magnético anômalo. Na escala de cores adotada para as imagens A e C, as cores avermelhadas representam altos valores de tório ou alta amplitude do sinal analítico, respectivamente, enquanto que as cores azuladas representam os baixos correspondentes. Na imagem ternária B, altos valores de Th, K e U apresentam-se com cores magenta, ciano e amarela, respectivamente. A cor final para um domínio com elevados teores de Th, U e K mostra-se preta, e branca se for um domínio de baixos teores nos três elementos.

Dados de campo demonstram que no Domínio Jari, e sobretudo no segmento sudoeste, os gnaisses dos complexos metamórficos de embasamento, e mesmo os leitos de leucossomas concordantes ao bandamento, apresentam conspícua foliação dúctil ( $S_1$ ) com direção NW-SE e mergulhos predominantemente entre 40 e 60°, principalmente para SW, em cujos planos identifica-se a lineação de estiramento ( $L_1$ ), com caimentos moderados para SW (Figura 3.15 A). Estas características estruturais (relação foliação/lineação) definem o caráter oblíquo da movimentação e permitem a caracterização de um sistema de cavalgamento oblíquo, com transporte tectônico de SW para NE. Dobras recumbentes com eixo paralelo à direção da foliação  $S_1$  ratificam a natureza convergente da movimentação (Figura 3.15 B).

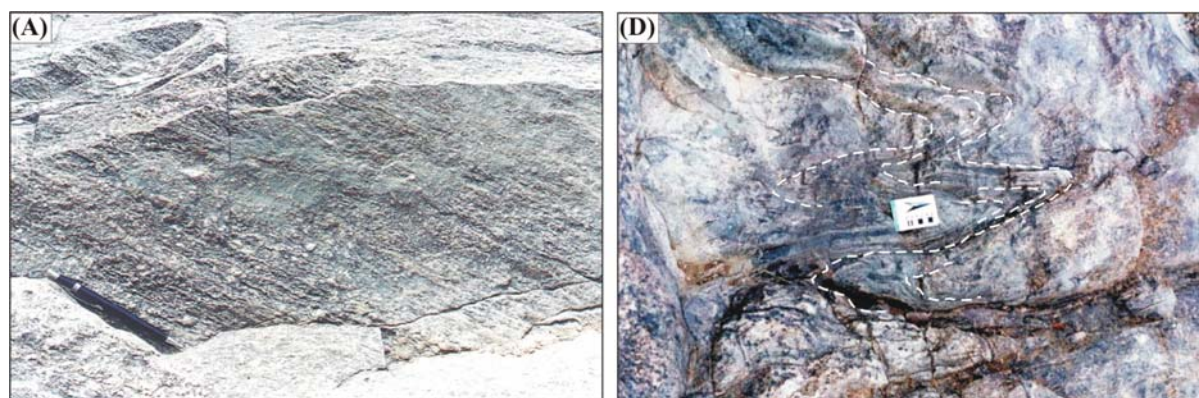


**Figura 3.15** - Feições estruturais observadas no setor sudoeste do Domínio Jari. (A) Lineação de estiramento mineral no plano da foliação gnáissica; (B) Dobras recumbentes com eixo ortogonal ao plano da foto, e paralelo à direção da foliação.

Este padrão estrutural pode ser modificado ao longo de zonas de cisalhamento transcorrentes, onde as rochas apresentam foliação milonítica ( $S_2$ ), com direção paralela a subparalela a  $S_1$  e com altos valores de mergulho. A lineação de estiramento sub-horizontal ( $L_2$ ) contida nos planos da foliação  $S_2$  definem o caráter direcional da movimentação. Localmente, é registrada a transposição da foliação  $S_1$  através de bandas de cisalhamento transcorrentes, que culmina com a paralelização dos elementos estruturais e desenvolvimento da foliação milonítica  $S_2$  (Figura 3.16), demonstrando que a movimentação transcorrente é posterior à fase de cavalgamento. Indicadores cinemáticos como foliação S-C, assimetria de porfiroclastos, *boudins* rotacionados, bandas de cisalhamento e dobras intrafoliais, sugerem principalmente o sentido dextral para a movimentação transcorrente.

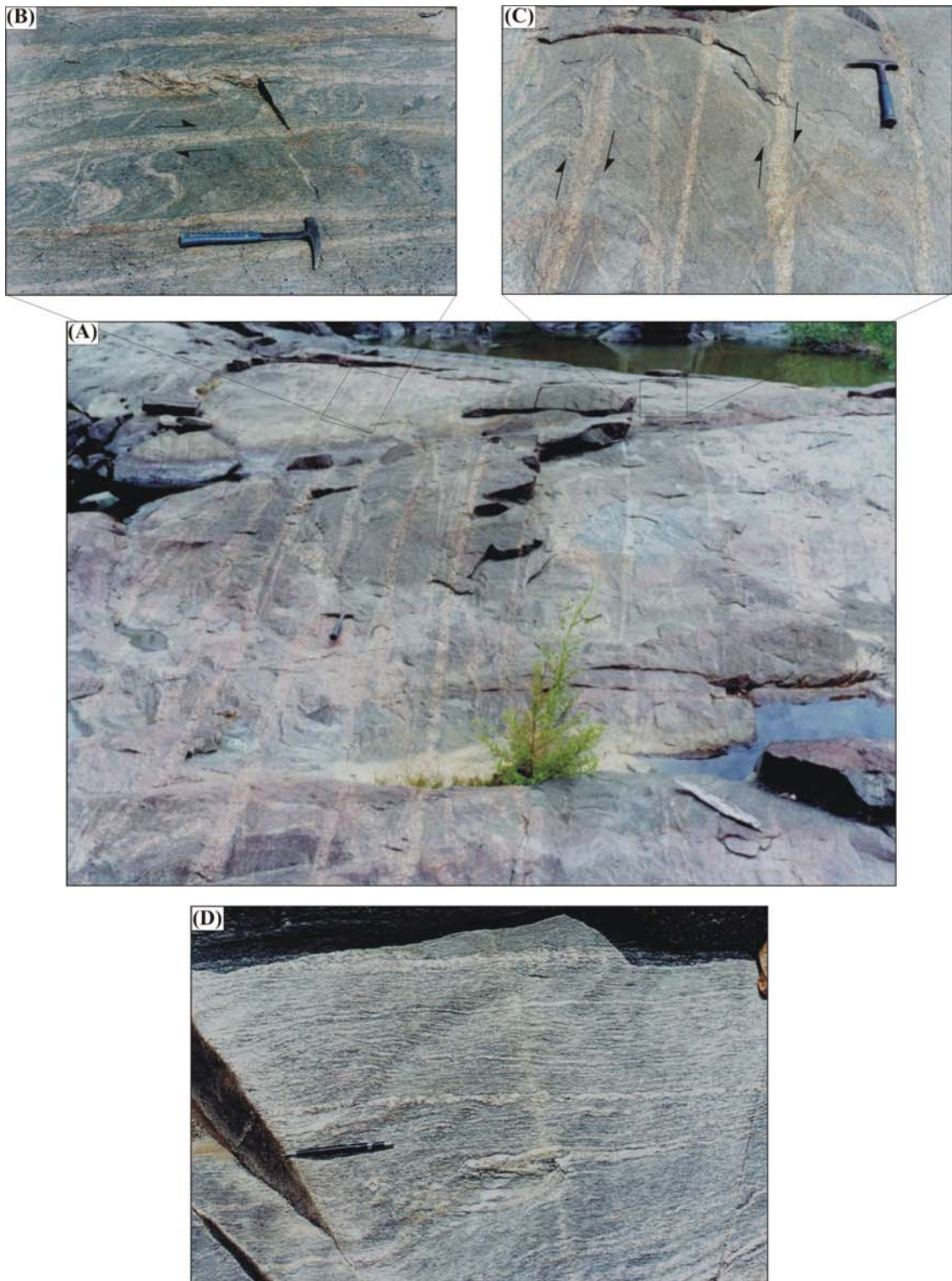


**Figura 3.16 -** (A) Feixe de bandas de cisalhamento transcorrentes paralelizadas recortando gnaisse do Complexo Guianense. (B) e (C) Detalhe das bandas de cisalhamento onde é observada a transposição da foliação gnáissica e o sentido dextral da movimentação transcorrente; (D) Foliação milonítica registrada no gnaisse, desenvolvida a partir da paralelização dos elementos estruturais através de bandas de cisalhamento transcorrentes. Todas as ilustrações referem-se ao mesmo afloramento.

Portanto, os megalineamentos observados em imagens aerogeofísicas e de outros sensores remotos podem ser caracterizados no campo como zonas de cavalgamento ou transcorrentes, que em alguns setores definem contatos tectônicos das faixas de rochas granulíticas. As zonas transcorrentes também definem limites tectônicos dos corpos granulíticos e de alguns plútons de granitóides. Na área estudada, o Lineamento Ipitinga representa a zona transcorrente mais expressiva, que demarca o limite entre os domínios Jari e Carecuru. Esta estrutura exerce forte controle sobre as rochas supracrustais do Grupo Ipitinga, que exibem, via de regra, foliação com altos ângulos de mergulho (Figura 3.10). Plútons granitóides seccionados pelo Lineamento Ipitinga ocorrem em corpos fortemente alongados, com foliação interna milonítica e de alto ângulo, e nas porções mais deformadas definem verdadeiros tectonitos L.

No Domínio Carecuru o padrão de deformação é heterogêneo, visto que neste domínio, zonas intensamente deformadas alternam-se a outras onde a deformação é incipiente, ou mesmo ausente. Este padrão é bem registrado nos granitóides cálcio-alcálicos que definem a Suíte Intrusiva Carecuru e nas seqüências vulcânicas das diversas faixas supracrustais, os quais têm localmente suas texturas ígneas primárias obliteradas pela estruturação milonítica. Este padrão estrutural heterogêneo também é refletido nos mapas magnéticos, onde setores de padrão magnético calmo, com superfícies magnéticas aplainadas, alternam-se a porções onde a incidência de anomalias magnéticas lineares é mais expressiva (Figura 3.14 B e C).

O Domínio Carecuru é caracteristicamente um segmento de baixos valores radiométricos, o que contrasta fortemente com o padrão radiométrico do Domínio Jari adjacente. Nos mapas do canal de tório e de composição ternária caracteriza-se pela predominância de cores azuladas (baixa radiação de Th) e esbranquiçadas (baixa radiação de Th, U e K), respectivamente, que refletem a composição primitiva dos principais grupos litológicos deste domínio, as rochas cálcio-alcálicas do Complexo Paru-Maratiá e da Suíte Intrusiva Cupixi, e as metavulcânicas predominantemente máficas que compõem as diversas faixas de supracrustais (Figura 3.14 A e B). Este padrão radiométrico é bruscamente modificado na região do Domínio Paru e nas áreas de ocorrência dos diversos plútons graníticos, que são caracteristicamente delineados por domínios de altos radiométricos (Figura 3.14 A). Portanto, a assinatura geofísica distintiva do Domínio Paru em relação às áreas adjacentes, fortalece a proposta de individualização daquele núcleo granulítico, também justificada pelo seu conteúdo litológico e padrão geocronológico, específicos e contrastantes em relação aos do Domínio Carecuru.

#### 4 – MOTIVAÇÃO DO TRABALHO E OBJETIVOS

Pode-se considerar que a área proposta para estudo apresenta características geológicas e posicionamento geográfico que a tornam estratégica para se compreender as relações entre os grandes segmentos de crosta arqueana e paleoproterozóica existentes na porção oriental do Cráton Amazônico, e que definem importantes províncias geocronológicas nas propostas vigentes de compartimentação do referido cráton. Seguindo-se a proposta de Tassinari & Macambira (2004), a área situa-se no domínio ensialico da Província Maroni-Itacaiúnas (paleoproterozóica), enquanto baseando-se na proposta de Santos et al. (2000), a mesma está localizada na região limítrofe entre as províncias Carajás (arqueana) e Transamazônica (paleoproterozóica) (Figuras 2.3 e 2.4).

Como demonstrado em capítulos anteriores, a retomada de estudos geológicos nesta área através do Projeto Promin-RENCA propiciou avanços importantes no conhecimento geológico. Neste sentido, uma das mais significativas contribuições trazidas pelo referido projeto foi a proposta de compartimentação tectônica apresentada por Ricci et al. (2001), que reconheceu distintos terrenos tectônicos na região. Esta proposta, além de ter subsidiado a definição ou redefinição de unidades estratigráficas que definem o arcabouço geológico da área enfocada, norteou os primeiros estudos geocronológicos realizados na mesma (Rosa-Costa et al. 2001, 2003), que tinham como objetivo primordial atribuir referências geocronológicas às unidades estratigráficas propostas e caracterizar preliminarmente o padrão geocronológico dos diferentes compartimentos tectônicos.

Como resultado dos trabalhos acima citados, foram reconhecidos na área de estudo os domínios Jari, Paru e Carecuru, e soube-se que a assembléia de embasamento dos domínios Jari e Paru tem padrão geocronológico predominantemente arqueano, contrastando com a assinatura paleoproterozóica do Domínio Carecuru. No entanto, os dados geológicos e geocronológicos disponíveis até o momento ainda não permitem assegurar se estes domínios tectônicos representam, de fato, segmentos crustais distintos, com assinatura isotópica característica e evolução geológica diferenciada.

Focalizando-se numa escala mais regional, constatam-se grandes incertezas na definição do limite entre o segmento arqueano que define a Província Amazônia Central ou a Província Carajás, segundo Tassinari & Macambira (2004) e Santos et al. (2000), respectivamente, e o

domínio paleoproterozóico representado pela Província Maroni-Itacaiúnas ou Transamazônica (definidas pelos mesmos autores, respectivamente). Na primeira proposta o limite é posicionado logo a norte da região de Carajás, enquanto na outra os autores estendem o domínio arqueano até a região central do Amapá. A região de intersecção representa uma faixa de mais de 500 km de extensão, que inclui o Domínio Carecuru, que representa uma área ainda pouco conhecida, face à escassez de levantamentos geológicos sistemáticos e aos dados geocronológicos restritos (Santos et al. 1988, Rosa-Costa et al. 2001, 2003, Macambira et al. 2001, 2003, Santos 2003, Faraco et al. 2005, Vasquez et al. 2005).

Diante deste cenário, configura-se como um dos principais objetivos desta pesquisa entender o significado geodinâmico dos terrenos tectônicos, através da caracterização dos processos de evolução crustal que atuaram no Arqueano e no Paleoproterozóico, e que são responsáveis pela configuração atual da área. Como consequência, vislumbra-se entender as relações existentes entre rochas arqueanas e paleoproterozóicas deste segmento do Cráton Amazônico, e apresentar subsídios às futuras propostas de compartimentação tectônica do referido cráton.

No Domínio Carecuru, a investigação será conduzida no sentido de acrescentar referências geocronológicas às principais unidades plutônicas, sobretudo aos granitóides cálcio-alcalinos do Complexo Paru-Maratiá e da Suíte Intrusiva Carecuru, e avaliar se os mesmos têm origem relacionada a acreção crustal juvenil no Paleoproterozóico, e/ou se envolve retrabalhamento de crosta arqueana. Enquanto que nos segmentos supostamente arqueanos, os domínios Jari e Paru, estudos complementares são necessários para avaliar a real extensão de crosta arqueana na região, principalmente através da datação de amostras provenientes das unidades que definem a assembléia de embasamento, e para definir os eventos de acreção e retrabalhamento crustal que atuaram neste éon e no Paleoproterozóico, durante o Ciclo Orogênico Transamazônico.

Avaliar o retrabalhamento de crosta arqueana durante a referida orogênese e seus produtos representa uma importante questão a ser discutida e também define mais um dos objetivos deste trabalho. Ênfase será dada a algumas unidades que constituem a assembléia de embasamento do Domínio Jari (os complexos Jari-Guaribas e Guianense), a qual representa uma notável

associação de alto grau metamórfico do tipo granulito-gnaiss-migmatito, e que, segundo demonstram os dados geocronológicos disponíveis, derivam de precursores arqueanos.

Neste sentido, será investigado se o metamorfismo de alto grau que afetou o segmento arqueano é produto de retrabalhamento ensiálico em orogenias arqueanas, ou se está vinculado ao Ciclo Orogênico Transamazônico, como registrado em outros domínios de alto grau da província paleoproterozóica em questão, a exemplo dos granulitos das Montanhas Bakhuis (Roever et al. 2003), no Suriname, do Complexo Imataca (Tassinari et al. 2004), na Venezuela, e da região de Tartarugalzinho (Avelar et al. 2001, 2003, Oliveira et al. 2002), na porção central do Amapá.

É importante ressaltar que, definir a idade do metamorfismo de alto grau representa talvez o objetivo mais imediato nesta linha de investigação termocronológica. No entanto, entender a qual processo tectônico e a que estágio da evolução orogênica o evento metamórfico está relacionado, também constitui uma relevante questão a ser abordada nesta pesquisa. Com isso, deseja-se fornecer os primeiros subsídios para o entendimento da evolução termotectônica da área enfocada.

No entanto, neste trabalho, a investigação da evolução termocronológica e termotectônica não se restringe ao terreno de alto grau metamórfico, ou seja, ao Domínio Jari. Consiste numa importante meta, entender, através da datação de minerais geocronômetros com temperaturas de bloqueio inferiores àquelas aceitáveis para o metamorfismo granulítico, a evolução tectono-termal dos diferentes domínios tectônicos no decorrer do Evento Transamazônico, com ênfase nos domínios Jari e Carecuru, e as possíveis diferenças com relação aos processos crustais que controlaram sua exumação e resfriamento termal.

Face à inexistência de um modelo de evolução geodinâmica para o segmento sudeste da Província Maroni-Itacaiúnas/Transamazônica, que leve em consideração a participação de terrenos arqueanos, uma vez que os modelos vigentes foram propostos para segmentos essencialmente juvenis (Vanderhaeghe et al. 1998, Delor et al. 2003a), discutir um modelo evolutivo baseado na integração de dados, a partir da caracterização dos principais estágios orogênicos do Evento Transamazônico, representa o objetivo final desta pesquisa.

## 5 – ATIVIDADES E PROCEDIMENTOS ANALÍTICOS

### 5.1 – TRABALHOS DE CAMPO E AMOSTRAGEM

No exercício de suas atividades funcionais na CPRM, a autora desta pesquisa participou de todas as etapas de campo desenvolvidas pelo Projeto Promin-RENCA, que culminaram com o mapeamento geológico em escala 1:250.000 da área do referido projeto. As atividades de campo foram realizadas em quatro etapas com cerca de 30 dias cada, nos anos de 2000 e 2001, quando foi possível caracterizar os principais conjuntos litológicos e aspectos estruturais das diversas unidades litoestratigráficas mapeadas e, em alguns casos, suas relações de contato.

Imagens geofísicas gamaespectométricas e magnetométricas dos projetos aerogeofísicos Jari-Rio Negro Leste I e II (CPRM/DNPM 1978, 1979) e RENCA (CPRM 1999), integradas a imagens dos sensores remotos JERS 1 e LANDSAT TM5, foram ferramentas importantes para subsidiar os trabalhos de campo, quando se procurou avaliar as relações existentes entre assinaturas aerogeofísicas, padrões de relevo, associações litológicas e padrões estruturais.

Vislumbrando-se o desenvolvimento desta pesquisa, durante os levantamentos de campo, ao tempo em que era feita a coleta de amostras necessárias à cartografia geológica de caráter regional desenvolvida pelo Projeto Promin-RENCA, realizou-se a coleta sistemática de amostras na área definida para esta tese, visando sua utilização em estudos mais específicos. Cerca de 600 amostras de rocha foram coletadas na área selecionada para esta pesquisa.

As atividades de campo foram desenvolvidas principalmente em perfis geológicos previamente programados ao longo dos principais cursos d'água da região, tais como os rios Jari, Ipitinga, Mapari, Carecuru, Iratapuru e Paru, e os igarapés Carecuruzinho, Fé em Deus e do Inferno. Devido às limitações de acesso a algumas áreas, também foram feitas observações pontuais em áreas de interflúvio, em clareiras planejadas em locais geologicamente estratégicos, cujo acesso só foi possível com utilização de helicóptero. No mapa do Anexo I estão plotadas todas as amostras coletadas na área de trabalho por ocasião do referido projeto, destacando-se os principais cursos d'água percorridos.

Dentre as amostras de rocha coletadas durante as atividades de campo, foram selecionadas 43 para utilização em análises laboratoriais, cuja localização, aferida através de GPS, pode ser observada na Figura 5.1 e no Anexo I.

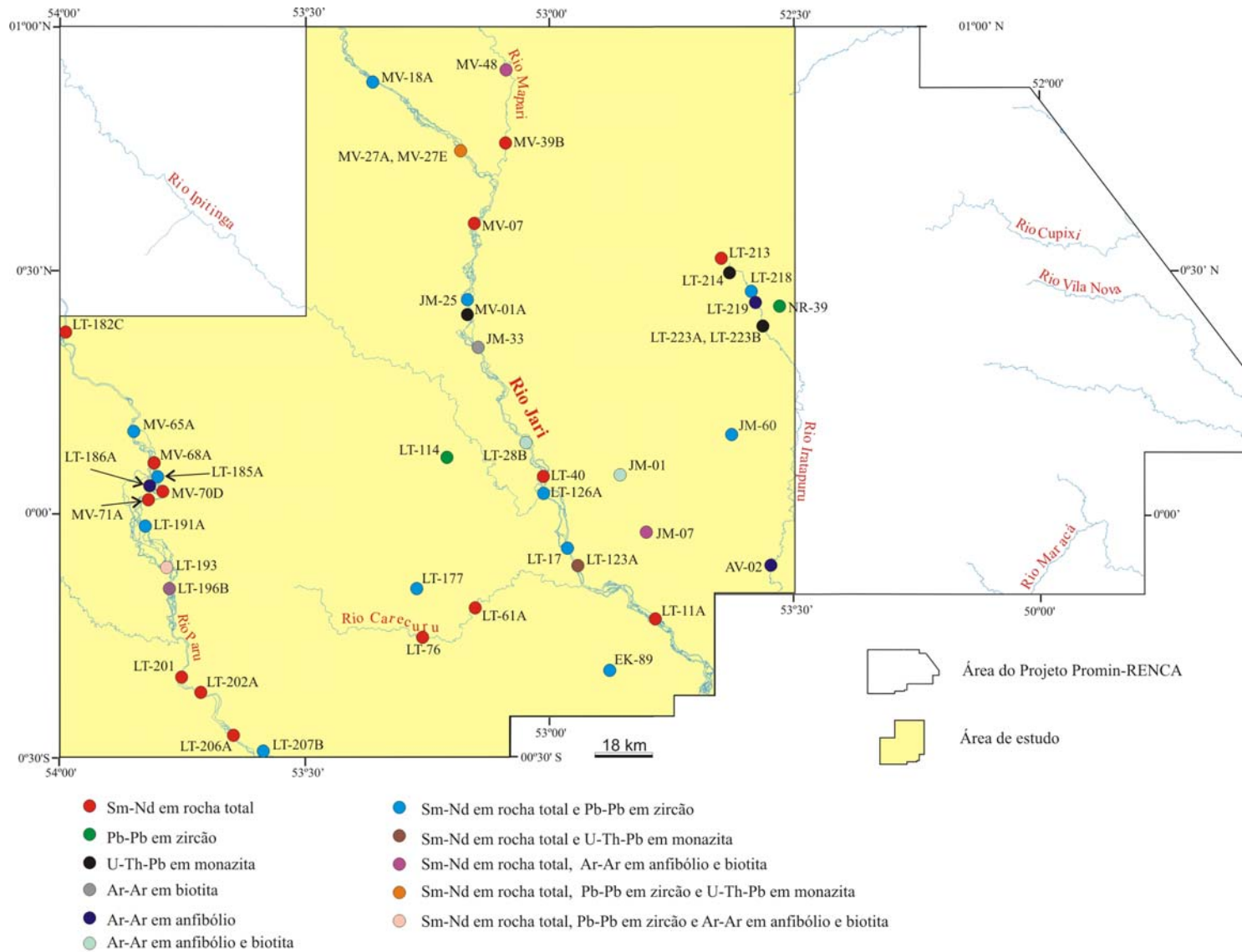


**Figura 5.1** - Mapa da área de estudo com a localização das amostras utilizadas no estudo geocronológico/isotópico, discriminadas conforme o tipo de material (rocha total ou mineral) e o método analítico empregado.

## 5.2 – ESTUDO PETROGRÁFICO

Durante o desenvolvimento do Projeto Promin-RENCA, foi realizado o estudo petrográfico de cerca de 250 lâminas delgadas relativas a amostras coletadas na área de trabalho. Este estudo consistiu basicamente na identificação e quantificação da mineralogia, na análise textural e na classificação petrográfica, seguindo propostas amplamente conhecidas (Streckeisen 1976, Best 1982, Le Maitre et al. 1989, Spear 1995, Passchier & Trow 1996, Robertson 1999).

Todas as lâminas petrográficas e amostras correspondentes foram reavaliadas detalhadamente nas fases iniciais desta pesquisa, quando foi feita a seleção daquelas adequadas para as análises laboratoriais subseqüentes. A seleção das amostras baseou-se em vários aspectos como, representatividade na área, potencial para solucionar problemas geológicos específicos, grau de alteração intempérica e presença de fases minerais de interesse.

Descrições petrográficas em detalhe e registros fotomicrográficos foram realizados nas amostras utilizadas em análises laboratoriais, bem como em outros exemplares representativos de cada unidade litoestratigráfica. As principais características petrográficas dos litotipos que definem as unidades estratigráficas abordadas neste estudo foram sinteticamente descritas no Capítulo 3. Nos capítulos 6, 7 e 8, referentes aos artigos científicos agregados nesta tese, são apresentadas descrições petrográficas sumarizadas de todas as amostras utilizadas em estudos isotópicos.

## 5.3 – PREPARAÇÃO DE AMOSTRAS

Técnicas convencionais de preparação de amostras foram empregadas para obtenção das frações de pó representativas de rocha total e de concentrados de minerais, como zircão, monazita, anfibólio e biotita. As amostras de rocha total foram obtidas através da trituração de aproximadamente 5 kg de rocha em britador de mandíbula, moagem em moinho de anéis/cilindro de todo o material, quarteamento, e subseqüente pulverização em moinho de esferas de cerca de 200 g, até a fração 200 #.

Para separação de zircão e monazita, após a moagem do material em moinho de anéis/cilindro, foi individualizada uma alíquota de aproximadamente 3 kg, através de etapas sucessivas de quarteamento, a qual foi submetida à lavagem, para eliminação das frações silte e argila, peneiramento e concentração de minerais pesados não magnéticos das frações 80-150 e 150-200  $\mu\text{m}$ , inicialmente utilizando-se bromofórmio como líquido pesado e, posteriormente,

com auxílio do separador magnético Franz. Finalmente, foi efetuada a separação manual dos cristais a partir dos concentrados finais, com auxílio de lupa binocular. Concentrados de anfibólio e biotita foram obtidos diretamente através de separação mecânica das frações granulométricas 350 – 500 e 500 – 1000  $\mu\text{m}$ , sob lupa binocular.

As atividades de preparação de amostras foram desenvolvidas em laboratórios da CPRM de Belém e Porto Alegre, e no Laboratório de Geologia Isotópica Pará-Iso e Oficina de Preparação de Amostras (OPA) do Centro de Geociências da UFPA.

#### 5.4 – MICROSCOPIA ELETRÔNICA

Duas etapas distintas de microscopia eletrônica de varredura foram realizadas ao longo deste trabalho. Na primeira etapa, com objetivo de identificar cristais de monazita dentre outros minerais pesados semelhantes, foram executadas imagens de elétrons retroespalhados (*Back-Scattered Electron* – BSE), sistematicamente acompanhadas de análises qualitativas por dispersão de energia (*Energy Dispersive Spectrometry* - EDS), as quais possibilitaram a avaliação dos aspectos morfológicos e texturais e a caracterização química preliminar dos cristais de monazita (Figura 5.2). Esta etapa foi realizada nos laboratórios de microscopia eletrônica do Centro de Geociências da UFPA e do Museu Paraense Emílio Goeldi, onde foram utilizados equipamentos modelo LEO-1430 e LEO-1450, respectivamente.

Na segunda etapa, foram novamente capturadas imagens de elétrons retroespalhados de cristais de monazitas, mas agora em seções polidas, com objetivo de investigar as características texturais internas dos mesmos, tais como padrão de zoneamento e presença de inclusões. Esta atividade subsidiou a seleção dos cristais para análises posteriores em microsonda eletrônica, bem como o posicionamento dos perfis analíticos a serem executados, e foi realizada no microscópio eletrônico modelo JSM-6100, em laboratório do BRGM, Orléans, França.

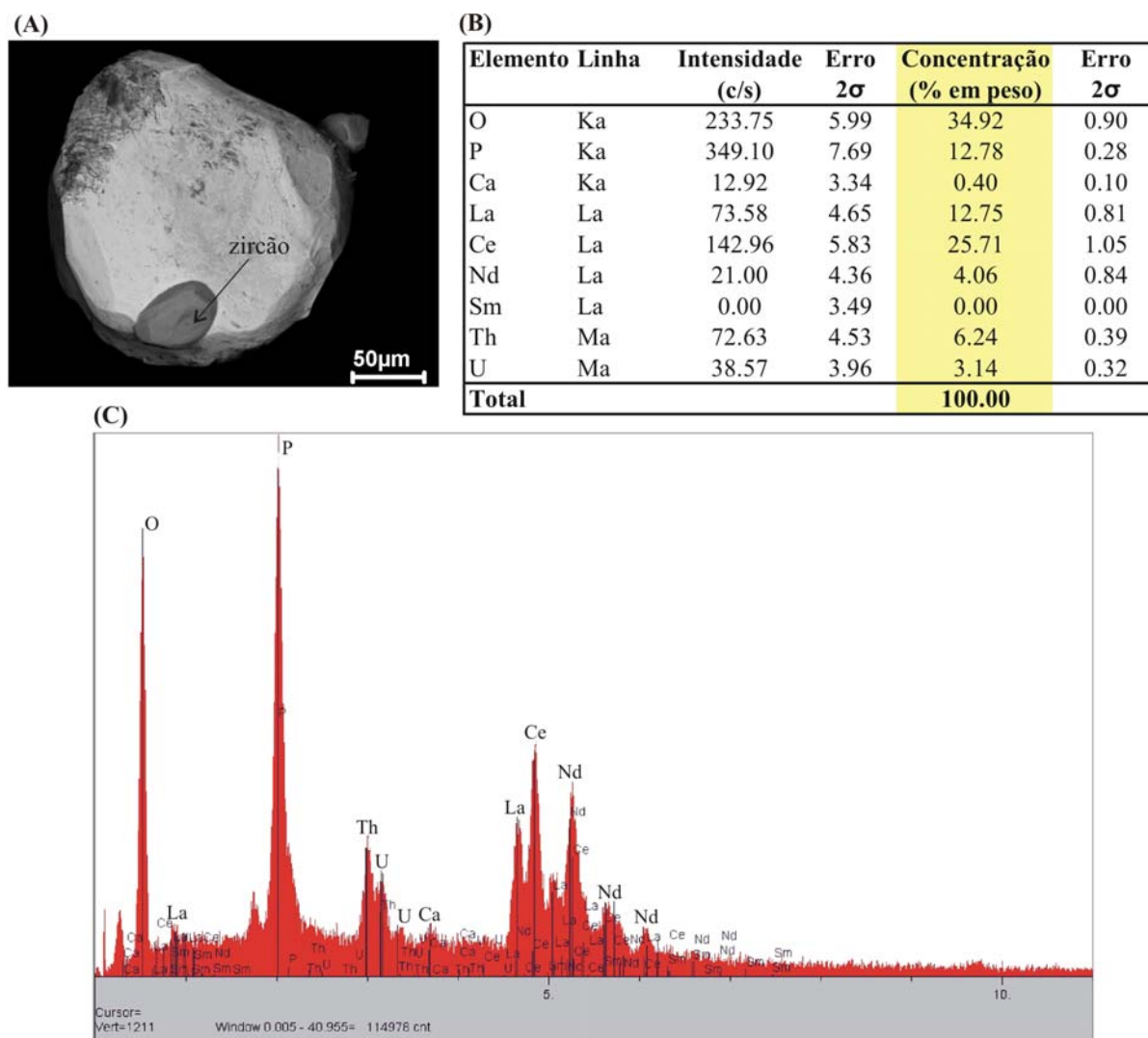


**Figura 5.2** - Síntese das informações obtidas na primeira fase analítica de cristais de monazita em microscópio eletrônico de varredura. **(A)** Imagem BSE, onde observa-se a “clareza” característica da monazita. Na imagem, os aspectos morfológicos e texturais do cristal podem ser avaliados, tratando-se neste exemplo de um grão arredondado, contendo cristal de zircão parcialmente incluso; **(B)** Tabela analítica resultante de análise EDS, que permite a caracterização da monazita como um fosfato de elementos terras raras leves, notadamente rico em Ce e La; **(C)** Difratoograma correspondente, mostrando padrão de distribuição dos picos típico da monazita, dentre os quais destacam-se os do P, O, Ce, La, Nd, Th e U.

## 5.5 – GEOCRONOLOGIA E GEOLOGIA ISOTÓPICA

Neste trabalho o estudo geocronológico/isotópico foi realizado segundo uma abordagem multimetodológica, direcionada ao entendimento das questões geológicas discutidas no capítulo anterior. O mapa da Figura 5.1 e Anexo I contêm a localização das amostras analisadas, assim como os métodos analíticos aplicados em cada uma delas.

### 5.5.1 – Evaporação de Pb em Monocristais de Zircão

Cristais de zircão provenientes de 17 amostras de rocha foram analisados de acordo com a metodologia proposta por Kober (1986, 1987), a qual permite a obtenção de idades a partir da razão  $^{207}\text{Pb}/^{206}\text{Pb}$ , corrigida para a presença do  $^{204}\text{Pb}$ , através de aquecimento de monocristais de zircão e medida diretamente no espectrômetro de massas, sem necessidade de separação química de Pb e U.

As análises foram realizadas em espectrômetro de massa modelo Finnigan MAT262, do Laboratório de Geologia Isotópica (Pará-Iso) do Centro de Geociências da UFPA. A adaptação da metodologia de Kober atualmente em rotina no referido laboratório, encontra-se detalhadamente descrita em Avelar (2002).

Uma das premissas fundamentais do método em questão é que, sendo a estrutura cristalina do zircão bastante resistente, este mineral pode preservar a assinatura isotópica da época de sua formação. No entanto, as idades obtidas através da razão  $^{207}\text{Pb}/^{206}\text{Pb}$  apenas representam verdadeiras idades de cristalização se o Pb analisado derivar de uma única fase do cristal de zircão, e se este não sofreu perda de Pb após sua cristalização. Como as razões Pb/U não são determinadas, a mais antiga idade  $^{207}\text{Pb}/^{206}\text{Pb}$  deve ser considerada apenas como uma idade mínima, entretanto, representará a idade de cristalização do zircão de uma rocha magmática quando repetidas medidas de  $^{207}\text{Pb}/^{206}\text{Pb}$  não variarem significativamente em vários cristais e em diferentes etapas de aquecimento em um grão (Kober et al. 1989; Ansdell & Kyser 1993; Karabinos & Gromet 1993; Kröner et al. 1999).

Eventos posteriores à cristalização do zircão, como metamorfismo e hidrotermalismo, podem provocar perda de Pb radiogênico (Kroner et al. 1994, Paquette et al. 1994), o que representa uma das maiores limitações do método em áreas com evolução polifásica. No entanto, devido às elevadas temperaturas de fechamento do sistema U-Th-Pb no zircão (Lee et al. 1997, Cherniack & Watson 2000), ele pode resistir isotopicamente fechado, mesmo durante eventos de alto grau metamórfico.

Portanto, este método foi utilizado com objetivo de estabelecer a cronologia dos eventos magmáticos que ocorreram no Arqueano e Paleoproterozóico, a partir da investigação da idade de cristalização de rochas ígneas ou dos protólitos ígneos de rochas metamórficas, em amostras representativas de unidades litoestratigráficas importantes e de domínios tectônicos distintos (vide Figura 6.2 e Apêndice 1 do Capítulo 6).

### 5.5.2 – Sm-Nd em Rocha Total

Análises isotópicas Sm-Nd foram realizadas em 32 amostras de rocha, no espectrômetro de massa Finnigan MAT 262 do Laboratório Pará-Iso. O método Sm-Nd foi inicialmente descrito por Lugmair (1974), sendo que as primeiras aplicações da metodologia para determinação isotópica do Nd em rochas ígneas devem-se a DePaolo & Wasserburg (1976 a, b) e Hamilton et al. (1977). Os procedimentos analíticos adotados por este laboratório para esta metodologia estão descritos em Moura (1992) e Avelar (2002).

A aplicação desta metodologia objetivou, sobretudo, o cálculo de idades modelo, que é feito a partir da regressão da razão  $^{143}\text{Nd}/^{144}\text{Nd}$  em função da razão  $^{147}\text{Nd}/^{144}\text{Nd}$ , até o intercepto desta regressão com a curva de evolução isotópica do Nd do manto superior em função do tempo geológico. O modelo de evolução isotópica adotado neste trabalho foi o denominado “manto empobrecido” (*Depleted Mantle*) de DePaolo (1981), o qual admite que o manto superior sofreu episódios sucessivos de diferenciação e fracionamento através da extração de magmas basálticos, tornando-se gradativamente mais empobrecido geoquimicamente e, conseqüentemente, aumentando a razão Sm/Nd, uma vez que o Nd é mais incompatível do que o Sm durante a fusão. Uma idade modelo representa o tempo desde que a razão  $^{143}\text{Nd}/^{144}\text{Nd}$  em uma rocha tinha composição similar à do DM, ou seja, a época em que a rocha diferenciou do manto. No entanto, a validade da idade modelo depende da premissa que a razão Sm/Nd não tenha sido modificada por processos intracrustais.

Também foi calculado o parâmetro petrogenético  $\epsilon_{\text{Nd}}$  para as amostras analisadas, que consiste basicamente na comparação da razão isotópica  $^{143}\text{Nd}/^{144}\text{Nd}$  de amostra analisada em relação à composição isotópica do reservatório condritico uniforme (CHUR) para o mesmo tempo. Segundo DePaolo (1988), se na época de formação da rocha o magma parental tiver uma razão isotópica mais elevada que a do CHUR, o valor de  $\epsilon_{\text{Nd}}$  será positivo, indicando que o mesmo originou-se a partir de uma fonte mantélica. Por outro lado, se uma rocha apresentar composição isotópica de Nd menor que a do CHUR, o valor de  $\epsilon_{\text{Nd}}$  será negativo, indicando fonte crustal para o magma parental.

As idades modelo podem ser interpretadas como idades de formação de crosta, mesmo em rochas que sofreram eventos de retrabalhamento crustal. No entanto, a interpretação de uma idade modelo pode ser complexa, especialmente se duas fontes (manto e crosta) participaram da formação de uma rocha e, neste caso, representa uma idade intermediária entre a época de

extração do manto e a idade da rocha recristalizada na crosta (modelo de mistura de fontes de Arndt & Goldstein 1987). Quando isto acontece, os valores de  $\epsilon_{Nd}$  flutuam entre valores positivos e negativos.

Este método foi empregado com objetivo de identificar os principais mecanismos de evolução crustal responsáveis pela estruturação atual dos domínios tectônicos, uma vez que de posse da idade modelo, do parâmetro  $\epsilon_{Nd}$  e da idade de cristalização de uma determinada rocha ou grupo de rochas, é possível avaliar se as mesmas são produto de acreção crustal juvenil ou de retrabalhamento de crosta mais antiga, ou ainda se são originárias de fontes mistas.

### 5.5.3 – U-Th-Pb em Monazitas

A base teórica para este método consiste na medida das concentrações de Th, U e Pb em cristais de monazita através de análises pontuais em microsonda eletrônica, e utilização diretamente no cálculo da idade ( $\tau$ ), através da solução da equação:

$$Pb = \frac{Th}{232} [\exp(\lambda^{232}\tau) - 1] 208 + \frac{U}{238.04} 0.09928$$

$$x [\exp(\lambda^{238}\tau) - 1] 206 + \frac{U}{238.04} 0.0072 \quad x [\exp(\lambda^{235}\tau) - 1] 207$$

Nesta equação, as concentrações de Pb, U, e Th estão em ppm, e  $\lambda^{232}$ ,  $\lambda^{235}$  e  $\lambda^{238}$  são as constantes de decaimento radioativo do  $^{232}Th$ ,  $^{235}U$  e  $^{238}U$ , respectivamente (Montel et al. 1996, Braun et al. 1998). É importante ressaltar que, neste trabalho, as idades calculadas e erros correspondentes seguiram o procedimento proposto por Cocherie & Albarede (2001) e Cocherie & Legendre (2006), cujas noções fundamentais são descritas no Capítulo 7.

O cálculo da idade por este método só é possível devido à monazita ser rica em Th e U (vide Figura 5.2), e o Pb radiogênico se acumular rapidamente, sendo que em menos de 100 Ma alcança um nível onde uma precisa medida pode ser realizada em microsonda eletrônica (Montel et al. 1996).

Portanto, em cada ponto de análise no cristal de monazita é obtida uma idade correspondente e, devido à alta resolução espacial da microsonda eletrônica, com feixe menor que 5  $\mu m$  de diâmetro, é possível obter um grande número de dados em um único cristal. Este procedimento, associado à observação de imagens BSE, permite relacionar as idades obtidas a

diferentes zonas do grão, e identificar se as mesmas são condizentes com uma única população de idades, sendo neste caso consistentes com um único evento geológico, ou se representam mais de uma população, portanto refletindo uma história geológica mais complexa.

No entanto, as idades calculadas por este método só terão significado geológico se: (1) o chumbo comum ( $^{204}\text{Pb}$ ) for negligenciável quando comparado à quantidade do Pb torogênico e uranogênico, (2) não houver perda de Pb radiogênico desde o fechamento do sistema, (3) não houver modificação das razões U/Th/Pb, exceto por decaimento radioativo, e (4) cada ponto analítico representar uma única idade (Montel et al. 1996, Cocherie et al. 2005).

Devido à elevada temperatura de bloqueio do sistema U-Th-Pb na monazita ( $\geq 700\text{ }^\circ\text{C}$ ), segundo Copeland et al. (1988), Parrish (1990), Suzuki et al. (1994), Bingen & Bremen (1998), Braun et al. (1998), Cherniack et al. (2002), Cocherie et al. (2005) e outros, e ao fato da difusão do Pb não ser significativa neste mineral (Parrish 1990), esta metodologia foi utilizada com objetivo de identificar a idade do metamorfismo granulítico e de eventos de migmatização que afetaram as rochas arqueanas que constituem a assembléia de embasamento do Domínio Jari. Para isso, foram analisados cristais de monazita provenientes de 7 amostras, incluindo gnaisses e leucossomas dos complexos Jari-Guaribas e Guianense. As análises foram realizadas com a microsonda eletrônica modelo CAMECA SX 50, em instalações laboratoriais do BRGM, Orléans, França.

#### 5.5.4 – $^{40}\text{Ar}$ - $^{39}\text{Ar}$ em Anfibólios e Biotitas

O método  $^{40}\text{Ar}$ - $^{39}\text{Ar}$  deriva diretamente do método  $^{40}\text{K}$ - $^{40}\text{Ar}$ , o qual mede a acumulação do elemento filho, o  $^{40}\text{Ar}$  radiogênico, a partir da desintegração natural do elemento pai, no caso o  $^{40}\text{K}$ , seguindo portanto a premissa fundamental dos demais métodos geocronológicos. No entanto, o método  $^{40}\text{Ar}$ - $^{39}\text{Ar}$ , cujos princípios foram estabelecidos por Merrihue (1965), Merrihue & Turner (1966) e Mitchell (1968), é baseado na formação de  $^{39}\text{Ar}$  por irradiação da amostra em reator nuclear, sob um fluxo de nêutrons suficientemente elevados, que induz a desintegração do  $^{39}\text{K}$ . Sabendo-se que a razão  $^{40}\text{K}/^{39}\text{K}$  representa uma proporção natural constante, a medida do  $^{39}\text{Ar}$  vai substituir a do  $^{40}\text{K}$  do método K-Ar convencional. A equação radiométrica final para o cálculo da idade baseia-se na razão  $^{40}\text{Ar}/^{39}\text{Ar}$  da amostra analisada e de um padrão com idade K-Ar conhecida (Monié 1984).

Foi utilizado o método *incremental heating technique*, no qual a extração do gás Ar é feita em etapas sucessivas de aquecimento, com cada etapa fornecendo uma idade independente. As medidas isotópicas foram realizadas no espectrômetro de massas modelo VG3600, em laboratório da Université de Montpellier 2, em Montpellier, França. Os procedimentos analíticos adotados por este laboratório estão descritos em Monié (1984) e Arnaud (1992).

Foram analisados hornblendas e/ou biotitas de 11 amostras provenientes de unidades estratigráficas representativas dos distintos domínios tectônicos (vide Figura 2 do Capítulo 8), tendo sido priorizadas amostras de complexos do embasamento no Domínio Jari, e de granitóides e gnaisses que representam o magmatismo plutônico cálcio-alcalino do Domínio Carecuru. Considerando-se que, as temperaturas de bloqueio do sistema K-Ar na hornblenda e biotita são estimadas em torno de 500-550°C e 300-350°C (Dodson 1973, Purdy & Jager 1976, Harrison 1981, Harrison et al. 1985, Baldwin et al. 1990, Dahl 1996), respectivamente, o método  $^{40}\text{Ar}$ - $^{39}\text{Ar}$  de datação foi empregado neste estudo com intuito primordial de entender a evolução termocronológica destes dois segmentos no Evento Transamazônico, e as possíveis diferenças com relação aos processos geodinâmicos que controlaram sua exumação e resfriamento termal.

## 6 – GEOCRONOLOGIA Pb-Pb POR EVAPORAÇÃO EM ZIRCÃO E GEOLOGIA ISOTÓPICA Sm-Nd EM ROCHA TOTAL

Neste capítulo, os dados obtidos pelos métodos de evaporação de Pb em zircão e Sm-Nd em rocha total serão apresentados e discutidos na forma de um artigo científico, aceito para publicação no periódico *Gondwana Research*, a ser editado em 2006. A abordagem principal deste artigo é a caracterização dos processos de evolução crustal que atuaram durante o arqueano e o paleoproterozóico nos domínios Jari, Carecuru e Paru, e a avaliação da extensão de crosta arqueana na região estudada.

### 6.1 – ZIRCON GEOCHRONOLOGY AND Sm-Nd ISOTOPIC STUDY: FURTHER CONSTRAINTS FOR THE ARCHEAN AND PALEOPROTEROZOIC GEODYNAMICAL EVOLUTION OF THE SOUTHEASTERN GUIANA SHIELD, NORTH OF AMAZONIAN CRATON, BRAZIL

Lúcia T. da Rosa-Costa<sup>a</sup>, Jean M. Lafon<sup>b</sup>, Claude Delor<sup>c</sup>

<sup>a</sup> CPRM – Geological Survey of Brazil, Belém,

<sup>b</sup> Pará-Iso Laboratory, Universidade Federal do Pará, Belém, Brazil

<sup>c</sup> BRGM, Orléans, France

#### Abstract

The northeastern part of the Guiana Shield, northern Amazonian Craton, in South America, represents a large orogenic belt developed during the Transamazonian orogenic cycle (2.26 – 1.95 Ga), which consists of extensive areas of Paleoproterozoic crust and two major Archean terranes: the Imataca Block, in Venezuela, and the here defined Amapá Block, in the north of Brazil.

Pb-evaporation on zircon and Sm-Nd on whole rock dating were provided on magmatic and metamorphic units from southwestern Amapá Block, in the Jari Domain, defining its long-lived evolution, marked by several stages of crustal accretion and crustal reworking. Magmatic activity occurred mainly at the Meso-Neoarchean transition (2.80-2.79 Ga) and during the Neoarchean (2.66-2.60 Ga). The main period of crust formation occurred during a protracted episode at the end of Paleoarchean and along the whole Mesoarchean (3.26-2.83 Ga). Conversely, crustal reworking processes have dominated in Neoarchean times. During the

Transamazonian event, the main geodynamic processes were related to reworking of older Archean crust, with minor juvenile accretion at about 2.3 Ga, during an early orogenic phase. Transamazonian magmatism consisted of syn- to late-orogenic granitic pulses, which were dated at 2.22 Ga, 2.18 Ga and 2.05-2.03 Ga. Most of the  $\epsilon_{Nd}$  values and  $T_{DM}$  model ages (2.52-2.45 Ga) indicate an origin of the Paleoproterozoic granites by mixing of juvenile Paleoproterozoic magmas with Archean components.

The Archean Amapá Block is limited in at southwest by the Carecuru Domain, a granitoid-greenstone terrane that had a geodynamic evolution mainly during the Paleoproterozoic, related to the Transamazonian event. In this latter domain, a widespread calc-alkaline magmatism occurred at 2.19-2.18 Ga and at 2.15-2.14 Ga, and granitic magmatism was dated at 2.10 Ga. Crustal accretion was recognized at about 2.28 Ga, in agreement with the predominantly Rhyacian crust-forming pattern of the Guiana Shield. Nevertheless,  $T_{DM}$  model ages (2.50-2.38 Ga), preferentially interpreted as mixed ages, and  $\epsilon_{Nd} < 0$ , point to some participation of Archean components in the source of the Paleoproterozoic rocks. In addition, the Carecuru Domain contains an oval-shaped Archean granulitic nucleus, named Paru Domain. In this domain, Neoproterozoic magmatism at about 2.60 Ga was produced by reworking of Mesoarchean crust, as registered in the Jari Domain. Crustal accretion events and calc-alkaline magmatism are recognized at 2.32 Ga and at 2.15 Ga, respectively, as well as charnockitic magmatism at 2.07 Ga.

The lithological association and the available isotopic data registered in the Carecuru Domain, suggests a geodynamic evolution model based on the development of a magmatic arc system during the Transamazonian orogenic cycle, which was accreted to the southwest border of the Archean Amapá Block.

**Key Words:** Archean, Paleoproterozoic, Transamazonian orogenesis, crustal evolution, Amazonian Craton

## 1 - Introduction

The Guiana Shield represents the northern segment of the Amazonian Craton, in South America, located on the northern edge of the Amazon Basin (Figure 1). With an area of nearly 1.5 million km<sup>2</sup>, it is one of the major Precambrian segments of the Western Gondwana. The eastern portion of the Guiana Shield consists of an exceptionally large Paleoproterozoic belt, exceeding 1200 km in length and 400 km in width, making it one of the largest Paleoproterozoic domains in the world. This belt extends from northern Brazil to eastern Venezuela, including French Guiana, Suriname and Guyana, and, in pre-Atlantic reconstructions, is correlated to the Eburnean domain in the West Africa Craton (Onstott and Hargraves, 1981; Onstott et al., 1984; Ledru et al., 1994; Zhao et al., 2002).

The geochronological pattern of this belt indicates that its evolution took place during the Transamazonian orogenic cycle (2.26 - 1.95 Ga), mainly in Rhyacian times (Gruau et al., 1985; Teixeira et al., 1989; Sato and Tassinari, 1997; Vanderhaeghe et al., 1998; Lafrance et al., 1999; Nogueira et al., 2000; Norcross et al., 2000; Tassinari et al., 2000; Voicu et al., 2000; Avelar, 2002; Avelar et al., 2003; Delor et al., 2003a,b; Roever et al., 2003). It consists mostly of gneissic-migmatitic-granulitic complexes, greenstone belts and granitoids, with variable chemical and structural features, defining several evolutionary episodes of juvenile crustal accretion, followed by crustal reworking. However, Archean remnants have been recognized, principally in eastern Venezuela (Montgomery and Hurley, 1978; Montgomery, 1979; Tassinari et al., 2001, 2004) and in some sectors of northwest Pará and centre-southwest Amapá states, in Brazil, (João and Marinho, 1982; Lima et al., 1982; Montalvão and Tassinari, 1984; Lafon et al., 1998; Ricci et al., 2002; Avelar et al., 2003; Rosa-Costa et al., 2003; Klein et al., 2003; Faraco et al., 2004).

The Transamazonian orogen corresponds to a remarkable geochronological province of the Amazonian Craton, named Maroni-Itacaiúnas (Cordani et al., 1979; Tassinari and Macambira, 2004) or Transamazonic (Santos et al., 2000), which was accreted to an Archean province unaffected by post-Archean orogens, the Central Amazonian or Carajás province (Figure 1 A and B).

Despite the difficulties of field access, due to dense rain forest and thick soil cover developed over the Precambrian substratum, the geological knowledge of this Paleoproterozoic belt has considerably been improved in recent years. Especially in French Guiana, where preserved Archean rocks are unknown, detailed mapping and geochronological program led to

the understanding of the geodynamic evolution of juvenile domains during Transamazonian orogenic cycle (Vanderhaeghe et al., 1998; Delor et al., 2003a,b).

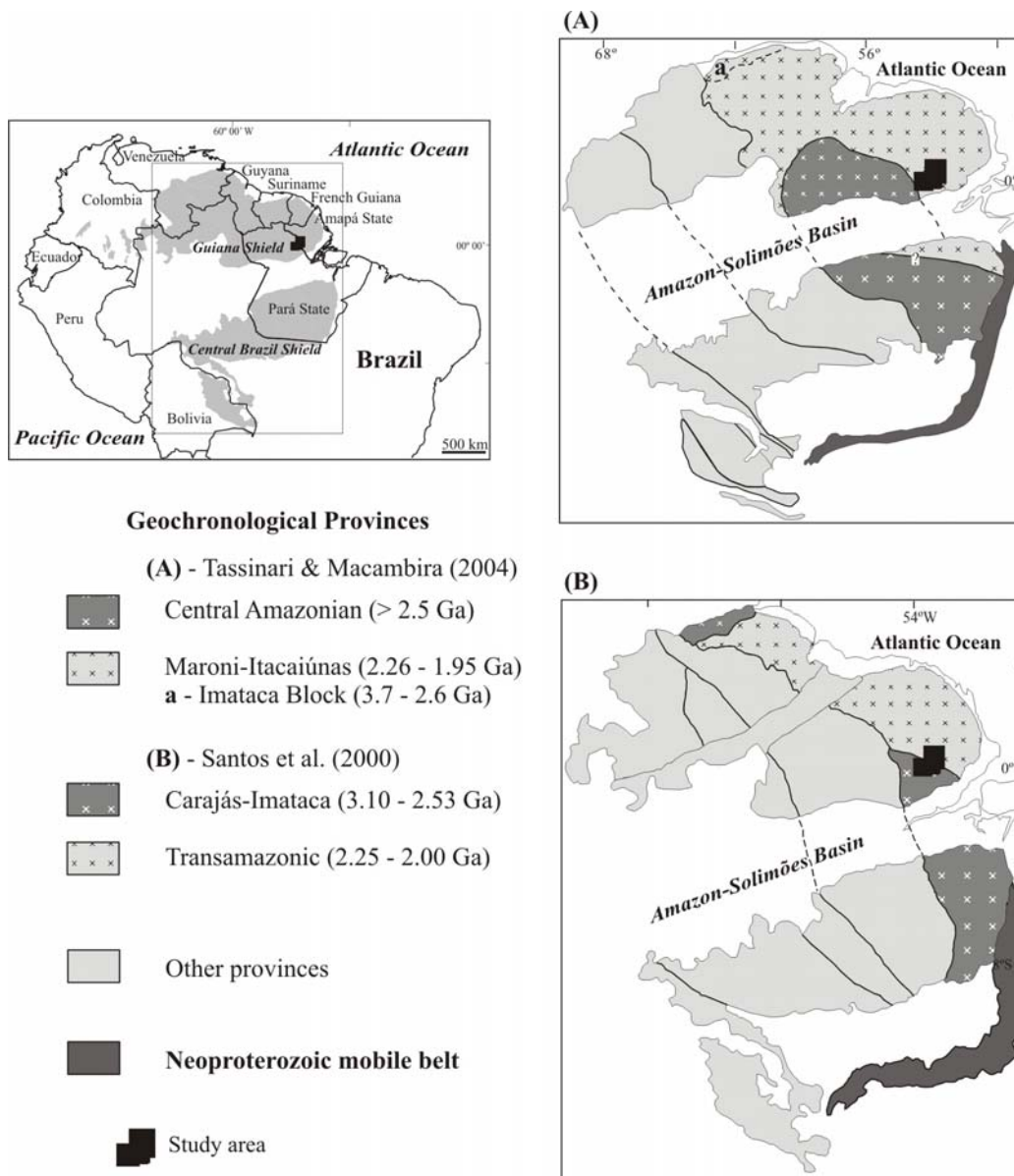


**Figure 1** – Location map and simplified sketch maps of the Amazonian Craton showing geochronological provinces according to proposals of (A) Tassinari and Macambira (2004) and (B) Santos et al. (2000).

However, concerning to more ensialic domains, even if Archean protoliths have been broadly recognized, as cited above, the nature, the geographical extension of the Archean segments and their relationships with Paleoproterozoic domains remain poorly understood. In addition, the occurrence of reworked Archean crust has promoted an extensive debate concerning to the location of the boundary between the Archean and Paleoproterozoic geochronological provinces of the eastern Amazonian Craton.

In NW Pará and SW Amapá states, geological mapping carried out by CPRM-Geological Survey of Brazil (see Carvalho et al., 2001 and Ricci et al., 2001), led to the recognition of juxtaposed geological domains, which present distinct lithological content, metamorphic history, geophysical and structural signatures (Ricci et al., 2001). Recent Pb-Pb and Sm-Nd dating indicated that these domains present, individually, dominating Archean or dominating Paleoproterozoic geochronological patterns (Pimentel et al., 2002; Ricci et al., 2002; Avelar et al., 2003; Rosa-Costa et al., 2003; Klein et al., 2003; Faraco et al., 2004).

This study is focused on the western portion of the area recently mapped by CPRM, where the Jari, Carecuru and Paru domains have been defined. An expressive group of single zircon Pb-evaporation ages and Sm-Nd  $T_{DM}$  model ages, acquired on igneous and metaigneous rocks from the different domains are presented, in order to identify the main crustal growth episodes and magmatic events in each domain and to discuss the main geodynamic processes responsible for the present-day configuration of the distinct domains, in the context of the major geochronological provinces of the Amazonian Craton.

## **2 - Precambrian Geological Setting and Previous Geochronology**

The tectonic models that have been proposed for the Amazonian Craton conceive the partitioning of this craton into large geochronological provinces that have distinctive ages, structural patterns and geodynamic evolution. In the current literature, two models prevail and are displayed in the Figure 1. The first one has been initially proposed by Cordani et al. (1979) and then refined by many authors (Teixeira et al., 1989; Sato and Tassinari, 1997; Tassinari and Macambira, 1999; Tassinari et al., 2000; Tassinari and Macambira, 2004), while the other was proposed by Santos et al. (2000).

The boundaries between provinces have been supported mainly by geochronological data. However, some of these limits are still under discussion, due to the lack of reliable geological and

geochronological information. Concerning to the northeastern portion of the craton, which coincides approximately with the eastern part of the Guiana Shield, the debate is focused on the extension of preserved or reworked Archean crust in the Paleoproterozoic domains.

According to the proposition of Tassinari and Macambira (2004), the eastern part of the Guiana Shield is included in the Maroni-Itacaiúnas Province, a widespread Paleoproterozoic belt accreted to an Archean block (the Central Amazonian Province) during the Transamazonian orogenic cycle. This province was defined as constituted of large areas of Paleoproterozoic crust, incorporating some remnants of an older Archean basement, such as the expressive allochthonous Imataca Block (3.7 – 2.6 Ga) in Venezuela (Montgomery and Hurley, 1978; Montgomery, 1979; Tassinari et al., 2001, 2004), or the restricted inliers that occur in Amapá state (Cupixi region - Montalvão and Tassinari, 1984; Sato and Tassinari, 1997 - and Tartarugalzinho region – João and Marinho, 1982; Lima et al., 1982; Lafon et al., 1998). The southern limit of the Maroni-Itacaiúnas Province with the Central Amazonian Province was positioned at the north of the Archean Carajás range, in Central Brazil Shield (Cordani et al., 1984).

The Transamazonian Province of Santos et al. (2000) roughly corresponds to the Maroni-Itacaiúnas Province. However, these authors excluded the Imataca Complex of the province and extended the Archean Carajás Province up to the southeastern most portion of Guiana Shield (Figure 1), incorporating the Archean inlier of the Cupixi region, in the Amapá state.

In French Guiana, a geodynamical model has been proposed by Vanderhaeghe et al. (1998), and refined by Delor et al. (2003a,b), to account for the Transamazonian evolution of juvenile sectors of the Paleoproterozoic belt. Vanderhaeghe et al. (1998) proposed a two-stage model, which follows the formation of an oceanic crust at 2.17 Ga. The first stage is related to crustal growth by magmatic accretion in a magmatic arc context, defined by calc-alkaline plutonism and greenstone belt formation between 2.14 and 2.11 Ga. The second stage is marked by crustal recycling and tectonic accretion, during oblique convergence between juvenile blocks, which was responsible for the formation of pull-apart basins and for the emplacement of high-K granites at 2.09-2.08 Ga.

According to Delor et al. (2003a), the earlier stage consists of the formation of juvenile oceanic crust between 2.26 and 2.20 Ga, followed by a stage of dominant TTG magmatism and development of greenstone belt sequences, between 2.18 and 2.13 Ga, in a scenario of island-arc, in response to a mainly southward-directed subduction. Granitic magmatism and migmatization

of earlier TTG-greenstone sequences occurred between 2.11 and 2.08 Ga due to the closure of island-arc basins. Formation of pull-apart basins is also associated to this stage. A further stage of oblique plate convergence, at 2.07-2.06 Ga, is marked by the production of metaluminous granites emplaced along strike-slip shear zones. These authors consider this stage synchronous with the metamorphic climax of the Ultra High Temperature (UHT) metamorphic event of the Bakhuis granulites, in Suriname (Delor et al., 2003b; Roever et al., 2003), which is also suspected in central and northern Amapá (Avelar et al., 2001; Lafon et al., 2001).

In face of the juvenile nature of the domains of the northeastern part of Guiana Shield, in recent years, Archean protoliths, dated between 3.3 and 2.6 Ga, have extensively been documented in its southeastern most portion (Pimentel et al., 2002; Ricci et al., 2002; Avelar et al., 2003; Klein et al., 2003; Rosa-Costa et al., 2003; Faraco et al., 2004). In this region, Archean records occur mainly between the border of Pará and Amapá states and the Tartarugal region (central of Amapá state), defining a more ensialic nature to this section of the Transamazonian orogen.

Field observations, together with map interpretations and petrographic studies, led Ricci et al. (2001) to propose a tectonic partitioning of the NW Pará and SW Amapá region into tectonic domains, bounded by first-order strike-slip shear zones, named from northeast to southwest, Cupixi-Tartarugal Grande Ancient Terrane, Jari Belt and Carecuru-Paru Orogen (Figure 2). These authors recognized that each domain has distinct lithological content, metamorphic history, geophysical and structural signatures, representing tectonostratigraphic terranes, sensu Howell (1995).

Rosa-Costa et al. (2003) renamed these terranes simply as “domains” and presented a new set of single zircon Pb-evaporation ages, which combined with previous published data (Montalvão and Tassinari, 1984; Sato and Tassinari, 1997; Pimentel et al., 2002; Ricci et al., 2002; Avelar et al., 2003), indicate a dominant Archean age pattern for the Cupixi and Jari domains, whereas the Carecuru Domain presents a dominant Paleoproterozoic age pattern. The latter includes an oval-shaped domain, named Paru, which also contains Archean rocks.

This study is focused on the Jari, Carecuru and Paru domains, corresponding to the centre-southwest portion of the area studied by Ricci et al. (2001). The main lithological units of these domains can be observed in the Figure 2, as well as the available geochronological records.

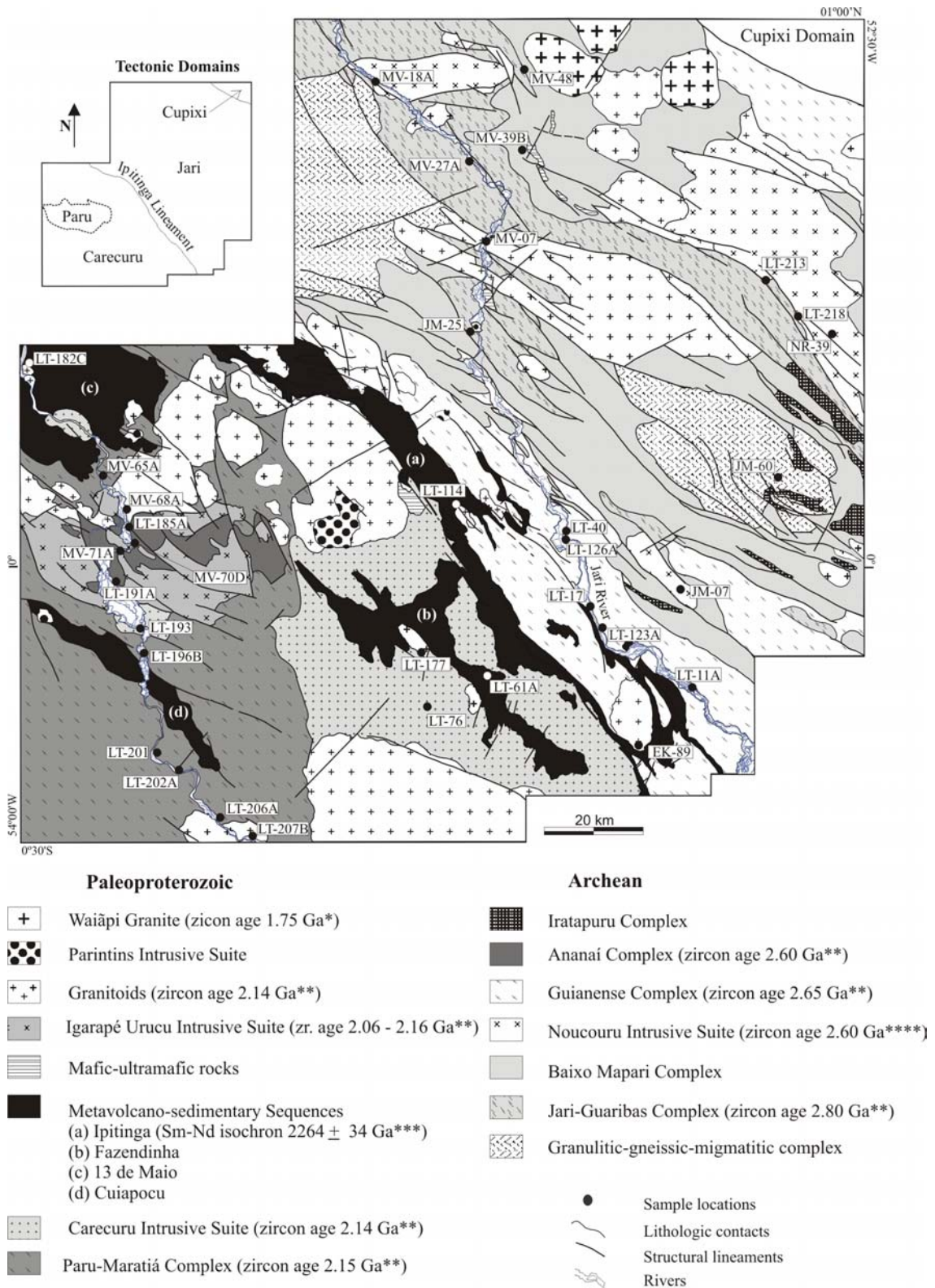


**Figure 2-** Geological map of the study area, showing the sites of the samples dated in this work. Geological map, stratigraphic arrange and tectonic subdivision (sketch on top-left) are based on Carvalho et al. (2001) and Ricci et al. (2001). Previous geochronological data compiled from: Vasquez and Lafon (2001)\*, Rosa-Costa et al. (2003)\*\*, McReath and Faraco (1997)\*\*\* and Ricci et al. (2002)\*\*\*\*.

The Jari Domain is a linear range, approximately 100 km wide, extending over the eastern boundary of the investigated area, interposed between the Cupixi and Carecuru domains. The Jari Domain is characterized by a conspicuous NW-SE ductile structuring, constituted mainly of high-grade rocks that are represented by the granulitic orthogneisses of the Jari-Guaribas Complex (enderbitic and charnockitic banded gneisses, with layers or enclaves of massive to foliated mafic granulites), mesoperthite and/or clinopyroxene-bearing granitic orthogneisses of the amphibolite-granulite transition facies included in the Baixo Mapari Complex, and catazonal granites grouped in the Noucouro Intrusive Suite (charnockites, enderbites and mesoperthite-bearing granites). Minor high-grade metasedimentary rocks occur as narrow belts, surrounded by orthogneisses, defining the Iratapuru Complex (aluminous gneisses and schists). Amphibolite-facies grey gneisses (mainly tonalitic and granodioritic gneisses) of the Guianense Complex are also included in the basement of the Jari Domain. High- to medium-grade gneisses that can not be inserted in specific stratigraphic units, complement the basement assemblage of the Jari Domain, and are informally referred to as granulitic-gneissic-migmatitic complex. All the metamorphic complexes are heterogeneously affected by migmatization and locally retrograded to amphibolite and greenschist facies metamorphism.

Neoproterozoic Pb-Pb zircon ages were obtained on enderbite gneiss of the Jari-Guaribas Complex and on granodioritic gneiss of the Guianense Complex (respectively  $2797 \pm 3$  Ma and  $2652 \pm 4$  Ma, Rosa-Costa et al., 2003) and on igneous charnoenderbite of the Noucouro Intrusive Suite ( $2605 \pm 6$  Ma - Ricci et al., 2002). In addition, a tonalitic gneiss of the Guianense Complex, yielded a Paleoproterozoic Pb-Pb zircon age ( $3321 \pm 11$  Ma - Klein et al., 2003).

The Carecuru Domain represents a Paleoproterozoic granitoid-greenstone domain. The plutonic assemblage is constituted mainly of diorites and tonalites, with minor granodiorites, composing a lithological association consistent to the calc-alkaline series (e.g. Lameyre and Bowden, 1982; Barbarin, 1999). These rocks are heterogeneously deformed, showing strongly penetrative foliation to preserved igneous texture, and are included in the Paru-Maratiá Complex, dated at  $2150 \pm 1$  Ma, and in the Carecuru Intrusive Suite, dated at  $2140 \pm 1$  Ma (Rosa-Costa et al., 2003). Concerning to the supracrustal sequences, the most expressive is the Ipitanga Group, which marks the boundary between the Jari and Carecuru domains. This group is composed of mafic-ultramafic metavolcanic schists, BIFs, metasedimentary schists and quartzites, metamorphosed under greenschist and amphibolite facies. Sm-Nd isochronic age date this

sequence at about  $2264 \pm 34$  Ma (McReath and Faraco, 1997). Minor undated supracrustal sequences (Fazendinha, 13 de Maio and Cuiapocu sequences), composed principally of mafic- to intermediated metavolcanics, occur as discontinuous strips, overlaying the plutonic units.

The Paru Domain represents an inlier within the Carecuru Domain, composed mainly of Neoproterozoic ( $2597 \pm 4$  Ma - Rosa-Costa et al, 2003) granulitic orthogneisses of the Ananaí Complex (enderbitic and charnoenderbitic gneisses, with minor mafic granulites) and Paleoproterozoic (2.16 - 2.06 Ga) intrusive charnockites and mesoperthite-granites, grouped in the Igarapé Urucu Intrusive Suite.

Plutons of granitoids with variable compositional and structural characteristics are widespread in all domains. They cross-cut metamorphic complexes or supracrustal sequences and represent different magmatic episodes of the Transamazonian Orogenic Cycle. The Parintins Intrusive Suite groups the late- to post-orogenic granitoids, composed mainly of granites and granodiorites, massive or weakly deformed. Moreover, several plutons, composed mainly by leucogranites, with minor granodiorites and tonalites are widespread. Due to the lack of conclusive geological information, they are informally referred as Granitoids. Preliminary Pb-Pb zircon dating of these plutons, registered a magmatic pulse at  $2146 \pm 3$  Ma in the Jari Domain (Rosa-Costa et al., 2003).

Post Transamazonian rocks are scarce in the investigated area, being restricted to three roughly circular plutons of A-type granites, referred as Waiãpi Granite, dated at  $1753 \pm 3$  Ma (Vasquez and Lafon, 2001).

### **3 - Geochronological Study**

#### *3.1 - Sampling and Experimental Procedure*

Geochronological investigations were carried out on gneisses, granitoids and metavolcanic rocks, which represent the key lithologic units of the Jari, Carecuru and Paru domains. The samples selected for the geochronological study were taken away from veins, migmatitic segregation and lithologic contacts, in order to avoid contamination. The sample locations are shown in the Figure 2. The geographic coordinates and brief sample descriptions are presented in the Appendix 1.

The geochronological study was based on zircon Pb-evaporation (Kober, 1986 and 1987) and whole rock Sm-Nd methods. All the isotopic analyses were carried out with a Finnigan

MAT262 mass spectrometer at the Laboratório de Geologia Isotópica (Pará-Iso) of the Universidade Federal do Pará (UFPA), Belém, Brazil. Sample preparation was done at laboratories of CPRM - Geological Survey of Brazil and UFPA.

Zircon crystals were dated using double Re filaments, and the isotopic data were acquired in the dynamic mode, using an ion-counting system. The Pb isotope compositions were determined through repeated analyses of several zircon grains from the sample, at increasing evaporation temperature steps. The  $^{207}\text{Pb}/^{206}\text{Pb}$  ratios were corrected from mass discrimination using a factor of  $0.12\% \pm 0.03$  per u.m.a., determined by repeated analyses of the NBS-982 “equal atoms” Pb standard. The calculation of common lead correction was done using the Pb composition of the Stacey and Kramers (1975) model, at the age of the grain. Analyses with  $^{206}\text{Pb}/^{204}\text{Pb}$  ratios lower than 2500 were eliminated to minimize the effects of common lead correction on the radiogenic isotopic ratios and they are not shown in the tables of data.

The Pb evaporation method usually provides very precise measurements of the  $^{207}\text{Pb}/^{206}\text{Pb}$  ratio, which enable the determination of a precise weighted average value for the age ( $\pm 1-5$  Ma) on a small number of grains. As Pb/U ratios are not determined, the oldest  $^{207}\text{Pb}/^{206}\text{Pb}$  age is a minimum age. However, the assumption that this age can represent a “concordant” crystallization age of zircon from magmatic rocks is strongly supported when repeated measurements of  $^{207}\text{Pb}/^{206}\text{Pb}$  do not vary significantly in several crystals and at different temperature steps in one grain (Kober et al., 1989; Ansdell and Kyser, 1993; Karabinos and Gromet, 1993; Kröner et al., 1999).

The age of each sample is calculated using the mean value of the  $^{207}\text{Pb}/^{206}\text{Pb}$  ratios at the highest temperature steps. When different temperature steps of the same grain furnish similar ages, all of them are included in the mean age calculation of this grain. Consequently, the confidence of the result depends on the number of grains with similar ages and, at least three grains with similar ages are necessary to define a crystallization age. Grains furnishing ages significantly lower are suspected to have suffered lead loss after crystallization and are arbitrarily discarded. In the same way, grains yielding isolated older ages are considered as inherited and, consequently, are also arbitrarily discarded. The weighted mean and the  $2\sigma$  errors on the age of the remaining zircon population were calculated following Gaudette et al. (1998). An age calculation using the Ludwig’s 2000 Isoplot program would furnish statistically indistinguishable

results as discussed in Delor et al. (2003a). Pb-evaporation age diagrams were drawn using the Isoplot program (Ludwig, 2004).

The chemical procedures for sample dissolution and Sm and Nd extraction have previously been described in Klein et al. (2005). The rock powders (~100 mg) were dissolved with a mixture of HF + HNO<sub>3</sub> in Teflon vessels at 220 °C. REE were separated from the other elements by cation exchange chromatography using a Biorad Dowex 50x8 resin in HCl and HNO<sub>3</sub> media. Then, Sm and Nd were separated from the REE by anion exchange chromatography on Biorad Dowex AG1x4 in HNO<sub>3</sub> – Methanol medium. A mixed <sup>150</sup>Nd - <sup>149</sup>Sm spike was introduced for determination of Sm and Nd concentrations. The isotopic measurements of Sm and Nd were performed in multi-collection static mode, using a Ta-Re double filament. The mean <sup>143</sup>Nd/<sup>144</sup>Nd value obtained during the study on repeated analyses of the La Jolla Standard was 0.511834 ± 18 (2σ) and the Nd data were normalized to a <sup>143</sup>Nd/<sup>144</sup>Nd ratio of 0.7219. The total blanks do not exceed 0.24 ng for Sm and 0.61 ng for Nd. Nd model ages for all the samples were calculated using the DePaolo (1981) model for a depleted mantle evolution (T<sub>DM</sub>), excluding those with <sup>147</sup>Sm/<sup>144</sup>Nd outside the range of 0.088-0.125, since a “single stage” Sm/Nd evolution is doubtful for the Sm/Nd system of these samples.

### 3.2 - Isotopic Results and Discussion

#### 3.2.1 - Zircon Ages – Constraining the magmatic events

Zircon populations from 16 rock samples have been investigated. The results are shown in Table 1, and organized according to their original domain and stratigraphic unit they belong to. Pb-evaporation diagrams of the dated samples are shown in the figures 3 and 4.

#### Jari Domain

Two samples of enderbite gneisses (JM-60 and MV-27A) from the Jari-Guaribas Complex were investigated in order to determine the age of the igneous precursor of the granulites. In sample JM-60, two distinct zircon populations were individualized: one defined by elongated and sub-euhedral grains and the other by rounded crystals. Nevertheless, both populations exhibit contrasted fine zoning, as classically observed in magmatic zircons. The isotopic data were collected on 15 zircons, which yielded ages ranging from 2760 to 3245 Ma. Due to the wide spread of the data (485 Ma), two ages were calculated separately. Three zircon

crystals with the oldest ages furnished a poorly constrained ( $USD = 3.5$ ) mean value of  $3238 \pm 6$  Ma, whereas an age of  $2788 \pm 2$  Ma ( $USD = 1.5$ ) was calculated with the other five grains. No relationships between shape and age of the grains have been observed.

These data permit two distinct interpretations: the age of 3.24 Ga represents the age of the igneous protolith and the age of 2.79 Ga indicates the time of the high-grade metamorphic event. Alternatively, both ages can be assumed as igneous ages, but the oldest being provided by inherited grains. The second hypothesis should be more acceptable since, in both zircon populations some crystals gave the same age at different steps of heating (e.g. grains JM60/03, JM60/06 and JM60/11), indicating that the zircon crystals registered individually a single geological event. In addition, strong variations of the  $^{208}\text{Pb}/^{206}\text{Pb}$  ratios compared to the  $^{207}\text{Pb}/^{206}\text{Pb}$  ratios of these grains are observed, which may be interpreted to reflect Th/U zonation during magmatic growth (Klotzli, 1999). Then, the age of  $2788 \pm 2$  Ma is interpreted as the age of the igneous precursor of the granulite and the age of  $3238 \pm 6$  Ma is considered as inherited from an oldest magmatic event. Furthermore, new geochronological data furnished by metamorphic zircon and monazite from granulites of the Jari-Guaribas Complex, dated the high-grade metamorphic event at about 2.1 Ga (Rosa-Costa et al., submitted), reinforcing our last interpretation.

The zircons from the enderbitic gneiss (MV-27A) are sub-euhedral, with external parts showing magmatic zoning. The 8 grains provided ages between  $2646 \pm 6$  Ma and  $2795 \pm 4$  Ma at the higher steps of temperature. A mean age of  $2790 \pm 8$  Ma ( $USD = 2.3$ ) was calculated from 3 grains, which is similar to the previous sample, even if it is not as well defined as that, and it is alike interpreted as the crystallization age of the protolith of the granulite. The younger and variable ages given by the other 5 grains are assumed to represent perturbations of the U-Pb system in these zircons, induced by younger, probably Transamazonian related geological events.

These new geochronological data obtained for rocks from the Jari-Guaribas Complex reinforce the existence of two distinct magmatic events in the Jari Domain, occurred during the Paleoproterozoic ( $\approx 3.24$  Ga) and at the Meso-Neoproterozoic transition ( $\approx 2.79 - 2.80$  Ga), which have already been identified at  $3321 \pm 11$  Ma and  $2797 \pm 3$  Ma by Klein et al. (2003) and Rosa-Costa et al. (2003), respectively.

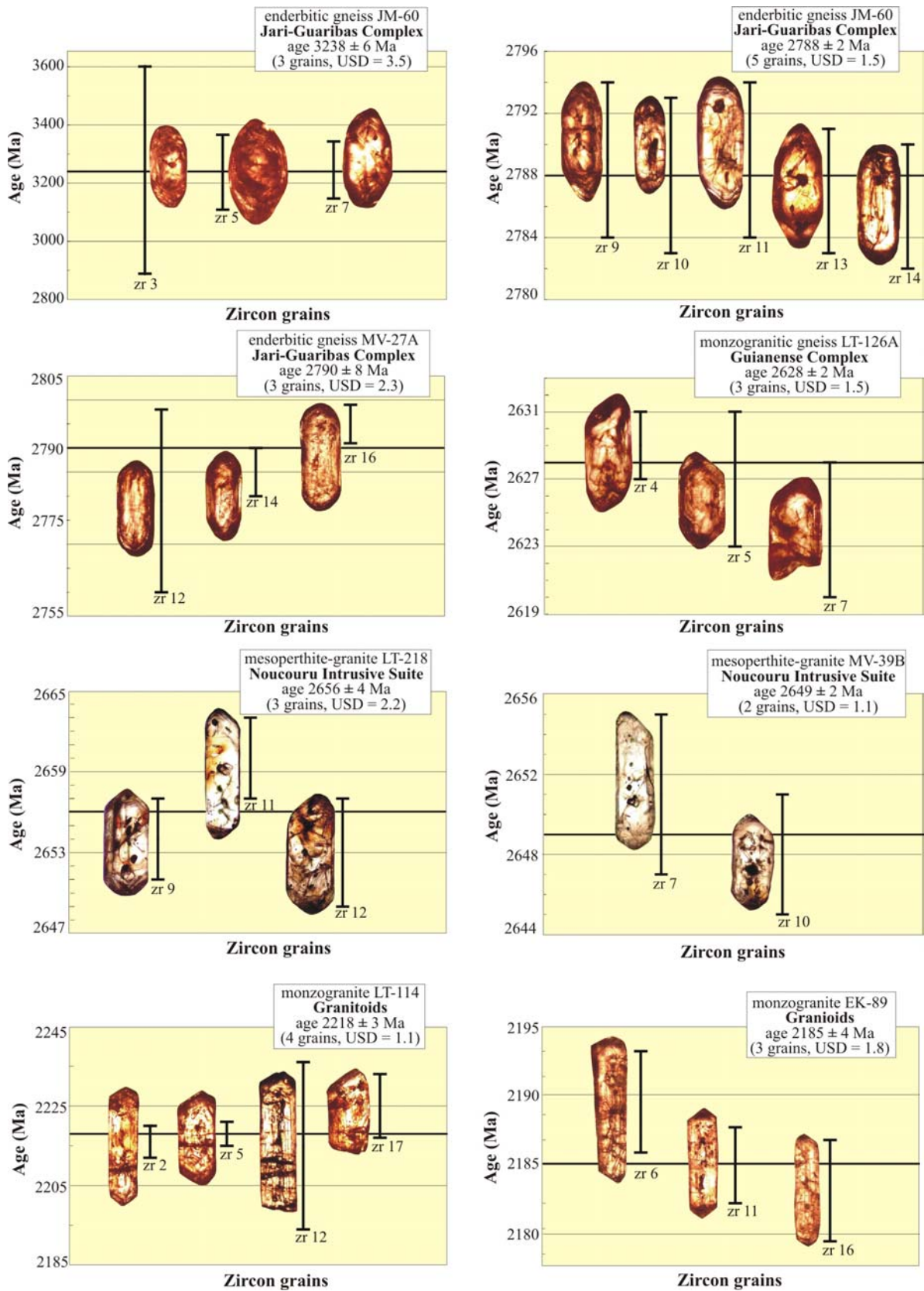


**Figure 3** – Pb-evaporation diagrams for the dated samples from the Jari Domain. The error bars correspond to the mean age value for each zircon grain.

A monzogranitic gneiss (sample LT-126A) of the Guianense Complex was analyzed and the dated zircons are euhedral to sub-euhedral, with visible magmatic zoning in their external parts. Seven zircon crystals yielded ages between  $2613 \pm 2$  Ma and  $2629 \pm 2$  Ma at temperature steps of 1500 °C and 1550 °C. The three oldest crystals provided a mean value of  $2628 \pm 2$  Ma (USD = 1.5), which is interpreted as giving the igneous age of the protolith. This age, added to the age of  $2652 \pm 4$  Ma previously obtained on a tonalitic gneiss from the same metamorphic complex (Rosa-Costa et al., 2003), confirms the existence of a Neoproterozoic magmatic event, at about 2.63-2.65 Ga, which is at about 150 Ma younger than the one identified in rocks from the Jari-Guaribas Complex.

Three different plutons of the Noucouuru Intrusive Suite were investigated, with the goal of dating the catazonal magmatic event that characterizes this suite. The dated samples consist of mesoperthite-granites (samples LT-218 and NR-39) and of a true charnockite (sample MV-18A). Zircons from the three distinct samples show similar textural characteristics. They are sub-euhedral crystals, exhibiting magmatic zoning and containing several mineral inclusions (rounded and acicular) in their inner parts.

In the sample LT-218, 8 zircon grains furnished ages ranging between  $2618 \pm 3$  Ma and  $2660 \pm 3$  Ma. Three crystals yielded a mean age of  $2656 \pm 4$  Ma (USD = 2.2). This age, even poorly constrained, can be considered as a good indication of the time of the catazonal magmatic event, occurred at about 2.66 Ma. Concerning to the sample NR-39, eight grains gave ages varying between  $2611 \pm 2$  Ma and  $2651 \pm 4$  Ma, and the two oldest grains furnished a mean age of  $2649 \pm 2$  Ma, considered as a minimum age. In the sample MV-18A, 8 grains yielded ages ranging from  $2522 \pm 3$  Ma to  $2625 \pm 4$  Ma at the highest steps of heating. As no reproducible ages were obtained, a mean age could not be calculated, and the oldest age of  $2625 \pm 4$  Ma is assumed as the minimum age for the crystallization of the rock.

This new set of ages, obtained from rocks of the Noucouuru Intrusive Suite, is significantly older than the age of  $2605 \pm 6$  Ma furnished by a garnet-bearing enderbite of that suite, which was collected from a pluton located in the southern part of the Jari Domain (Ricci et al., 2002). The geochronological data suggest a protracted period, of about 50 Ma, for the catazonal magmatism or, alternatively, this magmatism has occurred in distinct pulses during Neoproterozoic times.

In order to provide geochronological constraints for the widespread granitic magmatism registered in the Jari Domain, zircon populations from four distinct plutons were analyzed (samples LT-114, EK-89, JM-25 and LT-17). The studied plutons show distinct mineralogical composition, mode of occurrence and intensity of deformation (see Appendix 1).

Samples LT-114 and EK-89 were collected from two monzogranitic plutons located close to the boundary zone between the Jari and Carecuru domains. The former comes from a pluton that was strongly affected by the deformation imparted by the Ipitinga Lineament and that intruded the metavolcano-sedimentary rocks of the Paleoproterozoic Ipitinga Group. The latter is intrusive into the Neoproterozoic gneisses of the Guianense Complex as well as into metavolcano-sedimentary rocks correlated to the Ipitinga Group.

In both samples the zircon grains are euhedral, with well-developed pyramidal faces, and most of them are metamictic, showing transversal cracks and mineral inclusions. Several grains furnished high level of common lead ( $^{206}\text{Pb}/^{204}\text{Pb} < 2500$ ). Seventeen grains were analyzed from sample LT-114, and nine crystals yielded ages between  $2174 \pm 22$  Ma and  $2225 \pm 8$  Ma. A mean age of  $2218 \pm 3$  Ma (USD = 1.1) was calculated with the 4 oldest grains, and considered as being the age of crystallization of the granite.

For the sample EK-89, 16 grains were analyzed and only 6 crystals provided useful isotopic results. Among these, five crystals gave ages between  $2120 \pm 7$  Ma and  $2189 \pm 4$  Ma. A mean age of  $2185 \pm 4$  Ma (USD = 1.8) was calculated based on the 3 oldest grains, interpreted as the crystallization age. One grain yielded an age of  $2592 \pm 2$  Ma, attributed to inheritance from Archean source rocks.

The ages of  $2218 \pm 3$  Ma and  $2185 \pm 4$  Ma indicated the existence of eo-Transamazonian granitic magmatism events, not yet identified in other segments of the eastern Guiana Shield. For instance, in French Guiana, the period between 2.22 and 2.13 Ga is marked by tholeiitic and calc-alkaline magmatic events, related, respectively, to stages of oceanization and magmatic arc building (Delor et al., 2003a).

The sample JM-25 came from a small monzogranitic pluton of the Parintins Intrusive Suite. The zircon grains are euhedral, with pyramidal faces, showing magmatic zoning and several mineral inclusions. A narrow range of values was provided by 6 crystals, with ages between  $2042 \pm 3$  Ma and  $2053 \pm 4$  Ma. A mean age of  $2049 \pm 3$  Ma was calculated with 5 crystals, interpreted as the time of crystallization of the granite. However, 2 grains gave older

ages of  $2140 \pm 8$  Ma and  $2208 \pm 6$  Ma, and were considered as inherited crystals from reworked eo-Transamazonian source rocks.

The sample LT-17 was collected from a strongly mylonitized two-mica granite, emplaced along a NW-SE strike-slip zone that affects rocks of the Ipitinga Group and Guianense Complex. The zircon grains are clear, euhedral to sub-euhedral and some of them show few fractures and mineral inclusions in the inner parts. For this sample, six zircon grains furnished isotopic results only at the highest temperature steps. The ages vary from  $2027 \pm 5$  to  $2040 \pm 10$  Ma, producing a mean value of  $2030 \pm 2$  Ma (USD = 1.3), interpreted as the age of the granite.

The ages of  $2049 \pm 3$  Ma and  $2030 \pm 2$  Ma furnished by the samples JM-25 and LT-17 date the youngest magmatic events in the Jari Domain and are related to late stages of evolution of the Transamazonian orogenic cycle.

#### Carecuru Domain

Zircon populations from 4 samples of gneisses and granitoids of the Carecuru Domain have been dated and only Paleoproterozoic ages were obtained, confirming the previous assumption of Rosa-Costa et al. (2003), which admitted a dominant Paleoproterozoic age pattern for this domain.

Two samples, one from the Paru-Maratiá Complex (MV-65A) and the other from the Carecuru Intrusive Suite (LT-193), were dated in order to better constrain the age of the calc-alkaline magmatism in the Carecuru Domain. The zircons from the granodioritic gneiss MV-65A are euhedral with pyramidal faces or sub-euhedral with rounded terminations, and some of them exhibit magmatic zoning. Nine zircon grains furnished isotopic results, and 8 crystals yielded Paleoproterozoic ages between  $2191 \pm 6$  and  $2063 \pm 5$  Ma. The youngest ages were not considered for the age calculation. The three oldest grains provided a mean value of  $2191 \pm 2$  Ma (USD = 0.2), interpreted as the crystallization age of the igneous protolith. One grain gave an age of  $2784 \pm 6$  Ma, interpreted as inheritance, indicating contamination with Archean rocks in the source of the Paleoproterozoic magma.

The zircon grains from the diorite LT-193 are clear, sub-euhedral, containing rare mineral inclusions and fractures. They exhibit contrasted fine zoning, as frequently observed in magmatic zircons. Seven among 8 analyzed zircon grains yielded isotopic results, showing similar ages between the grains and, in some grains, between the heating steps. A mean age at  $2139 \pm 2$  Ma

(USD = 1.5) was calculated, considered as the crystallization age, which is in good agreement with the age of  $2140 \pm 1$  Ma, previously obtained on a diorite of the same suite (Rosa-Costa et al., 2003). No Archean component has been found in this sample.

These new data extend the time span for the calc-alkaline magmatism in the Carecuru Domain. Previous results furnished ages of 2.15 Ga and 2.14 Ga for this magmatism (Rosa-Costa et al., 2003). According to the geochronological results, the time between 2.19 and 2.14 Ga could represent a protracted period of calc-alkaline magmatism or, alternatively, two distinct pulses, occurring at about 2.19 Ga and at 2.15-2.14 Ga, the latter being the preferred interpretation. Anyway, the results are in good agreement with the two phases of calc-alkaline magmatism at 2.18-2.16 Ga and at 2.15-2.13 Ga, related to a magmatic arc context, characterized in French Guiana (Delor et al., 2003a).

As in the Jari Domain, several plutons of granitoids were characterized in the Carecuru Domain, which are constituted mainly of monzogranites and syenogranites, and display distinct structural characteristics, varying from weakly deformed to mylonitic.

Two granitic plutons (samples LT-177, LT-207B) were dated, in order to compare the granitic magmatism chronology between the different domains during the Transamazonian orogenic cycle. The sample LT-177 corresponds to a weakly deformed monzogranite, while sample LT-207B consists of a mylonitic syenogranite. Zircon grains from the sample LT-177 are euhedral, with well-developed pyramidal faces, exhibiting magmatic zoning and transversal fractures, being frequently broken. Zircon crystals from the granite LT-207B are sub-euhedral, often fractured and metamictic, although some of them are clear, with visible magmatic zoning. In both samples, 16 crystals were selected for analysis but, due to the metamictic nature of most of them, only 6 and 4 grains, respectively, furnished  $^{206}\text{Pb}/^{204}\text{Pb}$  ratio  $> 2500$ .

Two diachronous granitic pulses were revealed by the dated samples. The zircon crystals of the monzogranite LT-177 provided values between  $2157 \pm 17$  Ma and  $2179 \pm 3$  Ma. A mean age of  $2177 \pm 3$  Ma (USD = 1.5) was calculated with the 5 oldest grains, and interpreted as the crystallization age. This monzogranite is slightly younger than the calc-alkaline magmatic pulse dated at about 2.19 Ga, suggesting that it can represent more evolved rocks from the calc-alkaline series.

The 4 grains from the sample LT-207B yielded ages ranging from  $2081 \pm 5$  to  $2099 \pm 2$  Ma. A mean age of  $2098 \pm 2$  Ma was calculated with only 2 zircons, which is considered as the

minimum age of crystallization. In French Guiana this period also corresponds to a phase of granitic magmatism, with emplacement of plutons along shear zones, during a stage of oblique plate convergence.

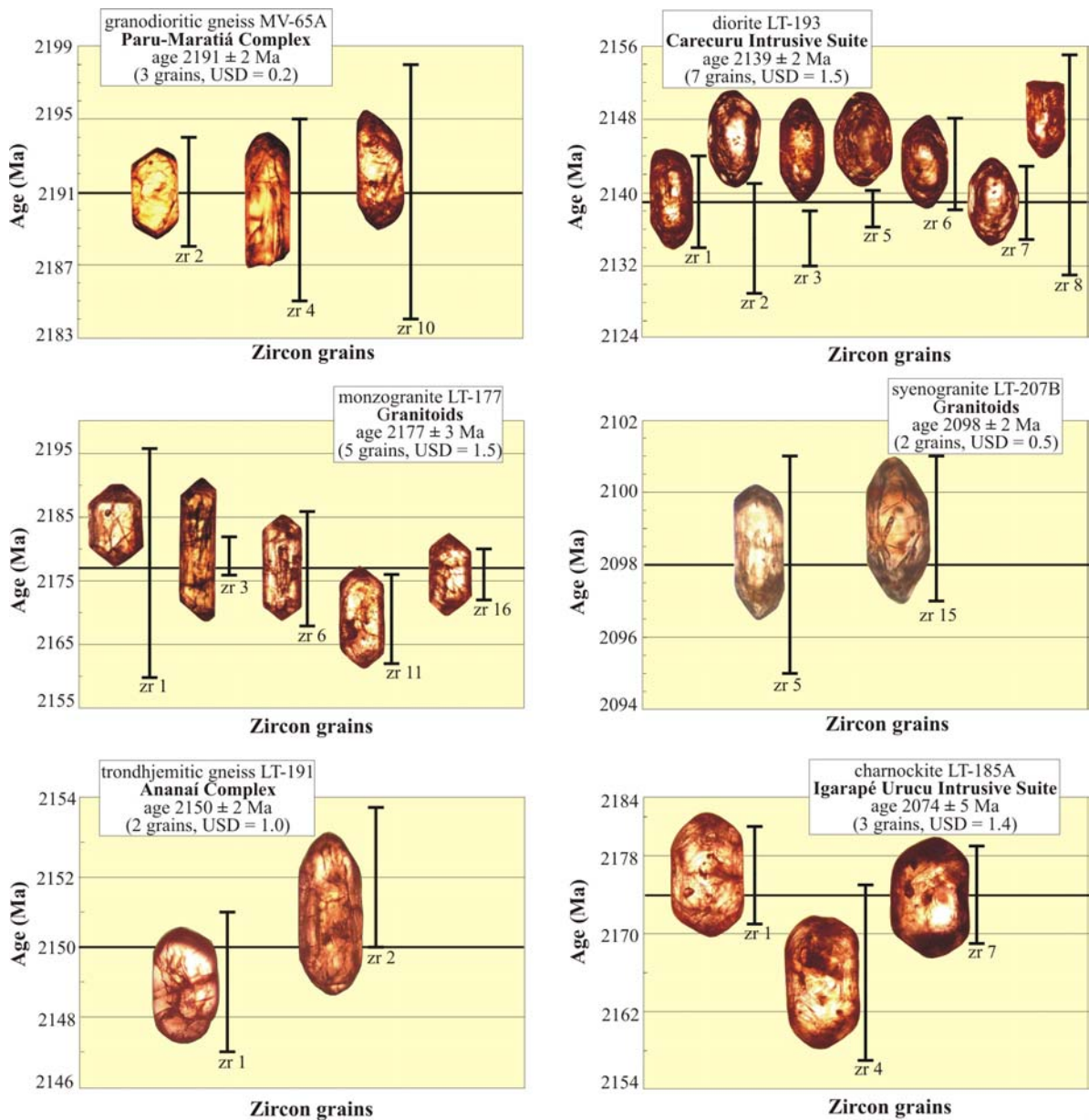


**Figure 4** – Pb-evaporation diagrams for the dated samples from the Carecuru and Paru domains. The error bars correspond to the mean age value for each zircon grain.

### Paru Domain

In this domain, two samples were investigated. The first one is a trondhjemitic gneiss (sample LT-191A) came from the Ananaí Complex, and the second one is a charnockite (sample LT-185A) from the Igarapé Urucu Intrusive Suite.

Zircon crystals from the trondhjemitic gneiss LT-191A are sub-euhedral with rounded terminations and fractured. In some grains magmatic zoning is visible. Eight grains furnished isotopic results and seven of them yielded ages between  $2127 \pm 3$  Ma and  $2152 \pm 2$  Ma in high steps of temperature. Three crystals yielded a mean value of  $2141 \pm 2$  Ma, while a mean age of  $2150 \pm 2$  Ma could be calculated with 2 other crystals. The latter is interpreted as the minimum age of crystallization of the igneous precursor. Such an age is similar to the age of 2.15-2.14 Ga of the calc-alkaline magmatism, characterized in the Carecuru Domain (Rosa-Costa et al., 2003 and this work).

The zircon grains from the charnockite LT-185A are typically rounded grains, showing magmatic zoning in the inner parts, with few mineral inclusions and often strongly metamictic. Among analyzed 12 grains, only 4 furnished useful isotopic results. The ages range from  $2052 \pm 4$  Ma to  $2076 \pm 5$  Ma and the 3 oldest grains provided a mean age of  $2074 \pm 5$  Ma (USD = 1.4), interpreted as the crystallization age. Although defined on a small number of grains, this age constrains the timing of the Paleoproterozoic charnockitic magmatism of the Igarapé Urucu Intrusive Suite, better than the previous geochronological dating available for this unit that furnished strongly variable ages, between  $2161 \pm 3$  Ma and  $2064 \pm 4$  Ma (Rosa-Costa et al., 2003). The new age at  $2074 \pm 5$  Ma is in agreement with the late-Transamazonian charnockitic magmatic events, dated between 2.07 and 2.05 Ga in other segments of the Guiana Shield and considered as indicators of the time of the high-grade metamorphism (Avelar et al., 2001; Lafon et al., 2001; Roeber et al., 2003).

### 3.2.2 - Sm-Nd Isotopic Data - Identifying events of crustal growth or reworking

The Sm-Nd isotopic results furnished by 32 samples are given in the Table 2. As all samples showed  $^{147}\text{Sm}/^{144}\text{Nd}$  ratios in the range of 0.08 to 0.13, the data were useful for calculation of  $T_{\text{DM}}$  model ages. In order to verify the reproducibility of the Sm-Nd isotopic analyses, the sample LT-207B was analyzed in duplicate and no differences of the Sm-Nd concentrations and isotopic composition were observed between the two analyses. The Table 2

also includes initial  $\epsilon_{Nd}$  values, calculated with the age of the emplacement provided by zircon Pb-evaporation method, obtained in this work or compiled from literature. When the zircon ages are not available, an estimation of the age is assumed, based on stratigraphic correlations.

### Jari Domain

Concerning to the Jari Domain, 16 samples were investigated, representing two major groups of rock: the Archean metamorphic complexes and the Paleoproterozoic granitoids. The  $T_{DM}$  model ages are clearly different between the two groups, as displayed in the  $\epsilon_{Nd}$  vs. Time diagram (Figure 5 A).

The first group includes samples from Archean metamorphic complexes (Jari-Guaribas, Baixo Mapari and Guianense) and igneous charnockites of the Noucouuru Intrusive Suite, which provided  $T_{DM}$  model ages ranging from 3.26 to 2.83 Ga, predominating ages between 3.26 to 2.92 Ga, and negative  $\epsilon_{Nd}$  values, between  $-3.97$  and  $-0.17$ . This range of model ages is in accordance with previous Nd data acquired in other Archean segments of the Guiana Shield, in its southeastern sector (3.06–3.01 Ga - Sato and Tassinari, 1997; 3.36–3.07 Ga - Pimentel et al., 2002; 3.29–2.90 Ga - Avelar et al., 2003) and northern sector (Imataca Complex, 3.23–2.80 Ga - Tassinari et al., 2001, 2004).

This coherent pattern supports the assumption that the interval between 3.26 and 2.83 Ga, which corresponds roughly to the Mesoarchean, can be considered as a protracted crust-forming episode, which is in agreement with the pattern of continental growth of the South America Platform during the Archean, based on Nd isotopic evolution (Cordani and Sato, 1999). The simultaneous determination of zircon ages and  $T_{DM}$  model ages allows the identification of two distinct geodynamic processes during Archean times in the Jari Domain. While juvenile crustal accretion is well documented since the end of the Paleoarchean and along the Mesoarchean, the lack of Neoarchean  $T_{DM}$  model ages and the negative  $\epsilon_{Nd}$  values of the magmatism dated at about 2.80-2.79 Ga and between 2.66-2.60 Ga, indicate that the Neoarchean evolution was preferentially related to ensialic reworking of older Paleo-Mesoarchean crust.

The second group is constituted of Paleoproterozoic granitoids that yielded  $T_{DM}$  model ages mainly between 2.52 and 2.45 Ga and  $\epsilon_{Nd}$  values between  $-0.87$  and  $-2.51$ . One exception is the leucogranite (sample EK-89) that furnished  $T_{DM}$  and  $\epsilon_{Nd}$  values of 2.30 Ga and  $+1.47$ , respectively.

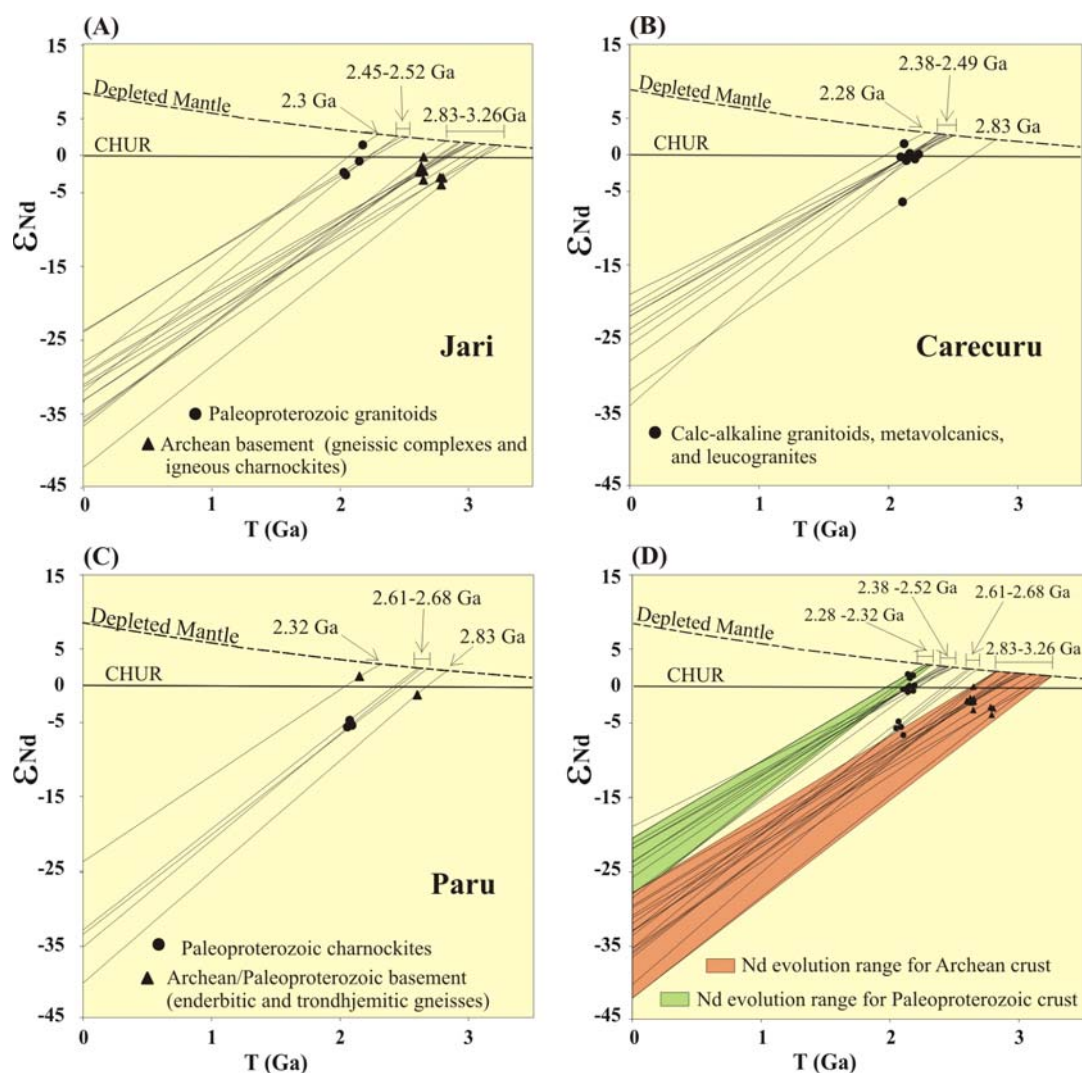


**Figure 5** – Diagrams of Nd isotopic evolution for rocks from the Jari (A), Carecuru (B) and Paru (C) domains, and (D) Nd isotopic evolution for all analyzed samples. The Nd evolution ranges for Archean and Paleoproterozoic crust are based on data acquired in this work.

A major Rhyacian crustal accretion event between 2.30 and 2.13 Ga has been recognized in southeastern Guiana Shield, from Guyana to northern Amapá region (Gruau et al., 1985; Lafrance et al., 1999; Nogueira et al., 2000; Voicu et al., 2000; Avelar, 2002; Roever et al., 2003). The Nd isotopic signature and the model age of the sample EK-89, which presents zircon age of  $2185 \pm 4$  Ma, indicate that its evolution is related to this regional period of crustal growth.

For the other samples of Paleoproterozoic granitoids, the Siderian  $T_{DM}$  ages of 2.52 to 2.45 Ga could indicate an older episode of crustal accretion at the Neoproterozoic – Paleoproterozoic

transition. However, the existence of such an event could be a misinterpretation of the Nd isotopic results as no other geological and geochronological arguments support this hypothesis for the Guiana Shield, as well as in its African counterpart (West African Craton).

Firstly, no significant geological activity (i.e. magmatism or metamorphism) is known in the Guiana Shield and in the West African Craton during Siderian (Boher et al., 1992; Kouamelan et al., 1997; Doumbia et al., 1998; Gasquet et al., 2003; Thiéblemont et al., 2004; Peucat et al., 2005). Even in global scale, Siderian is not recognized as an important period of crustal growth or of orogenic activities. In eastern Amazonian Craton, most of the geochronological records ranges between 3.3 Ga and 2.65 Ga and are lower than c.a. 2.30 Ga. Only few ages about 2.5 Ga have been registered, for instance, in the Carajás province, where some small plutons of granitoids were dated around 2.60-2.50 Ga (Machado et al., 1991; Souza et al., 1995). In the Guiana Shield, the Neoproterozoic magmatic activity is well constrained from 2.80 Ga to 2.60 Ga but ages younger than 2.60 Ga have not yet been recorded (Avelar et al., 2003; Rosa-Costa et al., 2003; this work). In the whole eastern Amazonia, Siderian zircon ages of  $2313 \pm 9$  Ma,  $2359 \pm 3$  Ma and  $2440 \pm 7$  Ma have only been reported northward from the Carajás Province (Faraco et al., 2003; Macambira et al., 2004; Vasquez et al., 2005), but no Siderian Sm-Nd model ages have been reported for any rocks of that region.

Therefore, even if the hypothesis of Siderian crustal accretion episode at the Paleoproterozoic - Neoproterozoic transition, as advocated by Faraco et al. (2004), cannot be excluded in the Jari Domain, we prefer to consider these  $T_{DM}$  ages and negative values of  $\epsilon_{Nd}$  in terms of mixing of two-components, with Paleoproterozoic juvenile mantle-derived magmas, contaminated by assimilation of Archean rocks or by interaction with magmas derived from Archean sialic sources, which are largely represented in the area. Such an hypothesis has been previously suggested by Avelar et al. (2003) to account for the late Neoproterozoic - Siderian  $T_{DM}$  ages of Paleoproterozoic granitoids from southeastern French Guiana. Siderian  $T_{DM}$  ages, slightly younger than those of rocks from the Jari domain, have been also locally registered in 2.07-2.05 Ga old granulites and pegmatites from the Bakhuis mountains in northwestern Suriname (Roever et al., 2003). The  $T_{DM}$  ages of 2.40-2.35 Ga and  $\epsilon_{Nd}$  values between +0.16 and -0.37 have been interpreted as recording an eo-Transamazonian crust-forming event with minor participation of reworked Archean crust.

### Carecuru Domain

Eleven samples representing all stratigraphic units were analyzed in this domain. Paleoproterozoic crystallization ages were provided or estimated for all investigated samples. The figure 5 B highlights three distinct isotopic patterns of Nd isotopic evolution furnished by the studied samples. Rhyacian crustal accretion event is also recognized in this domain, indicated by the model age of 2.28 Ga and  $\epsilon_{Nd}$  value of +1.63 furnished by the diorite LT-193. On the other hand, the syenogranite LT-207B, which has zircon age of  $2098 \pm 2$  Ma, exhibits a Nd  $T_{DM}$  age of 2.83 Ga, which is in agreement with the range of model ages furnished by Archean rocks of the Jari Domain. The strongly negative  $\epsilon_{Nd}$  value of -6.61 indicates that the origin of this granite is related to partial melting of Archean crust. This  $T_{DM}$  model age of 2.83 Ga confirms the presence of Archean remnants in the Carecuru Domain, also indicated by the occurrence of inherited Archean zircons in Paleoproterozoic rocks, for instance in metarhyolite (sample LT-182C - Rosa-Costa et al., 2002a) and granodioritic gneiss (sample MV-65A - this work). However, conversely to what occurs in the Jari Domain, no Archean rocks are preserved in the Carecuru Domain.

The most remarkable pattern is provided by a group of rocks, including calc-alkaline granitoids, metavolcanics and granites, which gave  $T_{DM}$  model ages ranging from 2.49 to 2.38 Ga and slightly negatives  $\epsilon_{Nd}$  values between -0.15 and -0.84, except in one sample (MV-65A), which gave a positive  $\epsilon_{Nd}$  value of +0.22. Like the rocks of the Jari Domain, these Siderian model ages can be interpreted in terms of crust-forming age or as a result of mixing between Paleoproterozoic juvenile magmas and minor Archean continental component. In the current case, the latter assumption is reinforced by the occurrence of inherited zircons in the metarhyolite and granodioritic gneiss, which furnished Archean Pb-Pb ages significantly older than their respective model ages (samples LT-182C:  $T_{DM} = 2.40$  Ga and inherited zircon age of  $2618 \pm 7$  Ma - Rosa-Costa et al., 2002a; sample MV-65A:  $T_{DM} = 2.45$  Ga and inherited zircon age of  $2784 \pm 6$  Ma).

### Paru Domain

In this domain, 2 gneisses of the Ananaí Complex were investigated, along with 3 charnockites that came from Igarapé Urucu Intrusive Suite.

The  $\epsilon_{Nd}$  vs. Time diagram (Figure 5 C) exhibits three clearly distinct patterns for the Nd isotopic evolution of the analyzed samples. The enderbitic gneiss MV-70D provided a Nd  $T_{DM}$

model age of 2.83 Ga and  $\epsilon_{\text{Nd}}$  value of -1.6 that, combined with the age of the magmatic precursor at 2.60 Ga, previously acquired on zircon from the same sample (Rosa-Costa et al., 2003), indicate that this gneiss was produced by reworking of Mesoarchean continental crust during Neoproterozoic. However, the trondhjemitic gneiss LT-191A yielded a Nd  $T_{\text{DM}}$  age of 2.32 Ga and  $\epsilon_{\text{Nd}}$  value of +1.17, characterizing the same eo-Transamazonian crustal accretion event that has been recognized in the other domains.

The 2.06-2.07 Ga charnockites furnished  $T_{\text{DM}}$  ages between 2.68 and 2.61 Ga, and negative  $\epsilon_{\text{Nd}}$  values between -5.89 and -4.80. The strongly negative  $\epsilon_{\text{Nd}}$  values indicate that the petrologic processes that originated these rocks include melting of an oldest crust during the Transamazonian orogenic event. This seems to be coherent if we consider that the formation of charnockites is related to the high grade event that affected the precursors of the surrounding Archean granulites of the Ananaí Complex. Nevertheless, if the charnockites are melting products of the enderbitic gneisses represented by sample MV-70D, which furnished a  $T_{\text{DM}}$  model age of 2.83 Ga, the Neoproterozoic model ages provided by the charnockites must be interpreted as mixed ages, produced by the participation of Archean and Paleoproterozoic components in the source of the charnockitic magma. A two-stage model for the Sm-Nd evolution of the source of charnockite with Sm-Nd fractionation during charnockitic magma formation would also account for  $T_{\text{DM}}$  ages (i.e. 2.68-2.61 Ga) younger than the  $T_{\text{DM}}$  age of the source rocks. However, the Sm-Nd ratios of both charnockites and enderbitic gneiss make this hypothesis unlikely. Alternatively, the  $T_{\text{DM}}$  ages of 2.68-2.61 Ga can correspond to the crust-formation time for the source of the charnockite, revealing a Neoproterozoic episode of crustal growth. Such an interpretation precludes the genetic relationship between charnockites and surrounding granulitic gneisses. The charnockitic magmas could be derived from younger (i.e. Neoproterozoic) and lower crustal segments accreted to the Mesoarchean segments by crustal underplating.

The diagram  $\epsilon_{\text{Nd}}$  vs. Time of the Figure 5 D summarizes the Nd evolution patterns provided by all rocks analyzed from the different domains. The evolution ranges of the rocks are highlighted in the diagram that present four intervals of  $T_{\text{DM}}$  model ages. Two of these intervals undoubtedly define crustal growth episodes that vary, between 3.26 and 2.83 Ga and between 2.32 Ga and 2.28 Ga. The first one is characterized mainly in the Archean basement of the Jari Domain, whereas the latter is related to a regional-scale eo-Transamazonian crustal accretion

event. The latter episode is recognized in all the domains but it represents a major event with significant production of crustal material only in the Carecuru Domain. The significance of the two other groups of Sm-Nd data, which present model age intervals of 2.52-2.38 Ga and 2.68-2.61 Ga is more questionable. Whether they represent two crust-forming episodes, respectively during Neoproterozoic and Archean times, or if they reflect mixed ages between Transamazonian juvenile and Archean components is an issue that needs to be addressed, even if the latter hypothesis seems to be better sustained by the available geological and geochronological constraints.

#### 4 – Geodynamical Implications

The new set of geochronological data, combined with those from previous geological and geochronological studies in the same area, demonstrate that the present-day configuration of the Jari, Carecuru and Paru domains results from a complex evolution, constrained by multi-stage crustal growth and reworking events.

The continental crust of the Jari Domain has a long-lived evolution, which started at the end of the Paleoproterozoic and continued until Neoproterozoic times (Figure 6). Zircon geochronology reveals three phases of magmatic activity during Archean, i.e. at about 3.32 Ga, at the Meso-Neoproterozoic transition, ca. 2.80-2.79 Ga, and during the Neoproterozoic, between 2.65 and 2.60 Ga. Nd  $T_{DM}$  model ages reveal that the main period of crust formation occurred at the end of the Paleoproterozoic and during the whole Mesooproterozoic, in a protracted episode between 3.26 and 2.83 Ga. Conversely, the combination of zircon geochronology and Nd model age data characterizes the Neoproterozoic as a period of crustal reworking, without significant production of juvenile crust.

Considering the superficial distribution of the Archean rocks in the Jari Domain, represented by the gneissic-granulitic-migmatitic basement assemblage (Figure 2), we can suppose that ca 70% of the crust was formed at that time. The available data indicate that Neoproterozoic rocks are almost restricted to plutons of granitoid and discrete supracrustal belts. During the Transamazonian orogenic cycle, the main geodynamical processes are related to reworking of older Archean crust, with minor juvenile accretion at about 2.3 Ga, associated to an early orogenic phase. Transamazonian magmatism consists of syn- to late-orogenic granitic pulses, which were dated at 2.22 Ga, 2.18 Ga, 2.15 Ga and 2.05 Ga to 2.03 Ga. Most of the

isotopic Nd signature and  $T_{DM}$  model ages (between 2.52 and 2.45 Ga) indicates an origin by mixing of juvenile Paleoproterozoic magmas with Archean crustal components.

Conversely, the geodynamical evolution of the Carecuru Domain took place only in Paleoproterozoic times, mainly during the Rhyacian (Figure 6). Eo-Transamazonian crustal accretion was recognized at about 2.28 Ga, in agreement with other Rhyacian crust forming ages registered in juvenile Transamazonian sectors of the Guiana Shield. Calc-alkaline magmatism is widespread, occurring apparently in two distinct pulses, at 2.19-2.18 Ga and at 2.15-2.14 Ga. Granitic magmatism was registered at 2.10 Ga, and can be envisaged as marking a stage of Paleoproterozoic crustal reworking in the Carecuru domain. Archean remnants are revealed by the model age of 2.83 Ga and by inherited zircon grains of some Paleoproterozoic rocks. However systematic  $T_{DM}$  model ages between 2.50 and 2.38 Ga with  $\epsilon_{Nd}$  slightly negative, preferentially interpreted as mixed ages, preclude any major participation of Archean components in the source of the Paleoproterozoic rocks.

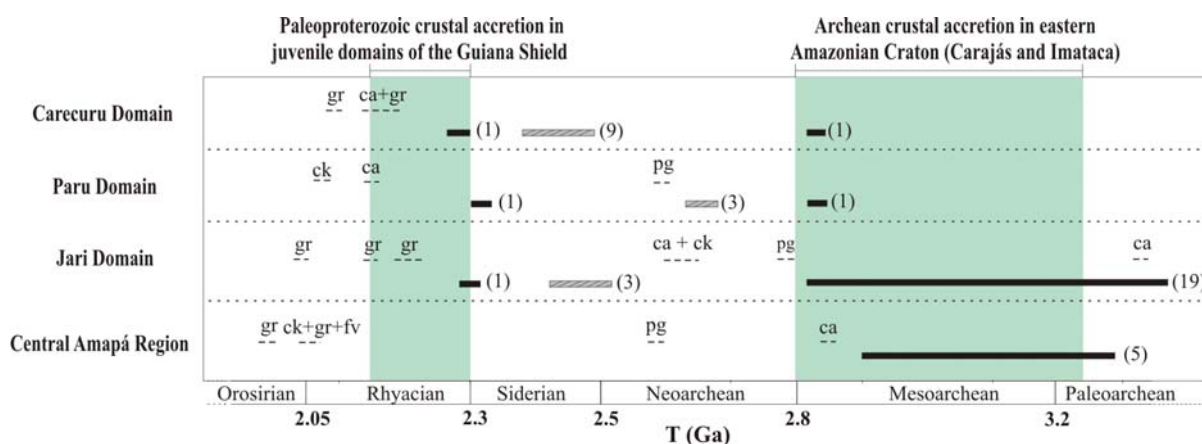


**Figure 6** – Summary of the main crustal growth episodes and magmatic pulses vs. time, registered in the investigated domains and in central Amapá region. Magmatic pulses (dashed lines) and crustal growth episodes (black bars) based on zircon ages and  $T_{DM}$  model ages, respectively. Conventions: ca–calc-alkaline, gr–granitic, ck–charnockitic, pg–precursor granulitic, fv–felsic volcanic, hatched grey bars – mixed  $T_{DM}$  model ages, (n) number of dated samples. Source of data: Avelar (2002), Avelar et al. (2003), Barros et al. (2004), Borges et al. (2002), Cordani and Sato (1999), Gruau et al. (1985), Klein et al. (2003), Lafrance et al. (1999), Macambira and Lafon (1995), Nogueira et al. (2000), Pimentel et al. (2002 and 2003), Ramö et al. (2002), Ricci et al. (2002), Roever et al. (2003), Rosa-Costa et al. (2002a and 2003), Santo and Tassinari (1997), Souza et al. (2001), Tassinari and Macambira (1999), Tassinari et al. (2001), Voicu et al. (2000).

The lithological association of the Carecuru Domain, i.e. large calc-alkaline plutons and mafic to intermediate volcanic rocks, is typical of subduction-related settings, being consistent with either a volcanic arc in oceanic environment or a magmatic arc at an active continental margin. However, the involvement of Archean crustal components shown by Nd isotopic signatures, added to the proximity of the adjacent Archean Jari Domain, strongly favors an origin in a magmatic arc setting.

Due to the scarcity of data, explanations concerning the tectonic significance of the Paru Domain in a Paleoproterozoic magmatic arc context are speculative. Some similarities can be recognized between the Paru and the Jari domains, which include  $T_{DM}$  model ages at about 2.83 Ga and Neoproterozoic magmatic events at about 2.6 Ga. However, besides contrasting geophysical and structural signatures between these domains (Rosa-Costa et al., 2002b), Paleoproterozoic calc-alkaline (2.15 Ga) and charnockitic (2.07 Ga) magmatism are known only in the former. At least two hypotheses can guide further investigations: 1) the Paru Domain represents a prolongation of the Jari Domain that was preserved in the roots of the magmatic arc; or 2) it is an allochthonous crustal fragment accreted to the magmatic arc during the Transamazonian orogenesis.

The next question to be addressed is the northeastern prolongation of the Archean continental crust. Several geochronological records of Archean rocks are known out of the limits of the investigated area, in the Cupixi region and vicinities ( $T_{DM}$  ages between 3.36 and 3.06 Ga - Sato and Tassinari, 1997 and Pimentel et al., 2002; zircon age of  $3321 \pm 11$  Ma - Klein et al., 2003), and more distant, in the Tartarugalzinho region, in the central portion of the Amapá state ( $T_{DM}$  ages between 3.29 and 2.9 Ga and zircon ages of  $\approx 2.60$  Ga - Lafon et al., 1998 and Avelar et al., 2003). As such, the available evidence points to the existence of an expressive and, probably, continuous NW-SE structured Archean continental landmass extending from the Pará/Amapá border to the north of Tartarugal region, here named Amapá Block (Figure 7). The limits proposed to this block coincide with major tectonic structures, which are outlined by large Paleoproterozoic supracrustal belts. However, in the areas where geological and geochronological informations are not available, the limit must be regarded with caution, since it was inferred mainly on the basis of aerogeophysical imagery.

The major arguments that favor the nature of the Amapá Block as a continental landmass during the Transamazonian orogenic cycle are: 1) the dominantly Archean geochronological

pattern; 2) the lack of significant Transamazonian accretion and magmatism related to subduction processes; 3) the Nd isotopic signature which strongly indicates an origin of Paleoproterozoic granites by reworking of Archean crust.

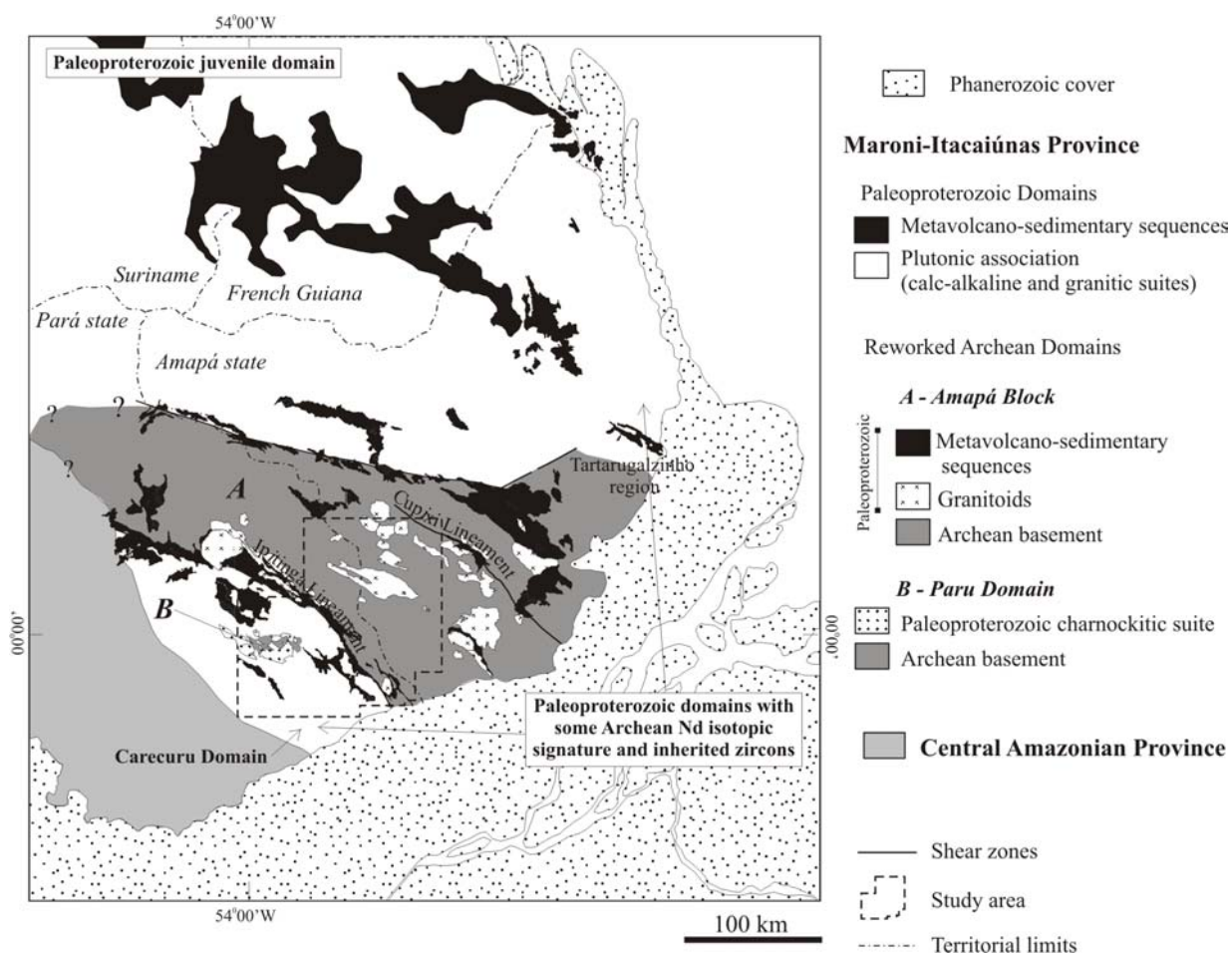


**Figure 7** – Sketch map showing distinct geochronological/tectonic domains of the eastern Guiana Shield, including the Amapá Block defined in this study. Designation of the geochronological provinces according to Tassinari and Macambira (2004).

Ricci et al. (2001) consider that the Jari Domain represents a tectonostratigraphic terrane, separated from the adjacent terranes by major NW-SE strike-slip shear zones: the Ipitinga Lineament, between the Carecuru and Jari terranes, and the Cupixi Lineament between the Jari and Cupixi terranes. The latter was originally named Cupixi-Tartarugal Grande Ancient Terrane, since it hosted the oldest dated rock in the southeastern Guiana Shield known until that time (2.85

Ga - Avelar et al., 2001). However, later geochronological studies have registered rocks older than 2.85 Ga in the Jari Domain (3.32 Ga - Klein et al., 2003; inherited zircon grains at about 3.24 Ga – this study). Therefore, a tectonic subdivision within the Archean block is still highly speculative, since there are not enough geological and geochronological arguments to support this hypothesis.

The recognition of an extended Archean landmass precludes previous statements that the Archean in the southeast of the Guiana Shield, was restricted to isolated remnants or inliers within Paleoproterozoic terrains (Tassinari and Macambira, 1999; Santos et al., 2000; Tassinari et al., 2000; Tassinari and Macambira 2004). In addition, these Archean remnants were previously interpreted as a possible northward prolongation of the Archean Carajás range, strongly affected by the Transamazonian orogenic cycle, as discussed by Avelar et al. (2003).

In this work we admit that the Amapá Block represents an independent continental landmass, rather than a northward prolongation of Carajás range, since the available geochronological data indicate distinct geodynamic evolution for these Archean segments. While a remarkable period of plutonic activity, between 2.80 and 2.60 Ga, took place during the Neoproterozoic in the Amapá Block, in the Carajás province this phase corresponds to predominantly rift-related volcanism and sedimentary deposition (Gibbs et al., 1986; Wirth et al., 1986; Machado et al., 1991; Trendall et al., 1998), with emplacement of some plutons of granitoids in the north of the province (Machado et al., 1991; Souza et al., 1995; Avelar et al., 1999; Barros et al., 2004). In addition, in terms of lithologic content, tectonic features and metallogenic history, the differences are also outstanding. Furthermore, north of the Carajás range, geochronological investigations showed widespread occurrence of Paleoproterozoic rocks (Macambira et al., 2001, 2004; Vasquez et al., 2005), in a magmatic arc environment (Macambira et al., 2001, 2004). This suggests the existence of a crustal segment extending from the north of the Carajás province to the southern border of the Amapá Block, which presents a geochronological pattern dominantly Paleoproterozoic. This segment includes the Carecuru Domain, and is related to the development of a magmatic arc system during the Transamazonian orogenic cycle.

In the same way, at north of the Amapá Block, Avelar et al. (2003) characterized a transitional zone, between the Archean Tartarugalzinho region and the juvenile Paleoproterozoic domains of the French Guiana. In that zone, zircon ages defined Paleoproterozoic magmatic

events between 2.19 and 2.09 Ga, but  $T_{DM}$  model ages, ranging from 2.75 to 2.39 Ga, indicate the existence of Archean components in the source of the Paleoproterozoic magmas. Some similarities can be outlined between the transitional zone described by Avelar et al. (2003) and the Carecuru Domain, for instance, calc-alkaline magmatism at about 2.19 Ga and the participation of Archean crust in the source of the Paleoproterozoic magmas. Moreover, in the northern portion of this transitional zone, Nogueira et al. (2000) dated tonalitic magmatism at 2.16 Ga and admitted that it is related to the development of a calc-alkaline magmatic arc.

Consequently, the Transamazonian orogenic cycle can be envisaged as a dominantly accretionary-type orogeny, responsible for the welding of several Archean continental landmasses (Carajás, Imataca Block, Amapá Block, and also the Kénéma Man domain in West Africa Craton) through arc systems (continental and oceanic), where reworking of continental crust and accretion of juvenile material played major roles. This major tectonic event resulted in the development of the extensive Paleoproterozoic belt of the northeast of the Amazonian Craton, which corresponds to the Maroni-Itacaiúnas Province or to the Transamazonic Province, according proposals of Tassinari and Macambira (2004) and Santos et al. (2000), respectively. As the major Archean blocks recognized within this belt, the Imataca Block and the here defined Amapá Block, are overprinted by the Transamazonian orogenesis, the proposal of Tassinari and Macambira (2004) is preferred since it is based on the age of the late orogenesis that affected the province. Nevertheless, the Amapá Block has to be incorporated in that model as an extensive Archean continental landmass instead of restricted Archean inliers.

## 5 – Acknowledgements

The field work, sampling and petrographic study were performed during the mapping program (RENCA Project) developed by CPRM-Belém that started the new geological approach in the studied area. The expertise help with sample processing and zircon separation received from M. R. Soares (CPRM-Belém) and L.A. Costa e Silva (CPRM-Porto Alegre) is greatly appreciated. E. Oliveira, R. Florencio, R. Monteiro and especially M. A. Galarza are acknowledged for continuous technical assistance during the geochronological analyses at the Pará-Iso Laboratory, Belém. E. Klein (CPRM-Belém) is thanked for his helpful comments and suggestions. We are also grateful to J.J. Peucat and C.C.G. Tassinari for their expert and

constructive reviews, which benefited substantially this article. This paper is a contribution to PRONEX/CNPq (Proj. 103/98 – Proc. 66.2103/1998-0).

## 6 – References

- Ansdell, K.M. and Kyser, T.K., 1993. Textural and chemical changes undergone by zircon during the Pb-evaporation technic. *American Mineralogist*, 78, 1663-1673.
- Avelar, V.G., 2002. Geocronologia Pb-Pb em zircão e Sm-Nd em rocha total da porção centro-norte do Estado do Amapá – Brasil: Implicações para a evolução geodinâmica do setor oriental do Escudo das Guianas. Tese de Doutorado, Universidade Federal do Pará.
- Avelar, V.G., Lafon, J.M., Correia Jr. F.C., Macambira, E.J.B., 1999. O magmatismo arqueano da região de Tucumã – Província Mineral de Carajás: novos dados geocronológicos. *Revista Brasileira de Geociências*, 29, 453-460.
- Avelar, V.G., Lafon, J.M., Delor, C., 2001. Geocronologia Pb-Pb em zircão e Sm-Nd em rocha total da porção centro-norte do Amapá. Implicações para a evolução geodinâmica do Escudo das Guianas. In: VII Simp. Geol. Amaz., Belém. CD ROM.
- Avelar, V.G., Lafon, J.M., Delor, C., Guerrot, C., Lahondère, D., 2003. Archean crustal remnants in the easternmost part of the Guiana Shield: Pb-Pb and Sm-Nd geochronological evidence for Mesoarchean versus Neoproterozoic signatures. *Géologie de la France*, 2-3-4, 83-100.
- Barbarin, B., 1999. A review of the relationships between granitoid types, their origins and their geodynamic environments. *Lithos*, 46, 605-626.
- Barros, C.E.M., Macambira, M.J.B., Barbey, P., Scheller, T., 2004. Dados isotópicos Pb-Pb em zircão (evaporação) e Sm-Nd do Complexo Granítico Estrela, Província Mineral de Carajás, Brasil: implicações petrológicas e tectônicas. *Revista Brasileira de Geociências*, 34, 531-538.
- Boher, M., Abouchami, W., Michard, A., Albarede, F., Arndt, N.T., 1992. Crustal growth in West Africa at 2.1 Ga. *Journal of Geophysical Research*, 97, 345-369.
- Borges, A.A.S., Lafon, J.M., Villas, R.N.N., 2002. Magmatismo Tardi-Transamazônico na Serra do Navio, região central do Amapá: evidências geocronológicas. In: XLI Cong. Bras. Geol., João Pessoa, Anais.
- Carvalho, J.M. de A., Rosa-Costa, L.T. da, Vasquez, M.L., Klein, E.L., Macambira, E.M.B., Vale, A.G., Ricci, P. dos S.F., 2001. Projeto Província Mineral da RENCA e Distrito Mineral do Ipitinga. CPRM - Serviço Geológico do Brasil, Belém, Mapa Geológico, escala 1:250.000.
- Cordani, U.G. and Sato, K., 1999. Crustal evolution of the South American Platform, based on Nd isotopic systematics on granitoid rocks. *Episodes*, 22, 67-173.
- Cordani, U.G., Tassinari, C.C.G., Kawashita, K., 1984. A Serra dos Carajás como região limítrofe entre províncias tectônicas. *Ciências da Terra*, 9, 6-11.
- Cordani, U.G., Tassinari, C.C.G., Teixeira, W., Basei, M.A.S., Kawashita, K., 1979. Evolução tectônica da Amazônia com base nos dados geocronológicos. In: II Cong. Geol. Chileno, Arica. *Actas*, 4, 137-148.

- Delor, C., Lahondère, D., Egal, E., Lafon, J.M., Cocherie, A., Guerrot, C., Rossi, P., Trufert, C., Theveniaut, H., Phillips, D., Avelar, V.G., 2003a. Transamazonian crustal growth and reworking as revealed by the 1:500,000-scale geological map of French Guiana (2<sup>nd</sup> edition). *Géologie de la France*, 2-3-4, 5-57.
- Delor, C., Roeber, E.W.F. De, Lafon, J.M., Lahondère, D., Rossi, P., Cocherie, A., Guerrot, C., Potrel, A., 2003b. The Bakhuis ultrahigh-temperature granulite belt (Suriname) : II. Implications for late Transamazonian crustal stretching in a revised Guiana Shield framework. *Géologie de la France*, 2-3-4, 207-230.
- DePaolo, D.J., 1981. Nd isotopic studies: some new perspectives on Earth structure and evolution. *EOS*, 62, 137-145.
- Doumbia, S., Pouclet, A., Kouamelan, A., Peucat, J.J., Vidal, M., Delor, C., 1998. Petrogenesis of juvenile-type Birimian (Paleoproterozoic) granitoids in Central Côte-d'Ivoire, West Africa: geochemistry and geochronology. *Precambrian Research*, 87, 33-63.
- Faraco, M.T.L., Marinho, P.A.C., Vale, A.G., Moura, C.V., Macambira, M.J.B., 2004. Idades modelo Sm-Nd e idade <sup>207</sup>Pb-<sup>206</sup>Pb em zircão no Distrito de Ipitanga, Reserva Nacional do Cobre e seus Associados-RENCA. In: XLII Cong. Bras. Geol., Araxá. CD-ROM.
- Faraco, M.T.L., Vale, A.G., Santos, J.O.S., Luzardo, R., Ferreira, A.L., Oliveira, M.A., Marinho, P.A.C., 2003. Levantamento geológico na região norte do Bloco Carajás: notícias preliminares. In: VIII Simp. Geol. Amaz., Manaus. CD-ROM.
- Gasquet, D., Barbey, P., Adou, M., Paquette, J.L., 2003. Structure, Sr-Nd isotope geochemistry and zircon U-Pb geochronology of the granitoids of the Dabakala area (Côte d'Ivoire): evidence for a 2.3 Ga crustal growth event in the Paleoproterozoic of West Africa? *Precambrian Research*, 127, 329-354.
- Gaudette, H.E., Lafon, J.M., Macambira, M.J.B., Moura, C.A.V., Scheller, T., 1998. Comparison of single filament Pb evaporation/ionization zircon ages with conventional U-Pb results: Examples from the Precambrian of Brazil. *Journal of South American Earth Sciences*, 11, 351-363.
- Gibbs, A.K., Wirth, K.R., Hirata, W.K., Olzewski, W.J., 1986. Age and composition of the Grão Pará Group volcanics, Serra dos Carajás. *Revista Brasileira de Geociências*, 16, 201-211.
- Gruau, G., Martin, H., Leveque, B., Capdevilla, R., 1985. Rb-Sr and Sm-Nd geochronology of Lower Proterozoic granite-greenstone terrains in French Guyane, South America. *Precambrian Research*, 30, 63-80.
- Howell, D.G., 1995. Principles of terrane analysis. New application for global tectonics. Chapman and Hall, 245p.
- João, X.S.J. and Marinho, P.A.C., 1982. Catametamorfitos Arqueanos da região centro-leste do Território Federal do Amapá. In: I Simp. Geol. Amaz., Belém.. Anais, 2, 207-228.
- Karabinos, P. and Gromet, L.P., 1993. Applications of single-grain zircon analysis to the detrital studies and age discrimination in igneous suites. *Geochimica and Cosmochimica Acta*, 57, 4257-4267.
- Klein, E.L., Moura, C.A., Pinheiro, B.L.S., 2005. Paleoproterozoic crustal evolution of the São Luís Craton, Brazil: evidence from zircon geochronology and Sm-Nd isotopes. *Gondwana Research*, 8, 1-10.
- Klein, E.L., Rosa-Costa, L.T. da, Lafon, J.M., 2003. Magmatismo Paleoarqueano (3,32Ga) na região do Rio Cupixi, SE do Amapá, SE do Escudo das Guianas. In: VII Simp. Geol. Amaz., Manaus. CD ROM.
- Klötzli, U.S., 1999. Th/U zonation in zircon derived from evaporation analysis: a model and its implications. *Chemical Geology*, 58, 325-333.

- Kober, B., 1986. Whole-grain evaporation for  $^{207}\text{Pb}/^{206}\text{Pb}$ -age-investigations on single zircons using a double-filament thermal ion source. *Contributions to Mineralogy and Petrology*, 93, 482-490.
- Kober, B., 1987. Single zircon evaporation combined with  $\text{Pb}^+$  emitter-bedding for  $^{207}\text{Pb}/^{206}\text{Pb}$ -age investigations using thermal ion mass spectrometry, and implications to zirconology. *Contributions to Mineralogy and Petrology*, 96, 63-71.
- Kober, B., Pidgeon, R.T., Lippolt, H.J., 1989. Single-zircon dating by stepwise Pb-evaporation constraints the Archean history of detrital zircons from the Jack Hills, Western Australia. *Earth and Planetary Sciences Letters*, 91, 286-296.
- Kouamelan, A.N., Delor, C., Peucat, J.-J., 1997. Geochronological evidence for reworking of Archean terrains during the Early Proterozoic (2.1 Ga) in the western Côte d'Ivoire (Man Rise–West Africa Craton). *Precambrian Research*, 86, 177-199.
- Kröner, A., Jaeckel, P., Brandl, G., Nemchin, A.A., Pidgeon, R.T., 1999. Single zircon ages for granitoid gneisses in the Central Zone of the Lompopo Belt, Southern Africa and geodynamic significance. *Precambrian Research*, 93, 299-337.
- Lafon, J.M., Rossi, P., Delor, C., Avelar, V.G., Faraco, M.T.L., 1998. Novas testemunhas de relíquias arqueanas na crosta continental paleoproterozóica da Província Maroni-Itacaiúnas (Sudeste do Escudo das Guianas). In: XL Cong. Bras. Geol., Belo Horizonte. Anais, p.64.
- Lafon, J.M., Rossi, P., Delor, C., Barbosa, O.S., 2001. Granulitos tardi-Transamazônicos (2,06 Ga) na região norte do Estado do Amapá: o charnoquito de Calçoene. In: VII Simp. Geol. Amaz., Belém. CD ROM.
- Lafrance, J., Bardoux, M., Voicu, G., Stevenson, R., Machado, N., 1999. Geological and metallogenic environments of gold deposits of the Guiana Shield: a comparative study between St. Élie (French Guiana) and Omai (Guyana). *Exploration and Mining Geology*, 8, 117-135.
- Lameyre, J. and Bowden, P., 1982. Plutonic rock types series: discrimination of various granitoid series and related rocks. *J. Volc. Geoth. Research*, 14, 169-196.
- Ledru, P., Johan, V., Milési, J.P., Tegye, M., 1994. Markers of the last stages of the Paleoproterozoic collision: evidence for a 2 Ga continent involving Caramuru-South Atlantic provinces. *Precambrian Research*, 69, 169-191.
- Lima, M.I.C., Oliveira, E.P., Tassinari, C.C.G., 1982. Cinturões granulíticos da porção setentrional do Craton Amazônico. In: I Simp. Geol. Amaz., Belém. Anais, 1, 147-162.
- Ludwig, K.R., 2004. Users manual for ISOPLOT/EX a geochronological toolkit for Microsoft Excel (version 3.1).
- Macambira, M.J.B., Barros, C.E.M., Silva, D.C.C., Santos, M.C.C., 2001. Novos dados geológicos e geocronológicos para a região ao norte da Província de Carajás, evidências para o estabelecimento do limite Arqueano-Paleoproterozóico no sudeste do Cráton Amazônico. In: VII Simp. Geol. Amaz., Belém. CD ROM.
- Macambira, M.J.B. and Lafon, J.M., 1995. Geocronologia da Província Mineral de Carajás: Síntese dos dados e novos desafios. *Boletim do Museu Paraense Emílio Goeldi, Série Ciências da Terra*, 7, 263-288.
- Macambira, M.J.B., Silva, D.C., Vasquez, M.L., Barros, C.E.M., 2004. Investigação do limite Arqueano-Paleoproterozóico ao norte da Província de Carajás, Amazônia Oriental. In: XLII Congr. Bras. Geol., Araxá, CD ROM.

- Machado, N., Lyndenmayer, Z., Krogh, T.E., Lindenmayer, D., 1991. U-Pb geochronology of Archean magmatism and basement reactivation in the Carajás area, Amazonian shield, Brazil. *Precambrian Research*, 49, 329-354.
- McReath, I. and Faraco, M.T.L., 1997. Sm/Nd and Rb/Sr systems in part of the Vila Nova metamorphic suite, northern Brazil. In: I, South Amer. Symp. Isotop. Geol., Campos do Jordão. Extended abstracts, 194-196.
- Montalvão, R.M.G. and Tassinari, C.C.G., 1984. Geocronologia pré-cambriana do Território Federal do Amapá (Brasil). In: II Simp. Geol. Amaz., Manaus. Anais, 54-57.
- Montgomery, C.W., 1979. Uranium-lead geochronology of the Archean Imataca Series, Venezuelan Guyana Shield. *Contributions to Mineralogy and Petrology*, 69, 167-176
- Montgomery, C.W. and Hurley, P.M., 1978. Total rock U-Pb and Rb-Sr systematics in the Imataca Series, Guyana Shield, Venezuela. *Earth and Planetary Sciences Letters*, 39, 281-290.
- Nogueira, S.A.A., Bettencourt, J.S., Tassinari, C.C.G., 2000. Geochronology of the Salamangone gold deposit host-rocks, Lourenço district, Amapá, Brazil. *Revista Brasileira de Geociências*, 30, 261-264.
- Norcross, C.E., Davis, D.W., Spooner, E.T.C., Rust, A., 2000. U-Pb and Pb-Pb age constraints on Paleoproterozoic magmatism, deformation and gold mineralization in the Omai area, Guyana Shield. *Precambrian Research*, 102, 69-86.
- Onstott, T.C. and Hargraves, R.B., 1981. Proterozoic transcurrent tectonics: paleomagnetic evidence from Venezuela and Africa. *Nature*, 289, 131-136.
- Onstott, T.C., Hargraves, R.B., York, D., Hall, C.M., 1984. Constraints on the motions of South American and African Shields during the Proterozoic, I.  $^{40}\text{Ar}/^{39}\text{Ar}$  and paleomagnetic correlations between Venezuela and Liberia. *Geological Society of American Bulletin*, 95, 1045-1054.
- Pecaut, J.-J., Capdevila, R., Drareni, A., Mahdjoub, Y., Kahoui, M., 2005. The Eglab massif in the West African Craton (Algeria), an original segment of the Eburnean orogenic belt: petrology, geochemistry and geochronology. *Precambrian Research*, 136, 309-352.
- Pimentel, M.M., Ferreira Filho, C.F., Spier, C.A., 2002. Estudo Sm-Nd do Complexo Máfico-Ultramáfico Bacuri, Amapá: idade da intrusão, metamorfismo e natureza do magma original. *Revista Brasileira de Geociências*, 32, 371-376.
- Pimentel, M.M., Lindenmayer, Z.G., Laux, J.H., Armstrong, R., Araújo, J.C., 2003. Geochronology and Nd isotope geochemistry of the Gameleira Cu-Au deposit, Serra dos Carajás, Brazil: 1.8 – 1.7 hydrothermal alteration and mineralization. *Journal of American Earth Sciences*, 15, 803-813.
- Ramö, O.T., Dall'agnol, R., Macamira, M.J.B., Leite, A.A.S., Oliveira, D.C., 2002. 1.88 Ga oxidized A-type granites of the Rio Maria region, eastern Amazonian Craton, Brazil: positively anorogenic! *Journal of Geology*, 110, 603-610.
- Ricci, P.S.F., Carvalho, J.M.A., Rosa-Costa, L.T., Klein, E.L., Vasquez, M.L., Vale, A.G., Macambira, E.M.B., Araújo, O.J.B., 2001. Geologia e recursos minerais do Projeto RENCA – Fase I. CPRM - Serviço Geológico do Brasil, Belém.
- Ricci, P.S.F., Carvalho, J.M.A., Rosa-Costa, L.T. da, Lafon, J.M., 2002. Plúton charnoenderbítico Arqueano intrusivo nos ortognaisses granulíticos do Cinturão Jari – Terreno Arqueano expressivo do sudeste do Escudo das Guianas. In: XLI Cong. Bras. Geol., João Pessoa. Anais, p.524.

- Roever, E.W.F. De, Lafon, J.M., Delor, C., Cocherie, A., Rossi, P., Guerrot, C., Potrel, A., 2003. The Bakhuis ultrahigh-temperature granulite belt (Suriname): I. petrological and geochronological evidence for a counterclockwise P-T path at 2.07-2.05 Ga. *Géologie de la France*, 2-3-4, 175-206.
- Rosa-Costa, L.T. da, Lafon, J.M., Cocherie, A., Delor, C., (submitted) Electron microprobe U-Th-Pb monazite dating deciphering the age of the high-grade metamorphic overprint on Archean rocks from Guiana Shield, north of Amazonian Craton, Brazil
- Rosa-Costa, L.T. da, Macambira, E.M.B., Vasquez, M.L., Lafon, J.M., Ricci, P.S.F., 2002a. Idades de rochas metavulcânicas félsicas do sudeste do Escudo das Guianas. In: II Simp. sobre Vulcanismo e Ambientes Associados, Belém. Boletim de Resumos e Roteiro de Excursão, p.46.
- Rosa-Costa, L.T. da, Ricci, P.S.F., Lafon, J.M., Vasquez, M.L., Carvalho, J.M.A., Klein, E.L., Macambira, E.M.B., 2003. Geology and geochronology of Archean and Paleoproterozoic domains of the southeastern Amapá and northwestern Pará, Brazil – southeastern Guiana Shield. *Géologie de la France*, 2-3-4, 101-120.
- Rosa-Costa, L.T. da, Vale, A.G., Silva, A.M., 2002b. Integração de dados aerogeofísicos e imagens de sensores remotos como ferramenta para o mapeamento geológico na Região Amazônica: o exemplo do Projeto Promin-RENCA. In: Klein, E.L., Vasquez, M.L., Rosa-Costa, L.T. da (Eds.), *Contribuições à Geologia da Amazônia*, 3, 227-243.
- Rosa-Costa, L.T. da, Vasquez, M.L., Carvalho, J.M.A., Ricci, P.S.F., Lafon, J.M., 2001. Geocronologia preliminar do Arqueano e Paleoproterozóico do NW do Pará/SW do Amapá – Escudo das Guianas. In: VII Simp. Geol. Amaz., Belém. CD ROM.
- Santos, J.O.S., Hartmann, L.A., Gaudette, H.E., Groves, D.I., Mcnaughton, N.J., Fletcher, I.R., 2000. A new understanding of the provinces of the Amazonian Craton based on integration of field mapping and U-Pb and Sm-Nd geochronology. *Gondwana Research*, 3, 453-488.
- Sato, K. and Tassinari, C.C.G., 1997. Principais eventos de acreção continental no Cráton Amazônico baseados em idade-modelo Sm-Nd, calculada em evoluções de estágio único e estágio duplo. In: Costa, M.L.C. and Angélica, R.S. (Eds.), *Contribuições à Geologia da Amazônia*, 1, 91-142.
- Souza, S.R.B., Macambira, M.J.B., Horbe, M.A., 1995. Geochronological and isotopic evidences of the influence of the Paleoproterozoic Pojuca Granite on the Cu-Zn (Au-Mo-Ag) deposit, Carajás province, Brazil. In: *Symp. Rapakivi Granites and Related Rocks*, Belém. Abstracts, 76.
- Souza, Z.S., Potrel, A., Lafon, J.M., Althoff, F.J., Pimentel, M.M., Dall'agnol, R., Oliveira, C.G., 2001. Nd, Pb and Sr isotopes in the Identidade Belt, an Archean greenstone belt of Rio Maria region (Carajás Province, Brazil): implications for the geodynamic evolution of the Amazonian Craton. *Precambrian Research*, 109, 293-315.
- Stacey, J.S. and Kramers, J.D., 1975. Approximation of terrestrial lead isotopic evolution by a two stage model. *Earth and Planetary Sciences Letters*, 26, 207-221.
- Tassinari, C.C.G. and Macambira, M.J.B., 1999. Geochronological provinces of the Amazonian Craton. *Episodes*, 22, 174-182.
- Tassinari, C.C.G. and Macambira, M.J.B., 2004. A evolução tectônica do Cráton Amazônico. In: Mantesso-Neto, V., Bartorelli, A., Carneiro, C.D.R., Brito Neves, B.B. (Eds.), *Geologia do Continente Sul-Americano: Evolução da Obra*

- de Fernando Flávio Marques de Almeida, 471-485.
- Tassinari, C.C.G., Bettencourt, J.S., Geraldes, M.C., Macambira, M.J.B., Lafon, J.M., 2000. The Amazonian Craton. In: Cordani, U.G., Milani, E.J., Filho, A.T. and Campos, D.A. (Eds.), *Tectonic Evolution of South America*, 41-95.
- Tassinari, C.C.G., Munhá, J.M.V., Teixeira, W., Palácios, T., Nutman, A.P., Sousa, C.S., Santos, A.P., Calado, B.O., 2004. The Imataca Complex, NW Amazonian Craton, Venezuela: crustal evolution and integration of geochronological and petrological cooling histories. *Episodes*, 27, 3-12.
- Tassinari, C.C.G., Teixeira, W., Nutman, A.P., Szabó, G.A., Mondin, M., Sato, K., 2001. Archean crustal evolution of the Imataca Complex, Amazonian Craton: Sm-Nd, Rb-Sr e U-Pb (SHRIMP) evidences. In: VII Simp. Geol. Amaz., Belém. CD ROM.
- Teixeira, W., Tassinari, C.C.G., Cordani, U.G., Kawashita, K., 1989. A review of the geochronology of the Amazonian Craton: Tectonic implications. *Precambrian Research*, 42, 213-227.
- Thiéblemont, D., Goujou, J.C., Ega, E., Cocherie, A., Delor, C., Lafon, J.M., Fanning, C.M., 2004. Archean evolution of the Leo Rise and its Eburnean reworking. *Journal of African Earth Sciences*, 39, 97-104.
- Trendall, A.F., Basei, M.A.S., Laeter, J.R., Nelson, D.R., 1998. SHRIMP zircon U-Pb constraints on the age of the Carajás formation, Grão Pará group, Amazon Craton. *Journal of South American Earth Sciences*, 11, 265-277.
- Vanderhaeghe, O., Ledru, P., Thiéblemont, D., Egal, E., Cocherie, A., Tegye, M., Milési, J.J., 1998. Contrasting mechanism of crustal growth Geodynamic evolution of the Paleoproterozoic granite-greenstone belts of French Guyana. *Precambrian Research*, 92, 165-193.
- Vasquez, M.L. and Lafon, J.M., 2001. Magmatismo tipo A de 1,75 Ga na porção oriental do Escudo das Guianas – Estados do Amapá e Pará, Brasil. In: VII Simp. Geol. Amaz., Belém. CD ROM.
- Vasquez, M.L., Macambira, M.J.B., Galarza, M.A. (2005) Granitóides Transamazônicos na região Iriri-Xingu, Pará – novos dados geológicos e geocronológicos. In: Horbe, M.A.C. & Souza, V.S. (Eds.) *Contribuições à Geologia da Amazônia*, v.4, p. 16-31.
- Voicu, G., Bardoux, M., Stevenson, R., Jébrak, M., 2000. Nd and Sr isotope study of hydrothermal scheelite and host rocks at Omai, Guiana Shield: implications for ore fluid source and flow path during the formation of orogenic gold deposits. *Mineralium Deposita*, 35, 302-314.
- Wirth, K.R., Gibbs, A.K., Olszewski, W.J., 1986. U-Pb ages of zircons from the Grão Pará Group and Serra dos Carajás Granite, Pará, Brazil. *Revista Brasileira de Geociências*, 16, 195-200.
- Zhao, G., Cawood, P.A., Simon, A.W., Sun, M., 2002. Review of global 2.1-1.8 Ga orogens: implications for a pre-Rodinia supercontinent. *Earth Sciences Reviews*, 59, 125-162.

**Table 1** - Zircon Pb-evaporation isotopic results for the dated samples. Values in bold were included in the age calculations.

Zircon grain	T(°C)	No. of ratios	$\frac{^{206}\text{Pb}}{^{204}\text{Pb}}$	$\frac{^{208}\text{Pb}}{^{206}\text{Pb}}$	2 $\sigma$	$\frac{^{207}\text{Pb}}{^{206}\text{Pb}}$	$\frac{^{207}\text{Pb}^*}{^{206}\text{Pb}^*}$	2 $\sigma$	step age (Ga)	2 $\sigma$	grain age (Ga)	2 $\sigma$
<b>Jari Domain</b>												
<b>Jari-Guaribas Complex / enderbitic gneiss (sample JM-60)</b>												
JM60/01	1450	12	5952	0.0950	1040	0.2219	0.2189	163	2973	12		
	1500	38	27778	0.1105	64	0.2090	0.2087	41	2896	3		
	1550	40	38462	0.0939	42	0.2168	0.2164	54	2955	4	2955	4
JM60/02	1450	32	6623	0.2200	128	0.1896	0.1875	47	2720	4		
	1500	32	45455	0.1609	42	0.1932	0.1930	40	2769	3		
	1550	38	55556	0.1770	46	0.1946	0.1943	29	2779	2	2779	2
JM60/03	<b>1500</b>	<b>36</b>	<b>19608</b>	<b>0.0605</b>	<b>76</b>	<b>0.2582</b>	<b>0.2575</b>	<b>51</b>	<b>3232</b>	<b>3</b>		
	<b>1550</b>	<b>8</b>	<b>27027</b>	<b>0.0984</b>	<b>55</b>	<b>0.2598</b>	<b>0.2594</b>	<b>174</b>	<b>3244</b>	<b>11</b>	<b>3233</b>	<b>6</b>
JM60/04	1450	34	111111	0.0627	53	0.2459	0.2459	43	3159	3		
	1500	8	> 1000000	0.1234	60	0.2491	0.2491	193	3180	12	3180	12
JM60/05	<b>1450</b>	<b>8</b>	<b>&gt; 1000000</b>	<b>0.0566</b>	<b>67</b>	<b>0.2470</b>	<b>0.2470</b>	<b>127</b>	<b>3166</b>	<b>8</b>		
	<b>1500</b>	<b>36</b>	<b>200000</b>	<b>0.0886</b>	<b>70</b>	<b>0.2583</b>	<b>0.2583</b>	<b>63</b>	<b>3237</b>	<b>4</b>	<b>3237</b>	<b>4</b>
JM60/06	1450	36	200000	0.1025	81	0.1948	0.1948	50	2783	4		
	1500	36	> 1000000	0.1229	190	0.1945	0.1945	47	2780	4		
	1550	8	> 1000000	0.1576	149	0.1953	0.1953	109	2787	9	2782	3
JM60/07	<b>1450</b>	<b>38</b>	<b>66667</b>	<b>0.0666</b>	<b>44</b>	<b>0.2532</b>	<b>0.2531</b>	<b>36</b>	<b>3204</b>	<b>2</b>		
	<b>1500</b>	<b>24</b>	<b>76923</b>	<b>0.0544</b>	<b>17</b>	<b>0.2531</b>	<b>0.2530</b>	<b>57</b>	<b>3204</b>	<b>4</b>		
	<b>1550</b>	<b>36</b>	<b>23810</b>	<b>0.0636</b>	<b>66</b>	<b>0.2600</b>	<b>0.2596</b>	<b>48</b>	<b>3245</b>	<b>3</b>	<b>3245</b>	<b>3</b>
JM60/08	1550	36	200000	0.1294	93	0.2261	0.2260	86	3025	6	3025	6
JM60/09	<b>1450</b>	<b>16</b>	<b>41667</b>	<b>0.2239</b>	<b>520</b>	<b>0.1957</b>	<b>0.1954</b>	<b>64</b>	<b>2789</b>	<b>5</b>	<b>2789</b>	<b>5</b>
	1500	40	333333	0.2147	61	0.1932	0.1932	33	2770	3		
JM60/10	<b>1450</b>	<b>8</b>	<b>41667</b>	<b>0.3656</b>	<b>653</b>	<b>0.1956</b>	<b>0.1951</b>	<b>124</b>	<b>2786</b>	<b>10</b>		
	<b>1500</b>	<b>38</b>	<b>250000</b>	<b>0.1928</b>	<b>74</b>	<b>0.1954</b>	<b>0.1954</b>	<b>60</b>	<b>2788</b>	<b>5</b>	<b>2788</b>	<b>5</b>
JM60/11	<b>1450</b>	<b>36</b>	<b>30303</b>	<b>0.1467</b>	<b>59</b>	<b>0.1954</b>	<b>0.1951</b>	<b>49</b>	<b>2786</b>	<b>4</b>		
	<b>1500</b>	<b>40</b>	<b>111111</b>	<b>0.1007</b>	<b>35</b>	<b>0.1953</b>	<b>0.1953</b>	<b>34</b>	<b>2787</b>	<b>3</b>		
	<b>1550</b>	<b>34</b>	<b>166667</b>	<b>0.1190</b>	<b>79</b>	<b>0.1960</b>	<b>0.1960</b>	<b>37</b>	<b>2794</b>	<b>3</b>	<b>2789</b>	<b>5</b>
JM60/12	1450	36	125000	0.1733	43	0.1868	0.1867	37	2714	3		
	1500	38	> 1000000	0.1557	42	0.1891	0.1891	29	2735	2		
	1550	32	> 1000000	0.1688	116	0.1920	0.1920	77	2760	7	2760	7
JM60/13	1450	36	22727	0.2152	191	0.1935	0.1930	40	2769	3		
	1500	36	> 1000000	0.2237	55	0.1926	0.1926	40	2765	3		
	<b>1550</b>	<b>40</b>	<b>125000</b>	<b>0.2522</b>	<b>65</b>	<b>0.1954</b>	<b>0.1953</b>	<b>44</b>	<b>2787</b>	<b>4</b>	<b>2787</b>	<b>4</b>
JM60/14	1450	16	26316	0.1394	200	0.1920	0.1914	42	2755	4		
	<b>1500</b>	<b>32</b>	<b>52632</b>	<b>0.1009</b>	<b>96</b>	<b>0.1953</b>	<b>0.1952</b>	<b>42</b>	<b>2786</b>	<b>4</b>	<b>2786</b>	<b>4</b>
JM60/15	1500	36	66667	0.1980	60	0.1915	0.1913	24	2753	2		
	1550	38	47619	0.1972	80	0.1924	0.1921	46	2761	4	2761	4
<b>Mean Age (grains Z9+Z10+Z11+Z13+Z14 - 244 ratios - USD 1.5)</b>									<b>2788 ± 2 Ma</b>			
<b>Mean Age (grains Z3+Z5+Z7 - 116 ratios - USD 3.5)</b>									<b>3238 ± 6 Ma</b>			

Table 1 (continued)

Zircon grain	T(°C)	No. of ratios	$\frac{^{206}\text{Pb}}{^{204}\text{Pb}}$	$\frac{^{208}\text{Pb}}{^{206}\text{Pb}}$	2 $\sigma$	$\frac{^{207}\text{Pb}}{^{206}\text{Pb}}$	$\frac{^{207}\text{Pb}^*}{^{206}\text{Pb}^*}$	2 $\sigma$	step age (Ga)	2 $\sigma$	grain age (Ga)	2 $\sigma$
<b>Jari-Guaribas Complex / enderbite gneiss (sample MV-27A)</b>												
MV27A/4	1500	32	5917	0.0522	43	0.1811	0.1792	66	2646	6	2646	6
MV27A/5	1450	38	5747	0.0544	129	0.1831	0.1811	25	2663	2		
	1500	8	7246	0.1557	82	0.1930	0.1913	57	2754	5	2754	5
MV27A/6	1450	36	12821	0.0378	26	0.1895	0.1885	25	2729	2	2729	2
MV27A/9	1450	8	8621	0.0254	48	0.1635	0.1621	128	2478	13	2478	13
MV27A/11	1450	16	5376	0.0724	134	0.1859	0.1838	79	2688	7	2688	7
MV27A/12	<b>1500</b>	<b>4</b>	<b>16949</b>	<b>0.0366</b>	<b>59</b>	<b>0.1950</b>	<b>0.1943</b>	<b>220</b>	<b>2779</b>	<b>19</b>	<b>2779</b>	<b>19</b>
MV27A/14	<b>1450</b>	<b>8</b>	<b>11905</b>	<b>0.0197</b>	<b>61</b>	<b>0.1960</b>	<b>0.1950</b>	<b>64</b>	<b>2785</b>	<b>5</b>	<b>2785</b>	<b>5</b>
MV27A/16	<b>1450</b>	<b>36</b>	<b>4739</b>	<b>0.0888</b>	<b>36</b>	<b>0.1987</b>	<b>0.1962</b>	<b>53</b>	<b>2795</b>	<b>4</b>	<b>2795</b>	<b>4</b>
<b>Mean Age (3 grains - 48 ratios - USD 2.3)</b>									<b>2790 ± 8 Ma</b>			
<b>Guianense Complex / monzogranitic gneiss (sample LT-126A)</b>												
LT126A/1	1450	38	8547	0.1382	172	0.1781	0.1767	38	2622	4		
	1500	36	12987	0.1306	188	0.1769	0.1759	66	2615	6	2621	6
LT126A/2	1450	30	2732	0.1444	82	0.1528	0.1481	56	2324	6		
	1500	26	76923	0.1416	102	0.1754	0.1752	30	2609	3		
	1550	36	50000	0.1526	50	0.1764	0.1761	33	2617	3	2617	3
LT126A/3	1450	38	4386	0.2095	460	0.1628	0.1598	228	2454	24		
	1500	38	23810	0.1869	42	0.1763	0.1757	21	2613	2	2613	2
LT126A/4	1450	16	15873	0.1480	62	0.1727	0.1719	82	2576	8		
	<b>1500</b>	<b>38</b>	<b>83333</b>	<b>0.1402</b>	<b>43</b>	<b>0.1776</b>	<b>0.1775</b>	<b>23</b>	<b>2630</b>	<b>2</b>		
	<b>1550</b>	<b>38</b>	<b>90909</b>	<b>0.1429</b>	<b>34</b>	<b>0.1773</b>	<b>0.1773</b>	<b>39</b>	<b>2628</b>	<b>4</b>	<b>2629</b>	<b>2</b>
LT126A/5	1450	38	12821	0.1282	88	0.1745	0.1735	37	2592	4		<b>4</b>
	<b>1500</b>	<b>36</b>	<b>47619</b>	<b>0.1347</b>	<b>39</b>	<b>0.1775</b>	<b>0.1772</b>	<b>40</b>	<b>2627</b>	<b>4</b>	<b>2627</b>	<b>4</b>
LT126A/6	1450	16	4651	0.0750	197	0.1662	0.1634	73	2492	8	2492	<b>8</b>
LT126A/7	1450	28	16949	0.0756	153	0.1755	0.1747	62	2604	6		<b>4</b>
	<b>1500</b>	<b>34</b>	<b>200000</b>	<b>0.0630</b>	<b>20</b>	<b>0.1770</b>	<b>0.1769</b>	<b>38</b>	<b>2624</b>	<b>4</b>	<b>2624</b>	<b>4</b>
<b>Mean Age (3 grains - 146 ratios - USD 1.5)</b>									<b>2628 ± 2 Ma</b>			
<b>Noucouuru Intrusive Suite / mesoperthite-granite (sample LT-218)</b>												
LTR218/1	1485	36	31250	0.1033	27	0.1790	0.1786	24	2641	2	2641	2
LTR218/4	1500	30	6897	0.1190	67	0.1799	0.1780	63	2635	6	2635	6
LTR218/5	1500	4	6211	0.1245	255	0.1811	0.1792	47	2645	4	2645	4
LTR218/6	1500	38	15625	0.1081	32	0.1771	0.1763	28	2618	3	2618	3
	1530	34	17544	0.1059	30	0.1758	0.1752	46	2608	4		
LTR218/7	1500	36	3367	0.1177	55	0.1812	0.1773	80	2628	7	2628	7
LTR218/9	<b>1500</b>	<b>36</b>	<b>2551</b>	<b>0.1242</b>	<b>64</b>	<b>0.1849</b>	<b>0.1801</b>	<b>38</b>	<b>2654</b>	<b>3</b>	<b>2654</b>	<b>3</b>
LTR218/11	1450	34	2865	0.1106	75	0.1804	0.1761	134	2617	13		
	<b>1500</b>	<b>30</b>	<b>13889</b>	<b>0.1110</b>	<b>32</b>	<b>0.1815</b>	<b>0.1807</b>	<b>34</b>	<b>2660</b>	<b>3</b>	<b>2660</b>	<b>3</b>
LTR218/12	<b>1500</b>	<b>34</b>	<b>5525</b>	<b>0.1205</b>	<b>33</b>	<b>0.1822</b>	<b>0.1800</b>	<b>41</b>	<b>2653</b>	<b>4</b>	<b>2653</b>	<b>4</b>
<b>Mean Age (3 grains - 100 ratios - USD 2.2)</b>									<b>2656 ± 4 Ma</b>			

Table 1 (continued)

Zircon grain	T(°C)	No. of ratios	$\frac{^{206}\text{Pb}}{^{204}\text{Pb}}$	$\frac{^{208}\text{Pb}}{^{206}\text{Pb}}$	2 $\sigma$	$\frac{^{207}\text{Pb}}{^{206}\text{Pb}}$	$\frac{^{207}\text{Pb}^*}{^{206}\text{Pb}^*}$	2 $\sigma$	step age (Ga)	2 $\sigma$	grain age (Ga)	2 $\sigma$
<b>Noucouuru Intrusive Suite / mesoperthite-granite (sample NR-39)</b>												
NR39/1	1500	28	14085	0.1084	87	0.1783	0.1774	37	2629	3	2629	3
NR39/2	1450	36	15385	0.0825	247	0.1684	0.1676	131	2534	13		
	1450	47	33333	0.0858	56	0.1689	0.1685	18	2543	2		
	1500	40	35714	0.1070	71	0.1772	0.1769	25	2624	2	2624	2
NR39/3	1500	38	27778	0.0963	37	0.1778	0.1774	27	2629	3	2629	3
NR39/4	1450	38	7299	0.1047	61	0.1767	0.1747	36	2604	3		
	1500	36	31250	0.1182	29	0.1791	0.1787	39	2641	4	2641	4
NR39/5	1450	10	10870	0.0941	143	0.1768	0.1753	47	2609	4		
	1500	36	25000	0.0985	33	0.1761	0.1756	23	2612	2	2611	2
NR39/6	1450	36	4484	0.0985	103	0.1669	0.1645	180	2503	18		
	1500	26	37037	0.1137	43	0.1785	0.1782	23	2636	2	2636	2
NR39/7	1450	4	5714	0.0908	83	0.1744	0.1722	47	2579	5		
	1450	38	13514	0.0920	62	0.1788	0.1780	50	2635	5		
	<b>1500</b>	<b>32</b>	<b>28571</b>	<b>0.0941</b>	<b>47</b>	<b>0.1802</b>	<b>0.1798</b>	<b>43</b>	<b>2651</b>	<b>4</b>	<b>2651</b>	<b>4</b>
NR39/10	1450	14	6944	0.0946	263	0.1748	0.1728	62	2586	6		
	<b>1485</b>	<b>40</b>	<b>76923</b>	<b>0.1005</b>	<b>103</b>	<b>0.1796</b>	<b>0.1794</b>	<b>93</b>	<b>2648</b>	<b>9</b>	<b>2648</b>	<b>9</b>
	<b>1500</b>	<b>40</b>	<b>21277</b>	<b>0.1216</b>	<b>85</b>	<b>0.1800</b>	<b>0.1794</b>	<b>32</b>	<b>2648</b>	<b>3</b>	<b>2648</b>	<b>3</b>
<b>Mean Age (2 grains - 112 ratios - USD 1.1)</b>									<b>2649 ± 2 Ma</b>			
<b>Noucouuru Intrusive Suite / charnockite (sample MV-18A)</b>												
MV18A/1	1450	30	2841	0.1032	38	0.1699	0.1656	57	2514	6	2514	6
MV18A/3	1450	34	3165	0.0961	65	0.1709	0.1667	94	2525	9		
	1500	24	6329	0.1143	169	0.1792	0.1769	47	2625	4	2625	4
MV18A/6	1450	34	5525	0.0838	61	0.1587	0.1564	97	2417	11	2417	11
MV18A/7	1500	34	8772	0.1208	38	0.1708	0.1694	22	2552	2	2552	2
MV18A/8	1450	34	6250	0.0933	44	0.1655	0.1634	108	2491	11		
	1500	36	25000	0.0891	38	0.1752	0.1746	23	2603	2	2603	2
MV18A/9	1450	16	3175	0.0942	51	0.1695	0.1656	137	2514	14		
	1500	32	5747	0.0861	108	0.1706	0.1684	31	2542	3	2542	3
MV18A/10	1450	6	3300	0.0972	162	0.1695	0.1657	58	2515	6	2515	6
MV18A/11	1450	6	33333	0.0881	151	0.1611	0.1607	71	2463	7		
	1500	22	32258	0.0934	42	0.1667	0.1664	30	2522	3	2522	3
<b>Granitoids / monzogranite (sample LT-114)</b>												
LT114/1	1500	38	2639	0.15759	77	0.14355	0.13853	26	2209	3	2209	3
LT114/2	<b>1500</b>	<b>20</b>	<b>2801</b>	<b>0.1531</b>	<b>183</b>	<b>0.1435</b>	<b>0.1391</b>	<b>33</b>	<b>2216</b>	<b>4</b>	<b>2216</b>	<b>4</b>
LT114/5	<b>1500</b>	<b>32</b>	<b>3311</b>	<b>0.1456</b>	<b>236</b>	<b>0.1432</b>	<b>0.1392</b>	<b>26</b>	<b>2218</b>	<b>3</b>	<b>2218</b>	<b>3</b>
LT144/09	1500	34	14286	0.1783	156	0.1385	0.1376	60	2197	8	2197	8
LT114/10	1450	38	2740	0.0880	44	0.1432	0.1383	31	2206	4	2206	4
LT114/11	1500	22	2564	0.1788	85	0.1413	0.1358	170	2174	22	2174	22
LT114/12	<b>1500</b>	<b>8</b>	<b>5682</b>	<b>0.1574</b>	<b>203</b>	<b>0.1413</b>	<b>0.1390</b>	<b>166</b>	<b>2215</b>	<b>21</b>	<b>2215</b>	<b>21</b>
LT114/15	1500	38	4386	0.1081	29	0.1410	0.1379	25	2201	3	2201	3
LT114/17	<b>1500</b>	<b>6</b>	<b>6623</b>	<b>0.0947</b>	<b>148</b>	<b>0.1417</b>	<b>0.1398</b>	<b>65</b>	<b>2225</b>	<b>8</b>	<b>2225</b>	<b>8</b>
<b>Mean Age (4 grains - 66 ratios - USD 1.1)</b>									<b>2218 ± 3 Ma</b>			

Table 1 (continued)

Zircon grain	T(°C)	No. of ratios	$\frac{^{206}\text{Pb}}{^{204}\text{Pb}}$	$\frac{^{208}\text{Pb}}{^{206}\text{Pb}}$	2 $\sigma$	$\frac{^{207}\text{Pb}}{^{206}\text{Pb}}$	$\frac{^{207}\text{Pb}^*}{^{206}\text{Pb}^*}$	2 $\sigma$	step age (Ga)	2 $\sigma$	grain age (Ga)	2 $\sigma$
<b>Granitoids / monzogranite (sample EK-89)</b>												
EK89/02	1450	8	5319	0.1452	348	0.1379	0.1354	131	2170	17	2170	17
EK89/03	1450	28	4292	0.0963	120	0.1539	0.1507	181	2354	20		
	1500	38	20833	0.1105	39	0.1741	0.1735	21	2592	2	2592	2
	1550	32	15625	0.1158	30	0.1720	0.1712	44	2570	4		
EK89/6	<b>1500</b>	<b>38</b>	<b>41667</b>	<b>0.1548</b>	<b>69</b>	<b>0.1373</b>	<b>0.1369</b>	<b>31</b>	<b>2189</b>	<b>4</b>	<b>2189</b>	<b>4</b>
EK89/10	1450	16	3268	0.1705	1683	0.1355	0.1316	51	2120	7	2120	7
EK89/11	<b>1500</b>	<b>32</b>	<b>11364</b>	<b>0.1612</b>	<b>166</b>	<b>0.1376</b>	<b>0.1365</b>	<b>22</b>	<b>2184</b>	<b>3</b>	<b>2184</b>	<b>3</b>
EK89/16	<b>1500</b>	<b>34</b>	<b>6711</b>	<b>0.2073</b>	<b>48</b>	<b>0.1384</b>	<b>0.1364</b>	<b>35</b>	<b>2182</b>	<b>4</b>	<b>2182</b>	<b>4</b>
Mean Age (3 grains - 104 ratios - USD 1.8)									2185 ± 4 Ma			
<b>Parintins Intrusive Suite / monzogranite (sample JM-25)</b>												
JMR25/1	1450	36	4525	0.1255	94	0.1291	0.1257	71	2039	10		
	<b>1500</b>	<b>32</b>	<b>22222</b>	<b>0.1805</b>	<b>699</b>	<b>0.1271</b>	<b>0.1266</b>	<b>33</b>	<b>2051</b>	<b>5</b>	<b>2051</b>	<b>5</b>
JMR25/2	1500	30	41667	0.1404	111	0.1334	0.1332	61	2140	8	2140	8
JMR25/3	1450	30	2770	0.0912	161	0.1431	0.1384	50	2208	6	2208	6
JMR25/4	1450	16	3226	0.1488	255	0.1265	0.1224	60	1992	9		
	<b>1500</b>	<b>30</b>	<b>52632</b>	<b>0.3638</b>	<b>206</b>	<b>0.1266</b>	<b>0.1263</b>	<b>26</b>	<b>2048</b>	<b>4</b>	<b>2048</b>	<b>4</b>
JMR25/6	1450	34	2513	0.2100	176	0.1296	0.1243	67	2019	10		
	<b>1500</b>	<b>36</b>	<b>10101</b>	<b>0.3258</b>	<b>133</b>	<b>0.1274</b>	<b>0.1261</b>	<b>24</b>	<b>2045</b>	<b>3</b>	<b>2045</b>	<b>3</b>
JMR25/8	<b>1500</b>	<b>30</b>	<b>32258</b>	<b>0.2502</b>	<b>108</b>	<b>0.1271</b>	<b>0.1267</b>	<b>31</b>	<b>2053</b>	<b>4</b>	<b>2053</b>	<b>4</b>
JMR25/9	<b>1485</b>	<b>22</b>	<b>9259</b>	<b>0.2245</b>	<b>69</b>	<b>0.1281</b>	<b>0.1267</b>	<b>31</b>	<b>2052</b>	<b>4</b>	<b>2052</b>	<b>4</b>
JMR25/12	1500	32	7092	0.1370	202	0.1277	0.1259	24	2042	3	2042	3
Mean Age (5 grains - 150 ratios - USD 1.8)									2049 ± 3 Ma			
<b>Granitoids / syenogranite (sample LT-17)</b>												
LT17/4	<b>1500</b>	<b>38</b>	<b>2833</b>	<b>0.3520</b>	<b>99</b>	<b>0.1303</b>	<b>0.1253</b>	<b>38</b>	<b>2034</b>	<b>5</b>	<b>2034</b>	<b>5</b>
LT17/6	<b>1500</b>	<b>38</b>	<b>7299</b>	<b>0.2966</b>	<b>187</b>	<b>0.1269</b>	<b>0.1251</b>	<b>17</b>	<b>2031</b>	<b>2</b>	<b>2031</b>	<b>2</b>
LT17/7	<b>1500</b>	<b>40</b>	<b>4902</b>	<b>0.1717</b>	<b>96</b>	<b>0.1278</b>	<b>0.1251</b>	<b>26</b>	<b>2030</b>	<b>4</b>	<b>2030</b>	<b>4</b>
LT17/10	<b>1500</b>	<b>10</b>	<b>23810</b>	<b>0.2915</b>	<b>124</b>	<b>0.1261</b>	<b>0.1258</b>	<b>72</b>	<b>2040</b>	<b>10</b>	<b>2040</b>	<b>10</b>
LT17/13	<b>1500</b>	<b>30</b>	<b>5236</b>	<b>0.3251</b>	<b>91</b>	<b>0.1273</b>	<b>0.1249</b>	<b>32</b>	<b>2027</b>	<b>5</b>	<b>2027</b>	<b>5</b>
LT17/14	<b>1500</b>	<b>22</b>	<b>6452</b>	<b>0.3406</b>	<b>102</b>	<b>0.1269</b>	<b>0.1248</b>	<b>34</b>	<b>2026</b>	<b>5</b>		
	<b>1550</b>	<b>28</b>	<b>6289</b>	<b>0.3711</b>	<b>97</b>	<b>0.1270</b>	<b>0.1250</b>	<b>48</b>	<b>2028</b>	<b>7</b>	<b>2027</b>	<b>4</b>
Mean Age (6 grains - 206 ratios - USD 1.3)									2030 ± 2 Ma			
<b>Carecuru Domain</b>												
<b>Paru-Maratiá Complex / granodioritic gneiss (sample MV-65A)</b>												
MV65A/1	1450	40	2513	0.0932	100	0.1241	0.1188	46	1938	7		
	1480	40	12821	0.1148	37	0.1369	0.1360	27	2177	3	2177	3
MV65A/2	1450	40	10526	0.0282	28	0.1308	0.1294	54	2090	7		
	<b>1500</b>	<b>30</b>	<b>33333</b>	<b>0.1123</b>	<b>37</b>	<b>0.1375</b>	<b>0.1371</b>	<b>22</b>	<b>2191</b>	<b>3</b>	<b>2191</b>	<b>3</b>
MV65A/4	1450	30	4082	0.0687	140	0.1336	0.1304	48	2103	7		
	<b>1500</b>	<b>34</b>	<b>52632</b>	<b>0.0893</b>	<b>25</b>	<b>0.1373</b>	<b>0.1370</b>	<b>39</b>	<b>2190</b>	<b>5</b>	<b>2190</b>	<b>5</b>

Table 1 (continued)

Zircon grain	T(°C)	No. of ratios	$\frac{^{206}\text{Pb}}{^{204}\text{Pb}}$	$\frac{^{208}\text{Pb}}{^{206}\text{Pb}}$	2 $\sigma$	$\frac{^{207}\text{Pb}}{^{206}\text{Pb}}$	$\frac{^{207}\text{Pb}^*}{^{206}\text{Pb}^*}$	2 $\sigma$	step age (Ga)	2 $\sigma$	grain age (Ga)	2 $\sigma$
<b>Paru-Maratiá Complex / granodioritic gneiss (sample MV-65A)</b>												
MV65A/5	1450	8	9259	0.0795	52	0.1962	0.1949	75	2784	6	2784	6
	1500	8	>1000000	0.1044	57	0.1900	0.1900	88	2742	8		
MV65A/6	1450	6	5814	0.0864	140	0.1376	0.1354	59	2169	8	2169	8
MV65A/7	1450	32	10000	0.0552	102	0.1319	0.1307	18	2107	2	2107	2
MV65A/9	1450	8	4016	0.0691	210	0.1328	0.1295	90	2091	12	2091	12
MV65A/10	1450	40	16949	0.0716	210	0.1330	0.1322	20	2128	3		
	1500	34	43478	<b>0.1133</b>	<b>57</b>	<b>0.1374</b>	<b>0.1371</b>	<b>57</b>	<b>2191</b>	<b>7</b>	<b>2191</b>	<b>7</b>
MV65A/13	1550	36	4386	0.0377	151	0.1303	0.1274	34	2063	5	2063	5
<b>Mean Age (3 grains - 98 ratios - USD 0.2)</b>									<b>2191 <math>\pm</math> 2 Ma</b>			
<b>Carecuru Intrusive Suite / diorite (sample LT-193)</b>												
LT193/1	1500	8	41667	0.1574	631	0.1307	0.1304	446	2103	60		
	1500	20	37037	<b>0.1663</b>	<b>132</b>	<b>0.1333</b>	<b>0.1330</b>	<b>39</b>	<b>2139</b>	<b>5</b>	<b>2139</b>	<b>5</b>
LT193/2	1450	28	5618	0.1635	96	0.1346	0.1322	33	2127	4		
	1500	36	12195	<b>0.1760</b>	<b>143</b>	<b>0.1338</b>	<b>0.1328</b>	<b>45</b>	<b>2135</b>	<b>6</b>	<b>2135</b>	<b>6</b>
LT193/3	1450	24	9901	<b>0.1526</b>	<b>286</b>	<b>0.1336</b>	<b>0.1328</b>	<b>24</b>	<b>2135</b>	<b>3</b>	<b>2135</b>	<b>3</b>
LT193/5	1500	40	14085	<b>0.1654</b>	<b>84</b>	<b>0.1340</b>	<b>0.133</b>	<b>19</b>	<b>2138</b>	<b>2</b>	<b>2138</b>	<b>2</b>
LT193/6	1500	36	50000	<b>0.1666</b>	<b>111</b>	<b>0.1334</b>	<b>0.1332</b>	<b>35</b>	<b>2140</b>	<b>5</b>		
	1550	34	43478	<b>0.1826</b>	<b>55</b>	<b>0.1339</b>	<b>0.1336</b>	<b>32</b>	<b>2145</b>	<b>4</b>	<b>2143</b>	<b>5</b>
LT193/7	1450	36	15625	<b>0.1461</b>	<b>65</b>	<b>0.1338</b>	<b>0.133</b>	<b>34</b>	<b>2138</b>	<b>4</b>		
	1500	30	35714	<b>0.1804</b>	<b>125</b>	<b>0.1335</b>	<b>0.1331</b>	<b>46</b>	<b>2139</b>	<b>6</b>	<b>2139</b>	<b>4</b>
LT193/8	1450	20	5917	<b>0.1822</b>	<b>73</b>	<b>0.1347</b>	<b>0.1328</b>	<b>109</b>	<b>2135</b>	<b>14</b>		
	1500	16	8696	<b>0.1755</b>	<b>75</b>	<b>0.1353</b>	<b>0.1338</b>	<b>85</b>	<b>2149</b>	<b>11</b>	<b>2144</b>	<b>13</b>
<b>Mean Age (7 grains - 292 ratios - USD 1.5)</b>									<b>2139 <math>\pm</math> 2 Ma</b>			
<b>Granitoids / monzogranite (sample LT-177)</b>												
LT177/1	1550	10	10753	0.1187	89	0.1376	0.1361	137	2178	18	2178	18
LT177/3	1500	32	26316	0.1275	32	0.1366	0.1361	20	2179	3	2179	3
LT177/5	1500	6	>1000000	0.1292	62	0.1345	0.1345	134	2157	17	2157	17
LT177/6	1450	18	3546	0.1489	90	0.1396	0.1360	71	2177	9	2177	9
LT177/11	1500	38	35714	0.1285	176	0.1357	0.1353	52	2169	7	2169	7
LT177/16	1500	40	7407	0.1134	50	0.1377	0.1359	28	2176	4	2176	4
<b>Mean Age (5 grains - 138 ratios - USD 1.5)</b>									<b>2177 <math>\pm</math> 3 Ma</b>			

Table 1 (continued)

Zircon grain	T(°C)	No. of ratios	$\frac{^{206}\text{Pb}}{^{204}\text{Pb}}$	$\frac{^{208}\text{Pb}}{^{206}\text{Pb}}$	2 $\sigma$	$\frac{^{207}\text{Pb}}{^{206}\text{Pb}}$	$\frac{^{207}\text{Pb}^*}{^{206}\text{Pb}^*}$	2 $\sigma$	step age (Ga)	2 $\sigma$	grain age (Ga)	2 $\sigma$
<b>Granitoids / syenogranite (sample LT-207B)</b>												
LT207B/2	1500	24	6452	0.0885	54	0.1314	0.1294	32	2090	4	2090	4
LT207B/4	1500	32	2688	0.0849	71	0.1336	0.1287	36	2081	5	2081	5
LT207B/5	<b>1500</b>	<b>32</b>	<b>5376</b>	<b>0.0850</b>	<b>63</b>	<b>0.1324</b>	<b>0.1300</b>	<b>21</b>	<b>2098</b>	<b>3</b>	<b>2098</b>	<b>3</b>
LT207B/15	<b>1500</b>	<b>32</b>	<b>7042</b>	<b>0.0919</b>	<b>44</b>	<b>0.1320</b>	<b>0.1300</b>	<b>18</b>	<b>2099</b>	<b>2</b>	<b>2099</b>	<b>2</b>
Mean Age (2 grains - 64 ratios - USD 0.5)									2098 ± 2 Ma			
<b>Paru Domain</b>												
<b>Ananaí Complex / trondhjemitic gneiss (sample LT-191A)</b>												
LT191A/1	1450	34	3401	0.1022	54	0.1350	0.1315	29	2118	4		
	<b>1500</b>	<b>38</b>	<b>24390</b>	<b>0.1134</b>	<b>27</b>	<b>0.1344</b>	<b>0.1339</b>	<b>16</b>	<b>2150</b>	<b>2</b>		
	<b>1550</b>	<b>8</b>	<b>18868</b>	<b>0.1134</b>	<b>139</b>	<b>0.1345</b>	<b>0.1338</b>	<b>95</b>	<b>2149</b>	<b>12</b>	<b>2149</b>	<b>2</b>
LT191A/2	1450	18	4926	0.1350	55	0.1353	0.1326	25	2133	3		
	<b>1500</b>	<b>34</b>	<b>26316</b>	<b>0.0715</b>	<b>30</b>	<b>0.1345</b>	<b>0.134</b>	<b>19</b>	<b>2152</b>	<b>2</b>	<b>2152</b>	<b>2</b>
LT191A/3	1450	32	10204	0.0547	167	0.1316	0.1303	46	2102	6	2102	6
LT191A/4	1450	32	8333	0.0966	48	0.1337	0.1322	21	2128	3	2128	3
LT191A/5	<b>1500</b>	<b>34</b>	<b>31250</b>	<b>0.0451</b>	<b>19</b>	<b>0.1335</b>	<b>0.1331</b>	<b>19</b>	<b>2140</b>	<b>2</b>		
	<b>1550</b>	<b>34</b>	<b>45455</b>	<b>0.0505</b>	<b>50</b>	<b>0.1336</b>	<b>0.1333</b>	<b>21</b>	<b>2142</b>	<b>3</b>	<b>2141</b>	<b>2</b>
LT191A/9	1450	36	5128	0.0851	56	0.1291	0.1263	55	2048	8	2048	8
LT191A/14	<b>1500</b>	<b>28</b>	<b>6711</b>	<b>0.0565</b>	<b>57</b>	<b>0.1351</b>	<b>0.1332</b>	<b>26</b>	<b>2141</b>	<b>3</b>	<b>2141</b>	<b>3</b>
LT191A/15	1450	34	8621	0.1025	56	0.1330	0.1315	17	2118	2		
	1500	40	41667	0.0880	45	0.1325	0.1321	23	2127	3	2127	3
LT191A/16	1450	34	43478	0.0991	12	0.1324	0.1322	37	2127	5		
	<b>1500</b>	<b>8</b>	<b>111111</b>	<b>0.0812</b>	<b>196</b>	<b>0.1332</b>	<b>0.1331</b>	<b>134</b>	<b>2140</b>	<b>18</b>	<b>2140</b>	<b>18</b>
Mean Age (Z1 + Z2 - 80 ratios - USD 1.0)									2150 ± 2 Ma			
Mean Age (Z5 + Z14 + Z16 - 104 ratios - USD 0.8)									2141 ± 2 Ma			
<b>Igarapé Urucu Intrusive Suite / charnockite (sample LT-185A)</b>												
LT185A/1	<b>1500</b>	<b>32</b>	<b>4405</b>	<b>0.1926</b>	<b>182</b>	<b>0.1314</b>	<b>0.1284</b>	<b>40</b>	<b>2076</b>	<b>5</b>	<b>2076</b>	<b>5</b>
LT185A/4	<b>1500</b>	<b>36</b>	<b>4329</b>	<b>0.2074</b>	<b>152</b>	<b>0.1305</b>	<b>0.1276</b>	<b>68</b>	<b>2066</b>	<b>9</b>	<b>2066</b>	<b>9</b>
LT185A/7	<b>1500</b>	<b>32</b>	<b>2564</b>	<b>0.2093</b>	<b>189</b>	<b>0.1343</b>	<b>0.1282</b>	<b>38</b>	<b>2074</b>	<b>5</b>	<b>2074</b>	<b>5</b>
LT185A/9	1500	36	2994	0.0994	25	0.1312	0.1266	26	2052	4	2052	4
Mean Age (3 grains - 92 ratios - USD 1.4)									2074 ± 5 Ma			

\* radiogenic

**Table 2** - Whole rock Sm-Nd isotopic data from the studied samples.  $T_{DM}$  ages were calculated using the DePaolo (1981) model for Nd evolution of the depleted mantle. References for the crystallization ages: 1 - this work, 2: Rosa-Costa et al. (2003); 3 - estimated age, 4 - Ricci et al. (2002).

Lithology/Sample	Stratigraphic Unit	Sm (ppm)	Nd (ppm)	$\frac{^{147}\text{Sm}}{^{144}\text{Nd}}$	$\frac{^{143}\text{Nd}}{^{144}\text{Nd}}$	$2\sigma$ ( $10^{-5}$ )	f (Sm/Nd)	$\epsilon_{\text{Nd}}(0)$	Zircon Age (Ga)	Ref.	$T_{DM}$ (Ga)	$\epsilon_{\text{Nd}}(t)$
<b>Jari Domain</b>												
enderbitic gneiss/JM-60		5.21	34.91	0.09022	0.51048	2	-0.5413	-42.19	2.79	1	<b>3.21</b>	<b>-3.97</b>
enderbitic gneiss/MV-48	Jari-Guaribas Complex	7.40	37.88	0.11810	0.51103	1	-0.3996	-31.33	2.80	2	<b>3.26</b>	<b>-3.12</b>
enderbitic gneiss/MV-27A		4.17	23.78	0.10601	0.51082	4	-0.4611	-35.46	2.79	1	<b>3.19</b>	<b>-2.91</b>
granitic gneiss/MV-39B	Baixo Mapari Complex	18.94	104.68	0.10941	0.51094	0.4	-0.4438	-33.12	2.65	3	<b>3.12</b>	<b>-3.38</b>
mesoperthite-granite/LT-218		17.17	86.33	0.12025	0.51121	1	-0.3887	-27.91	2.65	1	<b>3.04</b>	<b>-1.86</b>
mesoperthite-granite/LT-213	Noucoure Intrusive Suite	17.83	93.61	0.11515	0.51110	2	-0.4146	-29.94	2.65	3	<b>3.04</b>	<b>-2.15</b>
charnoenderbite/JM-07		11.5	60.88	0.11424	0.51112	1	-0.4192	-29.71	2.60	4	<b>2.99</b>	<b>-2.14</b>
charnockite/MV-18A		12.97	70.28	0.11156	0.51105	1	-0.4328	-31.00	2.62	1	<b>3.01</b>	<b>-2.31</b>
granodiotitic gneiss/LT-40		5.28	35.59	0.08976	0.51076	1	-0.5437	-36.63	2.65	2	<b>2.83</b>	<b>-0.17</b>
monzogranitic gneiss/LT-126A	Guianense Complex	6.45	40.94	0.09520	0.51078	1	-0.5160	-36.17	2.63	1	<b>2.94</b>	<b>-1.87</b>
tonalitic gneiss/LT-123A		2.33	14.80	0.09538	0.51080	2	-0.5151	-35.93	2.63	3	<b>2.92</b>	<b>-1.65</b>
granodioritic gneiss/LT-11A		14.95	85.93	0.10519	0.51094	0.6	-0.4652	-33.14	2.65	3	<b>2.99</b>	<b>-1.95</b>
monzogranite/EK-89		5.40	36.62	0.08917	0.51117	0.8	-0.5467	-28.66	2.18	1	<b>2.30</b>	<b>+1.47</b>
alkali feldspar-granite/MV-07	Granitoids	16.97	90.70	0.11308	0.51142	0.8	-0.4251	-23.86	2.15	1	<b>2.48</b>	<b>-0.87</b>
syenogranite/LT-17		4.48	23.55	0.11510	0.51142	1	-0.4148	-23.68	2.03	1	<b>2.52</b>	<b>-2.42</b>
monzogranite/JM-25	Parintins Intrusive Suite	4.89	34.43	0.08591	0.51100	1	-0.5632	-31.95	2.05	1	<b>2.45</b>	<b>-2.51</b>
<b>Carecuru Domain</b>												
granodioritic gneiss/MV-65A		2.87	14.46	0.12003	0.51154	0.8	-0.3898	-21.36	2.19	3	<b>2.45</b>	<b>+0.22</b>
granodioritic gneiss/LT-206A		1.77	14.27	0.07507	0.51089	3	-0.6184	-34.18	2.15	3	<b>2.38</b>	<b>-0.58</b>
tonalitic gneiss/LT-202A	Paru-Maratiá Complex	4.45	22.87	0.11773	0.51151	7	-0.4015	-21.96	2.15	2	<b>2.44</b>	<b>-0.15</b>
dioritic gneiss/LT-196B		4.36	23.67	0.11135	0.51142	3	-0.4339	-23.72	2.15	3	<b>2.43</b>	<b>-0.15</b>
diorite/LT-193	Carecuru Intrusive Suite	3.37	17.56	0.11595	0.51158	2	-0.4105	-20.58	2.14	1	<b>2.28</b>	<b>+1.63</b>
diorite/LT-76		3.89	19.61	0.11983	0.51151	0.5	-0.3908	-21.96	2.14	2	<b>2.50</b>	<b>-0.84</b>
metavolcanic/LT-182C	Supracrustal Sequences	7.80	45.67	0.10326	0.51131	0.8	-0.4750	-25.89	2.14	3	<b>2.40</b>	<b>-0.20</b>
metavolcanic/LT-61A		6.18	28.99	0.12890	0.51166	2	-0.3447	-19.00	2.14	3	<b>2.49</b>	<b>-0.36</b>
monzogranite/LT-177		6.65	40.65	0.09895	0.51120	1	-0.4969	-28.07	2.17	1	<b>2.46</b>	<b>-0.69</b>
syenogranite/LT207B	Granitoids	2.85	16.87	0.10211	0.51099	1	-0.4809	-32.09	2.1	1	<b>2.83</b>	<b>-6.61</b>
syenogranite/LT-207B		2.91	17.11	0.10274	0.51101	4	-0.4777	-31.76	2.1	1	<b>2.82</b>	<b>-6.45</b>
monzogranite/LT-201		3.54	19.88	0.10776	0.51138	0.8	-0.4522	-24.50	2.1	3	<b>2.40</b>	<b>-0.51</b>
<b>Paru Domain</b>												
enderbitic gneiss/MV-70D	Ananaí Complex	3.24	24.64	0.07963	0.51057	1.5	-0.5952	-40.32	2.6	2	<b>2.83</b>	<b>-1.16</b>
trondhjemitic gneiss/LT-191A		0.90	5.10	0.10612	0.51142	2	-0.4605	-23.86	2.15	1	<b>2.32</b>	<b>+1.17</b>
charnockite/LT-185A		24.62	165.49	0.08993	0.51094	2	-0.5428	-33.16	2.07	1	<b>2.61</b>	<b>-4.80</b>
charnockite/MV-71A	Igarapé Urucu Intrusive Suite	7.29	48.24	0.09138	0.51091	0.5	-0.5354	-33.73	2.06	2	<b>2.68</b>	<b>-5.89</b>
charnockite/MV-68A		27.61	198.88	0.08394	0.51082	2	-0.5733	-35.46	2.07	1	<b>2.63</b>	<b>-5.51</b>

## Appendix I

### *Description of dated samples*

Mineral abbreviations: plagioclase - pl, quartz - qz, alkali feldspar - Kfs, biotite - bt, hornblende - hb, orthopyroxene - opx, clinopyroxene - cpx, garnet - grt, opaque minerals - opq, apatite - ap, zircon - zr, sphene - sph, monazite-mz, allanite - al, epidote - ep, sericite - sr, chlorite-chl, muscovite - ms.

### **Jari-Guaribas Complex**

Samples JM-60 (N00°09'57''/W52°37'30.09''), MV-27A (N00°45'04.01''/W53°11'16.01''), MV-48 (N00°55'04.01''/W53°05'41.05'') – Enderbitic to charnoenderbitic gneisses, grey and medium-grained. The mineralogical assemblage in equilibrium is defined by antiperthitic pl, qz, bt, mesoperthitic Kfs, with minor cpx, opx and opq. Hornblende occurs only in the gneiss MV-48. Accessories are ap and zr, besides mz in the sample MV-27A. These rocks present pervasive foliation and in the sample MV-48 the compositional banding is well defined. Microscopically the texture is granoblastic (JM-60, MV-27A), with polygonal or interlobate contacts, or granolepidoblastic (MV-48). Mafic minerals are grouped in bands, with preferred orientation. Metamorphic retrogressions are chloritization of the bt, pyroxenes altered to bt or hb and pl to sr.

### **Baixo-Mapari Complex**

Sample MV-39 B (N00°46'01.01''/W53°05'32'') – Pink, medium-grained granitic gneiss. The mineralogy is composed of mesoperthitic Kfs, qz, hb, bt, pl, opq, and accessories are ap and zr. It presents a well defined banding, characterized microscopically by alternating granoblastic quartz-feldspatic and lepidoblastic mafic layers. Locally the pl is partially altered to sr.

### **Guianense Complex**

Samples LT-40 (N00°03'58.98''/W53°00'39.70''), LT-123A (S00°06'00.11''/W52°57'08.61''), LT-126A (N00°03'16.70''/W53°00'56.29'') – Medium-grained grey gneisses, classified in terms of igneous terminology, as tonalitic gneiss (LT-123A), granodioritic gneiss (LT-40) and mozogranitic gneiss (LT-126A). The mineralogy is pl, qz and Kfs, with variable amounts of bt. Accessories are ap, zr and al. The gneisses exhibit a well defined banding, produced by alternating of centimeter-scale bt-rich and quartz-feldspar-rich layers. Microscopically, the texture is defined by inter-layered granoblastic and lepidoblastic bands (LT-40, LT-126A) or is porphyroclastic (LT-123A).

Sample LT-11A (S00°14'07.30''/W52°45'36.91'') – A coarse-grained granodioritic augen gneiss, composed of pl, qz, bt, hb and Kfs. Accessories are sph, ap and zr. The texture is milonitic, defined by 1-3 cm long augens of Kfs or quartz-feldspatic aggregates, surrounded by strings of mafic minerals and medium-grained quartz-feldspatic long shaped aggregates. Metamorphic retrogressions in these gneisses are indicated by chloritization of the hb and bt, alteration of the bt to ms and sericitization of the pl.

**Noucouru Intrusive Suite**

Samples JM-07 (S00°02'25.81"/W52°48'18.12"), LT-213 (N00°30'58.57"/W52°38'02.52"), LT-218 (N00°27'38.74"/W52°35'40.23"), MV-18A (N00°53'33"/W53°21'43.02"), NR-39 (N00°25'42"/W52°31'49") – They are medium- to coarse-grained rocks, rose, greenish or brownish, massive or weakly deformed, classified as mesoperthite-granites (NR-39, LT-213, LT-218), charnockite (MV-18A) and gr-charnoenderbite (JM-07). The mineralogy is composed of mesoperthitic Kfs, qz, antiperthitic pl, bt, hb, opx, cpx, grt, opq, ap, zr, and al. Opx occurs in the samples JM-07 and MV-18A and cpx and gr only in the former. The texture can be inequigranular (LT-213, LT-218, MV-18A) with interlobate contacts, or porphyroclastic (JM-07), with medium-grained granuloblastic polygonal matrix.

**Paru-Maratiá Complex**

Samples LT-196B (S00°09'26.70"/W53°47'03.23"), LT-202A (S00°21'58.51"/W53°43'07.79"), LT-206A (S00°28'37.79"/W53°37'25.10"), MV-65A (N00°10'25.18"/W53°51'21.81") – Grey to pale grey and medium- to coarse-grained gneisses. The mineralogy is defined by pl, qz, Kfs, bt, hb, opq and grt. The hb occurs in the samples LT-196B and LT-202A, and the grt is present only in the sample MV-65A. The accessories are ap, zr and sph. In terms of igneous terminology they are classified as dioritic (LT-196B), tonalitic (LT-202A) and graodioritic (LT-206A, MV-65A). The texture is inequigranular interlobate (LT-206A), with qz recrystallised and preferred orientation of the bt, or protomylonitic (LT-196A, LT-201, LT-202A, MV-65A), defined by porphyroclasts of pl, Kfs or hb, within a fine- to medium-grained recrystallised matrix, containing polycrystalline ribbons of qz and mafic anastomosed bands. Retrograde alterations are pl sericitized, hb altered to bt or chl and primary bt to chl.

**Ananaí Complex**

Sample MV-70D (S00°02'31.69"/W53°47'32.31") – Leucoenderbitic gneiss, medium- to fine-grained, pale grey, where coexist in equilibrium pl, qz, opx, opq and cpx. Plagioclase is antiperthitic and coupled with qz defines about 90% of the rock. The pyroxenes are retrogressed to bt along cleavage planes. Accessories are ap and zr. The zr are small sub-rounded grains. In outcrop this granulite are clearly foliated, and microscopically present granuloblastic texture, with polygonal or interlobate contacts and pyroxenes showing a weak preferred orientation.

LT-191A (S00°01'31.31"/W53°50'03.41") – Pale grey and medium-grained trondhjemitic gneiss, defined by pl, qz, bt and opq. Quartz and pl represent more than 95% of the rock. The texture is inequigranular interlobate, with qz recrystallized in the boundaries and preferred orientation of the bt. Plagioclase is altered to white mica and bt to chl.

**Carecuru Intrusive Suite**

Samples LT-76 (S00°14'59.50"/W53°15'46") and LT-193 (N00°06'36.65"/W53°15'45.94") – They are diorites, grey to dark grey, medium- to coarse- grained. The sample LT-76 presents inequigranular hypidiomorphic to idiomorphic texture, and the sample LT-193 is weakly deformed, showing porphyroclastic texture. The mineralogy is composed of pl, hb, bt, qz, opq, sph, ap and zr.

### Igarapé Urucu Intrusive Suite

Samples LT-185A (N00°04'30.69"/W53°48'26.60"), MV-68A (N00°06'30.20"/W53°49'05.62"), MV-71A (N00°01'54.38"/W53°48'07.60") – Rose to pale brown, coarse grained igneous charnockites. The sample MV-71A presents porphyritic texture, defined by subhedral 0.5-2.0 cm long Kfs within a medium-grained matrix. The samples LT-185A and MV-68A are more deformed and the texture is porphyroclastic. Alkali-feldspar and qz represent about 50% of the assemblage, coexisting with minor bt, pl, hb, opx, cpx and opq. The Kfs is strongly mesoperthitic. The opx and cpx are in equilibrium with other minerals or are replaced by hb and bt along fractures and cleavages planes. Accessory minerals are zr, ap, sph and al.

### Granitoids

Samples EK-89 (S00°20'05.36"/W52°52'13.69"), LT-17 (S00°03'47.50"/W52°57'58.91"), LT-114 (N00°07'11.49"/W53°13'22.60"), LT-177 (S00°08'47.80"/W53°16'42.81"), LT-201 (S00°20'10"/W53°45'35.21"), LT-207B (S00°29'29.62"/W53°34'46.82"), MV-07 (N00°35'37.98"/W53°09'07.99") – They consist on pale rose to pale grey and medium- to coarse-grained leucogranites, weakly deformed or well foliated, composed of Kfs, qz, pl, with minor bt and opq, and the accessories are zr and ap. Based on quartz-feldspar ratios, they are classified as alkali feldspar-granite (MV-07), sienogranites (LT-17, LT-207B) and monzogranites (EK-89, LT-114, LT-177, LT-201). The granites EK-89, LT-177 and MV-07 present texture inequigranular hypidiomorphic, with qz variably recrystallised. The sample LT-17 contains bt and ms, besides grt, consisting in a typical two-mica granite. It presents milonitic texture, with porphyroclasts of Kfs in a matrix with quartz-feldspar recrystallized aggregates, polycrystalline ribbons of quartz and oriented strings of mica. The granite LT-114 is strongly striped, composed of alternating recrystallised quartz-feldspatic layers and quartz ribbons. In these rocks the pl is frequently altered to sr and ep and the bt is chloritized or transformed to ms. The granite LT-207B shows mylonitic texture.

### Parintins Intrusive Suite

Sample JM-25 (N00°22'27.11"/W53°59'39.59") – Pale grey, medium-grained and massive monzogranite, composed of qz, pl, Kfs, bt, opq, ap, zr and al. The texture is equigranular hypidiomorphic with interlobate contacts. Plagioclase is partially altered to white mica.

### Metavolcano-sedimentary Sequences

**Fazendinha** - sample LT-61A (S00°11'16.20"/W53°09'16.51") – Grey and fine-grained massive rock. The composition is dacitic, defined by pl, qz, Kfs, bt, ms and opq. The texture is porphyritic, with euhedral pl within a fine grained matrix.

**13 de Maio** - sample LT-182C (N00°26'11.83"/W53°10'40.07") – White, fine grained and foliated rock. The composition is dacitic to qz-andesitic (pl, qz, Kfs ?, opq, mica). Microscopically, the texture is mylonitic, defined by oriented porphyroclasts of pl within a quartz-feldspatic fine matrix, with bands of opaque minerals and strings of white mica.

## 7 – GEOCROLOGIA U-Th-Pb EM MONAZITAS

Idades químicas de monazitas obtidas pelo método U-Th-Pb serão apresentadas neste capítulo, as quais, associadas às informações estruturais, permitiram a identificação de dois importantes eventos de retrabalhamento de crosta arqueana no Bloco Amapá, que representam estágios distintos da evolução tectono-termal transamazônica na área estudada. Os resultados alcançados são apresentados na forma de um artigo científico, submetido ao *Journal of South American Earth Sciences*. A tabela relativa às análises U-Th-Pb em monazitas, a qual não foi incorporada ao referido artigo, é apresentada no Anexo II.

### 7.1 – ELECTRON MICROPROBE U-Th-Pb MONAZITE DATING OF THE TRANSAMAZONIAN HIGH-GRADE METAMORPHIC OVERPRINT ON ARCHEAN ROCKS FROM AMAPÁ BLOCK, SOUTHEASTERN GUIANA SHIELD, NORTHERN BRAZIL

Lúcia T. da Rosa-Costa<sup>a\*</sup>, Jean M. Lafon<sup>b</sup>, Alain Cocherie<sup>c</sup>, Claude Delor<sup>c</sup>

<sup>a</sup> CPRM – Geological Survey of Brazil, Belém, Brazil

<sup>b</sup> Laboratório Pará-Iso, Universidade Federal do Pará, Belém, Brazil

<sup>c</sup> BRGM, BP 6009, Orléans, France

#### Abstract

The Amapá Block, southeastern Guiana Shield, represents an Archean block involved in an exceptionally large Paleoproterozoic belt, with evolution related to the Transamazonian event (2.26-1.95 Ga). High spatial resolution dating using an electron-probe microanalyzer (EPMA) was employed to obtain U-Th-Pb chemical ages in monazites of seven rocks from the Archean basement from that block, which underwent granulite- and amphibolite-facies metamorphism. Pb-Pb zircon dating was also performed on one sample.

Monazite and zircon ages demonstrated that the metamorphic overprinting of the Archean basement occurred during the Transamazonian orogenesis, and two main tectono-thermal events were recorded. The first one was revealed by the monazite ages of  $2096 \pm 6$  Ma,  $2093 \pm 8$  Ma,  $2088 \pm 8$  Ma,  $2087 \pm 3$  Ma and  $2086 \pm 8$  Ma, and by the zircon age of  $2091 \pm 5$  Ma obtained in granulitic rocks. These concordant ages provided a reliable estimate of the time of the granulite-

facies metamorphism in the southwestern of Amapá Block and, coupled with petro-estructural data, suggest that it was contemporaneous to the development of a thrusting system associated to the collisional stage of the Transamazonian orogen, at about 2.10-2.09 Ga.

The later event, occurred under amphibolite-facies conditions, was testified by monazite ages of  $2056 \pm 7$  Ma and  $2038 \pm 6$  Ma, and is consistent with a late-orogenic stage marked by granitic emplacement and coeval migmatization of the Archean basement along strike-slip zones.

**Key Words:** Transamazonian Event, electron microprobe, U-Th-Pb dating, monazite, Amazonian Craton

### 1- Introduction

The eastern portion of the Guiana Shield, in South America, consists of an exceptionally large Paleoproterozoic belt, named Maroni-Itacaiúnas Province (Tassinari and Macambira, 2004), which evolved during the Transamazonian orogenic cycle (2.26 - 1.95 Ga) and that matches with the Eburnean orogen in West African Craton (Feybesse and Milesi, 1994; Ledru et al., 1994; Théveniaut et al., submitted). Despite the coherent Paleoproterozoic geochronological pattern of this belt, two major Archean domains have been documented in its northwestern and southeastern portions (Fig. 1), the Imataca Block in Venezuela (Montgomery and Hurley, 1978; Montgomery, 1979; Tassinari et al., 2001) and the Amapá Block in the north of Brazil (Rosa-Costa et al., in press). Granulitic complexes are widespread in the Archean blocks and also occur in Paleoproterozoic domains, as the well known granulites from the Bakhuis Mountains, in Suriname (Fig. 1).

Available geochronological data acquired on granulitic complexes from eastern Guiana Shield, which present both Archean and Paleoproterozoic protoliths, reveal that the high-grade metamorphism is related to late stages of the Transamazonian tectono-thermal event, since the metamorphic ages range mainly between 2.07 and 1.98 Ga (Avelar et al., 2001; Lafon et al., 2001; Oliveira et al., 2002; Roever et al., 2003; Enjolvy, 2004; Tassinari et al., 2004). In previous studies, the age of the high-grade metamorphism has been constrained by dating of metamorphic minerals from high-grade gneisses, as well as by dating of igneous charnockites frequently associated to them.

In the current literature, igneous charnockites have also been frequently described in granulite-facies metamorphic terrains and, in some cases, they represent coeval melting products of the high-grade metamorphic event (Bohlender et al., 1992; Newton, 1992; Ridley, 1992; Kouamelan et al., 1997). In the same way, igneous charnockites from eastern Guiana Shield, associated with high-grade complexes from both Paleoproterozoic (e.g. Bakhuis Mountains) and Archean (e.g. Tartarugalzinho region, eastern part of Amapá Block) domains have also been considered as produced during the Transamazonian granulitic event, since they were emplaced about 2.06-2.04 Ga (Avelar et al., 2001; Lafon et al., 2001; Roever et al., 2003; Enjolvy, 2004).

However, in the southwestern portion of the Archean Amapá Block, where this study is focused, the high-grade metamorphic assemblage is mainly composed of granulitic orthogneisses, which present igneous precursors dated at about 2.80 Ga, but also includes several charnockitic plutons that provided ages spreading from 2.65 to 2.60 Ga (Ricci et al., 2002; Rosa-Costa et al., 2003 and in press). Transamazonian-related igneous charnockites have never been found in that region up to now, and the Transamazonian overprint in Archean rocks is testified by the emplacement of several syn- to late-orogenic granitic plutons with ages ranging from 2.22 Ga to 2.03 Ga, which have Nd isotope signatures pointing to an origin involving reworking of Archean crust (Rosa-Costa et al., 2003 and in press).

The occurrence of Archean igneous charnockites compounding the high-grade assemblage and the undoubted Paleoproterozoic reworking of the Archean basement, point to a polymetamorphic evolution for the southwestern portion of the Amapá Block. Then, the purpose of this study is to constrain the age of the regional high-grade event that affected the Archean rocks, through the dating of monazite and zircon, with the aim of determining if the high-grade metamorphism is related to the overprint of Archean rocks during the Transamazonian orogenic cycle, as reported in other areas of the Guiana Shield, or whether it is associated with an older event that occurred during previous orogenies in Archean times, or both.

The geochronological approach is mainly based on the chemical U-Th-Pb method for dating of monazite using an electron probe microanalyzer (EPMA). This in-situ micro-dating technique has been successfully employed as a powerful tool for the understanding of metamorphic evolution of several orogenic belts (Suzuki and Adachi, 1991; Suzuki et al., 1994; Montel et al., 1996; Braun et al., 1998; Cocherie et al., 1998 and 2005; Suzuki and Adachi, 1998; Crowley and Ghent, 1999; Catlos et al., 2002; Foster and Parrish, 2003; Tickyj et al., 2004). The

Pb-evaporation method of dating is complementarily applied on zircon grains from a metamorphic rock.

## 2 - Regional Geological Background

The Guiana Shield represents the northern segment of the Amazonian Craton, in South America, located on the northern edge of the Amazon Basin (Fig. 1). The eastern portion of the Guiana Shield consists of an exceptionally large Paleoproterozoic belt that extends from northern Brazil to eastern Venezuela, including French Guiana, Suriname and Guyana, which corresponds to a remarkable geochronological province of the Amazonian Craton, the Maroni-Itacaiúnas Province (Cordani et al., 1979; Tassinari and Macambira, 2004).

The geochronological pattern of the Maroni-Itacaiúnas Province indicates that its evolution took place during the Transamazonian orogenic cycle (2.26 - 1.95 Ga), mainly in Rhyacian times (Gruau et al., 1985; Teixeira et al., 1989; Sato and Tassinari, 1997; Vanderhaeghe et al., 1998; Lafrance et al., 1999; Nogueira et al., 2000; Norcross et al., 2000; Tassinari et al., 2000; Voicu et al., 2000; Avelar, 2002; Delor et al., 2003a; Roever et al., 2003; Rosa-Costa et al., 2003 and in press). It essentially comprises Paleoproterozoic greenstone belts, calc-alkaline granitoids and granitic suites, migmatites and with minor granulitic complexes.

In addition, two major domains constituted mainly of Archean rocks have been documented along the Maroni-Itacaiúnas Province: 1) the Imataca Block, in Venezuela (Montgomery and Hurley, 1978; Montgomery, 1979; Tassinari et al., 2001), and 2) the Amapá Block, in the north of Brazil (Rosa-Costa et al., in press). These domains essentially include granulitic-gneissic-migmatitic complexes having Archean precursors (Lafon et al., 1998; Tassinari et al., 2001; Pimentel et al., 2002; Ricci et al., 2002; Avelar et al., 2003; Klein et al., 2003; Rosa-Costa et al., 2003 and in press; Faraco et al., 2004), and which have been intensely deformed, metamorphosed and intruded by plutons of granitoids during the Transamazonian orogenic cycle.

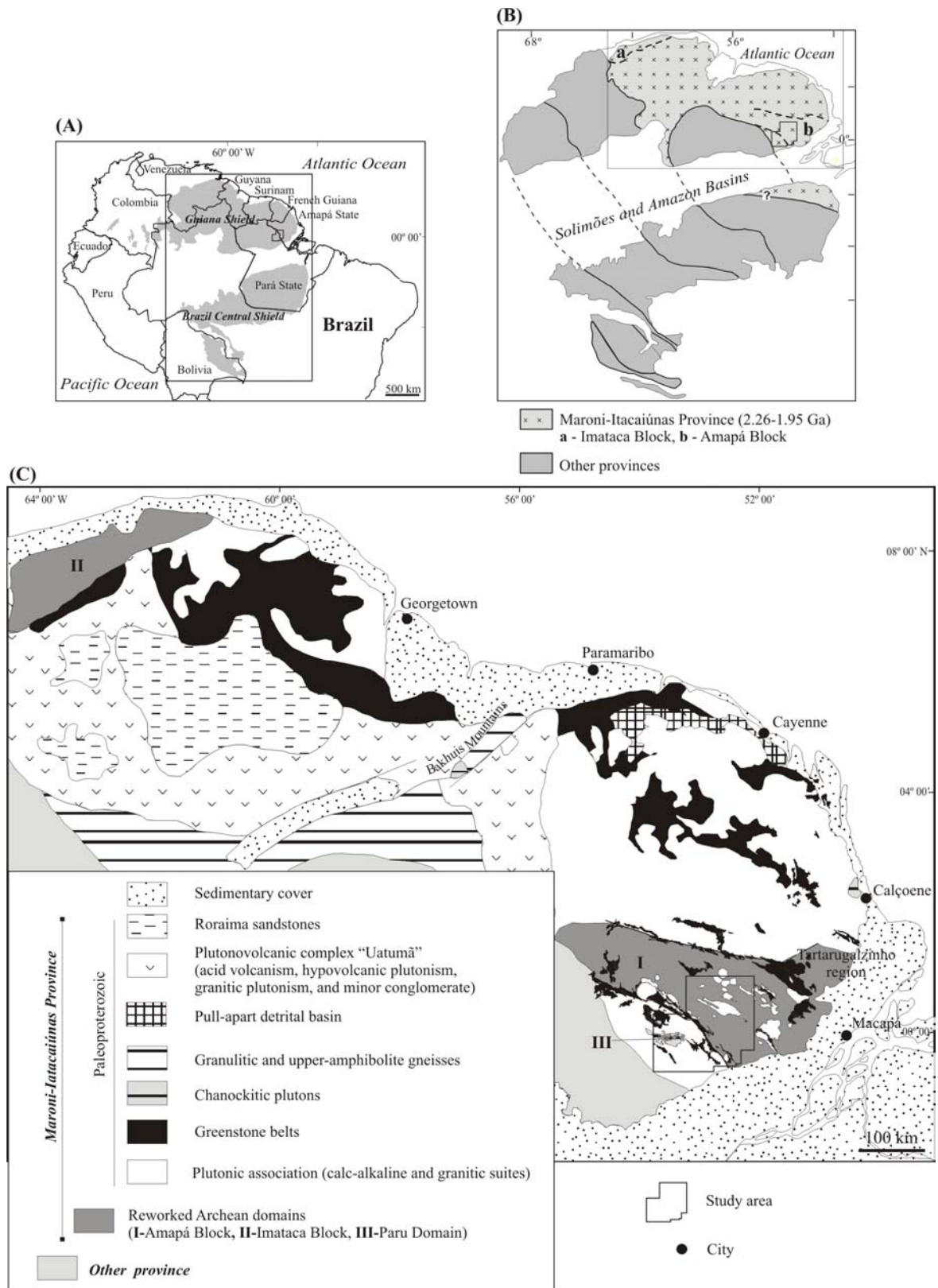


**Figure 1** – (A) Location map of the studied area; (B) Simplified sketch map showing the distribution of the geochronological provinces of the Amazonian Craton according to Tassinari and Macambira (2004); (C) Geological sketch map of the Guiana Shield, based on Delor et al. (2003b) and Rosa-Costa et al. (in press).

Granulite-facies rocks have been identified either in Paleoproterozoic or in Archean domains of the Maroni-Itacaiúnas Province, in: 1) the Guiana Central Granulitic belt, 2) the Imataca Block, 3) the Amapá Block and in 4) the Paru Domain. Furthermore, the occurrence of a 2.06 m.y. old charnockitic pluton (Lafon et al., 2001), at north of the Calçoene city (Fig. 1), suggests the existence of minor granulitic terrain in that region, not yet confirmed by the available geological data.

In the southwestern portion of the Amapá Block (Fig. 2), the high-grade basement rocks include: 1) granulitic orthogneisses from the Jari-Guaribas Complex (mainly enderbite and charnockitic banded gneisses, with minor mafic granulites) that have their igneous protoliths dated at about 2.8 Ga, and which enclose minor slivers of pelitic granulites (Rosa-Costa et al., 2003 and in press); 2) undated mesoperthite and/or clinopyroxene-bearing granitic orthogneisses, metamorphosed under amphibolite-granulite transition facies, included in the Baixo Mapari Complex; 3) undated paraderived granulites of the Iratapuru Complex (mainly aluminous gneisses and schists); 4) amphibolite-facies grey gneisses (mainly tonalitic and granodioritic) from the Guianense Complex, which have magmatic precursors dated at about 2.65 - 2.60 Ga (Rosa-Costa et al., 2003 and in press); and 5) several plutons of 2.65 - 2.60 m.y. old catazonal granites grouped in the Noucourou Intrusive Suite (Ricci et al., 2002; Rosa-Costa et al., in press). This suite is constituted of true charnockites, enderbites and mesoperthite-bearing granites, and supposedly marks the time of an Archean granulitic event. In addition, high- to medium-grade gneisses, with inferred Archean ages, which can not be inserted in any specific stratigraphic unit, are informally referred as granulitic-gneissic-migmatitic complex and also included in the basement assemblage of the Amapá Block.

The high-grade metamorphic complexes were heterogeneously affected by migmatization and locally retrograded to amphibolite-facies or even greenschist-facies metamorphism. Migmatization features are widespread in the basement rocks. Granitic leucosomes are common, and occur as layers concordant to the gneissic foliation, as discontinuous pods, or cross-cutting veins. Migmatization also occurred under granulite-facies metamorphic conditions, as indicated by the presence of orthopyroxene in some leucosomes (charnockitic leucosomes) from the Jari-Guaribas Complex.

There are not enough geochronological data in the investigated area that allow us to assume confidently that the migmatization occurred in Archean or during the Transamazonian orogenesis. However, the Transamazonian overprinting in the Archean basement is indicated by the emplacement of several Paleoproterozoic granitic plutons, dated at about 2.22 Ga, 2.18 Ga, 2.15 Ga, 2.05 Ga and 2.03 Ga, and which have Nd isotope signatures indicating an origin mainly by reworking of Archean crust (Rosa-Costa et al., 2003 and in press).

Granulites also occur within the Paru Domain, an oval-shaped Archean nucleus, composed of granulitic gneisses of the Ananaí Complex (mainly enderbites and charnoenderbites gneisses), which have igneous precursors dated at about 2.60 Ga (Rosa-Costa et al., 2003). These gneisses host catazonal plutons (charnockites, mesoperthite-bearing granites and enderbites) dated at around 2.07 Ga (Rosa-Costa et al., in press), which are grouped in the Igarapé Urucu Intrusive Suite.

The Paru Domain is located within the Carecuru Domain, a granitoid-greenstone terrane, developed in a magmatic arc setting that was accreted to the southwestern border of the Amapá Block during the Transamazonian event (Rosa-Costa et al., in press). It consists principally of calc-alkaline gneisses and granitoids, dated at 2.19-2.18 Ga and at 2.15-2.14 Ga, included, respectively, in the Paru-Maratiá Complex and in the Carecuru Intrusive Suite. The supracrustal sequences are constituted mainly by mafic and intermediated metavolcanics, but an expressive supracrustal belt, which marks the boundary between the Amapá Block and the Carecuru Domain, also comprises BIFs and paraderived rocks, composing the Ipitinga Group, dated at about 2.16 Ga (McReath and Faraco, 1997). In addition, several granitic plutons mark stages of crustal reworking in the Carecuru Domain, one of them dated at about 2.10 Ga.

Finally, the last magmatic manifestation known in the studied area is represented by emplacement of several plutons of A-type granites (Granito Waiãpi), dated around 1.75 Ga (Vasquez and Lafon, 2001).

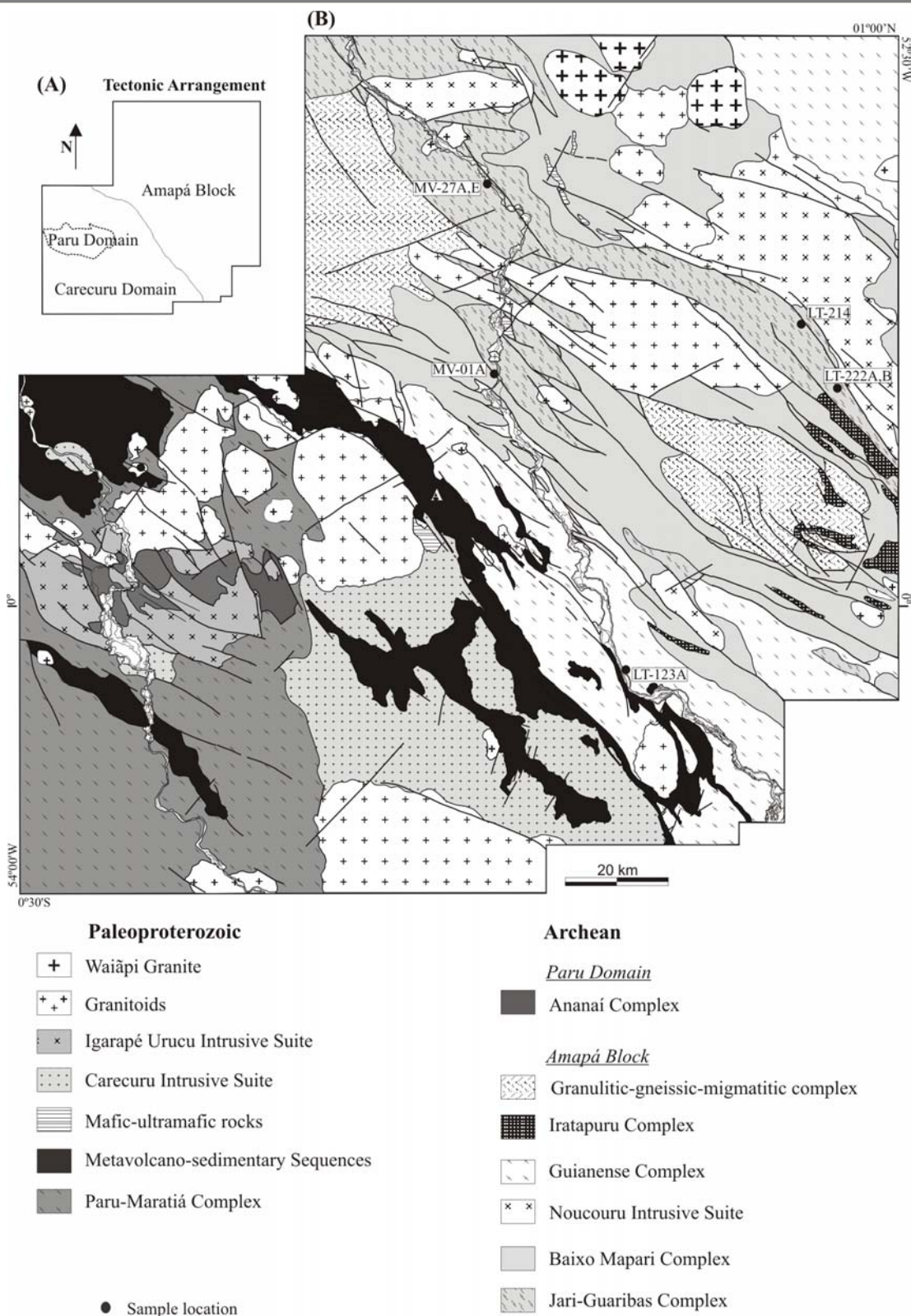


**Figure 2** – (A) Tectonic subdivision of the study area; (B) Geological map showing the sites of the samples dated in this work. Geological map, stratigraphic and tectonic arrangement based on Carvalho et al. (2001), Ricci et al. (2001) and Rosa-Costa et al. (in press).

### 3 - Analytical Procedure and Age Calculation

#### 3.1 - Sample Preparation

Monazite and zircon grains were separated in laboratories of the CPRM-Geological Survey of Brazil, by processing of about 5 kg of fresh rock, using standard techniques of concentration of heavy minerals that involved steel jaw-crusher, steel roller-mill, sifters, Franz magnetic separator and heavy liquids.

In order to identify the monazite grains among other similar accessory heavy minerals, back-scattered electron (BSE) imaging was carried out in electron microscopes (LEO-1430 and LEO-1450) at laboratories of the Universidade Federal do Pará (UFPA) and of the Museu Paraense Emílio Goeldi, both located in Belém, Brazil. Subsequently, eight to ten monazite grains from each sample were mounted in resin, grounded to approximately equatorial sections and then polished. In order to investigate the internal textural/compositional variations and the morphological features of all individualized monazite grains, BSE imaging was performed in a JSM-6100 electron microscope, at laboratory of the BRGM, Orléans, France. This BSE imaging was useful to select the grains and the domains within the grains to be analyzed.

Morphological and internal textural characteristics of the zircon grains were investigated using optical microscopy, which guided selection of the grains for analysis.

#### 3.2 - Monazite Dating

The analyses on monazite grains were carried out on a CAMECA SX 50 electron probe micro-analyzer (EPMA), equipped with five wave-length-dispersive spectrometers, at laboratory of the BRGM. The analytical procedure for monazite was detailed in Cocherie et al. (1998) and Cocherie and Legendre (2006). An accelerating voltage of 20 kV and a beam current of 200 nA were chosen as operating conditions (for all samples except MV-27A and MV-27E: 100 nA), giving a spot size of about 2  $\mu\text{m}$ . Counting times (peak + background) were 240 s for Pb, 200 s for U, and 40 s for all other elements. The X-ray lines used were  $\text{UM}\alpha$ ,  $\text{PbM}\alpha$ ,  $\text{ThM}\alpha$ ,  $\text{SiK}\alpha$ ,  $\text{CaK}\alpha$ ,  $\text{NdL}\beta$ ,  $\text{SmL}\alpha$ ,  $\text{CeL}\alpha$ ,  $\text{LaL}\alpha$ ,  $\text{PrL}\beta$ ,  $\text{GdL}\beta$ ,  $\text{YL}\alpha$ . A PaP correction program was used to correct matrix effects. The spectral interferences of  $\text{ThM}\beta$  on  $\text{UM}\alpha$ , and of Y on  $\text{PbM}\alpha$  were also corrected. The different interference corrections were validated by dating several monazite samples with this method and using conventional isotopic methods (see for instance Cocherie et al., 1998). According to this procedure, the calculated detection limits ( $2\sigma$ ) were 110 ppm for Pb,

105 ppm for U and 130 ppm for Th, the absolute error being taken as 110, 105 and 130 ppm, respectively. The two samples (MV-27A and MV-27E) being analyzed after applying a 100 nA current lead to error of 150 ppm for Pb, U and Th. A systematic minimum error of 2% was considered for concentrations >7500 ppm (Cocherie and Legendre, 2006). The major-element composition of monazite being relatively constant, it was not deemed necessary to calculate the detection limits for each individual analysis, which were thus taken as absolute error.

The standards were galena (PbS) for Pb, uraninite (UO<sub>2</sub>) for U and thorite (ThO<sub>2</sub>) for Th. For other element determinations, were used end-member synthetic phosphates (XPO<sub>4</sub>) for each REE and Y, apatite for Ca and andradite for Si. About 10-20 points were analyzed in each grain that represent about 120-140 points in each sample.

Age calculations were done using the Isoplot/Ex (3.1) program of Ludwig (2004) and a Microsoft Excel add-in program for determining U-Th-Pb ages from EPMA measurements (Pommier et al., 2002). All the calculations were done at 2 $\sigma$  level. U-Th-Pb weighted ages were calculated, according to the procedure proposed by Cocherie and Albarede (2001). This scheme uses a Th/Pb = f(U/Pb) isochron diagram to calculate an U-Th-Pb weighted average age based on a regression line, whose precision of the slope, depends on the variation of the Th/U ratios in the grains. The U-Th-Pb weighted average point of the population plotted in the Th/Pb = f(U/Pb) diagram is associated with an age that is related to the lowest error, as indicated by the calculated error envelope, which shows the evolution of the error along the regression line. The errors on Th/Pb and U/Pb are calculated using the error propagation formulas:  $\sigma_{\text{Th/Pb}} = (\sigma_{\text{Th}}^2 + \sigma_{\text{Pb}}^2)^{0.5}$  and  $\sigma_{\text{U/Pb}} = (\sigma_{\text{U}}^2 + \sigma_{\text{Pb}}^2)^{0.5}$  (Cocherie and Legendre, 2006). Th-Pb and U-Pb ages are also calculated separately at the intercepts of the regression line with the X and Y axes, respectively. If these two ages are similar within the errors and if the regression line is associated with a MSWD (Mean Squared Weighted Deviation) in agreement with a single age-population (Wendt and Carl 1991), then the system fulfils the requirements for calculation of the most precise and probable age at the centroid of the population (Cocherie and Albarède, 2001). Special care was taken on the MSWD, which must be below  $1+2/(2/f)^{0.5}$  (f: degree of freedom = number of analyses – number of dated events) in order to validate age calculation for a single age population (Wendt and Carl, 1991). In more complex cases, for instance in the case of polygenetic monazites that have more than one population of ages, the MSWD value increases and/or the U/Pb and Th/Pb ages are significantly different.

For each sample, before the U-Th-Pb age calculation in the Th/Pb = f(U/Pb) diagram, a simple average age was calculated using all individual ages and a weighted histogram representation was constructed with the Isoplot program. Coupled with BSE image observation, this initial procedure allows determination whether the calculated ages represent a single population of ages, then being consistent with a single geological event, or if they represent a bimodal population, reflecting a more complex geological history. Bimodal populations of ages, which can be produced by different successive or broadly dispersed events, were individually studied. Some rare spot analyses, statistically abnormal compared to the studied age population and not associated to specific domains of the crystal were rejected.

The three starting assumptions are: (1) common Pb is negligible as compared to the amount of thorogenic and uranogenic lead; (2) no radiogenic Pb loss has occurred since system closure; (3) a single age is involved at the size level of each individual spot analysis. After comparison with conventional isotopic U-Pb age determinations, it is now accepted that EPMA resolution allows us to avoid inclusions and altered domains that could potentially contain common Pb.

### 3.3 - Zircon Dating

The zircon geochronology was based on the Pb-evaporation method of Kober (1986 and 1987). The isotopic analyses were carried out on a Finnigan MAT262 mass spectrometer, at the Laboratório de Geologia Isotópica (Pará-Iso) of the UFPA, Belém, Brazil. Zircon crystals were dated using double Re filaments, and the isotopic data were acquired in the dynamic mode, using an ion-counting system. The Pb isotope compositions were determined through repeated analyses of several zircon grains from the sample, at increasing evaporation temperature steps. The  $^{207}\text{Pb}/^{206}\text{Pb}$  ratios were corrected from mass discrimination using a factor of  $0.12\% \pm 0.03$  per u.m.a., determined by repeated analyses of the NBS-982 “equal atoms” Pb standard. The calculation of common lead correction was done using the Pb composition of the Stacey and Kramers (1975) model, at the age of the grain. Analyses with  $^{206}\text{Pb}/^{204}\text{Pb}$  ratios lower than 2500 were eliminated to minimize the effects of common lead correction on the radiogenic isotopic ratios and they are not shown in the tables of data.

The Pb evaporation method usually provides very precise measurements of the  $^{207}\text{Pb}/^{206}\text{Pb}$  ratio, which enable the determination of a precise weighted average value for the age ( $\pm 1-5$  Ma) on a small number of grains. As Pb/U ratios are not determined, the oldest  $^{207}\text{Pb}/^{206}\text{Pb}$  age is a

minimum age. However, the assumption that this age can represent a “concordant” crystallization age of zircon from magmatic rocks is strongly supported when repeated measurements of  $^{207}\text{Pb}/^{206}\text{Pb}$  do not vary significantly in several crystals or at different temperature steps in one grain (Kober et al., 1989; Ansdell and Kyser, 1993; Karabinos and Gromet, 1993; Kröner et al., 1999).

The age of each sample is calculated using the mean value of the  $^{207}\text{Pb}/^{206}\text{Pb}$  ratios at the highest temperature steps. When different temperature steps of the same grain furnish similar ages, all of them are included in the mean age calculation of this grain. Consequently, the confidence of the result depends on the number of grains with similar ages and, at least three grains with similar ages are necessary to define a crystallization age. Grains furnishing ages significantly lower are suspected to have suffered lead loss after crystallization and are discarded. In the same way, grains yielding isolated older ages are considered as inherited and, consequently, are also discarded. The weighted mean and the  $2\sigma$  errors on the age of the remaining zircon population were calculated following Gaudette et al. (1998). The Pb-evaporation age diagram was drawn using the Isoplot program (Ludwig, 2004).

#### 4 - Sample, Monazite and Zircon Descriptions

Monazite grains from seven samples were investigated and their location is shown in Figure 2. The samples MV-27A, MV-27E, LT-214, LT-223A and LT-223B came from the Jari-Guaribas Complex, and the samples LT-123A and MV-01A came from the Guianense Complex. Zircons grains were also extracted from the sample MV-27E for dating.

Zircon geochronology defined an Archean age at about 2.8 Ga for the igneous precursor of the enderbitic gneiss MV-27A (Rosa-Costa et al., in press). Even if the other investigated gneisses, from the Jari-Guaribas or from the Guianense complexes, have not yet been dated, Archean ages are also suspected for their protoliths, based on the available geochronological data, field aspects and stratigraphical correlations (see Rosa-Costa et al., in press).

Gneisses and leucosomes of both complexes were chosen to be analyzed, in order to bracket the timing of the high-grade metamorphism and to constrain the age of related migmatization events. Their mineralogical composition, textural textures and mode of occurrence are briefly described below, as well as the micro-textural characteristics of some analyzed

monazite and zircon grains. Field features of the dated samples and the main textural aspects of the investigated monazites are displayed in the Figures 3 and 4.

Enderbitic gneiss MV-27A and charnockitic leucosome MV-27E – These samples represent a gneiss/leucosome pair, collected at the same outcrop (Fig. 3A). The gneiss MV-27A is grey and medium-grained, exhibiting a millimeter- to centimeter-scale compositional banding. The metamorphic mineralogical assemblage in equilibrium is antiperthitic plagioclase, quartz, biotite, mesoperthitic alkali-feldspar, with minor clinopyroxene, orthopyroxene and opaque minerals. Accessory minerals are monazite, apatite and zircon. Microscopically the texture is granoblastic, with polygonal or interlobate contacts and biotite showing preferred orientation.

The monazite grains display a well-rounded or slightly oval shape and occur as inclusions in plagioclase, quartz and biotite. Grain sizes range from 150 to 200  $\mu\text{m}$  in diameter. Most of the crystals show a weak concentric zonation under an optical microscope. BSE images reveal that the grains can be either unzoned or complexly zoned (Fig. 4 A, B).

The charnockitic leucosome MV-27E is a coarse grained rock, rose to pale rose, containing mesoperthitic alkali-feldspar, which represents 60% of the rock, besides quartz, plagioclase, orthopyroxene, biotite, monazite and zircon. The microtexture is inequigranular hypidiomorphic, with polygonal or interlobate contacts. In outcrop scale, this rock occurs as discontinuous foliation-concordant layers or pods (Fig. 3A), indicating that it is product of *in situ* partial melting of the enderbitic gneiss MV-27A. Monazite is an abundant accessory phase and occurs as prominent inclusions in plagioclase and quartz. The six monazites analyzed consist of well-rounded grains, with 100 to 250  $\mu\text{m}$  of diameter. BSE imaging reveals that the monazite grains are internally homogeneous, or display a simple concentric zoning, defined by a rounded core, surrounded by a slightly brighter rim (Fig. 4 C, D).

The zircon grains are rounded or subhedral (bipyramidal with rounded terminations), occurring as inclusions in plagioclase and quartz. The grains selected for analysis are clear, pale rose to light brown, presenting expressive oscillatory zoning, classically interpreted as evidence of magmatic crystal growth. A few mineral inclusions and primary cracks can be observed in the core (Fig. 4 E, F).

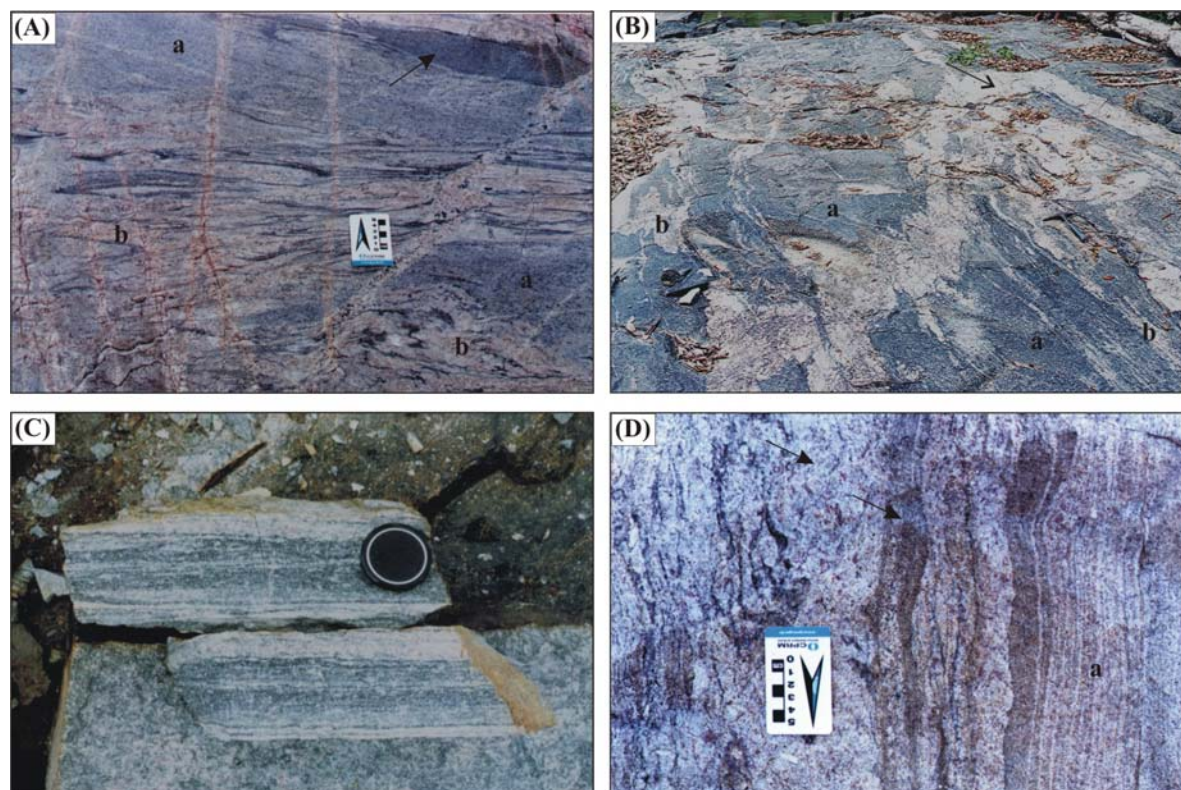


**Figure 3** – Field aspects of some of the dated samples: **(A)** Banded enderbite gneiss (**a** – sample MV-27A) containing enclaves of mafic granulite (arrow) and discontinuous and concordant layers of charnockitic leucosome (**b** – sample MV-27E); **(B)** Strongly migmatized tonalitic gneiss (**a** – sample LT-223A) containing granitic leucosomes that occur as foliation-concordant layers (**b** – sample LT-223B) and as cross-cutting veins (arrow); **(C)** Textural macroscopic aspect of the tonalitic gneiss LT-123A, which has centimeter-scale leucosome layers highlighting the banding; **(D)** Compositional banding observed in the station MV-01A by alternating melanosome (biotite and garnet-rich) and leucosome (quartz-feldspatic with garnet) layers (arrows). The dated granitic gneiss MV-01A was collected in zones like that marked in **a**.

Enderbite gneiss LT-214 – This rock is grey, fine- to medium grained, and exhibits a well-defined gneissic foliation. Sparse 1-3 cm thick quartz-feldspatic leucosome layers, concordant to the gneissic foliation, are observed in outcrop scale. The mineralogy is quartz, plagioclase, biotite, orthopyroxene, apatite, zircon and monazite. The micro-texture is granoblastic with interlobate contacts, presenting biotite with preferred orientation. The monazite occurs as inclusions in the plagioclase and quartz. The monazite grains are rounded (diameter ~ 200  $\mu\text{m}$ ) or display an ellipsoidal shape (about 200  $\mu\text{m}$  x 100  $\mu\text{m}$ ). Inclusions of zircon, apatite and alkali-feldspar are present in some of them. The monazites commonly show a sector zoning pattern, revealed by BSE imaging (Fig. 4 G).

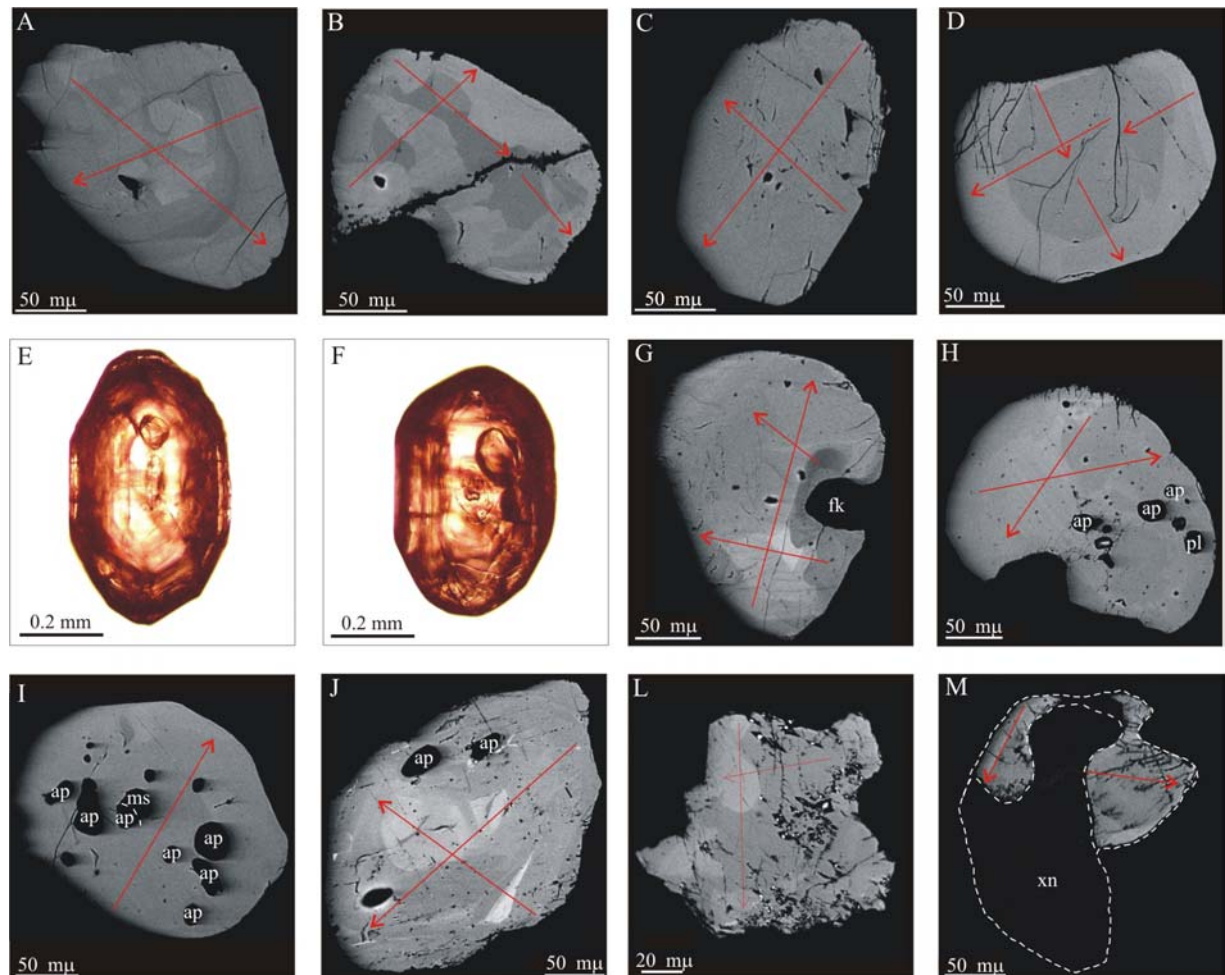


**Figure 4** – Back-scattered electron images and transmitted light images of representative monazite and zircon grains, respectively: (A) and (B) Gneiss MV-27A; (C) and (D) Monazites from the leucosome MV-27E; (E) and (F) Zircons from the leucosome MV-27E; (G) Gneiss LT-124; (H) Gneiss LT-223A; (I) Leucosome LT-223B; (J) Gneiss LT-123A; (L) and (M) Gneiss MV-01A. Morphological and textural aspects discussed in the text. Conventions: fk – alkali feldspar, ap – apatite, pl – plagioclase, ms – muscovite, xn – xenotime. Black arrows – analytical profiles.

Tonalitic gneiss LT-223A and granitic leucosome LT-223B – These samples represent a gneiss/leucosome pair. The gneiss LT-223A is constituted of plagioclase, quartz, biotite, alkali-feldspar, opaque minerals, apatite, zircon and monazite. Alkali-feldspar is locally mesoperthitic. The texture is porphyroclastic, defined by phenocrystals of plagioclase and quartz within a fine-grained matrix, composed by granoblastic quartzo-feldspatic aggregates, with polygonal or interlobed contacts, and strings of biotite with preferred orientation.

The leucosome LT-223B is a coarse-grained rock, composed by alkali-feldspar and quartz that constitute > 90% of the rock, besides biotite, plagioclase, monazite and zircon. The texture is mainly granoblastic to porphyroclastic in biotite-rich domains, with crystals showing interlobate and polygonal contacts. Quartz occurs in sub-grains aggregates, alkali-feldspar is locally mesophertitic and crystals of biotite exhibit preferred orientation.

Migmatization features are widespread in the outcrop where these samples were collected, which are represented by granitic leucosomes occurring as foliation-concordant layers and pods, and also as cross-cutting veins (Fig. 3B). The leucosome LT-223B is representative of foliation-concordant layers and shows unequivocal evidence of an origin related to *in situ* melting of the tonalitic gneiss LT-223A.

The metamorphic assemblage either in the gneiss or in the leucosome does not show definitive evidence that these rocks attained granulite-facies metamorphic conditions, as the surrounding granulitic gneisses that characterize the Jari-Guaribas Complex, but it is rather coherent with amphibolite-facies metamorphism.

The monazite grains of both samples are similar in their textural aspects. They are unzoned homogeneous grains, which occur mainly as rounded crystals, with diameters between 150µm and 250 µm. Inclusions occur frequently, mainly of apatite and minor allanite, alkali-feldspar, plagioclase, quartz, muscovite and chlorite (Fig. 4 H, I).

Tonalitic gneiss LT-123A – It consists of an amphibolite-facies grey gneiss, composed of plagioclase, quartz and alkali-feldspar and biotite, opaque minerals, apatite, zircon and monazite. Monazite occurs as inclusions within the quartz. Microscopically, the texture is mylonitic, defined by porphyroclasts of plagioclase and quartz, wrapped by a fine-grained matrix, containing elongated lenses of recrystallised quartz and feldspar and anastomosed strings of biotite. In outcrop, we observe quartz-feldspatic leucosomes containing abundant garnet that occur as foliation-concordant decimeter- to centimeter-scale layers, and which also present mylonitic texture (Fig. 3C). Eight grains of monazite selected for analysis display slightly rounded (~ 200-250 µm in diameter) or oval shapes (~ 150 x 250 µm). BSE images reveal a complex zoning pattern, highlighted by irregular bright domains. Some crystals present inclusions of apatite (Fig. 4 J).

Granitic gneiss MV-01A – It is a strongly migmatized gneiss, consisting of a mesosome defined by biotite- and garnet-rich fine-grained layers (melanosome) alternating with quartz-feldspatic medium- to coarse-grained layers (leucosome) (Fig. 3D). The whole mineralogy is represented by alkali-feldspar, quartz, plagioclase, biotite, garnet, monazite, zircon and xenotime. The biotites are chloritized and the feldspars are altered along cleavage planes and crystal boundaries. The monazite occurs in the interstices, between crystals of quartz and alkali feldspar, preferentially associated to leucosome layers. Monazite grains are rounded (~ 150-200  $\mu\text{m}$  of diameter) or present irregular shapes, with ragged crystal edges and embayment of the crystal faces, suggesting partial dissolution or interaction with fluids (Fig. 4M). Intergrowth relationships between monazite and xenotime are observed (Fig. 4L), but xenotime can also be found as inclusions in the monazite (Fig. 4M), indicating that the crystallization of the monazite has continued afterwards to the end of the xenotime crystallization. Apatite and zircon also occur as inclusions in the monazite grains.

## 5 - Geochronological Results

The appropriate analytical data are listed in the tables 1 and 2 and shown in U/Pb vs. Th/Pb isochron diagrams and in the Pb-evaporation diagram, displayed in the figures 5, 6, 7 and 9.

Enderbitic gneiss (MV-27A) and charnockitic leucosome (MV-27E)

In the enderbite gneiss MV-27A, U-Th-Pb EPMA traverses were conducted across nine monazite grains, with 141 spot analyses being analyzed. Th concentrations range between 2.0 and 9.0 wt.%. Pb and mainly U abundances are significantly lower, spreading between 0.26-0.95 wt.% and 0.01-0.18 wt.%, respectively. Individual calculated ages display a scatter between 2026 and 2182 Ma, provided by 137 measurements, whereas the other 4 spot analyses present isolated individual ages of 1944, 2210, 2269 and 2377 Ma, which were not discussed or included in the age calculation, since they are not statistically representative. The individual ages provided by the 137 spot analyses are considered as belonging to a single and unimodal population and are distributed along an average age of  $2096 \pm 6$  Ma (MSWD = 1.6), calculated at the centroid of the population on the Th/Pb vs. U/Pb diagram (Fig. 5 A). The Th/Pb and U/Pb ages of, respectively,  $2089 \pm 11$  Ma and  $2287 +228 -250$  Ma are indistinguishable within the errors, even if the U/Pb age is not very well defined. The spot analyses do not present a wide spread in the diagram,

defining a slope of the regression line of  $-4.30 \pm 0.63$  similar to the theoretical isochron within the analytical error. The MSWD is considered to agree with a single age group despite the fact that it is slightly above the maximum value of 1.25 defined by Wendt and Carl (1991).

Six monazite grains were analyzed in the charnockitic leucosome MV-27E, giving a total of 121 measurements, which were collected along 12 crosscuts. Element concentrations are similar to the sample MV-27A, even if in this sample, variations in Th concentrations are less expressive. Th concentrations range between 3.13 and 7.26 wt%, and U abundances range between 0.01 and 0.97. Pb abundances are rather lower and vary from 0.36 to 0.7 wt.%. Spot analyses (117 points) furnished individual ages spreading from 1988 to 2179 Ma and are considered as representing a unimodal population. Isolated ages of 1908, 1946, 2205 and 2207 Ma were provided by 4 remaining analytical points and were discarded. An average age of  $2088 \pm 8$  Ma (MSWD = 1.5) was calculated from the 117 individual ages and errors in the Th/Pb vs. U/Pb diagram (Fig. 5 B). Th/Pb ( $2083 \pm 18$  Ma) and U/Pb ( $2156 +254 -283$  Ma) ages are indistinguishable within the errors. The slight spread of the analytical points in the diagram, produced a slope of  $-3.98 \pm 0.69$  of the regression line. The MSWD is considered as in agreement with a single age group despite the fact that it is slightly above the maximum value of 1.25 defined by Wendt and Carl (1991). The statistical parameters indicate that the calculated age represents a unimodal population and dates a single event at about 2.09 Ga, which was also revealed in the previous sample of gneiss MV-27A, since both the ages are similar within the errors.

**Table 1** - Summary of electron microprobe data for analyzed monazites. The standard deviations show the range of U, Th and Pb variation for each sample. The mean isochron ages were calculated at the centroid of the population plotted in the Th/Pb vs. U/Pb isochron diagram. Error on age was calculated at 95 % confidence level.

Pb (ppm) $\pm \sigma$ std. deviation	U (ppm) $\pm \sigma$ std. deviation	Th (ppm) $\pm \sigma$ std. deviation	Th/U $\pm \sigma$ std. deviation	<b>Isochron age</b> <b><math>\pm 2\sigma</math> Ma</b>	No. of data
<b><i>Enderbitic gneiss MV-27A</i></b>					
6864 $\pm$ 1527	527 $\pm$ 362	68111 $\pm$ 16061	117 $\pm$ 48	<b>2096 <math>\pm</math> 6</b>	137
<b><i>Charnockitic leucosome MV-27E</i></b>					
4917 $\pm$ 796	603 $\pm$ 250	48185 $\pm$ 8824	74 $\pm$ 24	<b>2088 <math>\pm</math> 8</b>	117
<b><i>Enderbitic gneiss LT-214</i></b>					
9824 $\pm$ 2452	5197 $\pm$ 1418	80950 $\pm$ 20885	16 $\pm$ 5	<b>2087 <math>\pm</math> 3</b>	133
<b><i>Tonalitic gneiss LT-223A</i></b>					
3897 $\pm$ 1291	875 $\pm$ 258	36692 $\pm$ 13400	49 $\pm$ 33	<b>2086 <math>\pm</math> 8</b>	128
<i>Inherited zones</i>					
3262 $\pm$ 960	838 $\pm$ 194	28132 $\pm$ 9165	34 $\pm$ 9	<b>2215 <math>\pm</math> 28</b>	12
<b><i>Granitic leucosome LT-223B</i></b>					
4873 $\pm$ 931	630 $\pm$ 183	47470 $\pm$ 9405	88 $\pm$ 76	<b>2093 <math>\pm</math> 8</b>	114
<b><i>Tonalitic gneiss LT-123A</i></b>					
5030 $\pm$ 1646	1737 $\pm$ 513	46363 $\pm$ 16356	27 $\pm$ 7	<b>2038 <math>\pm</math> 6</b>	110
<i>Inherited zones</i>					
4685 $\pm$ 1333	1515 $\pm$ 411	41164 $\pm$ 12083	27 $\pm$ 5	<b>2132 <math>\pm</math> 25</b>	24
<b><i>Granitic gneiss MV-01A</i></b>					
12280 $\pm$ 1652	10588 $\pm$ 4780	87845 $\pm$ 12961	11 $\pm$ 7	<b>2056 <math>\pm</math> 7</b>	78
<i>Secondary group of ages</i>					
10915 $\pm$ 3114	9851 $\pm$ 6859	88235 $\pm$ 21445	17 $\pm$ 16	<b>1879 <math>\pm</math> 16</b>	8

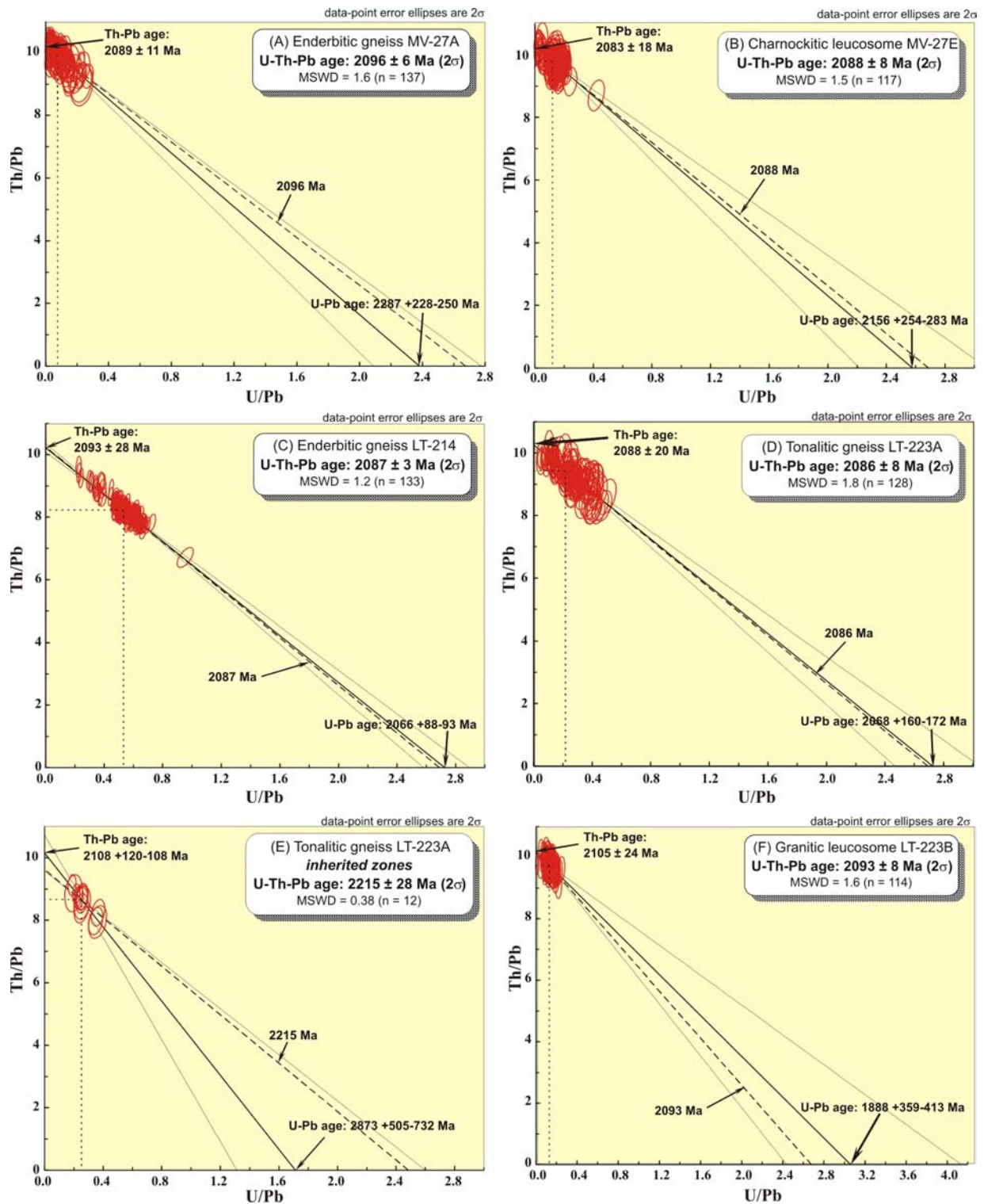


**Figure 5** – Th/Pb vs. U/Pb diagrams for monazites from five samples of the Jari-Guaribas Complex. Note that in all plots the real isochrons (dashed lines) are sub-parallel to the best regression line (heavy lines) and located between the two errors hyperbolas (thin lines). The intercept ages are similar within the analytical errors, allowing the calculation, in each sample, of the mean age at the centroid of the population.

In addition, 8 zircon grains from this charnockitic leucosome MV-27E were analyzed by Pb-evaporation method, and among them, seven crystals provided ages spreading between  $2045 \pm 50$  and  $2091 \pm 5$  Ma, at the higher steps of temperature of 1500 and 1550 °C (Table 2). A mean age of  $2091 \pm 5$  Ma (USD = 2.6) was calculated from three grains and is interpreted as the crystallization age of the charnockite (Fig. 6). The other 4 zircon grains furnished the youngest ages and were discarded from the age calculation, since they are suspected to have suffered lead loss after crystallization. Furthermore, one grain yielded an age of 2.24 Ga. Considering that zircon dating provided an age about 2.8 Ga for the igneous precursor of the gneiss MV-27A (Rosa-Costa et al. in press), and also that the leucosome is an *in situ* melting product of the that gneiss, the zircon dated about 2.24 Ga can be envisaged as an inherited Archean zircon, which lost most of its radiogenic lead during the melting. The zircon age provided by the leucosome MV-27E is in agreement with the age yielded by the monazites from the same sample and, consequently, is also concordant with the monazite ages from the gneiss MV-27A, reinforcing the existence of an event at about 2.09 Ga.

**Table 2** – Zircon Pb-evaporation isotopic results for the leucosome MV-27E. Values in bold were included in the age calculations.

Zircon grain	T(°C)	Nº of ratios	$\frac{^{206}\text{Pb}}{^{204}\text{Pb}}$	$\frac{^{208}\text{Pb}}{^{206}\text{Pb}}$	2 $\sigma$	$\frac{^{207}\text{Pb}}{^{206}\text{Pb}}$	$\frac{^{207}\text{Pb}^*}{^{206}\text{Pb}^*}$	2 $\sigma$	step age (Ga)	2 $\sigma$	grain age (Ga)	2 $\sigma$
MV27E/1	1450	12	8850	0.0373	13	0.1295	0.1279	57	2070	8		
	1500	36	76923	0.0499	29	0.1289	0.1287	2	2081	3	2081	3
<b>MV27E/2</b>	<b>1500</b>	<b>36</b>	<b>17857</b>	<b>0.0540</b>	<b>32</b>	<b>0.1301</b>	<b>0.1293</b>	<b>27</b>	<b>2089</b>	<b>4</b>	<b>2089</b>	<b>4</b>
MV27E/3	1500	36	52632	0.0461	86	0.1288	0.1285	44	2077	6	2077	6
MV27E/4	1500	34	28571	0.0479	38	0.1291	0.1286	17	2080	2	2080	2
MV27E/5	1500	40	7752	0.0743	62	0.1425	0.1407	46	2236	6	2236	6
MV27E/6	1500	8	4762	0.0498	542	0.1289	0.1261	358	2045	50	2045	50
<b>MV27E/7</b>	<b>1500</b>	<b>4</b>	<b>111111</b>	<b>0.0394</b>	<b>114</b>	<b>0.1296</b>	<b>0.1295</b>	<b>34</b>	<b>2091</b>	<b>5</b>	<b>2091</b>	<b>5</b>
<b>MV27E/9</b>	<b>1500</b>	<b>34</b>	<b>52632</b>	<b>0.0431</b>	<b>17</b>	<b>0.1295</b>	<b>0.1293</b>	<b>19</b>	<b>2088</b>	<b>3</b>		
	<b>1550</b>	<b>26</b>	<b>100000</b>	<b>0.0396</b>	<b>22</b>	<b>0.1301</b>	<b>0.1300</b>	<b>65</b>	<b>2098</b>	<b>9</b>	<b>2089</b>	<b>5</b>
<b>Mean Age (3 grains - 100 ratios - USD 2.6)</b>											<b>2091 ± 5 Ma</b>	

\*radiogenic

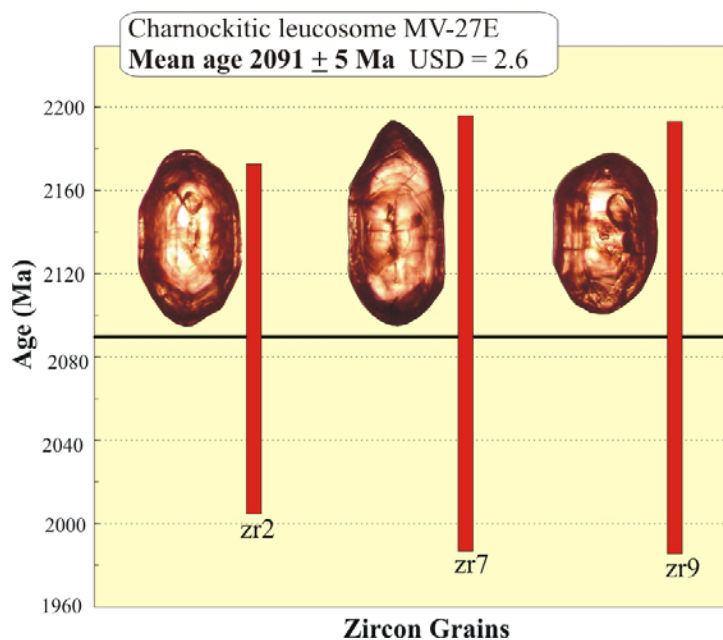


**Figure 6** – Pb-evaporation diagram for the leucosome MV-27E. The errors bars correspond to the mean age value on each zircon.

#### Enderbitic Gneiss LT-214

For this sample, 141 U-Th-Pb EPMA measurements were performed along traverses on eight monazite grains, yielding U, Th and Pb with strongly variables concentrations, especially the Th concentrations, which spread from 2.22 to 18.55 wt.%. U and Pb abundances range between 0.95 and 0.17 wt.% and 0.33 and 2.14 wt.%, respectively. Isolated ages of 1898 Ma, 1947 Ma and 2381 Ma were discarded. Furthermore, 5 additional spot analyses were also rejected statistically because their corresponding ellipses are significantly far from the especially very well defined error envelop (at 2007, 2009, 2010, 2194 and 2156 Ma) in the Th/Pb vs. U/Pb diagram. We can observe that the significant variation of the Th/U measured ratios, from 7 to 43, produced a wide spread of the points, giving a good precision on the slope ( $-3.75 \pm 0.27$ ) of the regression line (Fig. 5C). The U-Pb and Th-Pb ages of  $2066 +88 -93$  Ma and  $2093 \pm 28$  Ma, respectively, are similar within the errors. At the centroid of the population, an age of  $2087 \pm 3$  Ma is calculated, with MSWD = 1.2. This well defined age is interpreted as representing a single population of ages and, consequently, dates a single event at 2.09 Ga.

## Tonalitic gneiss LT-223A and granitic leucosome LT-223B

Eleven monazite grains from the tonalitic gneiss LT-223A were investigated, yielding a total of 140 measurements. Element concentrations are Th = 1.76-7.01 wt. %, U = 0.02-0.14 wt. % and Pb = 0.22-0.70 wt. %. The calculated individual ages present a scatter of about 300 Ma, varying from 1983 to 2282 Ma. From that, a bimodality of the age population can be suspected. An age of  $2095 \pm 9$  Ma was calculated from all the 140 measurements. This result is geologically acceptable, because it is in close agreement with the age provided by the previous samples, and fits with the event dated at about 2.09 Ga. Nevertheless, the calculated age is not statistically valid, since it is associated with a MSWD at 2.7 which is significantly above of the limit of 1.25 defined by Wendt and Carl (1991). A bimodality for the age population should be considered. We used the deconvolution of multiple age components algorithm (Sambridge and Compston, 1994) selecting the “Unmix Ages” option of Isoplot’s program from Ludwig (2004). Actually, a second group did not appear despite the group of several analyses, represented by their ellipse error in the Th/Pb vs U/Pb diagram, located significantly out of the error envelop on the same side of this envelop, showing a group of older analyses. Actually, the direct reduction of the individual ages and errors cannot lead to the same statistics as obtained from the Th/Pb vs U/Pb isochron diagram, because the error calculation on individual ages needs approximation and yields to a slight overestimate of the error. From the observation of all the 140 analyses in the Th/Pb vs U/Pb diagram, a main group represented by 128 measurements is identified after rejection of one young data (1986 Ma), besides a second minor group of 12 measurements in which the ages vary from 2169 to 2282 Ma.

The significant variation of the Th/U measured ratios lead to a good precision on the slope ( $-3.76 \pm 0.43$ ) of the regression line (Fig. 5D). The U-Pb and Th-Pb ages of  $2068 +160 -172$  Ma and  $2088 \pm 20$  Ma, respectively, are similar within the errors. Associated with an acceptable MSWD = 1.8, an age of  $2086 \pm 8$  Ma is calculated at the centroid of the population. This age is interpreted as representing a single population of ages and, consequently, dates a single event at 2.09 Ga.

The second group of 12 measurements leads to a larger error envelop associated with a large error on the slope of the regression line due to the reduced number of data (Fig. 5E). However, within the analytical error, the U-Pb and Th-Pb ages of  $2873 +505 -732$  Ma and  $2108 +120 -108$  Ma are in agreement with an age population dated at  $2215 \pm 28$  Ma at the centroid

(MSWD = 0.38). This age probably represents inheritance of an oldest event, suggesting a complex and polymetamorphic history for some monazite grains.

Several studies have shown that inheritance can be revealed for *in situ* measurements in monazite (Copeland et al., 1988; Montel et al., 1996; Cocherie et al., 1998 and 2005; Foster et al., 2002). However, in the focused case, conversely to the situation usually described in the literature, for instance by Cocherie et al. (1998), the two population of ages are not related to specific domains in a monazite grain, but they are rather randomly dispersed in all the analyzed grains.

#### Granitic leucosome LT-223B

In the leucosome LT-223B, six monazite grains were analyzed, yielding a total of 127 analyses. Th and Pb abundances range between 3.18-10.71 wt.% and 0.33-1.07 wt.%, respectively. U concentrations are remarkably low, varying between 0.01 and 0.09 wt. %. Four isolated points furnished ages of 1527 Ma and 2315 Ma, and Archean ages of 2527 Ma and 2646 Ma, and were not included in age calculations, since they are not statistically valid for interpretation. The first one can have suffered significant Pb loss while the three others can be shifted by common Pb contribution. The single remaining group of 123 measurements provided individual ages spreading between 2001 and 2187 Ma, distributed around the mean value of  $2092 \pm 8$  Ma calculated at the centroid with a MSWD = 2.0. We must admit that this high MSWD (2.0 instead of 1.26 expected for a single population of 123 measurements) indicates that some analyses are not statistically representative even if more than one population cannot be demonstrated. This is why we rejected 4 old data (between 2162 and 2187 Ma) and 5 young data (between 2001 and 2009 Ma) associated with ellipses out of the error envelop drawn in Th/Pb vs U/Pb diagram. The 114 remaining data do not spread widely because of the low and constant U content (Fig. 5F). However, the U-Pb and Th-Pb ages of  $1888 +359 -413$  Ma and  $2105 \pm 24$  Ma show that the regression line fits with the theoretical isochron within the analytical error associated with an acceptable MSWD = 1.6. The age population of  $2093 \pm 8$  Ma was calculated at the centroid. Taking into account the analytical errors, this age is similar to the age of  $2086 \pm 8$  Ma provided by the sample LT-223A, indicating that as the monazites from the gneiss LT-223A, as those from the leucosome LT-223B grew or were resetted during the same regional event occurred at about 2.09 Ga.

### Tonalitic gneiss LT-123A

The EPMA measurements were performed on eight monazite grains distributed along two traverses in each grain, giving 140 analytic points. Element concentrations are: Th = 2.03-10.62 wt.%, U = 0.06-0.45 wt.% and Pb = 0.22-0.92 wt. %. The individual ages display a wide spread, ranging from 1633 to 2234 Ma. Even after rejection of one old data (2234 Ma) and of 5 young statistically non representative measurements (1633 to 1921 Ma), the spread of the data indicates, at a first glance, that the ages do not represent a single population because the regression line calculated with the remaining 134 individual analyses yielded a MSWD of 2.9 in the diagram U/Pb vs. Th/Pb. Probably due to a slight over estimate of the individual ages, the “Unmix Ages” option of Isoplot cannot help to identify more than one population. Nevertheless, the high value of the MSWD is not statistically acceptable and indicates that the group does not represent a unimodal population. Then, two groups were arbitrarily individualized, which are envisaged as representing distinct unimodal populations. The major group is constituted of 110 spot analyses, with individual ages varying from 1962 to 2105 Ma, and the secondary group is represented by 24 measurements, which provided individual ages spreading between 2112 and 2173 Ma. The major population led to a weighted average age of  $2038 \pm 6$  Ma and a MSWD of 1.7 (Fig. 7A), registering a younger event, in order of 50-60 Ma, than that revealed in the precedent samples. The U/Pb and Th/Pb ages are similar within the errors, giving values of  $2016 +143 -154$  Ma and  $2042 \pm 27$  Ma, respectively. The spread of the Th/Pb ratios, which range from 11.07 to 48.23, gave a good precision on the slope of the regression line ( $-3.73 \pm 0.41$ ). Concerning the second group of ages, an age of  $2132 \pm 25$  Ma (MSWD = 0.35) was calculated with the 24 individual ages (Fig. 7B) at the centroid of the population. The regression line fits nicely with the corresponding theoretical isochron. This age can be considered as inheritance from an event older than 2.09 Ga.

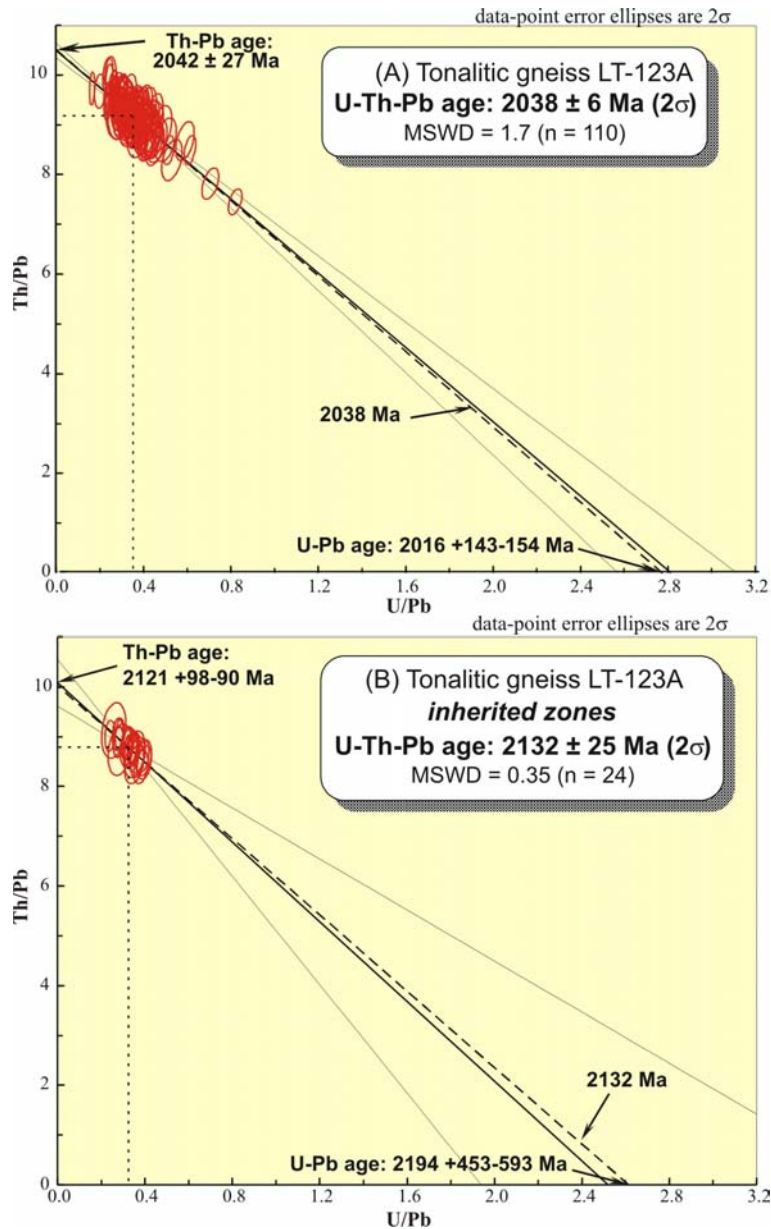


**Figure 7** – Th/Pb vs. U/Pb plots for eight monazite grains from the tonalitic gneiss LT-123A. The diagram (A) represents the main group of analytical points, whereas the diagram (B) is related to inherited domains in the grains. Heavy line: best regression line, dashed line: real isochron, thin lines: errors hyperbolas.

## Granitic gneiss MV-01A

Ninety-six measurements were performed on six monazite grains. The concentrations are rather uniform, ranging between 7.17 and 12.11 wt.%, and U and Pb abundances are similar, varying between 0.32-1.68 wt.% and 0.86-1.47 wt.%, respectively. The 96 individual ages range between 1623 and 2131 Ma, showing a scatter higher than 500 Ma. For the calculation of the ages, 3 points were initially discarded ( $1623 \pm 65$ ,  $1764 \pm 71$  and  $1794 \pm 72$  Ma), since they are supposed to have suffered radiogenic Pb loss. Using the Sambridge-Compston (1994) algorithm, the “Unmix Ages” option allows identification of two populations of ages from the remaining 93 spot analyses: the main group at about 2048 Ma and the second group at around 1890 Ma. (Fig. 8).

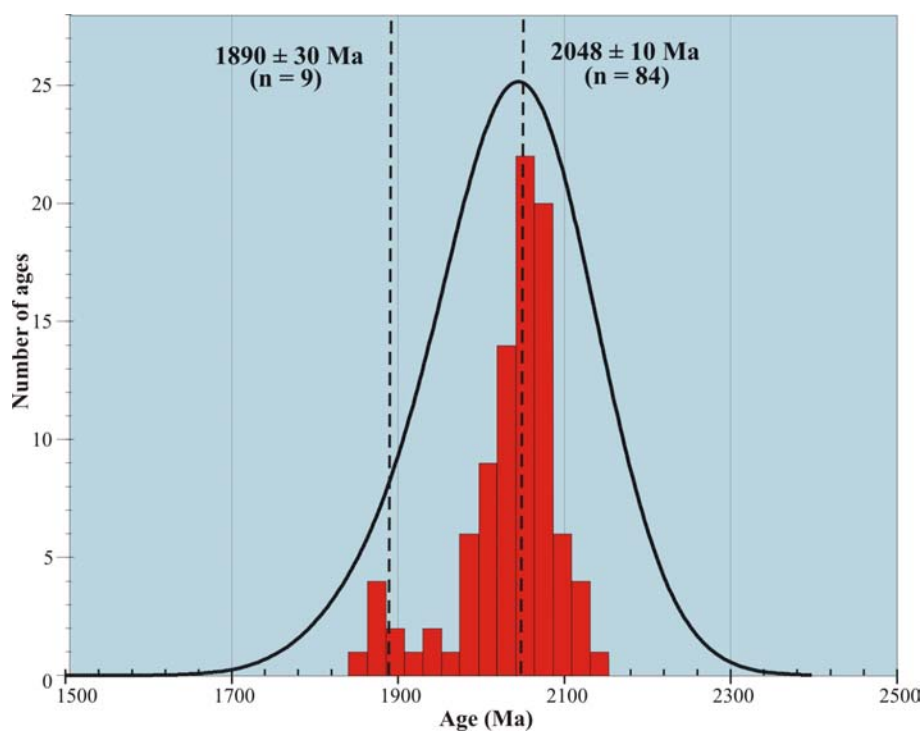


**Figure 8** – Age histogram representation of all individual ages ( $n = 93$ ) of monazites from the gneiss MV-01A showing two distinct group of ages.

Eight data ranging between these two groups were not considered because they probably suffered slight Pb diffusion at very small scale, similarly to that shown by Cocherie et al. (1998), they are meaningless in terms of a geological event. Thus the main group is defined by 78 measurements, with ages varying between 1985 and 2131 Ma. An average age of  $2056 \pm 7$  Ma

and a MSWD = 1.9 were calculated in the diagram U/Pb vs. Th/Pb (Fig. 9A). The large variation of the Th/U ratios, from 4.37 to 24.74, provided a wide spread of the points, giving a good precision on the slope of the regression line ( $-3.84 \pm 0.13$ ). The Th/Pb age of  $2049 \pm 22$  Ma is indistinguishable from the U/Pb age of  $2068 \pm 37$  Ma. The quality of this regression and mean age is also assessed by the very close location of the regression line compared to the theoretical isochron (Fig. 9A). Therefore, all statistical parameters are consistent and the calculated age marks an event at about 2.06 Ga.

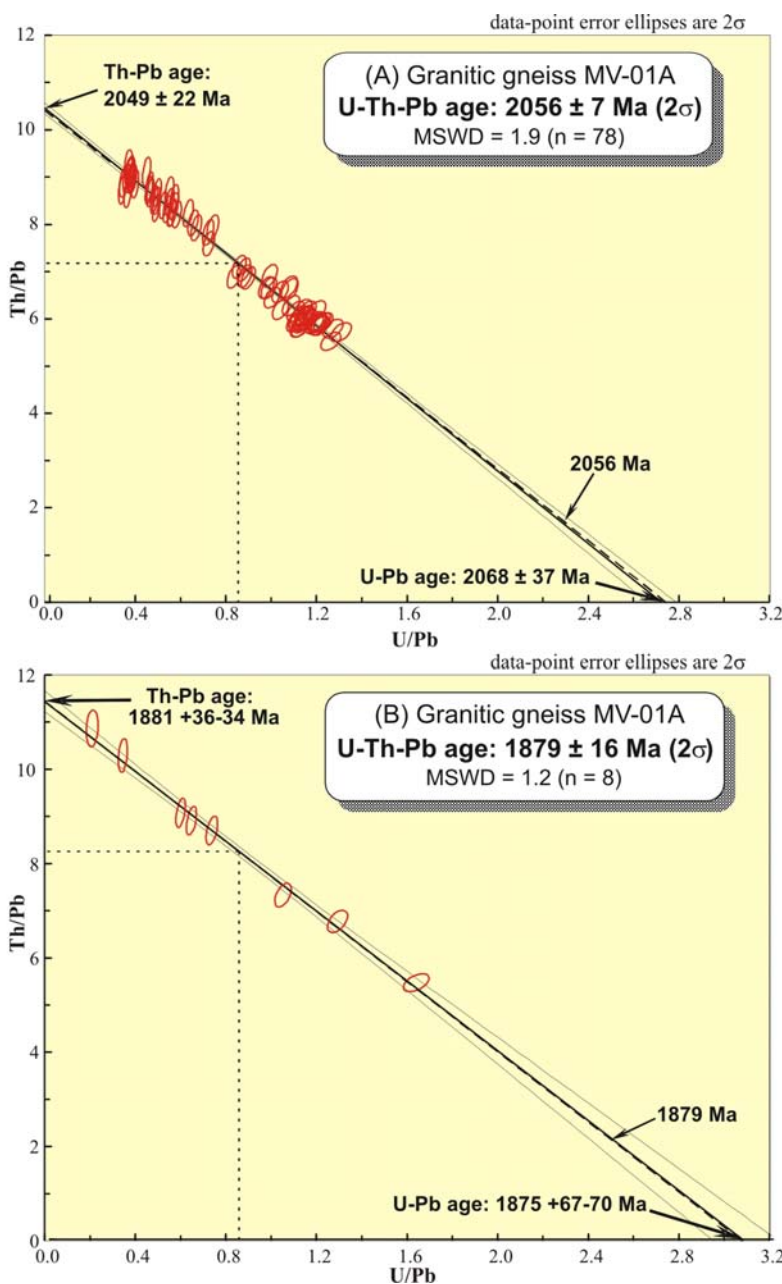


**Figure 9** – Th/Pb vs. U/Pb diagrams for six monazite grains from the granitic gneiss MV-01A, showing in (A) the plot referent to the main group of ages and in (B) the plot obtained with the secondary group of ages. Heavy line: best regression line, dashed line: real isochron, thin lines: errors hyperbolas.

The minor group is represented by 8 points, and provided a mean age of  $1879 \pm 16$  Ma (MSWD = 1.2) at the centroid of this population (Fig. 9B). We can notice the very nice spread of the data in the Th/Pb vs U/Pb diagram that determines a precise mean age despite the limited number of data.

## 6 - Discussion

### 6.1 - Interpretation of the geochronological data

The group of monazite ages obtained in this study indicates that the studied rocks experienced several stages of monazite growth, which possibly mark distinct tectono-thermal events that affected the Archean basement of the southwestern portion of the Amapá Block.

The enderbite gneiss MV-27A and the charnockitic leucosome MV-27E, furnished similar monazite ages of  $2096 \pm 6$  Ma and  $2088 \pm 8$  Ma, respectively. In addition, zircons from the sample MV-27E provided a mean age of  $2091 \pm 5$  Ma, interpreted as the crystallization age of the charnockite, which is also in agreement with the monazite ages from the same rock. The monazite and zircon ages, which are similar within the errors, make unambiguous the existence of a tectono-thermal event at about 2.09 Ga affecting the Archean basement of the southwestern portion of the Amapá Block. The next question to address is the geological meaning of the obtained ages and what is the meaning of the dated event in the metamorphic evolution of the area.

Interpretation of U-Pb mineral ages in high-grade metamorphic terranes relies on the concept of closure temperature ( $T_c$ ) for volume diffusion of the parent and radiogenic isotopes in a specific mineral or geochronometer (Dodson, 1973). This concept summarily predicts that, if during the metamorphic evolution the conditions of temperature exceed the  $T_c$  of a given geochronometer, the age obtained reflects the cooling through its blocking temperature.

The  $T_c$  of Th-U-Pb system in monazite has been largely accepted to be at least about  $700^\circ\text{C}$  (Parrish, 1990; Suzuki et al., 1994), but, some studies have shown that monazite can remain closed at temperatures higher than  $700^\circ\text{C}$ , if no fluid percolation is involved (Copeland et al., 1988; De Wolf et al., 1993; Kingsburg et al., 1993; Spear and Parrish, 1996; Braun et al., 1998; Cocherie et al., 2005), testifying that the  $T_c$  of the monazites can be significantly higher. Bingen and Bremen (1998) have shown that the U-Pb monazite ages, obtained in amphibolite- to granulite-facies rocks, can be preserved through metamorphic temperatures of about  $850^\circ\text{C}$ .

Finally, other studies (Braun et al., 1998; Cherniack et al., 2002) estimate the Tc of the monazite should be expected to be in order of 900°C, therefore, in the range of the Tc of U-Pb system in zircon (Lee et al., 1997; Cherniack and Watson, 2000).

It has been demonstrated that, in the U-Pb system in monazite may be reset by secondary replacement of newly grown monazite rather than by volume diffusion of Pb (De Wolf et al., 1993; Zhu et al., 1997, among others). Consequently, if diffusive Pb loss is not a common process in monazites (Parrish, 1990), a record of the prograde path of metamorphism and even of peak metamorphic conditions should be preserved.

Based on the considerations discussed above, we conclude that monazite ages from the granulites MV-27A and MV-27E may be interpreted as growth ages and, consequently, provides a reliable estimate of the age of the granulite-facies metamorphism that occurred at about 2.09 Ga, which possibly reached temperatures above 700°C. The zircon age of the leucosome MV-27E, which is similar to the monazite ages, reinforces this interpretation.

Zircon geochronology has been largely used to constrain the age of the high-grade metamorphism and commonly is interpreted as dating peak conditions of a metamorphic P-T path, in view of the high Tc of the zircon. In metamorphic rocks, protolithic zircons are accepted as the major carriers of zirconium for the formation of a new metamorphic zircon (Fraser et al., 1997; Robert and Finger, 1997). This implies that abundant zircon formation during the high-grade metamorphism occurs principally in connection with partial melting and subsequent magmatic crystallization. Consequently, the zircon age dates a phase of expressive melts in the partially molten rock, but this phase does not necessarily coincide with P-T peak of metamorphism, as demonstrated by Robert and Finger (1997).

Elucidative field data, described earlier, indicate that the charnockitic leucosome MV-27E is the product of *in situ* melting of the enderbite gneiss MV-27A during the high grade metamorphic event. The prominent oscillatory zoning observed in the zircon grains, generally seen as unequivocal evidence of magmatic crystal growth, fits with the field data, and thus, the zircon age can be confidently interpreted as dating a metamorphic stage involving partial melting. Furthermore, the metamorphic mineral assemblage (orthopyroxene-bearing) of the leucosome MV-27E strongly suggests that this migmatization event marks the time when peak metamorphic conditions were reached.

The monazite grains from the enderbite gneiss LT-214 furnished a well constrained average age of  $2087 \pm 3$  Ma, which is indistinguishable within the errors from the monazite and zircon ages from the samples MV-27A and MV-27E. Consequently, it is also interpreted as marking the granulite-facies metamorphic event registered in the previous samples.

The monazites from the tonalitic gneiss LT-223A recorded two distinct events, dated at  $2086 \pm 8$  Ma and at  $2215 \pm 28$  Ma, and a multistage growth history is suspected. The lowest age fits very well with the 2.09 m.y. old granulitic metamorphism previously discussed. Nevertheless, this gneiss shows a mineral assemblage consistent with amphibolite-facies metamorphism and there are no decisive indications that this sample had attained anytime granulite-facies metamorphic conditions, widely registered by the surrounding rocks.

Therefore, at least two possibilities can be envisaged: 1) this gneiss suffered granulitic metamorphism, but during the retrogressive metamorphic path, inverse metamorphic reactions re-adjusted the mineralogical assemblage to amphibolite-facies (for instance, through of the substitution of orthopyroxene by amphibole), or alternatively 2) the mineralogical assemblage of this rock testifies its position in upper crustal levels during the high-grade event, and for this reason granulite-facies conditions were not attained. The absence of petrographic features pointing to re-equilibration under amphibolite-facies conditions, in addition to the occurrence of inherited components older than 2.09 Ga in the monazites may be taken as evidence that the later hypothesis is more realistic. Anyway, the age at  $2086 \pm 8$  Ma reflects a stage of monazite growth coeval with the 2.09 Ga granulitic event.

We must address the discussion to the significance of the age of  $2215 \pm 28$  Ma also recorded by the monazites from the gneiss LT-223A, which possibly register an earlier event and, consequently, implies in the preservation of older components in the monazites.

In situ measurements have shown to be a powerful tool to identify older components in polygenetic monazites, which are frequently interpreted as inheritance of earlier magmatic or metamorphic thermal events (Montel et al., 1996; Zhu et al., 1997; Braun et al., 1998; Cocherie et al., 1998 and 2005; Crowley and Ghent, 1999; Tickyj et al., 2004). The recognition of inheritance in monazites is not doubt principally if a significant gap of time is registered between the age of the new and the old episodes of growth. However, inter- and intra-grain ages with less significant dispersion are frequently observed and this feature has been interpreted principally as produced

by episodic monazite grew during prograde and/or retrograde paths of a single metamorphic event (see Foster et al., 2000 and 2002).

In face of a difference higher than 100 Ma between the monazite ages of  $2086 \pm 8$  Ma and of  $2215 \pm 28$  Ma yielded by the gneiss LT-223A, the hypothesis that these ages reflects two distinct stages of monazite growth seems more coherent. Then, the U-Th-Pb data show that monazites from the gneiss LT-223A record unambiguously the prominent high-grade event occurred at about 2.09 Ga, but inheritance of an older event at around 2.21 Ga indicates that they were not completely reset during the youngest event. In view of the absence of elucidative data, the 2.21 m.y. old event can not be attributed to a granulitic event, as evoked for the youngest. However, the monazite age of  $2215 \pm 28$  Ma fits within the errors with a phase of granitic emplacement in the studied region, dated at  $2218 \pm 3$  Ma (Rosa-Costa et al., in press). The convergence of these geochronological data can be envisaged as evidence that the monazite age marks an earlier stage of migmatization coeval to granitic magmatism. This assumption is sustained by some studies that show the genetic relation between migmatization and granitic emplacement during orogenic stages of crustal reworking (Sawyer 1998, Milord et al. 2000, Solar and Brown 2001).

Monazite grains from the granitic leucosome LT-223B provided an age of  $2093 \pm 8$  Ga, which is also in accordance with the 2.09 m.y. old high grade event. Field features are consistent with local derivation of this leucosome, so, it is product of *in situ* melting of the gneiss LT-223A. Therefore, the age at  $2093 \pm 8$  Ma indicates that migmatization is contemporaneous to the high-grade metamorphic event.

The geochronological data provided by gneisses MV-01A and LT-123A, both from the Guianense Complex, recorded events younger, in order of 30-50 Ma, than the 2.09 m.y. old phase of granulite-facies metamorphism. In the gneisses MV-01A and LT-123A, prominent events were dated at  $2056 \pm 7$  Ma and at  $2038 \pm 6$  Ma, respectively. In addition, inherited components in monazites from sample LT-123A furnished an age at  $2132 \pm 25$  Ma. All monazite ages correspond within the errors to zircon ages furnished by neighboring granitic plutons, dated at  $2049 \pm 3$  Ma and  $2030 \pm 2$  Ma and (Rosa-Costa et al., in press) and at  $2146 \pm 3$  Ma (Rosa-Costa et al., 2003). Such a correlation, added to the widespread migmatization features observed in outcrop scale (see Fig. 3), strongly suggests that the monazite ages about 2.06 and 2.04 Ga can be interpreted as constraining migmatization events contemporaneous to granitic emplacement,

which occurred under amphibolite-facies metamorphic conditions. Inheritance from a previous event recognized in monazites from the gneiss LT-123A indicates that they were not completely reset during the latest event, and may also reflect an oldest migmatization event coeval to granitic magmatism about 2.13-2.14 Ga.

Especially in the gneiss MV-01A, a secondary age  $1879 \pm 16$  Ma was calculated. Some textural features document the interaction of this rock with hydrothermal fluids, as the prominent alteration of the feldspars along cleavage plans and grain boundaries. In addition, embayment of the crystal faces is a remarkable textural characteristic of the studied monazites (Fig. 4L), suggesting the interaction of the grains with fluid phases, leading to partial dissolution, which probably provoked elemental remobilization and, consequently, disturbing of the U-Th-Pb system. This is in agreement with investigations of Poitrasson et al. (1996) and Teufel and Heinrich (1997), which also emphasized the importance of hydrothermal activity in affecting the U-Th-Pb system of monazites. Thus, the significance of the lowest age is doubtful and it can not be confidently interpreted in terms of geological event. Nevertheless, we can not discard the possibility of the hydrothermal activity be related to the remarkable plutono-volcanic anorogenic event (Uatumã type) recorded in the central part of the Guiana Shield (Fig. 2), which is possibly synchronous to that dated at about 1.88-1.86 Ga in the central portion of the Brazil Central Shield (Santos et al. 2004, Dall'Agnol et al. 2005 and references therein).

## 6.2 - Geodynamical Implications

Distinct stages of the tectono-metamorphic evolution of the Archean basement in the southwestern portion of the Amapá Block were recognized in the studied samples, and dated at about 2.09 Ga and at 2.06 Ga and 2.04 Ga. The most prominent stage of monazite growth, recorded in monazites from high-grade gneisses and from a charnockitic leucosome of the Jari-Guaribas Complex, occurred at about 2.09 Ga and provides a reliable estimate of the age of the granulite-facies metamorphism. The 2.09 Ga monazite ages are in good agreement with the zircon age of a charnockitic leucosome, indicating that partial melting and migmatization have occurred during peak metamorphic conditions. However, in high-grade rocks that not reached granulitic temperatures, the monazites were not completely reset and preserved, locally, inheritance from an earlier event that occurred at about 2.21 Ga.

The other important stage, which occurred under amphibolite-facies conditions, was revealed by monazites from gneisses of the Guianense Complex that provided ages at about 2.06 Ga and 2.04 Ga, and which also registered inheritance of an older event at about 2.13 Ga.

The studied samples furnished only Paleoproterozoic ages, precluding the previous suspicion that Archean events could be also revealed. This indicates that, if the basement rocks from the Amapá Block were submitted to a high-grade event during Archean times, they were completely reset during the Paleoproterozoic overprinting. Then, based on the current data, we can not establish any genetic or chronological relationship between the Neoproterozoic (2.65-2.60 Ga) charnockitic magmatism (Noucouro Intrusive Suite) and the granulitic rocks of the region, as previously suspected (Rosa-Costa et al., 2003).

Comparing the obtained data with the available age records of other granulitic domains from eastern Guiana Shield, we observe that, in those areas, granulite-facies metamorphism has occurred in later stages of the Transamazonian orogenic cycle (Fig. 10A). In the Imataca Block, dating of metamorphic minerals has been used to constrain the time of the granulitic metamorphism at 2.05-1.98 Ga (Onstott et al., 1989; Tassinari et al., 2004). Roever et al. (2003) demonstrated that, the granulitic metamorphism in the Bakhuis Mountains, in Suriname, occurred at 2.07-2.05 Ga. Furthermore, in the northeastern portion of the Amapá Block, at Tartarugalzinho region, Oliveira et al. (2002) dated the high-grade event around 2.05-2.03 Ga, which is coeval to charnockitic emplacement occurred at about 2.05-2.04 Ga (Avelar et al., 2001; Enjolvy, 2004).

Differences concerning to the metamorphic conditions and the geodynamical processes that driven the high-grade metamorphism are also outstanding among the distinct granulitic terranes. In the Bakhuis Mountains, the metamorphism reached, at least locally, ultrahigh-temperature (UHT) conditions, following a counterclockwise path and attaining temperatures of about 950 °C, at 8.5-9 Kb (Roever et al., 2003). According to Delor et al. (2003b), the UHT metamorphic conditions were attained in response to mantle-driven thermal perturbation in a zone of maximum crustal stretching enhanced by sinistral shearing at continental scale, occurred between 2.07 and 2.05 Ga. In the Tartarugalzinho region, 2.05-2.04 m.y. old charnockitic magmatism is contemporaneous to the granulitic event of the Bakhuis Mountains and UHT metamorphic conditions were also evoked to explain the occurrence of charnockites in that region (Avelar et al., 2001). However, later petrologic investigations (Enjolvy, 2004) have estimated temperatures in order of 700-750 °C for the granulitic event, which are not compatible with UHT

metamorphism. Finally, in the Imataca Block, Tassinari et al. (2004) admitted that the granulites experienced peak-metamorphic conditions (750-800°C and 6-8 kbar) under a regime of transpressive thrusting and tectonic imbrication.

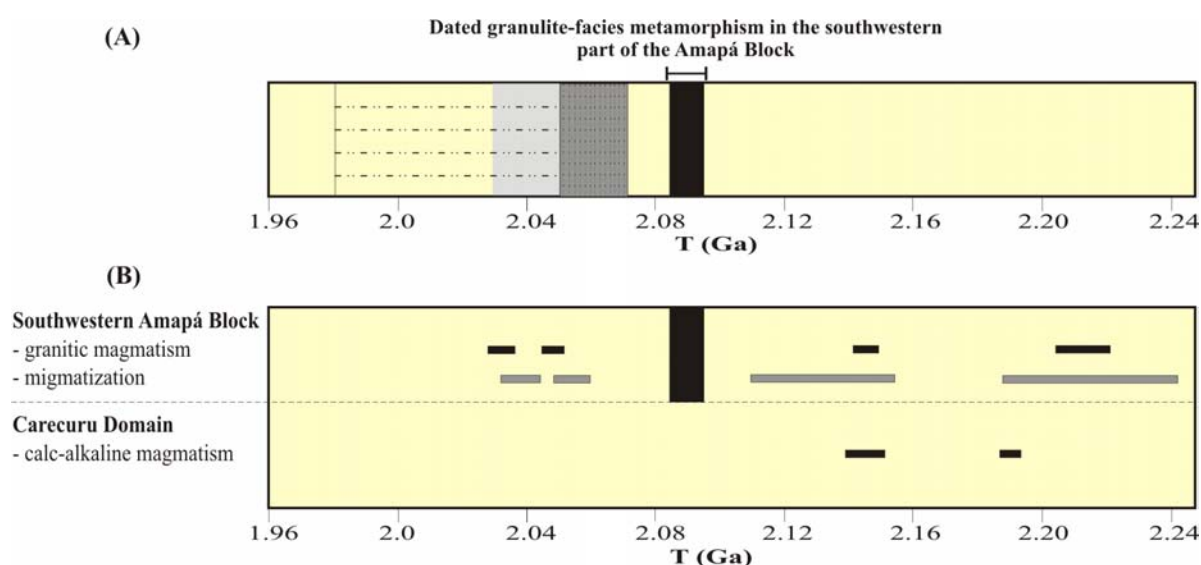


**Figure 10** – (A) Time of the high-grade metamorphism in granulitic domains from eastern Guiana Shield: southwestern Amapá Block – black column, Tartarugalzinho region – grey column, Imataca Block – horizontally hatched column, Bakhuis Mountains – dark grey and vertically hatched column. (B) Summary of the main geological events occurred during the Transamazonian tectono-thermal event in the southwestern portion of the Amapá Block and in the Carecuru Domain: granulitic metamorphism – black column, magmatism – black bars, migmatization – grey bars.

In the studied area, even if systematic petrological investigations and thermobarometric calculations were not performed, the set of data obtained in this study, added to available field and geochronological data brought some constraints for the tectono-metamorphic evolution of the Amapá Block.

The basement rocks from the southwestern part of the Amapá Block commonly exhibit pervasive NW-SE ductile foliation, dipping 40-60° SW, and stretching/mineral lineation with medium rakes predominantly to SW. This pattern is strongly disturbed along NW-SE transcurrent zones defined by steeply dipping mylonitic foliation and sub-horizontal lineation, marking the strike-slip movement. These structural features are coherent with a regime of oblique thrusting.

The penetrative character of the lineation, added to several kinematic indicators (e.g. S-C structures and rotated phenocrystals), indicate a general tectonic vergency from SW to NE. Apparently, the strike-slip zones development coincides with the final stages of the oblique movement, and produces reworking of the pre-existing fabrics (e.g. transposition of the banding).

Structural field features, added to the geochronological data, strongly indicate that the granulitic metamorphism was contemporaneous to the development of the thrusting system. For instance, the leucosomes MV-27E and LT-223B, both presenting monazite and zircon ages about 2.09 Ga, occur in layers concordant to the foliation of the parental gneisses (see Fig. 3A and B), and, specifically the latter presents mineral lineation parallel to the lineation of the hosting gneiss.

The structural pattern of the southwestern of Amapá Block, which registers an evolution from an early tangential tectonics to a dominantly transcurrent tectonics, is classically described as evidence of collision tectonics and testifies the oblique character of the collision. The development of this structural framework coeval to regional granulite-facies metamorphism about 2.09 Ga, is consistent with the paleomagnetic and  $^{40}\text{Ar}$ - $^{39}\text{Ar}$  data obtained in French Guiana by Théveniaut et al. (submitted). These authors admit that, during the Transamazonian orogenic cycle, an accretionary phase between 2.15 and 2.13 Ga, resulting from the convergence of West African (Man Shield) and Amazonian Archean plates (i.e. Amapá and Imatoca blocks), was followed by a collisional phase between 2.11 and 2.08 Ga that marks the end of the convergent cycle. In southwestern and eastern French Guiana, this collisional phase is accompanied by migmatization and granitic emplacement (Delor et al., 2003a; Lafon et al., 2003; Cocherie et al., 2005). Precedent palinspastic reconstructions involving Man and Guiana shields also evoke a collisional stage at about 2.1 Ga (Feybesse and Milési, 1994; Ledru et al., 1994).

The available geochronological data underline a gap of time in order of at least 30 Ma between the collisional phase and the latest stages of granitic emplacement and migmatization recorded in the investigated area. As above commented, the migmatization events revealed by dating of monazites from the gneiss MV-01A at  $2056 \pm 7$  Ma and from the gneiss LT-123A at  $2038 \pm 6$  Ma, are synchronous to emplacement of neighboring granitic plutons, respectively dated at  $2049 \pm 3$  Ma and  $2030 \pm 2$  Ma (Rosa-Costa et al., in press). All the dated samples are located around NW-SE strike-slip zones. Steeply dipping mylonitic foliation is recognized in the gneiss LT-123 and is described in the granite that furnished the age about 2.03 Ga (sample LT-17, see Rosa-Costa et al., in press), testifying to the strike-slip movement. Therefore, the

geochronological and structural data indicate that granitic emplacement and migmatization along strike-slip corridors mark a late-orogenic stage of the Transamazonian tectono-thermal event in the southwestern part of the Amapá Block.

This is consistent with the proposal of geodynamic evolution for the eastern Guiana Shield of Delor et al. (2003a and b), which consider that the period between 2.07 and 2.05 Ga is structurally characterized by transcurrent tectonics and marks a further stage of blockage of the oblique plate convergence between Amazonian and African Archean blocks. Records of this stage are granitic emplacement and metamorphism in French Guiana, UHT metamorphism with coeval charnockitic magmatism in the Bakhuis Mountains, and granulite-facies metamorphism and charnockitic emplacement in Tartarugalzinho region. If this model is confirmed, we may expect that the charnockitic pluton of the Paru Domain, dated at about 2.07 Ga (Rosa-Costa et al., in press), could also be a reflex of this regional event in the studied area.

Finally, in attempt to discuss the signification of the inherited ages in monazites from the gneisses LT-223A and LT-123A, some aspects of the Carecuru Domain have to be taken into account. According to Rosa-Costa et al. (in press), the Carecuru Domain represents a Paleoproterozoic magmatic arc that was accreted to the southern border of the Amapá Block during the Transamazonian orogenic cycle. Two distinct accretionary phases are indicated by calc-alkaline magmatism at 2.19-2.18 Ga and at 2.15-2.14 Ga (Rosa-Costa et al. 2003, in press). As discussed earlier, the monazite ages of  $2215 \pm 28$  Ma and of  $2132 \pm 25$  Ma are similar to the age of two distinct granitic pulses in the Amapá Block dated, respectively, at  $2218 \pm 3$  Ma and  $2146 \pm 3$  Ma (Rosa-Costa et al., 2003 and in press), and they are nearly synchronous to calc-alkaline magmatic pulses in the Carecuru Domain (e.g. granodioritic and dioritic pulses of  $2191 \pm 2$  Ma and  $2150 \pm 1$  Ma – Rosa-Costa et al., 2003 and in press). The convergence of the geochronological records (Fig. 10B) may be taken as evidence that, during the main phases of arc building in the Carecuru Domain, crustal reworking of the Archean basement rocks occurred in the Amapá Block, leading to migmatization and granitic emplacement.

## 7 - Acknowledgements

We thank L. A. Costa e Silva (CPRM-Porto Alegre) and M. R. Soares (CPRM-Belém) for their expert help with sample processing to monazite and zircon separation. C.N. Lamarão (UFPA, Belém), H.T. Costi (Museu Paraense Emílio Goeldi, Belém), J. Breton and C. Bény

(BRGM, Orléans) are acknowledged for acquiring of the BSE images. The continuous assistance provided by O. Legendre and C. Gilles (BRGM, Orléans) and by M. A. Galarza (Laboratório Pará-Iso, Belém) during the monazite and zircon analyses is greatly appreciated. David Fugate is thanked for his careful review of the English text.

The monazite analyzes were performed during a doctoral stage of the first author at BRGM, which was financially supported by CAPES (Coordenação de Aperfeiçoamento de Pessoal de Nível Superior), process BEX 2639/03-3. This paper is a contribution to PRONEX/CNPq (Proj. 103/98 – Proc. 66.2103/1998-0).

## 8 – References

- Ansdell, K.M. and Kyser, T.K., 1993. Textural and chemical changes undergone by zircon during the Pb-evaporation technic. *American Mineralogist*, 78, 1663-1673.
- Avelar, V.G., 2002. Geocronologia Pb-Pb em zircão e Sm-Nd em rocha total da porção centro-norte do Estado do Amapá – Brasil: Implicações para a evolução geodinâmica do setor oriental do Escudo das Guianas. Tese de Doutorado, CPGG-UFPA, Belém, 213 pg.
- Avelar, V.G., Lafon, J.M., Delor, C., 2001. Geocronologia Pb-Pb em zircão e Sm-Nd em rocha total da porção centro-norte do Estado do Amapá. Implicações pra a evolução geodinâmica do Escudo das Guianas. In: *Simp. Geol. Amaz.*, 7. Belém. Resumos Expandidos (CD ROM).
- Avelar, V.G., Lafon, J.M., Delor, C., Guerrot, C., Lahondère, D., 2003. Archean crustal remnants in the easternmost part of the Guiana Shield: Pb-Pb and Sm-Nd geochronological evidence for Mesoarchean versus Neoproterozoic signatures. *Geologie de la France* 2-3-4, 83-100.
- Bingen, B, and van Breemen, O., 1998. U-Pb monazite ages in amphibolite- to granulite-facies orthogneisses reflect hydrous mineral breakdown reactions: Sveconorwegian Province of SW Norway. *Contrib. Mineral. Petrol.* 132, 336-353.
- Bohlender, F., Van Reenen, D.D., Barton Jr., J.M., 1992. Evidence for metamorphic and igneous charnockites in the Sothern Marginal Zone of the Limpopo Belt. *Precambrian Research* 55, 429-449.
- Braun, I., Montel, J.M., Nicollet, C., 1998. Electron microprobe dating of monazites from high-grade gneisses and pegmatites of the Kerala Khondalite Belt, southern India. *Chemical Geology* 146, 65-85.
- Carvalho, J.M. de A., Rosa-Costa, L.T., Vasquez, M.L., Klein, E.L., Macambira, E.M.B., Vale, A.G., Ricci, P. Dos S.F., 2001. Projeto Província Mineral da RENCA e Distrito Mineral do Ipitinga - Carta geológica (escala 1:250.000). Belém, CPRM, (Programa de Levantamentos Geológicos Básicos).
- Catlos, E.J., Gilley, L.D., Harrison, T.M., 2002. Interpretation of monazite ages obtained via in situ analysis. *Chemical Geology* 188, 193-215.
- Cherniak, D.J. and Watson, E.B., 2000. Pb diffusion in zircon. *Chem. Geology*. 172, 5-24.

- Cherniak, D.J., Watson, E.B., Grove, M., Harrison, T.M., 2002. Pb diffusion in monazite. Abstract volume, The Geological Society of America Annual Meeting, Denver. Paper 138-5.
- Cocherie, A. and Albarède, F., 2001. An improved U-Th-Pb age calculation for electron microprobe dating of monazite. *Geochimica et Cosmochimica Acta* 65, 4509-4522.
- Cocherie, A. and Legendre, O., 2006. Potential minerals for determining U-Th-Pb chemical age using electron microprobe. *Lithos* (in press).
- Cocherie, A., Be Mezeme, E., Legendre, O., Fanning, C.M., Faure, M., Rossi, P. 2005. Electron-microprobe dating as a tool for determining the closure of Th-U-Pb systems in migmatitic monazites. *American Mineralogist* 90, 607-618.
- Cocherie, A., Legendre, O., Peucat, J.J., Kouamelan, A.N., 1998. Geochronology of polygenetic monazites constrained by in situ electron microprobe U-Th-total lead determination: implications for lead behaviour in monazite. *Geochimica et Cosmochimica Acta* 62, 2475-2497.
- Copeland, P., Parrish, R.R., Harrison, T.M., 1988. Identification of inherited radiogenic Pb in monazite and implications for U-Pb systematics. *Nature* 333, 760-763.
- Cordani, U.G., Tassinari, C.C.G., Teixeira, W., Basei, M.A.S., Kawashita, K., 1979. Evolução tectônica da Amazônia com base nos dados geocronológicos. In: II Congresso Geológico Chileno, Arica. *Actas*, 4, 137-148.
- Crowley, J.L. and Ghent, E.D., 1999. An electron microprobe study of the U-Th-Pb systematics of metamorphosed monazite: the role of Pb diffusion versus overgrowth and recrystallization. *Chemical Geology* 157, 285-302.
- Dall'Agnol, R., Teixeira, N.P., Ramo, O.T., Moura, C.A.V., Macambira, M.J.B., Oliveira, D.C. 2005. Petrogenesis of the Paleoproterozoic rapakivi A-type granites of the Archean Carajás metallogenic province, Brazil. *Lithos* 80, 101-129.
- De Wolf, C.P., Belshaw, N., O'Nions, R.K., 1993. A metamorphic history from micro-scale  $^{207}\text{Pb}/^{206}\text{Pb}$  chronometry of Archean monazite. *Earth Planet. Sci. Lett.* 120, 207-220.
- Delor, C., Lahondère, D., Egal, E., Lafon, J.M., Cocherie, A., Guerrot, C., Rossi, P., Trufert, C., Theveniaut, H., Phillips, D., Avelar, V.G., 2003a. Transamazonian crustal growth and reworking as revealed by the 1:500,000-scale geological map of French Guiana (2<sup>nd</sup> edition). *Geologie de la France* 2-3-4, 5-57.
- Delor, C., Roeber, E.W.F. De, Lafon, J.M., Lahondère, D., Rossi, P., Cocherie, A., Guerrot, C., Potrel, A., 2003b. The Bakhuis ultrahigh-temperature granulite belt (Suriname) : II. Implications for late Transamazonian crustal stretching in a revised Guiana Shield framework. *Geologie de la France* 2-3-4, 207-230.
- Dodson, M.H., 1973. Closure temperatures in cooling geochronological and petrological systems. *Contrib. Mineral. Petrol.* 40, 259-274.
- Enjolvy, R., 2004. Caractérisation géochronologique et pétrologique de l'événement fini-Transamazonien: étude en Guyane Française et en Amapá (Brésil). *Diplôme d'Etudes Approfondies, Université Montpellier II*, 42 p.
- Faraco, M.T.L., Marinho, P.A.C., Vale, A.G., Moura, C.V., Macambira, M.J.B., 2004. Idades modelo Sm-Nd e idade  $^{207}\text{Pb}$ - $^{206}\text{Pb}$  em zircão no Distrito de Ipitinga, Reserva Nacional do Cobre e seus Associados-RENCA. In: XLII Cong. Bras. Geol., Araxá. CD-ROM.

- Feybesse, J.L. and Milési, J.P., 1994. The Archean/Paleoproterozoic contact zone in West Africa: a mountain belt of décollement thrusting and folding on a continental margin related to 2.1 Ga convergence of Archean cratons? *Precambrian Research* 69, 199-227.
- Foster, G. and Parrish, R., 2003. Metamorphic monazite and the generation of P-T-t paths. In: Vance, D., Muller, W., Villa, I.M. (eds.) *Geochronology: linking the isotopic Record with petrology and textures*. Geological Society, London, Special Publication, v.220, 25-47.
- Foster, G., Gibson, H.D., Parrish, R.R., Horst-Wood, M.S.A., Fraser, J. Tindle, A., 2002. Textural, chemical and isotopic insight into the nature and behaviour of metamorphic monazite. *Chemical Geology* 191, 183-207.
- Foster, G., Kinny, P. Prince, C., Vance, D., Harris, N., 2000. The significance of monazite U-Th-Pb age data in metamorphic assemblages: a combined study of monazite and garnet chronometry. *Earth and Planetary Science Letters* 181, 327-340.
- Fraga, L.M.B., 2002. A associação anortosito-mangerito-granito rapakivi (AMG) do Cinturão Guiana Central, Roraima, e suas encaixantes paleoproterozóicas: evolução estrutural, geocronologia e petrologia. Tese de Doutorado, Curso de Pós-Graduação em Geologia e Geoquímica, Universidade Federal do Pará. 351p.
- Fraser, G., Elis, D., Eggins, S., 1997. Zirconium abundance in granulite-facies minerals, with implications for zircon geochronology in high-grade rocks. *Geology* 25, 607-610.
- Gaudette, H.E., Lafon, J.M., Macambira, M.J.B., Moura, C.A.V., Scheller, T., 1998. Comparison of single filament Pb evaporation/ionization zircon ages with conventional U-Pb results: Examples from the Precambrian of Brazil. *J. South American Earth Sci.* 11(4), 351-363.
- Gruau, G., Martin, H., Leveque, B., Capdevilla, R., 1985. Rb-Sr and Sm-Nd geochronology of Lower Proterozoic granite-greenstone terrains in French Guyane, South America. *Precambrian Research* 30, 63-80.
- João, X.S.J. and Marinho, P.A.C., 1982. Catametamorfitos Arqueanos da região centro-leste do Território Federal do Amapá. In: *Simp. Geol. Amaz.*, 1, Belém. Anais, v.2, pp. 207-228.
- Karabinos, P. and Gromet, L.P., 1993. Applications of single-grain zircon analysis to the detrital studies and age discrimination in igneous suites. *Geochimica and Cosmochimica Acta*, 57, 4257-4267.
- Kingsbury, J.A., Miller, C.F., Wooden, J.L., Harrison, M.T., 1993. Monazite paragenesis and U-Pb systematics in rocks of the eastern Mojave Desert, California, U.S.A.: implications for thermochronometry. *Chem. Geol.* 110, 147-167.
- Klein, E.L., Rosa-Costa, L.T., Lafon, J.M., 2003. Magmatismo Paleoarqueano (3,32Ga) na região do Rio Cupixi, SE do Amapá, SE do Escudo das Guianas. In: *Simpósio de Geologia da Amazônia*, 8. Manaus, CD ROM.
- Kober, B., 1987. Single zircon evaporation combined with  $Pb^+$  emitter-bedding for  $^{207}Pb/^{206}Pb$ -age investigations using thermal ion mass spectrometry, and implications to zirconology. *Contrib. Mineral. Petrology* 96, 63-71.
- Kober, B., Pidgeon, R.T., Lippolt, H.J., 1989. Single-zircon dating by stepwise Pb-evaporation constraints the Archean history of detrital zircons from the Jack Hills, Western Australia. *Earth and Planetary Science Letters*, 91, 286-296.
- Kröner, A., Jaeckel, P., Brandl, G., Nemchin, A.A., Pidgeon, R.T., 1999. Single zircon ages for granitoid gneisses in the Central Zone of the Lompopo Belt, Southern Africa and geodynamic significance. *Precambrian Research*, 93, 299-337.

- Kouamelan, A.N., Delor, C., Peucat, J.J., 1997. Geochronological evidence for reworking of Archean terrains during the Early Proterozoic (2.1 Ga) in the western Côte d'Ivoire (Man Rise – West African Craton). *Precambrian Research* 86, 177-199.
- Kober, B., 1986. Whole-grain evaporation for  $^{207}\text{Pb}/^{206}\text{Pb}$ -age-investigations on single zircons using a double-filament thermal ion source. *Contrib. Mineral. Petrology* 93, 482-490.
- Lafon J.M., Delor, C., Théveniaut H., Krymsky R., Tavares R.P.S., Roig J.Y., 2003. Isotopic deciphering of Rhyacian crustal evolution along the northern oyapok river: new constraints from Sm-Nd, U-Pb and Pb-Pb geochronology. In: *Simp. Geol. Amazônia*, 8, Manaus, Extended Abstract. CD-ROM.
- Lafon, J.M., Rossi, P., Delor, C., Avelar, V.G., Faraco, M.T.L., 1998. Novas testemunhas de relíquias arqueanas na crosta continental paleoproterozóica da Província Maroni-Itacaiúnas (Sudeste do Escudo das Guianas). In: *Cong. Bras. Geol.*, 40. Belo Horizonte, Anais., p.64.
- Lafon, J.M., Rossi, P., Delor, Barbosa, O.S., 2001. Granulitos tardi-Transamazônicos (2,06 Ga) na região norte do Estado do Amapá: o charnoquito de Calçoene. In: *Simp. Geol. Amaz.*, 7. Belém. CD ROM.
- Lafrance, J., Bardoux, M., Voicu, G., Stevenson, R. Machado, N., 1999. Geological and metallogenic environments of gold deposits of the Guiana Shield: a comparative study between St. Élie (French Guiana) and Omai (Guyana). *Exploration and Mining Geology* 8 (1-2), 17-135.
- Ledru, P., Johan, V., Milési, J.P. and Tegye, M., 1994. Markers of the last stages of the Paleoproterozoic collision: evidence for a 2 Ga continent involving Cúcum-South Atlantic provinces. *Precambrian Research* 69, 69-191.
- Lee, J.K.W., Williams, I.S., Ellis, D.J., 1997. Pb, U and Th diffusion in natural zircon. *Nature* 390, 159-162.
- Lima, M.I.C., Oliveira, E.P., Tassinari, C.C.G., 1982. Cinturões granulíticos da porção setentrional do Craton Amazônico. In: *I Simp. Geol. Amaz.*, Belém. Anais, 1, 147-162.
- Ludwig, K.R., 2004. Users manual for ISOPLOT/EX a geochronological toolkit for Microsoft Excel (version 3.1).
- McReath, I. and Faraco, M.T.L., 1997. Sm/Nd and Rb/Sr systems in part of the Vila Nova metamorphic suite, northern Brazil. In: *I South Amer. Symp. Isotop. Geol.*, Campos do Jordão. Extended abstracts, 194-196.
- Milord, I., Sawyer, E.W., Brown, M., 2000. Formation of diatexite migmatites and granites magma during anatexis of semi-pelitic metasedimentary rocks: an example from St. Malo, France. *Journal of Petrology* 42, 487-505.
- Montel, J.M., Foret, S., Veschambre, M. Nicollet, C., Provost, A., 1996. Electron microprobe dating of monazite. *Chemical Geology* 131, 37-53.
- Montgomery, C.W., 1979. Uranium-lead geochronology of the Archean Imataca Series, Venezuelan Guyana Shield. *Contrib. Min. Petrol.* 69, 167-176
- Montgomery, C.W. and Hurley, P.M., 1978. Total rock U-Pb and Rb-Sr systematics in the Imataca Series, Guyana Shield, Venezuela. *Earth Planet. Sci. Letters* 39, 281-290.
- Newton, R.C., 1992. An overview of charnockite. *Precam. Research* 55, 399-405.
- Nogueira, S.A.A., Bettencourt, J.S., Tassinari, C.C.G., 2000. Geochronology of the Salamangone gold deposit host-rocks, Lourenço district, Amapá, Brazil. *Rev. Brasil. Geoc.* 30 (2), 261-264.
- Norcross, C.E., Davis, D.W., Spooner, E.T.C., Rust, A., 2000. U-Pb and Pb-Pb age constraints on Paleoproterozoic

- magmatism, deformation and gold mineralization in the Omai area, Guyana Shield. *Prec. Res.* 102, 69-86.
- Oliveira, E.C., Lafon, J.M., Gioia, S.M.L., Pimentel, M.M., 2002. Implantação do método Sm-Nd para minerais metamórficos e sua aplicação em rochas da região central do Amapá, Sudeste do Escudo das Guianas. In: *Cong. Bras. Geol.*, 41. João Pessoa, SBG-NE, Anais, p.502.
- Onstott, T.C., Hall, C.M., York, D., 1989.  $^{40}\text{Ar}/^{39}\text{Ar}$  thermochronometry on the Imataca Complex, Venezuela. *Precambrian Research* 42, 255-291.
- Parrish, R.R., 1990. U-Pb dating of monazite and its application to geological problems. *Can. J. Earth Sci.* 27, 1435-1450.
- Pimentel, M.M., Ferreira Filho, C.F., Spier, C.A., 2002. Estudo Sm-Nd do Complexo Máfico-Ultramáfico Bacuri, Amapá: idade da intrusão, metamorfismo e natureza do magma original. *Revista Brasileira de Geociências* 32, 371-376.
- Poitrasson, F., Chenery, S., Bland, D.J., 1996. Contrasted monazite alteration and mechanisms and their geochemical implications. *Earth Planet. Sci. Lett.* 145, 79-96.
- Pommier A., Cocherie A. and Legendre O., 2002. EPMA Dating User's manual: Age calculation from electron probe microanalyser measurements of U-Th-Pb. BRGM, 9 p.
- Ricci, P.S.F., Carvalho, J.M.A., Rosa-Costa, L.T., Klein, E.L., Vasquez, M.L., Vale, A.G., Macambira, E.M.B., Araújo, O.J.B., 2001. Geologia e recursos minerais do Projeto RENCA – Fase I. Belém, CPRM.
- Ricci, P.S.F., Carvalho, J.M.A., Rosa-Costa, L.T., Lafon, J.M., 2002. Plúton charnoenderbítico Arqueano intrusivo nos ortognaisses granulíticos do Cinturão Jari – Terreno Arqueano expressivo do sudeste do Escudo das Guianas. In: *Cong. Bras. Geol.*, 41. João Pessoa, SBG-NE, Anais, p.524.
- Ridley, J., 1992. On the origins and tectonic significance of the charnockite suite of the Archean Limpopo Belt, Northern Marginal Zone, Zimbabwe. *Precambrian. Research* 55, 407-427.
- Robert, M. and Finger, F., 1997. Do U-Pb zircon ages from granulites reflect peak metamorphic conditions? *Geology* 25, 319-322.
- Roever, E.W.F. de, Kieft, C., Murray, E.E., Klein, E., Ducker, W.H., 1976. Surinamite, a new Mg-Al silicate from the Bakhuis Mountains, W Suriname. *American Mineralogist*, 61, 193-199.
- Roever, E.W.F. de, Lafon, J.M., Delor, C., Cocherie, A., Rossi, P., Guerrot, C., Potrel, A., 2003. The Bakhuis ultrahigh-temperature granulite belt (Suriname): I. petrological and geochronological evidence for a counterclockwise P-T path at 2.07-2.05 Ga. *Géologie de la France* 2-3-4, 175-206.
- Rosa-Costa, L.T., Lafon, J.M., Delor, C., in press. Zircon geochronology and Sm-Nd isotopic study: further constraints for the Archean and Paleoproterozoic geodynamic evolution of the southeastern Guiana Shield, north of Brazil. *Gondwana Research* (in press)
- Rosa-Costa, L.T., Ricci, P.S.F., Lafon, J.M., Vasquez, M.L., Carvalho, J.M.A., Klein, E.L., Macambira, E.M.B., 2003. Geology and geochronology of Archean and Paleoproterozoic domains of the southeastern Amapá and northwestern Pará, Brazil – southeastern Guiana Shield. *Géologie de la France* 2-3-4, 101-120.
- Sambridge, M.S. and Compston, W., 1994. Mixture modeling of multi-component data sets with application to ion-probe zircon ages. *Earth Planet. Sci. Lett.* 128, 373-390.

- Santos, J.O.S., Van Breemen, O.B., Groves, D.I., Hartmann, L.A., Almeida, M.E., McNaughton, N.J., Fletcher, I.R. 2004 . Timing and evolution of multiple Paleoproterozoic magmatic arcs in the Tapajós Domain, Amazon Craton: constraints from SHRIMP and TIMS zircon, baddeleyite and titanite U-Pb geochronology. *Precambrian Research*, 131, 73-109.
- Sato, K. and Tassinari, C.C.G., 1997. Principais eventos de acreção continental no Cráton Amazônico baseados em idade-modelo Sm-Nd, calculada em evoluções de estágio único e estágio duplo. In: Costa, M.L.C. and Angélica, R.S. (Eds.), *Contribuições à Geologia da Amazônia* 1, 91-142.
- Sawyer, E. W., 1998. Formation and evolution of granite magmas during crustal reworking, the significance of diatexis. *Journal of Petrology* 39, 1147-1167.
- Solar, G.S. and Brown, M., 2001. Petrogenesis of migmatites in Maine, USA: possible source of peraluminous leucogranite in plutons. *Journal of Petrology* 42, 789-823.
- Spear, F.S. and Parrish, R.R., 1996. Petrology and petrological cooling rates of the Valhalla Complex, British Columbia, Canada. *J. Petrol.* 37, 733-765.
- Stacey, J.S. and Kramers, J.D., 1975. Approximation of terrestrial lead isotopic evolution by a two stage model. *Earth and Planetary Sciences Letters* 26, 207-221.
- Suzuki, K. and Adachi, M., 1998. Denudation history of the high T/P Ryoke metamorphic belt, southwest Japan: constrains from CHIME monazite ages of gneisses and granitoids. *Journal of Metamorphic Geology* 16, 23-37.
- Suzuki, K. and Adachi, M., 1991. Precambrian provenance and Silurian metamorphism of the Tsubonosawa paragneiss in the South Kitakami terrane, Northeast Japan, revealed by the chemical Th-U-total Pb isochron ages of monazite, zircon and xenotime. *Geochemical Journal* 25, 357-376.
- Suzuki, K., Adachi, M., Kajizuka, I., 1994. Electron microprobe observations of Pb diffusion in metamorphosed detrital monazites. *Earth Planet. Sci. Lett.* 128, 391-405.
- Tassinari, C.C.G. and Macambira, M.J.B., 2004. A evolução tectônica do Cráton Amazônico. In: Mantesso-Neto, V., Bartorelli, A., Carneiro, C.D.R. and Brito Neves, B.B. (Eds.) *Geologia do Continente Sul-Americano: Evolução da Obra de Fernando Flávio Marques de Almeida*. pp. 471-485.
- Tassinari, C.C.G., Bettencourt, J.S., Geraldes, M.C., Macambira, M.J.B., Lafon, J.M., 2000. The Amazonian Craton. In: Cordani, U.G., Milani, E.J., Filho, A.T., Campos, D.A. (eds.) *Tectonic Evolution of South America*. Rio de Janeiro. In: Intern. Geol. Cong., 31. Rio de Janeiro. SBG. pp. 41-95.
- Tassinari, C.C.G., Munhá, J.M.V., Teixeira, W., Palácios, T., Nutman, A.P., Sousa, C.S., Santos, A.P., Calado, B.O., 2004. The Imataca Complex, NW Amazonian Craton, Venezuela: crustal evolution and integration of geochronological and petrological cooling histories. *Episodes* 27 (1), 3-12.
- Tassinari, C.C.G., Teixeira, W., Nutman, A.P., Szabó, G.A., Mondin, M., Sato, K., 2001. Archean crustal evolution of the Imataca Complex, Amazonian Craton: Sm-Nd, Rb-Sr e U-Pb (SHRIMP) evidences. In: *Simp. Geol. Amaz.*, 7. Belém. Resumos Expandidos (CD ROM).
- Teixeira, W., Tassinari, C.C.G., Cordani, U.G., Kawashita, K., 1989. A review of the geochronology of the Amazonian Craton: Tectonic implications. *Precambrian Research* 42, 213-227.

- Théveniaut, H., Delor, C., Lafon, J.M., Monié, P., Rossi, P., Lahondère, D., submitted. Paleoproterozoic (2155-2060 Ma) evolution of the Guiana Shield (Transamazonian event) in the light of new paleomagnetic data from French Guiana. Submitted to *Precambrian Research*.
- Tickyj, H., Hartmann, L.A., Vasconcellos, M.A.Z., Philipp, R.Y., Remus, M.V.D., 2004. Electron microprobe dating of monazite substantiates ages of major geological events in the southern Brazilian shield. *Journal of South American Earth Sciences* 16, 699-713.
- Tuefel, S. and Heinrich, W., 1997. Partial resetting of the U-Pb isotope system in monazite through hydrothermal experiments: a SEM and U-Pb study. *Chem. Geol.* 137, 273-281.
- Vanderhaeghe, O., Ledru, P., Thiéblemont, D., Egal, E., Cocherie, A., Tegye, M., Milési, J.J., 1998. Contrasting mechanism of crustal growth Geodynamic evolution of the Paleoproterozoic granite-greenstone belts of French Guyana. *Precambrian Research* 92, 165-193.
- Vasquez, M.L. and Lafon, J.M., 2001, Magmatismo tipo A de 1,75 Ga na porção oriental do Escudo das Guianas – Estados do Amapá e Pará, Brasil. In: *Simp. Geol. Amaz., 7. Belém. Resumos Expandidos (CD ROM)*.
- Voicu, G., Bardoux, M., Stevenson, R., Jébrak, M., 2000. Nd and Sr isotope study of hydrothermal scheelite and host rocks at Omai, Guiana Shield : implications for ore fluid source and flow path during the formation of orogenic gold deposits. *Mineralium Deposita* 35, 302-314.
- Wendt, I. and Carl, C., 1991. The statistical distribution of the mean squared weighted deviation. *Chemical Geology* 86, 275-285.
- Zhu, X.K., O’Nions, R.K., Belshaw, N.S., Gibb, A.J., 1997. Significance of in situ SIMS chronometry of zoned monazite from the Lewisian granulites, northwest Scotland. *Chem. Geol.* 135, 35-53.

## 8 – GEOCRONOLOGIA $^{40}\text{Ar}$ - $^{39}\text{Ar}$ EM ANFIBÓLIO E BIOTITA

Neste capítulo serão apresentados os dados obtidos pela datação de anfibólios e biotitas através do método  $^{40}\text{Ar}$ - $^{39}\text{Ar}$ , os quais, conjugados com outros dados geocronológicos e informações estruturais, permitiram definir preliminarmente os padrões de resfriamento regional dos distintos domínios tectônicos durante o Ciclo Orogênico Transamazônico, e associá-los a processos de exumação. Este capítulo compõe o último artigo científico relacionado a esta pesquisa, o qual foi submetido ao *Journal of South American Earth Sciences*.

### 8.1 – $^{40}\text{Ar}$ - $^{39}\text{Ar}$ GEOCHRONOLOGY ACROSS ARCHEAN AND PALEOPROTEROZOIC TERRANES FROM SOUTHEASTERN GUIANA SHIELD (NORTH OF AMAZONIAN CRATON, BRAZIL): EVIDENCE FOR CONTRASTING COOLING AND EXHUMATION HISTORIES

Lúcia T. da Rosa-Costa<sup>a</sup>, Patrick Monié<sup>b</sup>, Jean-Michel Lafon<sup>c</sup>, Nicolas O. Arnaud<sup>b</sup>

<sup>a</sup> CPRM – Geological Survey of Brazil, Belém, Brazil

<sup>b</sup> Laboratoire de Dynamique de la Lithosphère, UMR-CNRS 5573, Université Montpellier 2, Montpellier, France

<sup>c</sup> Laboratório de Geologia Isotópica Pará-Iso, Universidade Federal do Pará, Belém, Brazil

#### Abstract

A  $^{40}\text{Ar}/^{39}\text{Ar}$  geochronological study was performed on amphibole and biotite from representative units of distinct tectonic domains of the southeastern Guiana Shield, north of Amazonian Craton, the Amapá Block and the Carecuru Domain. In the Amapá Block, an Archean continental block involved in the Transamazonian orogeny (2.26 – 1.95 Ga), the investigated minerals, from rocks of the Archean high-grade basement assemblage, furnished Paleoproterozoic ages, indicating their complete resetting during the Transamazonian orogenic event. Amphibole ages are similar and vary from  $2133 \pm 25$  to  $2086 \pm 26$  Ma, and biotite ages spread mainly between  $2099 \pm 17$  and  $2073 \pm 14$  Ma. In the Carecuru Domain, which has geodynamic evolution related to a Paleoproterozoic magmatic arc setting during the Transamazonian event, calc-alkaline metagranitoids provided amphibole ages of  $2158 \pm 21$  Ma,  $2137 \pm 20$  Ma and  $2056 \pm 27$  Ma, and biotite ages of  $1853 \pm 13$  Ma and  $1970 \pm 15$  Ma.

The new  $^{40}\text{Ar}/^{39}\text{Ar}$  data, coupled with available geochronological records and petro-structural observations, allow delineate contrasting cooling and exhumation stories for the tectonic domains. In the Amapá Block, nearly vertical T-t paths reflect fast cooling rates around 67 °C/m.y. and 40 °C/m.y, which indicate a tectonically controlled exhumation, related to collisional stages of the Transamazonian orogeny. Conversely, in the Carecuru Domain, regional cooling rates in the order of 3-2.3 °C/m.y. suggest that the calc-alkaline granitoids underwent slow and monotonous cooling history since its emplacement until the biotite blocking. However, a local cooling rate of 100 °C/m.y. testifies magma emplacement in upper crustal levels or, alternatively, indicates differential uplift within the Carecuru Domain.

**Key Words:**  $^{40}\text{Ar}/^{39}\text{Ar}$  geochronology, T-t paths, Transamazonian Event, Guiana Shield, Amazonian Craton

## 1 - Introduction

During recent years, simultaneous petrological and geochronological investigations have been addressed for the reconstruction of the P-T-t paths of orogenic belts, in order to understand their metamorphic and tectonic evolution (England and Thompson, 1994; Thompson and England, 1994; Jolivet et al., 1996; Hawkins and Bowring, 1999; Liati and Gebauer, 1999). Mineral ages of metamorphic rocks are generally interpreted as the time of cooling through the closure temperature for volume diffusion of the parent and radiogenic isotopes (Dodson, 1973). The determination of ages in minerals with known closure temperatures has been widely used to constrain the cooling history (T-t path) of a given area in a temperature interval ranging from 150 to > 750°C, by combination of distinct geochronological methods (Moller et al., 2000; Baxter et al., 2002; Jung and Mezger, 2001, 2003). The  $^{40}\text{Ar}-^{39}\text{Ar}$  method has been mainly used to recover the cooling history of magmatic and metamorphic rocks over temperatures ranging from 550°C to 150°C. Comparing the cooling history (cooling time and cooling rate) of adjacent crustal portions in a given orogenic belt provides first order informations on the mechanisms that prevailed during the exhumation of rocks that equilibrated at various depths, and permits to link deep crustal and more superficial processes. Such thermochronological approach has been successfully employed in many orogenic belts (Monié et al., 1994, 1997; Bingen et al., 1998;

Morillon et al., 2000; Neves et al., 2000; Agard et al., 2002; Faure et al., 2002) and will be used in the present study to characterize the tectonic and thermal evolution of a portion of the southeastern Guiana Shield, northern Amazonian Craton.

In the northern part of the Amazonian Craton (Fig. 1), the Guiana Shield exposes an expressive orogenic belt extending along its eastern portion, which tectonic evolution is related to the Transamazonian orogenic cycle (2.26 – 1.95 Ga) and which matches with the Eburnean belt, in West Africa Craton (Feybesse and Milesi, 1994; Ledru et al., 1994; Théveniaut et al., submitted).

This belt corresponds to the Maroni-Itacaiúnas Province of Cordani et al. (1979) and Tassinari and Macambira (2004) that comprises large domains of Paleoproterozoic rocks, in which the geodynamic evolution involves juvenile crustal accretion during Rhyacian times (2300-2050 Ma), related to subduction settings, and subsequent crustal reworking (Gruau et al., 1985; Teixeira et al., 1989; Sato and Tassinari, 1997; Vanderhaeghe et al., 1998; Lafrance et al., 1999; Nogueira et al., 2000; Norcross et al., 2000; Voicu et al., 2000; Avelar, 2002; Delor et al., 2003; Roeber et al., 2003; Rosa-Costa et al., 2003, in press).

Moreover, the existence of two Archean blocks has been documented within the Maroni-Itacaiúnas Province, the Imataca Block in Venezuela (Montgomery and Hurley, 1978; Montgomery, 1979; Tassinari et al., 2001, 2004), and the Amapá Block, in northern Brazil (Rosa-Costa et al., in press). These blocks mainly consist of basement metamorphic complexes with Archean precursors, overprinted during the Transamazonian orogeny, when they have been deformed, cross-cut by several granitic plutons and experienced amphibolite- to granulite-facies metamorphism and migmatization (Sato and Tassinari, 1997; Lafon et al., 1998; Ricci et al., 2001, 2002; Tassinari et al., 2001, 2004, Oliveira et al., 2002; Pimentel et al., 2002; Avelar et al., 2003; Klein et al., 2003; Rosa-Costa et al., 2003, in press).

This study focuses on the southeasternmost part of the Maroni-Itacaiúnas Province, including the southwestern portion of the Amapá Block and part of an adjacent Paleoproterozoic terrane named Carecuru Domain (Fig. 1). The Amapá Block and the Carecuru Domain represent distinct crustal segments with outstanding differences in terms of age, lithological content, metamorphic grade and structural pattern (Ricci et al., 2001; Rosa-Costa et al., 2003, in press). The former is an Archean continental segment, which had a long-lived evolution marked by several episodes of crustal accretion and reworking that started at the end of the Paleoproterozoic and

continued until Paleoproterozoic times (Rosa-Costa et al., in press). Conversely, the latter is made of a Paleoproterozoic association of calc-alkaline granitoids and metavolcano-sedimentary sequences, interpreted as developed in an arc magmatic setting, which was accreted to the southern border of the Amapá Block during the Transamazonian orogenic cycle (Ricci et al., 2001; Rosa-Costa et al., in press).

In this paper, first hornblende and biotite  $^{40}\text{Ar}$ - $^{39}\text{Ar}$  dating has been conducted on rocks from representative lithological units of the Amapá Block and Carecuru Domain, in an attempt to provide a set of geochronological data to access the tectonothermal evolution of these two segments during the Transamazonian orogeny. Possible regional differences in the cooling and exhumation histories will be evaluated by comparing of biotite and amphibole ages from these two segments, in addition with available geochronological results, to better constrain cooling paths from high to low temperatures.

## 2 - Geological Setting

In the investigated area (Fig. 2), the basement of the Amapá Block consists of an Archean high-grade association which includes: 1) granulitic gneisses from the Jari-Guaribas Complex, represented mainly by enderbite and charnockitic orthogneisses derived from igneous protoliths dated at about 2.8 Ga (Rosa-Costa et al., 2003, in press), and which enclose minor slivers of mafic and pelitic granulites; 2) undated mesoperthite and/or clinopyroxene-bearing granitic orthogneisses, metamorphosed under amphibolite-granulite transitional facies, and included in the Baixo Mapari Complex; 3) undated paraderived granulites of the Iratapuru Complex (mainly aluminous gneisses and schists); 4) amphibolite-facies grey gneisses (mainly tonalitic and granodioritic) from the Guianense Complex, that derive from 2.65 - 2.60 Ga old magmatic precursors (Rosa-Costa et al., 2003, in press); and 5) several plutons of 2.65 - 2.60 Ga old catazonal granitoids (charnockites, enderbites and mesoperthite-bearing granites) grouped in the Noucouro Intrusive Suite (Ricci et al., 2002; Rosa-Costa et al., in press). In addition, high- to medium-grade gneisses, with inferred Archean ages, which can not be inserted in any specific stratigraphic unit, are informally referred as granulitic-gneissic-migmatitic complex and also included in the basement association of the Amapá Block.

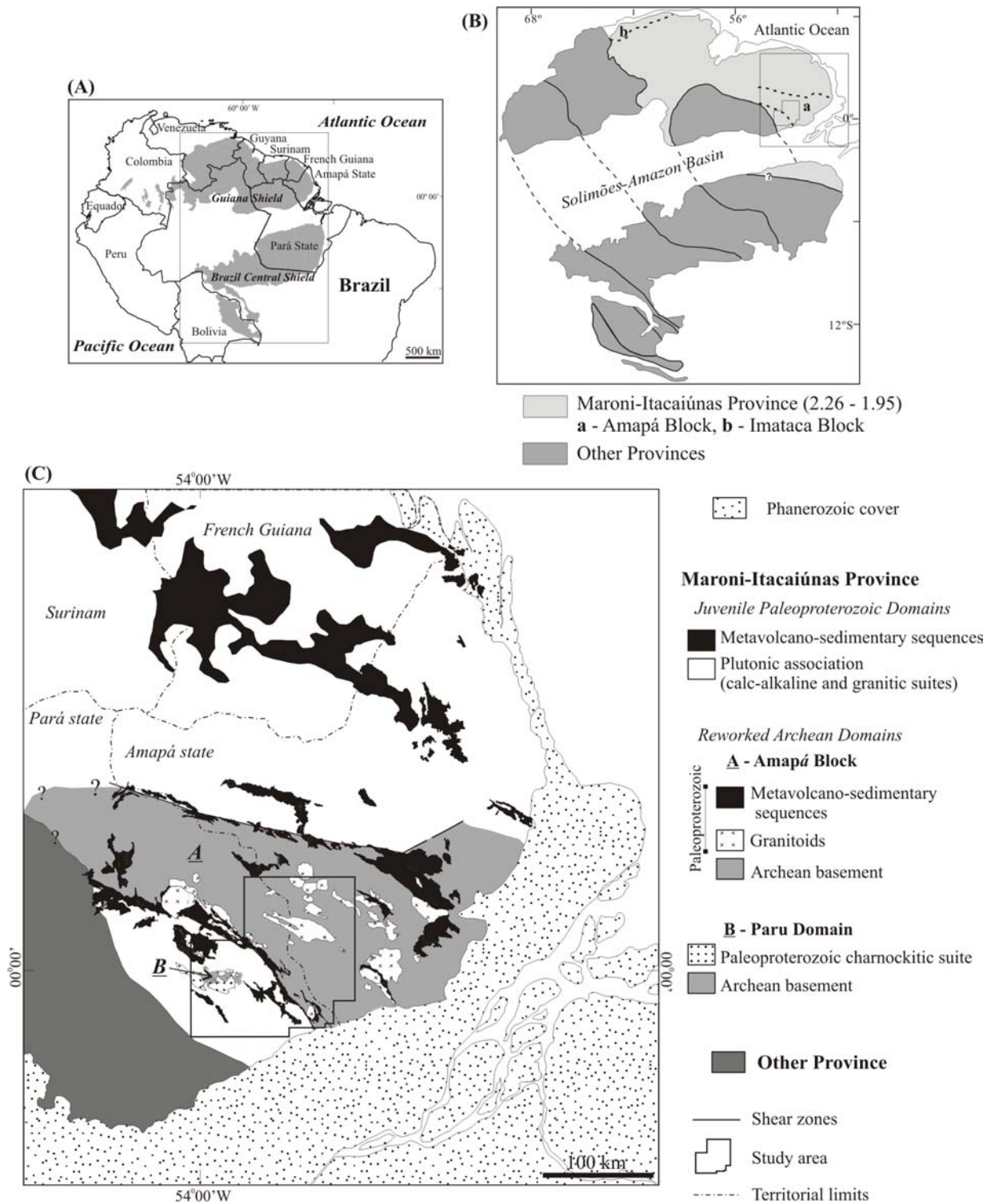


**Figure 1** – (A) Location map of the study area within the Amazonian Craton; (B) Simplified sketch map showing the distribution of the geochronological provinces of the Amazonian Craton according to the proposal of Tassinari and Macambira (2004), and (C) Geological sketch map of the southeastern Guiana Shield, based on Rosa-Costa et al. (in press).

The Transamazonian overprint in the Archean basement is indicated by the emplacement of several syn- to late-orogenic granitic plutons, dated at about 2.22 Ga, 2.18 Ga, 2.15 Ga, 2.05 Ga and 2.03 Ga, which have Nd isotope signatures pointing to an origin involving reworking of Archean crust (Rosa-Costa et al., 2003, in press). Furthermore, U-Th-Pb monazite dating performed on high-grade gneisses indicates that the granulite-facies metamorphism took place about 2.09 Ga ago, and marks late-orogenic migmatization events at about 2.06 Ga and 2.04 Ga, occurred under amphibolite-facies conditions and coeval to some episodes of granitic emplacement (Rosa-Costa et al., submitted)

The Carecuru Domain consists mainly of calc-alkaline gneisses and granitoids, dated around 2.19-2.18 Ga and 2.15-2.14 Ga, included in the Paru-Maratiá Complex and in the Carecuru Intrusive Suite. The Nd isotopic signature of these rocks reveals the participation of juvenile mantle-derived magmas and Archean components in the source of the calc-alkaline magmas (Rosa-Costa et al., in press). The supracrustal sequences are constituted mainly of mafic and intermediated metavolcanics, but a more expressive supracrustal belt, which composes the Ipitanga Group and that marks the boundary between the Amapá Block and the Carecuru Domain, also comprises BIFs and paraderived rocks. A Sm-Nd isochronic age dates this sequence at  $2264 \pm 34$  Ma (McReath and Faraco, 1997). Several granitic plutons cross-cut the calc-alkaline granitoids and supracrustal belts, one of them were being dated at about 2.10 Ga (Rosa-Costa et al., in press).

Furthermore, the Carecuru Domain contains an Archean inlier, named Paru Domain, composed essentially of granulitic gneisses of the Ananaí Complex, which are derived from 2.60 Ga old igneous precursors and that host charnockitic plutons of the Igarapé Urucu Intrusive Suite, dated at about 2.07 Ga (Rosa-Costa et al., 2003, in press).

The last known magmatic manifestation in the area is marked by emplacement of A-type granites (Waiãpi Granite), dated around 1.75 Ga (Vasquez and Lafon, 2001).

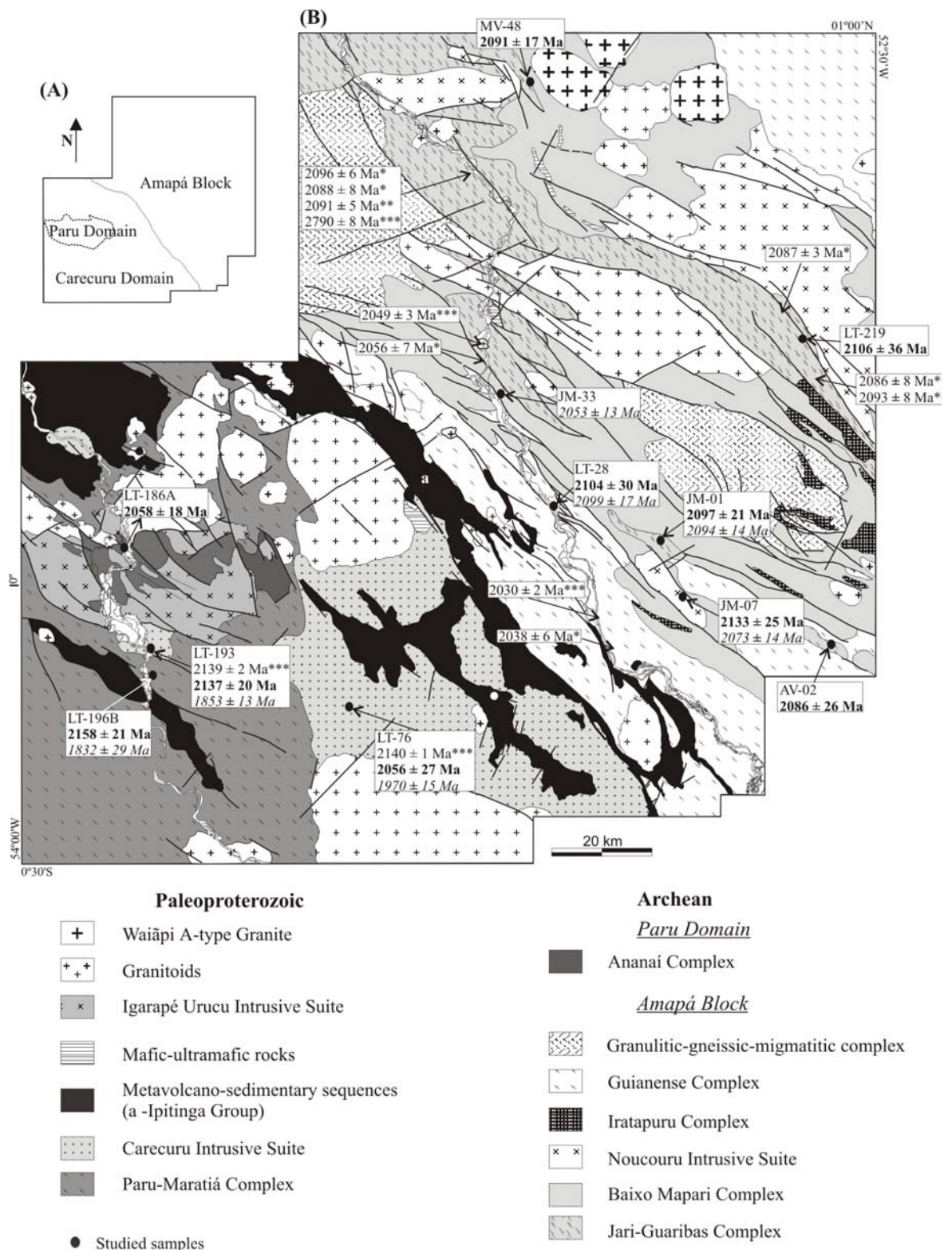


**Figure 2** – (A) Sketch map showing the tectonic subdivision of the studied area; (B) Geological map showing the amphibole (**bold**) and biotite (*italic*) ages of the samples dated in this work. This map also shows the monazite\* and zircon\*\* metamorphic ages compiled from Rosa-Costa et al. (submitted), and magmatic zircon\*\*\* ages from Rosa-Costa et al. (2003, in press). Map, stratigraphic arrangement and tectonic subdivision are based on Carvalho et al. (2001), Ricci et al. (2001) and Rosa-Costa et al. (in press).

### 3 - Sampling and Petrography

The  $^{40}\text{Ar}$ - $^{39}\text{Ar}$  study was performed on eleven samples from representative units of the different tectonic domains, selected according to the lithology, the available potassic minerals, the rock and mineral weathering and their geographic distribution. The location of the dated samples is shown in the Figure 2.

For the Amapá Block, five samples (MV-48, JM-01, AV-02, LT-219A, JM-33) of granulitic gneisses from the Jari-Guaribas Complex were selected, besides an enderbite (JM-07) from the Noucourou Intrusive Suite and a dioritic gneiss (LT-28B) from the Guianense Complex.

The samples MV-48 and JM-01 are enderbitic gneisses, composed of antiperthitic plagioclase, quartz, biotite, mesoperthitic alkali-feldspar, hornblende, and minor amounts of clino- and orthopyroxene, Fe-Ti oxides, apatite and zircon. These rocks present a well defined compositional banding and, microscopically, the texture is granolepidoblastic. The mafic granulites AV-02 and LT-219A are made of hornblende, plagioclase, clino- and orthopyroxene, Fe-Ti oxides and apatite, and present typical granulitic granoblastic texture.

The sample JM-33 is a medium-grained kinzigitic gneiss enclosed within the orthogranulites from the Jari-Guaribas Complex. This gneiss, with a grano-lepidoblastic microscopic texture, consists of quartz, antiperthitic plagioclase, biotite, sillimanite, cordierite, alkali-feldspar, garnet and Fe-Ti oxides, with minor zircon, monazite and spinel. It presents an evident compositional banding, which is modified by quartz-feldspatic leucosomes that occur as concordant or cross-cutting layers and streaks, interpreted as derived from *in situ* partial melting.

Zircon geochronology points to an Archean age at  $2797 \pm 3$  Ma for the igneous precursor of the enderbitic gneiss MV-48 (Rosa-Costa et al., 2003). Even if the other investigated gneisses from the Jari-Guaribas Complex have never been dated, an Archean age for the various protoliths is likely, based on the available geochronological data, field features and stratigraphical correlations (see Rosa-Costa et al., in press).

The sample JM-07 is a coarse-grained enderbite, constituted of antiperthitic plagioclase, quartz, mesoperthitic alkali-feldspar, biotite, hornblende, clino- and orthopyroxene, garnet, Fe-Ti oxides, apatite and zircon. It is weakly deformed, presenting porphyroclastic texture, defined by phenocrystals of mesoperthite and quartz dispersed within a medium-grained granoblastic matrix. Zircon dating defined the crystallization age of this rock at  $2605 \pm 6$  Ma (Ricci et al., 2002).

The dioritic gneiss LT-28B is a dark grey gneiss, defined by hornblende, biotite, plagioclase, quartz, Fe-Ti oxides, zircon and apatite. The texture is lepidoblastic and the mineralogical assemblage is compatible with amphibolite-facies metamorphic conditions. This rock is presumably Archean in age, since the available geochronological data indicate that the gneisses grouped in Guianense Complex derived from Archean igneous protoliths with ages ranging from 2.65 to 2.60 Ga (Rosa-Costa et al., 2003, in press).

Three samples (LT-196B, LT-76, LT-193) from the Carecuru Domain were investigated, which represent the widespread Paleoproterozoic calc-alkaline magmatism. The sample LT-196B is a dioritic gneiss from the Paru-Maratiá Complex, composed by plagioclase, quartz, biotite, hornblende, and accessories Fe-Ti oxides, titanite, apatite and zircon. The texture is protomylonitic, defined by porphyroclasts of plagioclase and hornblende within a medium-grained recrystallized matrix, containing polycrystalline ribbons of quartz and anastomosed strings of mafic minerals. Based on field correlations and on available geochronological data acquired in other samples of the focused stratigraphical unit (Rosa-Costa et al., 2003, in press), the crystallization age of this rock is assumed to be at around 2.15 - 2.14 Ga.

The samples LT-76 and LT-193 are grey to dark grey and medium- to coarse-grained diorites from the Carecuru Intrusive Suite, constituted of plagioclase, hornblende, biotite, quartz, Fe-Ti oxides, titanite, apatite and zircon. The sample LT-76 preserves an inequigranular hypidiomorphic- to idiomorphic igneous texture, while the sample LT-193 is weakly deformed and shows porphyroclastic texture. Zircon geochronology furnished magmatic ages for both samples at  $2140 \pm 1$  Ga (Rosa-Costa et al., 2003) and at  $2139 \pm 2$  Ma (Rosa-Costa et al., in press), respectively.

In addition, one sample (LT-186A) from the Paru Domain was studied. It is a medium-grained mafic granulite from the Ananaí Complex, composed of clinopyroxene, hornblende, plagioclase, orthopyroxene, quartz and Fe-Ti oxides, with zircon and apatite as accessory mineral phases, and exhibiting typical granoblastic granulitic texture. An Archean age is suspected for this rock, since an age at  $2597 \pm 4$  Ma was defined for the igneous protolith of a granulite from the Ananaí Complex (Rosa-Costa et al., 2003).

The gneisses and granitoids from the studied stratigraphical units show, commonly, evidences of hydrothermal alteration, which are indicated, for instance, by chloritization of the hornblendes and biotites. Then, a careful petrographic examination was carried out before

selection of the hornblende and biotite grains to be analyzed, in order to select only preserved minerals as well as to avoid grains containing mineral inclusions. Representative photos of some of the studied hornblendes and biotites are presented in the Figure 3, which shows the fresh nature of the dated minerals.

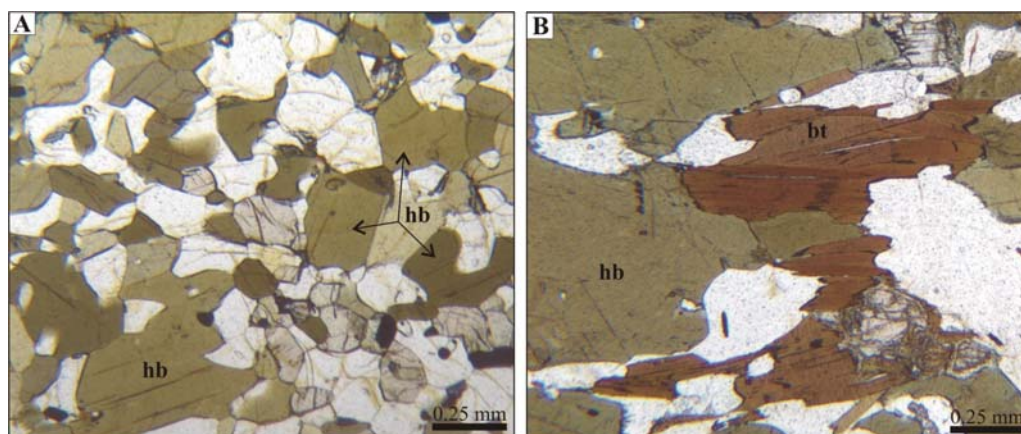


**Figure 3** – Photomicrographs showing representative hornblende (hb) and biotite (bt) crystals of some of the dated samples. (A) Mafic granulite AV-02, and (B) Enderbitic gneiss JM-01.

## 4 - $^{40}\text{Ar}$ - $^{39}\text{Ar}$ Dating

### 4.1 - Analytical Procedure

Bulk samples of hornblende and biotite were separated using standard techniques of concentration of minerals that involved steel jaw-crusher, steel roller-mill, sifters, magnetic separator and heavy liquids. Mineral concentrations were obtained by hand-picking under a binocular microscope from granulometric fractions  $> 350\mu\text{m}$ . The selection of the crystals to be analyzed was carefully performed considering the automorphic shape of the minerals. Final mineral purification was achieved by ultrasonic cleaning in acetone and posterior rinsing in distilled water.

The samples were irradiated at the McMaster reactor, Ontario, in the 5C position for 40 h under a  $10^{18}$  neutrons  $\text{cm}^{-2}\text{s}^{-1}$  flux. Irradiation interferences on K, Ca and Cl were corrected by irradiation of KCl and  $\text{CaF}_2$  pure salts. J factor was estimated by the use of duplicates of the Fish Canyon sanidine and MMHb-1 amphibole standards, with respective ages of 28.48 Ma and 520.4 Ma (Samson and Alexander, 1987; Schmitz and Bowring, 2001; Schmitz et al., 2003).

The samples were analyzed in laboratories of the Université de Montpellier 2, France, using bulk-sample step-heating technique. The minerals were loaded in aluminum packets into a double vacuum Staudacher type furnace, which temperature is calibrated by means of a thermocouple, and step heated. The gas was purified by the means of cold traps with liquid air and Al-Zr getters during 5 minutes. Once cleaned, the gas was introduced into a VG3600 mass spectrometer, and 1 minute was allowed for equilibration before analysis. Signals were measured by the mean of a Faraday cup with a resistor of  $10^{11}$  ohm for  $^{40}\text{Ar}$  and  $^{39}\text{Ar}$  while  $^{39}\text{Ar}$ ,  $^{38}\text{Ar}$ ,  $^{37}\text{Ar}$  and  $^{36}\text{Ar}$  were analyzed with a photomultiplier after interaction on a Daly plate. Gain between both collectors was estimated by duplicate analysis of  $^{39}\text{Ar}$  on both during each analysis, and also by statistical analysis on a period of several years. This gain is in average of 79 and is know at better than 1.5%. This error is included in the age calculation, along with analytical errors on each signal and errors on the blank values. Plateau ages are weighted mean ages which error takes the error on the J factor into account. The isochron ages are obtained in an inverse isochron diagram of  $^{36}\text{Ar}/^{40}\text{Ar}$  versus  $^{39}\text{Ar}/^{40}\text{Ar}$  (Roddick et al., 1980), which allows homogeneous excess components to be individualized in many occasions. Errors on age and intercept age include individual errors on each point and linear regression by York's method (York, 1969). The goodness of it relative to individual errors is measured by Mean Square Weighted Deviation (MSWD).

## 4.2 - Results

### *General Comments*

The calculated ages for the studied samples are summarized in the Table 1 and detailed  $^{40}\text{Ar}$ - $^{39}\text{Ar}$  analytical results are presented in the Table 2. Graphical representation of the data is displayed in the Figures 4 to 9.

The data were evaluated by simultaneous analysis of the  $^{40}\text{Ar}/^{39}\text{Ar}$  age spectra, K/Ca diagrams and  $^{36}\text{Ar}/^{40}\text{Ar}$  vs.  $^{39}\text{Ar}/^{40}\text{Ar}$  isotope correlations plots. Most of the samples displayed a nearly flat age spectra for a large percentage of the released  $^{39}\text{Ar}$ , producing ages representing weighted mean values for around 65% of the released gas. The flat portion of the release spectra is generally accompanied by constant K/Ca. The reproducibility of the Ar isotopic composition for successive heating steps consists in the fundamental argument that the isotopic system was not disturbed since the time of initial cooling (McDougall and Harrison, 1988). It is necessary to remark that this assumption is not valid in some special cases, for instance when the plateau age

records a posterior thermal event that provoked the total resetting of the isotopic system or when excess argon is homogeneously distributed within the dated minerals (e.g. Foland, 1983). Conversely, disturbed age spectra have been commonly interpreted as evidence for presence of extraneous  $^{40}\text{Ar}$  or of partial radiogenic  $^{40}\text{Ar}$  loss (Lanphere and Dalrymple, 1976; Harrison and McDougall, 1981), but other analytical or mineralogical phenomena can produce disturbed patterns of the age spectra (see Kelley and Turner, 1991; Lee et al., 1991; Wartho, 1995).

Some samples show strongly scattered release spectra, accompanied by variable K/Ca pattern, indicating that the Ar was released from different sites, for instance, from mineral inclusions, which were not detected through petrographic examination.

A general evaluation of the data show that the ages calculated in the age spectra and in the  $^{36}\text{Ar}/^{40}\text{Ar}$  vs.  $^{39}\text{Ar}/^{40}\text{Ar}$  isotope correlation plots are similar within limit of the errors for the most samples. Even in that samples showing disturbed release spectra, the corresponding gas fractions generally have a good alignment of the points in the isotope correlation plot and the age calculated do not differ markedly from the age calculated in the age spectra.

#### *Results from the Amapá Block*

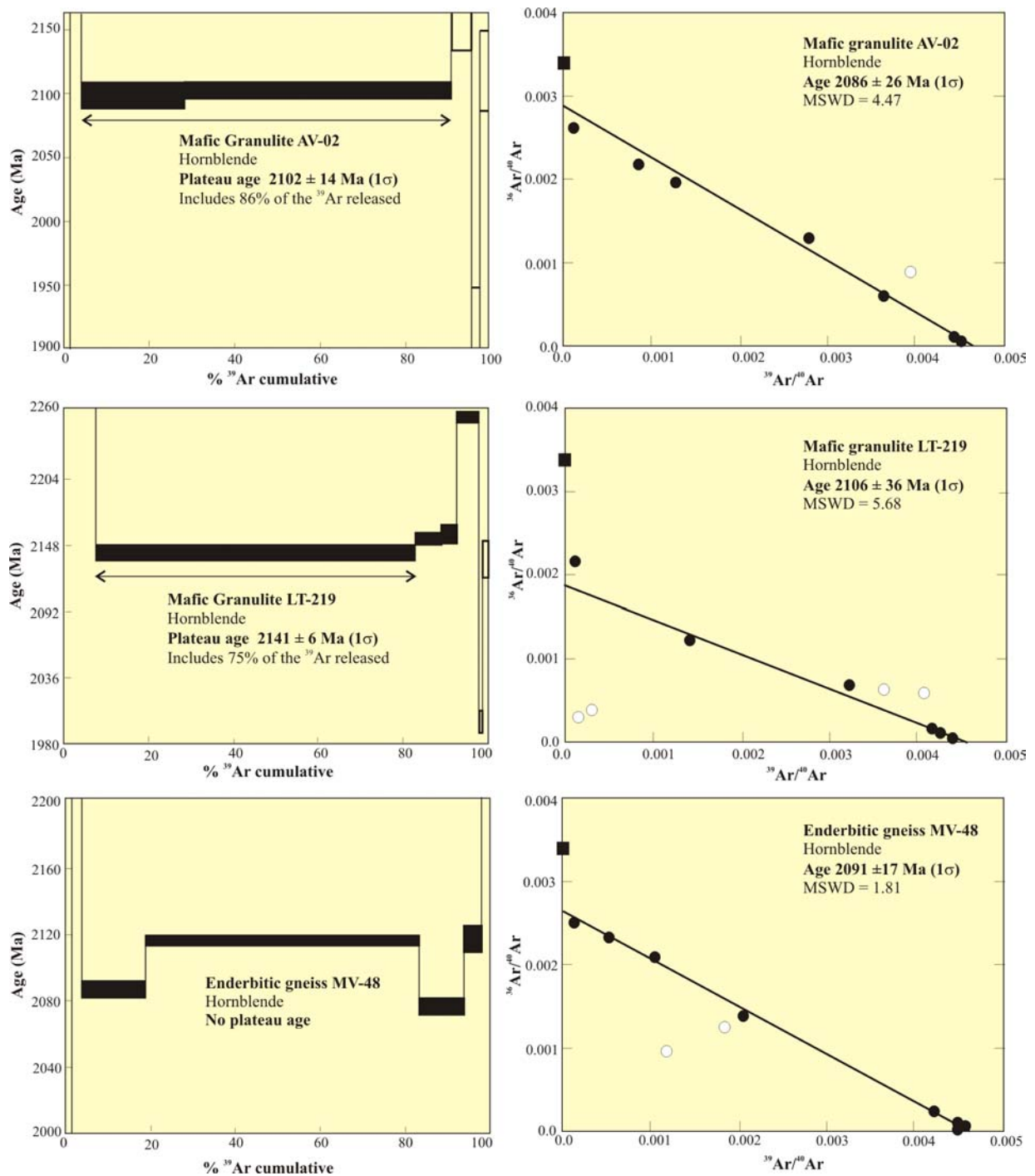
The Figures 4 to 6 show the age spectra and isotope correlation diagrams for hornblendes and biotites from rocks of representative units of the Archean basement assemblage of the Amapá Block. Hornblendes of the mafic granulites AV-02 and LT-219, both from the Jari-Guaribas Complex, displayed concave age spectra (saddle-shaped), with a rough stepwise age increase at low and high temperatures and minimum ages in the saddle. This release pattern is habitually considered as evidence that the mineral was affected by excess argon (Lanphere and Dalrymple, 1976; Harrison and McDougall, 1981). A two-step age at  $2102 \pm 14$  Ma (86% of the  $^{39}\text{Ar}$  released) and a single-step age at  $2141 \pm 6$  Ma (75% of the  $^{39}\text{Ar}$  released) were obtained in the age spectra of the granulites AV-02 and LT-219, respectively, and represent the minimum ages of the saddle. Intercept ages of  $2086 \pm 26$  Ma (MSWD = 4.47) and  $2106 \pm 36$  Ma (MSWD = 5.68) were calculated in the isotope correlation plot with 7 and 6 heating steps, for the same samples, respectively. Even if large MSWD values are associated with the intercept ages, which could render them partially meaningless, they are similar within the errors to the ages obtained in the age spectra and can be considered acceptable for geological interpretation.

Hornblende from the enderbitic gneiss MV-48 displayed a disturbed age spectrum but yielded a well-defined intercept age at  $2091 \pm 17$  Ma (MSWD = 1.81), calculated with 8 heating steps, which is in accordance with the previously discussed amphibole intercept ages furnished by the mafic granulites, reinforcing our interpretation that those ages are geologically significant.

In the enderbitic gneiss JM-01 a hornblende-biotite pair was analyzed. Biotite presented a convex age spectrum, characterized by low ages in the first heating increments, followed by a progressive climbing of the apparent ages in the medium section and a fall during high experimental temperatures. This is indicative of slightly chloritized biotite affected by  $^{39}\text{Ar}$  recoil during irradiation (Ruffet et al., 1991). A two-step age of  $2095 \pm 13$  Ma represents 60% of the released gas and is similar to the well-constrained intercept age of  $2094 \pm 14$  Ma (MSWD = 0.95) calculated in the isotope correlation plot with 8 heating steps. Hornblende provided a discordant age spectrum with excess argon released at low experimental temperature, followed by a flat section with concordant ages at  $2097 \pm 2$  Ma related to 66 % of the released gas. A similar age of  $2097 \pm 21$  Ma (MSWD = 0.85) was obtained with 6 heating steps in the isotope correlation plot. The biotite and hornblende ages from sample JM-01 are statistically similar, and agree with all ages above reported for the Amapá Block.

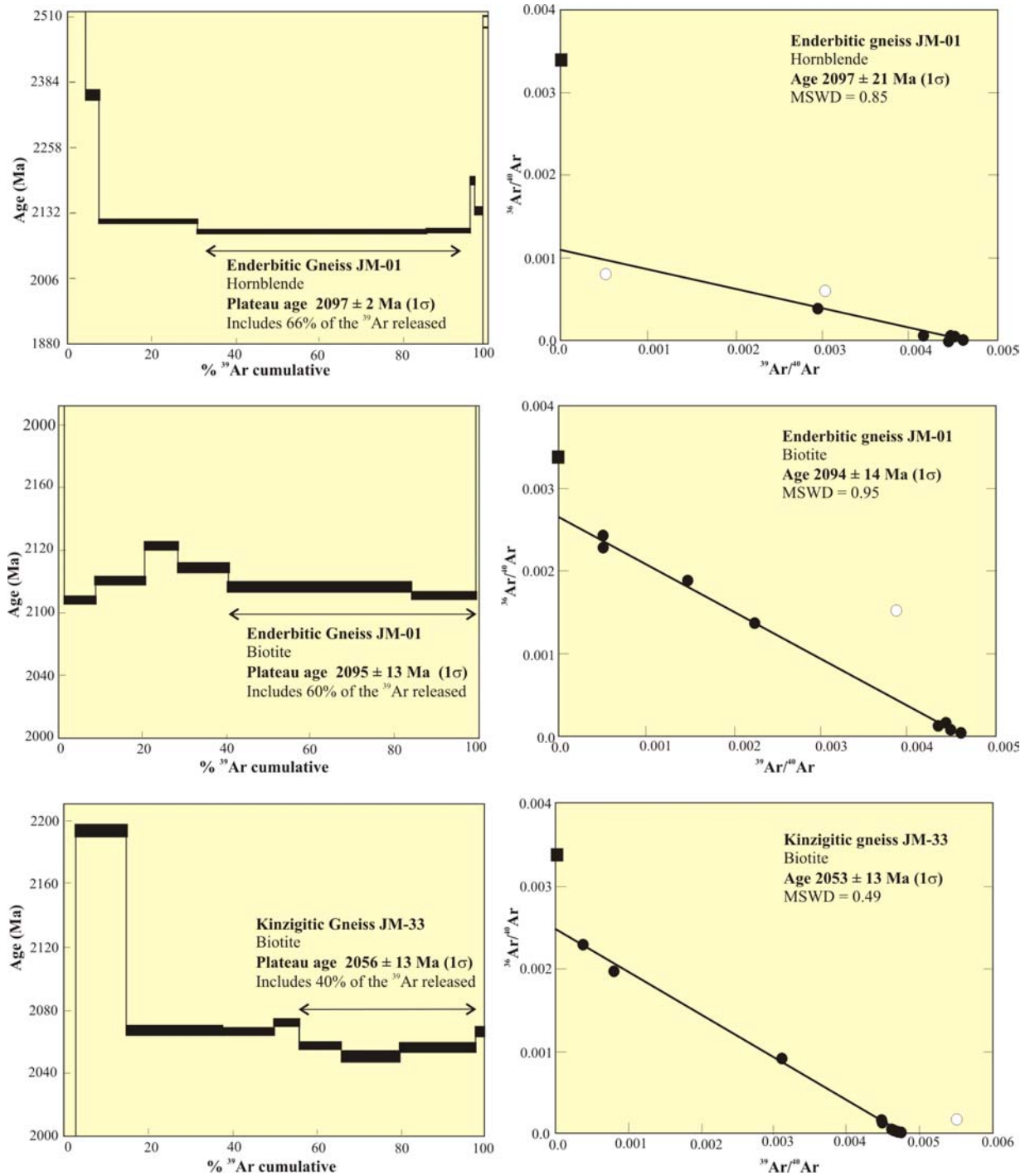
Biotites from the kinzigitic gneiss JM-33 displayed a concave age spectrum with minimum ages ranging from 2073 to 2050 Ma, providing a three-step age of  $2056 \pm 13$  Ma (40% of  $^{39}\text{Ar}$  released), which is similar to the intercept age of  $2053 \pm 13$  Ma (MSWD = 0.49) defined by 9 heating steps and obtained in the isotope correlation plot.

Hornblende and biotite from the enderbite JM-07 from the Noucouuru Intrusive Suite were analyzed. Biotite displayed a concordant age spectrum, characterized by a sharp increase of the age at low temperature, followed by a flat section over 90% of the released  $^{39}\text{Ar}$ . A well-defined plateau age of  $2076 \pm 13$  Ma was provided, which is consistent with an intercept age of  $2073 \pm 14$  Ma (MSWD = 0.76), calculated with 7 heating steps in the isotope correlation plot. For amphibole, argon was released irregularly with a single-step at  $2106 \pm 3$  Ma related to more than 80% of the gas released. An intercept age of  $2133 \pm 25$  Ma was calculated, which has to be considered with caution for geological interpretation, given the large MSWD value (3.27) and the fact that only 4 steps were considered in the calculation.



**Figure 4** – Age spectra and isotope correlation plots of hornblendes and biotites from rocks of the Jari-Guaribas Complex, Amapá Block

Figure 4 (continued)



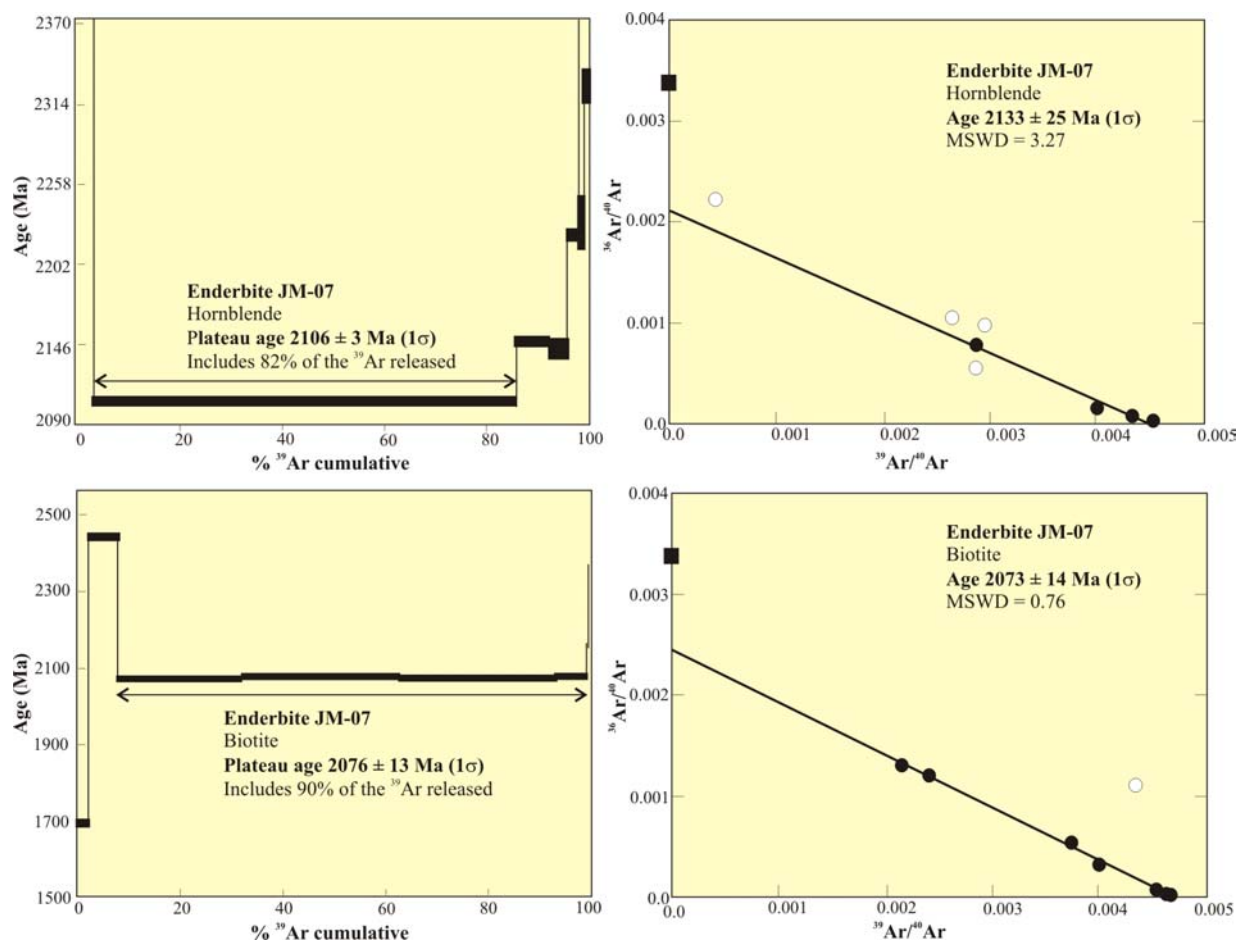


**Figure 5** – Age spectra and isotope correlation plots of hornblendes and biotites of the enderbite JM-07 from the Noucouru Intrusive Suite, Amapá Block

The dioritic gneiss LT-28B from Guianense Complex provided a concave amphibole age spectrum with a two-step minimum age of  $2087 \pm 13 \text{ Ma}$  that is related to more than 80% of the  $^{39}\text{Ar}$  released. This age is similar, within the limit of the errors, to the intercept age of  $2104 \pm 30$  (MSWD = 5.0) calculated in the isotope correlation plot with 7 heating steps.

Biotite displayed a very disturbed release spectrum, with strongly variable apparent ages ranging from 1986 to 2222 Ma. This release pattern can be attributed to recoil effects during irradiation by fast neutrons. Two steps furnished similar ages of  $2096 \pm 2 \text{ Ma}$  (third step, about 30% of the released  $^{39}\text{Ar}$ ) and  $2098 \pm 3 \text{ Ma}$  (sixth step, about 10% of the released  $^{39}\text{Ar}$ ). These

ages are similar to the intercept age of  $2099 \pm 17$  Ma (MSWD = 2.05) obtained in the isotope correlation plot with 9 heating steps, which is also concordant with the hornblende age obtained in the same sample.

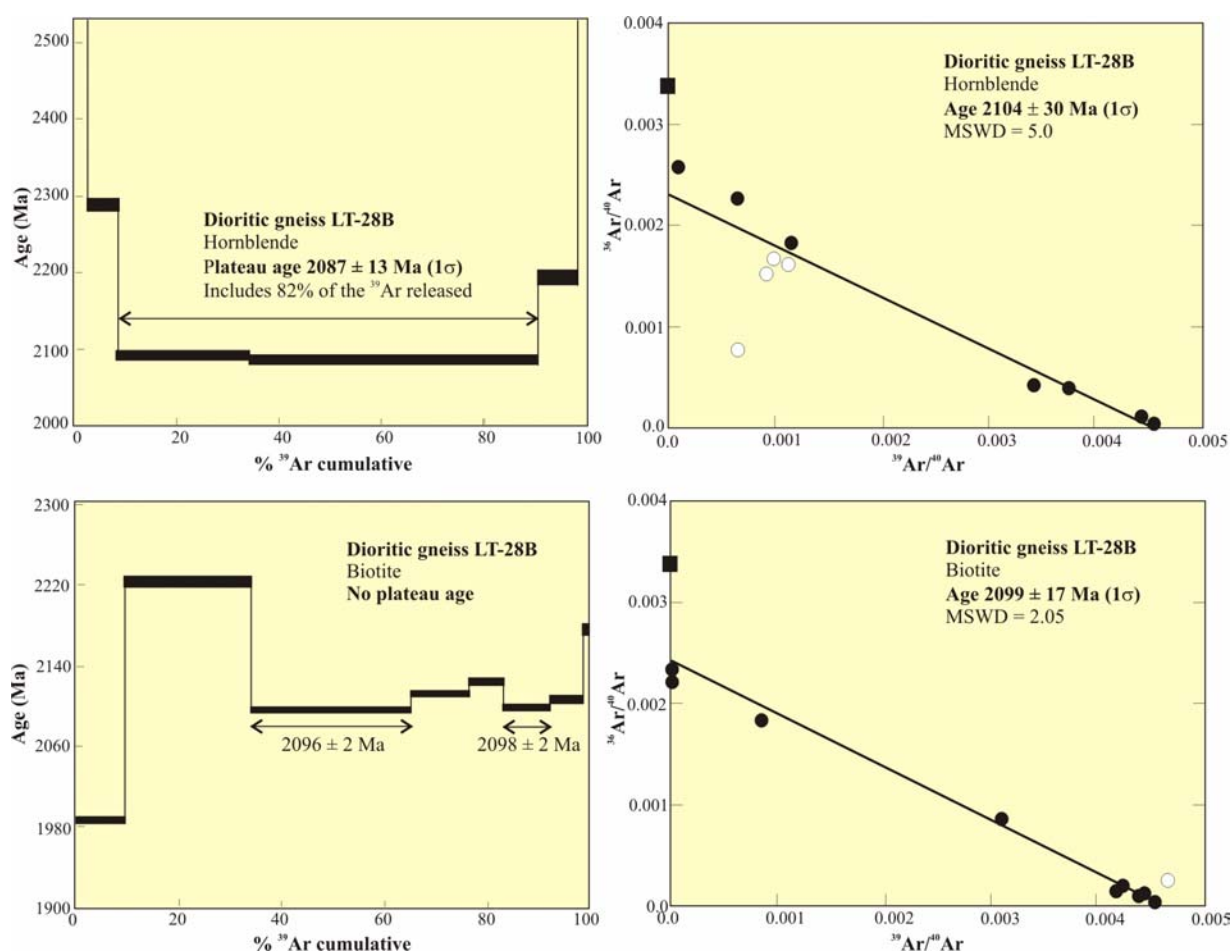


**Figure 6** – Age spectra and isotope correlation plots of hornblendes and biotites of the dioritic gneiss LT-28B from the Guianense Complex, Amapá Block

### *Results from the Carecuru Domain*

In three studied samples from the Carecuru Domain, hornblende-biotite pairs were simultaneously dated. The age spectra and isotope correlation plots for the studied minerals are shown in the Figures 7 and 8.

In the dioritic gneiss LT-196B, representative of the Paru-Maratiá Complex, the age spectrum of hornblende exhibited a flat pattern over more than 80% of the released gas, and

yields a two-step age of  $2149 \pm 13$  Ma related to constant K/Ca ratios. This age is indistinguishable from the intercept age of  $2158 \pm 21$  Ma (MSWD = 3.02), calculated with 8 heating steps in the isotope correlation plot. Biotite grains from the same sample displayed a strongly discordant age spectrum, accompanied by variable K/Ca pattern, with apparent ages ranging from 1630 to 1974 Ma. This scattered release spectrum can indicate that the Ar was released from different sites, for instance, from mineral inclusions, which were not detected through petrographic examination. This corresponds to an intercept age of  $1832 \pm 28$  Ma calculated with 6 heating steps in the isotope correlation plot, which is accompanied by a large MSWD value of 6.3, and that is considered meaningless for geological interpretation.

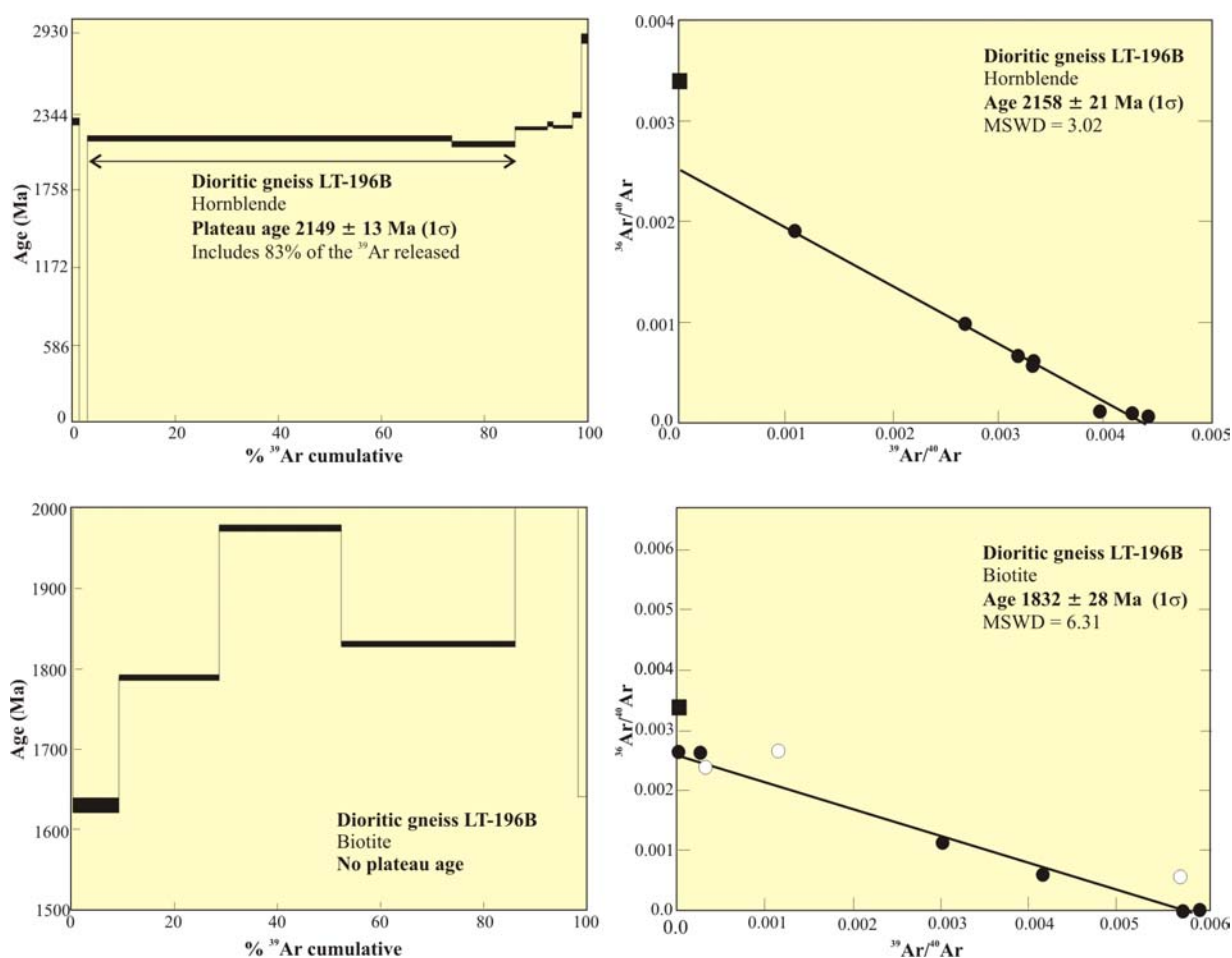


**Figure 7** – Age spectra and isotope correlation plots of hornblendes and biotites of the dioritic gneiss LT-196B from the Paru-Maratiá Complex, Carecuro Domain.

Concerning to the diorite LT-193 from the Carecuru Intrusive Suite, amphibole gave an apparently saddle-shaped age spectra with a plateau age of  $2133 \pm 14$  Ma related to 65% of the released gas in three successive steps. This age is similar to an intercept age of  $2137 \pm 20$  Ma (MSWD = 2.06) calculated with 4 heating steps. Biotite has an age spectrum that is suggestive of argon loss (McDougall and Harrison, 1988), with ages progressively climbing from a minimum of 1604 Ma to a maximum plateau-like age of  $1915 \pm 12$  Ma over 80% of the released  $^{39}\text{Ar}$ . The isotope correlation plot provided a younger intercept age of  $1853 \pm 13$  Ma (MSWD = 0.47) defined with 7 heating steps, with an initial  $^{40}\text{Ar}/^{36}\text{Ar}$  ratio of 417 pointing to the presence of excess argon.

Hornblende and biotite of diorite LT-76, from the same intrusive suite, yielded relatively discordant release spectra. Therefore, a two-step age of  $2068 \pm 14$  Ma (91 % of the released gas) and a single-step age of  $1953 \pm 2$  Ma (32% of the released gas) were obtained in the age spectra for amphibole and biotite, respectively, which are similar within the limit of the errors to their correspondent intercept ages of  $2056 \pm 27$  Ma (MSWD = 0.99) and  $1970 \pm 15$  (MSWD = 1.07). The hornblende intercept age is derived from only 4 heating steps and must be considered with caution for geological interpretation.

#### *Results from the Paru Domain*

$^{40}\text{Ar}$ - $^{39}\text{Ar}$  step-heating of hornblende from the mafic granulite LT-186A of the Ananaí Complex again produces a discordant and concave age spectrum with an intermediate plateau age of  $2051 \pm 13$  Ma for more than 80 % of the argon released in two heating steps. Seven gas fractions display a good linear array in the isotope correlation diagram (Figure 9), corresponding to an intercept age of  $2058 \pm 18$  Ma (MSWD = 1.91).

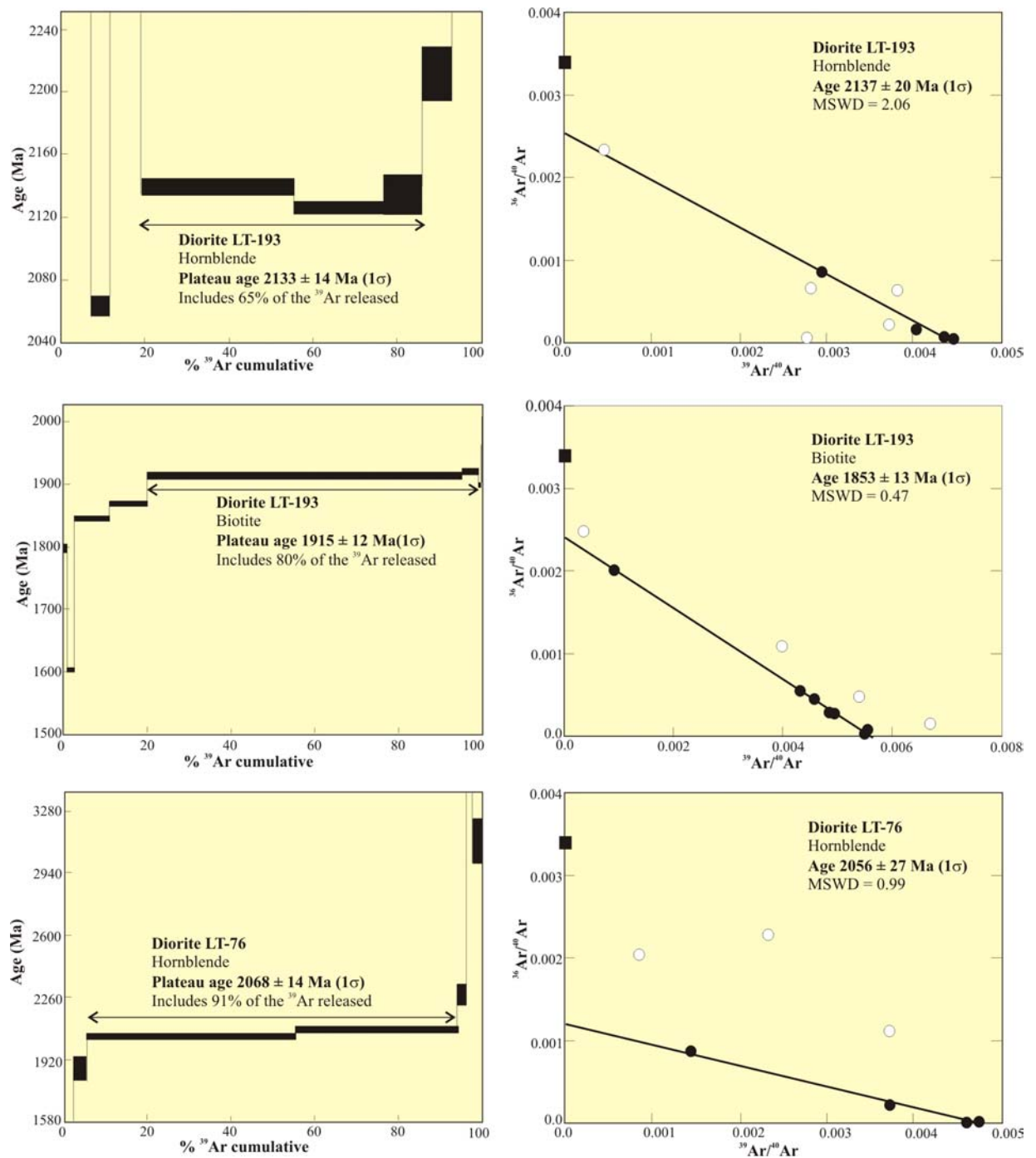


**Figure 8** – Age spectra and isotope correlation plots of hornblendes and biotites of the diorites LT-193 and LT-76 from the Carecuru Intrusive Suite, Carecuru Domain.

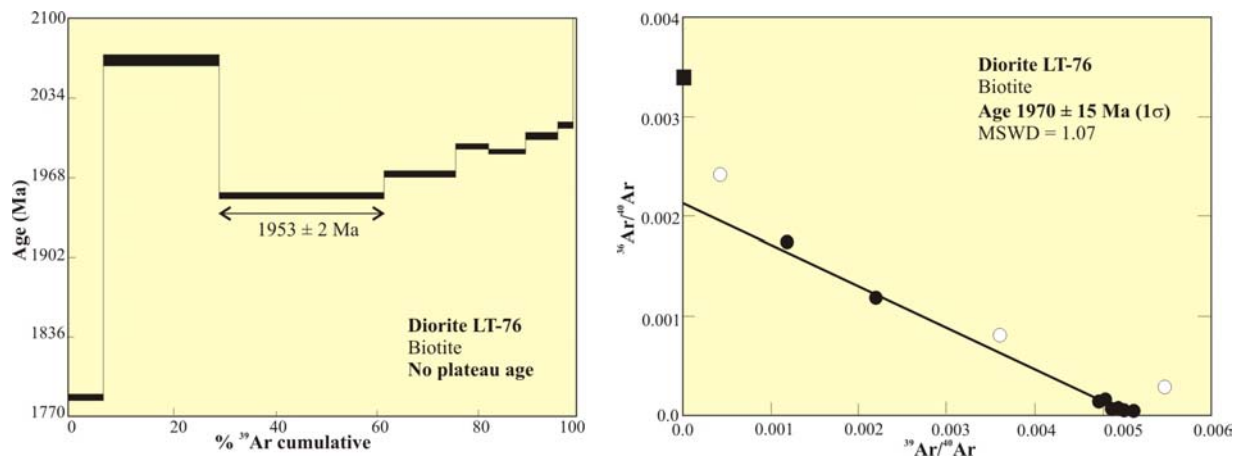


Figure 8 (continued)

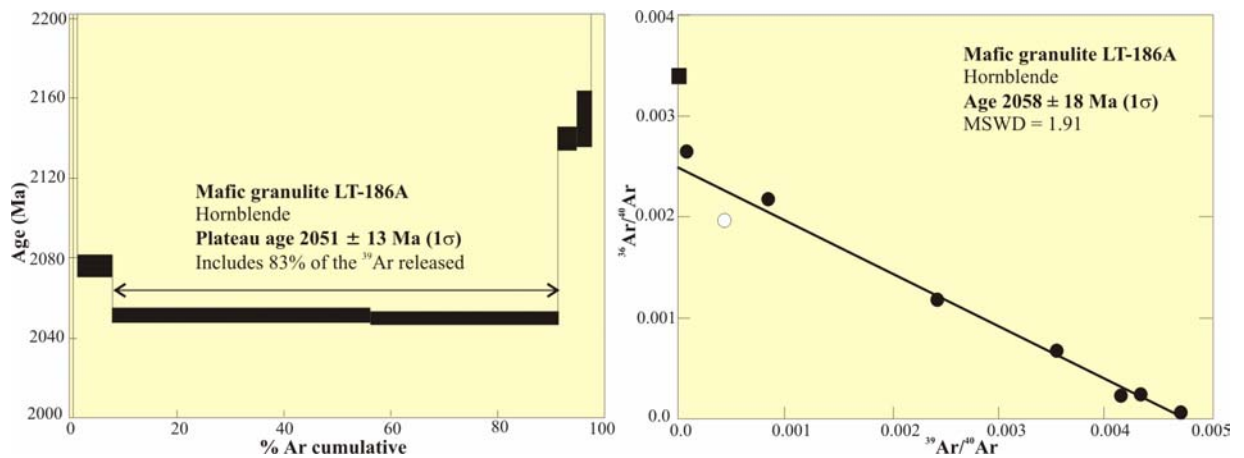


Figure 9 – Age spectra and isotope correlation plots of hornblendes and biotites of the mafic granulite LT-186A from the Ananaí Complex, Paru Domain.

**Table 1** – Mineral  $^{40}\text{Ar}/^{39}\text{Ar}$  ages (**bold**) calculated for the studied hornblendes and biotites in each tectonic domain, and available zircon and monazite ages compiled from Rosa-Costa et al. 2003<sup>1</sup>, in press<sup>2</sup>, submitted<sup>3</sup>, and from Ricci et al. 2002<sup>4</sup>

<b>Tectonic Domain</b>	<b>Stratigraphic Unit</b>	<b>Sample nº</b>	<b>Lithology</b>	<b>Mineral</b>	<b>Age (Ma)</b>
<b>Amapá Block</b>	Jari-Guaribas Complex	AV-02	mafic granulite	<b>hornblende</b>	<b>2086 ± 26</b>
		LT-219A	mafic granulite	<b>hornblende</b>	<b>2106 ± 36</b>
		MV-48	enderbitic gneiss	zircon	2770 ± 2 <sup>1</sup>
				<b>hornblende</b>	<b>2091 ± 17</b>
		JM-01	enderbitic gneiss	<b>hornblende</b>	<b>2097 ± 21</b>
				<b>biotite</b>	<b>2094 ± 14</b>
		JM-33	kinzigitic gneiss	<b>biotite</b>	<b>2053 ± 13</b>
		MV-27A	enderbitic gneiss	zircon	2790 ± 8 <sup>2</sup>
				monazite	2096 ± 6 <sup>3</sup>
		MV-27E	charnockitic leucosome	zircon	2091 ± 5 <sup>3</sup>
	monazite			2088 ± 8 <sup>3</sup>	
	LT-214	enderbitic gneiss	monazite	2087 ± 3 <sup>3</sup>	
	LT-223A	tonalitic gneiss	monazite	2086 ± 8 <sup>3</sup>	
	LT-223B	granitic leucosome	monazite	2093 ± 8 <sup>3</sup>	
			zircon	2605 ± 4 <sup>4</sup>	
Noucourou Intrusive Suite	JM-07	enderbite	<b>hornblende</b>	<b>2133 ± 25</b>	
			<b>biotite</b>	<b>2073 ± 14</b>	
Guianense Complex	LT-28B	dioritic gneiss	<b>hornblende</b>	<b>2104 ± 30</b>	
			<b>biotite</b>	<b>2099 ± 17</b>	
	LT-123A	tonalitic gneiss	monazite	2038 ± 6 <sup>3</sup>	
MV-01A	granitic gneiss	monazite	2056 ± 7 <sup>3</sup>		
<b>Carecuru Domain</b>	Paru-Maratiá Complex	LT-196B	dioritic gneiss	<b>hornblende</b>	<b>2158 ± 21</b>
			<b>biotite</b>	<b>1832 ± 29*</b>	
	Carecuru Intrusive Suite	LT-193	diorite	zircon	2139 ± 2 <sup>2</sup>
				<b>hornblende</b>	<b>2137 ± 20</b>
				<b>biotite</b>	<b>1853 ± 13</b>
LT-76	diorite	zircon	2140 ± 1 <sup>1</sup>		
		<b>hornblende</b>	<b>2056 ± 27</b>		
<b>biotite</b>	<b>1970 ± 15</b>				
<b>Paru Domain</b>	Ananaí Complex	LT-186A	mafic granulite	<b>hornblende</b>	<b>2058 ± 18</b>

\*meaningless

## 5 - Discussion

### 5.1 - Interpretation of the $^{40}\text{Ar}$ - $^{39}\text{Ar}$ Data

The  $^{40}\text{Ar}$ - $^{39}\text{Ar}$  data obtained in this work provide new time constraints on the Paleoproterozoic evolution of the southeastern part of Maroni-Itacaiúnas Province. The histogram representation displayed in the Figure 10 and the Table 1 summarizes all the ages obtained in this study. A preliminary evaluation of the data shows that, despite of they have been acquired on Archean and Paleoproterozoic rocks/domains, all biotite and amphibole ages lie in the interval between 2.1 and 1.8 Ga, predominantly around 2.1 Ga, demonstrating the importance of the Transamazonian orogenic cycle in the investigated area.

However, taken together, the  $^{40}\text{Ar}$ - $^{39}\text{Ar}$  ages display a significant scattering from  $2158 \pm 21$  Ma to  $2056 \pm 27$  Ma for amphibole, and from  $2099 \pm 17$  to  $1853 \pm 13$  Ma for biotite, producing a spread of about 100 Ma for amphibole and of more than 200 Ma for biotite and some amphibole-biotite pairs. On the other hand, inside each tectonic domain, and whatever the kind of rock analyzed, the ages are more clustered, suggesting that the temperature needed for isotopic closure of the K-Ar system was attained at different times in each domain, thus pointing to distinct cooling histories.

In the Amapá Block, most of the  $^{40}\text{Ar}$ - $^{39}\text{Ar}$  data show a clear maximum around 2.1 Ga (Fig. 10A). Amphibole ages vary from  $2133 \pm 25$  to  $2086 \pm 26$  Ma, being statistically similar within the limit of errors. The biotites also display similar ages, spreading between  $2099 \pm 17$  and  $2073 \pm 14$  Ma, with one exception being a slightly younger age at  $2053 \pm 13$  Ma obtained on the single paraderived studied rock.

Considering the Archean age of the igneous protoliths of the gneisses from the Amapá Block (Rosa-Costa et al., in press), and the lack of inherited Ar components in the dated minerals, the  $^{40}\text{Ar}$ - $^{39}\text{Ar}$  data indicate the complete resetting of the magmatic hornblende and biotite during the Transamazonian tectonothermal overprinting.

These results are in concordance with previous geochronological studies in the Amapá Block. U-Th-Pb monazite dating and Pb-evaporation zircon geochronology performed on gneisses from basement metamorphic complexes (Rosa-Costa et al., submitted) revealed that the Archean rocks suffered granulite-facies metamorphism around 2.09 Ga, and also bracketed late-orogenic migmatization events about 2.06 Ga and 2.04 Ga. Archean inheritance has not been recorded on zircon neither on monazite metamorphic grains.

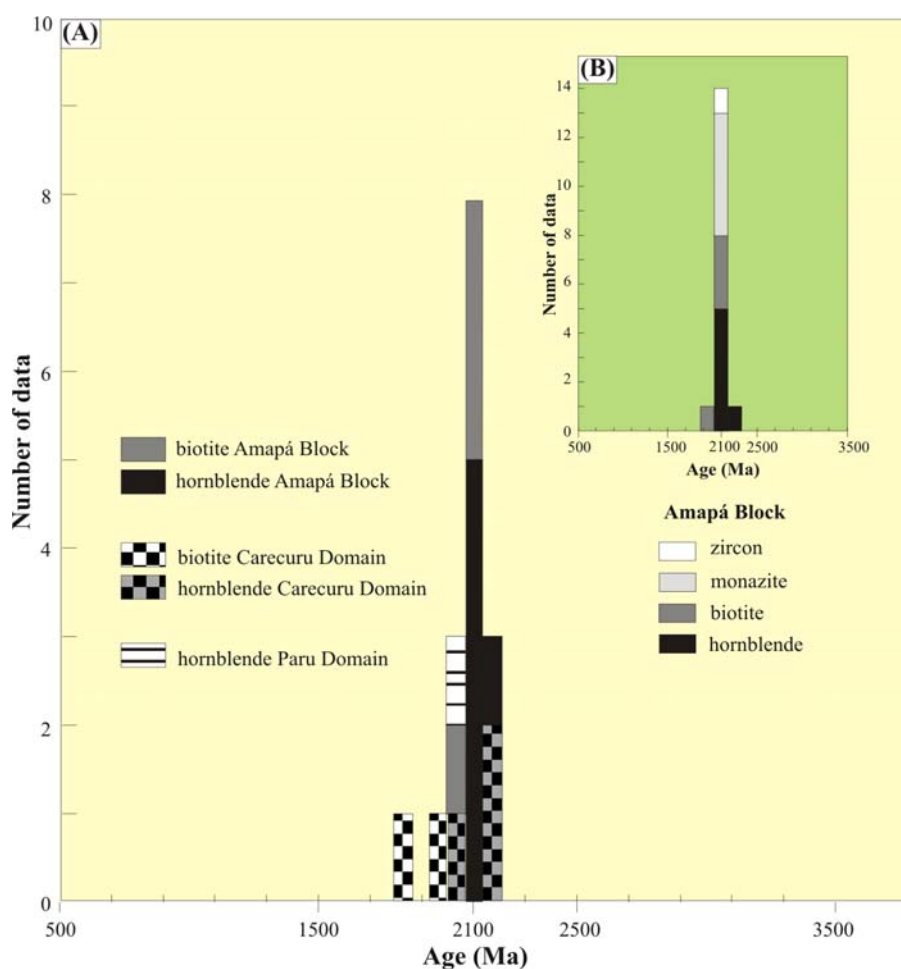


**Figure 10** – (A) Histogram representation of the  $^{40}\text{Ar}/^{39}\text{Ar}$  data obtained on hornblendes and biotites from rocks of the distinct tectonic domains. On top right, (B) histogram representation of zircon, monazite, hornblende and biotite metamorphic ages obtained in basement rocks of the Amapá Block. Zircon and monazite ages compiled from Rosa-Costa et al. (submitted).

On frequency histogram of the Figure 10B we present the available ages for metamorphic minerals of basement rocks from the focused tectonic block, also including the monazite and zircon age data of Rosa-Costa et al. (submitted), which are listed in the Table 1. It is clear that most of the mineral metamorphic ages lie around 2.1-2.09 Ga, which means that the  $^{40}\text{Ar}/^{39}\text{Ar}$  amphibole and biotite ages can be interpreted as registering exhumation and cooling following the granulite-facies metamorphism. The convergence of the ages around 2.1-2.09 Ga provided by distinct geochronometers, which have blocking temperatures varying approximately from 750 °C (monazite - Copeland et al., 1988) to 300 °C (biotite - Harrison et al., 1985), implies in fast

cooling rates. Moreover, the spatial distribution of the ages suggests that the isotopic closure for several isotopic systems was reached at the same time at least in large sections of the Amapá Block.

The isolated biotite age of about 2.05 Ga, provided by the paragneiss gneiss JM-33, can be envisaged as reflecting local reactivations, related to late-orogenic stages. Late-Transamazonian pulses of granitic magmatism and coeval migmatization events, dated between 2.06 and 2.04 Ga (Rosa-Costa et al., in press and submitted), have already been revealed by dating of zircon and monazite from granitic plutons and gneissic bodies located restrictedly in the neighboring area of the gneiss JM-33 (see Fig. 2), which are apparently controlled by late-orogenic transcurrent tectonics.

In the Carecuru Domain, the amphibole and biotite age pattern is significantly contrasting to that obtained in the adjacent Amapá Block. Similar amphibole ages of  $2158 \pm 21$  Ma and of  $2137 \pm 20$  Ma were acquired in two distinct samples, the dioritic gneiss LT-196B from the Paru-Maratiá Complex and the diorite LT-193 from the Carecuru Intrusive Suite. In the former, biotite furnished a meaningless age, and in the latter the biotite was dated at  $1853 \pm 13$  Ma. In the diorite LT-76, also from Carecuru Intrusive Suite, distinct ages have been recorded, since the hornblende was dated at  $2056 \pm 27$  Ma and the biotite at  $1970 \pm 15$  Ma. The contrasting ages measured in different sectors of the Carecuru Domain (see Fig. 2) suggest, at a first glance, that the cooling pattern can vary significantly along this tectonic domain, within a relatively small area.

This statement is reinforced when zircon and hornblende ages are compared among different sectors. It is notable that, in the diorite LT-193, the Pb-Pb zircon age of  $2139 \pm 2$  Ma and the  $^{40}\text{Ar}$ - $^{39}\text{Ar}$  hornblende age of  $2137 \pm 20$  Ma are similar within the limit of errors, and the former is interpreted as crystallization age (Rosa-Costa et al., 2003, in press). Considering that a dioritic magma crystallizes at about 750-800°C and that the estimated blocking temperature for U-Pb system of zircon is of, at least, 800°C (Cherniack and Watson, 2003), then the concordance of zircon and hornblende ages, the latter mineral having blocking temperature of 500-550°C (Harrison, 1981), clearly indicates that the magma experienced fast cooling immediately after its emplacement and the hornblende age marks a blunt temperature fall. Conversely, in the diorite LT-76, there is a remarkable gap of time between zircon and hornblende ages (see Table 1), which suggest that this rock experienced slow cooling from 750-800°C to 500-550°C over more than 80 Ma.

We must discuss the geological meaning of the biotite ages obtained in the Carecuru Domain. Concerning to the diorite LT-76, the age of  $1970 \pm 15$  Ma can be envisaged as marking the progressive cooling of this rock. The difference between zircon and hornblende ages in this sample, of about 85 Ma, is similar to that registered between the hornblende and biotite ages. In addition, the difference between the blocking temperatures of zircon and hornblende and of hornblende and biotite is about 200-250°C, indicating that the dioritic pluton cooled monotonously and maintained constant cooling rates since its emplacement.

It is likely that the biotite age of  $1853 \pm 13$  Ma yielded by the sample LT-193 do not registers magmatic cooling but some later thermal event that has induced a total isotopic resetting in biotite, evidencing its higher sensitivity to argon loss than hornblende that remained unaffected, due its higher retentivity for argon. A similar U-Th-Pb age at  $1879 \pm 16$  Ma was revealed by monazites of a high-grade gneiss from the Amapá Block, and interpreted as result of hydrothermal activity disturbing the U-Th-Pb system (Rosa-Costa et al., submitted). According to these authors, this hydrothermal event is possibly related to the remarkable plutono-volcanic anorogenic event (Uatumã type) recorded in the central portion of the Guiana Shield, which is admitted as synchronous to that dated at about 1.88-1.86 Ga in the central portion of the Brazil Central Shield (Santos et al., 2004, Dall'Agnol et al., 2005 and references therein).

It is necessary to remark that the fact of the biotite from diorite LT-76 yielded an older cooling age of 1970 Ma suggests that the 1.8 Ga thermal overprinting has affected, only locally, the Carecuru Domain.

Finally, in the Paru Domain, hornblende of the mafic granulite LT-186A from Ananaí Complex provided an age of  $2058 \pm 18$  Ma. This age is consistent within the errors with the Pb-Pb zircon age of  $2074 \pm 5$  Ga that marks the time of charnockite emplacement within the that high-grade complex (Rosa-Costa et al., in press). The age of the granulitic event that affected rocks from the Ananaí Complex remains an unsolved problem, leading to, at least, two possibilities for interpretation of the  $^{40}\text{Ar}$ - $^{39}\text{Ar}$  hornblende age: 1) the 2.07 m.y. old charnockitic magmatism marks a late-orogenic granulite-facies metamorphism, and the hornblende age can be envisaged as recording cooling following this high-grade event; or 2) the granulitic event occurred about 2.09 Ga, as in the Amapá Block, and the hornblende age records posterior disturbing in the K-Ar system, possibly provoked by emplacement of the 2.07 m.y. old

charnockites. Given the scarcity of data in the Paru Domain, confident interpretation of the age cannot be done.

## 5.2 - Cooling Rates Estimates and Tectonic Implications

In attempt to better understand the cooling history of the Amapá Block and Carecuru Domain,  $^{40}\text{Ar}$ - $^{39}\text{Ar}$  data from hornblende and biotite obtained in this research, together with available zircon ages for some of the investigated samples, were plotted in the Temperature vs. Time diagram shown in Figure 11.

Cooling rates can be estimated if the age of at least two distinct geochronometers having different blocking temperatures are known, and thus a temperature-time (T-t) path can be constructed. However, closure temperature for each mineral is not unique and depends on several intrinsic parameters, discussed by Dodson (1973), that include diffusion grain size, cooling rate and energy of activation. Therefore, the closure temperatures for hornblende and biotite adopted in this study must to be considered as only partially established. Based on several studies (Harrison, 1981; Baldwin et al., 1990; Dahl, 1996), closure temperature in the range of 500-550 °C is adopted for hornblende, and 300-350 °C is the accepted approximate blocking temperature for argon diffusion in biotite, in agreement with Dodson (1973), Purdy and Jager (1976) and Harrison et al. (1985).

The different age patterns registered in the southwestern Amapá Block and Carecuru Domain, above commented, do not converge to a regional single cooling path, but preferentially suggest that the rocks from distinct domains have cooled down at different cooling rates. In the southwestern Amapá Block, nearly vertical trends were defined by the available amphibole and biotite ages of the enderbite granulite JM-01 and of the dioritic gneiss LT-28B, reflecting fast cooling rates through the temperature interval from 500-550 °C to 300-350 °C, which were estimated around 67 °C/m.y. and 40 °C/m.y., respectively. The fast cooling rates and the convergence of the hornblende, biotite and monazite ages in the Amapá Block, the latter dating the granulite-facies metamorphism at about 2.09 Ga (Rosa-Costa et al., submitted), strongly indicates that the exhumation was rapid and tectonically controlled. Reliable monazite ages coupled with structural field data allowed Rosa-Costa et al. (submitted) to considerate the 2.09 m.y. old granulite-facies metamorphism in the southwestern Amapá Block as contemporaneous to the development of an oblique thrusting system. In that region, the high-grade basement rocks

commonly exhibit pervasive NW-SE ductile foliation, dipping systematically 40-60° SW, and stretching/mineral lineation with medium rakes predominantly to SW, indicating general tectonic vergency from SW to NE. This pattern is strongly disturbed along NW-SE transcurrent zones defined by steeply dipping mylonitic foliation and sub-horizontal lineation. Apparently, the strike-slip zones development coincides with the final stages of the oblique movement. Moreover, Rosa-Costa et al. (submitted) related this thrusting system to the collisional stage of the Transamazonian orogen, occurred at about 2.11-2.08 Ga (Feybesse and Milési, 1994; Ledru et al., 1994; Delor et al. 2003; Théveniaut et al., submitted).

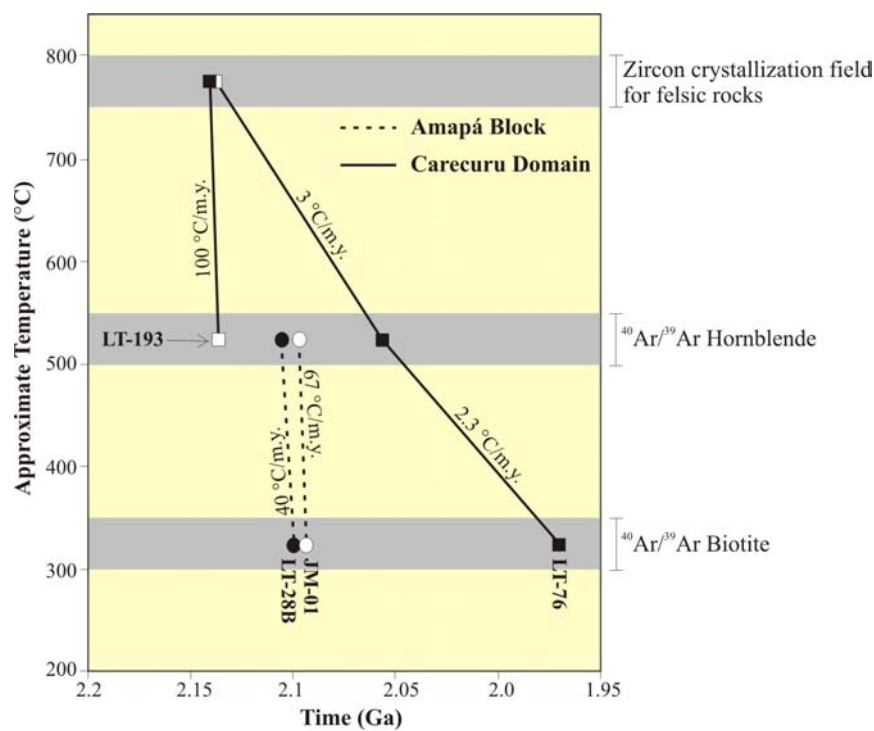


**Figure 11** – Temperature vs. Time diagram showing tentative cooling paths for Amapá Block and Carecuru Domain.

The structural pattern of the southwestern segment of the Amapá Block is similar to those observed in many orogenic belts, where crustal thickening is followed by transcurrent shear zones development, resulting in fast exhumation of deep parts of the orogen. This geodynamic model can account the convergence of the monazite, hornblende and biotite ages around 2.09-2.1 Ga and, consequently, the fast cooling rates estimated in this tectonic domain.

Conversely, in the Carecuru Domain, zircon and biotite ages of the diorite LT-76 led to an estimated cooling rate of about 2.6°C/m.y. from 2140 Ma to 1970 Ma. Hornblende age, even considered as fragile, is in good agreement with the estimated cooling rate based on zircon and biotite ages. Cooling rate calculation, taking into account the age around 2056 Ma for the hornblende, yielded values in order of 3°C/m.y. and 2.3°C/m.y. through the time intervals of 2140-2056 Ma and 2056-1970 Ma, respectively. The cooling path reported on Figure 11 shows that the dioritic pluton experienced slow cooling and underwent a monotonous cooling history since its emplacement until the biotite blocking, over the temperature interval of 750-300°C.

The slow cooling rate estimated for the diorite suggests that the regional cooling in the Carecuru Domain is not result of rapid and tectonically controlled exhumation, as defined in the Amapá Block, but it can be preferentially interpreted as result of exhumation by gradual uplift. This is coherent with the magmatic arc model proposed by Rosa-Costa et al. (in press) for this domain, where continental growth results mainly from lateral magmatic accretion, precluding significant tectonic crustal thickening. Furthermore, the calculated cooling rate is in accordance with those defined in French Guiana terrains that range between 2 and 5°C/m.y. (Nomade et al., 2001, 2002; Enjolvy, 2004; Théveniaut et al., submitted), which, as the Carecuru Domain, also represent Transamazonian accretionary domains from eastern Guiana Shield (see Delor et al., 2003).

Nevertheless, the nearly coincident zircon and hornblende ages of the diorite LT-193 led to an estimated cooling rate about 100°C/m.y., from 750°C to 500°C, for the 2139 to 2137 Ma period. This very fast cooling rate can be envisaged as result of rapid heat dissipation in the dioritic pluton, possibly provoked by magma emplacement in upper and colder crustal levels or, alternatively, can be interpreted as result of differential uplift within the Carecuru Domain, induced by vertical movement of structural blocks. Anyway, this cooling rate can not be considered as reflecting a regional cooling pattern, since there are no coherent geological arguments to support this hypothesis.

## 6 - Concluding Remarks

The set of  $^{40}\text{Ar}/^{39}\text{Ar}$  geochronological data obtained on amphibole and biotite from representative units of the Archean Amapá Block and Paleoproterozoic Carecuru Domain in southeastern Guiana Shield, coupled with available geochronological records and petro-structural

observations, allow delineate contrasting cooling and exhumation stories for these tectonic domains.

In the Archean Amapá Block, amphibole and biotite ages vary, respectively, from  $2133 \pm 25$  to  $2086 \pm 26$  Ma, and mainly between  $2099 \pm 17$  and  $2073 \pm 14$  Ma, indicating their total resetting during the Transamazonian orogenetic event. Nearly vertical T-t paths reflect fast cooling rates around  $67^\circ\text{C}/\text{m.y.}$  and  $40^\circ\text{C}/\text{m.y.}$ , which indicate a tectonically controlled exhumation, possibly provoked by oblique thrusting related to the collisional stages of the Transamazonian orogeny

In the Carecuru Domain, in which the geodynamic evolution is related to a Paleoproterozoic magmatic arc setting during the Transamazonian event, amphibole ages of  $2158 \pm 21$  Ma,  $2137 \pm 20$  Ma and  $2056 \pm 27$  Ma, and biotite ages of  $1853 \pm 13$  Ma and  $1970 \pm 15$  Ma were obtained. Regional cooling rates in the order of  $3\text{-}2.3^\circ\text{C}/\text{m.y.}$  suggest that the calc-alkaline granitoids underwent slow and monotonous cooling history since its emplacement until the biotite blocking. These cooling rates are coherent with a magmatic arc setting and are similar to those obtained in other Transamazonian accretionary domains from eastern Guiana Shield. However, a local cooling rate of  $100^\circ\text{C}/\text{m.y.}$  testifies magma emplacement in upper crustal levels or, alternatively, indicates differential uplift within the Carecuru Domain.

## 7 - Acknowledgements

The  $^{40}\text{Ar}\text{-}^{39}\text{Ar}$  analyzes were performed during a doctoral stage of the first author at Laboratoire de Dynamique de la Lithosphère, Université Montpellier 2, Montpellier, France, which was financially supported by CAPES (Coordenação de Aperfeiçoamento de Pessoal de Nível Superior), process BEX2639/03-3. Keila S. L. Teixeira is thanked for her expert help with sample processing. This paper is a contribution to PRONEX/CNPq (Proj. 103/98 – Proc. 66.2103/1998-0).

## 8 - References

- Agard, P., Monié, P., Jolivet, L., Goffé, B. 2002. Exhumation of the Schistes Lustrés complex: in situ laser probe  $^{40}\text{Ar}\text{-}^{39}\text{Ar}$  constraints and implications for the Western Alps. *Journal of Metamorphic Geology*, 20, 599-618.
- Avelar, V.G. 2002. Geocronologia Pb-Pb em zircão e Sm-Nd em rocha total da porção centro-norte do Estado do Amapá – Brasil: Implicações para a evolução geodinâmica do setor oriental do Escudo das Guianas. Tese de Doutorado, Curso de Pós-Graduação em Geologia e Geoquímica, Universidade Federal do Pará, 213 pg.

- Avelar, V.G., Lafon, J.M., Delor, C., Guerrot, C., Lahondère, D. 2003. Archean crustal remnants in the easternmost part of the Guiana Shield: Pb-Pb and Sm-Nd geochronological evidence for Mesoarchean versus Neoproterozoic signatures. *Geologie de la France*, 2-3-4, 83-100.
- Baldwin, S.L., Harrison, T.M., Fitz Gerald, J.D. 1990. The diffusion of  $^{40}\text{Ar}$  in metamorphic hornblende. *Contributions to Mineralogy and Petrology*, 105, 691-703.
- Baxter, E.F., Ague, J.J., DePaolo, D.J. 2002. Prograde temperature-time evolution in the Barrovian type locality constrained by Sm/Nd garnet ages from Glen Clova, Scotland. *Journal of the Geol. Society of London*, 159, 71-82.
- Bingen, B., Boven, A., Punzalan, L., Wijbrans, J.R., Demaiffe, D. 1998. Hornblende  $^{40}\text{Ar}$ - $^{39}\text{Ar}$  geochronology across terrane boundaries in the Sveconorwegian Province of S. Norway. *Precambrian Research*, 90, 159-185.
- Carvalho, J.M. de A., Rosa-Costa, L.T., Vasquez, M.L., Klein, E.L., Macambira, E.M.B., Vale, A.G., Ricci, P. Dos S.F. 2001. Projeto Província Mineral da RENCA e Distrito Mineral do Ipitinga - Carta geológica (escala 1:250.000). Belém, CPRM, (Programa de Levantamentos Geológicos Básicos).
- Cherniak, D.J. and Watson, E.B. 2003. Diffusion in zircon. In: Hancher, J.M. and Hoskin, P.W.O (Eds.) *Zircon. Reviews in Mineralogy and Geochemistry*, 53, 113-143.
- Copeland, P., Parrish, R.R., Harrison, T.M. 1988. Identification of inherited radiogenic Pb in monazite and implications for U-Pb systematics. *Nature*, 333, 760-763.
- Cordani, U.G., Tassinari, C.C.G., Teixeira, W., Basei, M.A.S., Kawashita, K. 1979. Evolução tectônica da Amazônia com base nos dados geocronológicos. In: II Congresso Geológico Chileno, Arica. *Actas*, 4, 137-148.
- Dahl, P.S. 1996. The effects of composition on retentivity of argon and oxygen in hornblende and related amphiboles: a field-test empirical model. *Geochimica and Cosmochimica Acta*, 60, 3687-3700.
- Dall'Agnol, R., Teixeira, N.P., Ramo, O.T., Moura, C.A.V., Macambira, M.J.B., Oliveira, D.C. 2005. Petrogenesis of the Paleoproterozoic rapakivi A-type granites of the Archean Carajás metallogenic province, Brazil. *Lithos* 80, 101-129.
- Delor, C., Lahondère, D., Egal, E., Lafon, J.M., Cocherie, A., Guerrot, C., Rossi, P., Trufert, C., Theveniaut, H., Phillips, D., Avelar, V.G. 2003. Transamazonian crustal growth and reworking as revealed by the 1:500,000-scale geological map of French Guiana (2<sup>nd</sup> edition). *Geologie de la France*, 2-3-4, 5-57.
- Dodson, M.H. 1973. Closure temperatures in cooling geochronological and petrological systems. *Contributions to Mineralogy and Petrology*, 40, 259-274.
- England, P.C. and Thompson, A.B. 1994. Pressure-temperature-time paths for regional metamorphism I. Heat transfer during the evolution of regions of thickened continental crust. *Journal of Petrology*, 25, 894-928.
- Enjolvy, R. 2004. Caractérisation géochronologique et pétrologique de l'événement fini-Transamazonien: étude en Guyane Française et em Amapá (Brésil). *Diplôme d'Etudes Approfondies, Université Montpellier II*, 42 p.
- Faure, M., Monié, P., Pin, C., Maluski, H., Leloix, C. 2002. Late Visean thermal event in the northern part of the French Massif Central: new  $^{39}\text{Ar}/^{40}\text{Ar}$  and Rb-Sr isotopic constraints on the Hercynian syn-orogenic extension. *International Journal of Earth Sciences*, 91, 53-75.

- Feybesse, J.L. and Milési, J.P. 1994. The Archean/Paleoproterozoic contact zone in West Africa: a mountain belt of décollement thrusting and folding on a continental margin related to 2.1 Ga convergence of Archean cratons? *Precambrian Research*, 69, 199-227.
- Foland, K.A. 1983.  $^{40}\text{Ar}$ - $^{39}\text{Ar}$  incremental heating plateaus for biotites with excess argon. *Chemical Geology*, 1, 3-21.
- Gruau, G., Martin, H., Leveque, B., Capdevilla, R. 1985. Rb-Sr and Sm-Nd geochronology of Lower Proterozoic granite-greenstone terrains in French Guyane, South America. *Precambrian Research*, 30, 63-80.
- Harrison, T.M. 1981. Diffusion of  $^{40}\text{Ar}$  in biotite. *Contributions to Mineralogy and Petrology*, 78, 324-331.
- Harrison, T.M. and MacDougall, I. 1981. Excess  $^{40}\text{Ar}$  in metamorphic rocks from Broken Hill, New South Wales: implications for  $^{40}\text{Ar}/^{39}\text{Ar}$  age spectra and the thermal history of the region. *Earth and Plan. Sci. Letters*, 55, 123-149.
- Harrison, M.T., Ducean, I., MacDougall, I. 1985. Diffusion of  $^{40}\text{Ar}$  in biotite: temperature, pressure and compositional effects. *Geochimica and Cosmochimica Acta*, 49, 2461-2468.
- Hawkins, D.P. and Bowring, S.A. 1999. U-Pb monazite, xenotime and titanite geochronological constraints on the prograde to post-peak metamorphic thermal history of Paleoproterozoic migmatites from the Grand Canyon, Arizona. *Contributions to Mineralogy and Petrology*, 134, 150-169.
- Jolivet, L., Goffé, B., Monié, P., Truffert-Luxey, C., Patriat, M., Bonneau, M. 1996. Miocene detachment in Crete and exhumation P-T-t paths of high-pressure metamorphic rocks. *Tectonics*, 15 (6), 1129-1153.
- Jung, S. and Mezger, K. 2001. Geochronology in migmatites – a Sm-Nd, U-Pb and Rb-Sr study from the Proterozoic Damara belt (Namibia): implications for polyphase development of migmatites in high-grade terranes. *Journal of Metamorphic Geology*, 19, 77-97.
- Jung, S. and Mezger, K. 2003. Petrology of basement dominated terranes: I. Regional metamorphic T-t path from U-Pb monazite and Sm-Nd garnet geochronology (Central Damara orogen, Namibia). *Chemical Geology*, 198, 223-247.
- Kelley, S.P. and Turner, G. 1991. Laser probe  $^{40}\text{Ar}$ - $^{39}\text{Ar}$  measurements of loss profiles within individual hornblende grains from the Giant Range Granite, northern Minnesota, USA. *Earth and Planetary Science Letters*, 107, 634-648.
- Klein, E.L., Rosa-Costa, L.T., Lafon, J.M. 2003. Magmatismo Paleoarqueano (3,32Ga) na região do Rio Cupixi, SE do Amapá, SE do Escudo das Guianas. In: *Simpósio de Geologia da Amazônia*, 8. Manaus, CD ROM.
- Lafon, J.M., Rossi, P., Delor, C., Avelar, V.G., Faraco, M.T.L. 1998. Novas testemunhas de relíquias arqueanas na crosta continental paleoproterozóica da Província Maroni-Itacaiúnas (Sudeste do Escudo das Guianas). In: *Cong. Bras. Geol.*, 40. Belo Horizonte, Anais., p.64.
- Lafrance, J., Bardoux, M., Voicu, G., Stevenson, R. Machado, N. 1999. Geological and metallogenic environments of gold deposits of the Guiana Shield: a comparative study between St. Élie (French Guiana) and Omai (Guyana). *Exploration and Mining Geology*, 8 (1-2), 117-135.
- Laiti, A. and Gebauer, D. 1999. Constraining the prograde and retrograde P-T-t path of Eocene HP rocks by SHRIMP dating different zircon domains: inferred rates of heating, burial, cooling and exhumation for central Rhodope, northern Greece. *Contributions to Mineralogy and Petrology*, 135, 340-354.
- Lanphere, M.A. and Dalrymple, G.B. 1976. Identification of excess  $^{40}\text{Ar}$  by the  $^{40}\text{Ar}/^{39}\text{Ar}$  age spectrum technique. *Earth and Planetary Science Letters*, 32, 141-148.

- Ledru, P., Johan, V., Milési, J.P. and Tegye, M. 1994. Markers of the last stages of the Paleoproterozoic collision: evidence for a 2 Ga continent involving circum-South Atlantic provinces. *Precambrian Research*, 69, 169-191.
- Lee, J.K.W., Onstott, T.C., Cashman, K.V., Cumbest, R.J., Johnson, D. 1991. Incremental heating of hornblende in vacuo: implications for  $^{40}\text{Ar}/^{39}\text{Ar}$  geochronology and the interpretation of thermal histories. *Geology*, 19, 872-876.
- MacDougall, I. and Harrison, T.M. 1988. *Geochronology and thermochronology by the  $^{40}\text{Ar}/^{39}\text{Ar}$  method*. Clarendon Press, Oxford, 212 pp.
- McReath, I. and Faraco, M.T.L. 1997. Sm/Nd and Rb/Sr systems in part of the Vila Nova metamorphic suite, northern Brazil. In: I, South Amer. Symp. Isotop. Geol., Campos do Jordão. Extended abstracts, 194-196.
- Moller, A., Mezger, K., Schenk, V. 2000. U-Pb dating of metamorphic minerals: Pan-African metamorphism and prolonged slow cooling of high pressure granulites in Tanzania, East Africa. *Precambrian Research*, 104, 123-146.
- Monié, P., Caby, R., Arthaud, M.H. 1997. The Neoproterozoic Brasiliano orogeny in northeast Brazil:  $^{40}\text{Ar}/^{39}\text{Ar}$  and petrostructural data from Ceará. *Precambrian Research*, 81, 241-264.
- Monié, O. Torres-Roldán, R.L., García-Casco, A. 1994. Cooling and exhumation of the Western Betic Cordilleras,  $^{40}\text{Ar}/^{39}\text{Ar}$  thermochronological constraints on a collapsed terrane. *Tectonophysics*, 238, 353-379.
- Montgomery, C.W. 1979. Uranium-lead geochronology of the Archean Imataca Series, Venezuelan Guyana Shield. *Contributions to Mineralogy and Petrology*, 69, 167-176.
- Montgomery, C.W. and Hurley, P.M. 1978. Total rock U-Pb and Rb-Sr systematics in the Imataca Series, Guyana Shield, Venezuela. *Earth and Planetary Sciences Letters*, 39, 281-290.
- Morillon, A.C., Féraud, G., Sosson, M., Ruffet, G., Crevola, G., Lerouge, G. 2000. Diachronous cooling on both sides of a major strike-slip fault in the Variscan Maures Massif (south-east France), as deduced from a detailed  $^{40}\text{Ar}/^{39}\text{Ar}$  study. *Tectonophysics*, 31, 103-126.
- Neves, S.P., Vauchez, A., Féraud, G. 2000. Tectono-thermal evolution, magma emplacement, and shear zone development in the Caruaru area (Borborema Province, NE Brazil). *Precambrian Research*, 99, 1-32.
- Nogueira, S.A.A., Bettencourt, J.S., Tassinari, C.C.G. 2000. Geochronology of the Salamangone gold deposit host-rocks, Lourenço district, Amapá, Brazil. *Revista Brasileira de Geociências*, 30 (2), 261-264.
- Nomade, S., Chen, Y., Féraud, G., Pouclet, A., Théveniaut, H. 2001. First paleomagnetic and  $^{40}\text{Ar}/^{39}\text{Ar}$  study of Paleoproterozoic rocks from the French Guyana (Camopi and Oyapok rivers), northeastern Guyana Shield. *Precambrian Research*, 109, 239-256.
- Nomade, S., Féraud, G., Chen, Y., Pouclet, A. 2002. Thermal and tectonic evolution of the Paleoproterozoic Transamazonian orogen as deduced from  $^{40}\text{Ar}/^{39}\text{Ar}$  and AMS along the Oyapok river (French Guyana). *Precambrian Research*, 114, 35-53.
- Norcross, C.E., Davis, D.W., Spooner, E.T.C., Rust, A. 2000. U-Pb and Pb-Pb age constraints on Paleoproterozoic magmatism, deformation and gold mineralization in the Omai area, Guyana Shield. *Precamb. Research*, 102, 69-86.
- Oliveira, E.C., Lafon, J.M., Gioia, S.M.L., Pimentel, M.M. 2002. Implantação do método Sm-Nd para minerais metamórficos e sua aplicação em rochas da região central do Amapá, Sudeste do Escudo das Guianas. In: Cong. Bras. Geol., 41. João Pessoa, SBG-NE, Anais, p.502.

- Pimentel, M.M., Ferreira Filho, C.F., Spier, C.A. 2002. Estudo Sm-Nd do Complexo Máfico-Ultramáfico Bacuri, Amapá: idade da intrusão, metamorfismo e natureza do magma original. *Revista Brasileira de Geociências*, 32, 371-376.
- Purdy, J.W., and Jager, E. 1976. K-Ar ages on rock-forming minerals from central Alps. Report of the Institute of Geology and Mineralogy, University of Padova, 30, 1-31.
- Ricci, P.S.F., Carvalho, J.M.A., Rosa Costa, L.T., Klein, E.L., Vasquez, M.L., Vale, A.G., Macambira, E.M.B., Araújo, O.J.B. 2001. Geologia e recursos minerais do Projeto RENCA – Fase I. Belém, CPRM.
- Ricci, P.S.F., Carvalho, J.M.A., Rosa-Costa, L.T Lafon, J.M. 2002. Plúton charnoenderbítico arqueano intrusivo nos ortognaisses granulíticos do Cinturão Jari – Terreno Arqueano expressivo do sudeste do Escudo das Guianas. In: Congresso Brasileiro de Geologia, 41. João Pessoa, SBG-NE, Anais, p.524.
- Roddick, J. C., Cliff, R. A., Rex, D.C. 1980. The evolution of excess argon in alpine biotites. *Earth and Planetary Sciences Letters*, 48, 185-208.
- Roever, E.W.F. de, Lafon, J.M., Delor, C., Cocherie, A., Rossi, P., Guerrot, C., Potrel, A. 2003. The Bakhuis ultrahigh-temperature granulite belt (Suriname): I. petrological and geochronological evidence for a counterclockwise P-T path at 2.07-2.05 Ga. *Géologie de la France*, 2-3-4, 175-206.
- Rosa-Costa, L.T., Lafon, J.M., Cocherie, A., Delor, C. submitted. Electron microprobe U-Th-Pb monazite dating of the Transamazonian high-grade metamorphic overprint on Archean rocks from Amapá Block, southeastern Guiana Shield, northern Brazil.
- Rosa-Costa, L.T., Lafon, J.M., Delor, C. in press. Zircon geochronology and Sm-Nd isotopic study: further constraints for the Archean and Paleoproterozoic geodynamic evolution of the southeastern Guiana Shield, north of Brazil. *Gondwana Research*.
- Rosa-Costa, L.T, Ricci, P.S.F., Lafon, J.M., Vasquez, M.L., Carvalho, J.M.A., Klein, E.L., Macambira, E.M.B. 2003. Geology and geochronology of Archean and Paleoproterozoic domains of the southeastern Amapá and northwestern Pará, Brazil – southeastern Guiana Shield. *Géologie de la France*, 2-3-4, 101-120.
- Ruffet, G., Féraud, G., Amouric, M. 1991. Comparison of  $^{40}\text{Ar}$ - $^{39}\text{Ar}$  conventional and laser dating of biotites from North Trégor Batholith. *Geochimica et Cosmochimica Acta*, 55, 1675-1688.
- Samson, S.D. and Alexander, E.C. 1987 . Calibration of the interlaboratory  $^{40}\text{Ar}$ - $^{39}\text{Ar}$  dating standard, MMhb-1. *Chemical Geology*, 66 (1-2), 27-34.
- Santos, J.O.S., Van Breemen, O.B., Groves, D.I., Hartmann, L.A., Almeida, M.E., McNaughton, N.J., Fletcher, I.R. 2004 . Timing and evolution of multiple Paleoproterozoic magmatic arcs in the Tapajós Domain, Amazon Craton: constraints from SHRIMP and TIMS zircon, baddeleyite and titanite U-Pb geochronology. *Precambrian Research*, 131, 73-109.
- Sato, K. and Tassinari, C.C.G. 1997. Principais eventos de acreção continental no Cráton Amazônico baseados em idade-modelo Sm-Nd, calculada em evoluções de estágio único e estágio duplo. In: Costa, M.L.C. and Angélica, R.S. (Eds.), *Contribuições à Geologia da Amazônia*. SBG-NO, pp. 91-142.

- Schmitz M. D. and Bowring S. A. 2001. U-Pb zircon and titanite systematics of the Fish Canyon Tuff: an assessment of high-precision U-Pb geochronology and its application to young volcanic rocks. *Geochimica et Cosmochimica Acta*, 65 (15), 2571-2587
- Schmitz M. D., Bowring S. A., Ludwig K. R., Renne P. R. 2003. Precise K-Ar,  $^{40}\text{Ar}$ - $^{39}\text{Ar}$ , Rb-Sr and U-Pb mineral ages from the 27.5 Ma Fish Canyon Tuff reference standard. *Chemical Geology*, 199 (3-4), 277-280.
- Tassinari, C.C.G. and Macambira, M.J.B. 2004. A evolução tectônica do Cráton Amazônico. In: Mantesso-Neto, V., Bartorelli, A., Carneiro, C.D.R. and Brito Neves, B.B. (Eds.) *Geologia do Continente Sul-Americano: Evolução da Obra de Fernando Flávio Marques de Almeida*. pp. 471-485.
- Tassinari, C.C.G., Munhá, J.M.V., Teixeira, W., Palácios, T., Nutman, A.P., Sousa, C.S., Santos, A.P., Calado, B.O. 2004. The Imataca Complex, NW Amazonian Craton, Venezuela: crustal evolution and integration of geochronological and petrological cooling histories. *Episodes*, 27 (1), 3-12.
- Tassinari, C.C.G., Teixeira, W., Nutman, A.P., Szabó, G.A., Mondin, M., Sato, K. 2001. Archean crustal evolution of the Imataca Complex, Amazonian Craton: Sm-Nd, Rb-Sr e U-Pb (SHRIMP) evidences. In: *Simpósio de Geologia da Amazônia, 7. Belém. Resumos Expandidos (CD ROM)*.
- Teixeira, W., Tassinari, C.C.G., Cordani, U.G., Kawashita, K. 1989. A review of the geochronology of the Amazonian Craton: Tectonic implications. *Precambrian Research*, 42, 213-227.
- Théveniaut, H., Delor, C., Lafon, J.M., Monié, P., Rossi, P., Lahondère, D. (submitted) Paleoproterozoic (2155-2060 Ma) evolution of the Guiana Shield (Transamazonian event) in the light of new paleomagnetic data from French Guiana. *Precambrian Research*.
- Thompson, A.B. and England, P.C. 1994. Pressure-temperature-time paths of regional metamorphism II. Their inference and interpretation using mineral assemblages in metamorphic rocks. *Journal of Petrology*, 25, 929-955.
- Vanderhaeghe, O., Ledru, P., Thiéblemont, D., Egal, E., Cocherie, A., Tegye, M., Milési, J.J. 1998. Contrasting mechanism of crustal growth Geodynamic evolution of the Paleoproterozoic granite-greenstone belts of French Guyana. *Precambrian Research*, 92, 165-193.
- Vasquez, M.L. and Lafon, J.M. 2001. Magmatismo tipo A de 1,75 Ga na porção oriental do Escudo das Guianas – Estados do Amapá e Pará, Brasil. In: *Simpósio de Geologia da Amazônia, 7. Belém, CD ROM*.
- Voicu, G., Bardoux, M., Stevenson, R., Jébrak, M. 2000. Nd and Sr isotope study of hydrothermal scheelite and host rocks at Omai, Guiana Shield : implications for ore fluid source and flow path during the formation of orogenic gold deposits. *Mineralium Deposita*, 35, 302-314.
- Wartho, J.A. 1995. Apparent argon diffusive loss  $^{40}\text{Ar}$ - $^{39}\text{Ar}$  age spectra in amphiboles. *Earth and Planetary Science Letters*, 134, 393-407.
- York, D. 1969. Least-square fitting of a straight line with correlated errors. *Earth and Planetary Sciences Letters*, 5, 320-324.

**Table 2** -  $^{40}\text{Ar}/^{39}\text{Ar}$  step-heating analytical results.  $^{40}\text{Ar}^*$  = radiogenic  $^{40}\text{Ar}$ .

Temp. (°C)	$^{40}\text{Ar}/^{39}\text{Ar}$	$^{38}\text{Ar}/^{39}\text{Ar}$	$^{37}\text{Ar}/^{39}\text{Ar}$	$^{36}\text{Ar}/^{39}\text{Ar}$ ( $10^{-3}$ )	Cum. % $^{39}\text{Ar}$	$^{40}\text{Ar}^*/^{39}\text{Ar}$	Age (Ma)	$\pm 1\sigma$ (Ma)
<b>Amapá Block</b>								
<b>AV-02 amphibole</b>				J= 0.010102				
700	9421.32	5.87	2.81	24582.22	1.49	2161.37	5644	663
800	782.93	0.25	1.51	1538.03	2.49	328.83	2641	127
900	1177.60	0.72	2.32	2563.01	4.49	420.98	2993	117
950	224.99	0.27	2.92	25.93	28.23	217.9	2099	9
1000	221.75	0.26	3.05	12.70	90.69	218.59	2103	6
1050	274.97	0.25	2.71	166.69	95.61	226.26	2146	13
1150	253.52	0.24	0.64	225.72	97.36	186.91	1913	34
1400	358.37	0.42	3.51	466.18	100	221.31	2118	31
<b>LT-219A amphibole</b>				J= 0.010102				
700	3134.06	0.79	3.53	1226.84	0.13	2778.08	6079	90
800	6141.44	0.00	0.02	1804.29	0.14	5608.32	7315	1877
900	8416.99	4.72	0.00	18245.08	0.25	3025.55	6228	377
950	700.38	0.34	1.48	853.46	7.86	448.69	3086	20
1000	226.80	0.11	1.50	5.64	83.17	225.42	2141	6
1050	234.55	0.12	1.37	24.40	89.48	227.6	2153	5
1100	239.88	0.11	1.20	40.12	93.09	228.26	2157	7
1150	308.88	0.16	1.34	210.84	98.24	246.86	2257	4
1200	244.20	0.17	1.59	148.18	99.29	200.69	1998	10
1400	275.57	0.16	0.63	173.50	100	224.41	2136	15
<b>MV-48 amphibole</b>				J= 0.010102				
500	1870.98	2.78	0.01	4308.72	0.05	597.74	3520	700
700	6842.45	4.06	1.96	17051.59	1.46	1806.11	5335	377
800	837.71	0.24	0	794.69	2.28	602.86	3534	43
900	484.46	0.47	1.34	666.70	3.92	287.76	2459	37
950	222.12	0.42	1.34	22.722	18.64	215.65	2086	5
1000	221.69	0.40	0.99	3.470	83.43	220.85	2116	2
1050	218.71	0.40	1.04	16.87	94.02	213.92	2076	5
1100	236.88	0.41	1.08	54.12	98.21	221.09	2117	8
1200	541.59	0.43	0.68	670.51	98.71	343.63	2702	105
1400	938.67	0.76	0	1959.43	100	359.64	2766	48
<b>JM-01 amphibole</b>				J= 0.010102				
700	1913.16	0.55	0.42	1607.81	4.13	1438.45	4948	11
800	328.14	0.22	0.00	205.17	7.29	267.49	2361	9
900	223.51	0.74	1.47	10.53	30.67	220.68	2115	3
950	217.98	0.78	1.47	3.15	85.54	217.33	2096	2
1000	221.05	0.71	1.44	12.36	96.18	217.67	2098	2
1050	240.49	1.12	2.34	19.98	97.29	235.06	2194	6
1100	224.08	1.07	2.07	0.01	98.74	224.49	2136	6
1200	183.98	1.29	2.76	0.03	99.16	184.45	1898	17
1400	337.82	0.94	1.61	138.98	100.00	297.14	2502	11

Table 2 ( continued)

Temp. (°C)	$^{40}\text{Ar}/^{39}\text{Ar}$	$^{38}\text{Ar}/^{39}\text{Ar}$	$^{37}\text{Ar}/^{39}\text{Ar}$	$^{36}\text{Ar}/^{39}\text{Ar}$ ( $10^{-3}$ )	Cum. % $^{39}\text{Ar}$	$^{40}\text{Ar}^*/^{39}\text{Ar}$	Age (Ma)	$\pm 1\sigma$ (Ma)
<b>JM-01 biotite</b>				J= 0.010102				
500	258.56	0.20	0.59	389.14	0.44	143.64	1617	13
600	2000.67	1.25	0.49	4560.49	1.29	653.26	3659	70
700	225.86	0.13	0.03	33.30	8.92	216.01	2088	3
800	222.31	0.12	0.04	14.22	20.49	218.09	2100	2
850	229.72	0.13	0.04	26.29	28.37	221.94	2122	3
900	222.58	0.13	0.03	10.07	40.36	219.59	2109	3
950	218.40	0.12	0.01	3.06	84.06	217.48	2097	2
1000	218.23	0.12	0.02	5.95	99.49	216.46	2091	2
1100	444.74	0.29	0.00	602.53	99.69	266.67	2357	45
1200	680.48	0.42	0.00	1273.04	99.87	304.28	2534	61
1400	1949.67	1.23	0.00	4674.97	100	568.19	3442	162
<b>JM-33 biotite</b>				J= 0.010102				
500	180.865	0.035	0.005	31.207	2.62	171.62	1814	3
600	321.331	0.091	0.001	292.363	14.68	234.92	2193	4
700	213.895	0.019	0.001	5.315	37.84	212.30	2067	3
800	215.278	0.021	0.001	10.312	49.71	212.21	2066	2
850	221.880	0.027	0.002	29.065	55.73	213.27	2073	2
900	213.551	0.023	0.001	9.246	65.87	210.80	2058	2
950	210.878	0.022	0.001	4.952	79.52	209.39	2050	3
1000	211.625	0.019	0.000	3.760	97.52	210.49	2056	2
1100	222.667	0.030	0.005	35.412	99.87	212.18	2066	3
1200	1251.891	0.781	0.000	2451.869	99.93	527.34	3328	127
1400	2749.484	1.593	0.000	6284.452	100.00	892.41	4157	78
<b>JM-07 amphibole</b>				J= 0.010102				
700	2311.87	1.29	0.38	5124.67	1.05	797.73	3976	87
800	348.87	0.26	0.57	192.26	3.21	292.18	2479	9
900	220.92	0.24	0.85	6.89	85.61	219.03	2106	3
950	230.71	0.24	0.80	14.64	92.25	226.53	2148	3
1000	231.03	0.24	0.78	18.41	95.65	225.73	2143	7
1050	249.65	0.25	1.10	32.20	97.7	240.35	2223	4
1100	347.73	0.34	1.47	269.16	98.07	268.52	2366	19
1200	338.63	0.26	0.62	326.86	98.85	242.16	2232	19
1400	377.72	0.31	0.59	397.14	100	260.48	2327	11
<b>JM-07 biotite</b>				J= 0.010102				
500	229.92	0.10	0.00	256.47	1.99	154.12	1694	7
600	465.32	0.21	0.05	613.09	7.73	284.14	2442	7
700	215.17	0.04	0.01	6.78	31.39	213.15	2072	2
800	216.08	0.04	0.01	5.39	62.6	214.47	2079	3
850	216.06	0.04	0.01	7.70	93.16	213.77	2075	3
900	220.11	0.04	0.07	19.08	98.95	214.46	2079	2
950	250.99	0.05	0.00	79.85	99.41	227.38	2152	10
1000	267.36	0.08	0.42	149.38	99.67	223.28	2129	24
1200	414.08	0.18	0.00	501.57	100	265.85	2353	15

Table 2 ( continued)

Temp. (°C)	$^{40}\text{Ar}/^{39}\text{Ar}$	$^{38}\text{Ar}/^{39}\text{Ar}$	$^{37}\text{Ar}/^{39}\text{Ar}$	$^{36}\text{Ar}/^{39}\text{Ar}$ ( $10^{-3}$ )	Cum. % $^{39}\text{Ar}$	$^{40}\text{Ar}^*/^{39}\text{Ar}$	Age (Ma)	$\pm 1\sigma$ (Ma)
<b>LT-28B amphibole</b>				J= 0.010102				
500	1523.39	1.33	4.74	1191.47	0.35	1175.2	4610	77
600	11449.21	7.59	2.94	29667.37	1.34	2687.81	6021	620
700	884.89	0.61	0.30	1443.04	1.72	458.56	3118	186
800	864.05	0.69	2.48	1596.69	2.2	392.99	2893	216
850	1081.36	1.27	1.28	1643.30	2.72	596.32	3517	111
900	291.62	0.84	1.07	132.15	8.67	252.79	2288	9
950	224.57	0.71	1.42	27.43	34.38	216.73	2092	4
1000	219.31	0.67	1.44	13.00	90.63	215.74	2087	2
1100	266.13	0.71	1.23	106.51	98.39	234.9	2193	9
1200	996.54	1.09	3.81	1696.74	99.21	496.59	3237	118
1400	1531.67	1.37	1.83	3505.19	100	496.57	3237	223
<b>LT-28B biotite</b>				J= 0.010102				
500	214.33	0.11	0.08	53.06	9.45	198.64	1986	3
600	322.06	0.17	0.04	276.82	34.09	240.25	2222	6
700	219.87	0.10	0.02	8.55	65.37	217.33	2096	2
800	226.85	0.10	0.05	22.76	76.54	220.11	2112	2
850	235.85	0.11	0.11	46.31	83.12	222.17	2123	3
900	224.94	0.11	0.03	24.43	92.16	217.70	2098	3
950	221.37	0.11	0.06	7.49	98.50	219.15	2106	3
1000	240.35	0.11	0.13	29.64	99.91	231.60	2175	5
1100	1181.13	0.88	2.24	2154.09	100.00	545.50	3380	135
1200	90398.20	55.72	0.10	198015.54	100.00	31886.61	10424	870
1400	-	20116.51	21.20	-	100.00	-	20738	1091
<b>Carecuru Domain</b>								
<b>LT-196B amphibole</b>				J= 0.010102				
700	314.47	0.17	0.24	212.39	1.33	251.75	2282	18
700	314.47	0.17	0.24	212.39	2.66	251.75	0	0
900	235.08	0.17	1.27	26.65	73.57	227.45	2153	3
950	226.67	0.17	1.16	19.03	85.99	221.26	2118	5
1000	252.48	0.17	1.11	30.57	92.11	243.67	2240	3
1050	301.35	0.19	0.99	175.13	93.47	249.80	2272	10
1100	300.44	0.21	0.88	187.21	97.00	245.30	2249	7
1200	372.79	0.25	1.11	371.06	98.87	263.37	2341	10
1400	923.87	0.53	0.78	1769.53	100.00	401.20	2923	37
<b>LT-196B biotite</b>				J= 0.010102				
400	3333.61	2.36	1.50	7983.69	0.05	975.45	4302	512
500	874.55	0.69	0.62	2303.67	0.53	193.91	1957	115
600	174.50	0.06	0.00	98.48	9.58	145.38	1630	9
700	167.83	0.03	0.00	0.00	28.89	167.81	1789	4
900	240.63	0.07	0.02	148.65	52.34	196.69	1974	5
1000	174.05	0.03	0.00	0.00	86.18	174.03	1830	4
1100	331.80	0.12	0.11	376.85	95.06	220.44	2114	6
1200	3873.12	2.29	0.09	10114.90	98.47	884.21	4142	136
1400	86036.66	51.42	0.00	225706.58	100.00	19340.35	9526	7296

Table 2 ( continued)

Temp. (°C)	$^{40}\text{Ar}/^{39}\text{Ar}$	$^{38}\text{Ar}/^{39}\text{Ar}$	$^{37}\text{Ar}/^{39}\text{Ar}$	$^{36}\text{Ar}/^{39}\text{Ar}$ ( $10^{-3}$ )	Cum. % $^{39}\text{Ar}$	$^{40}\text{Ar}^*/^{39}\text{Ar}$	Age (Ma)	$\pm 1\sigma$ (Ma)
<b>LT-193 amphibole</b>				J= 0.010102				
700	2243.94	1.37	0.54	5267.27	7.06	687.71	3740	119
800	262.07	0.09	0.21	170.69	11.67	211.66	2063	7
900	337.95	0.16	1.24	291.69	19.09	252.01	2284	14
950	227.90	0.12	2.08	11.26	55.84	224.98	2139	5
1000	224.49	0.12	2.77	8.00	76.99	222.67	2126	4
1050	229.46	0.12	2.93	20.06	85.81	224.12	2134	12
1100	248.07	0.13	2.71	35.45	93.08	238.16	2211	17
1150	269.30	0.14	2.92	59.73	98.09	252.28	2285	9
1200	354.69	0.20	4.16	235.07	99.63	286.23	2451	16
1400	357.32	0.36	5.63	25.36	100	351.44	2733	31
<b>LT-193 biotite</b>				J= 0.010102				
500	250.46	0.11	0.00	275.21	0.55	169.12	1798	7
600	184.95	0.04	0.00	92.84	0.81	157.5	1718	9
700	149.35	0.03	0.00	25.44	2.57	141.81	1604	4
800	180.49	0.03	0.02	14.77	10.93	176.11	1844	3
850	182.18	0.03	0.00	7.01	20.02	180.09	1870	3
875	205.51	0.03	0.00	62.65	95.16	186.98	1914	4
925	217.50	0.05	0.02	99.36	98.88	188.12	1921	2
950	202.79	0.04	0.00	60.33	99.67	184.95	1901	4
1000	232.65	0.05	0.27	132.86	99.84	193.42	1954	9
1100	1092.92	0.56	0.66	2197.86	99.94	443.66	3070	66
1400	2957.39	1.68	0.53	7384.40	100	775.57	3931	293
<b>LT-76 amphibole</b>				J= 0.010102				
700	429.79	0.30	0.51	978.84	2.22	140.6	1595	92
800	268.67	0.43	1.57	299.46	5.38	180.44	1872	63
900	211.14	0.36	0.98	8.07	55.35	208.93	2047	6
950	217.20	0.36	0.92	4.06	94.3	216.16	2089	5
1000	268.86	0.39	0.71	62.05	96.5	250.66	2277	57
1100	684.35	0.43	6.53	601.82	97.61	509.05	3275	149
1200	1156.12	0.76	0.00	2362.14	100	458.09	3117	121
<b>LT-76 biotite</b>				J= 0.010102				
500	182.48	0.06	0.03	51.02	7.24	167.39	1786	2
600	277.27	0.10	0.01	220.90	29.87	211.98	2065	4
700	194.92	0.05	0.02	5.62	62.27	193.24	1953	2
800	199.68	0.05	0.02	12.10	76.3	196.09	1970	2
850	208.77	0.06	0.10	30.01	82.68	199.9	1994	2
900	203.54	0.05	0.06	14.33	90	199.3	1990	2
950	205.50	0.05	0.11	13.75	96.39	201.43	2003	2
1000	211.10	0.05	0.11	27.83	99.4	202.88	2012	3
1100	456.77	0.17	0.94	537.46	99.7	298.17	2506	21
1200	839.59	0.27	1.83	1455.68	99.84	410.02	2954	92
1400	2390.84	1.39	4.08	5765.84	100	689.09	3743	137

Table 2 ( continued)

Temp. (°C)	<sup>40</sup> Ar/ <sup>39</sup> Ar	<sup>38</sup> Ar/ <sup>39</sup> Ar	<sup>37</sup> Ar/ <sup>39</sup> Ar	<sup>36</sup> Ar/ <sup>39</sup> Ar (10 <sup>-3</sup> )	Cum. % <sup>39</sup> Ar	<sup>40</sup> Ar*/ <sup>39</sup> Ar	Age (Ma)	± 1σ (Ma)
<i>Paru Domain</i>								
<b>LT-186A amphibole</b>				J= 0.010102				
700	10880.72	6.87	4.70	28500.27	0.75	2466.69	5872	682
800	2217.65	0.99	3.52	4336.09	0.91	938.67	4239	482
900	1173.94	0.73	0.43	2526.29	1.46	427.55	3015	168
950	229.60	0.11	2.33	54.70	8.03	213.88	2076	6
1000	212.03	0.11	3.57	10.51	55.88	209.6	2051	3
1050	211.40	0.11	3.28	8.92	91.15	209.39	2050	2
1100	239.91	0.11	2.63	51.68	94.87	225.16	2140	6
1200	281.32	0.12	3.00	186.19	97.45	226.91	2150	14
1400	412.14	0.18	0.98	488.19	100	268.09	2364	14

## 9 – CONSIDERAÇÕES FINAIS

O modelo evolutivo apresentado por Delor et al. (2003a), representa a mais recente proposta de evolução geodinâmica para a porção oriental do Escudo das Guianas. A referida proposta evolutiva é pautada em conceitos da tectônica de placas, envolve estágios de abertura oceânica, de formação de crosta continental relacionada a ambientes de subducção, precisamente em sistemas de arcos de ilha, e de fechamento oceânico, com retrabalhamento ensialico associado. O modelo proposto por estes autores foi fundamentado principalmente no acervo de dados geológicos e geocronológicos obtidos na Guiana Francesa, que representa um domínio juvenil da extensa faixa orogênica paleoproterozóica abordada neste estudo, cuja evolução está relacionada ao Ciclo Orogênico Transamazônico.

Os principais estágios evolutivos caracterizados por Delor et al. (2003a) também foram reconhecidos na área de estudo. No entanto, a delimitação de um bloco continental arqueano nesta região, o Bloco Amapá, requer a proposição de um modelo alternativo, que contemple o referido bloco tectônico e que leve em conta a participação de crosta arqueana na origem das rochas paleoproterozóicas.

Portanto, neste capítulo é apresentada uma proposta preliminar de evolução geodinâmica para a região estudada, na qual são discutidos os principais estágios evolutivos relacionados ao Evento Transamazônico. Na estruturação do modelo, três grandes estágios foram reconhecidos, os quais são ilustrados na Figura 9.1 e descritos a seguir:

### 1) Estágio Convergente Acrescionário (2,19 – 2,14 Ga)

Este estágio foi revelado no Domínio Carecuru, pelos gnaisses e granitóides cálcio-alcalinos que definem o Complexo Paru-Maratiá e a Suíte Intrusiva Carecuru, os quais foram originados a partir de dois pulsos magmáticos, sendo o primeiro ocorrido entre 2,19 e 2,18 Ga, e o mais jovem entre 2,15 e 2,14 Ga.

Estes eventos plutônicos podem ser correlacionados com aqueles identificados na Guiana Francesa, onde foram datados dois pulsos de magmatismo cálcio-alcalino, entre 2,19 e 2,16 Ga e 2,15 e 2,13 Ga (Delor et al. 2003a). Naquela região, sistemas de arcos de ilha são evocados para explicar o significado geodinâmico e a origem das rochas cálcio-alcalinas, que apresentam assinatura isotópica juvenil, definida por idades modelo  $T_{DM}$  riacianas e por valores de  $\epsilon_{Nd}$  sistematicamente positivos.

No Domínio Carecuru, embora também tenha sido reconhecida acreção juvenil riaciana nas rochas cálcio-alcálicas, visto que foi determinada uma idade  $T_{DM}$  em torno de 2,28 Ga associada a  $\epsilon_{Nd}$  positivo, prevalecem idades  $T_{DM}$  entre 2,50 e 2,38 Ga, acompanhadas por valores de  $\epsilon_{Nd}$  negativos, indicando que rochas mais antigas foram envolvidas nos processos petrogenéticos dos granitóides. Conseqüentemente, estas idades foram interpretadas em termos de mistura entre dois componentes, sendo magma juvenil cálcio-alcálico o principal componente, e o outro representado por crosta arqueana, com participação secundária.

Seguindo-se a classificação de Barbarin (1999), as rochas do Domínio Carecuru poderiam ser incluídas no grupo dos granitóides cálcio-alcálicos ricos em anfíbólio (tipo ACG), os quais, segundo este autor, têm fonte mista, pois envolvem na sua formação componentes derivados do manto e da crosta, e origem invariavelmente associada a ambientes envolvendo subducção de crosta oceânica.

Portanto, o conjunto de dados obtidos nas rochas cálcio-alcálicas do Domínio Carecuru, permitiu associar sua origem a um ambiente de arco magmático, originado sobre uma zona de subducção estabelecida durante a fase inicial da convergência entre blocos continentais arqueanos, provavelmente o Bloco Amapá, situado a leste, e outro fragmento continental a oeste, que poderia estar representado pelo núcleo arqueano Iricoumé, integrante da Província Amazônia Central, de Tassinari & Macambira (2004).

Embora tenham sido datados pulsos diacrônicos do magmatismo cálcio-alcálico, não foi detectada zonalidade espacial entre os corpos de granitóides de diferentes idades, o que não permite assegurar se os mesmos representam dois sistemas de arcos magmáticos, estabelecidos sucessivamente entre 2,19 Ga e 2,18 e entre 2,16 e 2,14, ou se, alternativamente, são produto de um contínuo episódio acrescionário, de 2,19 a 2,14 Ga.

Os registros deste estágio no Bloco Amapá, apontam que, enquanto dominavam processos acrescionários na sua margem meridional, retrabalhamento ensialítico ocorria nas suas porções mais internas, levando a migmatização do embasamento arqueano e produção de granitos, como sugerem as idades em torno de 2,2 Ga e 2,14 Ga fornecidas por plutons graníticos alojados em gnaisses do complexo Jari-Guaribas e Guianense, e as idades herdadas obtidas em monazitas provenientes destes mesmos complexos.

Dentro deste contexto tectônico, é necessário discutir o significado geodinâmico da expressiva seqüência metavulcano-sedimentar que define o Grupo Ipitinga. Faraco (1997) admite que as rochas metavulcânicas máfico-ultramáficas que constituem a porção basal deste grupo (Formação Igarapé do Inferno), têm como protólitos principalmente basaltos toleíticos e, subordinadamente, basaltos komatiíticos, cuja gênese estaria relacionada a um centro de extensão e expansão de fundo oceânico em um sistema de bacia retro-arco.

O modelo genético proposto por este autor para esta seqüência é compatível com o ambiente geodinâmico aqui discutido, que envolve a geração de arcos magmáticos. Entretanto, a imprecisa idade de  $2264 \pm 34$  Ma (MSWD = 37,4) calculada a partir de uma errócrona Sm-Nd para rochas metavulcânicas máficas e interpretada como idade do vulcanismo (McReath & Faraco 1997), não é consistente com o desenvolvimento de um sistema de arco magmático entre 2,19 e 2,14 Ga, pois um intervalo da ordem de 70 Ma deveria ser admitido entre o desenvolvimento da bacia retro-arco e a primeira fase acrescionária do arco magmático.

Pelo menos três hipóteses podem ser aventadas para explicar este diacronismo:

- 1) A bacia retro-arco estaria relacionada a um arco magmático mais antigo, desenvolvido em torno de 2,26 Ga, e cujas evidências ainda não foram comprovadas até agora na área estudada.
- 2) A idade de 2,26 Ga calculada para o vulcanismo máfico-ultramáfico estaria na verdade registrando um estágio oceânico de extensão limitada, com significado semelhante ao Estágio Oceânico Eo-Riaciano de Delor et al. (2003a), caracterizado na Guiana Francesa através da identificação de gabros e trondhjemitos toleíticos, datados em torno de 2,22-2,21 Ga.
- 3) A idade de 2,26 Ga é suficiente para confirmar a evolução transamazônica da seqüência vulcânica, mas não indica seguramente sua idade de formação.

Vários exemplos na literatura relatam dificuldades na datação de rochas máficas através do método Sm-Nd, a exemplo de Chauvel et al. (1985). Estes autores, estudando rochas vulcânicas máfico-ultramáficas da seqüência Kambalda, Bloco Yilgarn, na Austrália, demonstraram que a idade em torno de 3,2 Ga calculada numa isócrona Sm-Nd para estas rochas, reflete a época de separação do manto do magma parental, e é 500 Ma mais antiga que a verdadeira idade do vulcanismo, datado em torno de 2,7 Ga pelo método Pb-Pb.

A terceira hipótese parece ser a que mais se coaduna com os dados disponíveis, visto que, a idade de 2,26 Ga é compatível com o padrão regional eo-riaciano de acreção crustal,

amplamente registrado na faixa orogênica paleoproterozóica em questão. Portanto, na proposta evolutiva ora apresentada, admite-se que o desenvolvimento da bacia retro-arco está relacionado ao evento acrescionário, entre 2,19 e 2,14 Ga, embora as outras hipóteses discutidas não possam ser descartadas, face às limitações dos dados disponíveis.

Duas hipóteses distintas também são propostas para explicar o significado tectônico do Domínio Paru, de idade arqueana, dentro do contexto de sistema de arco magmático paleoproterozóico. Uma delas o admite como uma evidência do prolongamento da crosta continental arqueana do Bloco Amapá para oeste, preservada nas raízes do arco magmático, e a outra considera o referido domínio como um terreno alóctone, amalgamado ao arco magmático no Paleoproterozóico.

O reconhecimento de acreção crustal juvenil paleoproterozóica neste *inlier* arqueano, através da idade de cristalização de 2,15 Ga fornecida por um gnaisse cálcio-alcálico que apresenta idade  $T_{DM}$  de 2,32 Ga e  $\epsilon_{Nd}$  positivo, adicionado à identificação de componentes arqueanos na fonte das rochas cálcio-alcálicas do Domínio Carecuru, favorecem a primeira hipótese. Adicionalmente, algumas similaridades isotópicas são reconhecidas entre a crosta arqueana do Domínio Paru e do Bloco Amapá, como idades modelo  $T_{DM}$  em torno de 2,83 Ga e magmatismo neoarqueano em torno de 2,6 Ga. Logo, no modelo proposto o Domínio Paru é interpretado como parte da margem meridional do Bloco Amapá, fragmentada durante o desenvolvimento da bacia retro-arco Ipitinga e envolvido na evolução do arco magmático.

## 2) Estágio Colisional (2,10 – 2,08 Ga)

O estágio colisional foi estabelecido em função do fechamento do oceano que separava o Bloco Amapá e o outro segmento arqueano a oeste, que culminou com a colisão das duas massas continentais, e o desenvolvimento de um sistema de cavalgamento oblíquo na borda sudoeste do Bloco Amapá, que provocou o metamorfismo em condições de fácies granulito e o alçamento tectônico de porções infracrustais do embasamento arqueano.

Os principais marcadores geocronológicos e estruturais deste evento colisional são registrados na borda sudoeste do Bloco Amapá. O padrão estrutural observado neste setor é coerente com o desenvolvimento de um sistema de cavalgamento oblíquo, com transporte tectônico de SW para NE. Os dados estruturais demonstram a evolução de uma movimentação inicialmente oblíqua para uma tectônica com componentes predominantemente transcorrentes, o que

é classicamente aceito como evidência de colisão tectônica (Shackleton 1986). Adicionalmente, informações petro-estruturais associadas aos dados geocronológicos demonstram que o metamorfismo granulítico datado em torno de 2,09 Ga, através de monazitas e zircões provenientes de granulitos do Complexo Jari-Guaribas, é contemporâneo ao desenvolvimento do sistema de cavalgamento.

Outro importante argumento que favorece o cenário proposto são as idades obtidas em anfibólio e biotita de rochas da assembléia de embasamento, inclusive do Complexo Jari-Guaribas, que são similares às das monazitas, entre 2,10 e 2,08 Ga, indicando rápido resfriamento logo após o metamorfismo de fácies granulito. Taxas de resfriamento da ordem de 40 °C/Ma e 67 °C/Ma sugerem exumação tectônica de porções infracrustais do embasamento do Bloco Amapá, o que é consistente com o modelo de cavalgamento.

Em contrapartida, taxas de resfriamento regionais em torno de 3,0-2,3 °C/Ma foram calculadas para granitóides cálcio-alcálicos do Domínio Carecuru, para um intervalo de tempo entre 2,14 Ga e 1,97 Ga, o que sugere resfriamento lento e soerguimento gradual e, conseqüentemente, que durante o estágio colisional este segmento acrescionário não foi significativamente afetado. O único registro inequívoco deste estágio no Domínio Carecuru é o magmatismo granítico de 2,10 Ga, cuja gênese está relacionada a retrabalhamento de crosta arqueana, indicada pela idade  $T_{DM}$  de 2,83 Ga e pelo valor de  $\epsilon_{Nd}$  fortemente negativo.

Finalmente, a caracterização de uma fase colisional entre 2,10 e 2,08 Ga na área estudada é consistente com o quadro evolutivo regional do Ciclo Orogênico Transamazônico no Escudo das Guianas, visto que, além de também ter sido definido na Guiana Francesa, entre 2,11 e 2,08 Ga (Delor et al. 2003a), tentativas de reconstrução paleogeográficas envolvendo este escudo e o Escudo de Man, no Cráton Oeste Africano, também admitem uma fase colisional em torno de 2,1 - 2,0 Ga (Feybesse & Milési 1994, Ledru et al. 1994, Théveniaut et al. submetido).

#### c) Estágio Tardi-colisional (2,07 -2,03 Ga)

Neste estágio dominou tectônica transcorrente, que promoveu deformação, metamorfismo com migmatização associada, e colocação de pequenos plútons graníticos ao longo de extensas zonas de cisalhamento direcionais.

Na área de estudo, esta fase evolutiva foi registrada principalmente na porção sudeste do Bloco Amapá, onde monazitas provenientes de gnaisses fortemente migmatizados do Complexo

Guianense e apresentando pervasiva foliação milonítica de médio a alto ângulo de mergulho, revelaram eventos de migmatização em torno de 2,06 Ga e 2,04 Ga. Os gnaisses estudados, localizam-se nas proximidades de plútons graníticos nos quais foram obtidas idades de 2,05 e 2,03 Ga, que são similares, dentro dos limites de erros, àquelas que definiram os eventos de migmatização. Assim como os gnaisses citados, um dos plútons datados apresenta foliação milonítica de alto ângulo de mergulho, o que sugere colocação controlada por tectônica transcorrente.

Possivelmente, esta tectônica transcorrente ocorreu a partir de reativações locais de estruturas geradas durante o evento colisional, sejam de zonas de cavalgamento ou transcorrentes, e, aparentemente, tem abrangência restrita. Uma importante evidência é o fato das idades fornecidas por anfibólios e biotitas provenientes de rochas da assembléia de embasamento do sudoeste do Bloco Amapá, registrarem principalmente a idade do evento metamórfico de alto grau, ocorrido em torno de 2,09 Ga e relacionado à fase colisional. Apenas um paragneisse apresentou idade de biotita em torno de 2,05 Ga (amostra JM-33), o qual foi coletado nas proximidades do plúton granítico de 2,05 Ga e do gnaisse migmatizado a 2,06 Ga.

Este estágio também foi caracterizado por Delor et al. (2003a) na Guiana Francesa, entre 2,07 e 2,06 Ga, onde, da mesma forma que acontece na área de estudo, domina a tectônica transcorrente, com metamorfismo, migmatização e colocação de granitos ao longo grandes corredores de deformação. Estes autores admitem que, durante esta fase, o metamorfismo seguiu uma trajetória P-T anti-horária, similarmente àquela definida para os granulitos UHT das Montanhas Bakhuis, no Suriname, datados entre 2,07 e 2,05 Ga (Roever et al. 2003). Delor et al. (2003b), avaliando o registro deste estágio no contexto de toda porção oriental do Escudo das Guianas, sugerem que, à movimentação transcorrente, também estão relacionados segmentos onde predomina extensão crustal, nos quais altos gradientes termais podem ter sido alcançados em função de *upwelling* mantélico. Esse processo geodinâmico justifica as extremas condições de temperatura atingidas nas Montanhas Bakhuis, e também foi evocado para explicar a ocorrência do magmatismo charnoquítico de 2,05 Ga, que ocorre na região de Tartarugalzinho (Avelar et al. 2001), que integra a porção ocidental do Bloco Amapá.

Na área de estudo, embora ainda não tenham sido encontradas evidências decisivas de extensão relacionada ao estágio tardi-colisional, não se descarta essa possibilidade. Tectônica

extensional associada a elevados gradientes termais talvez explicasse o mecanismo de exumação dos gnaisses granulíticos do Complexo Ananaí, no Domínio Paru, a origem dos plutons charnoquíticos de 2,07 Ga da Suíte Intrusiva Igarapé Urucu, e o fato destas rochas charnoquíticas estarem freqüentemente isentas de deformação e em relação de mistura magmática com rochas máficas, de origem seguramente mantélica.

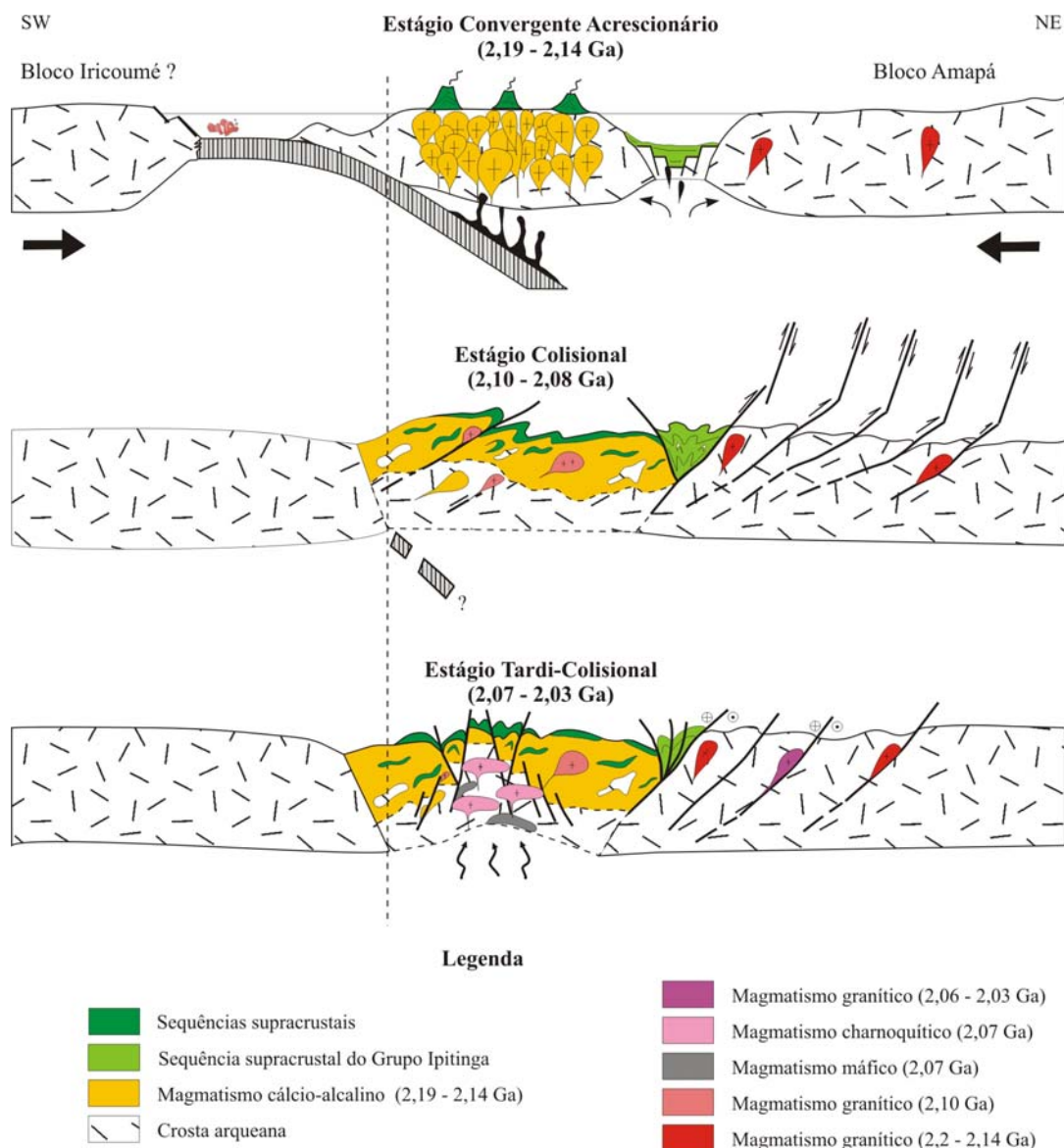


**Figura 9. 1** – Ilustração esquemática dos estágios evolutivos relacionados ao Ciclo Orogênico Transamazônico, reconhecidos na área de trabalho.

---

**REFERÊNCIAS BIBLIOGRÁFICAS**

- AGARD, P.; MONIÉ, P.; JOLIVET, L.; GOFFÉ, B. 2002. Exhumation of the Schistes Lustrés complex: in situ laser probe  $^{40}\text{Ar}$ - $^{39}\text{Ar}$  constraints and implications for the Western Alps. *J. Metamorph. Geol.*, **20**: 599-618.
- ALMEIDA, F.F.M.; HASUI, Y.; BRITO NEVES, B.B.; FUCK, P.A. 1981. Brazilian structural provinces: an introduction. *Earth Sci. Rev.*, **17**:1-29.
- ANSDELL, K.M. & KYSER, T.K. 1993. Textural and chemical changes undergone by zircon during the Pb-evaporation technic. *Am. Miner.*, **78**: 1663-1673.
- ARNAUD, N.O. 1992 . *Apports de la thermochronologie  $^{40}\text{Ar}$ - $^{39}\text{Ar}$  sur feldspath potassique a la connaissance de la tectonique cenozoique d'Asie*. 161 p. Université Blaise Pascal. Clermont-Ferrand II. (Tese de Doutorado)
- ARNDT, N.T. & GOLDSTEIN, S.L. 1987. Use and abuse of crust-formation ages. *Geology*, **15**: 893-895.
- AVELAR, V.G. 2002. Geocronologia Pb-Pb em zircão e Sm-Nd em rocha total da porção centro-norte do Estado do Amapá – Brasil: Implicações para a evolução geodinâmica do setor oriental do Escudo das Guianas. 213 p. Universidade Federal do Pará, Centro de Geociências, Pós-Graduação em Geologia e Geoquímica, Belém. (Tese de Doutorado).
- AVELAR, V.G.; LAFON, J.M.; CORREIA Jr. F.C.; MACAMBIRA, E.J.B. 1999. O magmatismo arqueano da região de Tucumã – Província Mineral de Carajás: novos dados geocronológicos. *Rev. Bras. Geoc.*, **29**: 453-460.
- AVELAR, V.G.; LAFON, J.M.; DELOR, C. 2001. Geocronologia Pb-Pb em zircão e Sm-Nd em rocha total da porção centro-norte do Estado do Amapá. Implicações pra a evolução geodinâmica do Escudo das Guianas. In: SIMPÓSIO DE GEOLOGIA DA AMAZÔNIA, 7, Belém, 2001. *Resumos Expandidos*, SBG-NO. CD ROM.
- AVELAR, V.G.; LAFON, J.M.; DELOR, C.; GUERROT, C.; LAHONDÈRE, D. 2003 . Archean crustal remnants in the easternmost part of the Guiana Shield: Pb-Pb and Sm-Nd geochronological evidence for Mesoarchean versus Neoarchean signatures. *Geologie de la France*, **2-3-4**:83-100.
- BALDWIN, S.L.; HARRISON, T.M.; FITZ GERALD, J.D. 1990. The diffusion of  $^{40}\text{Ar}$  in metamorphic hornblende. *Contr. Mineral. Petrol.*, **105**: 691-703.
- BARBARIN, B. 1999. A review of the relationships between granitoid types, their origins and their geodynamic environments. *Lithos*, **46**: 605-626.

- BARROS, A. M.; ARAÚJO, H.J.T.; TARAPANOFF, I.; MOREIRA, M.L.O.; PRADO, P. 1984 *Projeto Iratapuru (Área Cupixi) - Geologia Regional*. Goiânia, GEBAM/RADAMBRASIL, 205p. (Relatório Técnico).
- BARROS, C.E.M.; MACAMBIRA, M.J.B.; BARBEY, P.; SCHELLER, T. 2004. Dados isotópicos Pb-Pb em zircão (evaporação) e Sm-Nd do Complexo Granítico Estrela, Província Mineral de Carajás, Brasil: implicações petrológicas e tectônicas. *Rev. Bras. Geoc.*, **34**: 531-538.
- BAXTER, E.F.; AGUE, J.J.; DEPAOLO, D.J. 2002. Prograde temperature-time evolution in the Barrovian type locality constrained by Sm/Nd garnet ages from Glen Clova, Scotland. *J. Geol. Soc. London*, **159**: 71-82.
- BEN OTHMAN, D.; POLVÉ, M.; ALLEGRE, C.J. 1984. Nd-Sr isotopic composition of granulite and constraints on the evolution of the lower continental crust. *Nature*, **307**: 510-515.
- BEST, M.G. 1982. *Igneous and Metamorphic Petrology*. New York, W.H. Freeman & Company. 630p.
- BINGEN, B. & VAN BREEMEN, O. 1998. U-Pb monazite ages in amphibolite- to granulite-facies orthogneisses reflect hydrous mineral breakdown reactions: Sveconorwegian Province of SW Norway. *Contrib. Mineral. Petrol.*, **132**: 336-353.
- BINGEN, B.; BOVEN, A.; PUNZALAN, L.; WIJBRANS, J.R.; DEMAIFFE, D. 1998. Hornblende  $^{40}\text{Ar}$ - $^{39}\text{Ar}$  geochronology across terrane boundaries in the Sveconorwegian Province of S. Norway. *Precambrian Res.*, **90**: 159-185.
- BOHER, M.; ABOUCHAMI, W.; MICHARD, A.; ALBAREDE, F.; ARNDT, N.T. 1992. Crustal growth in West Africa at 2.1 Ga. *J. Geophys. Res.*, **97**: 345-369.
- BOHLENDER, F.; VAN REENEN, D.D.; BARTON Jr., J.M. 1992. Evidence for metamorphic and igneous charnockites in the Southern Marginal Zone of the Limpopo Belt. *Precambrian Res.*, **55**: 429-449.
- BORGES, A.A.S.; LAFON, J.M.; VILLAS, R.N.N. 2002. Magmatismo Tardi-Transamazônico na Serra do Navio, região central do Amapá: evidências geocronológicas. In: CONGRESSO BRASILEIRO DE GEOLOGIA, 41, João Pessoa. *Anais*, SBG-NE, p.435.
- BOSMA, W.; KROONENBERG, S.B.; MASS, K.; DE ROEVER, E.W.F. 1983. Igneous and metamorphic complexes of the Guiana Shield in Surinam. *Geol. Mijnbouw.*, **62**: 241-254.
- BRANDT, S.; KLEMD, R.; OKRUSCH, M. 2003. Ultrahigh-Temperature metamorphism and multistage evolution of garnet-orthopyroxene granulites from the Proterozoic Epupa Complex, NW Namibia. *J. Petrol.*, **44**(6): 1121-1144.

- 
- BRAUN, I.; MONTEL, J.M.; NICOLLET, C. 1998. Electron microprobe dating of monazites from high-grade gneisses and pegmatites of the Kerala Khondalite Belt, southern India. *Chem. Geol.*, **146**: 65-85.
- BRITO NEVES, B.B. & CORDANI, U.G. 1991. Tectonic evolution of South America during the Late Proterozoic. *Precambrian Res.*, **53**: 23-40
- CARVALHO, J.M.; ROSA-COSTA, L.T.; VASQUEZ, M.L.; KLEIN, E.L.; MACAMBIRA, E.M.B.; VALE, A.G.; RICCI, P.S.F. 2001. *Projeto Província Mineral da RENCA e Distrito Mineral do Ipitinga - Carta Geológica (escala 1:250.000)*. Belém, CPRM (Programa de Levantamentos Geológicos Básicos).
- CATLOS, E.J.; GILLEY, L.D.; HARRISON, T.M. 2002. Interpretation of monazite ages obtained via in situ analysis. *Chem. Geol.*, **188**: 193-215.
- CHAUVEL, C.; DUPRÉ, B.; JENNER, G.A. 1985. The Sm-Nd age of Kambalda volcanics is 500 Ma too old ! *Earth and Planetary Sciences Letters*, **74**:315-324.
- CHERNIAK, D.J. & WATSON, E.B. 2000. Pb diffusion in zircon. *Chem. Geol.*, **172**: 5-24.
- CHERNIAK, D.J. & WATSON, E.B. 2003. Diffusion in zircon. In: HANCHAR, J.M. & HOSKIN, P.W.O. (eds.) *Zircon*. Washington D.C., Mineralogical Society of America p. 113-143. (Reviews in Mineralogy and Geochemistry, 53).
- CHERNIAK, D.J.; WATSON, E.B.; GROVE, M.; HARRISON, T.M. 2002. Pb diffusion in monazite. In: GEOLOGICAL SOCIETY OF AMERICA ANNUAL MEETING, Denver. *Abstract Volume*, Paper 138-5.
- COCHERIE, A. & ALBARÈDE, F. 2001. An improved U-Th-Pb age calculation for electron microprobe dating of monazite. *Geochim. Cosmochim. Acta*, **65**: 4509-4522.
- COCHERIE, A. & LEGENDRE, O. 2006. Potential minerals for determining U-Th-Pb chemical age using electron microprobe. *Lithos* (no prelo).
- COCHERIE, A.; BE MEZEME, E.; LEGENDRE, O.; FANNING, C.M.; FAURE, M.; ROSSI, P. 2005. Electron-microprobe dating as a tool for determining the closure of Th-U-Pb systems in migmatitic monazites. *Am. Mineral.*, **90**: 607-618.
- COCHERIE, A.; LEGENDRE, O.; PEUCAT, J.J.; KOUAMELAN, A.N. 1998. Geochronology of polygenetic monazites constrained by in situ electron microprobe U-Th-totl lead determination: implications for lead behavior in monazite. *Geochim. Cosmochim. Acta*, **62**: 2475-2497.
- CONEY, P.J.; JONES, D.L.; MOMGER, J.W.H. 1980. Cordilleran suspect terranes. *Nature*, **288**: 329-333.

- 
- COPELAND, P.; PARRISH, R.R.; HARRISON, T.M. 1988. Identification of inherited radiogenic Pb in monazite band implications for U-Pb systematic. *Nature*, **333**: 760-763.
- CORDANI, U.G. & BRITO NEVES, B.B. 1982. The geologic evolution of South America during the Archean and Early Proterozoic. *Rev. Bras. Geoc.*, **12**: 78-88.
- CORDANI, U.G. & SATO, K. 1999. Crustal evolution of the South American Platform, based on Nd isotopic systematic on granitoid rocks. *Episodes*, **22**(3): 167-173.
- CORDANI, U.G.; SATO, K.; TEIXEIRA, W.; TASSINARI, C.C.G.; BASEI, M.A.S. 2000. Crustal evolution of the South American Platform. In: CORDANI, U.G.; MILANI, E.J.; FILHO, A.T.; CAMPOS, D.A. (eds.) *Tectonic Evolution of South America*. Rio de Janeiro, 31<sup>o</sup> International Geological Congress, SBG.
- CORDANI, U.G.; TASSINARI, C.C.G.; KAWASHITA, K. 1984. A Serra dos Carajás como região limítrofe entre províncias tectônicas. *Ciências da Terra*, **9**: 6-11.
- CORDANI, U.G.; TASSINARI, C.C.G.; TEIXEIRA, W.; BASEI, M.A.S.; KAWASHITA, K. 1979. Evolução tectônica da Amazônia com base nos dados geocronológicos. In: CONGRESSO GEOLÓGICO CHILENO, 2, Arica (Chile). *Actas*, p. 137-148.
- COSTA, J.B.S. & HASUI, Y. 1997. Evolução geológica da Amazônia. In: COSTA, M.L.C. & ANGÉLICA, R.S. (coords.) *Contribuição à Geologia da Amazônia*. Belém, SBG-NO, p.15-90.
- CPRM. 1999. *Projeto Aerogeofísico Reserva Nacional do Cobre e Associados (RENCA)*. Rio de Janeiro, 15v. 35p. (Relatório Final).
- CPRM/DNPM. 1978. Projeto Jari-Rio Negro Leste. Levantamentos aerogamaespectométrico e aeromagnetométrico: Território Federal do Amapá e Estado do Pará. Rio de Janeiro, 107p.
- CPRM/DNPM. 1979. Projeto Jari-Rio Negro Leste II. Levantamentos aerogamaespectométrico e aeromagnetométrico: Território Federal do Amapá e Estado do Pará. Rio de Janeiro, 66p.
- CROWLEY, J.L. & GHENT, E.D. 1999. An electron microprobe study of the U-Th-Pb systematics of metamorphosed monazite: the role of Pb diffusion versus overgrowth and recrystallization. *Chem. Geol.* **157**: 285-302.
- DAHL, P.S. 1996. The effects of composition on retentivity of argon and oxygen in hornblende and related amphiboles: a field-test empirical model. *Geochim. Cosmochim. Acta*, **6**: 3687-3700.
- DALL'AGNOL, R.; TEIXEIRA, N.P.; RAMO, O.T.; MOURA, C.A.V.; MACAMBIRA, M.J.B.; OLIVEIRA, D.C. 2005. Petrogenesis of the Paleoproterozoic rapakivi A-type granites of the Archean Carajás metallogenic province, Brazil. *Lithos*, **80**: 101-129.

- 
- De WOLF, C.P.; BELSHAW, N.; O'NIONS, R.K. 1993. A metamorphic history from micro-scale  $^{207}\text{Pb}/^{206}\text{Pb}$  chronometry of Archean monazite. *Earth Planet. Sci. Lett.*, **120**: 207-220.
- DELOR, C.; LAHONDÈRE, D.; EGAL, E.; LAFON, J.M.; COCHERIE, A.; GUERROT, C.; ROSSI, Ph.; TRUFERT, C.; THEVENIAUT, H.; PHILLIPS, D.; AVELAR, V.G. 2003a. Transamazonian crustal growth and reworking as revealed by the 1:500.000-scale geological map of French Guiana (2nd edition). *Géologie de la France*, **2-3-4**: 5-57.
- DELOR, C.; LAHONDÈRE, D.; EGAL, E.; MARTEAU, P. 2001. *Carte Géologique de la Guyane à 1/500000*. 2nd. ed., BRGM.
- DELOR, C.; ROEVER, E.W.F.; LAFON, J.M.; LAHONDÈRE, D.; ROSSI, P.; COCHERIE, A.; GUERROT, C.; POTREL, A. 2003b. The Bakhuis ultrahigh-temperature granulite belt (Suriname): II. Implications for late Transamazonian crustal stretching in a revised Guiana Shield framework. *Géologie de la France*, **2-3-4**: 207-230.
- DePAOLO, D.J. 1981. Nd isotopic studies: some new perspectives on Earth structure and evolution. *EOS*, **62**: 137-145.
- DePAOLO, D.J. 1988. *Neodymium isotope geochemistry – an introduction*. Berlim, Springer-Verlag. 187p.
- DePAOLO, D.J. & WASSERBURG, G.J. 1976a. Nd isotopic variations and petrogenetic models. *Geophys. Res. Lett.*, **3**: 249-252.
- DePAOLO, D.J. & WASSERBURG, G.J. 1976b. Inferences about magma sources and mantle structure from variations of  $^{143}\text{Nd}/^{144}\text{Nd}$ . *Geophys. Res. Lett.*, **3**: 743-747.
- DODSON, M.H. 1973. Closure temperatures in cooling geochronological and petrological systems. *Contr. Mineral. Petrol.*, **40**: 259-274.
- DOUMBIA, S.; POUCKET, A.; KOUAMELAN, A.; PEUCAT, J.J.; VIDAL, M.; DELOR, C. 1998. Petrogenesis of juvenile-type Birimian (Paleoproterozoic) granitoids in Central Côte-d'Ivoire, West Africa: geochemistry and geochronology. *Precambrian Res.*, **87**: 33-63.
- EGAL, E.; MILÉSI, J.P.; LEDRU, P.; CAUTRU, J.P.; FREYSSINET, P.; THIÉBLEMONT, D.; VERNHET, Y. 1994. *Ressources minérales et évolution lithostructurale de la Guyane. Carte thématique minière à 1/100.000, Feuille Cayenne*. Rapport BRGM, R 38019, 59p.
- EGAL, E.; MILÉSI, J.P.; VANDERHAEGHE, O.; LEDRU, P.; COCHERIE, C.; THIÉBLEMONT, D.; CAUTRU, J.P.; VERNHET, Y.; HOTTIN, A.M.; TEGYEY, M.; MARTEL-JANTIN, B. 1995. *Ressources minérales et évolution Lithostructurale de la Guyane. Carte thématique minière à 1/100.000, Feuille Régina*. Rapport BRGM, R 38458.

- ENGLAND, P.C. & THOMPSON, A.B. 1994. Pressure-temperature-time paths for regional metamorphism I. Heat transfer during the evolution of regions of thickened continental crust. *J. Petrol.*, **25**: 894-928.
- ENJOLVY, R. 2004. Caractérisation géochronologique et pétrologique de l'événement fini-Transamazonien: étude en Guyane Française et en Amapá (Brésil). 42 p. Université Montpellier II, Montpellier. (Diplôme d'Etudes Approfondies).
- FARACO, M.T.L. 1997. *Evolução petroquímico-metalogenética das rochas e mineralizações associadas à Suíte Vila Nova na Serra do Ipitinga (NW do Pará)*. 245p. Universidade Federal do Pará, Centro de Geociências, Pós-Graduação em Geologia e Geoquímica, Belém. (Tese de Doutorado).
- FARACO, M.T.L.; MARINHO, P.A.C.; VALE, A.G.; MOURA, C.V. 2004b. Corpo máfico-ultramáfico no Distrito de Ipitinga – Reserva Nacional de Cobre e Associados. In: CONGRESSO BRASILEIRO DE GEOLOGIA, 42, Araxá. *Resumos*, SBG. CD-ROM.
- FARACO, M.T.L.; MARINHO, P.A.C.; VALE, A.G.; MOURA, C.V.; MACAMBIRA, M.J.B. 2004a. Idades modelo Sm-Nd e idade  $^{207}\text{Pb}$ - $^{206}\text{Pb}$  em zircão no Distrito de Ipitinga, Reserva Nacional do Cobre e seus Associados - RENCA. In: CONGRESSO BRASILEIRO DE GEOLOGIA, 42, Araxá. *Resumos*, SBG. CD-ROM.
- FARACO, M.T.L.; VALE, A.G.; SANTOS, J.O.S.; LUZARDO, R.; FERREIRA, A.L.; OLIVEIRA, M.A.; MARINHO, P.A.C. 2003. Levantamento geológico na região norte do Bloco Carajás: notícias preliminares. In: SIMPÓSIO DE GEOLOGIA DA AMAZÔNIA, 8, Manaus. *Resumos Expandidos*, SBG-NO. CD-ROM.
- FARACO, M.T.L.; VALE, A.G.; SANTOS, J.O.S.; LUZARDO, R.; FERREIRA, A.L.; OLIVEIRA, M.A.; MARINHO, P.A.C. 2005. Levantamento geológico da região ao norte da Província Carajás. In: HORBE, M. C. & SOUSA, V.S. (eds.) *Contribuições à Geologia da Amazônia*. Manaus, SBG-NO, vol. 4, p. 32-43.
- FAURE, M.; MONIÉ, P.; PIN, C.; MALUSKI, H.; LELOIX, C. 2002. Late Visean thermal event in the northern part of the French Massif Central: new  $^{39}\text{Ar}/^{40}\text{Ar}$  and Rb-Sr isotopic constraints on the Hercynian syn-orogenic extension. *Internat. J. Earth Sci.*, **91**: 53-75.
- FEYBESSE, J.L. & MILÉSI, J.P. 1994. The Archean/Paleoproterozoic contact zone in West Africa: a mountain belt of décollement thrusting and folding on a continental margin related to 2.1 Ga convergence of Archean cratons? *Precambrian Res.*, **69**: 199-227.
- FOLAND, K.A. 1983.  $^{40}\text{Ar}$ - $^{39}\text{Ar}$  incremental heating plateau for biotites with excess argon. *Chem. Geol.*: **1**, 3-21.
- FOSTER, G. & PARRISH, R. 2003. Metamorphic monazite and the generation of P-T-t paths. In: VANCE, D.; MULLER, W.; VILLA, I.M. (eds.) *Geochronology: linking the isotopic*

---

*record with petrology and textures*. London, Geological Society, Special Publication, v. 220, p. 25-47.

- FOSTER, G.; GIBSON, H.D.; PARRISH, R.R.; HORST-WOOD, M.S.A.; FRASER, J.; TINDLE, A. 2002. Textural, chemical and isotopic insight into the nature and behaviour of metamorphic monazite. *Chem. Geol.*, **191**: 183-207.
- FOSTER, G.; KINNY, P.; PRINCE, C.; VANCE, D.; HARRIS, N. 2000. The significance of monazite U-Th-Pb age data in metamorphic assemblages: a combined study of monazite and garnet chronometry. *Earth Planet. Sci. Lett.*, **181**: 327-340.
- FRAGA, L.M.B. 2002. A associação anortosito-mangerito-granito rapakivi (AMG) do Cinturão Guiana Central, Roraima, e suas encaixantes paleoproterozóicas: evolução estrutural, geocronologia e petrologia. 351p. Universidade Federal do Pará, Centro de Geociências, Pós-Graduação em Geologia e Geoquímica, Belém. (Tese de Doutorado).
- FRASER, G.; ELIS, D.; EGGINS, S. 1997. Zirconium abundance in granulite-facies minerals, with implications for zircon geochronology in high-grade rocks. *Geology*, **25**: 607-610.
- FRIEND, C.R.L. & NUTMAN A.P. 2001. U-Pb zircon study of tectonically bounded blocks of 2940-2840- Ma crust with different metamorphic histories, Paamiut region, south-west Greenland: implications for the tectonic assembly of the North Atlantic Craton. *Precambrian Res.*, **105**:143-164.
- GASQUET, D.; BARBEY, P.; ADOU, M.; PAQUETTE, J.L. 2003. Structure, Sr-Nd isotope geochemistry and zircon U-Pb geochronology of the granitoids of the Dabakala area (Côte d'Ivoire): evidence for a 2.3 Ga crustal growth event in the Paleoproterozoic of West Africa? *Precambrian Res.*, **127**: 329-354.
- GAUDETTE, H.E.; LAFON, J.M.; MACAMBIRA, M.J.B.; MOURA, C.A.V.; SCHELLER, T. 1998. Comparison of single filament Pb evaporation/ionization zircon ages with conventional U-Pb results: Examples from the Precambrian of Brazil. *J. South Am. Earth Sci.*, **11**: 351-363.
- GIBBS, A.K. 1980. *Geology of the Barama-Mazaruni Supergroup of Guyana*. 375p. Harvard University, Cambridge. (Ph.D. Thesis).
- GIBBS, A.K. & OLSZEWSKI, W.J. 1982. Zircon U-Pb ages of Guyana greenstone-gneiss terrane. *Precambrian Res.*, **17**: 199-214.
- GIBBS, A.K.; WIRTH, K.R.; HIRATA, W.K.; OLZEWSKI, W.J. 1986. Age and composition of the Grão Pará Group volcanics, Serra dos Carajás. *Rev. Bras. Geoc.*, **16**: 201-211.

- 
- GRUAU, G.; MARTIN, H.; LEVEQUE, B.; CAPDEVILLA, R. 1985. Rb-Sr and Sm-Nd geochronology of Lower Proterozoic granite-greenstone terrains in French Guyane, South America. *Precambrian Res.*, **30**: 63-80.
- HAMILTON, P.J.; O'NIONS, R.K.; EVENSEN, N.M. 1977. Sm-Nd dating of Archean basic and ultrabasic volcanics. *Earth Planet. Sci. Lett.*, **36**: 263-268.
- HAMILTON, W.B. 1990. On terrane analysis. *Phil. Trans. R. Soc. London*, **A331**: 511-522.
- HARLEY, S.L. 1989. The origin of granulites: a metamorphic perspective. *Geol. Mag.*, **126** (3): 215-247.
- HARLEY, S.L. 1998. Ultrahigh temperature granulite metamorphism (1050°C, 12 Kbar) and decompression in garnet (Mg<sub>70</sub>)-orthopyroxene-sillimanite gneisses from Rauer Group, East Antarctica. *J. Metamorph. Geol.*, **16**:541-562.
- HARRISON, T.M. 1981. Diffusion of <sup>40</sup>Ar in biotite. *Contr. Mineral. Petrol.*, **78**: 324-331.
- HARRISON, T.M. & MacDOUGALL, I. 1981. Excess <sup>40</sup>Ar in metamorphic rocks from Broken Hill, New South Wales: implications for <sup>40</sup>Ar/<sup>39</sup>Ar age spectra and the thermal history of the region. *Earth Planet. Sci. Lett.*, **55**: 123-149.
- HARRISON, T.M.; DUCAN, I.; MacDOUGALL, I. 1985. Diffusion of <sup>40</sup>Ar in biotite: temperature, pressure and compositional effects. *Geochim. Cosmochim. Acta*, **49**: 2461-2468.
- HASUI, Y. & ALMEIDA, F.F.M. 1985. The Brazil Central Shield reviewed. *Episodes*, **8**(1): 29-37.
- HASUI, Y.; HARALY, N.L.E.; SCHOBENHAUS, C. 1984. Elementos geofísicos e geológicos da região amazônica: subsídios para o modelo geotectônico. In: SIMPÓSIO DE GEOLOGIA DA AMAZÔNIA, 2, Manaus. *Anais*, SBG-NO, p.129-148.
- HAWKINS, D.P. & BOWRING, S.A. 1999. U-Pb monazite, xenotime and titanite geochronological constraints on the prograde to post-peak metamorphic thermal history of Paleoproterozoic migmatites from the Grand Canyon, Arizona. *Contr. Mineral. Petrol.*, **134**: 150-169.
- HOWELL, D.G. 1995. *Principles of terrane analysis. New application for global tectonics*. 2ed. London. Chapman & Hall, 245p.
- JOÃO, X.S.J. & MARINHO, P.A.C. 1982. Catametamorfitos arqueanos da região centro-leste do Território Federal do Amapá. In: SIMPÓSIO DE GEOLOGIA DA AMAZÔNIA, 1, Belém. *Anais*, SBG-NO, v.2, p. 207-228.

- 
- JOÃO, X. S.J.; CARVALHO, J.M.A.; VALE, A.G.; FRIZZO, S.J.; MARTINS, R.C. 1979. *Projeto Rio Falsino*. Belém, DNPM-CPRM. v.1-A, 199 p. (Relatório Final).
- JOÃO, X.S.J.; FRIZZO, S.J.; MARINHO, P.A.C.; CARVALHO, J.M.A.; NETO, C.S.S.; SOUZA, A.N.; GUIMARÃES, L.R. 1978. *Geologia da região sudoeste do Amapá e norte do Pará: Projeto Sudoeste do Amapá*. DNPM/CPRM. 125p. (Série Geol. 10).
- JOLIVET, L.; GOFFÉ, B.; MONIÉ, P.; TRUFFERT-LUXEY, C.; PATRIAT, M.; BONNEAU, M. 1996. Miocene detachment in Crete and exhumation P-T-t paths of high-pressure metamorphic rocks. *Tectonics*, **15** (6): 1129-1153.
- JONES, D.L.; SILBERLING, N.J.; CONEY, P.J. 1986. Collision tectonics in the Cordillera of western N America: examples of Alaska. In: M.P. COWARD & A.C. RIES (eds) *Collision Tectonics*. Oxford, Geological Society, Special Publication, v.19, p. 367-387.
- JUNG, S. & MEZGER, K. 2001. Geochronology in migmatites – a Sm-Nd, U-Pb and Rb-Sr study from the Proterozoic Damara belt (Namibia): implications for polyphase development of migmatites in high-grade terranes. *J. Metamorph. Geol.*, **19**: 77-97.
- JUNG, S. & MEZGER, K. 2003. Petrology of basement dominated terranes: I. Regional metamorphic T-t path from U-Pb monazite and Sm-Nd garnet geochronology (Central Damara orogen, Namibia). *Chem. Geol.*, **198**: 223-247.
- KALSBECK, F. 2001. Geochemical comparison between Archean and Proterozoic orthogneisses from the Nagsugtoquidian orogen, West Greenland. *Precambrian Res.*, **105**:165-181.
- KARABINOS, P. & GROMET, L.P. 1993. Applications of single-grain zircon analysis to the detrital studies and age discrimination in igneous suites. *Geochim. Cosmochim. Acta*, **57**: 4257-4267.
- KELLEY, S.P. & TURNER, G. 1991. Laser probe  $^{40}\text{Ar}$ - $^{39}\text{Ar}$  measurements of loss profiles within individual hornblende grains from the Giant Rage Granite, northern Minnesota, USA. *Earth Planet. Sci. Lett.*, **107**: 634-648.
- KINGSBURY, J.A.; MILLER, C.F.; WOODEN, J.L.; HARRISON, M.T. 1993. Monazite paragenesis and U-Pb systematics in rocks of the eastern Mojave Desert, California, U.S.A.: implications for thermochronometry. *Chem. Geol.*, **110**: 147-167.
- KLEIN, E.L.; MOURA, C.A.; PINHEIRO, B.L.S. 2005. Paleoproterozoic crustal evolution of the São Luís Craton, Brazil: evidence from zircon geochronology and Sm-Nd isotopes. *Gondwana Research*, **8**: 1-10.
- KLEIN, E.L.; ROSA-COSTA, L.T.; LAFON, J.M. 2003. Magmatismo Paleoarqueano (3,32Ga) na região do Rio Cupixi, SE do Amapá, SE do Escudo das Guianas. In: SIMPOSIO DE

- 
- GEOLOGIA DA AMAZÔNIA, 8, Manaus. *Resumos Expandidos*, Manaus, SBG-NO. CD-ROM.
- KLÖTZLI, U.S. 1999. Th/U zonation in zircon derived from evaporation analysis: a model and its implications. *Chem. Geol.*, **58**: 325-333.
- KOBER, B., 1986. Whole-grain evaporation for  $^{207}\text{Pb}/^{206}\text{Pb}$ -age-investigations on single zircons using a double-filament thermal ion source. *Contr. Mineral. Petrol.*, **93**: 482-490.
- KOBER, B., 1987. Single zircon evaporation combined with  $\text{Pb}^+$  emitter-bedding for  $^{207}\text{Pb}/^{206}\text{Pb}$ -age investigations using thermal ion mass spectrometry, and implications to zirconology. *Contr. Mineral. Petrol.*, **96**: 63-71.
- KOBER, B.; PIDGEON, R.T.; LIPPOLT, H.J. 1989. Single-zircon dating by stepwise Pb-evaporation constrains the Archean history of detrital zircons from the Jack Hills, Western Australia. *Earth Planet. Sci. Lett.*, **91**: 286-296.
- KOUAMELAN, A.N.; DELOR, C.; PEUCAT, J.J. 1997. Geochronological evidence for reworking of Archean terrains during the Early Proterozoic (2.1 Ga) in the western Côte d'Ivoire (Man Rise – West African Craton). *Precambrian Res.*, **86**: 177-199.
- KRETZ, R. 1983. Symbols for rock-forming minerals. *Am. Mineral.*, **68**: 277-279.
- KRÖNER, A.; JAECKEL, P.; BRANDL, G.; NEMCHIN, A.A.; PIDGEON, R.T. 1999. Single zircon ages for granitoid gneisses in the Central Zone of the Limpopo Belt, Southern Africa and geodynamic significance. *Precambrian Res.*, **93**: 299-337.
- KRÖNER, A.; JAECKEL, P.; WILLIAMS, I.S. 1994. Pb-loss patterns in zircons from a high-grade metamorphic terrain as revealed by different dating methods: U-Pb and Pb-Pb ages for igneous and metamorphic zircons from northern Sri Lanka. *Precambrian Res.*, **66**: 151-186
- LAFON J.M.; DELOR, C.; THÉVENIAUT H.; KRYMSKY R.; TAVARES R.P.S.; ROIG J.Y. 2003. Isotopic deciphering of Rhyacian crustal evolution along the northern Oyapok river: new constraints from Sm-Nd, U-Pb and Pb-Pb geochronology. In: SIMPOSIO DE GEOLOGIA DA AMAZÔNIA, 8, Manaus. *Resumos Expandidos*, Manaus, SBG-NO. CD-ROM.
- LAFON, J.M.; ROSSI, P.; DELOR, C.; AVELAR, V.G.; FARACO, M.T.L. 1998. Novas testemunhas de relíquias arqueanas na crosta continental paleoproterozóica da Província Maroni-Itacaiúnas (Sudeste do Escudo das Guianas). In: CONGRESSO BRASILEIRO DE GEOLOGIA, 40, Belo Horizonte. *Anais*, SBG, p.64.
- LAFON, J.M.; ROSSI, P.; DELOR, C.; BARBOSA, O.S. 2001. Granulitos tardi-Transamazônicos (2,06 Ga) na região norte do Estado do Amapá: o charnoquito de

- 
- Calçoene. In: SIMPÓSIO DE GEOLOGIA DA AMAZÔNIA, 7, Belém. *Resumos Expandidos*, SBG-NO. CD ROM.
- LAFRANCE, J.; BARDOUX, M.; VOICU, G.; STEVENSON, R.; MACHADO, N. 1999. Geological and metallogenic environments of gold deposits of the Guiana Shield: a comparative study between St. Élie (French Guiana) and Omai (Guyana). *Exploration Mining Geol.*, **8** (1-2): 117-135.
- LAITI, A. & GEBAUER, D. 1999. Constraining the prograde and retrograde P-T-t path of Eocene HP rocks by SHRIMP dating different zircon domains: inferred rates of heating, burial, cooling and exhumation for central Rhodope, northern Greece. *Contr. Mineral. Petrol.*, **135**: 340-354.
- LAMEYRE, J. & BOWDEN, P. 1982. Plutonic rock types series: discrimination of various granitoid series and related rocks. *J. Vulcanol. Geoth. Res.*, **14**: 169-186.
- LANPHERE, M.A. & DALRYMPLE, G.B. 1976. Identification of excess  $^{40}\text{Ar}$  by the  $^{40}\text{Ar}/^{39}\text{Ar}$  age spectrum technique. *Earth Planet. Sci. Lett.*, **32**: 141-148.
- LE MAITRE, R.W.; BATEMMAN, P.; DUDEX, A.; KELLER, J.; LAMEYRE, J.; LE BASSABINE, P.A.; SCHMID, R.; SERENSEN, H.; STRECKEISEN, A.; WOOLWY, R.A.; ZANNETIN, B. 1989. *Recommendation of the IUGS, Subcomission of the Systematics of Igneous Rocks*. Oxford, Black Well Scientific Publications, 193p.
- LEDRU, P.; CALVEZ, J.Y.; MERCIER, D.; MAGNIEN, A. 1990. *Les conglomérats aurifères de Guyane Française: Dones géologiques complémentaires et géochronologie*. Note technique BRGM, 90, CSG. 7, 7p.
- LEDRU, P.; JOHAN, V.; MILÉSI, J.P.; TEGYEY, M. 1994. Markers of the last stages of the Paleoproterozoic collision: evidence for a 2,0 Ga continent involving circum-South Atlantic provinces. *Precambrian Res.*, **69**: 169-191.
- LEE, J.K.W.; ONSTOTT, T.C.; CASHMAN, K.V.; CUMBEST, R.J.; JOHNSON, D. 1991. Incremental heating of hornblende in vacuo: implications for  $^{40}\text{Ar}/^{39}\text{Ar}$  geochronology and the interpretation of thermal histories. *Geology*, **19**: 872-876.
- LEE, J.K.W.; WILLIAMS, I.S.; ELLIS, D.J. 1997. Pb, U and Th diffusion in natural zircon. *Nature*, **390**: 159-162.
- LIMA, M.I.C.; MONTALVÃO, R.M.G.; ISSLER, R.S.; OLIVEIRA, A.S.; BASEI, M.A.S.; ARAÚJO, J.F.V.; SILVA, G.G. 1974. Geologia. In: *Brasil Projeto RADAM. Folha NA/NB 22 Macapá*. Rio de Janeiro, I/120p. (Levantamentos de Recursos Naturais, 6).

- 
- LIMA, M.I.C.; OLIVEIRA, E.P.; TASSINARI, C.C.G. 1982. Cinturões granulíticos da porção setentrional do Craton Amazônico. In: SIMPÓSIO DE GEOLOGIA DA AMAZÔNIA, 1, Belém. *Anais*, SBG-NO, v.1, p. 147-162.
- LUDWIG, K.R., 2004. *User's manual for ISOPLOT/EX: a geochronological toolkit for Microsoft Excel (version 3.1)*. Berkeley Geochronology Center. Special Publication, 4, 71p.
- LUGMAIR, G.W. 1974. Sm-Nd ages: a new dating method. *Meteoritics*, **9**: 369.
- MACAMBIRA, M.J.B. & LAFON, J.M. 1995. Geocronologia da Província Mineral de Carajás: Síntese dos dados e novos desafios. *Bol. Museu Paraense Emílio Goeldi, Série Ciências da Terra*, **7**: 263-288.
- MACAMBIRA, M.J.B.; BARROS, C.E.M.; SILVA, D.C.C.; SANTOS, M.C.C. 2001 . Novos dados geológicos e geocronológicos para a região ao norte da Província de Carajás; evidências para o estabelecimento do limite Arqueano-Paleoproterozóico no sudeste do Cráton Amazônico. In: SIMPÓSIO DE GEOLOGIA DA AMAZÔNIA, 7, Belém, 2001. *Resumos Expandidos*, SBG-NO. CD-ROM.
- MACAMBIRA, M.J.B.; SILVA, D.C.; BARROS, C.E.M.; SCHELLER, T. 2003. New isotope evidences confirming the existence of a Paleoproterozoic terrain in the region at north of the Carajás Mineral Province. In: SOUTH AMERICAN SYMPOSIUM ON ISOTOPE GEOLOGY, 4, Salvador, 2003. *Short Papers*, p. 205-208.
- MACAMBIRA, M.J.B.; SILVA, D.C.; VASQUEZ, M.L.; BARROS, C.E.M. 2004. Investigação do limite Arqueano-Paleoproterozóico ao norte da Província de Carajás, Amazônia Oriental. In: CONGRESSO BRASILEIRO DE GEOLOGIA, 42, Araxá. *Resumos*, SBG. CD-ROM.
- MacDOUGALL, I. & HARRISON, T.M. 1988. *Geochronology and thermochronology by the  $^{40}\text{Ar}/^{39}\text{Ar}$  method*. Oxford, Clarendon Press. 212 p.
- MACHADO, N.; LYNDENMAYER, Z.; KROGH, T.E.; LINDENMAYER, D. 1991. U-Pb geochronology of Archean magmatism and basement reactivation in the Carajás area, Amazonian shield, Brazil. *Precambrian Res.*, **49**: 329-354.
- MACHADO FILHO, L.; RIBEIRO, M.W; MOREIRA, M.L.O.; TRINDADE, C.A.H.; HUCK, L. 1986 . *Projeto Iratapuru (Área Iratapuru) - Geologia Regional*. Goiânia, GEBAM/RADAM. 64 p.
- McREATH, I. & FARACO, M.T.L. 1997. Sm/Nd and Rb/Sr systems in part of the Vila Nova metamorphic suite, northern Brazil. In: SOUTH AMERICAN SYMPOSIUM ON ISOTOPE GEOLOGY, 1, Campos do Jordão, 1997. *Extended Abstracts*, p.194-196.

- 
- MEHNERT, K.R. 1968. *Migmatites and the origin of granitic rocks*. Amsterdam, Elsevier Publishing Company. 393p.
- MELO, A.F.F. & ARAÚJO, O.J.B. 1982. *Projeto Cuiapocu*. Belém, GEBAM/CPRM, v.1, 93p. (Relatório Final).
- MERRIHUE, C.M. 1965. Trace-element determinations and potassium-argon dating by mass spectroscopy of neutron-irradiated samples. *Trans. Amer. Geophys. Union*, **46**: 125.
- MERRIHUE, C.M & TURNER, G. 1966. Potassium-argon dating by activation with fast neutrons. *J. Geophys. Res.*, **71**: 2852-2857.
- MILÉSI, J.P.; EGAL, E.; LEDRU, P.; VERNHET, Y.; THIÉBLEMONT, D.; COCHERIE, A.; TEYGEY, M.; MARTEL-SANTIN, B.; LAGNY, P. 1995. Les minéralizations du Nord de la Guyane française dans leur cadre géologique. *Chronique de la Recherche Minière*, 518: 5-58.
- MILORD, I.; SAWYER, E.W.; BROWN, M. 2000. Formation of diatexite migmatites and granites magma during anatexis of semi-pelitic metasedimentary rocks: an example from St. Malo, France. *J. Petrol.*, **42**: 487-505.
- MITCHELL, J.G. 1968. The  $^{40}\text{Ar}$ - $^{39}\text{Ar}$  method for potassium-argon age determination. *Geochim. Cosmochim. Acta*, **32**: 781-790.
- MOLLER, A.; MEZGER, K.; SCHENK, V. 2000. U-Pb dating of metamorphic minerals: Pan-African metamorphism and prolonged slow cooling of high pressure granulites in Tanzania, East Africa. *Precambrian Res.*, **104**: 123-146.
- MONIÉ, P. 1984. Etude par la methode  $^{39}\text{Ar}$ - $^{40}\text{Ar}$  de la redistribution de l'argon dans les minéraux des socles anciens repris par l'orogenese Alpine. Application a la geochronologie des massifs de l'Argentera-Mecantour, du Mont-Rose et de la Grande Kabylie. Université de Montpellier II, Montpellier. (Tese de Doutorado).
- MONIÉ, P.; CABY, R.; ARTHAUD, M.H. 1997. The Neoproterozoic Brasiliano orogeny in northeast Brazil:  $^{40}\text{Ar}/^{39}\text{Ar}$  and petrostructural data from Ceará. *Precambrian Res.*, **81**: 241-264.
- MONIÉ, P.; TORRES-ROLDÁN, R.L.; GARCÍA-CASCO, A. 1994. Cooling and exhumation of the Western Betic Cordilleras,  $^{40}\text{Ar}/^{39}\text{Ar}$  thermochronological constraints on a collapsed terrane. *Tectonophysics*, **238**: 353-379.
- MONTALVÃO, R.M.G. & TASSINARI, C.C.G. 1984. Geocronologia pré-cambriana do Território Federal do Amapá (Brasil). In: SIMPÓSIO DE GEOLOGIA DA AMAZÔNIA, 2, Manaus, 1984. *Anais*, SBG, p.54-57.

- 
- MONTEL, J.M.; FORET, S.; VESCHAMBRE, M.; NICOLLET, C.; PROVOST, A. 1996. Electron microprobe dating of monazite. *Chem. Geol.*, **131**: 37-53.
- MONTGOMERY, C.W. 1979. Uranium-lead geochronology of the Archean Imataca Series, Venezuelan Guyana Shield. *Contr. Mineral. Petrol.*, **69**: 167-176
- MONTGOMERY, C.W. & HURLEY, P.M. 1978. Total rock U-Pb and Rb-Sr systematics in the Imataca Series, Guyana Shield, Venezuela. *Earth Planet. Sci. Lett.*, **39**: 281-290.
- MORILLON, A.C.; FÉRAUD, G.; SOSSON, M.; RUFFET, G.; CREVOLA, G.; LEROUGE, G. 2000. Diachronous cooling on both sides of a major strike-slip fault in the Variscan Maures Massif (south-east France), as deduced from a detailed  $^{40}\text{Ar}/^{39}\text{Ar}$  study. *Tectonophysics*, **31**: 103-126.
- MOURA, C.A.V. 1992. Geochronology and geochemistry of the basement orthogneisses of the Araguaia Belt, Brazil. 236p. University of New Hampshire. (Ph.D. Thesis)
- NEVES, S.P.; VAUCHEZ, A.; FÉRAUD, G. 2000. Tectono-thermal evolution, magma emplacement, and shear zone development in the Caruaru area (Borborema Province, NE Brazil). *Precambrian Res.*, **99**: 1-32.
- NEWTON, R.C., 1992. An overview of charnockite. *Precambrian Res.*, **55**: 399-405.
- NOGUEIRA, S.A.A.; BETTENCOURT, J.S.; TASSINARI, C.C.G. 2000. Geochronology of the Salamangone gold deposit host-rocks, Lourenço district, Amapá, Brazil. *Rev. Bras. Geoc.*, **30**(2): 261-264.
- NOMADE, S.; CHEN, Y.; FÉRAUD, G.; POUCKET, A.; THÉVENIAUT, H. 2001. First paleomagnetic and  $^{40}\text{Ar}/^{39}\text{Ar}$  study of Paleoproterozoic rocks from the French Guyana (Camopi and Oyapok rivers), northeastern Guyana Shield. *Precambrian Res.*, **109**: 239-256.
- NOMADE, S.; FÉRAUD, G.; CHEN, Y.; POUCKET, A. 2002. Thermal and tectonic evolution of the Paleoproterozoic Transamazonian orogen as deduced from  $^{40}\text{Ar}/^{39}\text{Ar}$  and AMS along the Oyapok river (French Guyana). *Precambrian Res.*, **114**: 35-53.
- NORCROSS, C.E.; DAVIS, D.W.; SPOONER, E.T.C.; RUST, A. 2000. U-Pb and Pb-Pb age constraints on Paleoproterozoic magmatism, deformation and gold mineralization in the Omai area, Guyana Shield. *Precambrian Res.*, **102**: 69-86.
- O'BRIEN, P.J. & ROTZLER, J. 2003. High-pressure granulites: formation, recovery of peak conditions and implications for tectonics. *J. Metamorph. Geol.*, **21**: 3-20.
- OLIVEIRA, E.C.; LAFON, J.M.; GIOIA, S.M.L.; PIMENTEL, M.M. 2002. Implantação do método Sm-Nd para minerais metamórficos e sua aplicação em rochas da região central do

- 
- Amapá, Sudeste do Escudo das Guianas. In: CONGRESSO BRASILEIRO DE GEOLOGIA, 41, João Pessoa, 2002. *Anais*, SBG-NE, p.502.
- OLSEWSKI, W.J.; GAUDETTE, H.E.; SANTOS, J.O. 1989. Isotopic age results from the shield areas of western Brazil. *GSA. Abstracts with Programs*, v.20, p. 76.
- ONSTOTT, T.C. & HARGRAVES, R.B. 1981. Proterozoic transcurrent tectonics: paleomagnetic evidence from Venezuela and Africa. *Nature*, **289**: 131-136.
- ONSTOTT, T.C. & YORK, D. 1989.  $^{40}\text{Ar}/^{39}\text{Ar}$  thermochronometry of the Imataca Complex, Venezuela. *Precambrian Res.*, **42**: 255-291.
- ONSTOTT, T.C.; HALL, C.M.; YORK, D. 1989.  $^{40}\text{Ar}/^{39}\text{Ar}$  thermochronometry on the Imataca Complex, Venezuela. *Precambrian Res.*, **42**: 255-291.
- ONSTOTT, T.C.; HARGRAVES, R.B.; YORK, D.; HALL, C.M. 1984. Constraints on the motions of South American and African Shields during the Proterozoic, I.  $^{40}\text{Ar}/^{39}\text{Ar}$  and paleomagnetic correlations between Venezuela and Liberia. *Geol. Soc. Am. Bull.*, **95**: 1045-1054.
- OUZEGANE, K & BOUZAMA, S. 1996. An example of ultra-high temperature metamorphism: orthopyroxene-sillimanite-garnet, sapphirine-quartz and spinel-quartz parageneses in Al-Mg granulites from In Hahaou, In Ouzzal, Hoggar. *J. Metamorph. Geol.*, **14**: 693-708.
- PAQUETTE, J.L.; NÉDELÉC, A.; MOINE, B. ; RAKOTONDRAZAFY, M. 1994. U-Pb, single zircon Pb-evaporation, and Sm-Nd isotopic study of a granulite domain in SE Madagascar. *J. Petrol.*, **102**: 523-538
- PARRISH, R.R. 1990. U-Pb dating of monazite and its application to geological problems. *Can. J. Earth Sci.*, **27**: 1435-1450.
- PASSCHIER, C.W. & TROUW, R.A.J. 1996. *Micro-tectonics*. Berlim, Springer-Verlag. 289p.
- PECAUT, J-J.; CAPDEVILA, R.; DRARENI, A.; MAHDJOUR, Y.; KAHOUI, M. 2005. The Eglab massif in the West African Craton (Algeria), an original segment of the Eburnean orogenic belt: petrology, geochemistry and geochronology. *Precambrian Res.*, **136**: 309-352.
- PIMENTEL, M.M.; FERREIRA FILHO, C.F.; SPIER, C.A. 2002. Estudo Sm-Nd do Complexo Máfico-Ultramáfico Bacuri, Amapá: idade da intrusão, metamorfismo e natureza do magma original. *Rev. Bras. Geoc.*, **32**: 371-376.
- PIMENTEL, M.M.; LINDENMAYER, ZG.; LAUX, J.H.; ARMSTRONG, R.; ARAÚJO, J.C. 2003. Geochronology and Nd isotope geochemistry of the Gameleira Cu-Au deposit, Serra

- 
- dos Carajás, Brazil: 1.8 – 1.7 hydrothermal alteration and mineralization. *J. Am. Earth Sci.*, **15**: 803-813.
- POITRASSON, F.; CHENERY, S.; BLAND, D.J. 1996. Contrasted monazite alteration and mechanisms and their geochemical implications. *Earth Planet. Sci. Lett.*, **145**: 79-96.
- POMMIER, A.; COCHERIE, A.; LEGENDRE, O. 2002. *EPMA Dating User's manual: Age calculation from electron probe microanalyser measurements of U-Th-Pb*. BRGM, 9 p.
- PRIEM, H.N.A.; BOELRIJK, N.A.I.M.; HEBEDA, E.H.; KROONEMBERG, S.B.; VERDURMEN, E.A.T.; VERSCHURE, R.H. 1977. Isotopic ages in the high grade metamorphic Coeroeni Group, southwestern Suriname. *Geol. Mijnbouw.*, **56**: 155-160
- PRIEM, H.N.A.; ROEVER, E.W.F.; BOSMA, W. 1980. A note on the age of the Paramacá metavolcanic in northwestern Suriname. *Geol. Mijnbouw*, **59**(2): 171-173.
- PURDY, J.W. & JAGER, E. 1976. *K-Ar ages on rock-forming minerals from central Alps*. University of Padova. Report of the Institute of Geology and Mineralogy, 30, p. 1-31.
- RAITH, M.; KARMAKAR, S.; BROWN, M. 1997. Ultra-high temperature metamorphism and multistage decompressional evolution of sapphirine granulites from the Palni Hill Ranges, southern India. *J. Metamorph. Geol.*, **15**: 379-399.
- RAMÕ, O.T.; DALL'AGNOL, R.; MACAMIRA, M.J.B.; LEITE, A.A.S.; OLIVEIRA, D.C. 2002. 1.88 Ga oxidized A-type granites of the Rio Maria region, eastern Amazonian Craton, Brazil: positively anorogenic! *J. Geol.*, **110**: 603-610.
- RICCI, P.S.F.; CARVALHO, J.M.A.; ROSA-COSTA, L.T.; KLEIN, E.L.; VASQUEZ, M.L.; VALE, A.G.; MACAMBIRA, E.M.B.; ARAÚJO, O.J.B. 2001. Geologia e recursos minerais do Projeto RENCA – Fase I. Belém, CPRM - Serviço Geológico do Brasil. p.
- RICCI, P.S.F.; CARVALHO, J.M.A.; ROSA-COSTA, L.T.; LAFON, J.M. 2002. Plúton charnoenderbítico arqueano intrusivo nos ortognaisses granulíticos do Cinturão Jari – Terreno Arqueano expressivo do sudeste do Escudo das Guianas. In: CONGRESSO BRASILEIRO DE GEOLOGIA, 41, João Pessoa. *Anais*, SBG-NE, p.524.
- RICCI, P.S.F.; CARVALHO, J.M.A.; ROSA-COSTA, L.T.; VASQUEZ, M.L.; LAFON, J.M. 2003. Review of some previously established high-grade terranes in southeastern Guyana Shield (Brazil) – unusually long history belts, domiform charnockitoid nuclei and isolated massifs. In SIMPOSIO DE GEOLOGIA DA AMAZÔNIA, 8, Manaus. *Resumos Expandidos*, SBG-NO. CD-ROM.
- RIDLEY, J., 1992. On the origins and tectonic significance of the charnockite suite of the Archean Limpopo Belt, Northern Marginal Zone, Zimbabwe. *Precambrian Res.*, **55**: 407-427.

- ROBERT, M. & FINGER, F. 1997. Do U-Pb zircon ages from granulites reflect peak metamorphic conditions? *Geology*, **25**: 319-322.
- ROBERTSON, S. 1999. *BGS rock classification scheme. Classification of metamorphic rocks*. British Geological Survey Research, Report RR 99-02, 24p.
- RODDICK, J. C.; CLIFF, R. A.; REX, D.C. 1980. The evolution of excess argon in alpine biotites. *Earth Planet. Sci. Lett.*, **48**: 185-208.
- ROEVER, E.W.F.; KIEFT, C.; MURRAY, E.E.; KLEIN, E.; DUCKER, W.H. 1976. Surinamite, a new Mg-Al silicate from the Bakhuis Mountains, W Suriname. *Am. Mineral.*, **61**: 193-199.
- ROEVER, E.W.F.; LAFON, J.M.; DELOR, C.; COCHERIE, A.; ROSSI, P.; GUERROT, C.; POTREL, A. 2003. The Bakhuis ultrahigh-temperature granulite belt (Suriname): I. petrological and geochronological evidence for a counterclockwise P-T path at 2.07-2.05 Ga. *Géologie de la France*, **2-3-4**: 175-206.
- ROSA-COSTA, L.T.; LAFON, J.M.; COCHERIE, A.; DELOR, C. Electron microprobe U-Th-Pb monazite dating of the Transamazonian high-grade metamorphic overprint on Archean rocks from Amapá Block, southeastern Guiana Shield, northern Brazil. (submetido ao *Journal of South America Earth Science*).
- ROSA-COSTA, L.T.; LAFON, J.M.; DELOR, C. 2006. Zircon geochronology and Sm-Nd isotopic study: further constraints for the Archean and Paleoproterozoic geodynamic evolution of the southeastern Guiana Shield, north of Brazil. *Gondwana Res.* (no prelo).
- ROSA-COSTA, L.T.; MACAMBIRA, E.M.B.; VASQUEZ, M.L.; LAFON, J.M.; RICCI, P.S.F. 2002a. Idades de rochas metavulcânicas félsicas do sudeste do Escudo das Guianas. In: SIMPÓSIO SOBRE VULCANISMO E AMBIENTES ASSOCIADOS, 2, Belém. *Boletim de Resumos e Roteiro de Excursão*, p. 46.
- ROSA-COSTA, L.T.; RICCI, P.S.F.; LAFON, J.M.; VASQUEZ, M.L.; CARVALHO, J.M.A.; KLEIN, E.L.; MACAMBIRA, E.M.B. 2003. Geology and geochronology of archean and paleoproterozoic domains of the southeastern Amapá and northwestern Pará, Brazil – southeastern Guyana Shield. *Géologie de la France*, **2-3-4**:101-120.
- ROSA-COSTA, L.T.; VALE, A.G.; SILVA, A.M. 2002b. Interpretação integrada de dados aerogeofísicos e imagens de sensores remotos como ferramenta para o mapeamento geológico na Região Amazônica: o exemplo do Projeto Promin-RENCA. In: KLEIN E.L.; VASQUEZ M.L.; ROSA-COSTA L.T. (eds.) *Contribuições à Geologia da Amazônia*. Belém, SBG-NO, v. 3, p. 227-243
- ROSA-COSTA, L.T.; VASQUEZ, M.L.; CARVALHO, J.M.A.; RICCI, P.S.F.; LAFON, J.M. 2001. Geocronologia preliminar do Arqueano e Paleoproterozóico do NW do Pará/SW do

- 
- Amapá – Escudo das Guianas. In: SIMPÓSIO DE GEOLOGIA DA AMAZÔNIA, 7, Belém. *Resumos Expandidos*, SBG-NO. CD ROM.
- RUFFET, G.; FÉRAUD, G.; AMOURIC, M. 1991. Comparison of  $^{40}\text{Ar}$ - $^{39}\text{Ar}$  conventional and laser dating of biotites from North Trégor Batholith. *Geochim. Cosmochim. Acta*, **55**: 1675-1688.
- SADOWSKI, G.R. & BETTENCOURT, J.S. 1996. Mesoproterozoic tectonic correlations between eastern Laurentia and the western border of the Amazon Craton. *Precambrian Res.*, **76**: 213-227.
- SAMBRIDGE, M.S. & COMPSTON, W. 1994. Mixture modeling of multi-component data sets with application to ion-probe zircon ages. *Earth Planet. Sci. Lett.*, **128**: 373-390.
- SAMSON, S.D. & ALEXANDER, E.C. 1987. Calibration of the interlaboratory  $^{40}\text{Ar}$ - $^{39}\text{Ar}$  dating standard, MMhb-1. *Chem. Geol.*, **66** (1-2): 27-34.
- SANTOS, J.O.S. 2003. Geotectônica do Escudo das Guianas e Brasil-Central. In: BIZZI, L.A.; SCHOBENHAUS, C.; VIDOTTI, R.M.; GONÇALVES, J.H. (eds.) *Geologia, Tectônica e Recursos Minerais do Brasil*. Brasília, CPRM, p. 169-226.
- SANTOS, J.O.S.; HARTMANN, L.A.; GAUDETTE, H.E.; GROVES, D.I.; McNAUGHTON, N.J.; FLETCHER, I.R. 2000. A new understanding of the provinces of the Amazon Craton based on integration of field mapping and U-Pb and Sm-Nd geochronology. *Gondwana Res.*, **3**(4): 453-488.
- SANTOS, M.V.; TASSINARI, C.C.G.; SOUZA FILHO, E.E.; TEIXEIRA, W.; RIBEIRO, A.C.O.; PAYOLLA, B.; VASCONI, A. 1988. Litoestratigrafia das rochas precambrianas na Bacia do Médio Rio Xingu, Altamira, Pará. In: SBG, Congresso Latino-Americano de Geologia, 7. Belém. *Extended Abstracts*. 363-377.
- SANTOS, J.O.S.; VAN BREEMEN, O.B.; GROVES, D.I.; HARTMANN, L.A.; ALMEIDA, M.E.; McNAUGHTON, N.J.; FLETCHER, I.R. 2004. Timing and evolution of multiple Paleoproterozoic magmatic arcs in the Tapajós Domain, Amazon Craton: constraints from SHRIMP and TIMS zircon, baddeleyite and titanite U-Pb geochronology. *Precambrian Res.*, **131**: 73-109.
- SATO, K. & TASSINARI, C.C.G. 1997. Principais eventos de acreção continental no Cráton Amazônico baseados em idade-modelo Sm-Nd, calculada em evoluções de estágio único e estágio duplo. In: COSTA, M.L.C. & ANGÉLICA, R.S. (coords.) *Contribuição à Geologia da Amazônia*. Belém, SBG-NO, p. 91-142.
- SAWYER, E. W. 1998. Formation and evolution of granite magmas during crustal reworking, the significance of diatexis. *J. Petrol.*, **39**: 1147-1167.

- SCHMITZ M. D. & BOWRING S. A. 2001. U-Pb zircon and titanite systematics of the Fish Canyon Tuff: an assessment of high-precision U-Pb geochronology and its application to young volcanic rocks. *Geochim. Cosmochim. Acta*, **65** (15): 2571-2587
- SCHMITZ M. D.; BOWRING S. A.; LUDWIG K. R.; RENNE P. R. 2003. Precise K-Ar, <sup>40</sup>Ar-<sup>39</sup>Ar, Rb-Sr and U-Pb mineral ages from the 27.5 Ma Fish Canyon Tuff reference standard. *Chem. Geol.*, **199** (3-4): 277-280.
- SCHOBENHAUS, C. & BRITO NEVES, B.B. 2003. A geologia do Brasil no contexto da Plataforma Sul-Americana. In: BIZZI, L.L.; SCHOBENHAUS, C.; VIDOTT, R.M.; GONÇALVES, J.H. (eds.) *Geologia, tectônica e Recursos Minerais do Brasil*. Brasília, CPRM. 674 p.
- SHACKLETON, R.M. 1986. Precambrian collision tectonics in Africa. In: M.P. COWARD & A.C. RIES (eds.) *Collision Tectonic*. Oxford, Geological Society Special Publication, v.19, p. 329-349.
- SOLAR, G.S. & BROWN, M. 2001. Petrogenesis of migmatites in Maine, USA: possible source of peraluminous leucogranite in plutons. *J. Petrol.*, **42**: 789-823.
- SOUZA, S.R.B.; MACAMBIRA, M.J.B.; HORBE, M.A. 1995. Geochronological and isotopic evidences of the influence of the Paleoproterozoic Pojuca Granite on the Cu-Zn (Au-Mo-Ag) deposit, Carajás province, Brazil. In: SYMPOSIUM RAPAKIVI GRANITES AND RELATED ROCKS, Belém. *Abstracts*, p.76.
- SOUZA, Z.S.; POTREL, A.; LAFON, J.M.; ALTHOFF, F.J.; PIMENTEL, M.M.; DALL'AGNOL, R.; OLIVEIRA, C.G. 2001. Nd, Pb and Sr isotopes in the Identidade Belt, an Archean greenstone belt of Rio Maria region (Carajás Province, Brazil): implications for the geodynamic evolution of the Amazonian Craton. *Precambrian Res.*, **109**: 293-315.
- SPEAR, F. 1995. *Metamorphic phase equilibria and pressure-temperature-time paths*. Washington D.C., Mineralogical Society of America. 799p.
- SPEAR, F.S. & PARRISH, R.R. 1996. Petrology and petrological cooling rates of the Valhalla Complex, British Columbia. *Can. J. Petrol.*, **37**: 733-765.
- SPIER, C. A. 1999 . Petrologia e metalogênese dos depósitos de cromita associados ao Complexo Máfico-Ultramáfico Bacuri, AP. 1999. 41p. Universidade de Brasília, Instituto de Geociências, Brasília. (Dissertação de Mestrado).
- SPIER, C.A. & FERREIRA FILHO, C. F. 1999. Geologia, estratigrafia e depósitos minerais do Projeto Vila Nova, Escudo das Guianas, Amapá, Brasil. *Rer. Bras. Geoc.*, **29**:173-178.
- STACEY, J.S. & KRAMERS, J.D. 1975. Approximation of terrestrial lead isotopic evolution by a two stage model. *Earth Planet. Sci. Lett.*, **26**: 207-221.

- St-ONGE, M. R.; SCOTT, D. J.; WODICKA, N. 2001. Terrane boundaries within Trans-Hudson Orogen (Quebec-Baffin segment), Canada: changing structural and metamorphic character from foreland to hinterland. *Precambrian Res.*, **107**: 75-91.
- STRECKEISEN, A.L. 1976. To each plutonic rock its proper name. *Earth Sci. Rev.*, **12**:1-33.
- SUZUKI, K. & ADACHI, M. 1991. Precambrian provenance and Silurian metamorphism of the Tsubonosawa paragneiss in the South Kitakami terrane, Northeast Japan, revealed by the chemical Th-U-total Pb isochron ages of monazite, zircon and xenotime. *Geochem. J.*, **25**: 357-376.
- SUZUKI, K. & ADACHI, M. 1998. Denudation history of the high T/P Ryoke metamorphic belt, southwest Japan: constrains from CHIME monazite ages of gneisses and granitoids. *J. Metamorph. Geol.*, **16**: 23-37.
- SUZUKI, K.; ADACHI, M.; KAJIZUKA, I. 1994. Electron microprobe observations of Pb diffusion in metamorphosed detrital monazites. *Earth Planet. Sci. Lett.*, **128**: 391-405.
- SWAPP, S.M. & ONSTOTT, T.C. 1989. P-T-time characterization of Transamazonian orogeny in the Imataca Complex, Venezuela. *Precambrian Res.*, **42**: 293-314.
- TASSINARI, C.C.G. 1996. O mapa geocronológico do cráton amazônico no Brasil: revisão dos dados isotópicos. 139p. Universidade de São Paulo, Instituto de Geociências, São Paulo. (Tese de Livre-docência).
- TASSINARI, C.C.G. & MACAMBIRA, M.J.B. 1999. Geochronological provinces of the Amazonian Craton. *Episodes*, **22**(3): 174-182.
- TASSINARI, C.C.G. & MACAMBIRA, M.J.B. 2004. A evolução tectônica do Cráton Amazônico. In: MANTESSO-NETO, V.; BARTORELLI, A.; CARNEIRO, C.D.R.; BRITO NEVES, B.B. (eds.) *Geologia do Continente Sul-Americano: Evolução da Obra de Fernando Flávio Marques de Almeida*. São Paulo, p. 471-485.
- TASSINARI, C.C.G.; BETTENCOURT, J.S.; GERALDES, M.C.; MACAMBIRA, M.J.B.; LAFON, J.M. 2000. The Amazonian Craton. In: CORDANI, U.G.; MILANI, E.J.; FILHO, A.T.; CAMPOS, D.A. (eds.) *Tectonic Evolution of South America*. Rio de Janeiro, 31<sup>o</sup> International Geological Congress, SBG. p. 41-95.
- TASSINARI, C.C.G.; MUNHÁ, J.M.V.; TEIXEIRA, W.; PALÁCIOS, T.; NUTMAN, A.P.; SOUSA, C.S.; SANTOS, A.P.; CALADO, B.O. 2004. The Imataca Complex, NW Amazonian Craton, Venezuela: crustal evolution and integration of geochronological and petrological cooling histories. *Episodes*, **27** (1): 3-12.
- TASSINARI, C.C.G.; TEIXEIRA, W.; NUTMAN, A.P.; SZABÓ, G.A.; MONDIN, M.; SATO, K. 2001. Archean crustal evolution of the Imataca Complex, Amazonian Craton: Sm-Nd,

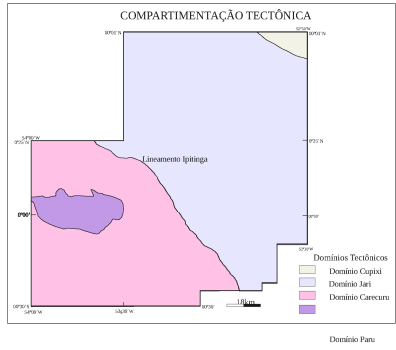
---

Rb-Sr e U-Pb (SHRIMP) evidences. In: SIMPÓSIO DE GEOLOGIA DA AMAZÔNIA, 7, Belém. *Resumos Expandidos*, SBG-NO. CD-ROM

- TAVARES, R.P.S.; LAFON, J.M.; DELOR, C.; THEVENIAUT, H.; KRYMSKY, R. 2003. Geocronologia Pb-Pb em monocristais de zircão e U-Pb em titanitas: evolução tardi-transamazônica da região de Oiapoque (fronteira Guiana Francesa – Norte do Amapá). In: CONGRESSO BRASILEIRO DE GEOQUÍMICA, 9, Belém. *Resumos Expandidos*, p. 746-748.
- TEIXEIRA, W.; OJIMA, S.K.; KAWASHITA, K. 1984. A evolução geocronológica de rochas metamórficas e ígneas da Faixa Móvel Maroni-Itacaiúnas, na Guiana Francesa. In: SYMPOSIUM AMAZÔNICO, 2, Manaus. *Actas*, p. 75-81.
- TEIXEIRA, W.; TASSINARI, C.C.G.; CORDANI, U.G.; KAWASHITA, K. 1989. A review of the geochronology of the Amazonian Craton: Tectonic implications. *Precambrian Res.*, **42**: 213-227.
- THÉVENIAUT, H.; DELOR, C.; LAFON, J.M.; MONIÉ, P.; ROSSI, P.; LAHONDÈRE, D. Paleoproterozoic (2155-2060 Ma) evolution of the Guiana Shield (Transamazonian event) in the light of new paleomagnetic data from French Guiana. Submetido a *Precambrian Research*).
- THIÉBLEMONT, D.; GOUJOU, J.C.; EGA, E.; COCHERIE, A.; DELOR, C.; LAFON, J.M.; FANNING, C.M. 2004. Archean evolution of the Leo Rise and its Eburnean reworking. *J. African Earth Sci.*, **39**: 97-104.
- THOMPSON, A.B. & ENGLAND, P.C. 1994. Pressure-temperature-time paths of regional metamorphism II. Their inference and interpretation using mineral assemblages in metamorphic rocks. *J. Petrol.*, **25**: 929-955.
- TICKYJ, H.; HARTMANN, L.A.; VASCONCELLOS, M.A.Z.; PHILIPP, R.Y.; REMUS, M.V.D. 2004. Electron microprobe dating of monazite substantiates ages of major geological events in the southern Brazilian shield. *J. South Am. Earth Sci.*, **16**: 699-713.
- TRENDALL, A.F.; BASEI, M.A.S.; LAETER, J.R.; NELSON, D.R. 1998. SHRIMP zircon U-Pb constraints on the age of the Carajás formation, Grão Pará group, Amazon Craton. *J. South Am. Earth Sci.*, **11**: 265-277.
- TUEFEL, S. & HEINRICH, W. 1997. Partial resetting of the U-Pb isotope system in monazite through hydrothermal experiments: a SEM and U-Pb study. *Chem. Geol.*, **137**: 273-281.
- VANDERHAEGHE, O.; LEDRU, P.; THIÉBLEMONT, D.; EGAL, E.; COCHERIE, A.; TEGYEY, M.; MILÉSI, J.J. 1998. Contrasting mechanism of crustal growth Geodynamic evolution of the Paleoproterozoic granite-greenstone belts of French Guyana. *Precambrian Res.*, **92**: 165-193.

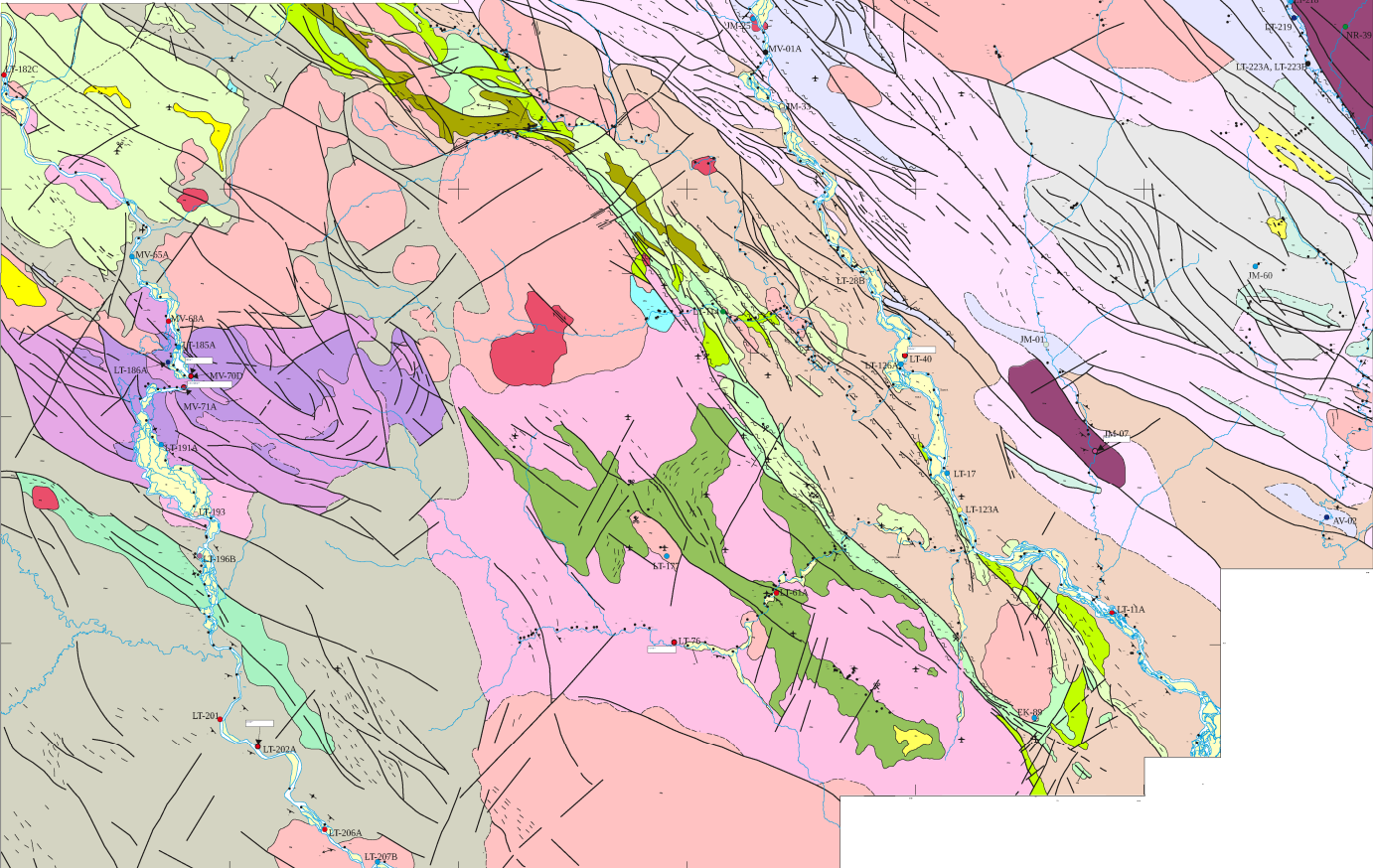
- VASQUEZ, M.L. & LAFON, J.M. 2001. Magmatismo tipo A de 1,75 Ga na porção oriental do Escudo das Guianas – Estados do Amapá e Pará, Brasil. In: SIMPÓSIO DE GEOLOGIA DA AMAZÔNIA, 7, Belém. *Resumos Expandidos*, SBG-NO. CD-ROM.
- VASQUEZ, M.L.; MACAMBIRA, M.J.B.; GALARZA, M.A. 2005. Granitóides Transamazônicos na região Iriri-Xingu, Pará – novos dados geológicos e geocronológicos. In: HORBE, M. C. & SOUSA, V.S. (eds.) *Contribuições à Geologia da Amazônia*. Manaus, SBG-NO, v.4, p. 16-31.
- VIGNOL, L.M. 1987. Etudes geochemiques des granulites du Brésil et de la zone d'Ivrea : les elements (K, Rb, Sr, Sm, Nd) et les isotopes radiogeniques (Sr, Nd). Université de Paris VII, Institute de Physique du Globe de Paris. (Diplome d'études approfondies de geochemie).
- VOICU, G.; BARDOUX, M.; STEVENSON, R. ; JÉBRAK, M. 2000. Nd and Sr isotope study of hydrothermal scheelite and host rocks at Omai, Guiana Shield: implications for ore fluid source and flow path during the formation of orogenic gold deposits. *Mineral. Dep.*, **35**: 302-314.
- WARTHÓ, J.A. 1995. Apparent argon diffusive loss  $^{40}\text{Ar}$ - $^{39}\text{Ar}$  age spectra in amphiboles. *Earth Planet. Sci. Lett.*, **134**: 393-407.
- WENDT, I. & CARL, C. 1991. The statistical distribution of the mean squared weighted deviation. *Chem. Geol.*, **86**: 275-285.
- WIRTH, K.R.; GIBBS, A.K.; OLSZEWSKI, W.J. 1986. U-Pb ages of zircons from the Grão Pará Group and Serra dos Carajás Granite, Pará, Brazil. *Rev. Bras. Geoc.*, **16**: 195-200.
- WIT, M. J; ROERING, C.; HART, R.J.; ARMSTRONG, A.R.; RONDE, C.E.J.; GREEN, R.W.E.; TREDoux, M.; PEBERDY, E.; HART, R.A. 1992. Formation of an archean continent. *Nature*, **357**: 553-562.
- YORK, D. 1969. Least-square fitting of a straight line with correlated errors. *Earth Planet. Sci. Lett.*, **5**: 320-324.
- ZHAO, G.; CAWOOD, P.A.; SIMON, A.W.; SUN, M. 2002. Review of global 2.1-1.8 Ga orogens: implications for a pre-Rodinia supercontinent. *Earth Sci. Rev.*, **59**: 125-162.
- ZHAO, G.; WILDE, S. A.; CAWOOD, P. A.; SUN, M. 2001. Archean blocks and their boundaries in the North China Craton: lithological, geochemical, structural and P-T path constraints and tectonic evolution. *Precambrian Res.*, **107**: 45-73.
- ZHU, X.K.; O'NIONS, R.K.; BELSHAW, N.S.; GIBB, A.J. 1997. Significance of in situ SIMS chronometry of zoned monazite from the Lewisian granulites, northwest Scotland. *Chem. Geol.*, **135**: 35-53.

N

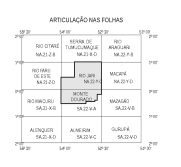


ANEXO I  
CARTA GEOLÓGICA

ERA	COBERTURAS SEDIMENTARES FANEROZÓICAS			
	DOMÍNIO PARU	DOMÍNIO CARECURU	DOMÍNIO JARI	DOMÍNIO CUIPIXI
P A L E O S O L I O	MAGMATISMO ANDRÓGENICO			
			Granito Walter (2,75 Ga)	
	MAGMATISMO OROGÊNICO			
			Suítas Intrusivas Pontais: granitos (trondhjemita e calcicamésio-basaltos)	
			Suítas Intrusivas Caracuru (2,14 Ga)	
			Suítas Intrusivas Caracuru (2,14 Ga): granitos com quartzos e xenólitos de granitos e granodioritos	
			Suítas Intrusivas Caracuru (2,14 Ga): granitos com quartzos e xenólitos de granitos e granodioritos	
			Suítas Intrusivas Caracuru (2,14 Ga): granitos com quartzos e xenólitos de granitos e granodioritos	
			Suítas Intrusivas Caracuru (2,14 Ga): granitos com quartzos e xenólitos de granitos e granodioritos	
			Suítas Intrusivas Caracuru (2,14 Ga): granitos com quartzos e xenólitos de granitos e granodioritos	
M E S O S O L O	ASSEMBLEIA DE EMBASAMENTO			
			Complexo PauAmará: Granitos e dioritos graníticos, trondhjemita e granodioritos, monzoníticos (2,18 Ga)	
			Complexo Araripe: Granitos e dioritos graníticos, trondhjemita e granodioritos, monzoníticos (2,18 Ga)	
			Complexo Araripe: Granitos e dioritos graníticos, trondhjemita e granodioritos, monzoníticos (2,18 Ga)	
			Complexo Araripe: Granitos e dioritos graníticos, trondhjemita e granodioritos, monzoníticos (2,18 Ga)	
			Complexo Araripe: Granitos e dioritos graníticos, trondhjemita e granodioritos, monzoníticos (2,18 Ga)	
			Complexo Araripe: Granitos e dioritos graníticos, trondhjemita e granodioritos, monzoníticos (2,18 Ga)	
			Complexo Araripe: Granitos e dioritos graníticos, trondhjemita e granodioritos, monzoníticos (2,18 Ga)	
			Complexo Araripe: Granitos e dioritos graníticos, trondhjemita e granodioritos, monzoníticos (2,18 Ga)	
			Complexo Araripe: Granitos e dioritos graníticos, trondhjemita e granodioritos, monzoníticos (2,18 Ga)	
NEO ARCAICO			Complexo Tucuruá: Granitos e dioritos graníticos, trondhjemita e granodioritos, monzoníticos com xenólitos em litas anfibolíticas (2,85 Ga)	



- Contato geológico
  - - - Contato aproximado
  - - - Contato sobre por ganho/empilhamento (carre de estereamento indicado)
  - - - Falha com cinemática indicada
  - ~ ~ ~ Linhaamento estrutural indeterminado
  - ~ ~ ~ Zona de cisalhamento transcorrente
  - ~ ~ ~ Zona de cisalhamento transcorrente distal
  - ~ ~ ~ Zona de cisalhamento transcorrente sinistral
  - ~ ~ ~ Zona de cisalhamento com reorientação oblíqua
  - ~ ~ ~ Zona de cisalhamento com reorientação oblíqua
  - ~ ~ ~ Anfibolite com carvão indicado
  - Triços de Falhação
  - + Falhação verticalizada
  - Falhação com mergulho nortado
  - Linhação de estiramento com carvão indicado
  - Linhação de estiramento com carvão nortado
  - Mina primária inativa
  - Campo primário ativo
  - Estação geológica
  - Rodovia: PO - 79 em projeto (Departamento de Estradas e Rodagem - DER RJ, 2007); Rodovia Costa do Sol (2007)
  - Pista de pouso
  - Drenagem
  - Limite de reserva indígena
  - Limite intermunicipal
- Amostras Libertadas e Meio Geocronológico Empregado**
- Sin-Nd em rocha total
  - Rb-Sr em zircão
  - U-Th-Pb em zircão
  - Ar-Ar em anfibolite
  - Ar-Ar em anfibolite
  - Ar-Ar em anfibolite e diorita
  - Sin-Nd em rocha total e Pb-Pb em zircão
  - Sin-Nd em rocha total e U-Th-Pb em zircão
  - Sin-Nd em rocha total, Ar-Ar em anfibolite e diorita
  - Sin-Nd em rocha total, Pb-Pb em zircão e Ar-Ar em rocha total
  - Sin-Nd em rocha total, Pb-Pb em zircão e Ar-Ar em anfibolite e diorita



Este mapa representa parte da área mapeada pelo Projeto PRECÁMBRIO-REINCA (CPRM 2001), cuja carta geológica e de salinidade de Cavalari et al. (2003) foram incorporados os resultados do estudo geocronológico realizado nesta tese.

ESCALA 1:250.000

PROJEÇÃO POLICÊNICA

Coordenadas: SAA de 140°

Coordenadas: SAA de 140°

Coordenadas: SAA de 140°

Coordenadas: SAA de 140°

2006

**ANEXO II - Valores de U, Th e Pb, razões e erros correspondentes obtidos por análises químicas de cristais monazita em microsonda eletrônica.**

REF	Idade Ma	Error Age Ma	U ppm	$\sigma$ %	Th ppm	$\sigma$ %	Pb ppm	$\sigma$ %	U/Pb	Error U/Pb %	Th/Pb	Error Th/Pb %	Corr.
<b>Gnaiss Enderbítico MV-27A</b>													
mv27al1g2t1	2169	158	560	26.79	34280	2.00	3700	4.05	0.15	27.09	9.26	4.52	0.13
mv27al1g2t2	2056	166	600	25.00	30750	2.00	3170	4.73	0.19	25.44	9.70	5.14	0.17
mv27al1g2t2	2156	192	630	23.81	25530	2.00	2820	5.32	0.22	24.40	9.05	5.68	0.20
mv27al1g2t2	2169	204	600	25.00	23590	2.00	2630	5.70	0.23	25.64	8.97	6.04	0.21
mv27al1g2t2	2089	168	500	30.00	30780	2.00	3190	4.70	0.16	30.37	9.65	5.11	0.14
mv27al1g2t2	2095	168	360	41.67	31630	2.00	3230	4.64	0.11	41.92	9.79	5.06	0.10
mv27al1g2t3	2068	93	340	44.12	92240	2.00	9030	2.00	0.04	44.16	10.21	2.83	0.03
mv27al2g4t1	2067	94	340	44.12	78490	2.00	7700	2.00	0.04	44.16	10.19	2.83	0.03
mv27al2g4t1	2123	97	260	57.69	79600	2.00	8000	2.00	0.03	57.73	9.95	2.83	0.02
mv27al2g4t1	2059	94	600	25.00	75430	2.00	7470	2.01	0.08	25.08	10.10	2.83	0.06
mv27al2g4t1	2143	97	800	18.75	77420	2.00	8070	2.00	0.10	18.86	9.59	2.83	0.07
mv27al2g4t1	2048	99	880	17.05	67400	2.00	6760	2.22	0.13	17.19	9.97	2.99	0.10
mv27al2g4t1	2161	98	820	18.29	73070	2.00	7710	2.00	0.11	18.40	9.48	2.83	0.08
mv27al2g4t1	2088	100	690	21.74	68430	2.00	6930	2.16	0.10	21.85	9.87	2.95	0.07
mv27al2g4t1	2114	100	440	34.09	70260	2.00	7110	2.11	0.06	34.16	9.88	2.91	0.04
mv27al2g4t1	2066	97	200	75.00	74190	2.00	7230	2.07	0.03	75.03	10.26	2.88	0.02
mv27al2g4t1	2116	85	0	100.00	83520	2.00	8260	2.00	0.00	100.0	10.11	2.83	0.01
mv27al1g4t2	2144	97	190	78.95	84920	2.00	8590	2.00	0.02	78.97	9.89	2.83	0.02
mv27al1g4t2	2076	94	400	37.50	81930	2.00	8090	2.00	0.05	37.55	10.13	2.83	0.04
mv27al1g4t2	2166	100	430	34.88	72030	2.00	7470	2.01	0.06	34.94	9.64	2.83	0.04
mv27al1g4t2	2107	99	1060	14.15	67860	2.00	7080	2.12	0.15	14.31	9.58	2.91	0.11
mv27al1g4t2	2114	101	400	37.50	69600	2.00	7030	2.13	0.06	37.56	9.90	2.92	0.04
mv27al1g4t2	2120	102	300	50.00	68580	2.00	6910	2.17	0.04	50.05	9.92	2.95	0.03
mv27al1g4t2	2110	103	510	29.41	66500	2.00	6750	2.22	0.08	29.50	9.85	2.99	0.06
mv27al1g4t2	2157	100	120	100.00	70360	2.00	7150	2.10	0.02	100.0	9.84	2.90	0.02
mv27al1g4t2	2172	113	510	29.41	58330	2.00	6130	2.45	0.08	29.51	9.52	3.16	0.06
mv27al1g4t2	2133	100	290	51.72	71870	2.00	7280	2.06	0.04	51.77	9.87	2.87	0.03
mv27al4g1t1	2093	96	260	57.69	78270	2.00	7750	2.00	0.03	57.73	10.10	2.83	0.02
mv27al4g1t1	2100	115	450	33.33	54930	2.00	5560	2.70	0.08	33.44	9.88	3.36	0.06
mv27al4g1t1	2178	137	420	35.71	43000	2.00	4550	3.30	0.09	35.87	9.45	3.86	0.08
mv27al4g1t1	2124	139	590	25.42	40630	2.00	4260	3.52	0.14	25.67	9.54	4.05	0.12
mv27al4g1t1	2063	118	520	28.85	51590	2.00	5160	2.91	0.10	28.99	10.00	3.53	0.08
mv27al4g1t1	2107	111	880	17.05	55750	2.00	5820	2.58	0.15	17.24	9.58	3.26	0.12
mv27al4g1t1	2124	119	1140	13.16	48700	2.00	5270	2.85	0.22	13.46	9.24	3.48	0.17
mv27al4g1t1	2139	99	160	93.75	74240	2.00	7490	2.00	0.02	93.77	9.91	2.83	0.02
mv27al4g1t2	2060	98	200	75.00	72560	2.00	7050	2.13	0.03	75.03	10.29	2.92	0.02
mv27al4g1t2	2149	105	170	88.24	67090	2.00	6810	2.20	0.02	88.26	9.85	2.98	0.02
mv27al4g1t2	2217	138	700	21.43	41940	2.00	4640	3.23	0.15	21.67	9.04	3.80	0.13
mv27al4g1t2	2154	149	740	20.27	36240	2.00	3940	3.81	0.19	20.62	9.20	4.30	0.16
mv27al4g1t3	2114	153	670	22.39	34880	2.00	3700	4.05	0.18	22.75	9.43	4.52	0.16
mv27al4g1t3	2182	153	600	25.00	35850	2.00	3900	3.85	0.15	25.29	9.19	4.34	0.13
mv27al4g1t3	2156	145	560	26.79	38580	2.00	4110	3.65	0.14	27.03	9.39	4.16	0.12
mv27al4g1t3	2170	133	310	48.39	45670	2.00	4760	3.15	0.07	48.49	9.59	3.73	0.05
mv27al4g1t3	2047	129	1050	14.29	42170	2.00	4410	3.40	0.24	14.69	9.56	3.95	0.20
mv27al4g3t1	2050	96	280	53.57	74000	2.00	7180	2.09	0.04	53.61	10.31	2.89	0.03
mv27al4g3t1	2100	97	310	48.39	74210	2.00	7400	2.03	0.04	48.43	10.03	2.85	0.03
mv27al4g3t1	2039	97	230	65.22	73440	2.00	7070	2.12	0.03	65.25	10.39	2.92	0.02
mv27al4g3t1	2072	98	230	65.22	73340	2.00	7180	2.09	0.03	65.25	10.21	2.89	0.02
mv27al4g3t1	2078	98	270	55.56	73150	2.00	7200	2.08	0.04	55.59	10.16	2.89	0.03
mv27al4g3t1	2090	99	290	51.72	71810	2.00	7120	2.11	0.04	51.77	10.09	2.90	0.03
mv27al4g3t1	2028	96	220	68.18	73500	2.00	7030	2.13	0.03	68.22	10.46	2.92	0.02
mv27al4g3t1	2172	100	160	93.75	74700	2.00	7660	2.00	0.02	93.77	9.75	2.83	0.02
mv27al4g3t1	2039	93	230	65.22	82590	2.00	7940	2.00	0.03	65.25	10.40	2.83	0.02
mv27al4g3t1	2078	94	320	46.88	81820	2.00	8060	2.00	0.04	46.92	10.15	2.83	0.03
mv27al4g3t1	2060	94	340	44.12	82220	2.00	8030	2.00	0.04	44.16	10.24	2.83	0.03
mv27al4g3t1	2075	90	80	100.00	76580	2.00	7450	2.01	0.01	100.0	10.28	2.84	0.01

## ANEXO II (continuação)

REF	Idade Ma	Error Age Ma	U ppm	$\sigma$ %	Th ppm	$\sigma$ %	Pb ppm	$\sigma$ %	U/Pb	Error U/Pb %	Th/Pb	Error Th/Pb %	Corr.
mv27al4g3t1	2091	87	40	100.00	77740	2.00	7610	2.00	0.01	100.0	10.22	2.83	0.01
mv27al4g3t1	2077	85	20	100.00	76810	2.00	7460	2.01	0.00	100.0	10.30	2.84	0.01
mv27al4g3t1	2060	95	250	60.00	76820	2.00	7480	2.01	0.03	60.03	10.27	2.83	0.02
mv27al4g3t1	2090	85	20	100.00	77760	2.00	7600	2.00	0.00	100.0	10.23	2.83	0.01
mv27al4g3t1	2119	97	190	78.95	76510	2.00	7650	2.00	0.02	78.97	10.00	2.83	0.02
mv27al4g3t1	2171	99	190	78.95	81320	2.00	8340	2.00	0.02	78.97	9.75	2.83	0.02
mv27al4g3t1	2091	90	90	100.00	85660	2.00	8400	2.00	0.01	100.0	10.20	2.83	0.01
mv27al4g3t1	2063	94	480	31.25	77390	2.00	7630	2.00	0.06	31.31	10.14	2.83	0.05
mv27al5g1t1	2112	97	420	35.71	75290	2.00	7590	2.00	0.06	35.77	9.92	2.83	0.04
mv27al5g1t1	2143	106	350	42.86	64900	2.00	6640	2.26	0.05	42.92	9.77	3.02	0.04
mv27al5g1t1	2084	114	1440	10.42	49990	2.00	5400	2.78	0.27	10.78	9.26	3.42	0.21
mv27al5g1t1	2073	92	1240	12.10	86590	2.00	8840	2.00	0.14	12.26	9.80	2.83	0.12
mv27al5g1t1	2082	108	740	20.27	58790	2.00	5990	2.50	0.12	20.42	9.81	3.20	0.10
mv27al5g1t1	2124	109	740	20.27	58900	2.00	6130	2.45	0.12	20.42	9.61	3.16	0.09
mv27al5g1t1	2109	99	1050	14.29	67100	2.00	7010	2.14	0.15	14.45	9.57	2.93	0.11
mv27al5g1t1	2138	104	840	17.86	64460	2.00	6770	2.22	0.12	17.99	9.52	2.98	0.09
mv27al5g1t1	2152	107	770	19.48	61480	2.00	6490	2.31	0.12	19.62	9.47	3.06	0.09
mv27al5g1t1	2090	109	190	78.95	61340	2.00	6060	2.48	0.03	78.99	10.12	3.18	0.02
mv27al5g1t1	2045	105	580	25.86	61930	2.00	6120	2.45	0.09	25.98	10.12	3.16	0.07
mv27al5g1t1	2093	91	1680	8.93	95340	2.00	9950	2.00	0.17	9.15	9.58	2.83	0.15
mv27al5g1t1	2140	103	640	23.44	65780	2.00	6830	2.20	0.09	23.54	9.63	2.97	0.07
mv27al5g1t1	2093	95	370	40.54	82540	2.00	8210	2.00	0.05	40.59	10.05	2.83	0.03
mv27al5g1t1	2106	97	150	100.00	77640	2.00	7700	2.00	0.02	100.0	10.08	2.83	0.01
mv27al5g1t2	2140	94	100	100.00	75820	2.00	7630	2.00	0.01	100.0	9.94	2.83	0.01
mv27al5g1t2	2081	92	1920	7.81	76310	2.00	8130	2.00	0.24	8.06	9.39	2.83	0.18
mv27al5g1t2	2117	98	530	28.30	72450	2.00	7370	2.04	0.07	28.37	9.83	2.85	0.05
mv27al5g1t2	2055	97	610	24.59	71480	2.00	7080	2.12	0.09	24.68	10.10	2.91	0.06
mv25al5g2t1	2192	124	150	100.00	51730	2.00	5370	2.79	0.03	100.0	9.63	3.44	0.02
mv25al5g2t1	2047	114	310	48.39	55470	2.00	5410	2.77	0.06	48.47	10.25	3.42	0.05
mv25al5g2t1	2099	113	340	44.12	57020	2.00	5720	2.62	0.06	44.20	9.97	3.30	0.05
mv25al5g2t1	2117	146	550	27.27	37800	2.00	3950	3.80	0.14	27.54	9.57	4.29	0.12
mv25al5g2t1	2176	147	630	23.81	37620	2.00	4080	3.68	0.15	24.09	9.22	4.19	0.13
mv25al5g2t1	2086	109	680	22.06	58360	2.00	5940	2.53	0.11	22.20	9.82	3.22	0.09
mv25al5g2t1	2081	95	450	33.33	79240	2.00	7870	2.00	0.06	33.39	10.07	2.83	0.04
mv25al5g2t1	2085	106	390	38.46	62670	2.00	6250	2.40	0.06	38.54	10.03	3.12	0.05
mv25al5g2t1	2115	107	400	37.50	63210	2.00	6400	2.34	0.06	37.57	9.88	3.08	0.05
mv25al5g2t1	2073	100	390	38.46	69370	2.00	6860	2.19	0.06	38.52	10.11	2.96	0.04
mv27al5g2t2	2094	130	540	27.78	44760	2.00	4580	3.28	0.12	27.97	9.77	3.84	0.10
mv27al5g2t2	2162	135	250	60.00	44590	2.00	4610	3.25	0.05	60.09	9.67	3.82	0.05
mv27al5g2t2	2088	117	550	27.27	52650	2.00	5340	2.81	0.10	27.42	9.86	3.45	0.08
mv27al5g2t2	2092	97	710	21.13	71790	2.00	7280	2.06	0.10	21.23	9.86	2.87	0.07
mv27al5g2t2	2026	115	650	23.08	52560	2.00	5200	2.88	0.13	23.26	10.11	3.51	0.10
mv27al5g2t2	2105	119	510	29.41	52230	2.00	5330	2.81	0.10	29.55	9.80	3.45	0.08
mv27al5g2t2	2067	104	530	28.30	64190	2.00	6390	2.35	0.08	28.40	10.05	3.08	0.06
mv27al5g2t2	2144	121	300	50.00	52700	2.00	5400	2.78	0.06	50.08	9.76	3.42	0.05
mv27al5g2t2	2096	116	330	45.45	54700	2.00	5480	2.74	0.06	45.54	9.98	3.39	0.05
mv27al5g3at1	2045	93	270	55.56	82690	2.00	7990	2.00	0.03	55.59	10.35	2.83	0.03
mv27al5g3at1	2122	97	300	50.00	78880	2.00	7940	2.00	0.04	50.04	9.93	2.83	0.03
mv27al5g3at1	2055	93	420	35.71	79940	2.00	7820	2.00	0.05	35.77	10.22	2.83	0.04
mv27al5g3at1	2097	95	850	17.65	77070	2.00	7870	2.00	0.11	17.76	9.79	2.83	0.08
mv27al5g3at1	2100	95	680	22.06	79740	2.00	8080	2.00	0.08	22.15	9.87	2.83	0.06
mv27al5g3at1	2069	94	560	26.79	81590	2.00	8090	2.00	0.07	26.86	10.09	2.83	0.05
mv27al5g3at1	2106	96	480	31.25	80960	2.00	8150	2.00	0.06	31.31	9.93	2.83	0.05
mv27al5g3at1	2075	94	490	30.61	81520	2.00	8080	2.00	0.06	30.68	10.09	2.83	0.05
mv27al5g3at1	2174	99	490	30.61	80260	2.00	8360	2.00	0.06	30.68	9.60	2.83	0.05
mv27al5g3at1	2070	94	670	22.39	80730	2.00	8050	2.00	0.08	22.48	10.03	2.83	0.06
mv27al5g3at1	2056	93	610	24.59	79280	2.00	7830	2.00	0.08	24.67	10.13	2.83	0.06
mv27al5g3at1	2088	92	1240	12.10	89260	2.00	9170	2.00	0.14	12.26	9.73	2.83	0.12
mv27al5g3at1	2074	92	1380	10.87	86320	2.00	8870	2.00	0.16	11.05	9.73	2.83	0.13

**ANEXO II (continuação)**

REF	Idade Ma	Error Age Ma	U ppm	$\sigma$ %	Th ppm	$\sigma$ %	Pb ppm	$\sigma$ %	U/Pb	Error U/Pb %	Th/Pb	Error Th/Pb %	Corr.
mv27al5g3at1	2042	92	680	22.06	80560	2.00	7920	2.00	0.09	22.15	10.17	2.83	0.06
mv27al5g3at1	2120	96	580	25.86	81810	2.00	8330	2.00	0.07	25.94	9.82	2.83	0.05
mv27al5g4t1	2037	91	1720	8.72	74930	2.00	7740	2.00	0.22	8.95	9.68	2.83	0.16
mv27al5g4t1	2103	95	1120	13.39	76820	2.00	7970	2.00	0.14	13.54	9.64	2.83	0.10
mv27al5g4t1	2075	94	920	16.30	76070	2.00	7710	2.00	0.12	16.43	9.87	2.83	0.09
mv27al5g4t1	2059	94	530	28.30	76940	2.00	7590	2.00	0.07	28.37	10.14	2.83	0.05
mv27al5g4t1	2117	92	100	100.00	86730	2.00	8620	2.00	0.01	100.0	10.06	2.83	0.01
mv27al5g4t1	2061	93	320	46.88	86070	2.00	8400	2.00	0.04	46.92	10.25	2.83	0.03
mv27al5g4t1	2054	93	210	71.43	86820	2.00	8400	2.00	0.03	71.46	10.34	2.83	0.02
mv27al5g4t1	2040	90	110	100.00	85840	2.00	8210	2.00	0.01	100.0	10.46	2.83	0.01
mv27al5g4t2	2050	92	780	19.23	82000	2.00	8130	2.00	0.10	19.33	10.09	2.83	0.07
mv27al5g4t2	2080	94	630	23.81	80860	2.00	8090	2.00	0.08	23.89	10.00	2.83	0.06
mv27al5g4t2	2049	93	220	68.18	84190	2.00	8130	2.00	0.03	68.21	10.36	2.83	0.02
mv27al5g4t2	2059	93	330	45.45	84040	2.00	8200	2.00	0.04	45.50	10.25	2.83	0.03
mv27al5g4t2	2043	93	400	37.50	80200	2.00	7790	2.00	0.05	37.55	10.30	2.83	0.04
mv27al5g4t2	2019	91	710	21.13	78580	2.00	7650	2.00	0.09	21.22	10.27	2.83	0.07
mv27al5g4t2	2097	96	580	25.86	76760	2.00	7740	2.00	0.07	25.94	9.92	2.83	0.05
mv27al5g4t2	2128	95	1770	8.47	73900	2.00	8030	2.00	0.22	8.71	9.20	2.83	0.16
mv27al5g4t2	2130	108	800	18.75	59780	2.00	6260	2.40	0.13	18.90	9.55	3.12	0.10
mv27al5g4t2	2030	104	640	23.44	62310	2.00	6130	2.45	0.10	23.56	10.16	3.16	0.08
mv27al5g4t2	2083	94	1040	14.42	77430	2.00	7920	2.00	0.13	14.56	9.78	2.83	0.10
mv27al5g4t2	2090	84	0	100.00	97490	2.00	9520	2.00	0.00	100.0	10.24	2.83	0.01

**Leucossoma Charnoquítico MV-27E**

mv27el1g2t1	2052	119	800	18.75	49180	2.00	5000	3.00	0.16	18.99	9.84	3.61	0.13
mv27el1g2t1	2083	127	850	17.65	44560	2.00	4650	3.23	0.18	17.94	9.58	3.80	0.15
mv27el1g2t1	2093	133	340	44.12	44520	2.00	4480	3.35	0.08	44.24	9.94	3.90	0.06
mv27el1g2t1	2016	118	1000	15.00	48650	2.00	4930	3.04	0.20	15.31	9.87	3.64	0.17
mv27el1g2t1	2086	121	1060	14.15	47070	2.00	4980	3.01	0.21	14.47	9.45	3.62	0.17
mv27el1g2t1	2157	127	850	17.65	46070	2.00	4980	3.01	0.17	17.90	9.25	3.62	0.14
mv27el1g2t1	2140	130	670	22.39	44970	2.00	4760	3.15	0.14	22.61	9.45	3.73	0.12
mv27el1g2t1	2065	128	740	20.27	44700	2.00	4580	3.28	0.16	20.53	9.76	3.84	0.14
mv27el1g2t1	2176	131	790	18.99	43980	2.00	4790	3.13	0.16	19.24	9.18	3.72	0.14
mv27el1g2t1	2131	131	780	19.23	43860	2.00	4670	3.21	0.17	19.50	9.39	3.78	0.14
mv27el1g2t2	1988	135	590	25.42	40860	2.00	3990	3.76	0.15	25.70	10.24	4.26	0.13
mv27el1g2t2	2104	123	780	19.23	47660	2.00	4980	3.01	0.16	19.47	9.57	3.62	0.13
mv27el1g2t2	2048	129	900	16.67	42730	2.00	4410	3.40	0.20	17.01	9.69	3.95	0.17
mv27el1g2t2	2036	125	870	17.24	44810	2.00	4570	3.28	0.19	17.55	9.81	3.84	0.16
mv27el1g2t2	2086	123	910	16.48	46920	2.00	4910	3.05	0.19	16.76	9.56	3.65	0.15
mv27el1g2t2	1999	121	240	62.50	50180	2.00	4760	3.15	0.05	62.58	10.54	3.73	0.04
mv27el1g2t2	2040	124	970	15.46	45390	2.00	4670	3.21	0.21	15.79	9.72	3.78	0.17
mv27el1g2t2	2123	139	1020	14.71	38510	2.00	4210	3.56	0.24	15.13	9.15	4.09	0.21
mv27el1g2t2	2010	135	780	19.23	40060	2.00	4030	3.72	0.19	19.59	9.94	4.23	0.17
mv27el1g2t2	2032	127	830	18.07	43910	2.00	4460	3.36	0.19	18.38	9.85	3.91	0.16
mv27el2g1t1	2016	135	560	26.79	41390	2.00	4090	3.67	0.14	27.04	10.12	4.18	0.12
mv27el2g1t1	2128	134	600	25.00	43020	2.00	4510	3.33	0.13	25.22	9.54	3.88	0.11
mv27el2g1t1	2036	98	640	23.44	68630	2.00	6750	2.22	0.09	23.54	10.17	2.99	0.07
mv27el2g1t1	2090	141	550	27.27	39390	2.00	4050	3.70	0.14	27.52	9.73	4.21	0.12
mv27el2g1t1	2035	136	570	26.32	41030	2.00	4100	3.66	0.14	26.57	10.01	4.17	0.12
mv27el2g1t1	2139	135	590	25.42	42810	2.00	4510	3.33	0.13	25.64	9.49	3.88	0.11
mv27el2g1t1	2087	129	670	22.39	44740	2.00	4610	3.25	0.15	22.62	9.70	3.82	0.12

## ANEXO II (continuação)

REF	Idade Ma	Error Age Ma	U ppm	$\sigma$ %	Th ppm	$\sigma$ %	Pb ppm	$\sigma$ %	U/Pb	Error U/Pb %	Th/Pb	Error Th/Pb %	Corr.
mv27el2g1t1	2041	131	790	18.99	42370	2.00	4320	3.47	0.18	19.30	9.81	4.01	0.16
mv27el2g1t1	2149	134	510	29.41	43600	2.00	4580	3.28	0.11	29.59	9.52	3.84	0.09
mv27el2g1t1	2035	100	220	68.18	69520	2.00	6680	2.25	0.03	68.22	10.41	3.01	0.02
mv27el2g1t2	2036	129	510	29.41	44920	2.00	4450	3.37	0.11	29.60	10.09	3.92	0.10
mv27el2g1t2	2067	128	810	18.52	44170	2.00	4560	3.29	0.18	18.81	9.69	3.85	0.15
mv27el2g1t2	2161	135	470	31.91	43480	2.00	4580	3.28	0.10	32.08	9.49	3.84	0.09
mv27el2g1t2	2035	128	710	21.13	43980	2.00	4430	3.39	0.16	21.40	9.93	3.93	0.14
mv27el2g1t2	2089	134	660	22.73	42260	2.00	4370	3.43	0.15	22.99	9.67	3.97	0.13
mv27el2g1t2	2091	135	710	21.13	41520	2.00	4320	3.47	0.16	21.41	9.61	4.01	0.14
mv27el2g1t2	2098	134	690	21.74	42340	2.00	4410	3.40	0.16	22.00	9.60	3.95	0.13
mv27el2g1t2	2150	89	0	100.0	69370	2.00	6980	2.15	0.00	100.0	9.94	2.94	0.02
mv27el2g1t2	2103	99	210	71.43	72170	2.00	7170	2.09	0.03	71.46	10.07	2.89	0.02
mv27el2g2t1	2069	134	580	25.86	42300	2.00	4300	3.49	0.13	26.10	9.84	4.02	0.12
mv27el2g2t1	2035	123	830	18.07	46580	2.00	4720	3.18	0.18	18.35	9.87	3.75	0.15
mv27el2g2t1	2121	130	590	25.42	44730	2.00	4660	3.22	0.13	25.63	9.60	3.79	0.11
mv27el2g2t1	2067	127	750	20.00	45230	2.00	4640	3.23	0.16	20.26	9.75	3.80	0.14
mv27el2g2t1	2093	125	740	20.27	46470	2.00	4820	3.11	0.15	20.51	9.64	3.70	0.13
mv27el2g2t1	2106	124	730	20.55	47490	2.00	4950	3.03	0.15	20.77	9.59	3.63	0.12
mv27el2g2t1	2077	131	720	20.83	43040	2.00	4440	3.38	0.16	21.11	9.69	3.93	0.14
mv27el2g2t1	2054	137	620	24.19	40420	2.00	4100	3.66	0.15	24.47	9.86	4.17	0.13
mv27el2g2t1	2079	150	1510	9.93	31330	2.00	3600	4.17	0.42	10.77	8.70	4.62	0.35
mv27el2g2t1	2077	88	0	100.0	68850	2.00	6680	2.25	0.00	100.0	10.31	3.01	0.02
mv27el2g2t2	2063	100	140	100.0	69040	2.00	6700	2.24	0.02	100.0	10.30	3.00	0.02
mv27el2g2t2	2083	110	180	83.33	60270	2.00	5930	2.53	0.03	83.37	10.16	3.22	0.02
mv27el2g2t2	2084	139	670	22.39	39770	2.00	4120	3.64	0.16	22.68	9.65	4.15	0.14
mv27el2g2t2	2043	137	780	19.23	39620	2.00	4060	3.69	0.19	19.58	9.76	4.20	0.17
mv27el2g2t2	2078	135	680	22.06	41620	2.00	4290	3.50	0.16	22.33	9.70	4.03	0.14
mv27el2g2t2	2019	137	670	22.39	39640	2.00	3970	3.78	0.17	22.70	9.98	4.28	0.15
mv27el2g2t2	2120	127	590	25.42	46370	2.00	4820	3.11	0.12	25.61	9.62	3.70	0.10
mv27el2g2t2	2179	124	710	21.13	48720	2.00	5250	2.86	0.14	21.32	9.28	3.49	0.11
mv27el2g2t2	2037	100	170	88.24	69100	2.00	6630	2.26	0.03	88.26	10.42	3.02	0.02
mv27el2g3t1	2051	98	200	75.00	72690	2.00	7030	2.13	0.03	75.03	10.34	2.92	0.02
mv27el2g3t1	2084	126	880	17.05	45440	2.00	4750	3.16	0.19	17.34	9.57	3.74	0.15
mv27el2g3t1	2079	124	560	26.79	47820	2.00	4850	3.09	0.12	26.96	9.86	3.68	0.10
mv27el2g3t1	2076	132	830	18.07	42330	2.00	4410	3.40	0.19	18.39	9.60	3.95	0.16
mv27el2g3t2	2072	121	670	22.39	49330	2.00	5020	2.99	0.13	22.59	9.83	3.60	0.11
mv27el2g3t2	2140	130	660	22.73	45120	2.00	4770	3.14	0.14	22.94	9.46	3.73	0.12
mv27el2g3t2	1998	129	560	26.79	43850	2.00	4280	3.50	0.13	27.01	10.25	4.04	0.11
mv27el2g3t2	2092	131	590	25.42	43990	2.00	4520	3.32	0.13	25.64	9.73	3.87	0.11
mv27el2g3t2	2105	130	720	20.83	44310	2.00	4630	3.24	0.16	21.08	9.57	3.81	0.13
mv27el2g3t2	2093	105	200	75.00	65180	2.00	6450	2.33	0.03	75.04	10.11	3.07	0.02
mv27el2g3t2	2121	103	120	100.0	65290	2.00	6520	2.30	0.02	100.0	10.01	3.05	0.02
mv27el2g3t2	2150	107	330	45.45	63560	2.00	6520	2.30	0.05	45.51	9.75	3.05	0.04
mv27el2g3t3	2108	126	310	48.39	48440	2.00	4890	3.07	0.06	48.48	9.91	3.66	0.05
mv27el2g3t3	2076	139	420	35.71	41100	2.00	4140	3.62	0.10	35.90	9.93	4.14	0.09
mv27el2g3t3	2170	133	700	21.43	43780	2.00	4720	3.18	0.15	21.66	9.28	3.75	0.12
mv27el2g3t3	2119	129	730	20.55	45050	2.00	4740	3.16	0.15	20.79	9.50	3.74	0.13
mv27el2g3t4	2122	126	720	20.83	46830	2.00	4920	3.05	0.15	21.06	9.52	3.65	0.12
mv27el2g3t4	2168	129	650	23.08	46170	2.00	4940	3.04	0.13	23.28	9.35	3.64	0.11
mv27el2g3t4	2048	130	770	19.48	42900	2.00	4380	3.42	0.18	19.78	9.79	3.97	0.15
mv27el2g3t4	2124	113	230	65.22	58120	2.00	5860	2.56	0.04	65.27	9.92	3.25	0.03
mv27el2g3t4	2070	111	290	51.72	58270	2.00	5740	2.61	0.05	51.79	10.15	3.29	0.04

**ANEXO II (continuação)**

REF	Idade Ma	Error Age Ma	U ppm	$\sigma$ %	Th ppm	$\sigma$ %	Pb ppm	$\sigma$ %	U/Pb	Error U/Pb %	Th/Pb	Error Th/Pb %	Corr.
mv27el3g2t1	2063	135	790	18.99	40610	2.00	4200	3.57	0.19	19.32	9.67	4.09	0.16
mv27el3g2t1	2041	137	590	25.42	40500	2.00	4070	3.69	0.14	25.69	9.95	4.19	0.13
mv27el3g2t1	2068	122	610	24.59	48640	2.00	4920	3.05	0.12	24.78	9.89	3.65	0.10
mv27el3g2t1	2119	120	720	20.83	50430	2.00	5270	2.85	0.14	21.03	9.57	3.48	0.11
mv27el3g2t1	2070	127	490	30.61	46440	2.00	4670	3.21	0.10	30.78	9.94	3.78	0.09
mv27el3g2t1	2090	122	790	18.99	48400	2.00	5020	2.99	0.16	19.22	9.64	3.60	0.13
mv27el3g2t1	2069	127	680	22.06	45240	2.00	4620	3.25	0.15	22.30	9.79	3.81	0.12
mv27el3g2t1	2075	132	710	21.13	42810	2.00	4410	3.40	0.16	21.40	9.71	3.95	0.14
mv27el3g2t1	2097	139	800	18.75	39410	2.00	4160	3.61	0.19	19.09	9.47	4.12	0.17
mv27el3g2t1	2139	140	700	21.43	39990	2.00	4270	3.51	0.16	21.71	9.37	4.04	0.14
mv27el3g2t2	2035	126	740	20.27	45010	2.00	4540	3.30	0.16	20.54	9.91	3.86	0.14
mv27el3g2t2	2099	126	820	18.29	45900	2.00	4810	3.12	0.17	18.56	9.54	3.70	0.14
mv27el3g2t2	2097	130	560	26.79	44800	2.00	4600	3.26	0.12	26.98	9.74	3.83	0.10
mv27el3g2t2	2189	137	510	29.41	42990	2.00	4610	3.25	0.11	29.59	9.33	3.82	0.09
mv27el3g2t2	2119	129	560	26.79	45490	2.00	4720	3.18	0.12	26.97	9.64	3.75	0.10
mv27el3g2t2	2178	131	620	24.19	45180	2.00	4850	3.09	0.13	24.39	9.32	3.68	0.11
mv27el3g2t2	2070	127	720	20.83	44950	2.00	4610	3.25	0.16	21.09	9.75	3.82	0.13
mv27el3g2t2	2089	130	730	20.55	43830	2.00	4550	3.30	0.16	20.81	9.63	3.86	0.14
mv27el3g2t2	2171	123	720	20.83	49280	2.00	5290	2.84	0.14	21.03	9.32	3.47	0.11
mv27el3g2t2	2149	131	490	30.61	45460	2.00	4760	3.15	0.10	30.77	9.55	3.73	0.09
mv27el3g2t1	2029	92	10	100.0	63470	2.00	6010	2.50	0.00	100.0	10.56	3.20	0.02
mv27el3g2t1	2121	98	90	100.0	67940	2.00	6770	2.22	0.01	100.0	10.04	2.98	0.02
mv27el3g2t1	2068	105	130	100.0	62560	2.00	6090	2.46	0.02	100.0	10.27	3.17	0.02
mv27el3g2t1	2090	109	450	33.33	59720	2.00	6000	2.50	0.08	33.43	9.95	3.20	0.06
mv27el3g2t1	2031	119	790	18.99	49140	2.00	4940	3.04	0.16	19.23	9.95	3.64	0.13
mv27el3g2t1	2077	121	760	19.74	48640	2.00	5000	3.00	0.15	19.96	9.73	3.61	0.13
mv27el3g2t1	2041	128	550	27.27	45370	2.00	4520	3.32	0.12	27.47	10.04	3.87	0.10
mv27el3g2t1	2149	130	600	25.00	45340	2.00	4790	3.13	0.13	25.20	9.47	3.72	0.10
mv27el3g2t1	1994	124	730	20.55	45570	2.00	4490	3.34	0.16	20.82	10.15	3.89	0.14
mv27el3g2t1	2040	127	570	26.32	45640	2.00	4550	3.30	0.13	26.52	10.03	3.86	0.11
mv27el3g2t1	2085	128	720	20.83	44890	2.00	4640	3.23	0.16	21.08	9.67	3.80	0.13
mv27el3g2t1	2070	127	660	22.73	45390	2.00	4630	3.24	0.14	22.96	9.80	3.81	0.12
mv27el3g2t2	2051	105	300	50.00	64160	2.00	6250	2.40	0.05	50.06	10.27	3.12	0.04
mv27el3g2t2	2116	107	230	65.22	63810	2.00	6400	2.34	0.04	65.26	9.97	3.08	0.03
mv27el3g2t2	2046	103	180	83.33	66130	2.00	6380	2.35	0.03	83.37	10.37	3.09	0.02
mv27el3g2t2	2123	125	570	26.32	48080	2.00	4990	3.01	0.11	26.49	9.64	3.61	0.09
mv27el3g2t3	2127	132	310	48.39	45570	2.00	4650	3.23	0.07	48.49	9.80	3.80	0.06
mv27el3g2t3	2097	138	480	31.25	41430	2.00	4240	3.54	0.11	31.45	9.77	4.06	0.10

**Gnaiss Enderbítico LT-214**

lt21411g2t1	2075	84	4670	2.25	70870	2.00	8591	2.00	0.54	3.01	8.25	2.83	0.47
lt21411g2t1	2071	83	9500	2.00	185460	2.00	21427	2.00	0.44	2.83	8.66	2.83	0.50
lt21411g2t1	2104	84	5070	2.07	88030	2.00	10561	2.00	0.48	2.88	8.34	2.83	0.49
lt21411g2t1	2065	83	7290	2.00	130690	2.00	15276	2.00	0.48	2.83	8.56	2.83	0.50
lt21411g2t1	2123	85	5420	2.00	90450	2.00	11036	2.00	0.49	2.83	8.20	2.83	0.50
lt21411g2t1	2119	87	3750	2.80	86590	2.00	10001	2.00	0.37	3.44	8.66	2.83	0.41
lt21411g2t2	2115	86	4600	2.28	76280	2.00	9281	2.00	0.50	3.03	8.22	2.83	0.47
lt21411g2t2	2101	86	3860	2.72	69650	2.00	8287	2.00	0.47	3.38	8.40	2.83	0.42
lt21411g2t2	2078	83	7480	2.00	135820	2.00	15943	2.00	0.47	2.83	8.52	2.83	0.50
lt21411g2t2	2083	83	6220	2.00	113660	2.00	13367	2.00	0.47	2.83	8.50	2.83	0.50
lt21411g2t3	2142	86	6890	2.00	118660	2.00	14542	2.00	0.47	2.83	8.16	2.83	0.50

## ANEXO II (continuação)

REF	Idade Ma	Error Age Ma	U ppm	$\sigma$ %	Th ppm	$\sigma$ %	Pb ppm	$\sigma$ %	U/Pb	Error U/Pb %	Th/Pb	Error Th/Pb %	Corr.
lt21411g2t3	2098	85	4290	2.45	70600	2.00	8526	2.00	0.50	3.16	8.28	2.83	0.45
lt21411g2t3	2083	85	4120	2.55	72460	2.00	8576	2.00	0.48	3.24	8.45	2.83	0.44
lt21411g2t4	2194	88	5340	2.00	91290	2.00	11503	2.00	0.46	2.83	7.94	2.83	0.50
lt21411g2t4	2071	85	3990	2.63	71310	2.00	8366	2.00	0.48	3.31	8.52	2.83	0.43
lt21411g2t4	2067	84	4080	2.57	71370	2.00	8386	2.00	0.49	3.26	8.51	2.83	0.43
lt21411g3t1	2037	81	5260	2.00	65770	2.00	8143	2.00	0.65	2.83	8.08	2.83	0.50
lt21411g3t1	2119	85	4890	2.15	59960	2.00	7793	2.00	0.63	2.93	7.69	2.83	0.48
lt21411g3t1	2073	83	5340	2.00	73310	2.00	9062	2.00	0.59	2.83	8.09	2.83	0.50
lt21411g3t1	2094	84	5580	2.00	82470	2.00	10149	2.00	0.55	2.83	8.13	2.83	0.50
lt21411g3t1	2137	85	6640	2.00	107310	2.00	13272	2.00	0.50	2.83	8.09	2.83	0.50
lt21411g3t1	2093	84	6290	2.00	98180	2.00	11944	2.00	0.53	2.83	8.22	2.83	0.50
lt21411g3t1	2029	81	6590	2.00	100070	2.00	11829	2.00	0.56	2.83	8.46	2.83	0.50
lt21411g3t1	2069	83	6030	2.00	90150	2.00	10925	2.00	0.55	2.83	8.25	2.83	0.50
lt21411g3t1	2024	81	5310	2.00	71350	2.00	8629	2.00	0.62	2.83	8.27	2.83	0.50
lt21411g3t2	2074	83	5580	2.00	72850	2.00	9114	2.00	0.61	2.83	7.99	2.83	0.50
lt21411g3t2	2073	83	5910	2.00	82340	2.00	10146	2.00	0.58	2.83	8.12	2.83	0.50
lt21411g3t2	2062	82	5570	2.00	74430	2.00	9201	2.00	0.61	2.83	8.09	2.83	0.50
lt21411g3t2	2072	83	5390	2.00	74420	2.00	9183	2.00	0.59	2.83	8.10	2.83	0.50
lt21411g3t2	2090	84	5290	2.00	74400	2.00	9233	2.00	0.57	2.83	8.06	2.83	0.50
lt21411g3t2	2152	86	5110	2.05	71250	2.00	9152	2.00	0.56	2.87	7.79	2.83	0.49
lt21411g3t2	2100	84	5460	2.00	73140	2.00	9221	2.00	0.59	2.83	7.93	2.83	0.50
lt21411g3t2	2057	82	5370	2.00	83060	2.00	9931	2.00	0.54	2.83	8.36	2.83	0.50
lt21411g3t2	2123	85	5910	2.00	94130	2.00	11590	2.00	0.51	2.83	8.12	2.83	0.50
lt21411g3t2	2086	83	5530	2.00	83520	2.00	10195	2.00	0.54	2.83	8.19	2.83	0.50
lt21411g5t1	2024	81	7440	2.00	147930	2.00	16624	2.00	0.45	2.83	8.90	2.83	0.50
lt21411g5t1	2097	84	5720	2.00	100250	2.00	11961	2.00	0.48	2.83	8.38	2.83	0.50
lt21411g5t1	2056	83	4780	2.20	76820	2.00	9112	2.00	0.52	2.97	8.43	2.83	0.48
lt21411g5t1	2086	84	4610	2.28	74040	2.00	8926	2.00	0.52	3.03	8.29	2.83	0.47
lt21411g5t1	2108	85	4620	2.27	74240	2.00	9053	2.00	0.51	3.03	8.20	2.83	0.47
lt21411g5t1	2063	83	5100	2.06	79290	2.00	9502	2.00	0.54	2.87	8.34	2.83	0.49
lt21411g5t1	2102	86	4290	2.45	67540	2.00	8244	2.00	0.52	3.16	8.19	2.83	0.45
lt21411g5t1	2080	85	4430	2.37	60390	2.00	7507	2.00	0.59	3.10	8.04	2.83	0.46
lt21411g5t1	2090	84	5570	2.00	79150	2.00	9803	2.00	0.57	2.83	8.07	2.83	0.50
lt21411g5t1	2104	84	5040	2.08	72290	2.00	9001	2.00	0.56	2.89	8.03	2.83	0.49
lt21411g5t1	2123	85	5000	2.10	77480	2.00	9592	2.00	0.52	2.90	8.08	2.83	0.49
lt21411g5t2	2051	82	6670	2.00	114070	2.00	13342	2.00	0.50	2.83	8.55	2.83	0.50
lt21411g5t2	2088	84	5530	2.00	93980	2.00	11223	2.00	0.49	2.83	8.37	2.83	0.50
lt21411g5t2	2131	87	4210	2.49	67390	2.00	8324	2.00	0.51	3.20	8.10	2.83	0.44
lt21411g5t2	2059	84	4420	2.38	61910	2.00	7565	2.00	0.58	3.11	8.18	2.83	0.46
lt21411g5t2	2129	85	5590	2.00	90360	2.00	11131	2.00	0.50	2.83	8.12	2.83	0.50
lt21411g5t2	2094	84	5080	2.07	74150	2.00	9150	2.00	0.56	2.88	8.10	2.83	0.49
lt21411g5t2	2101	84	4960	2.12	75000	2.00	9225	2.00	0.54	2.91	8.13	2.83	0.49
lt21411g5t3	2070	83	5240	2.00	86610	2.00	10296	2.00	0.51	2.83	8.41	2.83	0.50
lt21411g5t3	2097	84	5020	2.09	85630	2.00	10267	2.00	0.49	2.89	8.34	2.83	0.49
lt21411g5t3	2105	87	3810	2.76	60350	2.00	7370	2.00	0.52	3.41	8.19	2.83	0.42
lt21411g5t3	2043	85	3540	2.97	59880	2.00	6989	2.00	0.51	3.58	8.57	2.83	0.40
lt21411g7t1	2126	86	4890	2.15	64620	2.00	8287	2.00	0.59	2.93	7.80	2.83	0.48
lt21411g7t1	2120	85	5090	2.06	67040	2.00	8575	2.00	0.59	2.87	7.82	2.83	0.49
lt21411g7t1	2088	84	5320	2.00	71230	2.00	8924	2.00	0.60	2.83	7.98	2.83	0.50
lt21411g7t1	2138	86	4960	2.12	69730	2.00	8876	2.00	0.56	2.91	7.86	2.83	0.49
lt21411g7t1	2093	84	5350	2.00	69230	2.00	8765	2.00	0.61	2.83	7.90	2.83	0.50
lt21411g7t1	2087	83	5520	2.00	70670	2.00	8940	2.00	0.62	2.83	7.91	2.83	0.50

## ANEXO II (continuação)

REF	Idade Ma	Error Age Ma	U ppm	$\sigma$ %	Th ppm	$\sigma$ %	Pb ppm	$\sigma$ %	U/Pb	Error U/Pb %	Th/Pb	Error Th/Pb %	Corr.
lt21411g7t1	2137	85	6800	2.00	112270	2.00	13826	2.00	0.49	2.83	8.12	2.83	0.50
lt21411g7t1	2136	85	6850	2.00	106650	2.00	13278	2.00	0.52	2.83	8.03	2.83	0.50
lt21411g7t1	2084	83	5680	2.00	78560	2.00	9752	2.00	0.58	2.83	8.06	2.83	0.50
lt21411g7t1	2072	83	5600	2.00	76830	2.00	9494	2.00	0.59	2.83	8.09	2.83	0.50
lt21411g8t1	2074	86	3060	3.43	81610	2.00	9031	2.00	0.34	3.97	9.04	2.83	0.36
lt21411g8t1	2033	88	2160	4.86	52620	2.00	5765	2.00	0.37	5.26	9.13	2.83	0.27
lt21411g8t1	2108	92	2070	5.07	52140	2.00	5917	2.00	0.35	5.45	8.81	2.83	0.26
lt21411g8t1	2096	90	2320	4.53	60190	2.00	6760	2.00	0.34	4.95	8.90	2.83	0.29
lt21411g8t1	2103	88	2230	4.71	85450	2.00	9235	2.00	0.24	5.12	9.25	2.83	0.28
lt21411g8t1	2076	87	2710	3.87	83840	2.00	9129	2.00	0.30	4.36	9.18	2.83	0.32
lt21411g8t1	2082	87	2650	3.96	77290	2.00	8496	2.00	0.31	4.44	9.10	2.83	0.32
lt21411g8t2	2084	94	2620	4.01	41430	2.00	5004	2.20	0.52	4.57	8.28	2.97	0.36
lt21411g8t2	2052	88	2660	3.95	48080	2.00	5570	2.00	0.48	4.43	8.63	2.83	0.32
lt21411g8t2	2083	88	2090	5.02	86180	2.00	9159	2.00	0.23	5.41	9.41	2.83	0.26
lt21411g8t2	2072	86	2890	3.63	85280	2.00	9315	2.00	0.31	4.15	9.16	2.83	0.34
lt21411g8t2	2106	91	2250	4.67	55280	2.00	6286	2.00	0.36	5.08	8.79	2.83	0.28
lt21411g8t2	2062	88	2400	4.38	54850	2.00	6158	2.00	0.39	4.81	8.91	2.83	0.29
lt21411g8t2	2034	88	2160	4.86	51260	2.00	5639	2.00	0.38	5.26	9.09	2.83	0.27
lt21411g8t2	2111	92	2130	4.93	47230	2.00	5464	2.01	0.39	5.32	8.64	2.84	0.27
lt21411g8t2	2046	88	1710	6.14	72890	2.00	7579	2.00	0.23	6.46	9.62	2.83	0.22
lt21411g9t1	2125	85	6800	2.00	106250	2.00	13145	2.00	0.52	2.83	8.08	2.83	0.50
lt21411g9t1	2094	84	6750	2.00	109140	2.00	13199	2.00	0.51	2.83	8.27	2.83	0.50
lt21411g9t1	2120	85	7140	2.00	115820	2.00	14186	2.00	0.50	2.83	8.16	2.83	0.50
lt21411g9t1	2055	82	6300	2.00	93700	2.00	11282	2.00	0.56	2.83	8.31	2.83	0.50
lt21411g9t1	2098	84	6200	2.00	87040	2.00	10852	2.00	0.57	2.83	8.02	2.83	0.50
lt21411g9t1	2043	82	6140	2.00	80400	2.00	9885	2.00	0.62	2.83	8.13	2.83	0.50
lt21411g9t1	2058	82	5680	2.00	76100	2.00	9386	2.00	0.61	2.83	8.11	2.83	0.50
lt21411g9t1	2048	82	5770	2.00	73950	2.00	9158	2.00	0.63	2.83	8.08	2.83	0.50
lt21411g9t1	2077	83	5830	2.00	72910	2.00	9225	2.00	0.63	2.83	7.90	2.83	0.50
lt21411g9t1	2065	83	5050	2.08	67730	2.00	8381	2.00	0.60	2.88	8.08	2.83	0.49
lt21411g9t2	2072	119	3140	3.34	22090	2.00	3292	3.34	0.95	4.73	6.71	3.89	0.61
lt21411g9t2	2052	82	5870	2.00	80550	2.00	9850	2.00	0.60	2.83	8.18	2.83	0.50
lt21411g9t2	2108	84	5720	2.00	74470	2.00	9492	2.00	0.60	2.83	7.85	2.83	0.50
lt21411g9t2	2102	84	5150	2.04	64900	2.00	8307	2.00	0.62	2.86	7.81	2.83	0.50
lt21411g9t3	2082	86	3070	3.42	79990	2.00	8915	2.00	0.34	3.96	8.97	2.83	0.36
lt21411g9t3	2115	85	6360	2.00	103780	2.00	12669	2.00	0.50	2.83	8.19	2.83	0.50
lt21411g9t3	2139	86	8000	2.00	139280	2.00	17008	2.00	0.47	2.83	8.19	2.83	0.50
lt21411g9t3	2099	84	7210	2.00	109490	2.00	13441	2.00	0.54	2.83	8.15	2.83	0.50
lt21411g9t3	2104	84	6220	2.00	94420	2.00	11620	2.00	0.54	2.83	8.13	2.83	0.50
lt21411g9t3	2076	83	5650	2.00	87240	2.00	10544	2.00	0.54	2.83	8.27	2.83	0.50
lt21411g10t1	2100	84	5370	2.00	64600	2.00	8353	2.00	0.64	2.83	7.73	2.83	0.50
lt21411g10t1	2068	83	6210	2.00	69420	2.00	8981	2.00	0.69	2.83	7.73	2.83	0.50
lt21411g10t1	2092	84	6430	2.00	76790	2.00	9901	2.00	0.65	2.83	7.76	2.83	0.50
lt21411g10t1	2106	84	6430	2.00	77730	2.00	10070	2.00	0.64	2.83	7.72	2.83	0.50
lt21411g10t1	2088	84	5040	2.08	71270	2.00	8827	2.00	0.57	2.89	8.07	2.83	0.49
lt21411g10t1	2068	83	6860	2.00	80480	2.00	10287	2.00	0.67	2.83	7.82	2.83	0.50
lt21411g10t1	2094	84	6420	2.00	75380	2.00	9772	2.00	0.66	2.83	7.71	2.83	0.50
lt21411g10t2	2091	84	4870	2.16	71110	2.00	8760	2.00	0.56	2.94	8.12	2.83	0.48
lt21411g10t2	2065	83	6020	2.00	71840	2.00	9133	2.00	0.66	2.83	7.87	2.83	0.50
lt21411g10t2	2028	81	7090	2.00	76440	2.00	9768	2.00	0.73	2.83	7.83	2.83	0.50
lt21411g10t2	2085	84	5030	2.09	74090	2.00	9085	2.00	0.55	2.89	8.16	2.83	0.49
lt21411g10t2	2088	84	6390	2.00	78710	2.00	10052	2.00	0.64	2.83	7.83	2.83	0.50

**ANEXO II (continuação)**

REF	Idade Ma	Error Age Ma	U ppm	$\sigma$ %	Th ppm	$\sigma$ %	Pb ppm	$\sigma$ %	U/Pb	Error U/Pb %	Th/Pb	Error Th/Pb %	Corr.
lt2141lg10t2	2092	84	6530	2.00	77740	2.00	10034	2.00	0.65	2.83	7.75	2.83	0.50
lt2141lg10t2	2073	83	6630	2.00	76550	2.00	9851	2.00	0.67	2.83	7.77	2.83	0.50
lt2141lg10t2	2118	85	6260	2.00	71120	2.00	9413	2.00	0.67	2.83	7.56	2.83	0.50
lt2141lg10t2	2080	83	6150	2.00	70880	2.00	9160	2.00	0.67	2.83	7.74	2.83	0.50
lt2141lg11t1	2049	83	4540	2.31	58880	2.00	7277	2.00	0.62	3.06	8.09	2.83	0.46
lt2141lg11t1	2096	84	6620	2.00	106180	2.00	12874	2.00	0.51	2.83	8.25	2.83	0.50
lt2141lg11t1	2061	82	5590	2.00	89730	2.00	10679	2.00	0.52	2.83	8.40	2.83	0.50
lt2141lg11t1	2047	83	4730	2.22	62960	2.00	7727	2.00	0.61	2.99	8.15	2.83	0.47
lt2141lg11t1	2117	85	4970	2.11	69540	2.00	8766	2.00	0.57	2.91	7.93	2.83	0.49
lt2141lg11t2	2097	84	5110	2.05	84260	2.00	10167	2.00	0.50	2.87	8.29	2.83	0.49
lt2141lg11t2	2093	85	4690	2.24	73520	2.00	8938	2.00	0.52	3.00	8.23	2.83	0.47
lt2141lg11t2	2084	84	5050	2.08	82550	2.00	9910	2.00	0.51	2.88	8.33	2.83	0.49
lt2141lg11t2	2110	84	6350	2.00	96540	2.00	11914	2.00	0.53	2.83	8.10	2.83	0.50
lt2141lg11t2	2089	84	6330	2.00	100300	2.00	12146	2.00	0.52	2.83	8.26	2.83	0.50
lt2141lg11t2	2108	84	6270	2.00	97650	2.00	11982	2.00	0.52	2.83	8.15	2.83	0.50
lt2141lg11t2	2076	83	6160	2.00	91910	2.00	11182	2.00	0.55	2.83	8.22	2.83	0.50
lt2141lg11t2	2068	83	5700	2.00	87090	2.00	10500	2.00	0.54	2.83	8.29	2.83	0.50
lt2141lg11t2	2070	83	5020	2.09	78700	2.00	9451	2.00	0.53	2.89	8.33	2.83	0.49
lt2141lg11t2	2073	83	5220	2.01	77890	2.00	9464	2.00	0.55	2.84	8.23	2.83	0.50

**Gnaiss Tonalítico LT-223A***Grupo 1*

lt223al1g1t1	2112	126	990	10.61	31090	2.00	3443	3.20	0.29	11.08	9.03	3.77	0.24
lt223al1g1t1	2023	122	1060	9.91	31400	2.00	3341	3.29	0.32	10.44	9.40	3.85	0.27
lt223al1g1t1	2065	119	1010	10.40	33700	2.00	3620	3.04	0.28	10.83	9.31	3.64	0.23
lt223al1g1t1	2126	117	1090	9.63	34840	2.00	3879	2.84	0.28	10.04	8.98	3.47	0.23
lt223al1g1t1	2062	104	1270	8.27	40840	2.00	4397	2.50	0.29	8.64	9.29	3.20	0.23
lt223al1g1t1	2050	104	1240	8.47	41060	2.00	4378	2.51	0.28	8.83	9.38	3.21	0.22
lt223al1g1t2	2077	112	1070	9.81	36970	2.00	3982	2.76	0.27	10.19	9.28	3.41	0.22
lt223al1g1t2	2009	132	530	19.81	30430	2.00	3038	3.62	0.17	20.14	10.02	4.14	0.16
lt223al1g2t1	2038	90	970	10.82	63470	2.00	6384	2.00	0.15	11.01	9.94	2.83	0.13
lt223al1g2t1	2072	91	900	11.67	68930	2.00	7000	2.00	0.13	11.84	9.85	2.83	0.12
lt223al1g2t1	2103	92	1090	9.63	70150	2.00	7304	2.00	0.15	9.84	9.60	2.83	0.14
lt223al1g2t1	2153	102	450	23.33	48890	2.00	5100	2.16	0.09	23.43	9.59	2.94	0.07
lt223al1g2t1	2116	101	720	14.58	48110	2.00	5030	2.19	0.14	14.75	9.56	2.96	0.11
lt223al1g2t1	2162	116	210	50.00	41100	2.00	4241	2.59	0.05	50.07	9.69	3.28	0.04
lt223al1g2t1	2074	108	350	30.00	43880	2.00	4378	2.51	0.08	30.11	10.02	3.21	0.07
lt223al1g2t1	2128	95	850	12.35	55440	2.00	5842	2.00	0.15	12.51	9.49	2.83	0.11
lt223al1g2t1	2073	93	830	12.65	57220	2.00	5844	2.00	0.14	12.81	9.79	2.83	0.11
lt223al1g2t1	2094	94	880	11.93	53960	2.00	5608	2.00	0.16	12.10	9.62	2.83	0.12
lt223al1g2t2	2153	96	900	11.67	57920	2.00	6185	2.00	0.15	11.84	9.36	2.83	0.12
lt223al1g2t2	2055	92	860	12.21	57440	2.00	5823	2.00	0.15	12.37	9.86	2.83	0.11
lt223al1g2t2	2028	106	540	19.44	43500	2.00	4307	2.55	0.13	19.61	10.10	3.24	0.10
lt223al1g2t2	2112	113	220	47.73	41870	2.00	4217	2.61	0.05	47.80	9.93	3.29	0.04
lt223al1g2t2	2002	102	470	22.34	45910	2.00	4451	2.47	0.11	22.48	10.32	3.18	0.09
lt223al1g2t2	2129	103	810	12.96	46110	2.00	4899	2.25	0.17	13.16	9.41	3.01	0.13
lt223al1g2t2	2076	103	640	16.41	45840	2.00	4681	2.35	0.14	16.57	9.79	3.09	0.11
lt223al1g2t2	2024	99	600	17.50	47960	2.00	4741	2.32	0.13	17.65	10.12	3.06	0.10
lt223al1g2t2	2083	102	820	12.80	45470	2.00	4729	2.33	0.17	13.01	9.62	3.07	0.14
lt223al1g3t1	2073	153	900	11.67	22940	2.00	2552	4.31	0.35	12.44	8.99	4.75	0.31
lt223al1g3t1	2083	156	820	12.80	22660	2.00	2509	4.38	0.33	13.53	9.03	4.82	0.29

**ANEXO II (continuação)**

REF	Idade Ma	Error Age Ma	U ppm	$\sigma$ %	Th ppm	$\sigma$ %	Pb ppm	$\sigma$ %	U/Pb	Error U/Pb %	Th/Pb	Error Th/Pb %	Corr.
lt223al1g3t1	2191	150	770	13.64	24950	2.00	2865	3.84	0.27	14.17	8.71	4.33	0.24
lt223al1g3t1	2047	149	1010	10.40	23210	2.00	2583	4.26	0.39	11.23	8.99	4.70	0.34
lt223al1g3t1	2165	166	940	11.17	20430	2.00	2436	4.51	0.39	12.05	8.39	4.94	0.34
lt223al1g3t1	2164	153	1130	9.29	22360	2.00	2705	4.07	0.42	10.14	8.27	4.53	0.36
lt223al1g3t1	2111	156	1200	8.75	20880	2.00	2514	4.38	0.48	9.78	8.31	4.81	0.41
lt223al1g3t1	1998	140	1070	9.81	24970	2.00	2702	4.07	0.40	10.62	9.24	4.54	0.34
lt223al1g3t1	2086	145	1020	10.29	24550	2.00	2771	3.97	0.37	11.03	8.86	4.44	0.32
lt223al1g4t1	2188	158	1070	9.81	21630	2.00	2640	4.17	0.41	10.66	8.19	4.62	0.35
lt223al1g4t1	2100	157	1000	10.50	21670	2.00	2501	4.40	0.40	11.38	8.66	4.83	0.35
lt223al1g4t1	2133	168	540	19.44	21870	2.00	2388	4.61	0.23	19.98	9.16	5.02	0.21
lt223al1g4t1	2055	170	710	14.79	20310	2.00	2206	4.99	0.32	15.61	9.20	5.37	0.30
lt223al1g4t2	2011	152	1030	10.19	22150	2.00	2442	4.50	0.42	11.14	9.07	4.93	0.37
lt223al1g4t2	2144	179	820	12.80	18630	2.00	2184	5.04	0.38	13.76	8.53	5.42	0.34
lt223al1g8t1	2105	143	890	11.80	25890	2.00	2882	3.82	0.31	12.40	8.98	4.31	0.27
lt223al1g8t1	2017	144	1050	10.00	24160	2.00	2646	4.16	0.40	10.83	9.13	4.61	0.35
lt223al1g8t1	2031	142	1150	9.13	24350	2.00	2720	4.04	0.42	9.99	8.95	4.51	0.36
lt223al1g8t2	2055	142	1110	9.46	24700	2.00	2773	3.97	0.40	10.26	8.91	4.44	0.35
lt223al1g8t2	2161	151	1120	9.38	22910	2.00	2753	4.00	0.41	10.19	8.32	4.47	0.35
lt223al1g8t2	2067	146	1140	9.21	23440	2.00	2680	4.10	0.43	10.08	8.75	4.57	0.37
lt223al1g8t2	1998	140	1130	9.29	24680	2.00	2695	4.08	0.42	10.15	9.16	4.55	0.36
lt223al1g8t2	2123	157	1150	9.13	21070	2.00	2528	4.35	0.45	10.11	8.33	4.79	0.39
lt223al1g8t3	2056	165	1000	10.50	19830	2.00	2267	4.85	0.44	11.57	8.75	5.25	0.39
lt223al1g8t3	2045	168	1090	9.63	18840	2.00	2192	5.02	0.50	10.86	8.59	5.40	0.43
lt223al1g8t3	2098	145	850	12.35	25230	2.00	2791	3.94	0.30	12.97	9.04	4.42	0.27
lt223al1g9t1	2010	92	1210	8.68	51010	2.00	5209	2.11	0.23	8.93	9.79	2.91	0.17
lt223al1g9t1	2060	95	1420	7.39	48180	2.00	5152	2.14	0.28	7.70	9.35	2.93	0.20
lt223al1g9t1	2033	90	1380	7.61	53450	2.00	5566	2.00	0.25	7.87	9.60	2.83	0.18
lt223al1g9t1	2122	111	950	11.05	39400	2.00	4271	2.58	0.22	11.35	9.23	3.26	0.18
lt223al1g9t1	1988	103	970	10.82	41960	2.00	4225	2.60	0.23	11.13	9.93	3.28	0.19
lt223al1g9t2	2134	117	610	17.21	37850	2.00	4010	2.74	0.15	17.43	9.44	3.39	0.13
lt223al1g9t2	2081	107	990	10.61	40740	2.00	4327	2.54	0.23	10.91	9.41	3.23	0.18
lt223al1g9t2	2106	110	1050	10.00	38970	2.00	4230	2.60	0.25	10.33	9.21	3.28	0.20
lt223al1g9t2	2169	105	910	11.54	44190	2.00	4843	2.27	0.19	11.76	9.12	3.03	0.14
lt223al1g9t2	2049	91	1340	7.84	52790	2.00	5535	2.00	0.24	8.09	9.54	2.83	0.17
lt223al1g9t2	2111	107	860	12.21	41860	2.00	4454	2.47	0.19	12.46	9.40	3.18	0.15
lt223al1g9t2	2159	108	990	10.61	41850	2.00	4613	2.38	0.21	10.87	9.07	3.11	0.17
lt223al1g9t2	2084	106	1060	9.91	41120	2.00	4396	2.50	0.24	10.22	9.35	3.20	0.19
lt223al1g11t1	2069	142	850	12.35	25900	2.00	2814	3.91	0.30	12.96	9.20	4.39	0.27
lt223al1g11t1	2111	154	750	14.00	23700	2.00	2622	4.20	0.29	14.62	9.04	4.65	0.26
lt223al1g11t1	2082	146	640	16.41	26060	2.00	2772	3.97	0.23	16.88	9.40	4.44	0.21
lt223al1g11t1	2047	177	540	19.44	19770	2.00	2084	5.28	0.26	20.15	9.49	5.64	0.24
lt223al1g11t1	2111	131	900	11.67	29820	2.00	3282	3.35	0.27	12.14	9.09	3.90	0.24
lt223al1g11t1	2015	123	870	12.07	31960	2.00	3312	3.32	0.26	12.52	9.65	3.88	0.23
lt223al1g11t1	2108	136	750	14.00	28540	2.00	3094	3.56	0.24	14.44	9.22	4.08	0.21
lt223al1g11t2	2136	141	880	11.93	26700	2.00	3004	3.66	0.29	12.48	8.89	4.17	0.26
lt223al1g11t2	2010	128	1080	9.72	29040	2.00	3103	3.54	0.35	10.35	9.36	4.07	0.30
lt223al1g11t2	2003	153	620	16.94	23910	2.00	2451	4.49	0.25	17.52	9.76	4.91	0.23
lt223al1g11t2	2136	127	1050	10.00	30720	2.00	3471	3.17	0.30	10.49	8.85	3.75	0.26
lt223al1g11t2	2150	153	900	11.67	23410	2.00	2703	4.07	0.33	12.36	8.66	4.53	0.30
lt223al1g11t2	2114	146	720	14.58	25800	2.00	2822	3.90	0.26	15.10	9.14	4.38	0.23
lt223al1g11t2	2188	157	700	15.00	23690	2.00	2704	4.07	0.26	15.54	8.76	4.53	0.23
lt223al1g11t2	2101	152	820	12.80	23790	2.00	2644	4.16	0.31	13.46	9.00	4.62	0.28

## ANEXO II (continuação)

REF	Idade Ma	Error Age Ma	U ppm	$\sigma$ %	Th ppm	$\sigma$ %	Pb ppm	$\sigma$ %	U/Pb	Error U/Pb %	Th/Pb	Error Th/Pb %	Corr.
lt223al2g2t1	2134	102	270	38.89	50290	2.00	5123	2.15	0.05	38.95	9.82	2.93	0.04
lt223al2g2t1	2088	97	440	23.86	52450	2.00	5279	2.08	0.08	23.95	9.94	2.89	0.06
lt223al2g2t1	2123	95	720	14.58	58190	2.00	6051	2.00	0.12	14.72	9.62	2.83	0.10
lt223al2g2t1	2037	91	810	12.96	58610	2.00	5861	2.00	0.14	13.12	10.00	2.83	0.11
lt223al2g2t1	2134	94	900	11.67	64410	2.00	6773	2.00	0.13	11.84	9.51	2.83	0.12
lt223al2g2t1	2116	100	410	25.61	50060	2.00	5106	2.15	0.08	25.70	9.80	2.94	0.06
lt223al2g2t1	2061	99	540	19.44	49020	2.00	4914	2.24	0.11	19.57	9.98	3.00	0.09
lt223al2g2t1	2044	101	680	15.44	46220	2.00	4654	2.36	0.15	15.62	9.93	3.10	0.12
lt223al2g2t1	2025	101	610	17.21	46890	2.00	4648	2.37	0.13	17.38	10.09	3.10	0.10
lt223al2g2t1	2125	103	370	28.38	48490	2.00	4959	2.22	0.07	28.46	9.78	2.99	0.06
lt223al2g2t2	2092	104	570	18.42	45600	2.00	4669	2.36	0.12	18.57	9.77	3.09	0.10
lt223al2g2t2	2099	101	570	18.42	48300	2.00	4950	2.22	0.12	18.55	9.76	2.99	0.09
lt223al2g2t2	2103	104	510	20.59	46290	2.00	4740	2.32	0.11	20.72	9.77	3.06	0.08
lt223al2g2t2	2054	90	790	13.29	66940	2.00	6704	2.00	0.12	13.44	9.98	2.83	0.11
lt223al2g2t2	2089	92	970	10.82	61900	2.00	6403	2.00	0.15	11.01	9.67	2.83	0.13
lt223al2g2t2	2102	93	1020	10.29	60840	2.00	6360	2.00	0.16	10.49	9.57	2.83	0.13
lt223al2g2t2	2078	92	880	11.93	60430	2.00	6189	2.00	0.14	12.10	9.76	2.83	0.12
lt223al2g2t2	2124	94	860	12.21	61260	2.00	6409	2.00	0.13	12.37	9.56	2.83	0.11
lt223al2g2t2	2058	95	850	12.35	50790	2.00	5190	2.12	0.16	12.53	9.79	2.91	0.12
lt223al2g2t2	2063	93	640	16.41	56290	2.00	5657	2.00	0.11	16.53	9.95	2.83	0.09
lt223al2g4t1	2174	136	1400	7.50	25750	2.00	3170	3.47	0.44	8.26	8.12	4.01	0.36
lt223al2g4t1	2082	139	1130	9.29	25690	2.00	2917	3.77	0.39	10.03	8.81	4.27	0.33
lt223al2g4t2	2092	119	1090	9.63	33600	2.00	3691	2.98	0.30	10.08	9.10	3.59	0.25
lt223al2g4t2	2077	127	1090	9.63	30000	2.00	3312	3.32	0.33	10.19	9.06	3.88	0.28
lt223al2g4t2	2013	125	1180	8.90	29570	2.00	3194	3.44	0.37	9.54	9.26	3.98	0.31
lt223al2g4t2	2042	128	1150	9.13	28920	2.00	3170	3.47	0.36	9.77	9.12	4.00	0.31
lt223al2g4t2	1988	123	1270	8.27	29790	2.00	3203	3.43	0.40	8.95	9.30	3.97	0.33
lt223al2g4t2	2006	128	1160	9.05	28470	2.00	3072	3.58	0.38	9.73	9.27	4.10	0.32
lt223al2g5t1	2039	158	470	22.34	23550	2.00	2411	4.56	0.19	22.80	9.77	4.98	0.18
lt223al2g5t1	1983	143	550	19.09	26460	2.00	2636	4.17	0.21	19.54	10.04	4.63	0.19
lt223al2g5t1	2036	144	680	15.44	26020	2.00	2717	4.05	0.25	15.96	9.58	4.52	0.23
lt223al2g5t1	2122	112	1080	9.72	37550	2.00	4136	2.66	0.26	10.08	9.08	3.33	0.21
lt223al2g5t1	2006	109	1340	7.84	36520	2.00	3888	2.83	0.34	8.33	9.39	3.46	0.28
lt223al2g5t1	2087	121	1290	8.14	31710	2.00	3571	3.08	0.36	8.70	8.88	3.67	0.30
lt223al2g5t1	2064	114	1150	9.13	35370	2.00	3829	2.87	0.30	9.57	9.24	3.50	0.25
lt223al2g5t1	2053	113	1070	9.81	36210	2.00	3859	2.85	0.28	10.22	9.38	3.48	0.23
lt223al2g5t1	2034	113	1040	10.10	35990	2.00	3789	2.90	0.27	10.51	9.50	3.53	0.23
lt223al2g6t1	2133	146	810	12.96	25590	2.00	2863	3.84	0.28	13.52	8.94	4.33	0.25
lt223al2g6t1	2111	129	610	17.21	31980	2.00	3386	3.25	0.18	17.52	9.44	3.81	0.16
lt223al2g6t1	2138	125	800	13.13	32890	2.00	3596	3.06	0.22	13.48	9.15	3.65	0.19
lt223al2g6t1	2140	129	520	20.19	32870	2.00	3490	3.15	0.15	20.44	9.42	3.73	0.13
lt223al2g6t1	2141	127	750	14.00	32210	2.00	3514	3.13	0.21	14.35	9.17	3.71	0.18
lt223al2g6t1	2090	126	820	12.80	31740	2.00	3405	3.23	0.24	13.21	9.32	3.80	0.21
lt223al2g6t1	2052	128	720	14.58	31350	2.00	3264	3.37	0.22	14.97	9.60	3.92	0.19
lt223al2g6t1	2138	129	870	12.07	30910	2.00	3424	3.21	0.25	12.49	9.03	3.78	0.22
lt223al2g6t1	2156	130	880	11.93	30650	2.00	3435	3.20	0.26	12.35	8.92	3.78	0.22
lt223al1g4t2	2175	178	910	11.54	18560	2.00	2248	4.89	0.40	12.53	8.26	5.29	0.36

**ANEXO II (continuação)**

REF	Idade Ma	Error Age Ma	U ppm	$\sigma$ %	Th ppm	$\sigma$ %	Pb ppm	$\sigma$ %	U/Pb	Error U/Pb %	Th/Pb	Error Th/Pb %	Corr.
<i>Grupo 2</i>													
lt223al1g1t2	2217	120	940	11.17	35350	2.00	4052	2.71	0.23	11.50	8.72	3.37	0.19
lt223al1g4t1	2232	177	610	17.21	20330	2.00	2375	4.63	0.26	17.83	8.56	5.04	0.24
lt223al2g4t1	2211	146	1090	9.63	24630	2.00	2989	3.68	0.36	10.31	8.24	4.19	0.31
lt223al1g4t2	2277	190	800	13.13	17580	2.00	2213	4.97	0.36	14.03	7.94	5.36	0.33
lt223al1g8t1	2194	141	800	13.13	27490	2.00	3143	3.50	0.25	13.58	8.75	4.03	0.22
lt223al1g8t2	2282	162	960	10.94	21940	2.00	2752	4.00	0.35	11.64	7.97	4.47	0.31
lt223al1g8t3	2190	176	790	13.29	19540	2.00	2317	4.75	0.34	14.11	8.43	5.15	0.31
lt223al1g9t2	2206	104	1090	9.63	44590	2.00	5044	2.18	0.22	9.88	8.84	2.96	0.16
lt223al1g11t1	2195	129	910	11.54	31140	2.00	3564	3.09	0.26	11.94	8.74	3.68	0.22
lt223al1g11t1	2277	165	670	15.67	22510	2.00	2686	4.10	0.25	16.20	8.38	4.56	0.23
lt223al1g11t2	2216	189	430	24.42	19240	2.00	2172	5.07	0.20	24.94	8.86	5.45	0.19
lt223al1g11t2	2219	138	840	12.50	28590	2.00	3312	3.32	0.25	12.93	8.63	3.88	0.22
<b>Leucossoma Granítico LT-223B</b>													
lt223bl1g1t1	2095	109	570	18.42	41900	2.00	4315	2.55	0.13	18.60	9.71	3.24	0.11
lt223bl1g1t1	2032	109	470	22.34	42000	2.00	4149	2.65	0.11	22.50	10.12	3.32	0.09
lt223bl1g1t1	2071	111	420	25.00	41360	2.00	4154	2.65	0.10	25.14	9.96	3.32	0.08
lt223bl1g1t1	2034	110	540	19.44	40470	2.00	4034	2.73	0.13	19.63	10.03	3.38	0.11
lt223bl1g1t1	2057	115	610	17.21	38050	2.00	3876	2.84	0.16	17.45	9.82	3.47	0.13
lt223bl1g1t1	2187	114	530	19.81	40970	2.00	4407	2.50	0.12	19.97	9.30	3.20	0.10
lt223bl1g1t1	2114	112	410	25.61	41580	2.00	4264	2.58	0.10	25.74	9.75	3.26	0.08
lt223bl1g1t1	2172	109	560	18.75	43660	2.00	4659	2.36	0.12	18.90	9.37	3.09	0.10
lt223bl1g1t1	2085	104	530	19.81	45870	2.00	4663	2.36	0.11	19.95	9.84	3.09	0.09
lt223bl1g1t1	2015	99	470	22.34	49140	2.00	4784	2.30	0.10	22.46	10.27	3.05	0.08
lt223bl1g1t2	2122	103	530	19.81	47380	2.00	4901	2.24	0.11	19.94	9.67	3.01	0.08
lt223bl1g1t2	2176	112	400	26.25	42450	2.00	4483	2.45	0.09	26.36	9.47	3.17	0.07
lt223bl1g1t2	2123	121	370	28.38	36750	2.00	3788	2.90	0.10	28.53	9.70	3.53	0.08
lt223bl1g1t2	2164	116	190	55.26	41160	2.00	4243	2.59	0.04	55.32	9.70	3.27	0.04
lt223bl1g1t2	2029	100	710	14.79	46880	2.00	4692	2.34	0.15	14.97	9.99	3.08	0.12
lt223bl1g1t2	2036	99	910	11.54	46530	2.00	4748	2.32	0.19	11.77	9.80	3.06	0.15
lt223bl1g1t2	2035	101	760	13.82	45960	2.00	4637	2.37	0.16	14.02	9.91	3.10	0.13
lt223bl1g1t2	2119	101	340	30.88	50440	2.00	5126	2.15	0.07	30.96	9.84	2.93	0.05
lt223bl1g2t1	2131	128	350	30.00	34150	2.00	3537	3.11	0.10	30.16	9.65	3.70	0.09
lt223bl1g2t1	2067	108	770	13.64	41310	2.00	4269	2.58	0.18	13.88	9.68	3.26	0.15
lt223bl1g2t1	2089	112	840	12.50	38790	2.00	4097	2.68	0.21	12.79	9.47	3.35	0.17
lt223bl1g2t1	2059	107	820	12.80	41570	2.00	4296	2.56	0.19	13.06	9.68	3.25	0.15
lt223bl1g2t1	2092	102	860	12.21	45220	2.00	4741	2.32	0.18	12.43	9.54	3.06	0.14
lt223bl1g2t1	2082	105	890	11.80	42910	2.00	4503	2.44	0.20	12.05	9.53	3.16	0.16
lt223bl1g2t2	2109	104	950	11.05	43570	2.00	4653	2.36	0.20	11.30	9.36	3.10	0.16
lt223bl1g2t2	2097	109	710	14.79	41620	2.00	4344	2.53	0.16	15.00	9.58	3.23	0.13
lt223bl1g2t2	2098	115	770	13.64	37730	2.00	3986	2.76	0.19	13.91	9.46	3.41	0.16
lt223bl1g2t2	2073	127	720	14.58	31760	2.00	3340	3.29	0.22	14.95	9.51	3.85	0.19
lt223bl1g2t2	2063	104	920	11.41	43010	2.00	4480	2.46	0.21	11.67	9.60	3.17	0.16
lt223bl1g2t2	2174	113	680	15.44	39980	2.00	4337	2.54	0.16	15.65	9.22	3.23	0.13
lt223bl1g2t2	2050	113	590	17.80	38740	2.00	3920	2.81	0.15	18.02	9.88	3.45	0.13
lt223bl1g2t2	2025	115	590	17.80	37320	2.00	3735	2.94	0.16	18.04	9.99	3.56	0.14
lt223bl1g2t2	2035	114	930	11.29	36490	2.00	3799	2.90	0.24	11.66	9.61	3.52	0.20
lt223bl1g4t1	2133	115	640	16.41	38780	2.00	4114	2.67	0.16	16.62	9.43	3.34	0.13
lt223bl1g4t1	2148	109	760	13.82	42210	2.00	4536	2.43	0.17	14.03	9.31	3.14	0.13
lt223bl1g4t1	2135	115	510	20.59	39410	2.00	4130	2.66	0.12	20.76	9.54	3.33	0.10

**ANEXO II (continuação)**

REF	Idade Ma	Error Age Ma	U ppm	$\sigma$ %	Th ppm	$\sigma$ %	Pb ppm	$\sigma$ %	U/Pb	Error U/Pb %	Th/Pb	Error Th/Pb %	Corr.
lt223bl1g4t1	2165	117	510	20.59	38490	2.00	4099	2.68	0.12	20.76	9.39	3.35	0.10
lt223bl1g4t1	2162	128	340	30.88	34410	2.00	3615	3.04	0.09	31.03	9.52	3.64	0.08
lt223bl1g4t1	2087	122	550	19.09	34940	2.00	3610	3.05	0.15	19.33	9.68	3.64	0.13
lt223bl1g4t1	2096	120	490	21.43	36560	2.00	3763	2.92	0.13	21.63	9.72	3.54	0.11
lt223bl1g4t1	2046	107	850	12.35	41050	2.00	4228	2.60	0.20	12.62	9.71	3.28	0.16
lt223bl1g5t1	2092	100	490	21.43	49650	2.00	5037	2.18	0.10	21.54	9.86	2.96	0.07
lt223bl1g5t2	2073	93	700	15.00	57000	2.00	5775	2.00	0.12	15.13	9.87	2.83	0.09
lt223bl1g5t2	2065	106	560	18.75	43480	2.00	4397	2.50	0.13	18.92	9.89	3.20	0.10
lt223bl1g5t2	2129	96	810	12.96	54750	2.00	5760	2.00	0.14	13.12	9.51	2.83	0.11
lt223bl1g5t3	2128	99	570	18.42	50550	2.00	5247	2.10	0.11	18.54	9.63	2.90	0.08
lt223bl1g5t3	2113	102	540	19.44	48110	2.00	4955	2.22	0.11	19.57	9.71	2.99	0.08
lt223bl1g5t3	2114	94	650	16.15	60620	2.00	6237	2.00	0.10	16.28	9.72	2.83	0.09
lt223bl1g5t3	2147	97	590	17.80	57330	2.00	5986	2.00	0.10	17.91	9.58	2.83	0.08
lt223bl1g5t4	2075	88	780	13.46	107070	2.00	10662	2.00	0.07	13.61	10.04	2.83	0.10
lt223bl1g5t4	2065	97	670	15.67	50660	2.00	5129	2.14	0.13	15.82	9.88	2.93	0.10
lt223bl1g5t4	2103	104	500	21.00	46270	2.00	4736	2.32	0.11	21.13	9.77	3.07	0.08
lt223bl1g5t4	2054	95	820	12.80	51260	2.00	5212	2.11	0.16	12.98	9.84	2.91	0.12
lt223bl1g5t4	2054	98	470	22.34	50950	2.00	5056	2.18	0.09	22.45	10.08	2.96	0.07
lt223bl1g5t5	2085	95	610	17.21	53710	2.00	5456	2.02	0.11	17.33	9.84	2.84	0.08
lt223bl1g5t5	2103	91	690	15.22	89570	2.00	9062	2.00	0.08	15.35	9.88	2.83	0.09
lt223bl1g5t5	2152	107	550	19.09	44750	2.00	4718	2.33	0.12	19.23	9.48	3.07	0.09
lt223bl1g5t5	2024	103	650	16.15	44420	2.00	4426	2.49	0.15	16.34	10.04	3.19	0.12
lt223bl1g6t1	2088	101	710	14.79	47470	2.00	4895	2.25	0.15	14.96	9.70	3.01	0.11
lt223bl1g6t1	2051	97	440	23.86	51770	2.00	5114	2.15	0.09	23.96	10.12	2.94	0.07
lt223bl1g6t1	2066	94	860	12.21	52230	2.00	5355	2.05	0.16	12.38	9.75	2.87	0.12
lt223bl1g6t1	2165	100	460	22.83	51430	2.00	5392	2.04	0.09	22.92	9.54	2.86	0.06
lt223bl1g6t1	2101	95	460	22.83	54790	2.00	5552	2.00	0.08	22.91	9.87	2.83	0.06
lt223bl1g6t1	2155	96	990	10.61	56070	2.00	6039	2.00	0.16	10.79	9.28	2.83	0.13
lt223bl1g6t1	2104	95	710	14.79	54230	2.00	5599	2.00	0.13	14.92	9.69	2.83	0.09
lt223bl1g6t1	2144	99	690	15.22	50550	2.00	5336	2.06	0.13	15.36	9.47	2.87	0.10
lt223bl1g6t1	2091	100	530	19.81	49420	2.00	5027	2.19	0.11	19.93	9.83	2.96	0.08
lt223bl1g6t1	2057	94	270	38.89	56430	2.00	5516	2.00	0.05	38.94	10.23	2.83	0.04
lt223bl1g6t2	2103	94	1080	9.72	55330	2.00	5843	2.00	0.18	9.93	9.47	2.83	0.14
lt223bl1g6t2	2058	99	350	30.00	50040	2.00	4934	2.23	0.07	30.08	10.14	3.00	0.06
lt223bl1g6t2	2099	96	740	14.19	51560	2.00	5334	2.06	0.14	14.34	9.67	2.87	0.10
lt223bl1g6t2	2102	94	780	13.46	57770	2.00	5967	2.00	0.13	13.61	9.68	2.83	0.10
lt223bl1g6t2	2158	97	780	13.46	54050	2.00	5763	2.00	0.14	13.61	9.38	2.83	0.10
lt223bl1g6t2	2110	97	560	18.75	52140	2.00	5354	2.05	0.10	18.86	9.74	2.87	0.08
lt223bl1g6t2	2042	95	670	15.67	52270	2.00	5223	2.11	0.13	15.81	10.01	2.90	0.10
lt223bl1g6t2	2102	95	480	21.88	54420	2.00	5525	2.00	0.09	21.97	9.85	2.83	0.06
lt223bl1g7t1	2082	101	790	13.29	46530	2.00	4819	2.28	0.16	13.49	9.66	3.03	0.13
lt223bl1g7t1	2078	111	740	14.19	39430	2.00	4100	2.68	0.18	14.44	9.62	3.35	0.15
lt223bl1g7t1	2083	96	850	12.35	51290	2.00	5306	2.07	0.16	12.53	9.67	2.88	0.12
lt223bl1g7t1	2074	101	800	13.13	46500	2.00	4798	2.29	0.17	13.32	9.69	3.04	0.13
lt223bl1g7t1	2041	102	640	16.41	45520	2.00	4567	2.41	0.14	16.58	9.97	3.13	0.11
lt223bl1g7t2	2101	114	770	13.64	38100	2.00	4029	2.73	0.19	13.91	9.46	3.38	0.16
lt223bl1g7t3	2171	107	1040	10.10	42450	2.00	4720	2.33	0.22	10.36	8.99	3.07	0.17
lt223bl1g7t3	2093	106	870	12.07	42860	2.00	4517	2.44	0.19	12.31	9.49	3.15	0.15
lt223bl1g7t3	2156	107	900	11.67	42990	2.00	4687	2.35	0.19	11.90	9.17	3.08	0.15
lt223bl1g7t3	2055	109	640	16.41	40910	2.00	4157	2.65	0.15	16.62	9.84	3.32	0.13
lt223bl1g9t1	2039	100	900	11.67	46050	2.00	4706	2.34	0.19	11.90	9.78	3.08	0.15
lt223bl1g9t1	2066	99	850	12.35	48060	2.00	4948	2.22	0.17	12.55	9.71	2.99	0.13

**ANEXO II (continuação)**

REF	Idade Ma	Error Age Ma	U ppm	$\sigma$ %	Th ppm	$\sigma$ %	Pb ppm	$\sigma$ %	U/Pb	Error U/Pb %	Th/Pb	Error Th/Pb %	Corr.
lt223bl1g9t1	2056	98	510	20.59	50230	2.00	5008	2.20	0.10	20.71	10.03	2.97	0.08
lt223bl1g9t1	2060	101	660	15.91	47030	2.00	4764	2.31	0.14	16.08	9.87	3.05	0.11
lt223bl1g9t1	2057	103	880	11.93	43880	2.00	4535	2.43	0.19	12.18	9.68	3.14	0.15
lt223bl1g9t1	2141	106	490	21.43	45670	2.00	4762	2.31	0.10	21.55	9.59	3.06	0.08
lt223bl1g9t1	2083	97	720	14.58	50980	2.00	5227	2.10	0.14	14.73	9.75	2.90	0.10
lt223bl1g9t2	2175	95	70	100.00	58130	2.00	5946	2.00	0.01	100.0	9.78	2.83	0.01
lt223bl1g9t2	2141	107	560	18.75	44150	2.00	4637	2.37	0.12	18.90	9.52	3.10	0.10
lt223bl1g9t2	2103	106	650	16.15	44040	2.00	4572	2.41	0.14	16.33	9.63	3.13	0.11
lt223bl1g9t2	2078	101	720	14.58	46730	2.00	4802	2.29	0.15	14.76	9.73	3.04	0.12
lt223bl1g9t2	2107	101	570	18.42	48480	2.00	4990	2.20	0.11	18.55	9.72	2.98	0.09
lt223bl1g9t2	2073	104	590	17.80	45250	2.00	4597	2.39	0.13	17.96	9.84	3.12	0.10
lt223bl1g9t2	2109	101	540	19.44	48330	2.00	4967	2.21	0.11	19.57	9.73	2.98	0.08
lt223bl1g9t2	2115	105	860	12.21	43590	2.00	4635	2.37	0.19	12.44	9.40	3.10	0.15
lt223bl1g9t2	2030	110	470	22.34	41240	2.00	4074	2.70	0.12	22.50	10.12	3.36	0.10
lt223bl1g10t1	2069	99	530	19.81	49840	2.00	5010	2.20	0.11	19.93	9.95	2.97	0.08
lt223bl1g10t1	2052	108	560	18.75	42390	2.00	4264	2.58	0.13	18.93	9.94	3.26	0.11
lt223bl1g10t1	2055	92	710	14.79	59960	2.00	6009	2.00	0.12	14.92	9.98	2.83	0.09
lt223bl1g10t1	2105	94	450	23.33	61190	2.00	6188	2.00	0.07	23.42	9.89	2.83	0.06
lt223bl1g10t1	2077	101	440	23.86	48290	2.00	4847	2.27	0.09	23.97	9.96	3.02	0.07
lt223bl1g10t1	2070	102	540	19.44	46900	2.00	4732	2.32	0.11	19.58	9.91	3.07	0.09
lt223bl1g10t1	2072	111	430	24.42	41380	2.00	4161	2.64	0.10	24.56	9.94	3.31	0.09
lt223bl1g10t1	2187	115	460	22.83	40550	2.00	4336	2.54	0.11	22.97	9.35	3.23	0.09
lt223bl1g10t2	2127	105	450	23.33	46660	2.00	4812	2.29	0.09	23.45	9.70	3.04	0.07
lt223bl1g10t2	2074	109	420	25.00	42520	2.00	4273	2.57	0.10	25.13	9.95	3.26	0.08
lt223bl1g10t2	2123	96	590	17.80	56910	2.00	5874	2.00	0.10	17.91	9.69	2.83	0.08
lt223bl1g10t2	2062	92	520	20.19	60320	2.00	5997	2.00	0.09	20.29	10.06	2.83	0.07
lt223bl1g10t2	2073	94	560	18.75	55660	2.00	5595	2.00	0.10	18.86	9.95	2.83	0.07
lt223bl1g10t2	2092	102	410	25.61	47860	2.00	4831	2.28	0.08	25.71	9.91	3.03	0.07
lt223bl1g10t2	2152	105	550	19.09	45970	2.00	4841	2.27	0.11	19.23	9.50	3.03	0.09
lt223bl1g10t2	2066	115	570	18.42	38010	2.00	3875	2.84	0.15	18.64	9.81	3.47	0.12

**Gnaiss Tonalítico LT-123A***Grupo 1*

lt123al1g1t1	1983	85	1950	5.38	61020	2.00	6316	2.00	0.31	5.74	9.66	2.83	0.25
lt123al1g1t1	2011	86	1990	5.28	72280	2.00	7482	2.00	0.27	5.64	9.66	2.83	0.25
lt123al1g1t1	2057	86	2160	4.86	87830	2.00	9219	2.00	0.23	5.26	9.53	2.83	0.27
lt123al1g1t1	2029	87	1930	5.44	61370	2.00	6499	2.00	0.30	5.80	9.44	2.83	0.24
lt123al1g1t1	1988	84	1950	5.38	79230	2.00	8019	2.00	0.24	5.74	9.88	2.83	0.25
lt123al1g1t1	2064	110	1340	7.84	36600	2.00	4018	2.74	0.33	8.30	9.11	3.39	0.27
lt123al1g1t1	2059	114	1690	6.21	32700	2.00	3759	2.93	0.45	6.87	8.70	3.54	0.35
lt123al1g1t1	1990	104	1500	7.00	38700	2.00	4112	2.67	0.36	7.49	9.41	3.34	0.29
lt123al1g1t1	1972	111	2100	5.00	30880	2.00	3561	3.09	0.59	5.88	8.67	3.68	0.44
lt123al1g1t2	2027	89	1660	6.33	52170	2.00	5527	2.00	0.30	6.63	9.44	2.83	0.21
lt123al1g1t2	2012	105	1620	6.48	37380	2.00	4080	2.70	0.40	7.02	9.16	3.36	0.31
lt123al1g1t2	2050	102	1460	7.19	41130	2.00	4466	2.46	0.33	7.60	9.21	3.17	0.25
lt123al1g1t2	2022	86	2000	5.25	71520	2.00	7456	2.00	0.27	5.62	9.59	2.83	0.25
lt123al1g1t2	2078	88	2060	5.10	82000	2.00	8721	2.00	0.24	5.48	9.40	2.83	0.26
lt123al1g1t2	2063	89	1900	5.53	57070	2.00	6193	2.00	0.31	5.88	9.21	2.83	0.24
lt123al1g2t1	1990	96	1420	7.39	45580	2.00	4723	2.33	0.30	7.75	9.65	3.07	0.23
lt123al1g2t1	1980	83	2470	4.25	78240	2.00	8073	2.00	0.31	4.70	9.69	2.83	0.30
lt123al1g2t1	2039	103	1630	6.44	39400	2.00	4336	2.54	0.38	6.92	9.09	3.23	0.29

**ANEXO II (continuação)**

REF	Idade Ma	Error Age Ma	U ppm	$\sigma$ %	Th ppm	$\sigma$ %	Pb ppm	$\sigma$ %	U/Pb	Error U/Pb %	Th/Pb	Error Th/Pb %	Corr.
lt123al1g2t1	2058	102	1430	7.34	41380	2.00	4497	2.45	0.32	7.74	9.20	3.16	0.24
lt123al1g2t1	1969	84	1860	5.65	76810	2.00	7684	2.00	0.24	5.99	10.00	2.83	0.24
lt123al1g2t1	2060	88	2040	5.15	67200	2.00	7207	2.00	0.28	5.52	9.32	2.83	0.26
lt123al1g2t2	1991	105	1740	6.03	36260	2.00	3973	2.77	0.44	6.64	9.13	3.42	0.34
lt123al1g2t2	2081	100	1800	5.83	41690	2.00	4719	2.33	0.38	6.28	8.83	3.07	0.28
lt123al1g2t2	2012	111	1510	6.95	34280	2.00	3752	2.93	0.40	7.55	9.14	3.55	0.32
lt123al1g2t2	1967	113	1490	7.05	33130	2.00	3548	3.10	0.42	7.70	9.34	3.69	0.34
lt123al1g2t2	2019	99	1700	6.18	41470	2.00	4510	2.44	0.38	6.64	9.20	3.15	0.28
lt123al1g2t2	2087	104	1460	7.19	40690	2.00	4509	2.44	0.32	7.59	9.02	3.15	0.25
lt123al1g2t2	2029	102	1490	7.05	40930	2.00	4408	2.50	0.34	7.48	9.29	3.20	0.26
lt123al1g2t2	2036	87	2060	5.10	66040	2.00	7014	2.00	0.29	5.48	9.42	2.83	0.26
lt123al1g2t2	2032	86	2260	4.65	66270	2.00	7093	2.00	0.32	5.06	9.34	2.83	0.28
lt123al1g2t3	1996	84	2830	3.71	71670	2.00	7658	2.00	0.37	4.21	9.36	2.83	0.34
lt123al1g2t3	2032	88	1780	5.90	56890	2.00	6032	2.00	0.30	6.23	9.43	2.83	0.23
lt123al1g2t3	2084	103	1570	6.69	40220	2.00	4497	2.45	0.35	7.12	8.94	3.16	0.27
lt123al1g2t3	2057	88	1900	5.53	65380	2.00	6969	2.00	0.27	5.88	9.38	2.83	0.24
lt123al1g2t3	2027	86	2160	4.86	72760	2.00	7652	2.00	0.28	5.26	9.51	2.83	0.27
lt123al1g2t3	2046	88	1940	5.41	65760	2.00	6981	2.00	0.28	5.77	9.42	2.83	0.25
lt123al1g2t3	1998	86	1710	6.14	63400	2.00	6504	2.00	0.26	6.46	9.75	2.83	0.22
lt123al1g5t1	1962	101	1680	6.25	38930	2.00	4134	2.66	0.41	6.79	9.42	3.33	0.31
lt123al1g5t1	2001	109	1220	8.61	37290	2.00	3908	2.81	0.31	9.06	9.54	3.45	0.25
lt123al1g5t1	2052	94	1050	10.00	50640	2.00	5233	2.10	0.20	10.22	9.68	2.90	0.15
lt123al1g5t1	2062	133	1110	9.46	27540	2.00	3057	3.60	0.36	10.12	9.01	4.12	0.31
lt123al1g5t1	2063	98	1480	7.09	44340	2.00	4812	2.29	0.31	7.45	9.21	3.04	0.23
lt123al1g5t2	2082	89	2500	4.20	55600	2.00	6334	2.00	0.39	4.65	8.78	2.83	0.30
lt123al1g5t2	2069	93	1740	6.03	47730	2.00	5250	2.10	0.33	6.39	9.09	2.90	0.24
lt123al1g5t2	2052	141	1200	8.75	24400	2.00	2773	3.97	0.43	9.61	8.80	4.44	0.37
lt123al1g5t2	2007	128	1140	9.21	28510	2.00	3070	3.58	0.37	9.88	9.29	4.10	0.32
lt123al1g5t2	2020	116	1460	7.19	32450	2.00	3577	3.08	0.41	7.82	9.07	3.67	0.33
lt123al1g5t2	2017	109	1570	6.69	35330	2.00	3880	2.83	0.40	7.26	9.11	3.47	0.32
lt123al1g6t1	1987	88	2030	5.17	50050	2.00	5343	2.06	0.38	5.57	9.37	2.87	0.27
lt123al1g6t1	2105	100	1540	6.82	43220	2.00	4830	2.28	0.32	7.19	8.95	3.03	0.24
lt123al1g6t1	2027	93	1610	6.52	47620	2.00	5077	2.17	0.32	6.87	9.38	2.95	0.23
lt123al1g6t1	2034	88	1980	5.30	54350	2.00	5869	2.00	0.34	5.67	9.26	2.83	0.25
lt123al1g6t1	2085	88	2440	4.30	80290	2.00	8725	2.00	0.28	4.75	9.20	2.83	0.30
lt123al1g6t2	2101	91	1830	5.74	58540	2.00	6433	2.00	0.28	6.08	9.10	2.83	0.23
lt123al1g6t2	2059	111	1350	7.78	35860	2.00	3940	2.79	0.34	8.26	9.10	3.43	0.27
lt123al1g6t2	2021	98	1860	5.65	41900	2.00	4613	2.38	0.40	6.13	9.08	3.11	0.30
lt123al1g6t2	1994	85	1990	5.28	73850	2.00	7558	2.00	0.26	5.64	9.77	2.83	0.25
lt123al1g6t2	1995	95	1360	7.72	46520	2.00	4802	2.29	0.28	8.05	9.69	3.04	0.21
lt123al1g6t2	2045	96	1740	6.03	44610	2.00	4886	2.25	0.36	6.44	9.13	3.01	0.26
lt123al1g6t2	2051	86	3150	3.33	51900	2.00	6112	2.00	0.52	3.89	8.49	2.83	0.36
lt123al1g6t3	2002	97	1660	6.33	43380	2.00	4634	2.37	0.36	6.76	9.36	3.10	0.27
lt123al1g6t3	2023	94	1830	5.74	45610	2.00	4957	2.22	0.37	6.15	9.20	2.99	0.27
lt123al1g7t1	2077	130	1650	6.36	25820	2.00	3113	3.53	0.53	7.28	8.29	4.06	0.42
lt123al1g7t1	2023	129	1530	6.86	26510	2.00	3047	3.61	0.50	7.75	8.70	4.13	0.41
lt123al1g7t1	2053	132	1390	7.55	26200	2.00	3016	3.65	0.46	8.39	8.69	4.16	0.38
lt123al1g7t1	1968	99	1470	7.14	41940	2.00	4351	2.53	0.34	7.58	9.64	3.22	0.26
lt123al1g7t1	2009	86	2060	5.10	59740	2.00	6322	2.00	0.33	5.48	9.45	2.83	0.26
lt123al1g7t1	2070	95	1950	5.38	44600	2.00	5028	2.19	0.39	5.81	8.87	2.96	0.28
lt123al1g7t1	2073	106	1630	6.44	38120	2.00	4290	2.56	0.38	6.93	8.89	3.25	0.29
lt123al1g7t1	1979	94	1850	5.68	44040	2.00	4703	2.34	0.39	6.14	9.36	3.08	0.29

## ANEXO II (continuação)

REF	Idade Ma	Error Age Ma	U ppm	$\sigma$ %	Th ppm	$\sigma$ %	Pb ppm	$\sigma$ %	U/Pb	Error U/Pb %	Th/Pb	Error Th/Pb %	Corr.
lt123al1g7t1	2042	101	2960	3.55	32770	2.00	4192	2.62	0.71	4.41	7.82	3.30	0.47
lt123al1g7t1	2093	96	2010	5.22	44150	2.00	5066	2.17	0.40	5.66	8.71	2.95	0.28
lt123al2g1t1	2033	119	1390	7.55	31150	2.00	3453	3.19	0.40	8.20	9.02	3.76	0.33
lt123al2g1t1	2074	130	1410	7.45	26970	2.00	3132	3.51	0.45	8.23	8.61	4.04	0.37
lt123al2g1t1	2084	148	1010	10.40	23680	2.00	2679	4.11	0.38	11.18	8.84	4.57	0.33
lt123al2g1t1	2021	146	1130	9.29	23160	2.00	2586	4.25	0.44	10.22	8.96	4.70	0.38
lt123al2g1t1	2052	121	1480	7.09	30020	2.00	3412	3.22	0.43	7.79	8.80	3.79	0.35
lt123al2g1t1	1995	127	1460	7.19	27070	2.00	3029	3.63	0.48	8.06	8.94	4.15	0.39
lt123al2g1t2	2035	87	1940	5.41	66430	2.00	7005	2.00	0.28	5.77	9.48	2.83	0.25
lt123al2g1t2	2092	106	1530	6.86	38910	2.00	4374	2.51	0.35	7.31	8.90	3.21	0.27
lt123al2g1t2	2048	150	1050	10.00	22800	2.00	2560	4.30	0.41	10.88	8.91	4.74	0.36
lt123al2g1t2	2033	98	1790	5.87	42620	2.00	4684	2.35	0.38	6.32	9.10	3.08	0.28
lt123al2g1t2	2086	99	1620	6.48	43060	2.00	4798	2.29	0.34	6.87	8.97	3.04	0.25
lt123al2g2t1	2009	103	1800	5.83	37790	2.00	4176	2.63	0.43	6.40	9.05	3.31	0.33
lt123al2g2t1	1981	107	1520	6.91	36370	2.00	3884	2.83	0.39	7.47	9.36	3.47	0.31
lt123al2g2t1	2048	88	1820	5.77	70710	2.00	7417	2.00	0.25	6.11	9.53	2.83	0.23
lt123al2g2t1	2093	108	1750	6.00	36250	2.00	4198	2.62	0.42	6.55	8.64	3.30	0.32
lt123al2g2t1	2070	110	1760	5.97	34760	2.00	4007	2.75	0.44	6.57	8.67	3.40	0.34
lt123al2g2t1	2031	83	4480	2.34	40720	2.00	5464	2.01	0.82	3.09	7.45	2.84	0.46
lt123al2g2t2	2054	89	2100	5.00	50380	2.00	5595	2.00	0.38	5.39	9.00	2.83	0.26
lt123al2g2t2	2083	92	1570	6.69	52130	2.00	5654	2.00	0.28	6.98	9.22	2.83	0.20
lt123al2g2t2	2093	102	1650	6.36	40710	2.00	4597	2.39	0.36	6.80	8.86	3.12	0.27
lt123al2g2t2	1965	107	1730	6.07	35260	2.00	3821	2.88	0.45	6.72	9.23	3.51	0.35
lt123al2g2t2	2059	100	1680	6.25	41770	2.00	4627	2.38	0.36	6.69	9.03	3.11	0.27
lt123al2g2t2	2097	115	1570	6.69	33100	2.00	3831	2.87	0.41	7.28	8.64	3.50	0.32
lt123al2g2t2	2062	109	1380	7.61	36900	2.00	4057	2.71	0.34	8.08	9.10	3.37	0.27
lt123al2g3t1	1987	83	3670	2.86	50890	2.00	5992	2.00	0.61	3.49	8.49	2.83	0.41
lt123al2g3t1	2068	87	1800	5.83	106240	2.00	10919	2.00	0.16	6.17	9.73	2.83	0.23
lt123al2g3t1	2049	171	650	16.15	20340	2.00	2181	5.04	0.30	16.92	9.33	5.43	0.28
lt123al2g3t1	2011	104	1410	7.45	39110	2.00	4165	2.64	0.34	7.90	9.39	3.31	0.27
lt123al2g3t1	2103	96	1520	6.91	47490	2.00	5239	2.10	0.29	7.22	9.06	2.90	0.21
lt123al2g3t1	2087	92	1730	6.07	51430	2.00	5656	2.00	0.31	6.39	9.09	2.83	0.22
lt123al2g3t2	2014	99	1840	5.71	41020	2.00	4505	2.44	0.41	6.21	9.11	3.16	0.30
lt123al2g3t2	2023	106	1710	6.14	36570	2.00	4061	2.71	0.42	6.71	9.01	3.37	0.32
lt123al2g3t2	2083	132	1040	10.10	28200	2.00	3129	3.51	0.33	10.69	9.01	4.04	0.29
lt123al2g3t2	2051	172	630	16.67	20160	2.00	2159	5.10	0.29	17.43	9.34	5.47	0.27
lt123al2g3t2	1971	100	1060	9.91	43320	2.00	4342	2.53	0.24	10.22	9.98	3.23	0.19
lt123al2g3t2	2011	95	1460	7.19	46830	2.00	4907	2.24	0.30	7.53	9.54	3.00	0.22
lt123al2g3t2	2079	91	1790	5.87	54980	2.00	6001	2.00	0.30	6.20	9.16	2.83	0.23
lt123al2g3t2	2043	104	1590	6.60	38900	2.00	4282	2.57	0.37	7.09	9.08	3.26	0.29
<i>Grupo 2</i>													
lt123al1g1t1	2148	94	1640	6.40	52310	2.00	5890	2.00	0.28	6.71	8.88	2.83	0.21
lt123al1g1t1	2112	91	1900	5.53	60330	2.00	6674	2.00	0.28	5.88	9.04	2.83	0.24
lt123al1g1t1	2120	104	1470	7.14	40670	2.00	4589	2.40	0.32	7.53	8.86	3.12	0.24
lt123al1g2t1	2143	90	2610	4.02	70730	2.00	8094	2.00	0.32	4.49	8.74	2.83	0.31
lt123al1g5t1	2137	148	990	10.61	24250	2.00	2804	3.92	0.35	11.31	8.65	4.40	0.31
lt123al1g5t1	2150	95	1410	7.45	53060	2.00	5883	2.00	0.24	7.71	9.02	2.83	0.18
lt123al1g5t1	2117	94	1520	6.91	49970	2.00	5522	2.00	0.28	7.19	9.05	2.83	0.20
lt123al1g5t1	2115	98	1410	7.45	45810	2.00	5062	2.17	0.28	7.76	9.05	2.95	0.21
lt123al1g5t2	2156	107	1650	6.36	38630	2.00	4537	2.42	0.36	6.81	8.51	3.14	0.27
lt123al1g5t2	2121	114	1560	6.73	33930	2.00	3957	2.78	0.39	7.28	8.57	3.42	0.31

**ANEXO II (continuação)**

REF	Idade Ma	Error Age Ma	U ppm	$\sigma$ %	Th ppm	$\sigma$ %	Pb ppm	$\sigma$ %	U/Pb	Error U/Pb %	Th/Pb	Error Th/Pb %	Corr.
lt123al1g6t1	2119	107	1690	6.21	37670	2.00	4373	2.52	0.39	6.70	8.62	3.21	0.29
lt123al1g6t1	2134	123	1170	8.97	31560	2.00	3598	3.06	0.33	9.48	8.77	3.65	0.27
lt123al1g6t2	2144	95	1590	6.60	51070	2.00	5735	2.00	0.28	6.90	8.90	2.83	0.20
lt123al1g6t2	2120	97	1640	6.40	45630	2.00	5145	2.14	0.32	6.75	8.87	2.93	0.23
lt123al1g6t4	2115	94	1860	5.65	47540	2.00	5405	2.04	0.34	6.00	8.80	2.85	0.24
lt123al1g6t4	2113	95	1840	5.71	46290	2.00	5266	2.09	0.35	6.08	8.79	2.89	0.25
lt123al2g1t1	2140	110	1420	7.39	37150	2.00	4265	2.58	0.33	7.83	8.71	3.26	0.26
lt123al2g1t2	2131	116	1430	7.34	33850	2.00	3920	2.81	0.36	7.86	8.64	3.45	0.29
lt123al2g1t2	2173	140	1080	9.72	26090	2.00	3077	3.58	0.35	10.36	8.48	4.10	0.30
lt123al2g2t1	2167	112	1610	6.52	35480	2.00	4227	2.60	0.38	7.02	8.39	3.28	0.29
lt123al2g2t2	2137	109	1710	6.14	36540	2.00	4309	2.55	0.40	6.65	8.48	3.24	0.30
lt123al2g3t1	2171	165	710	14.79	21750	2.00	2489	4.42	0.29	15.44	8.74	4.85	0.26
lt123al2g3t2	2115	96	1830	5.74	45670	2.00	5206	2.11	0.35	6.11	8.77	2.91	0.25
lt123al2g3t2	2116	165	620	16.94	21950	2.00	2406	4.57	0.26	17.54	9.12	4.99	0.24

**Gnaiss Granítico MV-10A***Grupo 1*

mv0lag1t1	2033	81	16750	2.00	81380	2.00	13730	2.00	1.22	2.83	5.93	2.83	0.50
mv0lag1t1	2043	82	16440	2.00	81550	2.00	13718	2.00	1.20	2.83	5.94	2.83	0.50
mv0lag1t1	2043	82	16620	2.00	81310	2.00	13760	2.00	1.21	2.83	5.91	2.83	0.50
mv0lag1t1	2052	82	16570	2.00	80400	2.00	13721	2.00	1.21	2.83	5.86	2.83	0.50
mv0lag1t1	2047	82	16720	2.00	80450	2.00	13745	2.00	1.22	2.83	5.85	2.83	0.50
mv0lag1t1	2046	82	16390	2.00	80570	2.00	13630	2.00	1.20	2.83	5.91	2.83	0.50
mv0lag1t1	2026	81	16760	2.00	80690	2.00	13619	2.00	1.23	2.83	5.92	2.83	0.50
mv0lag1t1	2059	82	15630	2.00	80350	2.00	13426	2.00	1.16	2.83	5.98	2.83	0.50
mv0lag1t2	2022	81	17110	2.00	77790	2.00	13435	2.00	1.27	2.83	5.79	2.83	0.50
mv0lag1t2	2073	83	16810	2.00	73510	2.00	13310	2.00	1.26	2.83	5.52	2.83	0.50
mv0lag1t2	2012	80	16620	2.00	72610	2.00	12700	2.00	1.31	2.83	5.72	2.83	0.50
mv0lag2t3	2097	84	14480	2.00	77170	2.00	12975	2.00	1.12	2.83	5.95	2.83	0.50
mv0lag2t3	2111	84	14920	2.00	76930	2.00	13218	2.00	1.13	2.83	5.82	2.83	0.50
mv0lag2t3	2093	84	14560	2.00	75960	2.00	12860	2.00	1.13	2.83	5.91	2.83	0.50
mv0lag2t3	2005	80	14670	2.00	75460	2.00	12229	2.00	1.20	2.83	6.17	2.83	0.50
mv0lag2t3	2116	85	13950	2.00	72180	2.00	12418	2.00	1.12	2.83	5.81	2.83	0.50
mv0lag2t3	2058	82	14430	2.00	71590	2.00	12142	2.00	1.19	2.83	5.90	2.83	0.50
mv0lag2t3	2061	82	7810	2.00	114690	2.00	13889	2.00	0.56	2.83	8.26	2.83	0.50
mv0lag3t1	2081	83	15320	2.00	79800	2.00	13431	2.00	1.14	2.83	5.94	2.83	0.50
mv0lag3t1	2070	83	13490	2.00	72820	2.00	11997	2.00	1.12	2.83	6.07	2.83	0.50
mv0lag3t1	2038	82	14780	2.00	80340	2.00	12964	2.00	1.14	2.83	6.20	2.83	0.50
mv0lag3t1	2121	85	10800	2.00	89090	2.00	12936	2.00	0.83	2.83	6.89	2.83	0.50
mv0lag3t1	2052	82	13730	2.00	72580	2.00	11943	2.00	1.15	2.83	6.08	2.83	0.50
mv0lag3t1	2083	83	13820	2.00	74420	2.00	12366	2.00	1.12	2.83	6.02	2.83	0.50
mv0lag3t1	2067	83	8250	2.00	121120	2.00	14713	2.00	0.56	2.83	8.23	2.83	0.50
mv0lag3t1	2047	82	7280	2.00	86200	2.00	10874	2.00	0.67	2.83	7.93	2.83	0.50
mv0lag3t1	1990	80	5010	2.10	79250	2.00	9101	2.00	0.55	2.90	8.71	2.83	0.49
mv0lag3t2	2058	82	13600	2.00	78480	2.00	12500	2.00	1.09	2.83	6.28	2.83	0.50
mv0lag3t2	2059	82	14920	2.00	79020	2.00	13045	2.00	1.14	2.83	6.06	2.83	0.50
mv0lag3t2	2107	84	14760	2.00	79150	2.00	13346	2.00	1.11	2.83	5.93	2.83	0.50
mv0lag3t2	2032	81	15290	2.00	81300	2.00	13190	2.00	1.16	2.83	6.16	2.83	0.50
mv0lag3t2	2080	83	15210	2.00	79780	2.00	13375	2.00	1.14	2.83	5.96	2.83	0.50
mv0lag3t2	2061	82	15310	2.00	80560	2.00	13345	2.00	1.15	2.83	6.04	2.83	0.50
mv0lag3t2	2079	83	15510	2.00	80700	2.00	13571	2.00	1.14	2.83	5.95	2.83	0.50

## ANEXO II (continuação)

REF	Idade Ma	Error Age Ma	U ppm	$\sigma$ %	Th ppm	$\sigma$ %	Pb ppm	$\sigma$ %	U/Pb	Error U/Pb %	Th/Pb	Error Th/Pb %	Corr.
mv0lag3t2	2065	83	15650	2.00	86890	2.00	14115	2.00	1.11	2.83	6.16	2.83	0.50
mv0lag3t2	2039	82	6070	2.00	74420	2.00	9267	2.00	0.66	2.83	8.03	2.83	0.50
mv0lag5t1	1997	80	15120	2.00	93620	2.00	14019	2.00	1.08	2.83	6.68	2.83	0.50
mv0lag5t1	2004	80	15180	2.00	92950	2.00	14032	2.00	1.08	2.83	6.62	2.83	0.50
mv0lag5t1	2066	83	6370	2.00	109800	2.00	12927	2.00	0.49	2.83	8.49	2.83	0.50
mv0lag5t1	2051	82	5960	2.00	110670	2.00	12762	2.00	0.47	2.83	8.67	2.83	0.50
mv0lag5t2	2066	83	6210	2.00	109400	2.00	12831	2.00	0.48	2.83	8.53	2.83	0.50
mv0lag5t2	2032	81	6170	2.00	107460	2.00	12399	2.00	0.50	2.83	8.67	2.83	0.50
mv0lag5t2	2060	82	6760	2.00	108450	2.00	12902	2.00	0.52	2.83	8.41	2.83	0.50
mv0lag5t2	2039	82	14670	2.00	92710	2.00	14108	2.00	1.04	2.83	6.57	2.83	0.50
mv0lag5t2	2083	83	12330	2.00	96280	2.00	13939	2.00	0.88	2.83	6.91	2.83	0.50
mv0lag5t2	2064	83	12290	2.00	98460	2.00	13989	2.00	0.88	2.83	7.04	2.83	0.50
mv0lag5t2	2012	80	13260	2.00	92280	2.00	13354	2.00	0.99	2.83	6.91	2.83	0.50
mv0lag6t1	2131	88	3320	3.16	84670	2.00	9706	2.00	0.34	3.74	8.72	2.83	0.38
mv0lag6t1	2099	87	3280	3.20	84070	2.00	9473	2.00	0.35	3.77	8.87	2.83	0.37
mv0lag6t1	2053	85	3500	3.00	82040	2.00	9133	2.00	0.38	3.61	8.98	2.83	0.39
mv0lag6t1	2012	83	3230	3.25	80970	2.00	8740	2.00	0.37	3.82	9.26	2.83	0.37
mv0lag6t1	2093	84	6000	2.00	101680	2.00	12179	2.00	0.49	2.83	8.35	2.83	0.50
mv0lag6t1	2063	83	7330	2.00	112610	2.00	13531	2.00	0.54	2.83	8.32	2.83	0.50
mv0lag6t1	2005	80	6420	2.00	95920	2.00	11231	2.00	0.57	2.83	8.54	2.83	0.50
mv0lag6t1	2047	82	6310	2.00	119610	2.00	13712	2.00	0.46	2.83	8.72	2.83	0.50
mv0lag6t1	2031	81	6160	2.00	117200	2.00	13313	2.00	0.46	2.83	8.80	2.83	0.50
mv0lag6t2	2049	84	3630	2.89	84090	2.00	9358	2.00	0.39	3.52	8.99	2.83	0.40
mv0lag6t2	2127	87	3560	2.95	84200	2.00	9730	2.00	0.37	3.56	8.65	2.83	0.40
mv0lag6t2	2041	84	3300	3.18	80460	2.00	8856	2.00	0.37	3.76	9.09	2.83	0.38
mv0lag6t2	2070	86	3270	3.21	80900	2.00	9022	2.00	0.36	3.78	8.97	2.83	0.37
mv0lag6t2	2028	84	3280	3.20	78840	2.00	8634	2.00	0.38	3.77	9.13	2.83	0.37
mv0lag6t2	2037	84	3390	3.10	81840	2.00	9001	2.00	0.38	3.69	9.09	2.83	0.38
mv0lag6t2	2058	84	3640	2.88	85760	2.00	9569	2.00	0.38	3.51	8.96	2.83	0.40
mv0lag6t2	2065	84	3970	2.64	88110	2.00	9949	2.00	0.40	3.32	8.86	2.83	0.43
mv0lag6t2	1985	81	4210	2.49	85140	2.00	9343	2.00	0.45	3.20	9.11	2.83	0.44
mv0lag7t1	2017	81	8250	2.00	107220	2.00	13018	2.00	0.63	2.83	8.24	2.83	0.50
mv0lag7t1	2069	83	9890	2.00	103540	2.00	13639	2.00	0.73	2.83	7.59	2.83	0.50
mv0lag7t1	2000	80	9450	2.00	100970	2.00	12736	2.00	0.74	2.83	7.93	2.83	0.50
mv0lag7t1	2081	83	10990	2.00	83960	2.00	12227	2.00	0.90	2.83	6.87	2.83	0.50
mv0lag7t2	2083	83	12790	2.00	82100	2.00	12731	2.00	1.00	2.83	6.45	2.83	0.50
mv0lag7t2	2063	83	11840	2.00	80590	2.00	12097	2.00	0.98	2.83	6.66	2.83	0.50
mv0lag7t2	2102	84	12270	2.00	73060	2.00	11779	2.00	1.04	2.83	6.20	2.83	0.50
mv0lag7t2	2058	82	11750	2.00	78930	2.00	11870	2.00	0.99	2.83	6.65	2.83	0.50
mv0lag7t2	2066	83	10210	2.00	84420	2.00	11888	2.00	0.86	2.83	7.10	2.83	0.50
mv0lag7t2	2030	81	9740	2.00	105550	2.00	13488	2.00	0.72	2.83	7.83	2.83	0.50
mv0lag7t2	2056	82	6940	2.00	97560	2.00	11890	2.00	0.58	2.83	8.21	2.83	0.50
mv0lag7t2	2033	81	6990	2.00	102590	2.00	12241	2.00	0.57	2.83	8.38	2.83	0.50
mv0lag7t2	2029	81	6570	2.00	100740	2.00	11889	2.00	0.55	2.83	8.47	2.83	0.50
<i>Grupo 2</i>													
mv0lag1t2	1861	74	15100	2.00	79110	2.00	11679	2.00	1.29	2.83	6.77	2.83	0.50
mv0lag1t2	1901	76	6480	2.00	97990	2.00	10794	2.00	0.60	2.83	9.08	2.83	0.50
mv0lag2t3	1862	74	21740	2.00	72540	2.00	13253	2.00	1.64	2.83	5.47	2.83	0.50
mv0lag5t2	1910	76	13890	2.00	96750	2.00	13197	2.00	1.05	2.83	7.33	2.83	0.50
mv0lag6t1	1860	78	2500	4.20	74480	2.00	7237	2.00	0.35	4.65	10.29	2.83	0.30
mv0lag6t2	1849	85	1070	9.81	55450	2.00	5101	2.16	0.21	10.05	10.87	2.94	0.16
mv0lag7t1	1899	76	8710	2.00	119710	2.00	13435	2.00	0.65	2.83	8.91	2.83	0.50
mv0lag7t2	1880	75	9320	2.00	109850	2.00	12624	2.00	0.74	2.83	8.70	2.83	0.50